Further titles in this series:
Volumes 2, 3, 5, 6, 7, 9, 10, 13, 16 and 26 are out of print

1. G. SANGLERAT — THE PENETROMETER AND SOIL EXPLORATION
4. R. SILVESTER — COASTAL ENGINEERING, 1 and 2
8. L.N. PERSEN — ROCK DYNAMICS AND GEOPHYSICAL EXPLORATION
   Introduction to Stress Waves in Rocks
11. H.K. GUPTA AND B.K. RASTOGI — DAMS AND EARTHQUAKES
12. F.H. CHEN — FOUNDATIONS ON EXPANSIVE SOILS
14. B. VOIGHT (Editor) — ROCKSLIDES AND AVALANCHES, 1 and 2
15. C. LOMNITZ AND E. ROSENBLUETH (Editors) — SEISMIC RISK AND ENGINEERING DECISIONS
17. A.P.S. SELVADURAI — ELASTIC ANALYSIS OF SOIL-FOUNDATION INTERACTION
18. J. FEDA — STRESS IN SUBSOIL AND METHODS OF FINAL SETTLEMENT CALCULATION
19. Á. KÉZDI — STABILIZED EARTH ROADS
20. E.W. BRAND AND R.P. BRENNER (Editors) — SOFT-CLAY ENGINEERING
21. A. MYSLIVE AND Z. KYSELA — THE BEARING CAPACITY OF BUILDING FOUNDATIONS
22. R.N. CHOWDHURY — SLOPE ANALYSIS
23. P. BRUUN — STABILITY OF TIDAL INLETS
    Theory and Engineering
24. Z. BAŽANT — METHODS OF FOUNDATION ENGINEERING
25. Á. KÉZDI — SOIL PHYSICS
    Selected Topics
27. D. STEPHENSON — ROCKFILL IN HYDRAULIC ENGINEERING
28. P.E. FRIVIK, N. JANBU, R. SAETERSDAL AND L.I. FINBORUD (Editors) — GROUND FREEZING 1980
29. P. PETER — CANAL AND RIVER LEVÉES
30. J. FEDA — MECHANICS OF PARTICULATE MATERIALS
    The Principles
31. Q. ZÁRUBA AND V. MENCL — LANDSLIDES AND THEIR CONTROL
    Second completely revised edition
32. I.W. FARMER (Editor) — STRATA MECHANICS
33. L. HOBST AND J. ZAJÍC — ANCHORING IN ROCK AND SOIL
    Second completely revised edition
34. G. SANGLERAT, G. OLIVARI AND B. CAMBOU — PRACTICAL PROBLEMS IN SOIL MECHANICS AND FOUNDATION ENGINEERING, 1 and 2
35. L. RÉTHÁTI — GROUNDWATER IN CIVIL ENGINEERING
36. S.S. VYALOV — RHEOLOGICAL FUNDAMENTALS OF SOIL MECHANICS
37. P. BRUUN (Editor) — DESIGN AND CONSTRUCTION OF MOUNDS FOR BREAKWATERS AND COASTAL PROTECTION
38. W.F. CHEN AND G.Y. BALADI — SOIL PLASTICITY
    Theory and Implementation
39. E.T. HANRAHAN — THE GEOTECTONICS OF REAL MATERIALS: THE ϵ_g, ϵ_k METHOD
40. J. ALDORF AND K. EXNER — MINE OPENINGS
    Stability and Support
41. J.E. GILLOTT — CLAY IN ENGINEERING GEOLOGY
42. A.S. CAKMAK (Editor) — SOIL DYNAMICS AND LIQUEFACTION
42. A.S. CAKMAK (Editor) — SOIL-STRUCTURE INTERACTION
44. A.S. CAKMAK (Editor) — GROUND MOTION AND ENGINEERING SEISMOLOGY
45. A.S. CAKMAK (Editor) — STRUCTURES, UNDERGROUND STRUCTURES, DAMS, AND STOCHASTIC METHODS
46. L. RÉTHÁTI — PROBABILISTIC SOLUTIONS IN GEOTECTONICS
47. B.M. DAS — THEORETICAL FOUNDATION ENGINEERING
48. W. DERSKI, R. IZBICKI, I. KISIEL AND Z. MROZ — ROCK AND SOIL MECHANICS
49. T. ARIMAN, M. HAMADA, A.C. SINGHAL, M.A. HAROUN AND A.S. CAKMAK (Editors) — RECENT ADVANCES IN LIFELINE EARTHQUAKE ENGINEERING
50. B.M. DAS — EARTH ANCHORS
51. K. THIEL — ROCK MECHANICS IN HYDROENGINEERING
52. W.F. CHEN AND X.L. LIU — LIMIT ANALYSIS IN SOIL MECHANICS
53. W.F. CHEN AND E. MIZUNO — NONLINEAR ANALYSIS IN SOIL MECHANICS
54. F.H. CHEN — FOUNDATIONS ON EXPANSIVE SOILS
55. J. VERFEL — ROCK GROUTING AND DIAPHRAGM WALL CONSTRUCTION
56. B.N. WHITTAKER AND D.J. REDDISH — SUBSIDENCE
    Occurrence, Prediction and Control
57. E. NONVEILLER — GROUTING, THEORY AND PRACTICE
58. V. KOLÁŘ AND I. NĚMEC — MODELLING OF SOIL-STRUCTURE INTERACTION
59A. R.S. SINHA — UNDERGROUND STRUCTURES
    Design and Instrumentation

DEVELOPMENTS IN GEOTECHNICAL ENGINEERING, 52

LIMIT ANALYSIS IN SOIL MECHANICS

W.F.CHEN

Purdue University, School of Civil Engineering, West Lafayette, IN 47907, U.S.A.

and

X.L. LIU

Department of Civil Engineering, Tsinghua University, Beijing, PRC

ELSEVIER
Amsterdam — Oxford — New York — Tokyo 1990

DEVELOPMENTS IN GEOTECHNICAL ENGINEERING, 52

LIMIT ANALYSIS IN SOIL MECHANICS

ELSEVIER SCIENCE PUBLISHERS B.V.
Sara Burgerhartstraat 25
P.O. Box 211, 1000 AE Amsterdam, The Netherlands

Distributors for the United States and Canada:

ELSEVIER SCIENCE PUBLISHING COMPANY INC.
655, Avenue of the Americas
New York, NY 10010, U.S.A.

Library of Congress Cataloging-in-Publication Data

Chen, Wai-Fah, 1936-
Limit analysis in soil mechanics / W.F. Chen and X.L. Liu.
p. cm. -- (Developments in geotechnical engineering ; 52)
Includes bibliographical references.
ISBN 0-444-43042-3 (Elsevier Science Pub.)
1. Soil mechanics. 2. Plastic analysis (Engineering)
3. Earthquake engineering. I. Liu, X. L. II. Title. III. Series.
TA710.C5332 1990
624.1'5136--dc20 90-35193
CIP

ISBN 0-444-43042-3 (Vol. 52)

Printed in The Netherlands

PREFACE

Limit analysis is concerned with the development of efficient methods for computing the collapse or limit load of structures in a direct manner. It is therefore of intense practical interest to practicing engineers. There have been an enormous number of applications in metal structures. Applications of limit analysis to reinforced concrete structures are more recent and are given in two recent books (W.F. Chen, 'Plasticity in Reinforced Concrete', McGraw-Hill, 1982; M.P. Nielsen, 'Limit Analysis and Concrete Plasticity', Prentice-Hall, 1984). Applications to typical stability problems in soil mechanics have been the most highly developed aspect of limit analysis so that the basic techniques and many numerical results were summarized in the 1975 book by Chen entitled 'Limit Analysis and Soil Plasticity', Elsevier. About 250 pages in this 1975 book were devoted to applying limit analysis to the well-known 'classical' stability problems in soil mechanics: bearing capacity of footings, lateral earth pressure problems, and stability of slopes. Many limit analysis solutions were presented and compared with solutions from conventional limit equilibrium analysis and slip-line solutions. In several instances, especially in bearing capacity problems, such a level of reliability and completeness was achieved that limit analysis solutions were given in comprehensive graphs and tables greatly facilitating the practical application of the results.

However, most of the applications of limit analysis to soil mechanics problems before 1975 were limited to soil statics. Further, it is a surprise to note that relatively little work was carried out by researchers and engineers before 1975 to apply limit analysis to earth pressure problems. During the last ten years, our understanding of the perfect plasticity and the associated flow rule assumption on which limit analysis is based has increased considerably and many extensions and advances have been made in applications of limit analysis to the area of soil dynamic, in particular, to earthquake-induced slope failure and landslide problems and to earthquake-induced lateral earth pressures on rigid retaining structures. This is not therefore just another book which presents limit analysis in a new style. Instead, its purpose is in part to discuss the validity of the upper bound work (or energy) method of limit analysis in a form that can be appreciated by a practicing soil engineer, and in part to provide a compact and convenient summary of recent advances in the applications of limit analysis to earthquake-induced stability problems in soil mechanics.

For reasons of brevity, and because it is assumed that the reader has had some

contact with the 1975 book on 'Limit Analysis and Soil Plasticity' by the first author, the emphasis in the first part of this book is focussed therefore on the physical justification of limit analysis of perfect plasticity in application to soils from the viewpoint of a soil engineer, rather than on the mathematical rigorousness from the viewpoint of a continuum mechanician. To this end, some practical limits on soils are suggested in the use of limit analysis method. Details of the application of the upper bound work (or energy) method to stability problems in soil mechanics in general and to earthquake-induced earth pressures and slope failures in particular are made with extensive numerical results presented in graphs and tables. Since extensive references to the work of limit analysis in soil mechanics before 1975 were already given in the 1975 book cited, only the references relevant to the recent work will be given in this book.

The scope of the book is indicated by the contents. The first part of the book sets out initially to describe the basic concept and technique of limit analysis and the assumptions on which it is based (Chapter 2), going on to examine, on the basis of idealized test conditions, the behavior and strength of soils, and leading to show why the limit analysis technique is applicable to soils, especially for the cohesionless soils (Chapter 3).

The upper bound work method is then applied and used to predict the lateral earth pressures subjected to static forces (Chapter 4) as well as to earthquake forces (Chapter 5). Practical design considerations of rigid retaining structures made using this analysis are then summarized in Chapter 6. A brief description of the application of the work method to determine the bearing capacity of strip footings on a half-space follows of a rigorous upper bound analysis capable of dealing with foundations on anisotropic and nonhomogeneous soils (Chapter 7).

The analysis method based on the concept put forward by N.M. Newmark in his 1965 Rankine lecture entitled 'Effects of Earthquakes on Dams and Embankments', (Geotechnique, Vol. 15, No. 2), is then developed. The method is used to predict the stability of a slope and its possible movement under a design earthquake (Chapters 8, 9, 10). In the slope stability analysis, the logarithmic spiral rotational failure mechanism is frequently utilized to provide a least upper-bound solution. However, this failure mechanism is appropriate only for the material that follows the popular linear Mohr-Coulomb failure criterion. We cannot immediately apply the linear limit analysis method to a nonlinear failure problem. In many practical problems such as the frozen gravel embankments used in offshore arctic engineering, the material is known to be highly nonlinear in its failure criterion. It is necessary therefore to investigate the stability problems and to develop practical solution methods based upon a general nonlinear failure criterion. This is described in Chapter 11.

Much of the research on soil mechanics, plasticity and earthquake-induced slope failure and landslide problems, sponsored by the National Science Foundation at Purdue University, provided a background for the book and has been drawn on freely. The book contains many results first presented in the form of technical

reports and later as Ph.D. dissertations, prepared under various phases of research projects, related to this subject. It is a pleasure for Professor Chen to acknowledge his indebtedness to many of his students and friends, particularly Drs. C.J. Chang, M.F. Chang, X.L. Liu, W.O. McCarron, E. Mizuno, A.F. Saleeb, T. Sawada, E. Yamaguchi and Messrs. S.W. Chan, O.Y. Wang and X.J. Zhang for their excellent work concerning specific topics included in the book. Mr. T.K. Huang read the entire manuscript and gave us many useful suggestions.

West Lafayette, Indiana — W.F. Chen
December 1988 — X.L. Liu

CONTENTS

Chapter 8 EARTHQUAKE-INDUCED SLOPE FAILURE AND LANDSLIDES

Chapter 9 SEISMIC STABILITY OF SLOPES IN NONHOMOGENEOUS, ANISOTROPIC SOILS AND GENERAL DISCUSSIONS

Chapter 10 ASSESSMENT OF SEISMIC DISPLACEMENT OF SLOPES

Chapter 11 STABILITY ANALYSIS OF SLOPES WITH GENERALIZED FAILURE CRITERION

Chapter 1

INTRODUCTION

1.1 Introduction

The main objectives of stress analysis in soil mechanics are to ensure that the soil mass under consideration shall have a suitable factor of safety against ultimate failure or collapse, that it shall meet the service requirements when subjected to its design working load. To this end, the analysis of problems in soil mechanics is generally divided into two distinct groups – the *stability problems* and the *elasticity problems*. They are then treated in two separate and unrelated ways. The stability problems deal with the condition of ultimate failure of a mass of soil: problems of earth pressure, bearing capacity, and stability of slopes most often are considered in this group. The most important feature of such problems is the determination of the loads which will cause failure of the soil mass. Solutions to these problems can often be obtained by simple statics by assuming failure surface of various simple shapes – plane, circular, or logspiral – and by using Coulomb's failure criterion. This is known as the *limit equilibrium method* in soil mechanics.

The earliest contribution to this method was made in 1773 by Coulomb who proposed the Coulomb criterion for soils and also established the important concept of limiting equilibrium to a continuum and applied it to determine the pressure of a fill on a retaining wall. Later, in 1857, Rankine investigated the limiting equilibrium of an infinite body and developed the theory of earth pressure in soil mechanics. In this historical development, the introduction of *stress-strain relations* or *constitutive relations* of soils was obviated by the restriction to the consideration of limiting equilibrium and the appeal to the extremum principle. Subsequent developments by Fellenius (1926) and Terzaghi (1943), among many others, have made the limit equilibrium method a working tool with which many engineers develop their own practical solutions. Perhaps the most striking feature of this approach is that no matter how complex the geometry of a problem or loading condition is, it is always possible to obtain some approximate but realistic solution.

The elasticity problems, on the other hand, deal with stress and deformation of the soil at working load level when no failure of the soil is involved. Stresses at points in a soil mass under a footing, or behind a retaining wall, deformations around tunnels or excavations, and all settlement problems belong in this group. Solutions to these problems are often obtained by using the theory of linear elastici-

ty. This approach is rational for problems at short-term working load level, but limited by the assumed elasticity of the soils whose properties approach most nearly those of a time-independent elastic material. While time-dependent effects are significantly large, introducing long-term working stresses over a given period, it is obviously wrong to design a structure on the basis of this time-independent Hooke's law for soils. In this case the design must consider the influence of time on the deformations. This is known as *creep*. Such a behavior may be modelled as viscoelastic and the theory of viscoelasticity may be applied to obtain solutions.

Intermediate between the elasticity problems and the stability problems mentioned above are the problems known as progressive failure. *Progressive failure problems* deal with the elastic – plastic transition from the initial linear elastic state to the ultimate failure state of the soil by plastic flow. The essential constituent in obtaining the solution of a progressive failure problem is the explicit introduction of stress-strain or constitutive relations of soils which must be considered in any solution of a solid mechanics problem.

As mentioned previously, for a long time, solutions in soil mechanics have been based upon Hooke's law of linear elasticity for describing soil behavior under working loading conditions and Coulomb's law of perfect plasticity for describing soil behavior under collapse state because of simplicity in their respective applications. It is well known that soils are not linearly elastic and perfectly plastic for the entire range of loading of practical interest. In fact, actual behavior of soils is known to be very complicated and it shows a great variety of behavior when subjected to different conditions. Drastic idealizations are therefore essential in order to develop simple mathematical constitutive models for practical applications. For example, time-independent idealization is necessary in order to apply the theories of elasticity and plasticity to problems in soil mechanics.

It must be emphasized here that not one mathematical model can completely describe the complex behavior of real soils under all conditions. Each soil model is aimed at a certain class of phenomena, captures their essential features, and disregards what is considered to be of minor importance in that class of applications. Thus, a constitutive model meets its limits of applicability where a disregarded influence becomes important. This is why Hooke's law has been used so successfully in soil mechanics to describe the general behavior of soil media under short-term working load conditions, while the Coulomb's law of perfect plasticity providing good predictions of soil behavior near ultimate strength conditions, because plastic flow at this ultimate load level attains a dominating influence, whereas elastic behavior becomes of relatively minor importance.

For the most part, the concept of *perfect plasticity* has been used extensively in conventional soil mechanics in assessing the collapse load in stability problems The standard and widely known technique used in conventional soil mechanics is the limit equilibrium method. However, it neglects altogether the important fact that

the stress-strain relations constitute an essential part in a complete theory of continuum mechanics of deformable solids. Modern *limit analysis method*, however, takes into consideration, in an idealized manner, the stress-strain relations of soils. This idealization, termed normality or flow rule, establishes the limit theorems on which limit analysis is based. Within the framework of perfect plasticity and the associated flow rule assumption, the approach is rigorous and the techniques are competitive with those of limit equilibrium approach. In several instances, especially in slope stability analysis, earth pressure problems, and bearing capacity calculations, such a level and completeness has been achieved and firmly established in recent years that the limit analysis method can be used as a working tool for design engineers to solve everyday problems (Chen, 1975).

Most of the early applications of limit analysis of perfect plasticity to soil mechanics problems have been limited to soil statics. Recent works attempt to extend this method to soil dynamics, in particular to earthquake-induced stability problems. Recent results show convincingly that the upper-bound analysis method can be applied to soils for obtaining reasonably accurate solutions of slope failures and lateral earth pressures subjected to earthquake forces. Different aspects of these advances were reported in several recent books, theses, conference proceedings, and state-of-the-art reports. This includes the books by Bazant (1985), Desai and Gallagher (1983), and Dvorak and Shield (1984); the theses by C.J. Chang (1981), Saleeb (1981), M.F. Chang (1981), Chan (1980), Mizuno (1981) and McCarron (1985); the Conference Proceedings by ASCE (Yong and Ko, 1981, Yong and Selig, 1982), and the state-of-the-art reports by Chen (1980, 1984), and Chen and Chang (1981), among others.

The main virtue of the application of the upper-bound techniques of limit analysis to stability problems in soil mechanics is that no matter how complex the shape of a soil mass or loading configuration is, it is always possible to obtain a realistic value of the failure or collapse load. When this is coupled with its other merits, namely, that it is relatively simple to apply, that it is a limit state or collapse state method and that many of the solutions predicted by the method have been substantiated by experiments or by numerical calculations through the well-established computer-based methods, it can be appreciated that it is a working tool with which every engineer should be conversant.

The objective of this book, therefore, is to describe the recent applications of the upper-bound techniques of limit analysis to stability problems in soil mechanics in detail, beginning with the historical review of the subject and the assumptions on which it is based and covering the numerous developments which have taken place since 1975. The book does not include what may be termed 'standard limit analysis methods and solutions' which have been previously covered in the book entitled 'Limit Analysis and Soil Plasticity' by Chen (1975).

Before the upper-bound techniques of limit analysis are described in detail, the

basic assumptions of the limit theorems on which the limit analysis is based are first reviewed in Chapter 2 and the range of validity of these assumptions in the context of soils is then critically examined and assessed in Chapter 3 from the stress-dilatancy and from the energy point of view. In the subsequent chapters, the upper-bound limit analysis method is applied to obtain solutions of the earth pressure on rigid retaining walls subjected to static and seismic loadings (Chapters 4, 5 and 6), of the bearing capacity of strip footings on nonhomogeneous, anisotropic soil (Chapter 7), and of the seismic stability of slopes (Chapters 8, 9 and 10).

Although, the upper-bound limit analysis method can be applied to solve stability problems with any type of failure criterion, almost all solutions that are at present known, are based on the well-known linear Mohr-Coulomb failure criterion. However, in many practical problems in geotechnical engineering, such as the frozen gravel embankments used in offshore arctic engineering, experimental data have shown that the frozen gravel follows a highly nonlinear failure criterion. We cannot apply directly the techniques developed in the linear limit analysis to the nonlinear failure problems. It is therefore necessary to investigate the soil stability problems and to develop practical solution methods based upon a general nonlinear failure criterion. Fortunately, in recent years, the application of the variational calculus in soil mechanics makes it possible to combine the upper-bound limit analysis method with the conventional limit equilibrium method and leads to the development of a realistic and practical method for the solution of a class of stability problems in nonlinear soil mechanics. This is described in detail in Chapter 11.

1.2 A short historical review of soil plasticity

Before the techniques of limit analysis are described in the chapters that follow, it is important to appreciate that the limit analysis is indeed a great simplification of the true behavior of soil mass. In order to get these simplifications or assumptions in true perspective, we shall present in this section a brief summary of the current advances in the applications of the theory of plasticity to problems in soil mechanics. A general examination of soil plasticity is followed in the subsequent sections by a detailed description of the three basic subjects that are closely interrelated. These are:

1. Idealized stress-strain relations for soil;
2. Limit analysis for collapse load; and
3. Finite-element analysis for progressive failure behavior of soil mass.

In this way, some of the interrelationships between the limit analysis of perfect plasticity and the finite-element analysis of work-hardening plasticity are demonstrated, and their power and their relative merits and limitations for practical applications are evaluated.

In the 1950s, major advances were made in the theory of metal plasticity by the development of (a) fundamental *theorems of limit analysis*; (b) Drucker's postulate or definition of *stability of material*; and (c) the concept of *normality condition* or *associated flow rule*. The theory of limit analysis of perfect plasticity leads to practical methods that are needed to estimate the load-carrying capacity of structures in a more direct manner. The concept of a stable material provides a unified treatment and broad point of view of the stress-strain relations of plastic solids. The normality condition provides the necessary connection between the yield criterion or loading function and the plastic stress-strain relations. All these have led to a rigorous basis for the theory of classical plasticity, and laid down the foundations for subsequent notable developments.

The initial applications of the classical theory of plasticity were almost exclusively concerned with perfectly plastic metallic solids such as mild steel which behaves approximately like a perfectly plastic material (Prager and Hodge, 1950). For these materials, the angle of internal friction ϕ is zero, no plastic volume change occurs and the only material property is the shear strength k or cohesion c in the terminology of soil mechanics. Numerical calculations were restricted to the method of characteristics based on the theory of the plane slip-line field analysis to derive the stress and velocity distribution in the plastic region (Hill, 1950). Since the plane slip-line field analysis is rarely applicable to structures, exact and approximate calculations of the plastic collapse load were made exclusively by the methods of limit analysis (Drucker, 1960).

The development of the modern theory of soil plasticity, as the new field was called, was strongly influenced by the well-established theory of metal plasticity. Soil mechanics specialists have been preoccupied with extending these concepts to answer the complex problems of soil behavior. Tresca's yield condition, used widely in metal plasticity, can be regarded as a special case of the condition of Coulomb on which the important concept of the limiting equilibrium of a soil medium had been firmly established in soil mechanics.

It is relatively straightforward matter to extend the method of characteristics to cover Coulomb material where c and ϕ can either remain constant (Sokolovskii, 1965) or vary throughout the stress field in some specified manner (Booker and Davis, 1972). In the theory of limit equilibrium, the introduction of stress-strain relations was obviated by the restriction to the consideration of equations of equilibrium and a yield condition. This produces what appears to be and sometimes is static determinacy for the solutions of slip-line field equations. However, in many soil–structure interaction problems, the boundary conditions involve rates of displacement and the slip line equations are generally statically indeterminate. The key to obtain a valid solution for such cases requires the basic knowledge of the stress-strain relations. Otherwise, a so-called solution is merely a guess.

The general theory of limit analysis, developed in the early 1950s, considers the stress-strain relation of a soil in an idealized manner. This idealization, termed nor-

mality or the associated flow rule, establishes the limit theorems on which limit analysis is based. Although the applications of limit analysis to problems in soil mechanics are relatively recent, there have been an enormous number of practical solutions available (Chen, 1975). Many of the solutions obtained by the method are remarkably good when comparing with the existing results for which satisfactory solutions already exist. As a result of this development, the meaning of the limit equilibrium solutions in the light of the upper- and lower-bound theorems of limit analysis becomes clear.

The first major advance in the extension of metal plasticity to soil plasticity was made in the paper 'Soil Mechanics and Plastic Analysis or Limit Design' by Drucker and Prager (1952). In this paper, the authors extended the Mohr-Coulomb criterion to three-dimensional soil mechanics problems. The Mohr-Coulomb criterion was interpreted by Drucker (1953) as a modified Tresca as well as an extended von Mises yield criterion. The yield criterion obtained by Drucker and Prager for the later case is now known as the Drucker-Prager model or the extended von Mises model.

One of the main stumbling blocks in the further development of the stress-strain relations of soil based on the Drucker-Prager type or Mohr-Coulomb type of yield surfaces to define the limit of elasticity and beginning of a continuing irreversible plastic deformation was the excessive prediction of dilation, which was the result of the use of the associated flow rule. It became necessary, therefore, to extend classical plasticity ideas to a 'non-associated' form in which the plastic potential and yield surfaces are defined separately (Davis, 1968). However, this modification eliminated the validity of the use of limit theorems for bounding collapse loads and created doubts about the uniqueness of solutions. Attempts have been made to revise the bouding theorems and to resolve the uniqueness problem, but to date not much success has been achieved through this route (Palmer, 1973).

In 1957, an important advance was made in the paper 'Soil Mechanics and Work-Hardening Theories of Plasticity' by Drucker, Gibson and Henkel (1957). In this paper the authors introduced the concept of work-hardening plasticity into soil mechanics. There are two important innovations in the paper. The first is the introduction of the idea of a work-hardening cap to the perfectly plastic yield surface such as the Coulomb type or Drucker-Prager type of yield criterion. The second innovation is the use of current soil density (or voids ratio, or plastic compaction) as the state variable or the strain-hardening parameter to determine the successive loading cap surfaces.

These ideas have led to in turn to the generation of many soil models, most notably the development of the critical-state soil mechanics at Cambridge University, U.K. These new soil models have grown increasingly complex as additional experimental data have been gathered, interpreted, and matched. This extension marks the beginning of the modern development of a consistent theory of soil plasticity (Chen, 1975; Chen and Baladi, 1985).

1.3 Idealized stress-strain relations for soil

Soil mechanics along with all other branches of mechanics of solids requires the consideration of geometry or compatibility and of equilibrium or dynamics. The essential set of equations that differentiate the soil from other solids is the relation between stress and stain. The behavior of soils is very complicated. The attempt to incorporate the various features of soil properties in a single mathematical model is not likely to be successful, but even if such a model could be constructed, it would be far too complex to serve as the basis for the solution of practical geotechnical engineering problems. Simplifications and idealizations are essential in order to produce simpler models that can represent those properties that are essential to the considered problem. Thus, any such simpler models should not be expected to be valid over a wide range of conditions.

The need for mathematical simplicity in the description of the mechanical properties of solids is understood quite well for metals where so much research effort has been expended by so many investigators. Yet even for metals, the simple idealizations such as perfect plasticity, isotropic hardening, kinematic hardening, and mixed hardening are frequently used in solving practical problems. The same situation is to be expected for the stress-strain modeling of soil which is a far more complex material.

Drastic idealizations are valuable not only for the ease of treatment of practical engineering problems but also conceptually for a clear physical understanding of the essential features of the complex behavior of a material under certain conditions. Therefore, for soils, as for metals, perfect plasticity is still an excellent design assumption, while very complex stress-strain relations of soil which require an ever increasing elaboration in detail of a mathematical description may be approximated crudely by simple isotropic, kinematic, or mixed hardening models. Thus, the isotropic hardening cap models and Cambridge models, the kinematic hardening nested yield surfaces models, or the mixed hardening bounding surface models that have been proposed and developed in recent years are all within the realms of this simplification (Chen and Baladi, 1985). In the sections that follow, some of these developments are briefly described and, hopefully, unified within the same framework of physically and mathematically well-established theory of work-hardening plasticity.

The use of work-hardening plasticity theories in soil mechanics has been developed for about thirty years, since publication of the classical paper by Drucker et al. (1957). Most of the research has been conducted by engineers working in the area of soil statics. Recently, attention has been focused on the use of these models in soil dynamics (Chen, 1980). The objective of this section is to set forth the state-of-the-art with respect to elastic-plastic stress-strain relations of soils. In doing so, it achieves not only the purpose of surveying the current research activity that has

been going on very actively in this field in recent years, but also the survey gives the best indications of future problems that may result from the observations of the trend of recent developments.

One of the main problems in the theory of plasticity is to determine the nature of the subsequent yield surfaces. This post-yielding response is described by the hardening rule which specifies the rule for the evolution of the loading surfaces during the course of plastic deformations. Indeed, the assumption made concerning the hardening rule introduces a major distinction among various plasticity models developed for soils in recent years.

1.3.1 Hardening (softening) rules

There are several hardening rules that have been proposed to describe the growth of subsequent yield surfaces for strain-hardening (softening) materials. The choice of a specific rule depends primarily on the ease with which it can be applied and its ability to represent the hardening behavior of a particular material. In general, three types of hardening rules have been commonly utilized (Chen, 1982). These are: (1) isotropic hardening; (2) kinematic hardening; and (3) mixed hardening. In an isotropic hardening model, the initial yield surface is assumed to expand (or contract) uniformly without distortion as plastic flow continues. On the other hand, the kinematic hardening rule assumes that, during plastic deformations, the loading surface translates without rotation as rigid body in the stress space, maintaining the size and shape of the initial yield surface. This rule provides a means of accounting for the Bauschinger effect, which refers to one particular type of directional anisotropy induced by plastic deformations; namely that an initial plastic deformation of one sign reduces the resistance of the material with respect to a subsequent plastic deformation of the opposite sign. Therefore, kinematic hardening models are particularly suitable for materials with pronounced Bauschinger effect such as soils under cyclic and reversed types of loading.

A combination of isotropic and kinematic hardening models leads to a more general hardening rule, and therefore provides for more flexibility in describing the hardening behavior of the material. For a mixed (combined) hardening model, the loading surface experiences translation as well as expansion (contraction) in all directions, and different degrees of Bauschinger effect may be simulated. Kinematic and mixed types of hardening rules are generally known as anisotropic hardening models.

In the last few years, several plasticity models with more complex hardening rules combining the concepts of kinematic and isotropic hardening have been developed and applied to describe the behavior of soils under cyclic loading (Chen and Baladi, 1985).

1.3.2 Perfect plasticity models

Perfect plasticity is an appropriate idealization for a structural metal because it captures the essential features of its behavior. This includes small tangent modulus when compared with elastic modulus, when loading in the plastic range, and the unloading response is elastic. However, perfect plasticity is not nearly appropriate for soils. Some of the troubles and their justifications for adoption of this idealization for practical use were discussed in the paper 'Concepts of Path Independence and Material Stability for Soils' by Drucker (1966).

For the most part, the concept of perfect plasticity has been used extensively in the past in conventional soil mechanics in assessing the collapse load in stability problems. Different widely known techniques have been employed to obtain numerical solutions in these cases; such as the slip-line method (Sokolovskii, 1965), and the limit equilibrium method (Terzaghi, 1943). For the later case, the simple ideas of perfect plasticity have found their direct application in many practical geotechnical engineering problems.

In addition to these classical methods, the more rigorous approach of modern limit analysis of perfect plasticity has been applied to a wide variety of practical stability problems. Using the well-known Coulomb yield criterion and its associated flow rule, many solutions have been obtained (Chen, 1975). Recently, the stability analysis has been extended to include the earthquake loading, employing the pseudo-static force method (see Chapters 5, 9 and 10). It should be emphasized here that the useful application of these techniques has not been exhausted. New and striking applications are not only possible but to be encouraged strongly, because of their simplicity and power in helping us reach an understanding of, and feel for, a problem. Further, some predictions of this enormous idealization are very good. Much more value will be uncovered as engineers who have need for particular results apply the methods of limit analysis and design to their own special problems.

1.4 Limit analysis for collapse load

Limit analysis is concerned with the development of efficient methods for computting the *collapse load* in a direct manner. It is therefore of intense practical interest to practicing engineers. There have been an enormous number of applications in metal structures. Applications of limit analysis to reinforced concrete structures are more recent and are given in a recent book by Chen (1982) as well as a colloquium proceedings (IABSE, 1979). Applications to typical stability problems in soil mechanics have been the most highly developed aspect of limit analysis so that the basic techniques and many numerical results have been summarized in the book by Chen (1975). Extensive references to the work before 1975 are also given in the book cited. An up-to-date reference to recent work on the applications of limit analysis

to earth pressure, bearing capacity and slope stability problems can be found in the ASCE Proceedings (Yong and Ko, 1981; Yong and Selig, 1982), among many others.

It is true, as in most fields of knowledge, that many of the basic ideas of perfect plasticity and limit analysis have been used extensively and fruitfully in the past in conventional soil mechanics through experimental studies and engineering intuition. Here, the standard and widely known techniques of the slip-line method and the limit equilibrium method, among others, come to mind immediately, and these methods also have been mentioned previously.

The slip-line method uses the Coulomb criterion as the yield condition for soil. From the basic slip-line differential equations, the slip-line network can be constructed and the collapse load determined. Examples of this approach are the solutions presented in the book by Sokolovskii (1965).

The limit equilibrium method can be best described as an approximate approach to the construction of the slip-line field. It generally entails the assumption of the failure surface of various simple configurations from which it is possible to solve problems by simple statics. Terzaghi (1943) cited some examples of this approach.

Although these methods are widely used in geotechnical practice, they neglect altogether the important fact that the stress-strain relations constitute an essential consideration in a complete theory of any branch of the continuum mechanics of deformable solids. Modern limit analysis methods take into consideration, in an idealized manner, the stress-strain relations of soils in the present case. This idealization, termed normality or associated flow rule, establishes the limit theorems on which limit analysis is based. Within the framework of perfect plasticity and the associated flow rule assumption, the approach is rigorous and the techniques are competitive with those of limit equilibrium approach. In several instances, especially

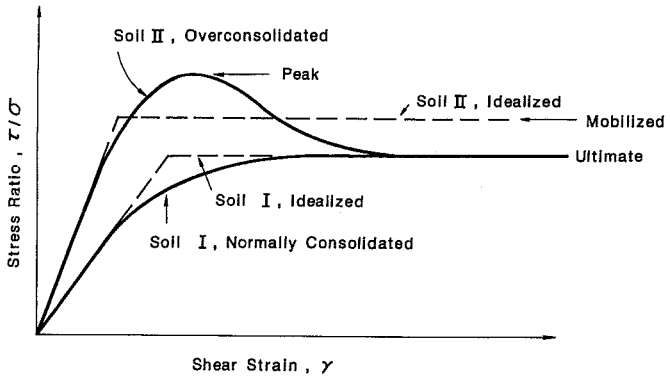

Fig. 1.1. Typical stress-strain curves and perfectly plastic idealizations.

in slope stability analysis, earth pressure problems and bearing capacity calculations, such a level of reliability and completeness has been achieved and firmly established in recent years that the limit analysis method can be used as a working tool for design engineers to solve everyday problems.

Although the perfectly plastic idealization for soil is of real value for many stability problems in soil mechanics, the idealization is severe and it is necessary to guard against improper interpretation. Since the perfect plastic idealization ignores the real work-hardening or softening of the soil beyond the arbitrarily chosen yield stress level (Fig. 1.1), it must therefore be interpreted as an average value with the meaning that no more than small plastic deformation takes place in the so-called elastic range but large plastic deformation occurs in the collapse state. In the following section, we shall illustrate this concept of perfect plasticity, i.e., plasticity without work-hardening, by presenting some typical progressive failure solutions of strip footings on an overconsolidated stratum of clay using the finite-element analysis with perfectly plastic models and work-hardening plastic models, and also by comparing these solutions with the limit analysis of perfect plasticity. Further discussions on the validity of limit analysis in application to soils will be critically examined in Chapter 3. In the strip footing example that follows, emphasis is placed on the comparison of failures modes and limit loads by the almost 'exact' finite-element analyses with those assumed in the limit analysis and limit equilibrium methods.

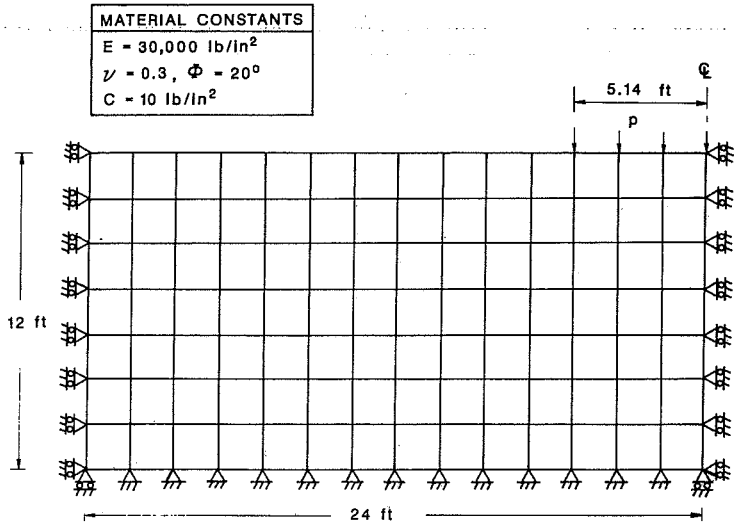

Fig. 1.2. Analytical model for shallow stratum of clay.

1.5 Finite-element analysis for progressive failure behavior of soil mass

As an illustration for some justifications of the perfect plasticity idealization for soils, we shall present here a summary of the recent finite-element solutions of strip footings on an overconsolidated stratum of clay. These computer-based solutions include:

1. The analyses of flexible and smooth footings on clay by the *perfectly plastic models* with different methods of determining the material constants. These material constants define the appropriate level of plastic flow for soils as shown schematically by the simple stress-strain curves of Fig. 1.1.
2. The analyses of rigid and rough footings on clay by the *work-hardening plastic cap models*. The cap models have been used widely and successfully in recent years in the geotechnical engineering research and applications.

Details of the plasticity modeling for soils and finite-element implementation for computer solutions are given elsewhere (Chen and Baladi, 1985). Herein, only the highlights of the numerical results of the response of clay to footing loads are reported and compared with the limit analysis solutions.

1.5.1 Flexible and smooth strip footings

The problem used for the analyses is a 10.28 ft (3.13 m) wide strip footing (Fig. 1.2) bearing on a shallow stratum supported by a rigid and perfectly rough base. The horizontal extent of the stratum is set at 24 ft (7.32 m) from the footing center and the depth of the stratum is 12 ft (3.66 m). The vertical boundary is assumed to be perfectly smooth and rigid. The uniform mesh as shown in Fig. 1.2 is used. The finite-element mesh consists of 120 nodes and 98 rectangular elements.

(a) Analyses by D-P models with different material constants

In this section, the response of the clay stratum to footing loads is analyzed by the Drucker-Prager perfectly plastic model, for which the determination of the material constants is made in several different ways. The following mechanical properties of clay are used: Young's modulus $E = 3 \times 10^4$ psi (2.07×10^5 kPa), Poisson's ratio $\nu = 0.3$, cohesion $c = 10$ psi (69 kPa), angle of internal friction $\phi = 20°$. In the present analysis, the effect of soil weight is neglected or the unit weight of soil $\gamma = 0$ pcf. For the Drucker-Prager model, a careful selection of the material constants α and k in the yield function $\alpha I_1 + \sqrt{J_2} = k$ is required so that it matches to some extend with the well-known Coulomb criterion (Chen and Mizuno, 1979). In the Drucker-Prager model, $I_1 = \sigma_x + \sigma_y + \sigma_z$ is the first invariant of stress tensor σ_{ij}, and J_2 is the second invariant of stress deviatoric tensor s_{ij}. Herein, three types of material constants are used in the analysis with the associated flow rule. These constants are obtained from matching the Drucker-Prager model with the Coulomb model along the compressive meridian (triaxial compression test), along the tensile meridian (triaxial extension test), and under the plane strain condition (plane strain test), respectively (see the inset of Fig. 1.3). The corresponding values of the material constants α and k are 0.149 and 12.25 psi (84.53 kPa), 0.118 and 9.74 psi (67.21 kPa), and 0.112 and 9.22 psi (63.62 kPa), respectively.

Load-displacement curves. The complete load-displacement response of the strip footing is shown in Fig. 1.3 where the applied pressure is plotted vs. the centerline displacement directly beneath the footing for each case. The circles plotted in Fig. 1.3 correspond to some actual computed points obtained from the small deforma-

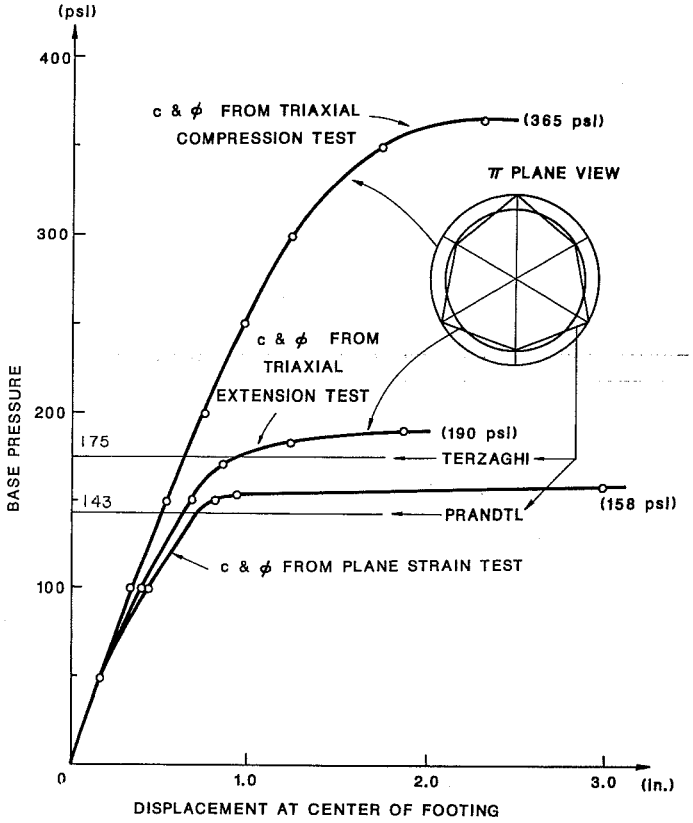

Fig. 1.3. Load-displacement curves by the Drucker-Prager perfectly plastic models with different material constants (flexible and smooth footing).

tion analysis. As can be seen, the analysis using material constants matched with the compressive meridian of the Coulomb criterion in three-dimensional space results in a collapse load (365 psi or 2520 kPa) which is almost twice that of the other analyses (158, 190 psi or 1090, 1310 kPa). This load-displacement curve is characterized by a linear elastic response up to approximately 150 psi and a nonlinear elastic-plastic response to the collapse load. On the other hand, the Drucker-Prager criterion with material constants matched with the tensile meridian of the Coulomb criterion predicts a collapse load (190 psi) which is somewhat higher than that of 175 psi given by Terzaghi (1943). Further, the collapse load (158 psi) predicted by the Drucker-Prager criterion matched with the Coulomb criterion in the plane strain condition is, as expected, almost the same as that of 152 psi predicted by the Coulomb criterion (Zienkiewicz et al., 1975). This load is close to the loads (175 and 143 psi) given by the Terzaghi and Prandtl solutions.

As a result, the analysis with the material constants matched with the compressive meridian of the Coulomb criterion in three-dimensional stress space does not agree with the well-known solution of Terzaghi and Prandtl. The important point to be noted here in using the perfectly plastic Drucker-Prager model is the careful selection of material constants. In order for this criterion to represent a proper generalization of the Coulomb or modified Coulomb criteria under multi-dimensional stress states, its material constants α and k must be properly defined. These constants should not be treated as fixed expressions for all types of applications. Rather, their choice depends on the particular problems to be solved. Further

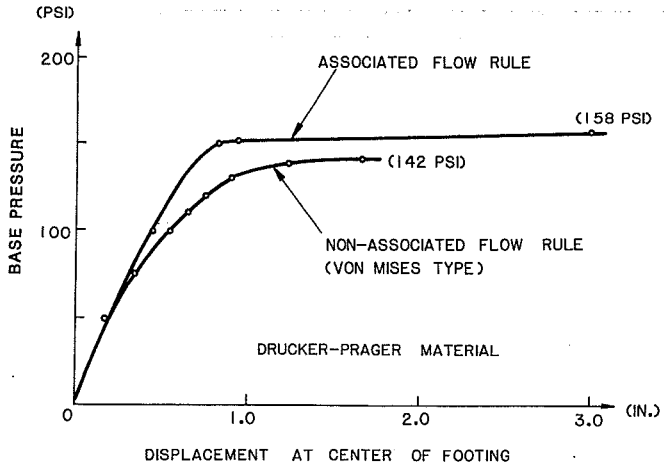

Fig. 1.4. Load-displacement curves by the Drucker-Prager perfectly plastic models with associated and non-associated flow rules (flexible and smooth footing).

discussions on the choice of material constants can be found in the paper by Chen and Mizuno (1979).

(b) Analysis by D-P model with non-associated flow rule

In this section, the Drucker-Prager perfectly plastic model with a non-associated flow rule is utilized so that comparisons can be made with the analyses by the associated flow rule model reported in the previous section. For the case of the associated flow rule, the material constants α and k obtained from matching the Coulomb model in plane strain condition are used in the yield function F and the

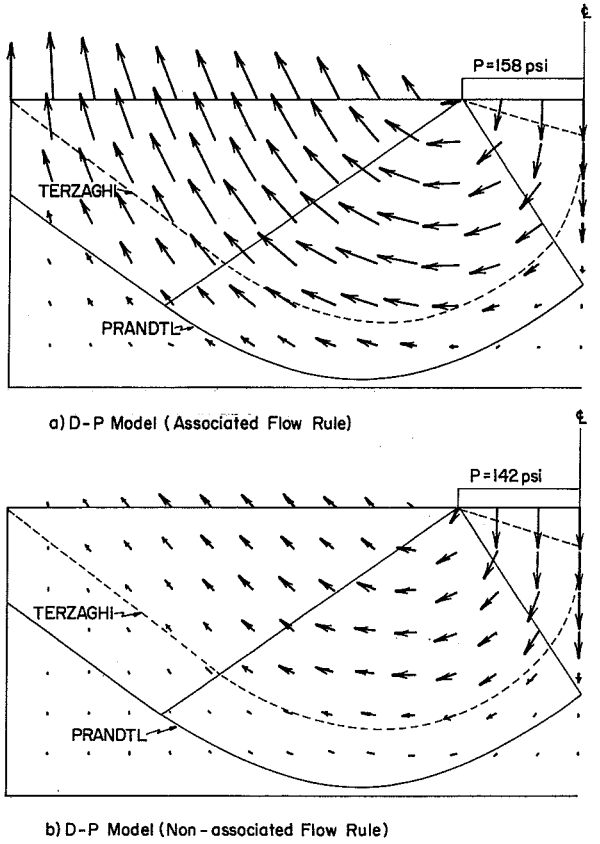

Fig. 1.5. Velocity fields by the Drucker-Prager perfectly plastic models at the numerical limit load (flexible and smooth footings).

potential function $\psi = F$. For the case of a non-associated flow rule, the yield function is the same as that for the associated flow rule case, but a von Mises type of function (no plastic volumetric strain) is used as the potential function (Mizuno and Chen, 1983).

Load-displacement curves. Figure 1.4 shows the load-displacement curves predicted by both flow rule cases. These curves are the same up to an applied load of 40 psi (276 kPa) because the state of stress in all elements at this load level is still within the elastic region. Then, as the load is gradually increased, their behavior becomes different. The load-displacement curve for the associated flow rule case bends sharply at a load of 150 psi and reaches a plastic limit load of 158 psi. On the other hand, the curve for the non-associated flow rule case deviates gradually from the associated flow rule curve at a load of 40 psi, and exhibits a significantly nonlinear response to its collapse load of 142 psi. This collapse load is less than that of the associated flow rule case. This collapse load agrees quite well with the loads of 143 and 147 psi given by the solutions of Prandtl, and of Coulomb with a non-associated flow rule (Zienkiewicz et al., 1975).

(c) Velocity fields of perfect plasticity

In Fig. 1.5, the velocity fields at the collapse load are presented for both cases. The broken and solid lines in the figure are outlines of Terzaghi and Prandtl velocity fields, respectively. The magnitude and direction of velocity at each node is represented by an arrow, and the displacement increment at the center of the footing is taken as a normalized unit length. As shown in Fig. 1.5a, the numerically obtained velocity field for the associated flow rule material is seen to be in a fair agreement with that of the Terzaghi and Prandtl solutions. Further, it can be seen that the magnitude of the velocity becomes gradually larger along the slip flow in 'the radial shearing zone' and 'near surface zone' of the Prandtl mechanism. This is due to the nature of dilatancy in soil during plastic flow.

In the other case, the velocity field (Fig. 1.5b) for the non-associated flow rule material appears to agree with that of the Terzaghi solution. In this case, the magnitude of velocity becomes gradually smaller, or remains nearly the same, along the slip flow in the 'radial shearing zone'. Here, because the von Mises type of potential function is assumed, no dilatancy occurs during the plastic flow. The velocity field in Fig. 1.5(b) is consistent with this condition.

(d) Analyses of cap models with associated flow rule

In this section, the strain-hardening plane cap and elliptic cap models with the associated flow rule are employed to solve the same problem. The material constants W and D in the hardening function $\epsilon_{kk}^{p} = W(e^{Dx} - 1)$ (Chen and Baladi, 1985) are assumed to be 0.003 (the maximum compaction of plastic volumetric strain ϵ_{kk}^{p})

and 6.042×10^{-5} ft^2/lb (1.26×10^{-6} Pa^{-1}), respectively. The location of the cap is determined by the value x. In addition, the shape ratio of an elliptic cap, R, is assumed to be 4. Further, the initial intersection of both cap hardening surfaces with the I_1-axis is situated at the point of -6700 psf on that axis. In this analysis, these caps are allowed to expand and contract as the plastic volumetric strain increases and decreases.

As for the yield surface, the Drucker-Prager type of yield surface based on material constants matched with the Coulomb criterion in the plane strain condition is used.

Note that since the weight of clay is not considered, the initial state of stress inside the clay stratum is set at the origin in $I_1 - \sqrt{J_1}$ space at the beginning of the analysis.

Load-displacement curves. In Fig. 1.6, the load-displacement curves for the cap models are compared with those obtained previously. Initially, all the curves are the same. After some yielding, the plane cap model curve deviates significantly from the Drucker-Prager model curves at approx. 40 psi (276 kPa), and thereafter rises to a load of 139 psi. Beyond this point the iterative procedure of the computer solution does not converge. Thus, this load is approximately the collapse load. Compared with the collapse loads discussed in the previous sections, the present estimated collapse load agrees quite well with that of 142 psi predicted by the Drucker-Prager non-associated flow rule model, and with that of 143 psi given by the Prandtl solution.

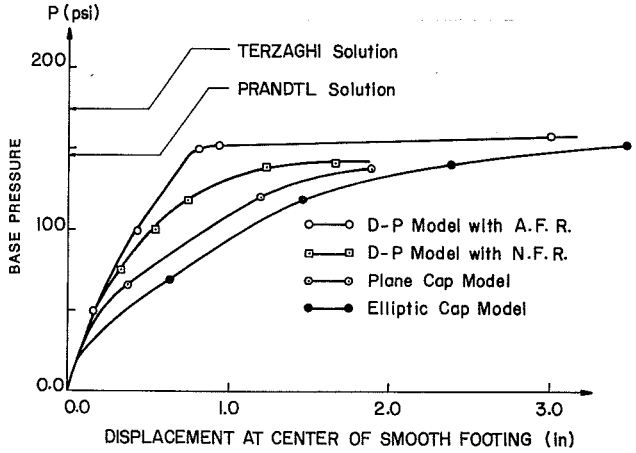

Fig. 1.6. Load-displacement curves by the Cap and Drucker-Prager models (flexible and smooth footing).

On the other hand, the elliptic cap model curve starts to deviates significantly at a much earlier load of 25 psi. This is because the elastic zone developed in the elliptic cap model is smaller, in compressive $I_1 - \sqrt{J_2}$ space, than that of the plane cap model. However, the curve behaves in a similar manner to that of the plane cap model and asymptotically approaches the curves predicted by the Drucker-Prager associated flow rule model.

(e) Velocity fields of work-hardening plasticity

The velocity fields corresponding to the last load increment for both cap models are shown in Fig. 1.7. For the plane cap model, the velocity field (Fig. 1.7a) agrees

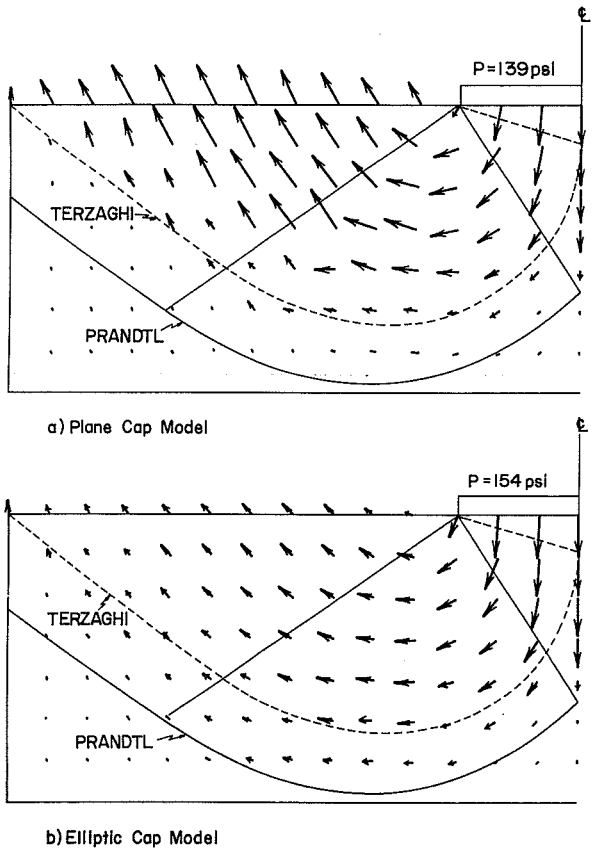

Fig. 1.7. Velocity fields by the Cap models at numerical limit load (flexible and smooth footing).

quite well with that of the Terzaghi solution (broken line). The magnitude of the velocity is large inside the triangular zone along the free boundary surface. The velocity field appears to lie between those predicted by the various Drucker-Prager models.

The velocity field predicted by the elliptic cap model corresponds reasonably well with the Prandtl field (Fig. 1.7b). The magnitude of the velocity becomes gradually smaller along the slip-flow direction from the footing surface to the free boundary surface. Since the stress states lie either in a corner zone or a hardening cap zone for almost all the elements, little dilatancy is expected. Thus, the velocity field is close to that predicted by the Drucker-Prager non-associated flow rule model.

1.5.2 Rigid and rough strip footings

In this section, the previous soil – structure interaction problem between footing and ground is changed from a flexible and smooth boundary to a rigid and rough boundary. The displacements beneath the footing are assumed to be vertically uniform. As a result of this change, the incremental displacement method is used in the finite-element analysis with the initial stress procedure. Note that the footing pressure in this section is defined as the average pressure under the footing.

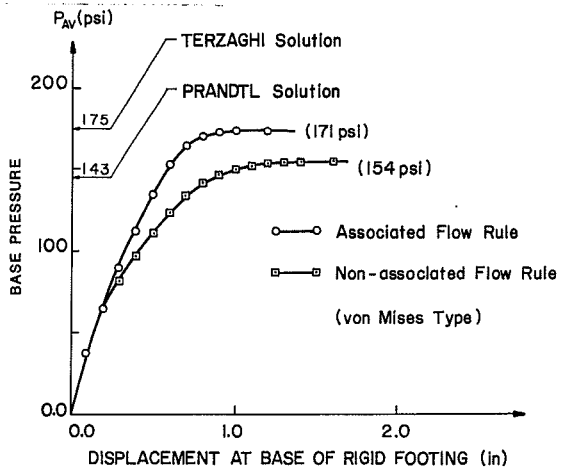

Fig. 1.8. Load-displacement curves by the Drucker-Prager models with associated and non-associated flow rules (rigid and rough footings).

(a) Analyses by D-P models

Here, the results such as load-displacement curves and velocity fields predicted by the Drucker-Prager models are presented.

Load-displacement curves. Figure 1.8 shows the load-displacement curves predicted by the Drucker-Prager models. The curve for the associated flow rule case rises linearly to about 65 psi (449 kPa), then exhibits mild nonlinear behavior and finally a severe reduction of the stiffness. The model predicts a much stiffer curve compared with that of the flexible and smooth footing problem. The collapse load is approximately 171 psi which is quite close to Terzaghi's solution (175 psi) but

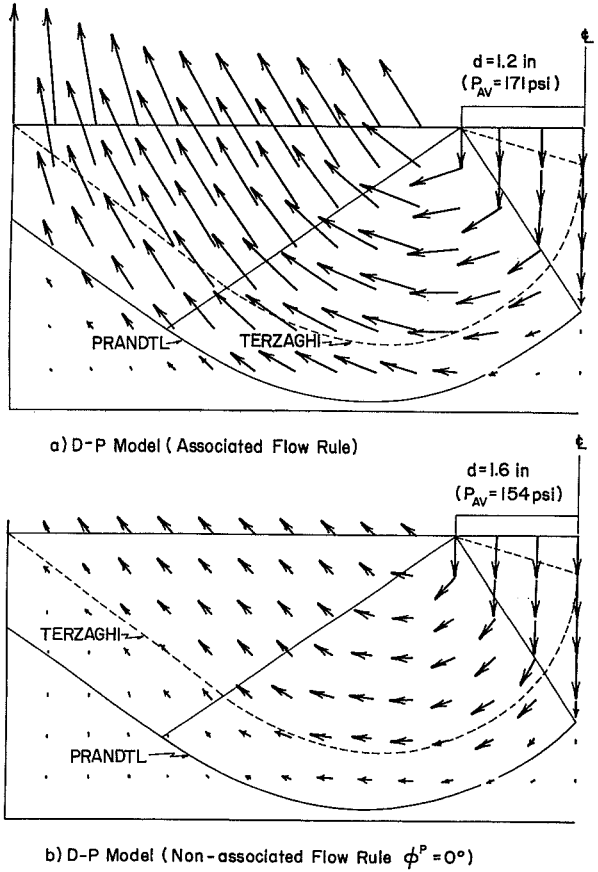

Fig. 1.9. Velocity fields by the Drucker-Prager models at the numerical limit load (rigid and rough footing).

considerably higher than 158 psi as predicted by the same model for the flexible and smooth footing problem.

The curve corresponding to the non-associated flow rule case deviates from the associated flow rule curve at a load of 65 psi, and then shows a nonlinear behavior until it reaches a collapse load of approximately 154 psi. The collapse load lies between those of 158 and 142 psi predicted by the same models for the flexible and smooth footing problem. Also, this load is close to that of 143 psi given by the Prandtl solution.

Velocity fields. The velocity fields for both models at the last displacement increment are shown in Fig. 1.9. The magnitude and direction of velocity at each node is denoted by an arrow and, the uniform displacement increment at the base of the footing is taken as a normalized unit length. Figure 1.9a shows the velocity field predicted by the associated flow rule model. The velocity field agrees quite well with that of the Prandtl solution, as represented by the solid line. The magnitude of the velocity field is much larger than that predicted by the same model for the flexible and smooth footing problem. Further, its magnitude at the free surface becomes two or three times that beneath the footing. This is due to the large amount of dilatancy at this displacement increment.

The velocity field predicted by the model with a non-associated flow rule (Fig. 1.9b) has a relatively small and uniform magnitude in the 'radial shearing zone' and the 'near-surface zone'. The velocity field agrees well with that of the Prandtl solu-

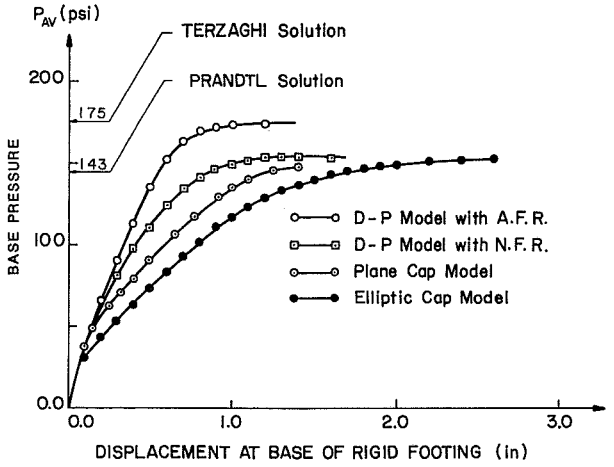

Fig. 1.10. Load-displacement curves by the Cap and Drucker-Prager models (rigid and rough footing).

tion. As expected, dilatancy in the stratum is restricted at this increment, as can be seen from the velocity field on the surface.

In the present analysis, the direction of the velocity in the 'triangle rigid zone' beneath the footing in the Prandtl mechanism is found to be vertically downward (Fig. 1.9), while the corresponding velocity in the flexible and smooth footing problem is not uniformly vertical (Fig. 1.5).

(b) Analyses by cap models

Herein, results predicted by cap models are presented.

Load-displacement curves. The load-displacement curves predicted by both cap models are shown in Fig. 1.10, and compared with those predicted by the Drucker-

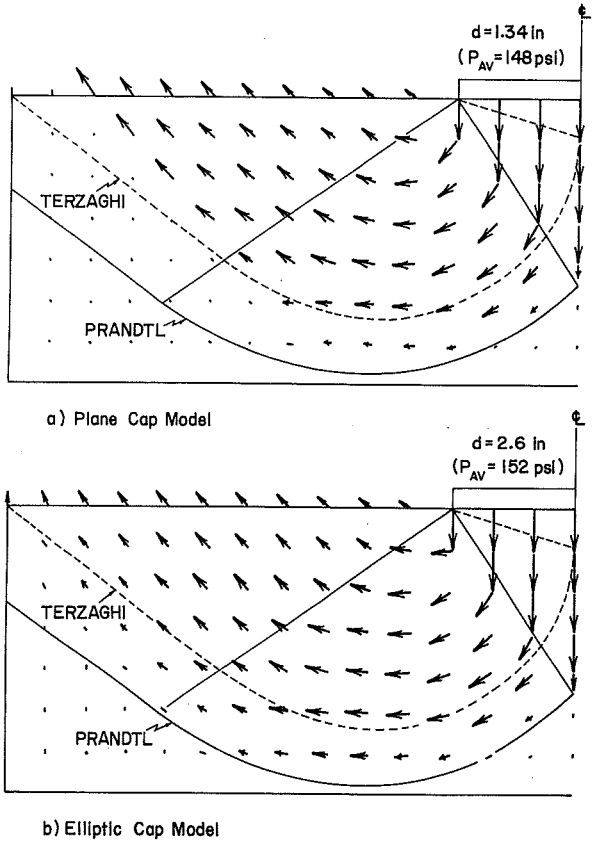

Fig. 1.11. Velocity fields by the Cap models at the numerical limit load (rigid and rough footing).

Prager models. Initially, all the curves are similar. After yielding, the cap model curves start to deviate from each other. Here, as in the Drucker-Prager models, these curves are stiffer than those of the flexible and smooth footing problem (Fig. 1.6). For the plane cap model, yielding starts at about 40 psi (276 kPa). Thereafter, the cap surface expands, hardens, and reaches the collapse state at 148 psi. This load is quite close to those (143 psi, 154 psi) predicted by the Prandtl solution and the Drucker-Prager model with the non-associated flow rule. Note that this collapse load is slightly higher than that (139 psi) predicted by the same model for the flexible and smooth footing problem.

As for the elliptic cap model, yielding starts at 30 psi, and reaches the collapse load of 152 psi, which is greater than that (143 psi) of the Prandtl solution but quite close to that (148 psi) predicted by the plane cap model.

Velocity fields. The velocity fields associated with both models are presented in Fig. 1.11. The velocity field predicted by the plane cap model (Fig. 1.11a) agrees quite well with that of Terzaghi solution in the 'radial shearing zone' and 'near free surface zone'. However, the velocity under the footing follows that of the Prandtl field and its direction is almost vertical.

The velocity field predicted by the elliptic cap model (Fig. 1.11b) agrees quite well with that of the Prandtl solution. Its magnitude is comparable to that of the plane cap model.

Both models have much less dilatancy than that required by the Drucker-Prager model with the associated flow rule.

1.5.3 Summary remarks

In this section, the Drucker-Prager models, with the associated flow rule as well as a non-associated flow rule, and cap models are applied to obtain solutions for problems of flexible smooth, and rigid rough footings resting on a stratum of clay. From the cases studied, the following observations can be made:

a. The load displacement curves predicted by the Drucker-Prager perfectly plastic models are found to be much stiffer than those predicted by the cap models.
b. All the collapse loads obtained from the matching of the Drucker-Prager model with the Coulomb model under the plane strain conditions lie between the solutions of Terzaghi and Prandtl.
c. The velocity fields predicted by the plane cap model for both types of footing problems do not agree with that of the Prandtl solution in the 'radial shearing zone' and 'near the free surface zone'. The velocity fields predicted by the Drucker-Prager and elliptic cap models agree well with that of the Prandtl solution for both footing problems.

References

Bazant, Z.P. (Editor), 1985. Mechanics of Geomaterials. John Wiley, London, 611 pp.

Booker, J.R. and Davis, E.H., 1972. A note of a plasticity solution to the stability of slopes in homogeneous clay. Geotechnique, 22: 509–513.

Chan, S.W., 1980. Perfect plasticity upper bound limit analysis of the stability of a seismic-infirmed earthslope. M.S. Thesis, Sch. of Mech. Engl., Purdue Univ., West Lafayette, IN, 129 pp.

Chang, C.J., 1981. Seismic safety analysis of slopes. Ph.D. Thesis, Sch. of Civ. Eng., Purdue Univ., West Lafayette, IN, 125 pp.

Chang, M.F., 1981. Static and seimic lateral earth pressures on rigid retaining structures. Ph.D. Thesis, Sch. of Civ. Eng., Purdue Univ., West Lafayette, IN, 465 pp.

Chen, W.F., 1975. Limit Analysis and Soil Plasticity. Elsevier, Amsterdam, 638 pp.

Chen, W.F., 1980. Plasticity in soil mechanics and landslides. J. Eng. Mech. Div., ASCE, 106 (EM3): 443–464.

Chen, W.F., 1982. Plasticity in Reinforced Concrete. McGraw-Hill, New York, NY, 474 pp.

Chen, W.F., 1984. Soil mechanics, plasticity and landslides. In: G.J. Dvorak and R.T. Shield (Editors), Mechanics of Material Behavior. Elsevier, Amsterdam, pp. 31–58.

Chen, W.F. and Baladi, G.Y., 1985. Soil Plasticity: Theory and Implementation. Elsevier, Amsterdam, 231 pp.

Chen, W.F. and Chang, M.F., 1981. Limit analysis in soil mechanics and its applications to lateral earth pressure problems. Solid Mech. Arch., 6 (3): 331–399.

Chen, W.F. and Mizuno, E., 1979. On material constants for soil and concrete models. Proc. 3rd ASCE/EMD Specialty Conf., Austin, Tx, pp. 539–542.

Davis, E.H., 1968. Theories of plasticity and the failure of soil masses. In: I.K. Lee (Editor), Soil Mechanics: Selected Topics. Butterworths, London, pp. 341–380.

Desai, C.S. and Gallagher, R.H. (Editors), 1983. Constitutive Laws for Engineering Materials: Theory and Application. John Wiley, London, 691 pp.

Drucker, D.C., 1953. Limit analysis of two- and three-dimensional soil mechanics problems. J. Mech. Phys. Solids, 1: 217–226.

Drucker, D.C., 1960. Plasticity. In: J.N. Goodier and N.J. Hoff (Editors), Structural Mechanics. Pergamon Press, London, pp. 407–455.

Drucker, D.C., 1966. Concepts of path independence and material stability for soils. In: J. Kravtchenko and P.M. Sirieys (Editors), Rheol. Mecan. Soils Proc. IUTAM Symp. Grenoble. Springer, Berlin, pp. 23–43.

Drucker, D.C. and Prager, W., 1952. Soil mechanics and plastic analysis or limit design. Q. Appl. Math., 10(2): 157–165.

Drucker, D.C., Gibson, R.E. and Henkel, D.J., 1957. Soil Mechanics and Work Hardening Theories of Plasticity. Trans. 122, ASCE, New York, NY, pp. 338–346.

Dvorak, G.J. and Shield, R.T. (Editors), 1984. Mechanics of Material Behavior. Elsevier, Amsterdam, 383 pp.

Fellenius, W.O., 1926. Mechanics of Soils. Statika Gruntov, Gosstrollzdat.

Hill, R., 1950. The Mathematical Theory of Plasticity. Clarendon Press, Oxford, 355 pp.

IABSE, 1979, Proc. Colloq. on Plasticity in Reinforced Concrete, Copenhagen, May 21–23, IABSE Publ., Zurich.

McCarron, W.O., 1985. Soil plasticity and finite element applications. Ph.D. Thesis, School of Civil Engineering, Purdue Univ., West Lafayette, IN, 266 pp.

Mizuno, E., 1981. Plasticity modeling of soils and finite element applications. Ph.D. Thesis, Sch. of Civ. Eng., Purdue Univ., West Lafayette, IN, 320 pp.

Mizuno, E. and Chen, W.F., 1981a. Plasticity models for soils – Comparison and discussion, pp. 328–351. Also: Plasticity models for soils, pp. 553–591. Proc. Workshop on Limit Equilibrium, Plasticity and Generalized Stress-Strain in Geotechnical Engineering, McGill University, 28–30 May 1980, R.K. Yong and H.Y. Ko (Editors), ASCE, New York, NY, 871 pp.

Mizuno, E. and Chen, W.F., 1981b. Plasticity models and finite element implementation. Proc. Symp. Implementation of Computer Procedures and Stress-Strain Laws in Geotechnical Engineering, Chicago, IL, 3–6 August 1981, Two-Volume Proceedings, Acorn Press, Durham, NC, pp. 519–534.

Mizuno, E. and Chen, W.F., 1982. Analysis of soil response with different plasticity models. In: R.N. Yong and E.T. Selig (Editors), Proc. of the Symp. Applications of Plasticity and Generalized Stress-Strain in Geotechnical Engineering. ASCE, New York, NY, pp. 115–138.

Mizuno, E. and Chen, W.F., 1983. Cap models for clay strata to footing loads. Comput Struct., 17 (4): 511–528.

Palmer, A.C. (Editor), 1973. Proc. Symp. on the Role of Plasticity in Soil Mechanics. Cambridge Univ. Press, Cambridge, England, 314 pp.

Parry, R.H.G. (Editor), 1972. Roscoe Memorial Symp.: Stress-Strain Behavior of Soils, Henly-on-Thames. Cambridge Univ., Cambridge, England, 752 pp.

Prager, W. and Hodge, P.G., 1950. Theory of Perfectly Plastic Solids. Wiley, New York, NY, 264 pp.

Saleeb, A.F., 1981. Constitutive models for soils in landslides. Ph.D. Thesis, Sch. Civ. Eng. Purdue Univ., West Lafayette, IN.

Sokolovskii, V.V., 1965. Statics of Granular Media. Pergamon, New York, NY, 232 pp.

Terzaghi, K., 1943. Theoretical Soil Mechanics. John Wiley, New York, NY, 510 pp.

Yong, R.N. and Ko, H.Y. (Editors), 1981. Limit Equilibrium, Plasticity and Generalized Stress-Strain in Geotechnical Engineering. ASCE, New York, NY, 871 pp.

Yong, R.N. and Selig, E.T. (Editors), 1982. Application of Plasticity and Generalized Stress-Strain in Geotechnical Engineering. ASCE, New York, NY, 356 pp.

Zienkiewicz, O.C., Humpheson, C. and Lewis, R.W., 1975. Associated and non-associated visco-plasticity and plasticity in soil mechanics. Geotechnique 25 (4): 671–689.

Chapter 2

BASIC CONCEPTS OF LIMIT ANALYSIS

2.1 Introduction

There are three basic conditions needed for the solution of a boundary value problem in the mechanics of deformable solids: the stress equilibrium equations, the stress-strain relations, and the compatibility equations relating strain to displacement. In general, an infinity of stress states will satisfy the stress boundary conditions, the equilibrium equations and the yield criterion alone, and an infinite number of displacement modes will be compatible with a continuous distortion of the continuum satisfying the displacement boundary conditions. Here, as in the theory of elasticity, use has to be made of the stress-strain relations to determine whether given stress and displacement states correspond and a unique solution results. For an elastic-plastic material, however, there is as a rule a three-stage development in a solution, when the applied loads are gradually increased in mangitude from zero, namely, the initial elastic response, the intermediate contained plastic flow and finally the unrestricted plastic flow. The complete solution by this approach is likely to be cumbersome for all but the simplest problems, and methods are needed to furnish to load-carrying capacity estimation in a more direct manner. Limit analysis is the method which enables a definite statement to be made about the collapse load without carrying out the step-by-step elastic-plastic analysis.

The limit analysis method considers the stress-strain relationship of a soil in an idealized manner. This idealization, termed *normality* (or the *associated flow rule*), establishes the limit theorems on which limit analysis is based. Within the framework of this assumption, the approach is rigorous and the techniques are in some instances being much simpler. The plastic limit theorems may conveniently be employed to obtain upper and lower bounds of the collapse load for stability problems in soil mechanics.

The conditions required to establish an upper- or lower-bound solution to the collapse load are essentially as follows:

(1) *Lower-bound theorem.* The loads, determined from a distribution of stress alone, that satisfies: (a) the equilibrium equations; (b) the stress boundary conditions; and (c) no where violates the yield criterion, are not greater than the actual collapse load. The distribution of stress has been termed a *statically admissible stress field* for the problem under consideration. Thus, the lower-bound theorem may be

restated as follows: If a statically admissible stress distribution can be found, uncontained plastic flow will not occur at a lower load. It can be seen that the lower-bound technique considers only equilibrium and yield. It gives no consideration to soil kinematics.

(2) *Upper-bound theorem.* The loads, determined by equating the external rate of work to the internal rate of dissipation in an assumed velocity field, that satisfies: (a) the velocity boundary conditions; and (b) the strain and velocity compatibility conditions, are not less than the actual collapse load. The dissipation of energy in plastic flow associated with such a field can be computed from the idealized flow rule. The velocity field satisfying the above conditions has been termed a *kinematically admissible velocity field.* Hence, the upper-bound theorem states that if a kinematically admissible velocity field can be found, uncontained plastic flow must have taken place previously. It can be seen that the upper-bound technique considers only velocity modes and energy dissipations. The stress distribution need not be in equilibrium.

By a suitable choice of stress and velocity fields, the above two theorems thus enable the required collapse load to be bracketed as closely as seems necessary for the problem under consideration.

In view of the uncertainties inherent in all engineering problems, and the essential role of judgement in their solution, it is clear that the approximate nature of the method is no basic handicap. The real difficulty is the possible discrepancy between the plastic deformation properties of the ideal and the real material, which often exhibits some degree of work softening, and may not follow the associated flow rule. Since the assumptions regarding the mechanical properties of the material under investigation determine the range of validity of the theory of limit analysis, a complete and concise statement of the assumptions used in this theory will be presented and illustrated.

2.2 Index notation

Usually, we use the three mutually perpendicular coordinate axes by the familiar notation x, y and z. For future convenience, however, these three mutually perpendicular axes will be denoted by x_1, x_2, and x_3 as a dual notation. Accordingly, each of the components of a force vector (or displacement vector) and the vector itself is represented by the symbol T_i (or u_i) where i takes on the values 1, 2, and 3:

$$T_i = \begin{bmatrix} T_x \\ T_y \\ T_z \end{bmatrix} = \begin{bmatrix} T_1 \\ T_2 \\ T_3 \end{bmatrix} \tag{2.1}$$

Similarly, each of the components of a stress tensor (or strain tensor) and the tensor

itself will be represented by the symbol σ_{ij} (or ϵ_{ij}) where i and j take on the values 1, 2, and 3:

$$\sigma_{ij} = \begin{bmatrix} \sigma_x & \tau_{xy} & \tau_{xz} \\ \tau_{yx} & \sigma_y & \tau_{yz} \\ \tau_{zx} & \tau_{zy} & \sigma_z \end{bmatrix} = \begin{bmatrix} \sigma_{11} & \sigma_{12} & \sigma_{13} \\ \sigma_{21} & \sigma_{22} & \sigma_{23} \\ \sigma_{31} & \sigma_{32} & \sigma_{33} \end{bmatrix} \tag{2.2}$$

The symmetry of the stress tensor, $\sigma_{12} = \sigma_{21}$, etc., is symbolized by $\sigma_{ij} = \sigma_{ji}$.

In the following, we will often encounter sums in which a certain subscript pair is 'summed' from 1 to 3. It will be inconvenient to write summation signs and so we here introduce a summation convention which consists essentially in merely dropping the summation sign.

The summation convention can be understood as that whenever a subscript occurs twice in the same term, the subscript is to be summed from 1 to 3. Thus:

$$\sum_{i=1}^{3} T_i u_i = T_i u_i = T_1 u_1 + T_2 u_2 + T_3 u_3 \tag{2.3a}$$

$$\sum_{i=1}^{3} \sum_{j=1}^{3} \sigma_{ij}\epsilon_{ij} = \sigma_{ij}\epsilon_{ij} = (\sigma_{11}\epsilon_{11} + \sigma_{12}\epsilon_{12} + \sigma_{13}\epsilon_{13}) + (\sigma_{21}\epsilon_{21} + \sigma_{22}\epsilon_{22} + \sigma_{23}\epsilon_{23}) + (\sigma_{31}\epsilon_{31} + \sigma_{32}\epsilon_{32} + \sigma_{33}\epsilon_{33}) \tag{2.3b}$$

Such repeated subscripts are often called *dummy* subscripts because of the fact that the particular letter used in the subscripts is not important; thus $T_i u_i = T_j u_j$ or $\sigma_{ij}\epsilon_{ij} = \sigma_{mn}\epsilon_{mn}$. The subscript index which occurs only 'once' in a term is called *free* subscript. A free subscript also takes the values 1, 2, 3 but repeats the equation for three times. For example, the equation $T_i = \sigma_{ji} n_j$ (or $T_i = \sigma_{mi} n_m$) implies the following three simultaneous equations:

$$\begin{aligned} T_1 &= \sigma_{11} n_1 + \sigma_{21} n_2 + \sigma_{31} n_3 \\ T_2 &= \sigma_{12} n_1 + \sigma_{22} n_2 + \sigma_{32} n_3 \\ T_3 &= \sigma_{13} n_1 + \sigma_{23} n_2 + \sigma_{33} n_3 \end{aligned} \tag{2.4}$$

2.3 The perfectly plastic assumption and yield criterion

Figure 2.1 shows a typical stress-strain diagram for soils. The stress-strain behavior of most real soils is characterized by an initial linear portion and a peak stress followed by softening to a residual stress. Usually, the stress-strain diagram given above is associated with a simple shear test or a triaxial compression test. In limit analysis, it is necessary to ignore the strain softening feature of the stress-strain diagram and to take the stress-strain diagram to consist of two straight lines as shown by the dashed lines in Fig. 2.1. A hypothetical material exhibiting this proper-

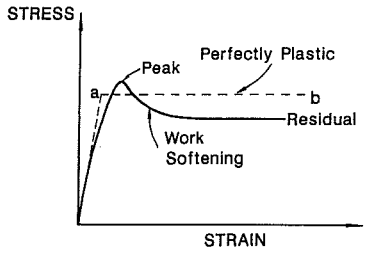

Fig. 2.1. Stress-strain relationship for ideal and real soils.

ty of continuing plastic flow at constant stress is called an *perfectly plastic material.*

It should be noted that the constant stress level used in limit analysis applications where perfect plasticity assumption is made may be chosen to represent the average stress in an appropriate range of strain. Thus the validity of the assumption of perfect plasticity may be wider than might appear possible at first glance. The choice of the level of the constant stress is not an absolute one, but is determined by the most significant features of the problem to be solved.

It is important to know the behavior of the soil for a complex stress state. In particular it is necessary to have an idea of what conditions characterize the change of the material from an elastic state to a flow state or yield (as the horizontal line a-b in Fig. 2.1). Here the question arises of a possible form of the condition which characterizes the transition of a soil from an elastic state to a plastic flow state with a complex stress state. This condition, satisfied in the flow state, is called the perfect plasticity condition or the *yield criterion.*

It is generally assumed that plastic flow occurs when, on any plane at any point in a mass of soil, the set of stress components σ_{ij} reaches a yield surface which can be mathematically expressed as a yield function f in the stress space. In other words, each element of general bodies is assumed to be governed by a yield function f. For a perfectly plastic material, f depends only on the set of stress components σ_{ij} but not on the strain components ϵ_{ij}. Plastic flow can occur only when the yield function is satisfied:

$$f(\sigma_{ij}) = 0 \tag{2.5}$$

Stress states for which $f(\sigma_{ij}) > 0$ are excluded, and $f(\sigma_{ij}) < 0$ corresponds to elastic behavior.

The term yield surface is used to emphasize the fact that three or more components of stress σ_{ij} may be taken as coordinate axes. A two-dimensional picture only is drawn, however, as shown in Fig. 2.2. The yield surface thus is represented by a yield curve or actually becomes a yield curve when two independent com-

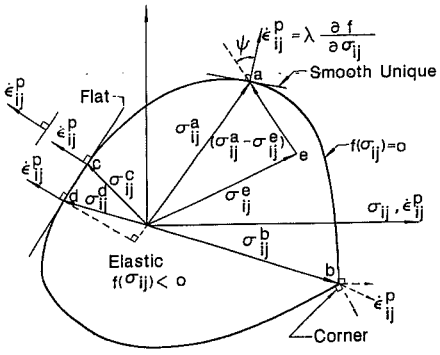

Fig. 2.2. Pictorial representation of yield surface and flow rules.

ponents of stress are studied. It is helpful to visualize a state of stress in a nine-dimensional stress space as a point in the two-dimensional picture, shown in Fig. 2.2, as a vector whose components are the nine σ_{ij}.

For materials, which satisfy the definition of Drucker's stability postulate for *stable material,* the yield surface must be convex. It will be proved later.

2.4 The kinematic assumption on soil deformations and flow rule

It is known that plastic flow occurs when a stress-point in stress space, represented by a vector from the origin, reaches the perfectly plastic yield surface. When this condition is met, then, what is the kinematics of the plastic flow? It is immediately clear that we cannot say anything about the total plastic strain ϵ^p_{ij} because the magnitude of the plastic flow is unlimited. In this case, the strain rates $\dot{\epsilon}_{ij}$ instead of strains ϵ_{ij} are needed. The total strain rate $\dot{\epsilon}_{ij}$ is composed of elastic and plastic parts:

$$\dot{\epsilon}_{ij} = \dot{\epsilon}^e_{ij} + \dot{\epsilon}^p_{ij} \tag{2.6}$$

The $\dot{\epsilon}^e_{ij}$ are related to the $\dot{\sigma}_{ij}$ through Hooke's law only. The $\dot{\epsilon}^p_{ij}$ depend on the state of stress through an appropriate kinematic assumption on the deformations.

In discussing plastic strain rates, we need to define the directions of the axes of principal plastic strain rates. The coordinate axes of the stress space already referred to for the yield surface can also be used to represent simultaneously plastic strain rates as well as stresses, each axis of σ_{ij} being an axis of the corresponding plastic strain rate component of $\dot{\epsilon}^p_{ij}$. Thus, a point in this space also specifies a plastic strain rate state. Figure 2.2 shows this combined stress and strain rate plot. For

isotropic materials, we expect the axes of principal strain rates to coincide with the axes of principal stresses. In other words, a rectangular element of isotropic material under simple compression would be expected during any plastic flow to deform in such a way that its faces remained mutually perpendicular.

For stable materials that are defined by Drucker, it can be shown later that the vector representing the plastic strain rate $\dot{\epsilon}_{ij}^{p}$ has the direction of the outward normal to the yield surface $f(\sigma_{ij}) = 0$. It can be written in the general form:

$$\dot{\epsilon}_{ij}^{p} = \lambda \frac{\partial f}{\partial \sigma_{ij}} \tag{2.7}$$

where $\lambda > 0$ is a positive scalar proportionality factor. Equation (2.7) is called the *associated flow rule* or '*normality*' because it is associated (or connected) with the yield surface of the perfect plastic material. If λ is known, the $\dot{\epsilon}_{ij}^{p}$ can be obtained. From Eq. (2.6), the total strain rate $\dot{\epsilon}_{ij}$ can be calculated without difficulty.

2.5 The stability postulate of Drucker

Considering the symbolic uniaxial stress-strain curves in Fig. 2.3, there are three types of materials in Drucker's sense:

1. In cases (a) to (c) in this figure, the stress σ is uniquely determined from the strain ϵ, and the converse is also true. An additional stress $\dot{\sigma} > 0$ gives rise to an additional strain $\dot{\epsilon} > 0$, with the product $\dot{\sigma}\dot{\epsilon} > 0$. That is, the additional stress $\dot{\sigma}$ does positive work on the additional strain $\dot{\epsilon}$ which is represented by the shaded triangle in the diagrams. Material of this kind is called *stable*.

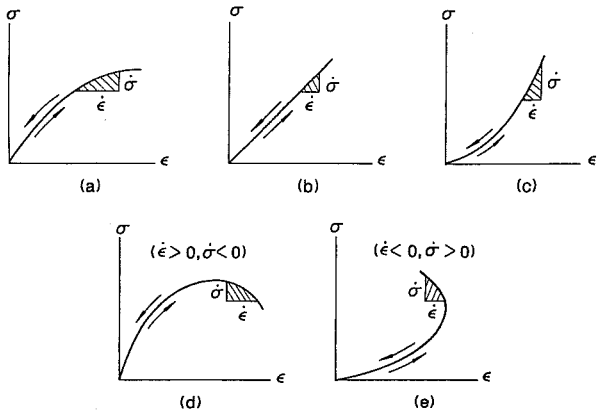

Fig. 2.3. Stable and unstable stress-strain curves. (a), (b) and (c) Stable materials, $\dot{\sigma}\dot{\epsilon} > 0$. (d) and (e) Unstable materials, $\dot{\sigma}\dot{\epsilon} < 0$.

2. In case (d), the deformation curve has a descending branch, where the strain increases with decreasing stress. Although the stress σ is uniquely determined from the value of the strain ϵ, the converse is not generally true. On the descending branch, the additional stress does negative work on the additional strain $\dot{\epsilon}$, i.e. $\dot{\sigma}\dot{\epsilon} < 0$. Such a material is called *unstable*.
3. In case (e), the strain decreases with increasing stress, so that the stress, σ, can not be uniquely determined from the value of the strain ϵ and again, $\dot{\sigma}\dot{\epsilon} < 0$ and the material is called *unstable*.

From this simple uniaxial stress-strain behavior, Drucker extended the concept of stable material to the general stress state, and obtained some very useful results. This is described in the forthcoming.

Suppose that an external agency slowly applies and then removes additional forces to a already loaded body without any temperature change. For a stable material as defined by Drucker's stability postulate, it should be that (a) positive work is done by the external agency during the application of the added set of stresses on the changes in strains and (b) nonnegative net work is done by the external agency over the cycle of application and removal.

It is emphasized here that the work referred to is only the work done by the added set of stresses on the 'change' in strains it produces, not the total stresses on strains. For example, in case (d) of Fig. 2.3, although $\dot{\sigma}\dot{\epsilon} < 0$, the work done by the total stress is positive.

As shown in Fig. 2.4, the stress state moves from A to B and from C to D, they correspond to elastic behavior. However, the stress state moves from E to G along the yield surface or remains on E or G, they show plastic behavior.

Assume at time $t = 0$, $\overset{0}{\sigma}_{ij}$ are any set of stresses, in equilibrium with F_i in the body and with the external forces T_i on the surface. If the external forces are added at time t, the stress state reaches the yield surface and becomes σ_{ij}, and then moves along the yield surface (Fig. 2.4b). When the time shifts to $t + \Delta t$, the stress state is $\sigma_{ij} + \Delta\sigma_{ij}$. If the external forces are removed at $t = t^*$, the stress state will return to $\overset{0}{\sigma}_{ij}$ again.

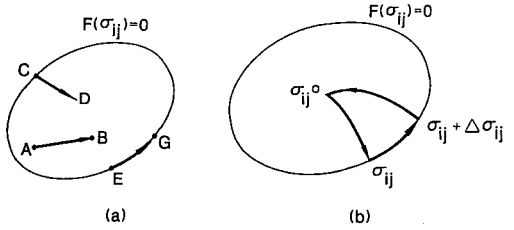

Fig. 2.4. Stress state in the stress space.

The work done over the cycle of addition and removal of the additional set of forces has the form:

$$\Delta W_t = \int_0^t \sigma_{ij}\ \dot{\epsilon}_{ij}\ dt + \int_t^{t+\Delta t} \sigma_{ij}\ \dot{\epsilon}_{ij}\ dt + \int_{t+\Delta t}^{t^*} \sigma_{ij}\ \dot{\epsilon}_{ij}\ dt \tag{2.8}$$

$$[\text{from } \sigma_{ij}^0 \text{ to } \sigma_{ij}] \qquad [\text{from } \sigma_{ij} \text{ to } \sigma_{ij} + \Delta\sigma_{ij}] \qquad [\text{from } \sigma_{ij} + \Delta\sigma_{ij} \text{ to } \sigma_{ij}^0]$$

Since the total strain rate $\dot{\epsilon}_{ij}$ is composed of elastic and plastic parts $\dot{\epsilon}_{ij} = \dot{\epsilon}_{ij}^e + \dot{\epsilon}_{ij}^p$, it follows that:

$$\Delta W_t = \int_0^t \sigma_{ij}\,\dot{\epsilon}_{ij}^e\ dt + \int_t^{t+\Delta t} \sigma_{ij}(\dot{\epsilon}_{ij}^e + \dot{\epsilon}_{ij}^p)\ dt + \int_{t+\Delta t}^{t^*} \sigma_{ij}\,\dot{\epsilon}_{ij}^e\ dt$$

$$= \oint \sigma_{ij}\,\dot{\epsilon}_{ij}^e\ dt + \int_t^{t+\Delta t} \sigma_{ij}\,\dot{\epsilon}_{ij}^p\ dt = \int_t^{t+\Delta t} \sigma_{ij}\,\dot{\epsilon}_{ij}^p\ dt \tag{2.9}$$

in which $\oint \sigma_{ij}\dot{\epsilon}_{ij}^e\ dt$ indicates the integration of the elastic work over the entire load cycle, it must be zero for an elastic material. Note that the loading cycle starts not from $\sigma_{ij} = 0$, but from σ_{ij}^0. Thus, the work done by σ_{ij}^0 during this load cycle must be subtracted:

$$\Delta W_0 = \int_t^{t+\Delta t} \sigma_{ij}^0\,\dot{\epsilon}_{ij}^p\ dt \tag{2.10}$$

The total plastic work over the load cycle is:

$$\Delta W_t - \Delta W_0 = \int_t^{t+\Delta t} (\sigma_{ij} - \sigma_{ij}^0)\,\dot{\epsilon}_{ij}^p\ dt \tag{2.11}$$

The rate of plastic work or dissipation of energy is defined as:

$$\lim_{\Delta t \to 0} \frac{\Delta W_t - \Delta W_0}{\Delta t} = \lim_{\Delta t \to 0} \frac{\int_t^{t+\Delta t} (\sigma_{ij} - \sigma_{ij}^0)\,\dot{\epsilon}_{ij}^p\ dt}{\Delta t}$$

If $\Delta t > 0$ and is very small, it can be written as:

$$\lim_{\Delta t \to 0} \frac{\Delta W_t - \Delta W_0}{\Delta t} = (\sigma_{ij} - \sigma_{ij}^0)\,\dot{\epsilon}_{ij}^p \tag{2.12}$$

From the *stability postulate* of Drucker, we obtain:

$$(\sigma_{ij} - \sigma_{ij}^0)\,\dot{\epsilon}_{ij}^p \geq 0 \tag{2.13}$$

Condition (2.13) has very significant implications and restrictions on the shape of the yield surface and the flow rule, among others.

2.6 Restrictions imposed by Drucker's stability postulate – convexity and normality

It will be shown that the Drucker's stability postulate in fact imposes the requirements of convexity for the yield surface and of normality for the flow rule. This will be pictorially described below.

Referring to Fig. 2.5a, we note that:

$$(\sigma_{ij} - \sigma_{ij}^0) = \vec{AB} \tag{2.14}$$

and

$$\dot{\epsilon}_{ij}^p = \vec{BC} \tag{2.15}$$

Condition (2.13) requires that:

$$(\sigma_{ij} - \sigma_{ij}^0)\,\dot{\epsilon}_{ij}^p = |\vec{AB}|\,|\vec{BC}|\cos\theta \geq 0 \tag{2.16}$$

where θ is the angle between the two vectors $\vec{AB}$ and $\vec{BC}$. Equation (2.16) states that the value of $\cos\theta$ could not be less than zero, i.e., the angle θ must not larger than 90°. In other words, for a yield surface $f(\sigma_{ij}) = 0$ fixed in a three-dimensional stress space, each tangent plane to the yield surface must never intersect the surface but lies on one side of the surface at all points (Fig. 2.5a); otherwise, the condition, $\cos\theta \geq 0$ could be violated. As a result of this restriction, the yield surface of stable materials must be convex. If the yield surface is nonconvex, as shown in Fig. 2.5b, it is easy to choose a state of stress inside the surface to make $\theta > 90°$. Thus, Eq. (2.16) can not be satisfied.

Consider any existing initial state of stress σ_{ij}^0 inside the convex surface $f(\sigma_{ij}) = 0$. No matter where it is, the angle θ between the vectors $(\sigma_{ij} - \sigma_{ij}^0)$ and $\dot{\epsilon}_{ij}^p$ must be equal to or less than 90° to meet the requirement of Drucker's postulate. In this case, the only possibility for an arbitrary stress state vector $(\sigma_{ij} - \sigma_{ij}^0)$ is to require the vector $\dot{\epsilon}_{ij}^p$ normal to the yield surface; otherwise, the angle θ may be larger than 90°. This restriction is known as the 'normality' or 'associated flow rule' for the plastic strain rate vector $\dot{\epsilon}_{ij}^p$.

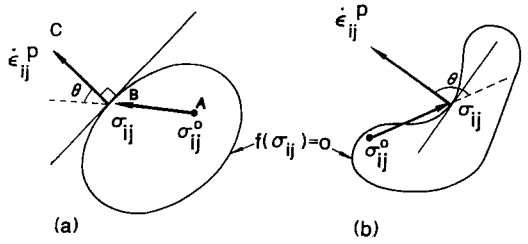

Fig. 2.5. Convex yield surface for stable materials.

2.7 The assumption of small change in geometry and the equation of virtual work

The key to prove the theorems of limit analysis and to apply them is the use of the equation of virtual work. It is well known that the application of virtual work equation requires the assumption of no appreciable change in geometry. In limit analysis, it is assumed that changes in geometry of the body that occur at the instant of collapse are small, in the sense that, in all calculations, original undeformed dimensions will be used in the equilibrium equations. That is, if equilibrium equations are established for the original state of the problem, it will be assumed that the overall dimensions at the incipient of collapse will alter by negligible amounts, so that the same equations can be used to describe the deformed state of the problem.

The equation of virtual work deals with two separate and unrelated sets: equilibrium set and compatible set. Equilibrium set and compatible (or geometry) set are brought together, side by side but independently, in the *equation of virtual work*:

Equilibrium set

$$\int_A T_i \dot{u}_i^* \, dA + \int_V F_i \dot{u}_i^* \, dV = \int_V \sigma_{ij} \dot{\epsilon}_{ij}^* \, dV \tag{2.17}$$

Compatible set

Here integration is over the whole area, A or volume V, of the body. The quantities T_i, F_i are external forces on the surface and body forces in a body, respectively. σ_{ij} are any set of stresses, real or otherwise, in equilibrium with F_i in the body and with the external forces T_i on the surface. Referring to Fig. 2.6a, a valid equilibrium set must therefore satisfy the following equilibrium equations:

$$\text{At surface points} \quad T_i = \sigma_{ji} n_j \tag{2.18}$$

$$\text{At interior points} \quad \frac{\partial \sigma_{ji}}{\partial x_j} + F_i = 0 \tag{2.19}$$

$$\sigma_{ji} = \sigma_{ij} \tag{2.20}$$

where n_i is the outward-drawn unit normal vector to a surface element.

Similarly, the strain rate $\dot{\epsilon}_{ij}^*$ represents any set of strain or deformations compatible with the real or imagined (virtual) displacement rate $\dot{u}_i^*$ of the points of applications of the external forces T_i or the points of displacements corresponding to the body forces F_i. Referring to Fig. 2.6b, a continuous distortion of a body compatible with an assumed displacement field must satisfy the following strain and displacement rate compatibility relation:

$$2\,\dot{\epsilon}_{ij}^* = \frac{\partial \dot{u}_i^*}{\partial x_j} + \frac{\partial \dot{u}_j^*}{\partial x_i} \tag{2.21}$$

The important point to keep in mind is that neither the equilibrium set T_i, F_i, σ_{ij} (Fig. 2.6a) nor the compatible set $\dot{u}_i^*$, $\dot{\epsilon}_{ij}^*$ (Fig. 2.6b) need be the actual state, nor need the equilibrium and compatible sets be related in any way to each other. Here, the asterisk for the compatible set is used to emphasize the point that these two sets are completely independent. When the actual or real states (which satisfy both equilibrium and compatibility) are substituted in the equation of virtual work, the asterisk will be omitted.

Any equilibrium set may be substituted in Eq. (2.17). In particular, an increment or rate of change of forces and interior stresses $\dot{T}_i$, $\dot{F}_i$, $\dot{\sigma}_{ij}$ may be used as an equilibrium set:

$$\int_A \dot{T}_i \dot{u}_i^* \, dA + \int_V \dot{F}_i \dot{u}_i^* \, dV = \int_V \dot{\sigma}_{ij} \dot{\epsilon}_{ij}^* \, dV \tag{2.22}$$

Equation (2.22) is a virtual work equation in rate form. The two forms of virtual work

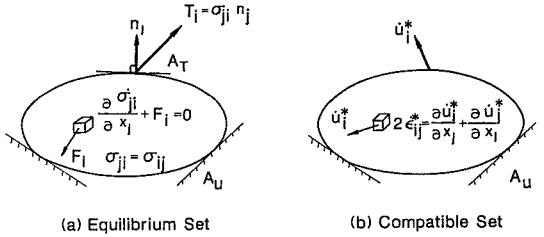

Fig. 2.6. Two independent sets in the equation of virtual work.

(Eqs. 2.17 and 2.22) will be used later in proving the theorems of limit analysis. It should be remembered that the virtual work equation carries the implication, which will hold throughout the book, that all displacements are sufficiently small for the original undeformed configuration of the problem to be used in setting up the equations of the system.

2.8 Theorems of limit analysis

Figure 2.7 shows a typical load-displacement curve as it might be measured for a surface footing test. The curve consists of an elastic portion; a region of transition from mainly elastic to mainly plastic behavior; a plastic region, in which the load increases very little while the deflection increases manifold; and finally, a work-hardening region. In a case such as this, there exists no physical collapse load. However, to know the load at which the footing will deform excessively has obvious practical importance. For this purpose, indealizing the soil as a perfectly plastic medium and neglecting the changes in geometry lead to the condition in which displacements can increase without limit while the load is held constant as shown in Fig. 2.7. A load computed on the basis of this ideal situation is called *plastic limit load*. This hypothetical limit load usually gives a good approximation to the physical *plastic collapse load* or the load at which deformations become excessive. The methods of limit analysis furnish bounding estimates to this hypothetical limit load.

The theorems of limit analysis can be established directly for a general body if the body possesses the following ideal properties:

1. The material exhibits perfect or ideal plasticity, i.e., work-hardening or work-softening does not occur. This implies that stress point can not move outside the yield surface, so the vector $\dot{\sigma}_{ij}$ must be tangential to the yield surface whenever plastic strain rates are occurring.

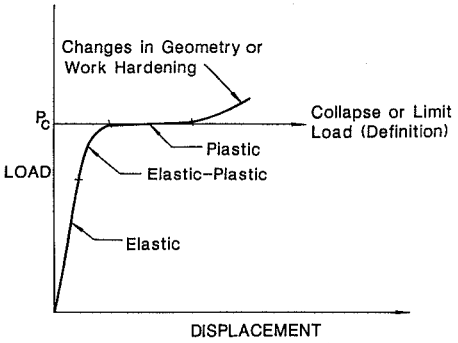

Fig. 2.7. A typical plastic collapse phenomenon and definition of limit load.

2. The yield surface is convex and the plastic strain rates are derivable from the yield function through the associated flow rule (normality). It follows from the perfect plasticity and the normality condition that $\dot{\sigma}_{ij}\dot{\epsilon}^{p}_{ij} = 0$.
3. Changes in geometry of the body that occur at the limit load are insignificant, hence the equations of virtual work can be applied.

In summary, the limit load is defined as the plastic collapse load of an ideal body having the ideal properties listed above, and replacing the actual one.

Before we proceed to prove the limit theorems, we need to prove first the following statement:

When the limit load is reached and the deformation proceeds under constant load, all stresses remain constant; only plastic (not elastic) increments of strain occur.

Thus the application of the elastic-perfectly plastic stress-strain rate relation becomes formally the same as the use of the rigid-perfectly plastic stress-strain rate relation. It should be noted that in this case the elastic strain increments are proved to be zero, they are not neglected.

A direct proof of this statement starts with the equation of virtual work (Eq. 2.22) in rate form for the stress rates $\dot{\sigma}^{c}_{ij}$ and strain rate $\dot{\epsilon}^{c}_{ij}$ in the body at the limit load and continuous displacement rates $\dot{u}_i{}^{c}$. The superscript c emphasizes the fact that all the quantities used in what follows are the actual state at collapse or limit load. The equation of virtual work is:

$$\int_{A_T} \dot{T}^{c}_{i}\dot{u}^{c}_{i}\,dA + \int_{A_u} \dot{T}^{c}_{i}\dot{u}^{c}_{i}\,dA + \int_{V} \dot{F}^{c}_{i}\dot{u}^{c}_{i}\,dV = \int_{V} \dot{\sigma}^{c}_{ij}\dot{\epsilon}^{c}_{ij}\,dV \tag{2.23}$$

In this equation the load system at collapse consists of body force rates $\dot{F}^{c}_{i}$ (per unit volume) and surface traction rates $\dot{T}^{c}_{i}$ (per unit area). Each component $\dot{T}^{c}_{i}$ is specified on the surface area A_T and each component of displacement rate $\dot{u}^{c}_{i}$ is prescribed to be zero on area A_u.

Now, at the limit load, the left-hand side of Eq. (2.23) vanishes, by our definition, $\dot{F}^{c}_{i} = 0$ everywhere; $\dot{T}^{c}_{i} = 0$ on A_T and $\dot{u}^{c}_{i} = 0$ on A_u. Since total strain rate $\dot{\epsilon}^{c}_{ij}$ consists of elastic and plastic parts, $\dot{\epsilon}^{c}_{ij} = \dot{\epsilon}^{ec}_{ij} + \dot{\epsilon}^{pc}_{ij}$, it follows from Eq. (2.23) that:

$$\int_{V} \dot{\sigma}^{c}_{ij}\,(\dot{\epsilon}^{ec}_{ij} + \dot{\epsilon}^{pc}_{ij})\,dV = 0 \tag{2.24}$$

But it follows from the ideal properties (a) and (b) that $\dot{\sigma}^{c}_{ij}\dot{\epsilon}^{pc}_{ij} = 0$. Therefore;

$$\int_{V} \dot{\sigma}^{c}_{ij}\dot{\epsilon}^{ec}_{ij}\,dV = 0 \tag{2.25}$$

Since $\dot{\sigma}_{ij}^{c}\dot{\epsilon}_{ij}^{ec}$ is a positive quantity when $\dot{\sigma}_{ij}^{c} \neq 0$ for any elastic materials, the vanishing of the integral in Eq. (2.25) requires that $\dot{\sigma}_{ij}^{c} = 0$ throughout the body. Therefore, there is no change in stress, and correspondingly no elastic change in strain during deformation at the limit load. All deformation is plastic. This statement states that elastic characteristics plays no part in the collapse at the limit load.

The lower- and upper-bound limit theorems will now be stated and proved here (Drucker et al., 1952).

Theorem I (lower bound) – If an equilibrium distribution of stress σ_{ij}^{E} covering the whole body can be found which balances the applied loads T_i on the stress boundary A_T and is everywhere below yield $f(\sigma_{ij}^{E}) < 0$; then the body at the loads T_i, F_i will not collapse.

To prove the theorem, assume it false. We show that this leads to a contradiction. If the body at the loads T_i, F_i collapses, a collapse pattern associated with the actual stresses, strain rates and displacement rates, σ_{ij}^{c}, $\dot{\epsilon}_{ij}^{c}$ and $\dot{u}_i^{c}$ exists. This collapse pattern corresponds to the collapse loads T_i on A_T and F_i in V, with $\dot{u}_i^{c} = 0$ on A_u. Two equilibrium systems would exist, T_i, F_i, σ_{ij}^{c} and T_i, F_i, σ_{ij}^{E}. From virtual work equation (2.17):

$$\int_{A_T} T_i^{c}\dot{u}_i^{c}\,dA + \int_{V} F_i^{c}\dot{u}_i^{c}\,dV = \int_{V} \sigma_{ij}^{c}\dot{\epsilon}_{ij}^{c}\,dV$$

$$\int_{A_T} T_i^{c}\dot{u}_i^{c}\,dA + \int_{V} F_i^{c}\dot{u}_i^{c}\,dV = \int_{V} \sigma_{ij}^{E}\dot{\epsilon}_{ij}^{c}\,dV$$

Hence:

$$\int_{V} (\sigma_{ij}^{c} - \sigma_{ij}^{E})\,\dot{\epsilon}_{ij}^{c}\,dV = 0$$

Since at collapse, all deformation is plastic, it follows that:

$$\int_{V} (\sigma_{ij}^{c} - \sigma_{ij}^{E})\,\dot{\epsilon}_{ij}^{pc}\,dV = 0 \qquad (2.26)$$

In view of the fact that convvexity and normality properties require $(\sigma_{ij}^{c} - \sigma_{ij}^{E})\,\dot{\epsilon}^{pc} > 0$ for σ_{ij}^{E} below yield (Eq. 2.13). A sum of positive terms cannot vanish. Therefore, Eq. (2.26) cannot be true and the lower-bound theorem is proved. If $f(\sigma_{ij}^{E}) = 0$ is permitted the body may be at the point of collapse.

The lower-bound theorem expresses the ability of the ideal body to adjust itself to carry the applied loads if at all possible.

Theorem II (upper bound) – If a compatible mechanism of plastic deformation $\dot{\epsilon}_i^{p*}$, $\dot{u}_i^{p*}$ is assumed, which satisfies the condition, $\dot{u}_i^{p*} = 0$ on the displacement boundary A_u; then loads T_i, F_i determined by equating the rate at which the external forces do work

$$\int_{A_T} T_i\dot{u}_i^{p*}\,dA + \int_{V} F_i\dot{u}_i^{p*}\,dV \qquad (2.27)$$

to the rate of internal dissipation

$$\int_{V} \sigma_{ij}^{p*}\dot{\epsilon}_{ij}^{p*}\,dV \qquad (2.28)$$

will be either higher or equal to the actual limit load.

Again, assume the theorem false, then we show that this leads to a contradiction. If the loads so computed are less than the actual limit load, then the body will not collapse at this load. An equilibrium distribution of stress σ_{ij}^{E} everywhere below yield $f(\sigma_{ij}^{E}) < 0$ must therefore exist (converse of lower-bound theorem mentioned above). From virtual work equation (2.17):

$$\int_{A_T} T_i\dot{u}_i^{p*}\,dA + \int_{V} F_i\dot{u}_i^{p*}\,dV = \int_{V} \sigma_{ij}^{E}\dot{\epsilon}_{ij}^{p*}\,dV \qquad (2.29)$$

Since T_i and F_i are computed by Eqs. (2.27) and (2.28), it follows that:

$$\int_{V} (\sigma_{ij}^{p*} - \sigma_{ij}^{E})\,\dot{\epsilon}_{ij}^{p*}\,dV = 0 \qquad (2.30)$$

The convexity and normality properties require, however, $(\sigma_{ij}^{p*} - \sigma_{ij}^{E})\,\dot{\epsilon}_{ij}^{p*} > 0$ for σ_{ij}^{E} below yield. This leads to a contradiction and thus proves Theorem II.

The upper-bound theorem states that if a path of failure exists the ideal body will not stand up.

Some corollaries follow immediately from the lower-bound theorem because the original stress distribution is admissible in the modified situation.

Corollary I – Initial stresses or deformations have no effect on the plastic limit or collapse load provided the geometry is essentially unaltered.

Corollary II – Addition of (weightless) material to a body without any change in the position of the applied loads cannot result in a lower collapse load.

Corollary III – Increasing (decreasing) the yield strength of the material in any region cannot weaken (strengthen) the body.

Corollary IV – A limit load computed from a convex yield surface which circumscribes the actual surface will be an upper bound on the actual limit load. A

limit load computed from an inscribed surface will be a lower bound on the actual collapse load.

2.9 Limit theorems for materials with non-associated flow rules

An essential point in the proofs of the limit theorems given earlier is the inequality (2.13). This inequality is a direct consequence of the normality condition or the associated flow rule. Without this inequality, the theorems cannot be proven in general. This normality relationship between a yield surface and its associated plastic strain rate vector, or the so-called associated flow rule is known to be a property of several wide classes of materials satisfying certain thermodynamic conditions (Drucker, 1951; Il'yushin, 1961).

The inequality (2.13) does not hold, for frictional materials and systems, and hence the limit theorems of plastic materials do not apply here. In this section, we shall examine first the frictional material, and then go on to see how we can, nevertheless, obtain a limited amount of useful information about friction effects by use of the theorems derived for materials with associated flow rule. Finally, limit theorems for a class of materials with nonassociated flow rules are derived.

A simple frictional system to which normality does not apply is illustrated in Fig. 2.8. Figure 2.8a shows a block resting on a rough horizontal surface and subjected to two forces, a horizontal force Q and a vertical force P. The coefficient of friction between the block and the surface is μ. Then, the 'yield surface' in P-Q load space for the system is $Q = \mu P$, which is a straight line. If the forces on the block are represented by a point below the straight line, the block will not move; if they are represented by a point on the line, an infinitesimal force increment directed upward will cause the block to slide. This is analogous to a yield surface for a perfectly plastic material. Any sliding of the block along the horizontal plane gives a corresponding increment of irreversible displacement. The displacement of the block is in the direction of the horizontal force Q, and there is no displacement in the direction corresponding to the vertical force P. The displacement increment vector for the block superimposed in the P-Q load space will be parallel to the Q-axis, and thus not normal to the 'yield surface' except in the special case $\mu = 0$, i.e., frictionless sliding. It is clear from this example that, the limit theorems cannot be applied in general for frictional materials. However, there are some special cases for which the limit theorems of plastic bodies can still fully apply. They are: (a) the coefficient of friction is zero; (b) there is no relative motion or separation at the frictional interferface. As shown in Fig. 2.8, normality does apply for a smooth or frictionless material and no relative movement at the frictional interface implies that any 'sliding' must be of the plastic kind. With this background it is intuitively clear that:

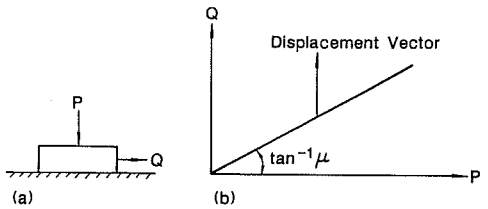

Fig. 2.8. Friction model.

Theorem III – Any set of loads which produces collapse of an assemblage of elastic-plastic bodies with frictional interfaces for the condition of no relative motion at the interfaces will produce collapse for the case of finite friction.

No relative motion is a more inclusive than infinite friction because separation is not permitted.

Theorem IV – Any set of loads which will not cause collapse of an assemblage of elastic-plastic bodies with frictional interfaces when all coefficients of friction at the interfaces are zero will not produce collapse with any values of the coefficients.

According to the frictional theorems, the limit load is bounded below by the limit load for the same bodies with zero friction on the interface. It is bounded above by the limit load for no relative motion at the interfaces. Hence, in a lower-bound calculation, if we take the footing base or retaining wall interface to be a plane of principal stress; then our calculation is 'safe' for a 'smooth' footing or wall and hence also for a footing or wall with finite friction. Further, in an upper-bound calculation, if we assume a mechanism having no relative motion at the footing base or wall interface, then, our calculation is 'unsafe' for a 'rough' footing or wall and hence also for a footing or wall with finite friction. From the frictional theorems, it can be seen that the special treatment is to enlarge the range between upper and lower bounds derived for materials with associated flow rule.

In some of the stability problems considered in this book, the range between upper and lower bounds corresponding to these two 'extreme' conditions is not affected much by the question of whether the footing or retaining wall is rough or smooth. This indicates that friction is of only secondary importance in the determination of the limit load. In some other cases, however, we find that there is a large difference between the bounds corresponding to rough and smooth footings or walls; this then indicates that friction plays an important role, and it may be necessary to use approximate intuitive method for assessing the effect of any particular coefficient of friction.

As mentioned before, the limit theorems developed earlier for materials with

associated flow rule are inapplicable for materials with non-associated flow rules. However, we can prove the following theorem which may have practical relevance to the material having the same yield criterion but with a non-associated flow rule.

Theorem V (Upper Bound) – Any set of loads which produces collapse for the material with associated flow rule will produce collapse for the same material with non-associated flow rules.

This follows readily from the fact that statically admissible stress solutions are independent of the flow rule (see Eqs. 2.18 to 2.20) so that the stress field corresponding to the actual collapse load for the material with non-associated flow rules must also be statically admissible for the same material with associated flow rule. It follows immediately from the lower-bound theorem that the actual collapse load for the material with non-associated flow rules must therefore be less than or equal to the actual collapse load for the same material with associated flow rule. The result has been discussed and applied by a number of investigators, e.g., Radenkovic (1961), Sacchi and Save (1968), Mroz and Drescher (1969), and Collins (1969, 1973).

In what follows a lower-bound theorem for perfectly plastic materials with non-associated flow rules will be developed (DeJong, 1964; Palmer, 1966). In Fig. 2.9, a single yield surface, not necessarily smooth or convex, is shown. It is assumed that at each point on this yield surface the directions of the plastic strain rate vector, not necessarily normal to the yield surface, are known. Through each point on the yield surface, $f(\sigma_{ij}) = 0$, we construct the hyperplane perpendicular to the direction of the plastic strain rate vector at that point (Fig. 2.9). If the direction at a point is non-unique, construct hyperplanes perpendicular to each of the admissible plastic

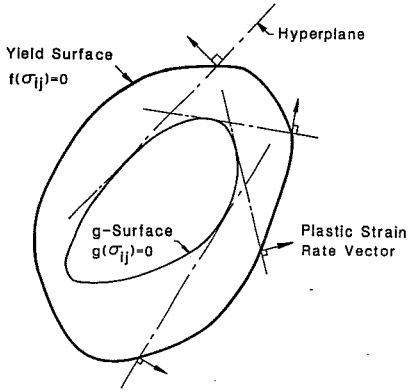

Fig. 2.9. Construction of g-surface.

strain rate directions. Either these hyperplanes have an envelope which is a surface completely within the yield surface, or they do not. If they do not, the limit theorem which follows cannot be applied. If they do, the surface is necessarily convex, by a well-known theorem in convex set theory (Eggleston, 1958). Denoting stress by σ_{ij} this envelope or new surface can be represented by $g(\sigma_{ij}) = 0$, in such a way that at points within it $g(\sigma_{ij}) < 0$ and outside it $g(\sigma_{ij}) > 0$; it will be called the g-surface. We now state and prove the following lower-bound theorem:

Theorem VI (Lower Bound) – If an equilibrium stress distribution $\overset{E}{\sigma}_{ij}$ covering the whole body can be found which balances the applied loads on the stress boundary surface and is everywhere below yield $g(\overset{E}{\sigma}_{ij}) < 0$, then the body will not collapse.

The proof follows exactly the proof of the lower-bound theorem (Theorem I) given earlier. From the definition of the g-surface, it follows that the inequality (2.13) is applicable for the new yield surface $g(\sigma_{ij}) = 0$. If the normality condition does hold, then the g-surface is identical with the yield surface $f(\sigma_{ij}) = 0$ and this theorem reduces to the lower-bound theorem (Theorem I).

2.10 The upper-bound method

In the following two sections we shall discuss in more detail some of the basic techniques of applying these upper- and lower-bound theorems. Herein we shall illustrate the applications of these techniques by means of relatively simple examples; more complex applications will be taken up in later chapters.

As stated in the upper-bound theorem, the imposed loads cannot be carried by the soil mass if for any assumed failure mechanism the rate of work done by the external forces exceeds the internal rate of dissipation. Equating of external to internal rate of work for any such valid mechanism thus gives a unsafe upper bound on the collapse or limit load. The equation formed in this way is called the work equation for a particular assumed mechanism. The conditions required to establish such an upper-bound solution are essentially as follows:

1. A valid mechanism of collapse must be assumed which satisfies the mechanical boundary conditions.
2. The expenditure of energy by the external loads (including soil weights) due to the small displacement defined by the assumed mechanism must be calculated.
3. The internal dissipation of energy by the plastically deformed regions which is associated with the mechanism must be calculated.
4. The most critical or least upper-bound solution corresponding to a particular layout of the assumed mechanism must be obtained by the work equation.

Any mechanism is said to be 'valid' if the small change in displacement within the

body (or velocity field) due to the mechanism is 'compatible' or 'kinematically admissible'. In other words, the mechanism must be continuous in the sense that no gaps or overlaps develop within the body and the direction of the strains which is defined by the mechanism must in turn define the yield stresses required to calculate the dissipation. This is known as the yield criterion and its associated flow rule.

It should be mentioned that discontinuous fields of stress and velocity may be used in applying lower- and upper-bound theorems. *Discontinuous stress fields* are actually very useful in deriving lower bounds. Surfaces of stress discontinuity are clearly possible provided the equilibrium equations are satisfied at all points of these surfaces. Surfaces of velocity discontinuity can also be admitted, provided the energy dissipation is properly computed. Rigid-body sliding of one part of the body against the other part is a well-known example. This discontinuous surface should be regarded as the limiting case of continuous velocity fields, in which one or more velocity components change very rapidly across a narrow transition layer, which is replaced by a discontinuity surface as a matter of convenience. *Discontinuous velocity fields* not only prove convenient but often are contained in actual collapse mode or mechanism. This is in a marked contrast to the stress situation where discontinuity is useful and permissible but rarely resembles the actual state.

Before the solution of a particular mechanism can be found, however, the work equation must be formed by equating the external rate of work due to the external applied loads and soil weight to the internal dissipation of energy in the plastically deformed region. Since these two quantities of work or energy have to be calculated separately before they are equated, the way in which these quantities are calculated shall be presented separately.

Once the work equation is formed, the collapse or limit load may be solved in terms of the variables that define the assumed mechanism. The final step in the analysis is to seek the particular layout or the value of the variables which is the least or the most critical. By the use of differential calculus, the magnitudes of the variables which give the most critical solution can generally be found. The algebraic technique, when it can be applied, gives a general solution applicable to all size of body of the particular mechanism assumed. This method can only be used, however, when the plot of load vs. variable parameters has a stationary minimum value. Sometimes, because of the physical conditions imposed on the parameters, there will not be a stationary minimum value within the valid range of a particular parameter. In such a case, the value of the least upper bound is not governed by the stationary minimum condition.

An alternative to the differential calculus technique is to try certain values of distances or angles which are treated as variables and several values of upper-bound solution can be obtained directly by the work equation. Visual inspection of the magnitude of the various solutions enables the most critical answer to be selected. Since many solutions are not very sensitive to a particular layout of a mechanism

and further the valid ranges of variable parameters are already considered in the trial values, the method may be used conveniently in all circumstances.

As an alternative to the algebraic technique, an arithmetic process can be used in which several particular layouts corresponding to a particular assumed mechanism are each examined in turn, each solution being obtained directly and arithmetically by the work equation. The most critical answer can then be selected. Since this technique can be combined with graphical constructions of various layouts and mechanisms, it can be used conveniently in problems involving complex geometry.

Both the algebraic and arithmetic methods, and indeed a combination of both methods, are each most suitable for certain types of problems.

An illustrative example

As an example of application of the upper-bound method we try to find the critical height, H_{cr}, of a vertical cut in a cohesive (c-ϕ) soil (Fig. 2.10) which follows the Mohr-Coulomb yield criterion and its associated flow rule. The unit weight of the soil is γ. Here, we restrict our discussion to the plane strain case. The dimension perpendicular to the plane of the book will be taken as unity, but all motion is supposed in the plane. The critical height is defined as the height at which the unsupported vertical cut, as illustrated in the figure, will collapse due to its own weight.

We assume first that the failure occurs by sliding along a plane making an angle β with the vertical. A limiting condition is reached when the rate at which the gravity forces are doing work is equal to the rate of energy dissipation along the surface of sliding. The rate of work done by the gravity force is the vertical component of the velocity multiplied by the weight of the soil wedge:

$$\tfrac{1}{2}\,\gamma\,H^2\,\tan\beta\;v\,\cos(\phi+\beta) \tag{2.31}$$

where v is the velocity of the soil, ϕ is called the angle of internal friction of the soil.

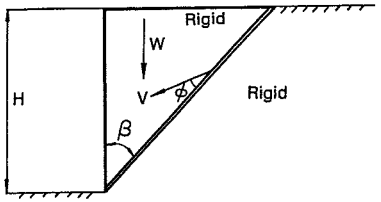

Fig. 2.10. Critical height of a vertical cut.

The Mohr-Coulomb yield criterion assumes that plastic flow occurs when, on any plane at any point in a mass of soil, the shear stress τ reaches an amount that depends linearly upon the cohesion stress c, and the normal stress, σ:

$$\tau = c + \sigma \tan\phi \tag{2.32}$$

where σ is a compressive stress, and c, ϕ are material constants (Fig. 2.11). If now a stress state, represented by a vector from the origin, is increased from zero, yielding will be incipient when the vector reaches the curve (two straight lines). For a perfectly plastic material, the vector representing the stress state at any given point can never protrude beyond the curve, since it is an unattainable stress state for a perfectly plastic soil. We shall now obtain in a convenient fashion a geometrical interpretation of the flow rule. As we assumed before, in the (σ, τ) stress coordinates, the corresponding plastic strain rates $(\dot{\epsilon}^p, \dot{\gamma}^p)$ are set out parallel to the same directions, respectively. In order to associate each strain rate vector with the corresponding stress vector, we plot it with the corresponding stress point as a floating origin. Figure 2.11 shows this combined stress and strain rate plot. The associated flow rule requires that the plastic strain rate vector be normal to the yield curve when their corresponding axes are superimposed. It can be seen from Fig. 2.12 that the perfectly plastic idealization with associated flow rule is illustrated by a block shearing on

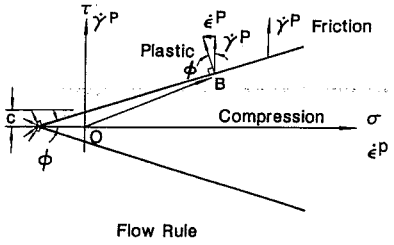

Fig. 2.11. Plastic strain rate is normal to yield curve for perfectly plastic theory, but parallel to τ-axis for frictional theory.

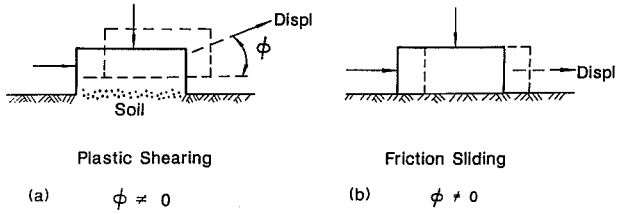

Fig. 2.12. Difference between plastic shearing and frictional sliding.

a horizontal plane. Volume expansion is seen to be a necessary accompaniment to shearing deformation according to the idealization. This theory was proposed by Drucker and Prager (1952) and generalized later by Drucker (1953), and Shield (1955a).

We shall now evaluate the rate of dissipation of energy, D, along the sliding plane. The mode of deformation in the transition layer shown in Fig. 2.13 is a combination of shear flow parallel to the layer with extension normal to it. The shear strain rate $\dot{\gamma}$ which is assumed to be uniform in the layer is equal to $\delta u/t$ and the normal strain rate $\dot{\epsilon}$ is equal to $\delta v/t$, so the rate of dissipation of energy per unit volume is equal to $\tau\dot{\gamma} - \sigma\dot{\epsilon}$, τ and σ (here taken to be positive in compression) being the shear and normal stresses, respectively. The volume of the layer is numerically equal to $t \times 1 \times 1 = t$ (see Fig. 2.13), so:

$$D = (\tau\dot{\gamma} - \sigma\dot{\epsilon})t = (\tau\delta u - \sigma\delta v)$$

or:

$$D = \delta u(\tau - \sigma \tan\phi) \tag{2.33}$$

Since the Mohr-Coulomb yield criterion must be satisfied in the plastic layer it follows from Eq. (2.32) that:

$$D = \delta u\, c \tag{2.34}$$

This equation states that the rate of dissipation of energy per unit area of discontinuous surfaces of the narrow transition layer of Mohr-Coulomb material is simply the product of the cohesion stress, c, and the tangential velocity change, δu, across the layer. It should be noted that the expression is independent of the layer thickness, so t may be taken as small as we please, including zero as a matter of con-

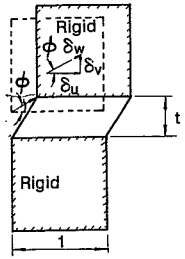

Fig. 2.13. The mode of deformation in the narrow transition layer of Mohr-Coulomb material.

venience. Thus, the rate of energy dissipated along the discontinuity surface in Fig. 2.10 is:

$$\frac{H}{\cos\beta}\, v\, (\cos\phi)\, c \tag{2.35}$$

Equating the rate of external work (Eq. 2.31) to the rate of internal energy dissipation (Eq. 2.35) gives:

$$H = \frac{2c}{\gamma}\,\frac{\cos\phi}{\sin\beta\,\cos(\phi + \beta)} \tag{2.36}$$

If β is minimized then:

$$\beta_{cr} = \tfrac{1}{4}\pi - \tfrac{1}{2}\phi \tag{2.37}$$

and

$$H_{cr} = (4c/\gamma)\,\tan\,(\tfrac{1}{4}\pi + \tfrac{1}{2}\phi) \tag{2.38}$$

This is the same value obtained by the conventional Rankine analysis (limit equilibrium analysis). See for example Terzaghi's book (1943).

An improved upper-bound solution may be obtained by considering a different mechanism, i.e., a rotational discontinuity (logarithmic spiral) instead of the

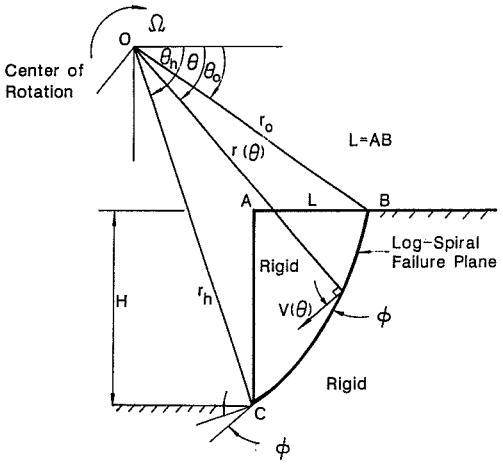

Fig. 2.14. Rotational failure mechanism for the critical height of a vertical cut.

translation discontinuity (plane surface) used above. Such an analysis requires an expression for the rate of dissipation of energy along a logarithmic spiral surface as well as an expression for the external rate of work done by the weight of the rotating soil mass. Since these expressions are useful for many applications in soil mechanics, details of the calculations are treated as a typical illustrative example.

The rotational discontinuity mechanism used here is shown in Fig. 2.14. The triangular-shaped region A-B-C rotates as a rigid body about the center of rotation O (as yet undefined) with the angular velocity Ω. The materials below the logarithm surface BC remain at rest. Thus, the surface BC is a thin layer surface of velocity discontinuity. The assumed mechanism can be specified completely by three variables. For the sake of convenience, we shall select the slope angles θ_0 and θ_h of the chords OB and OC, respectively and the height H of the vertical cut. Since the equation for the logarithmic spiral surface is given by:

$$r(\theta) = r_0 \exp[(\theta - \theta_0)\,\tan\phi] \tag{2.39}$$

the length of OC is:

$$r_h = r(\theta_h) = r_0 \exp[(\theta_h - \theta_0)\,\tan\phi] \tag{2.40}$$

From the geometrical relations, it can easily be shown that the ratios, H/r_0 and L/r_0, may be expressed in terms of the angles θ_0 and θ_h in the forms:

$$H = r_h \sin\theta_h - r_0 \sin\theta_0 \tag{2.41}$$

or

$$H/r_0 = \sin\theta_h \exp[(\theta_h - \theta_0)\,\tan\phi] - \sin\theta_0 \tag{2.42}$$

and

$$L = r_0 \cos\theta_0 - r_h \cos\theta_h \tag{2.43}$$

or

$$L/r_0 = \cos\theta_0 - \cos\theta_h \exp[(\theta_h - \theta_0)\,\tan\phi] \tag{2.44}$$

A direct integration of the rate of external work due to the soil weight in the region A-B-C is very complicated. An easier alternative is to use the method of superposition by first finding the rates of work, $\dot{W}_1$, $\dot{W}_2$ and $\dot{W}_3$ due to the soil weight in the regions O-B-C, O-A-B, and O-A-C, respectively. The rate of external

work for the required region A-B-C is then found by the simple algebraic summation, $\dot{W}_1 - \dot{W}_2 - \dot{W}_3$. We now proceed to compute the respective expressions for each of the three regions.

Considering first the logarithmic spiral region O-B-C, a differential element of the region is shown in Fig. 2.15a. The rate of external work done by this differential element is:

$$d\dot{W}_1 = (\Omega \tfrac{2}{3} r \cos\theta)\,(\gamma \tfrac{1}{2} r^2\, d\theta) \tag{2.45}$$

integration over the entire area, we obtain:

$$\dot{W}_1 = \tfrac{1}{3}\gamma\,\Omega \int_{\theta_0}^{\theta_h} r^3 \cos\theta\, d\theta$$

$$= \gamma\, r_0^3\, \Omega \int_{\theta_0}^{\theta_h} \tfrac{1}{3} \exp[3(\theta - \theta_0)\tan\phi] \cos\theta\, d\theta \tag{2.46}$$

or

$$\dot{W}_1 = \gamma\, r_0^3\, \Omega\, f_1\,(\theta_h, \theta_0) \tag{2.47}$$

where the function $f_1(\theta_h,\theta_0)$ is defined as:

$$f_1(\theta_h,\theta_0) = \frac{(3\tan\phi\cos\theta_h + \sin\theta_h)\exp[3(\theta_h - \theta_0)\tan\phi] - 3\tan\phi\cos\theta_0 - \sin\theta_0}{3(1 + 9\tan^2\phi)} \tag{2.48}$$

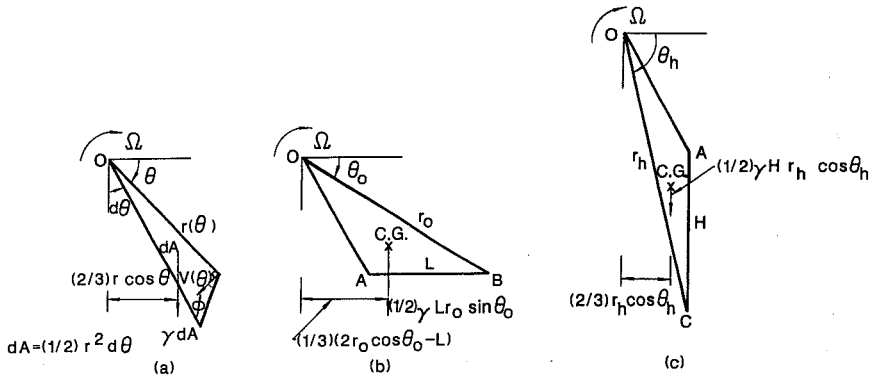

Fig. 2.15. Detail calculations for Fig. 2.14.

Consider next the triangular region O-A-B shown separately in Fig. 2.15b. The rate of work done by the weight of the region is:

$$\dot{W}_2 = (\tfrac{1}{2}\gamma\, L\, r_0 \sin\theta_0)\,[\tfrac{1}{3}(2r_0\cos\theta_0 - L)]\,\Omega \tag{2.49}$$

where the first bracket represents the total weight of the region and the other represents the vertical component of the velocity at the center of gravity of the region. The horizontal distance from the center of gravity to the vertical line passing through the point O is obtained by taking the mean horizontal distance of the points O, A, and B. This is represented in the second bracket above. Rearranging the terms in Eq. (2.49), we obtain:

$$\dot{W}_2 = \gamma\, r_0^3\, \Omega\, f_2\,(\theta_h,\theta_0) \tag{2.50}$$

where the function $f_2\,(\theta_h,\theta_0)$ is defined as:

$$f_2\,(\theta_h,\theta_0) = \tfrac{1}{6}\frac{L}{r_0}\left(2\cos\theta_0 - \frac{L}{r_0}\right)\sin\theta_0 \tag{2.51}$$

and L/r_0 is a function of θ_h and θ_0 (see Eq. 2.44).

A similar technique can be used for the triangular area O-A-C as shown separately in Fig. 2.15c. It is found that:

$$\dot{W}_3 = \gamma\, r_0^3\, \Omega\, f_3\,(\theta_h,\theta_0) \tag{2.52}$$

where the function $f_3(\theta_h,\theta_0)$ is defined as:

$$f_3(\theta_h,\theta_0) = \tfrac{1}{3}\frac{H}{r_0}\cos^2\theta_h \exp[2(\theta_h - \theta_0)\tan\phi] \tag{2.53}$$

and H/r_0 is a function of θ_h and θ_0 (see Eq. 2.42).

The magnitude of the rate of work done by the soil weight in the required region O-B-C is now obtained by the simple algebraic summation:

$$\dot{W}_1 - \dot{W}_2 - \dot{W}_3 = \gamma\, r_0^3\, \Omega(f_1 - f_2 - f_3) \tag{2.54}$$

The internal dissipation of energy occurs along the discontinuity surface BC (Fig. 2.14). The differential rate of dissipation of energy along the surface may be found by multiplying the differential area, $r d\theta/\cos\phi$, of this surface by the cohesion c times the tangential discontinuity in velocity, $v\cos\phi$, across the surface of discontinuity,

Eq. (2.34). The total internal dissipation of energy is then found by integration over the whole surface:

$$\int_{\theta_0}^{\theta_h} c(v\cos\phi)\frac{r\,d\theta}{\cos\phi} = \frac{cr_0^2\Omega}{2\tan\phi}\{\exp[2(\theta_h - \theta_0)\tan\phi] - 1\} \tag{2.55}$$

Equating the external rate of work, Eq. (2.54), to the rate of internal energy dissipation, Eq. (2.55), gives:

$$H = \frac{c}{\gamma} f(\theta_h,\theta_0) \tag{2.56}$$

where $f(\theta_h,\theta_0)$ is defined as:

$$f(\theta_h,\theta_0) = \frac{[\exp\{2(\theta_h - \theta_0)\tan\phi\} - 1]\,[\sin\theta_h \exp\{(\theta_h - \theta_0)\tan\phi\} - \sin\theta_0]}{2\tan\phi\,(f_1 - f_2 - f_3)} \tag{2.57}$$

By the upper-bound theorem of limit analysis, Eq. (2.56) gives an upper bound for the critical value of the height. The function $f(\theta_h,\theta_0)$ has a minimum value when θ_h and θ_0 satisfy the conditions:

$$\frac{\partial f}{\partial\theta_h} = 0, \qquad \frac{\partial f}{\partial\theta_0} = 0 \tag{2.58}$$

Solving these equations and substituting the values of θ_h and θ_0 thus obtained into Eq. (2.56), we obtain a least upper bound for the critical height, H_{cr}, of the vertical cut.

To avoid lengthy computations, these simultaneous equations may be solved by a semi-graphic method. The function $f(\theta_h,\theta_0)$ is found to have a minimum value near the point $\theta_0 = 40°$, $\theta_h = 65°$ for the case $\phi = 20°$, where it has the value 3.83 $\tan(\frac{1}{4}\pi + \frac{1}{2}\phi)$ for all values of ϕ, so that:

$$H_{cr} = (3.83c/\gamma)\tan(\tfrac{1}{4}\pi + \tfrac{1}{2}\phi) \tag{2.59}$$

is an upper bound for the critical height of the vertical cut. The value 3.83 in Eq. (2.59) is an improvement of the previous solution 4.0 as given in Eq. (2.38).

This is the same value obtained by Fellenius (1927) using the conventional limit equilibrium method.

In the laboratory, soil may exhibit the ability to resist tension. In the field, however, the presence of water or tensile cracks near the surface may destroy the tensile strength of the soil. Hence, the tensile strength of soil is not reliable and it

may be neglected. This is a conservative idealization. The Mohr-Coulomb yield criterion is modified by the tension cut-off as shown in Fig. 2.16, in which the requirement of zero-tension is met by the circle termination as shown (the upper half of the yield curve is ODB).

As the soil is unable to resist tension, the introduction of a tensile crack in a failure mechanism is permissible. No energy is dissipated in the formation of a simple tension crack; both normal and shear stress are zero on the plane of separation (see the origin in Fig. 2.16).

The rotational mechanism containing a simple-tension crack and a homogeneous shearing zone A-B-C is shown in Fig. 2.17. Failure due to tipping over of the soil 'slab' of thickness Δ about point A with an angular velocity ω is possible. The region A-B-C of homogeneous shearing, $\dot{\gamma}$, is the field shown in Fig. 2.18b which indicates that $\omega = \dot{\gamma}$.

To understand the homogeneous shearing zone of Fig. 2.18b, we consider, the rate of dissipation of energy, D, per unit volume of the simple shear flow shown in Fig. 2.18a. This simple shear can be easily visualized as a series of narrow transition layers of the type discussed before. Each of these layers is bounded by horizon-

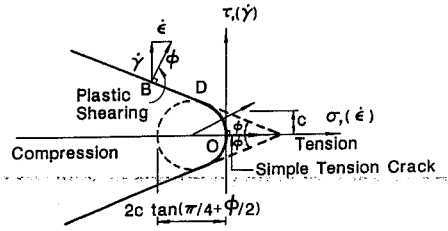

Fig. 2.16. Modified Mohr-Coulomb criterion with zero-tension cut-off.

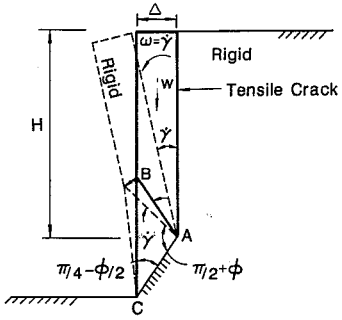

Fig. 2.17. Rotational mechanism containing a simple tension crack and the homogeneous shearing zone for soil unable to take tension.

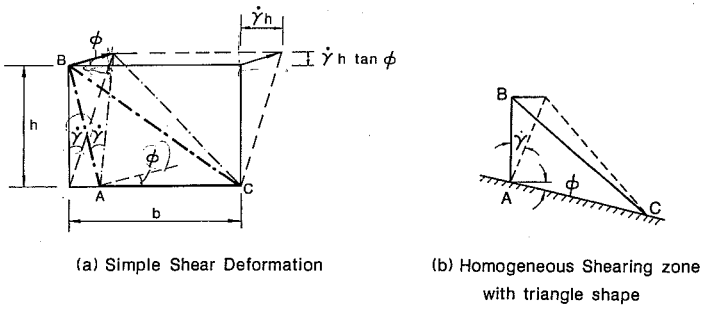

(a) Simple Shear Deformation

(b) Homogeneous Shearing zone with triangle shape

Fig. 2.18. Homogeneous shearing zone.

tal parallel straight lines corresponding to a relative translation of the adjacent masses of soil. The simple shear deformation designed by $\dot{\gamma}$ is accompanied by the vertical normal strain rate, $\dot{\gamma}\tan\phi$. The rate of dissipation of energy is equal to $\tau\dot{\gamma} - \sigma\dot{\gamma}\tan\phi$ per unit volume, τ and σ being the shear and normal stresses, respectively. Since the Mohr-Coulomb yield criterion must be satisfied in the field of flow, it follows that:

$$D = \tau\dot{\gamma} - \sigma\dot{\gamma}\tan\phi = c\dot{\gamma} \tag{2.60}$$

For the example problem, where the triangle A-B-C of Fig. 2.18b is a portion of the parallelogram of Fig. 2.18a, it follows that Eq. (2.60) gives $D = c\dot{\gamma} = c\omega$. The total rate of dissipation of internal energy for unit dimension perpendicular to the paper is just D times the area of the triangle ABC or:

$$(c\omega)\ [\Delta^2 \tan(\tfrac{1}{4}\pi + \tfrac{1}{2}\phi)] \tag{2.61}$$

The rate of external work done by gravity is the weight of the soil moving downward as the 'slab' rotates about A, multiplied by the velocity, which is ω ($\frac{1}{2}\Delta$):

$$W \simeq \tfrac{1}{2}\,\gamma\,\Delta^2\,H\,\omega \tag{2.62}$$

If the rate of external work is equated to the dissipation, it yields:

$$H_{cr} = (2c/\gamma)\tan(\tfrac{1}{4}\pi + \tfrac{1}{2}\phi) \tag{2.63}$$

This confirms Terzaghi's solution (1943) for a tensile crack extending the full height of the bank.

2.11 The lower-bound method

The lower-bound method of limit analysis is different from the upper-bound method in that the equilibrium equation and yield condition instead of the work equation and failure mechanism are considered. Moreover, whereas the development of the work equation from an assumed collapse mechanism is always clear, many engineers find the construction of a plastic equilibrium stress field to be quite unrelated to physical intuition. Without physical insight there is trouble in finding effective ways to alter the stress fields when they do not give a close bound on the collapse or limit load. Often the user employs the existing stress fields from well-known texts or the more recent technical literature as a magic handbook and tries to fit his problem to the particular solutions he finds. Intuition and innovation seem discouraged by unfamiliarity and apparent complexity. Although the discontinuous fields of stress which will be drawn and discussed in this Section are simpler to visualize, they too are not often employed in an original manner by the design engineer. Yet, in fact, the concepts are familiar to the civil engineer in his terms and can be utilized by the designer as a working tool. This was described in some details by Chen (1975).

Most of the early work on the construction of a stress field is concerned with the pure cohesive soil for which $\phi = 0$, or Tresca material, the self-weight of the material being assumed to be insignificant. Actually, there are only limited practically important problems in soil mechanics for which this assumption is justified. Further, as a rule for Mohr-Coulomb material, the stress field involves both applied forces and the self-weight of soil mass. While a number of simple stress fields of this type have been obtained during recent years, general methods allowing for the self-weight of soil have not yet been developed. However, progress in its extension to soils with some different yield surfaces is anticipated in the near future.

As stated in the lower-bound theorem, if an equilibrium state of stress below yield can be found which satisfies the stress boundary conditions, then the loads imposed can be carried without collapse by a stable body composed of elastic-perfectly plastic material. Any such field of stress thus gives a safe or lower bound on the collapse or limit load. The stress field satisfying all these conditions is called statically admissible stress field. The conditions required to establish such a lower-bound solution are essentially as follows:

a. A complete stress distribution or stress field must be found, everywhere satisfying the differential equation of equilibrium.
b. The stress field at the boundary must satisfy the stress boundary conditions.
c. The stress field must nowhere violate the yield condition.

From these rules it can be seen therefore that a lower-bound technique is based entirely on equilibrium and yield conditions but it must not, however, be confused that the limit equilibrium method or slip-line field gives a lower-bound solution. It is

worth pointing out here that in the limit equilibrium method or slip-line field, the stress state is specified only either along the slip lines or in a local plastic stress zone around the load and not everywhere in the soil mass, as required by item (a), and therefore a limit equilibrium solution or a slip-line solution does not give a complete equilibrium solution. Further, even if a complete equilibrium solution extended from the slip-line field into the rigid regions can be found, it remains to be demonstrated that such a stress distribution will not violate the yield condition in the rigid regions, as required by item (c). Hence, the slip-line field solution strictly should only be regarded as an upper-bound solution, though, it seems most likely that it could be completed. It should also be noted that the stress distribution associated with an assumed collapse mechanism in the upper-bound calculation need not be in equilibrium, and is only defined in the deforming regions of the collapse mode.

It has already been mentioned previously that discontinuous fields of stress and velocity may be used in applying the lower- and upper-bound theorems. Similarly, discontinuous fields of stress are found to be especially useful in deriving lower bounds. Here, as in a discontinuous velocity situation, surfaces of stress discontinuity are clearly possible, provided the equilibrium equations of stresses are satisfied at all points of these surfaces. If the stress fields are chosen for convenience to be at yield in some regions rather than below, the load so obtained may be the collapse

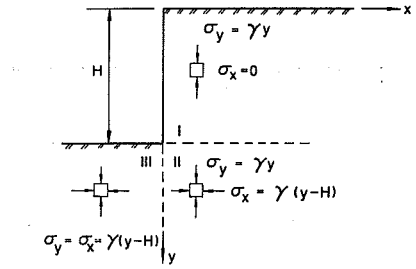

Fig. 2.19. A lower-bound stress field for the stability of a vertical cut.

load itself. Although such a discontinuous stress situation is useful and permissible in lower-bound calculation, it is rarely the actual state. This is in a marked contrast to the velocity situation where discontinuity is not only found useful and convenient in upper-bound calculation but often is contained in actual collapse mode or mechanism.

An illustrative example

Let us now attempt a lower-bound solution of the same slope stability problem-critical height of a vertical cut with soil unable to take tension, by constructing a simple discontinuous stress field which does not violate the yield condition. The simplest possible equilibrium distribution of stress is found by having a horizontal plane of discontinuity between Zones I and II and a vertical plane of discontinuity between Zones II and III as shown in Fig. 2.19a. Assuming the state of stress in Zones I, II, and III to be uniaxial compression, biaxial compression, and hydrostatic compression, respectively. Figure 2.19b shows the corresponding Mohr circles for each zone. The Mohr-Coulomb yield condition with tension cut-off is satisfied when the circles representing Zone I at ground level meet the yield lines M_0M_1 and M_0M_2. Therefore:

$$\tfrac{1}{2}\gamma H = c\cos\phi + \tfrac{1}{2}\gamma H \sin\phi \tag{2.64}$$

Since this discontinuous stress field satisfies equilibrium everywhere in the soil mass and the boundary conditions, which in this case require both normal and shear to be zero on all surfaces, and nowhere exceeds the Mohr-Coulomb yield criterion with zero-tension cut-off, by the lower bound theorem of limit analysis, the value H computed from Eq. (2.64) is therefore a lower bound for the critical height:

$$H_{cr} = (2c/\gamma)\tan(\tfrac{1}{4}\pi + \tfrac{1}{2}\phi) \tag{2.65}$$

Since this lower bound agrees with the previous upper-bound solution (Eq. 2.63), the exact value of the critical height, which neglects the tensile stress of soil, is Eq. (2.65) or Eq. (2.63). It must be borne in mind however that the coincidence of upper and lower bounds provided by the velocity field, Fig. 2.17, and the stress field, Fig. 2.19a, is by no means indicating that the two discontinuous fields are the actual state. Once again it is worth pointing out that in the limit analysis there is no theoretical restriction that the assumed stress field or velocity field need have some similarity to the actual state, although generally speaking, the closer the assumed state to the actual state is, the more realistic the resulting answer will be.

References

Chen, W.F., 1975. Limit Analysis and Soil Plasticity, Elsevier Amsterdam, 638 pp.

Collins, I.F., 1969. The upper-bound theorem for rigid/plastic solids generalized to include Coulomb friction. J. Mech. Phys. Solids, 17: 323 – 338.

Collins, I.F., 1973. A note on the interpretation of Coulomb's analysis of the thrust on a rough retaining wall in terms of the limit theorems of plasticity theory. Geotechnique, 23(3): 442 – 447. Discussion by J.L. Justo, Geotechnique, 24(1): 106 – 108.

DeJong, D.J.G., 1964. Lower-bound collapse theorem and lack of normality of strain-rate to yield surface for soils. In: J. Kravtchenko and P.M. Sirirys (Editors), Rheology and Soil Mechanics, IUTAM Symp., Grenoble. Springer, Berlin, 1966, pp. 69 – 75.

Drucker, D.C., 1951. A more fundamental approach to stress-strain relations. Proc. 1st U.S. Natl. Congr. Appl. Mech. American Society of Mechanical Engineers, pp. 487 – 491.

Drucker, D.C., 1953. Limit analysis of two- and three-dimensional soil mechanics problems. J. Mech. Phys. Solids, 1: 217 – 226.

Drucker, D.C., Greenberg, J.H. and Prager, W., 1952. Extended limit design theorems for continuous media. Q. Appl. Mech., 10(2): 381 – 389.

Drucker, D.C. and Prager, W., 1952. Soil mechanics and plastic analysis or limit design. Q. Appl. Math., 10(2): 157 – 165.

Eggleston, H.G., 1958. Convexity. Cambridge University Press, London.

Fellenius, W., 1927. Erdstatische Berechnungen. Ernst, Berlin (revised ed., 1939, 48 pp.).

Il'yushin, A.A., 1961. O postulate plastichnosti (On the postulate of plasticity). Prikl. Mat. Mekh., 25: 503 – 507.

Mroz, Z. and Drescher, A., 1969. Limit plasticity approach to some cases of flow of bulk solids. J. Eng. Ind., 51: 537 – 564.

Palmer, A.C., 1966. A limit theorem for materials with non-associated flow laws. J. Mecanique, 5(2): 217 – 222.

Prager, W., 1952a. The general theory of limit design. Proc. 8th Int. Congr. Appl. Mech., Istanbul. Faculty of Science, Univ. Istanbul, II, pp. 65 – 72.

Prager, W., 1952b. On the kinematics of soils. Colloques Junius Massau, Comite National de Mécanique Théorique et Appliquée, Brussels, pp. 3 – 8.

Radenkovic, D., 1961. Théorie des Charges Limitées, Extension à la Mécanique des Sols. Séminaires de Plasticité. Ecole Polytechnique, Publ. Sci. Tech., 116.

Sacchi, G. and Save, M.A., 1968. A note on the limit loads of non-standard materials. Meccanica, 3: 43 – 45.

Shield, R.T., 1955a. On Coulomb's law of failure in soils. J. Mech. Phys. Solids, 4(1): 10 – 16.

Shield, R.T., 1955b. On the plastic flow of metals under conditions of axial symmetry. Proc. R. Soc. London, Ser. A, pp. 233 – 267.

Terzaghi, K., 1943. Theoretical Soil Mechanics. Wiley, New York, NY., 510 pp.

Chapter 3

VALIDITY OF LIMIT ANALYSIS IN APPLICATION TO SOILS

3.1 Introduction

While the *limit equilibrium method* has been widely used for solving stability problems in soil mechanics for more than 200 years, the application of the *limit analysis method*, that was originally developed for metals, to soil medium is a recent one (e.g. Finn, 1967; Chen, 1975). Although the use of the upper-bound techniques of limit analysis for solving stability problems is promising, there is, however, much controversy on its applicability to soils. The required limit analysis assumption on normality condition leads to a much too large dilatation for frictional ($\phi \neq 0$) soils during plastic flow than that can be explained experimentally. This has been the center of the dispute. Previous investigators, such as Chen (1975), have concentrated on how the techniques of limit analysis can be applied to solve soil stability problems. However, little work has been done on why these techniques are applicable to soils, especially for cohesionless soils. It is one of the major purposes of this chapter to examine the applicability of the upper-bound limit analysis method as applied to soil medium (Chen and Chang, 1981).

In the first part of this chapter, the principle of effective stresses and the mechanical behavior of soils are briefly discussed. Some suggested yield criteria are introduced. In the latter part of this chapter, the basic assumptions of the limit theorems on which the limit analysis is based and the range of validity of these assumptions in the context of soils are critically discussed, following the work of Chen and Chang (1981). Meanwhile, a simple, vertical cut slope problem is presented to illustrate the effect of pure friction or perfect plasticity idealization on the collapse load analysis for a naturally existed, partially frictional and partially dilating soil.

3.2 Soil – a multiphase material

In its general sense, the term *soil* refers to the unaggregated or uncemented granular material consisting of both mineral and organic particles. In many materials classified as soils, cementing between grains may exist to some slight degree and therefore may contribute to the mechanical characteristics of the

granular material. However, if the material is to be classified as soil, this cementation should not be such as to cause the granular material to assume a rocklike form.

Generally, soil is a multiphase material comprised of mineral grains, air voids and water. Therefore, the mathematical characterization of their mechanical behavior should ideally be based on a consideration of the behavior of individual constituent elements and their interaction. This type of mathematical formulation has been made using the particulate mechanics approach (Harr, 1977), in which the 'macroscopic' continuum stress-strain behaviors are studied in terms of the more basic 'microscopic' interactions of many particles, including the use of probabilistic theory to handle the probabilistic nature of the interparticle contact relationships. Such an approach in studying soil behavior can be rather complex and would not be particularly fruitful in engineering applications.

For most practical applications, the scale of the geometry of interest of the soil mass is very large. Thus, the 'microscopic' effects can be averaged and the soil can be idealized as a continuum, and its mechanical behavior can then be studied within the framework of *continuum mechanics*. All the discussions in this book are based on this latter approach, that is, a phenomenological approach on a macroscopic level.

Although soils are treated as ideal continua, the particulate nature of real soils with respect to the effects of pore water and pore air pressures in saturated and partially saturated soils on their deformational and strength characteristics must be emphasized. The *principle of effective stresses* (Terzaghi, 1943) is therefore fundamental in the discussion of the mechanical behavior of soils.

In general, soils are divided into two main groups, *cohesionless* and *cohesive soils*. Cohesionless soils may be defined as those in which intrinsic interparticle forces or bounds have a negligible effect on the mechanical behavior of the soil. This category includes rockfill, gravels, sands, and coarse silts. According to the state of packing of the grains, cohesionless soils may further be classified as loose or dense material.

On the other hand, in cohesive soils, interparticle forces or bonds make a significant contribution to the mechanical behavior of the soil. Included in this category are soils such as clays, clayey silts, and boulder clays and tills. Depending on the stress history of the cohesive soils, they may be classified as overconsolidated or normally consolidated soils. Many qualitative similarities exist between the behavior of normally and overconsolidated cohesive soils, and that of loose and dense cohesionless soils, respectively.

The mechanical behavior of soil materials under externally applied loads is quite complicated, and it has been a subject of research for many years. The complexity stems mainly from the fact that, unlike the properties of most engineering materials, deformational and strength characteristics of soils are greatly affected by such factors as soil structure (e.g., grain size, grain shape, surface texture, mineralogy, cementation or bonding), density, water content, drainage conditions, degree of

void saturation, loading rate, confining pressure, loading (or stress) history, current stress state, and inherent and stress (or strain)-induced anisotropy. In many cases, it may be possible to take account of several of these factors (e.g., soil structure, density, water content, drainage conditions, degree of saturation) by selecting soil specimens and testing conditions that duplicate the field conditions as closely as possible. However, even when this is done, it is always found that the behavior of soil under the various stress paths and loading histories encountered in the field is substantially different. Therefore, new or improved laboratory testing devices capable of providing for a wide range of stress paths and modes of deformations are essential in the development and the proper assessment of the applicability of various *constitutive models* utilized to describe the behavior of soil materials. For this purpose, a number of investigators have recently developed multiaxial or 'truly' triaxial test devices in which the three principal stresses and strains acting on a soil sample can be independently controlled and measured.

As a multiphase material, soil can be visualized as a skeleton of solid particles enclosing continuous voids that contain water and/or air. For the range of stresses usually encountered in practice, the individual solid particles and water can be considered *incompressible*; air, on the other hand, is highly compressible. As a result of the applied stresses, the volume of soil skeleton as a whole can change owing to rearrangement of the solid particles into new positions, mainly by rolling and sliding, with a corresponding change in forces acting between particles. The actual compressibility of the soil skeleton depends on the structural arrangement of the solid particles.

In a fully saturated soil, since water is considered to be incompressible, a change in volume is possible only if some of the water can escape from (or flow into) the voids (i.e., under drained condition). When drainage of water is not allowed in a

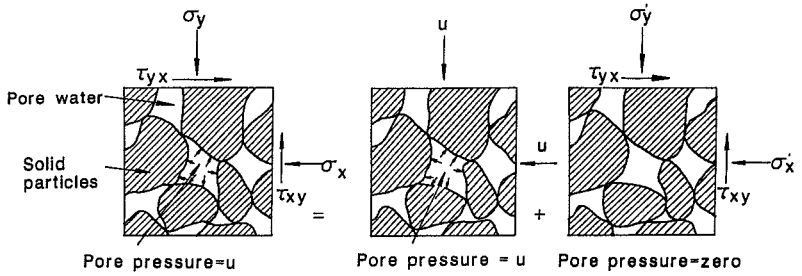

Fig. 3.1. Total and effective stresses in saturated soils.

saturated soil, volume changes cannot occur, and the soil is defined to be under undrained condition. In a dry or a partially saturated soil, a change in volume is always possible owing to the compressibility of the air in the voids, provided that there is scope for particles rearrangement.

Shear stresses can be resisted only by the skeleton of solid particles, by means of forces developed at the interparticle contacts. However, the resistance to normal stresses is provided by two components: the first is the stress carried by the skeleton of solid particles, and the second is the stress carried by the pore pressure. The latter component in turn is divided into two parts, the *pore water pressure* and the *pore air pressure.*

The principle of effective stress (Terzaghi, 1943; Bishop and Blight, 1963) provides the relation between the total stresses, σ_{ij}, acting at any point in a soil mass, the stresses carried by the skeleton of solid particles (interparticle stresses), referred to as the effective stresses, and the pressure in the pore fluid (water and air).

In a fully saturated soil (Fig. 3.1), the principle of effective stress can be expressed mathematically as (Terzaghi, 1943):

$$\sigma_{ij} = \sigma'_{ij} + u\delta_{ij} \tag{3.1}$$

where σ_{ij} is the total stress tensor, σ'_{ij} is the effective stress tensor, u is the pore water pressure, and δ_{ij} is the Kronecker delta. The components of δ_{ij} are 1 if $i = j$ and 0 if $i \neq j$.

In the case of partially saturated soils, part of the voids is occupied by water and the other part by air. The pore fluid pressure, u, consists of two parts: pore water pressure, u_w, and pore air pressure, u_a. For such cases, the following effective stress equation has been proposed (Bishop and Blight, 1963):

$$\sigma_{ij} = \sigma'_{ij} + [u_a - \chi (u_a - u_w)]\, \delta_{ij} \tag{3.2}$$

where χ is a dimensionless parameter, to be determined experimentally, which is primarily related to the degree of saturation of the soil (i.e., χ is proportional to the pore volume occupied by the water phase). The term $(u_a - u_w)$ is a measure of the suction in the soil. The relation in Eq. (3.2) can be conveniently expressed in the same form as Eq. (3.1), in which case u represents the total pore pressure for the combined effect of the pore air pressure and the pore water pressure; that is:

$$u = u_a - \chi(u_a - u_w) \tag{3.3}$$

For a fully saturated soil $\chi = 1$ and Eq. (3.2) degenerates to Eq. (3.1); and for a completely dry soil $\chi = 0$.

The principle of effective stress is fundamental to a proper description of deformational and strength characteristics of saturated and partially saturated soils. According to Terzaghi (1943), 'All measurable effects of a change of stress, such as compression, distortion, and a change of shearing resistance, are exclusively due to changes in the effective stresses'. On this basis, all soil deformations are assumed to be caused by the effective stresses.

In practice, the use of Eq. (3.2) for a three-phase soil material is not convenient owing to the presence of the parameter χ. Therefore, in most practical applications, soils are treated as two-phase materials; in which cases only fully saturated or completely dry soils are considered. Furthermore, when studying the behavior of fully saturated soils, two different situations are encountered in terms of the pore water pressure variable, that is, *drained and undrained conditions.*

When the stresses are applied so slowly that the induced excess pore pressures are negligible, the soil is said to be in a drained condition. Hence the only pore pressures (if any) are steady-state pressures due to a preexisting seepage pattern or simply a hydrostatic pressure. Any changes in the applied total stresses result in identical changes in the effective stresses.

On the other hand, under an *undrained condition*, the loads are assumed to be applied very rapidly so that the excess water pressure induced by the applied loading does not have time to dissipate. No volumetric strains, i.e., no volume change can occur in such case; the soil element undergoes shear strain only. Therefore, an undrained condition is often termed a *constant volume condition.* Precisely, undrained condition implies no change in water content; and constant volume condition is an approximation based on the incompressibility assumption for pore water and solid particles.

The behavior of saturated soils under both fully drained and fully undrained conditions can be described by *time-independent constitutive models.* In the subsequent parts in this book, only time-independent behavior of soils are considered.

Under the general partially drained condition, the induced excess pore pressures are functions of both the total stresses due to the applied loads and the elapsed time, which is a time-dependent case. Throughout this book, the discussions are limited to dry or fully saturated soils under drained or undrained conditions. Partially saturated soils or partially drained conditions are not considered.

Drained and undrained conditions of saturated soils represent two of the most important situations in may practical geotechnical applications. For instance, stability or progressive failure analysis involving saturated cohesionless soils are often carried out based on a fully drained assumption, since cohesionless soils have high permeability and drainage normally takes place so fast in such cases. Nevertheless, undrained deformational and strength characteristics of cohesionless soils are of prime interest in the study of problems involving rapid loadings as, for example, underground shaking during an earthquake. In these cases, such phenomena as *liquefaction* of large masses of saturated cohesionless soil are extremely important

since they can result in catastrophic failures in earth structures (e.g., landslides, and failure of waterfront retaining structures).

Both drained and undrained behavior characteristics are relevant in problems involving cohesive soils. For example, stability analyses of earth structures such as footings and retaining walls at the end of construction, before the induced excess pore water pressure dissipates, are usually based on undrained conditions (often called immediate stability analyses). Drained conditions are relevant in the long-term stability analyses, corresponding to the situation when all the excess pore water pressures have dissipated.

3.3 Mechanical behavior of soils

Characteristics of soil deformational behavior have been the subject of research for many years. Only the essential point and characteristics of typical soil behavior are briefly described in the following.

The qualitative typical volumetric behavior of dry or saturated drained soils under hydrostatic loading and unloading conditions is shown in Fig. 3.2. It is clear from this figure that soils, in general, exhibit a nonlinear behavior under hydrostatic loading and unloading. Upon unloading to the initial stress state, only a small part of volumetric strains is recovered (elastic or reversible strains), whereas the other part remains as permanent (irreversible or plastic) strain.

Qualitative typical stress-strain response curves for soils obtained under drained

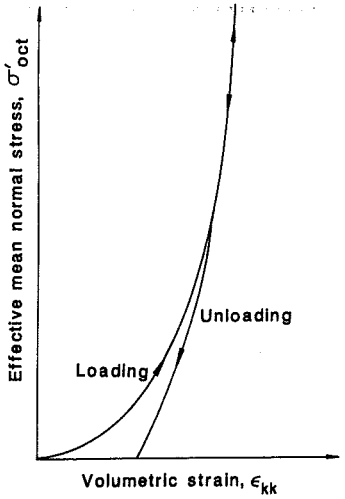

Fig. 3.2. Typical behavior of a dry or drained soil under hydrostatic loading and unloading.

triaxial compression conditions are given in Fig. 3.3. This is the most commonly used test in soil mechanics. The test is performed on a cylindrical sample, on which two of the principal stresses are kept constant (e.g., $\sigma_2 = \sigma_3 =$ constant) while the third principal stress σ_1 is increased. Typically, the stress-strain behavior of dense sands or overconsolidated clays is similar to that of curves 1 in Fig. 3.3, whereas curves 2 in this figure are typical for loose sands or normally consolidated clays. The curves in Fig. 3.3 demonstrate the great influence of the initial state of consolidation (compaction) of the soil on the stress-strain response.

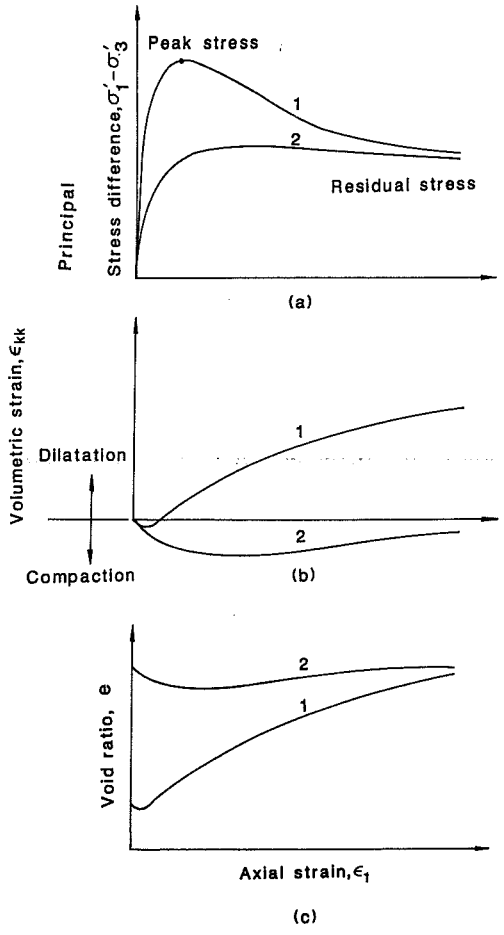

Fig. 3.3. Typical behavior of saturated soils tested under drained conventional triaxial compression test conditions. (1) Dense sand or overconsolidated clay; (2) loose sand or normally consolidated clay.

Dense sands and overconsolidated clays have higher stiffnesses and higher peak stresses than those for loose sands and normally consolidated clays. After peak stresses (Fig. 3.3a), the stress-strain curves for dense and loose soils are distinctly different. Loose soils show very little or no reduction in shear strength with increasing strain beyond the peak, and their behavior can be characterized as strain-hardening behavior, whereas the dense soils exhibit a more brittle strain softening behavior with a marked post-peak falloff in shear strength. At very large strains (i.e., the end of the test in a strain-controlled test), both dense and loose soils eventually reach the same constant ultimate (or residual) shearing resistance.

Irrespective of the original state of consolidation (loose or dense), the volumetric strains are initially compressive (compaction), but after peak stresses, the dense samples show a considerable amount of dilation, whereas the loose specimens con-

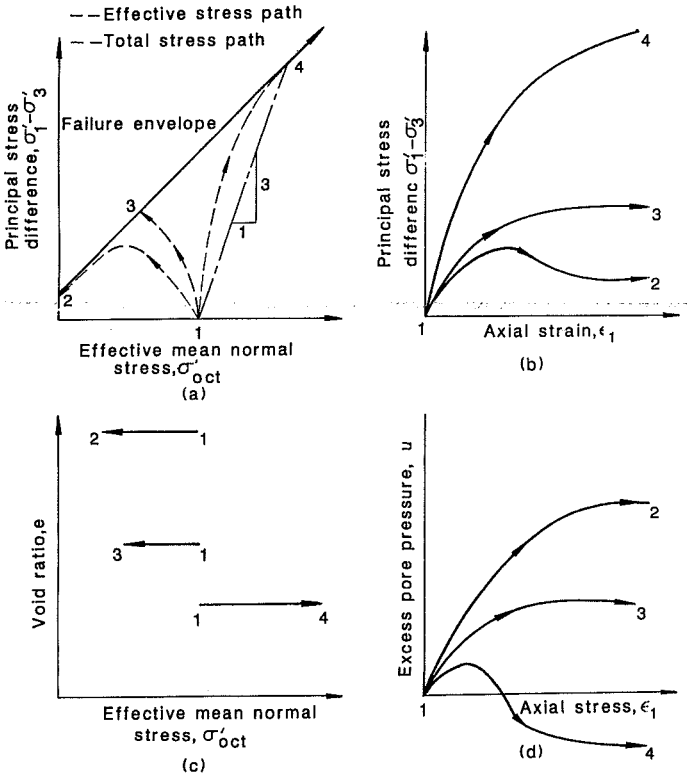

Fig. 3.4. Typical behavior of saturated soils under undrained conventional triaxial compression test conditions.

tinue to compress (Fig. 3.3b). At very large strains, the volumes for both dense and loose samples eventually approach a constant unique ultimate value. The condition under which strains continue to increase without further changes in the shearing resistance and void ratio has been termed the *critical state* (Hvorslev, 1937). As can be seen from Fig. 3.3, the ultimate values of the shearing strength and the *void ratio* (or *specific volume*) corresponding to this condition are independent of the initial state of consolidation of the soil.

Qualitative typical stress-strain pore-pressure response curves for three different saturated soils tested under undrained conventional triaxial compression are given in Fig. 3.4. In this figure, the three soil samples are first isotropically consolidated to the same effective mean normal stress level, Point 1, and then subjected to increasing axial stress σ_1. The stress-strain curves 2 show typical response of a normally consolidated clay or very loose sand. In these curves, the peak shear strength is developed at a relatively small axial strain compared to the value of the strain at the end of the test (Fig. 3.4b). After the peak, the curve shows strain softening behavior, and the residual shear strength at very large strains is small compared to the peak value. Because of the volume contraction tendency in loose soils, the induced excess pore pressure increases as the test progresses, leading to a substantial decrease in the effective stresses which causes the decrease in the shear strength.

Curves 4 in Fig. 3.4 depict behavior typical of dense sands and heavily overconsolidated clays. The strength of the material increases continuously with strain hardening. Owing to the tendency of volume expansion in the dense soils, the effective stresses increase with increasing applied stresses (Fig. 3.4a). The pore water pressure reaches its maximum value at a relatively small strain, then decreases and eventually becomes negative (Fig. 3.4d).

Within the extreme limits of the dense and loose soil behaviors, various intermediate responses can be observed (curve 3 in Fig. 3.4) depending mainly on the initial state of consolidation of the material. Obviously the void ratio remains constant under undrained condition since no volumetric strain can occur (Fig. 3.4c).

The effect of the confining pressure (σ_3) on the behavior of soil can be shown by considering the stress-strain-volume change curves in Fig. 3.5 obtained from drained triaxial compression tests on loose and dense sands. As can be seen, the behavior changes from strain softening to strain hardening, and the strains at peak failure stresses increase as the confining pressure increases. This change in the behavior is particularly pronounced for the initially dense sand. The volumetric strains become more compressive with increasing confining pressure.

With increasing confining pressure σ_3, although the peak deviatoric stress $\sigma_1 - \sigma_3$ increases, the peak stress ratio σ_1/σ_3 decreases. Corresponding to a particular value of initial void ratio, the confining pressure that results in no volume change at failure is called the *critical confining pressure*. Also, for a particular value of σ_3, there is a corresponding value of the initial void ratio at which no volume change

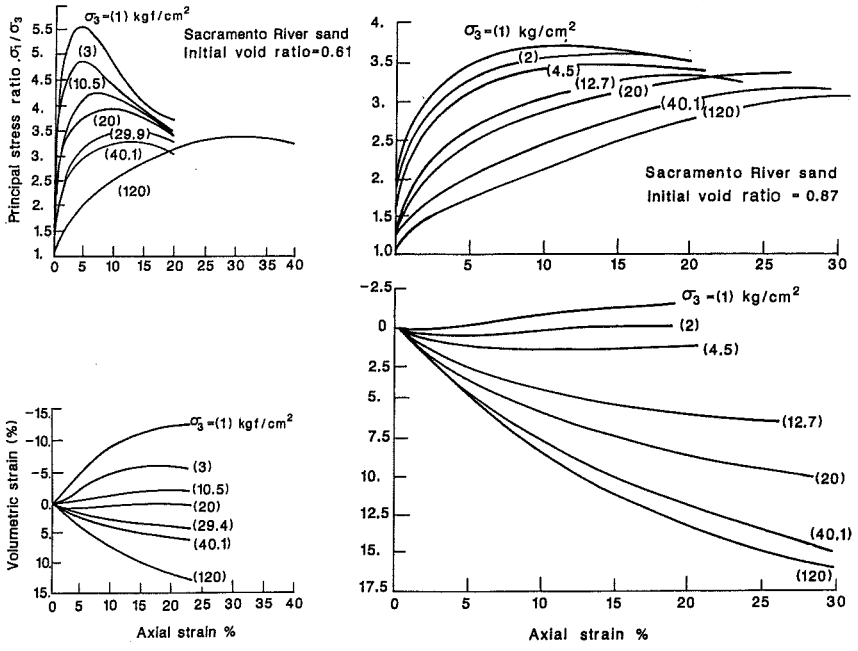

(a) Dense sand (b) Loose sand

Fig. 3.5. Effect of the confining pressure (σ_3) on the stress-strain-volume change curves (Lee and Seed, 1967).

occurs at failure. This void ratio is termed the *critical void ratio* (Lee and Seed, 1967).

Irrespective of the initial void ratio, a particular soil element may exhibit contractive or dilative behavior depending on the value of the confining pressure. For tests under confining pressures larger than the critical, the behavior is generally of the strain hardening type with compressive volumetric strains at failure, whereas for confining pressures below the critical value, the stress-strain curves show, in general, decreasing shear strength after the peak with volume expansion at failure. Therefore, the characterization of soil behavior as loose (contractive, strain hardening) or dense (dilative, strain softening) depends on the initial state of consolidation of the soil as well as the magnitude of the confining pressure.

The influence of the intermediate principal stress (σ_2) on the behavior of soils can be illustrated by Fig. 3.6, which shows the stress-strain curves of sand obtained by Cornforth (1964) from conventional triaxial compressive tests ($\sigma_2 = \sigma_3$ = cons-

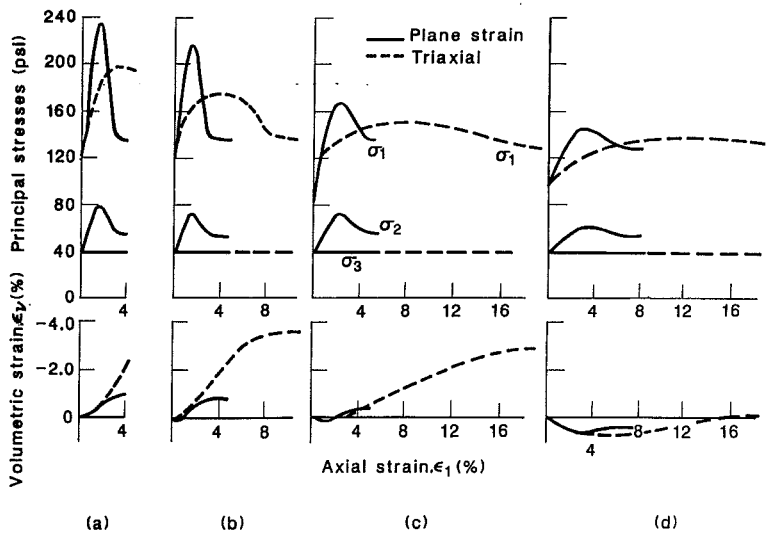

Fig. 3.6. Stress-strain curves in triaxial compression and plane strain tests for sand with different initial porosities (Cornforth, 1964). The relative density, D_r in (a) D_r = 80%, (b) D_r = 65%, (c) D_r = 40%, (d) D_r = 15%.

tant), and plane strain tests for which σ_2 is a variable. The results shown in this figure indicate that the stress-strain curves in the plane strain tests are stiffer than the corresponding curves in the triaxial compression test up to failure stresses. The peak failure values of σ_1 are higher in the plane strain tests for all values of initial relative density, D_r. However, the residual values of σ_1 seem to be approximately the same for both tests. Volumetric strains near failure in plane strain tests are less sensitive than those in the triaxial tests, particularly for loose samples (Fig. 3.6c and d).

One of the most important characteristics of the behavior of soils is the *stress-path dependency*. The stress-strain behaviors of a soil element in loading and unloading are entirely different. This has been demonstrated in Fig. 3.2 for the nonlinear behavior under hydrostatic compression. The same is certainly true under other stress paths, as can be seen, for example, from the results of a triaxial compression test on sand in Fig. 3.7.

The nonlinear deformations in soils are basically *inelastic*. Except at very low stress levels, only a small part of the strains is recovered upon unloading from any given stress state. The recoverable strains represent the *elastic* component of the total strains. These elastic strains are mainly due to the elastic deformations of the individual solid particles in a soil material element. The irrecoverable strains, on the

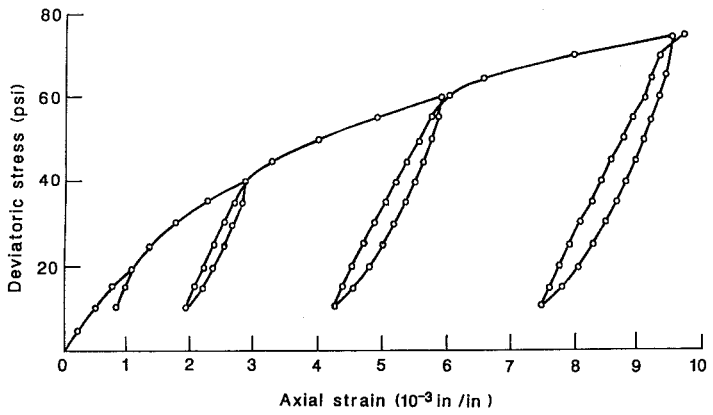

Fig. 3.7. Typical primary loading-unloading-reloading curves for air-dry Ottawa sand in triaxial compression test (Makhlouf and Stewart, 1965).

other hand, are called the *plastic* strains, and they are caused by the deformations resulting from sliding, rearrangement, and crushing of particles. These plastic deformations cause a change in the internal structure of the soil element.

Experimental work has indicated that, at very low stress levels, the strains produced by loading and reloading are mainly elastic. The plastic deformations due to particle slippage upon unloading from such low stress levels are very small; the unloading and reloading curves follow essentially the same linear paths with very small hysteresis loops. At high stress levels, hysteresis loops are observed upon unloading and reloading with almost constant slope of the hysteresis loops. However, with increasing stress levels, and particularly when failure states are approached, the hysteresis loops become wider. Large slip plastic strains are produced upon unloading from such high stress levels. The rebound curves become nonlinear and the slope of the hysteresis loops decreases.

3.4 Soil failure surfaces

Failure conditions and strength parameters are very important in the solution of stability problems in soil mechanics. As has been demonstrated previously, two values of the shear strength, the peak (maximum) and the residual (ultimate), are required in order to characterize the strain softening materials, such as overconsolidated clays and dense sands at low confining pressures. The term failure is used herein to define the limiting peak (or maximum) stress conditions. Therefore, only those parameters related to the peak (maximum) strength are relevant in the following discussion.

It should be emphasized, however, that in problems involving such soils as dense sands and overconsolidated clays, both peak and residual strength parameters are needed. In this case, the actual maximum shear stress mobilized at overall failure of a soil mass lies between the two limits of the peak and residual values (Bishop, 1972).

In the following, various strength characteristics are discussed with reference to the shape of the failure envelope in Mohr's diagrams and the trace of the cross section of the failure surface in the deviatoric plane. In the Mohr diagram the normal stress σ and the shearing stress τ are used as coordinates. The deviatoric plane is a plane perpendicular to the hydrostatic axis ($\sigma_1 = \sigma_2 = \sigma_3$) in the principal stress space whose coordinates are σ_1, σ_2, and σ_3.

From a plot of Mohr's circles corresponding to various failure stress states (in terms of effective principal stresses, $\sigma_1' \geq \sigma_2' \geq \sigma_3'$), the Mohr's failure envelope can be obtained as the common tangent curve to these circles, as shown in Fig. 3.8. In general, the failure envelopes are curved, particularly for dense soils, such as dense sand or overconsolidated clay. In many cases, if only a limited range of hydrostatic (confining) pressures is of interest, the failure envelope may be approximated by a straight line. In these cases, the familiar strength parameters, the *cohesion, c'*, and the *friction angle, ϕ'*, can be obtained as the intercept at the origin and the slope of the failure line, respectively. The primes here are used to emphasize that c' and ϕ' are *effective strength parameters.*

Figure 3.9 shows Mohr's failure envelope obtained from actual test results on sand and clay. The tests have been carried out over a wide range of confining pressures. At low effective confining pressures, the envelopes are curved, indicating a rapid decrease in the friction angle with increasing pressures. In the high stress range, the failure envelopes progressively flatten until a constant value of ϕ' is attained at very high pressures. This value of ϕ' at very high confining pressures is

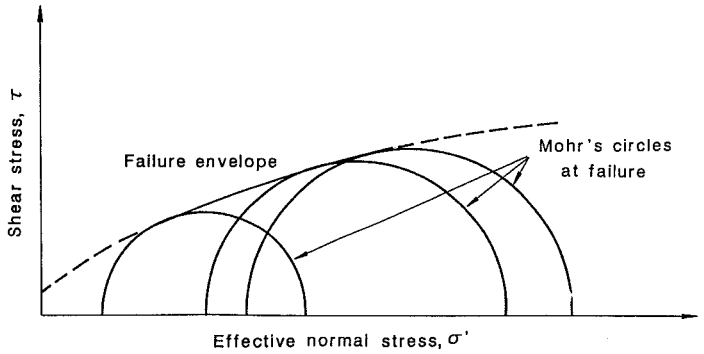

Fig. 3.8. Typical Mohr's failure envelope for soils.

the same for both dense or loose materials (Fig. 3.9a), which indicates that the effect of the initial state of compaction is eliminated at high pressures.

As can be seen from Fig. 3.9b, dense soil shows a marked increase in the measured values of ϕ' at low confining pressures. This is mainly caused by the effect of particle interlocking due to the increased tendency of dilatation in this range of low stresses. At higher confining pressure, the crushing of the particles becomes more significant and causes a decrease in dilatancy, which in turn results in a decrease in friction angle. However, at very high confining pressures, particles crushing and

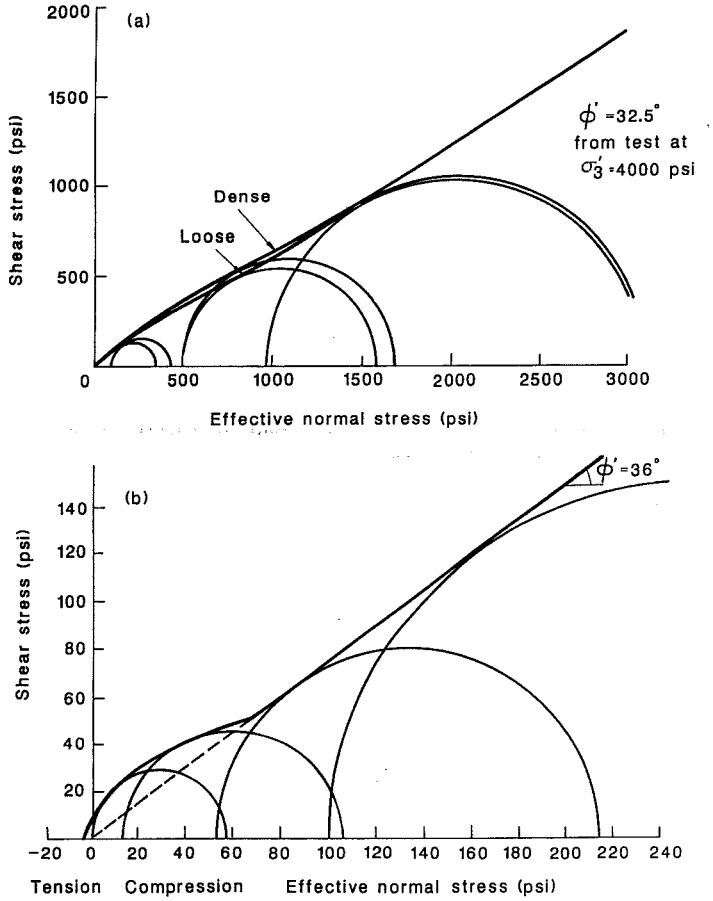

Fig. 3.9. Mohr's failure envelopes from drained triaxial tests on sand and clay (Bishop, 1972). (a) Ham River sand; (b) undisturbed Toulnustoue clay.

rearrangement require a considerable amount of energy, which causes an increase in the shear strength (i.e., increase in measured ϕ') until a constant value of ϕ' is ultimately reached. A schematic illustration of the various contributions (sliding, dilatancy, crushing, and rearrangement of particles) to the shear strength of cohesionless soils at different confining stresses is given in Fig. 3.10.

Curvature of the failure envelopes for soils has been observed by many in-

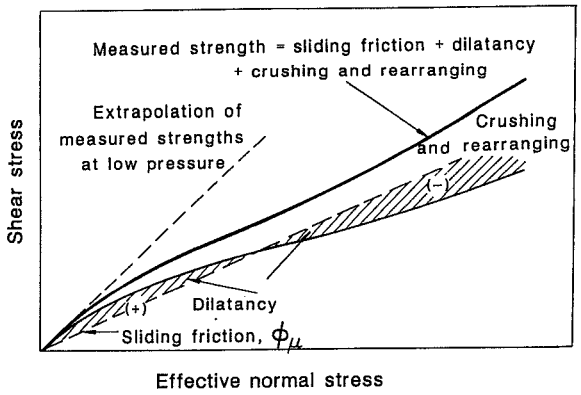

Fig. 3.10. Schematic illustration of contributions to strength of cohesionless soils (Lee and Seed, 1967).

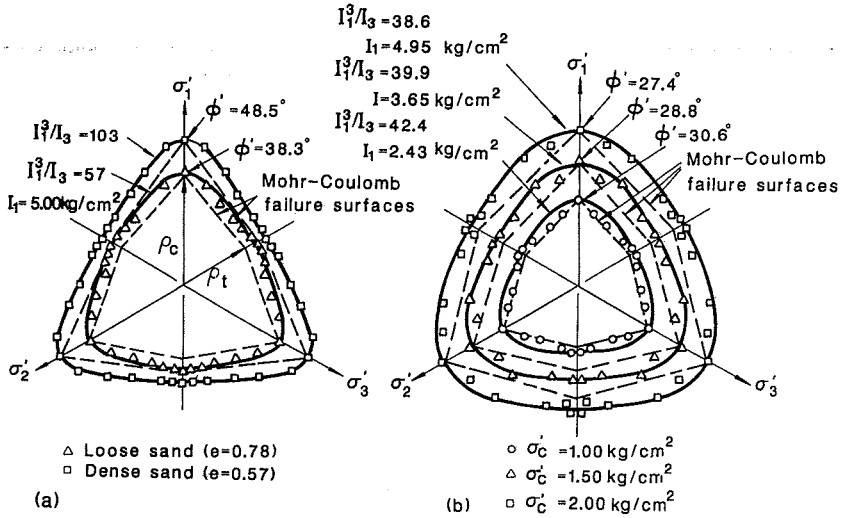

Fig. 3.11. General characteristics of the traces of the failure surface on the deviatoric planes (Lade and Musante, 1977). (a) Monterey No. 0 sand; (b) Grundite clay.

vestigators. It should be emphasized, however, that the stress ranges encountered in most civil engineering applications are not very high. In such cases, only the type of curvature observed at low and moderate pressure values is of interest. Furthermore, with only a limited range of pressures considered, a linear approximation of the failure envelope is often possible.

General characteristics of the traces of the failure surfaces for sand and clay are illustrated in Fig. 3.11. The experimental points have been obtained from triaxial compression and extension tests (drained tests for sand and consolidated-undrained tests for clay) with constant b values which is defined as the relative position of σ_2 with respect to σ_1 and σ_3 as:

$$b = \frac{\sigma_2 - \sigma_3}{\sigma_1 - \sigma_3} \tag{3.4}$$

From Fig. 3.11, two distinct failure surfaces for sand are obtained depending on the initial void ratio e of the sample. Dense samples exhibit larger shear strength, and consequently larger ϕ' value in triaxial compression, resulting in a larger size of the trace of failure surface in the deviatoric plane. For clay, the strength increases with increasing consolidation pressure, σ_c' (Fig. 3.11b).

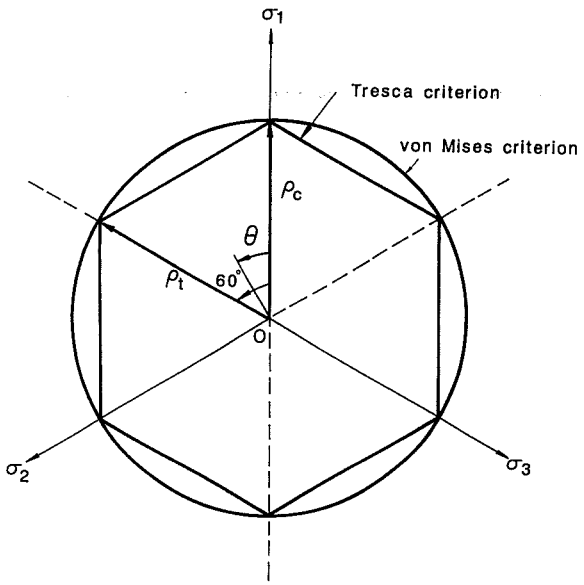

Fig. 3.12. Trace of the failure surface in the deviatoric plane for Tresca and von Mises criteria.

Based on the results shown in Fig. 3.11 and those of other experimental works, it can be concluded that the traces of the failure surface in the deviatoric planes are smooth, curved, noncircular and convex with $\varrho_c/\varrho_t > 1$, where indexes c and t correspond to the compressive ($\theta = 0°$) and the tensile ($\theta = 60°$) meridians, respectively, as shown in Fig. 3.12. The curvature of these traces clearly indicates the influence of the intermediate principal stress on the shearing strength of soils ($0 \leq b \leq 1$). In general, this influence is more pronounced at low and moderate values of confining pressures. But for high confining pressures the effect is almost negligible, as can be seen from Fig. 3.13, where the friction angles in both triaxial compression ($b = 0$) and plane strain ($0 < b < 1$) tests approach approximately the same value.

Within the limits of the available experimental data, it appears that failure surfaces for soils are independent of the loading path, except possibly for the effects of stress histories involving cyclic loading which cause strength increase due to densification of the soil.

Various aspects of the complicated stress-strain behavior and strength of real soils unders different loading and drainage conditions have been described above. To

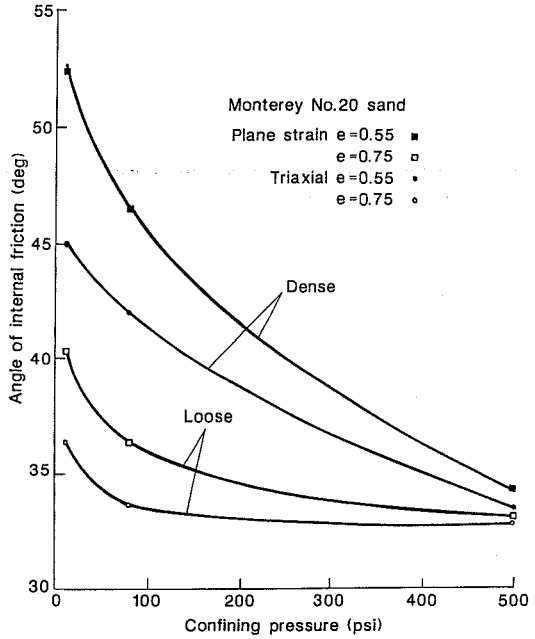

Fig. 3.13. Variations of friction angles in plane strain and triaxial compression with confining pressure (Marachi, 1969).

summarize, hydrostatic (confining) pressure sensitivity and effect of the intermediate principal stress are important factors in formulating the failure criteria for soils.

In the following, several failure criteria proposed for soils are described. Throughout this and the subsequent sections, unless otherwise stated, all stresses are effective stresses, σ'_{ij}, together with the associated strength parameters, c' and ϕ'. For convenience, the primes are not written.

3.4.1 Tresca criterion (one-parameter model)

This criterion was originally developed and used as a yielding condition for metals. According to this criterion, failure occurs when the maximum shear stress at a point reaches a critical value k. Mathematically, this criterion can be expressed as:

$$\tfrac{1}{2}\,|\sigma_1 - \sigma_3| = k \tag{3.5}$$

where k is a constant to be determined experimentally which respresents the failure (yield) stress in pure shear, and σ_1 and σ_3 are the major and minor principal stresses, respectively ($\sigma_1 \geq \sigma_2 \geq \sigma_3$). Equation (3.5) can be written in terms of the stress invariant J_2 and θ (Fig. 3.12) as follows ($0° \leq \theta \leq 60°$):

$$\tfrac{1}{2}\,(\sigma_1 - \sigma_3) = \tfrac{1}{3}\sqrt{3}\,\sqrt{J_2}\,[\cos\theta - \cos(\theta + \tfrac{2}{3}\pi)] = k \tag{3.6}$$

where

$$J_2 = \tfrac{1}{6}\,[(\sigma_1 - \sigma_2)^2 + (\sigma_2 - \sigma_3)^2 + (\sigma_3 - \sigma_1)^2] \tag{3.7a}$$

$$\cos 3\theta = \tfrac{3}{2}\sqrt{3}\,(J_3/J_2^{3/2}) \tag{3.7b}$$

$$J_3 = \tfrac{1}{27}\,(2\sigma_1 - \sigma_2 - \sigma_3)\,(2\sigma_2 - \sigma_3 - \sigma_1)\,(2\sigma_3 - \sigma_1 - \sigma_2) \tag{3.7c}$$

Expanding Eq. (3.6), we have:

$$f(J_2,\theta) = \sqrt{J_2}\,\sin(\theta + \tfrac{1}{3}\pi) - k = 0 \tag{3.8}$$

or identically in terms of the variables ϱ, θ (Fig. 3.12):

$$f(\varrho,\theta) = \varrho\,\sin(\theta + \tfrac{1}{3}\pi) - \sqrt{2}\,k = 0 \tag{3.9}$$

Since the effect of hydrostatic pressure on the failure surface is not considered in this criterion, Eqs. (3.8) and (3.9) are independent of the hydrostatic pressure. In the principal stress space, the Tresca failure criterion corresponds to a prism whose generator is parallel to the hydrostatic axis, and whose cross section in the deviatoric plane is a regular hexagon, as shown in Fig. 3.12.

Clearly, the Tresca criterion has many obvious shortcomings in connection with its application to soil materials. First, according to this criterion, shearing strength is independent of the hydrostatic (confining) pressure, which is certainly not true for soils in general. Second, the criterion predicts the same failure stresses in compression and tension. According to experimental evidence, soils are generally characterized by smaller tensile than compressive strength. In addition, the effect of the intermediate principal stress is not accounted for.

However, there are certain problems for which adequate results can be obtained using Tresca failure criterion, in particular, problems involving saturated soils under undrained conditions, when the analysis is performed in terms of the total stresses. The type of analysis in such cases is often referred to as $\phi = 0$ analysis. In agreement with the experimental observations, shearing strength of saturated soils during undrained loading is independent of the imposed hydrostatic (or mean) total stress component; and therefore the Tresca failure criterion may be utilized. In these cases, the constant k in Eqs. (3.5) to (3.9) represents the undrained shear strength, c_u ($\phi_u = 0$), which can be determined, for example, from the results of undrained triaxial tests.

3.4.2 von Mises criterion (one-parameter model)

This criterion states that failure takes place when the stress invariant J_2 (Eq. 3.7a) reaches a limiting value. Mathematically, this failure criterion can be expressed as:

$$f(J_2) = J_2 - k^2 = 0 \tag{3.10}$$

or

$$f(\varrho) = \varrho - \sqrt{2}\,k = 0 \tag{3.11}$$

In terms of the principal stresses σ_1, σ_2, and σ_3, these expressions reduce to:

$$(\sigma_1 - \sigma_2)^2 + (\sigma_2 - \sigma_3)^2 + (\sigma_3 - \sigma_1)^2 = 6k^2 \tag{3.12}$$

where k is the failure (or yield) stress in pure shear.

In the principal stress space, the von Mises failure surface represents a circular cylinder whose generator is parallel to the hydrostatic axis ($\sigma_1 = \sigma_2 = \sigma_3$). If both

von Mises and *Tresca criteria* are made to agree along the compressive and tensile meridians, ϱ_c ($\theta = 0°$) and ϱ_t ($\theta = 60°$), respectively, then the trace of the von Mises surface in the deviatoric plane is a circle circumscribing the Tresca hexagon (Fig. 3.12). In such cases, the maximum difference in the predicted failure stresses is along the simple shear meridian ($\theta = 30°$), where the ratio between the predicted failure shear stresses for the von Mises and Tresca criteria is $2/\sqrt{3} = 1.15$. On the other hand, if the two criteria are matched in simple shear (same k values), then the von Mises circle inscribes the Tresca hexagon, and the maximum deviation between the predictions of the two criteria will be along the compressive ($\theta = 0°$) and tensile ($\theta = 60°$) meridians.

When applied to soil materials, the von Mises failure criterion suffers from the same shortcomings mentioned previously for the Tresca criterion, namely, the same predicted strength in tension and compression and the independence of the hydrostatic pressure. Again, as for the Tresca criterion, undrained strength of saturated soils can be adequately approximated by the von Mises failure condition. In fact, the von Mises criterion is mathematically more convenient to use in most practical applications since the corners (singularities) on the hexagon of Tresca surface may cause mathematical difficulties and possible numerical complications.

3.4.3 Lade-Duncan criterion (one-parameter model)

Based on the experimental triaxial test results, Lade and Duncan (1975) have proposed a one-parameter failure criterion for cohesionless soils. This criterion accounts for many of the observed strength characteristics such as hydrostatic pressure sensitivity, effect of the intermediate principal stress, and noncircular trace on the deviatoric plane. However, the failure surface has straight failure envelopes in Mohr's diagram. Consequently, it can be applied to cases in which only a limited range of hydrostatic (confining) pressures is of interest, where the curvature of the failure envelope can be neglected. Further improvement of this failure criterion has been made by Lade (1977) by adding an additional degree of freedom to the model, taking into account the curvature of the failure envelope for cohesionless soils. This same failure model also has been applied to normally consolidated clays (Lade, 1979). In what follows a brief description of the one-parameter criterion is presented. The more refined two-parameter criterion is discussed in the next section.

The failure surface in the one parameter model is expressed in term of stress invariants I_1 and I_3, respectively, as follows:

$$f(I_1, I_3) = I_1^3 - k_1 I_3 = 0 \tag{3.13}$$

where k_1 is a constant that depends on the initial void ratio, and I_1 and I_3 are expressed in terms of the principal stresses as:

$$I_1 = \sigma_1 + \sigma_2 + \sigma_3 \tag{3.14}$$

$$I_3 = \sigma_1\sigma_2\sigma_3 \tag{3.15}$$

In the principal stress space, the shape of the failure surface defined by the equations above is conical, with the apex of the cone at the origin of the stress axes, as shown in the inset of Fig. 3.14. Also shown in this figure are the deviatoric cross sections of the failure surfaces corresponding to $k_1 = I_1^3/I_3 = 41.7$, 62.5, and 115.3 (i.e. corresponding to $\phi = 30°$, 40° and 50° in conventional triaxial compression). As can be seen, the deviatoric traces of this failure surface have the same

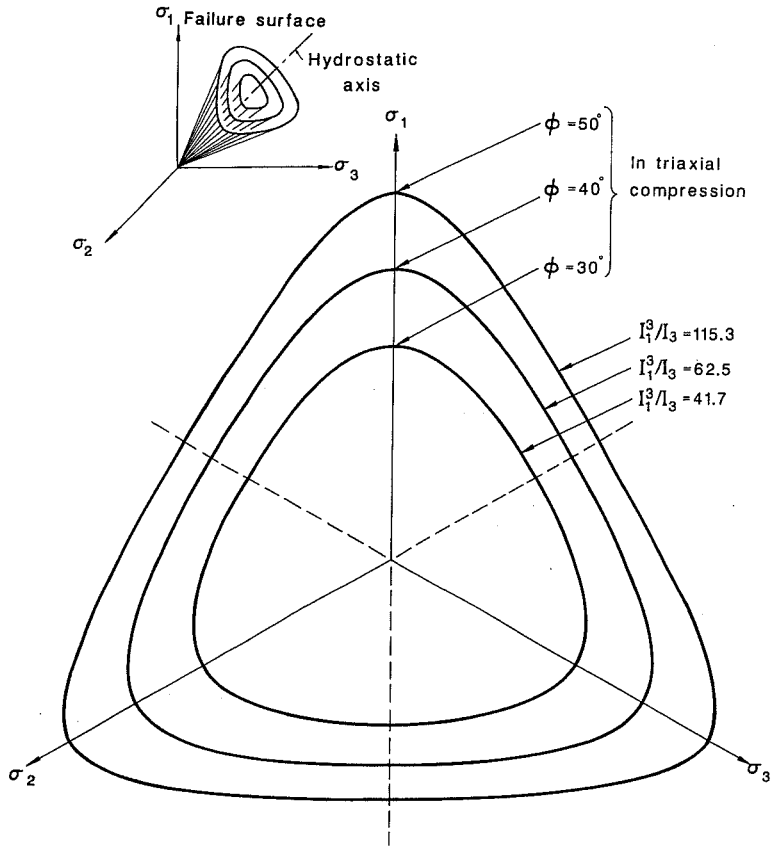

Fig. 3.14. General shape and deviatoric cross sections of the one-parameter failure model of Lade and Duncan (1975).

general shape as those determined experimentally (Fig. 3.11). For smaller values of k_1 the deviatoric traces are more circular, and they become increasingly triangular with increasing values of k_1.

It can be seen that the present failure criterion has only one parameter k_1, which can easily be determined from the results of conventional triaxial compression tests.

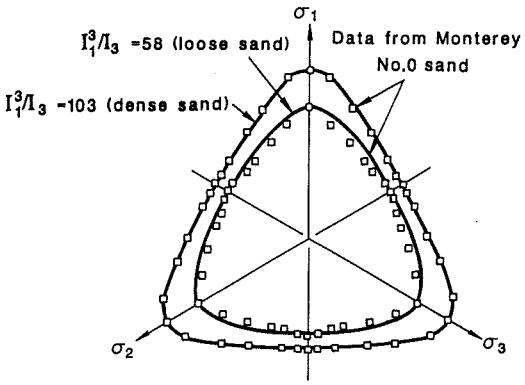

Fig. 3.15. Comparison of the experimental and calculated results of the failure traces on the deviatoric plane for Monterey No. 0 sand (Lade and Duncan, 1975).

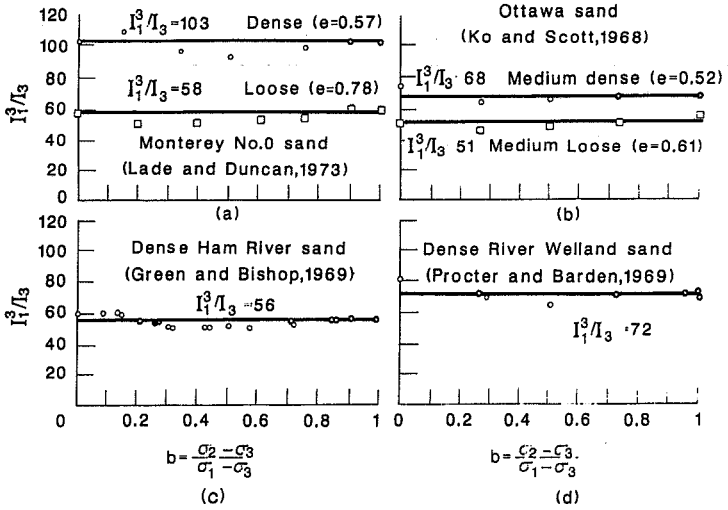

Fig. 3.16. Comparison of failure criterion results with experimental data from cubical triaxial tests on four different sands (Lade and Duncan, 1975).

Certainly, simple identification of the model parameter fom standard test data is of great advantage in practical applications. Besides, this failure criterion involves the stress invariant I_1 and I_3. Thus, it accounts for the effects of the hydrostatic pressure and the intermediate principal stress on the strength of the soil. The traces of the failure surface in the meridian plane (θ = constant) are straight. That is, the present model implies that Mohr's failure envelope is a straight line; the strength parameter ϕ is thus assumed to be constant and does not change with the confining pressure.

In Figs. 3.15 and 3.16, the experimental results for dense and loose Monterey No. 0 sand are compared to the results obtained using Eq. (3.13) with values of k_1 determined from triaxial compression tests. As may be seen, reasonably good agreement is obtained for both dense and loose sand, although there is some scatter. The failure criterion overestimates the strength of the loose sand at intermediate values of b, whereas, it expresses the strength of dense sand quite accurately for all values of b.

3.4.4 Mohr-Coulomb criterion (two-parameter model)

The criterion of Mohr (1900) states that failure is governed by the following relation:

$$|\tau| = f(\sigma) \tag{3.16}$$

where the limiting shearing stress, τ, in a plane depends only on the normal stress, σ, in the same plane at a certain point, and where Eq. (3.16) is the failure envelope for the corresponding Mohr's circles. The failure envelope $f(\sigma)$ is an experimentally determined function. According to Mohr's criterion, failure of the material occurs for all states of stress for which the largest of Mohr's circles is just tangent to the failure envelope. This means that the intermediate principal stress, σ_2 ($\sigma_1 \geq \sigma_2 \geq \sigma_3$), has no influence on the failure condition.

The simplest form of the Mohr failure envelope is the straight line such as that shown in Fig. 3.17b. The equation for the straight line envelope is given by Eq. (2.32), in which c and ϕ are known as the strength parameters of the material; c represents the *cohesion* and ϕ represents the *angle of internal friction*.

The failure criterion associated with Eq. (2.32) is referred to as the *Mohr-Coulomb criterion*. This criterion is currently the most widely used for soils in practical applications owing to its extreme simplicity and good accuracy.

In terms of the principal stresses ($\sigma_1 \geq \sigma_2 \geq \sigma_3$), the failure condition (2.32) is identical to:

$$\sigma_1 \frac{(1 - \sin\phi)}{2c\cos\phi} - \sigma_3 \frac{(1 + \sin\phi)}{2c\cos\phi} = 1 \qquad \text{for } c \neq 0 \tag{3.17}$$

In terms of the stress invariants I_1, J_2, and θ, Eq. (3.17) can be written in the following form:

$$f(I_1,J_2,\theta) = -\tfrac{1}{3} I_1 \sin\phi + \sqrt{J_2}\sin\left(\theta + \frac{\pi}{3}\right) - \frac{1}{\sqrt{3}}\sqrt{J_2}\cos\left(\theta + \frac{\pi}{3}\right)\sin\phi - c\cos\phi = 0 \qquad (3.18)$$

In the principal stress space, the Mohr-Coulomb criterion represents an irregular hexagonal pyramid, as shown in Fig. 3.17a. The traces of failure surface in the meridian planes are straight lines, and its deviatoric trace is an *irregular hexagon*. A family of deviatoric cross sections for different values of ϕ is shown in Fig. 3.18a. The compression and extension failure envelopes (compressive, $\theta = 0°$, and tensile, $\theta = 60°$, meridians) are illustrated in Fig. 3.18b.

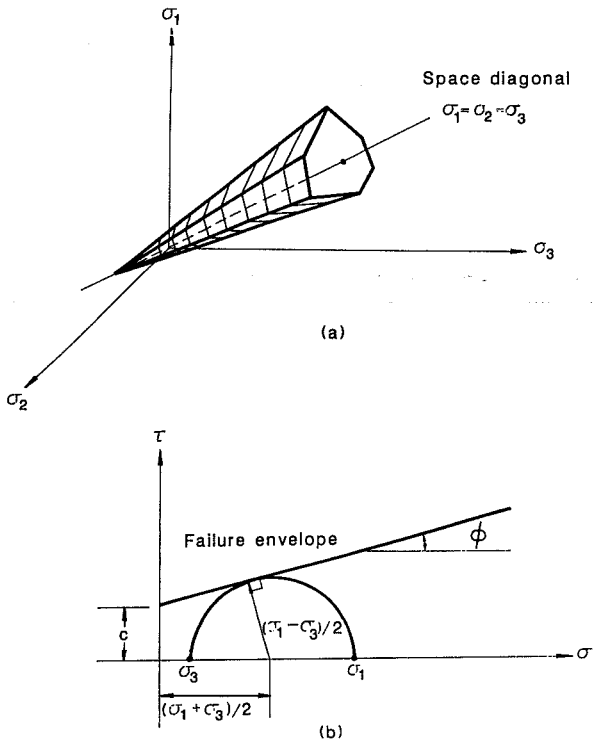

Fig. 3.17. Mohr-Coulomb criterion in principal stress space and Mohr's diagram. (a) Principal stress space, (b) Mohr's diagram.

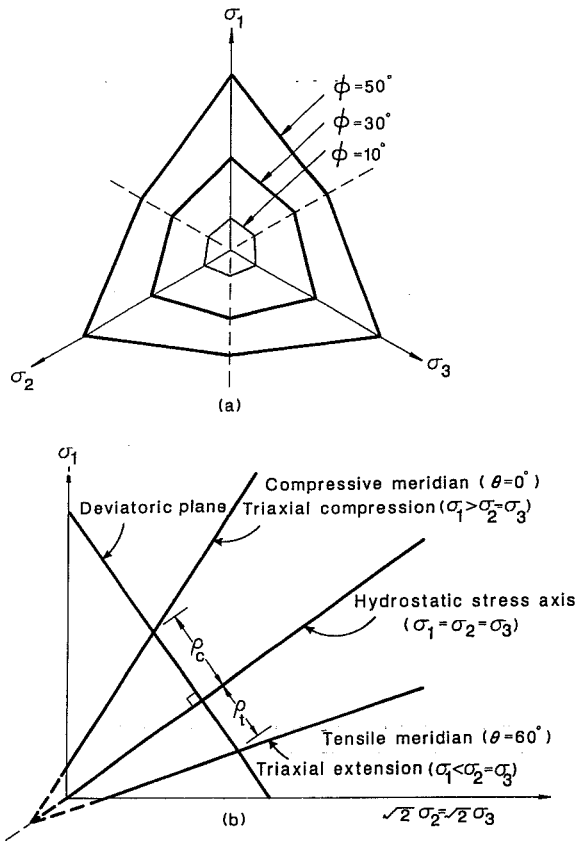

Fig. 3.18. Traces of Mohr-Coulomb failure surface in the deviatoric and triaxial planes. (a) Deviatoric plane, (b) triaxial plane.

In connection with its use for soils, the Mohr-Coulomb failure criterion has two main shortcomings. First, it assumes that the intermediate principal stress has no influence on failure, which is contrary to the experimental evidence (Figs. 3.6, 3.11, and 3.13). Second, the meridians and the failure envelope in the Mohr's diagram are straight lines, which implies that the strength parameter ϕ does not change with the confining (or hydrostatic) pressure. This approximation is reasonable only for a limited range of confining pressures; but it certainly becomes poorer as the range of pressures of interest becomes wider, as may be seen in Figs. 3.9 and 3.13. In addition, the failure surface has corners (or singularities) which are known to be difficult to handle in the numerical analysis.

However, this criterion is still one of the widely used failure models, mainly because it is simple and it yields reasonably accurate results for many practical problems in which only a limited range of confining pressures is encountered. This criterion has been successfully utilized in a considerable amount of numerical applications for a variety of geotechnical engineering problems.

3.4.5 Drucker-Prager criterion (two-parameter model)

Fundamentally, both the Tresca and von Mises failure criteria are in contrast with the experimental results for soils in the dependence upon the hydrostatic stress component (I_1). Therefore, attempts have been made to generalize these criteria by incorporating such hydrostatic pressure dependence for applications to soil media. For example, on the basis of the Tresca criterion, Drucker (1953) proposed an *extended Tresca criterion*, which is a two-parameter criterion and can be written as:

$$\max\left[\tfrac{1}{2}\,|\sigma_1-\sigma_2|,\ \tfrac{1}{2}\,|\sigma_2-\sigma_3|,\ \tfrac{1}{2}\,|\sigma_3-\sigma_1|\right] = k + \alpha I_1 \tag{3.19}$$

or, for $\sigma_1 \geq \sigma_2 \geq \sigma_3$ we have:

$$\tfrac{1}{2}\,(\sigma_1-\sigma_3) = k + \alpha I_1 \tag{3.20}$$

where k and α are material constants to be determined experimentally. In the principal stress space, the failure surface corresponding to the extended Tresca criterion is a right-hexagonal pyramid whose deviatoric cross section is a regular hexagon (Fig. 3.19). Here, as in the Mohr-Coulomb criterion, the extended Tresca failure surface has corners, and therefore it is not mathematically convenient for use in three-dimentional problems.

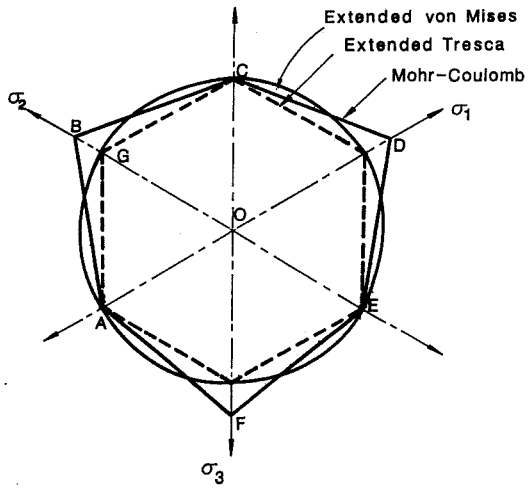

Fig. 3.19. Section of the yield surface by the π-plane ($\sigma_1 + \sigma_2 + \sigma_3 = 0$).

The second extended criterion, which was developed by Drucker and Prager (1952) as a simple modification of the von Mises model, is most frequently used in practical applications. This criterion is known as the *extended von Mises failure criterion*. In terms of the stress invariants I_1 and J_2, the extended von Mises criterion can be written as:

$$f(I_1,J_2) = \sqrt{J_2} - \alpha I_1 - k = 0 \tag{3.21}$$

where the two parameters α and k are material constants, which can be determined from test results.

The extended von Mises criterion failure surface in the principal stress space is shown in Fig. 3.20a. This surface is clearly a right circular cone with the space diagonal (hydrostatic stress axis, $\sigma_1 = \sigma_2 = \sigma_3$) as its axis. The traces of the failure surface on the meridian (θ = constant) and deviatoric planes are illustrated in Figs. 3.20b and 3.20c. The extended von Mises failure surface can be looked upon as a smooth Mohr-Coulomb surface or as an extension of the von Mises surface for hydrostatic pressure-dependent materials such as soils.

In view to its use for soil strength modeling, the main characteristics of the extended von Mises criterion can be summarized in the following: First, the failure criterion is simple. It has only two parameters k and α, which can be readily determined from conventional triaxial tests. Second, the failure surface is smooth and is therefore mathematically convenient to use in three-dimensional applications. Third, it accounts for the effect of the hydrostatic pressure on soil strength. However, since the traces of the failure surface on the meridian planes (θ = constant) are straight line, reasonable results are expected only for a limited range of hydrostatic pressure, when the curvature in the failure envelope may be neglected (Figs. 3.9 and 3.10). Fourth, since the failure criterion is independent of θ, the trace of the failure surface on the deviatoric plane is circular. This contradicts the experimental results shown in Fig. 3.11. Fifth, unlike the Mohr-Coulomb criterion, the influence of the intermediate principal stress is considered in the extended von Mises criterion. However, unless care is taken in selecting the material parameters α and k from test results, there is no guarantee that this influence will be correctly represented. For example, for soils with $c = 0$ and $\phi > 36.9°$ the extended von Mises and extended Tresca failure criteria may yield unrealistic results when they are matched to the Mohr-Coulomb criterion along the compression meridian ($\theta = 0°$) (Chen and Saleeb, 1982). For example, in this case, when the stress state approaches

$\theta = 60°$, the corresponding failure stress states will lie in the negative effective stress space, which is clearly impossible for a cohesionless soil.

There are several ways to approximate the Mohr-Coulomb hexagonal surface by the extended von Mises cone. If, for example, the two surfaces are made to agree along the compressive meridian ($\theta = 0°$) shown as point A in Fig. 3.21, the two sets of material constants (α, k and c, ϕ) are related by:

$$\alpha = \frac{2\sin\phi}{\sqrt{3}\,(3 - \sin\phi)}, \qquad k = \frac{6c\cos\phi}{\sqrt{3}\,(3 - \sin\phi)} \tag{3.22}$$

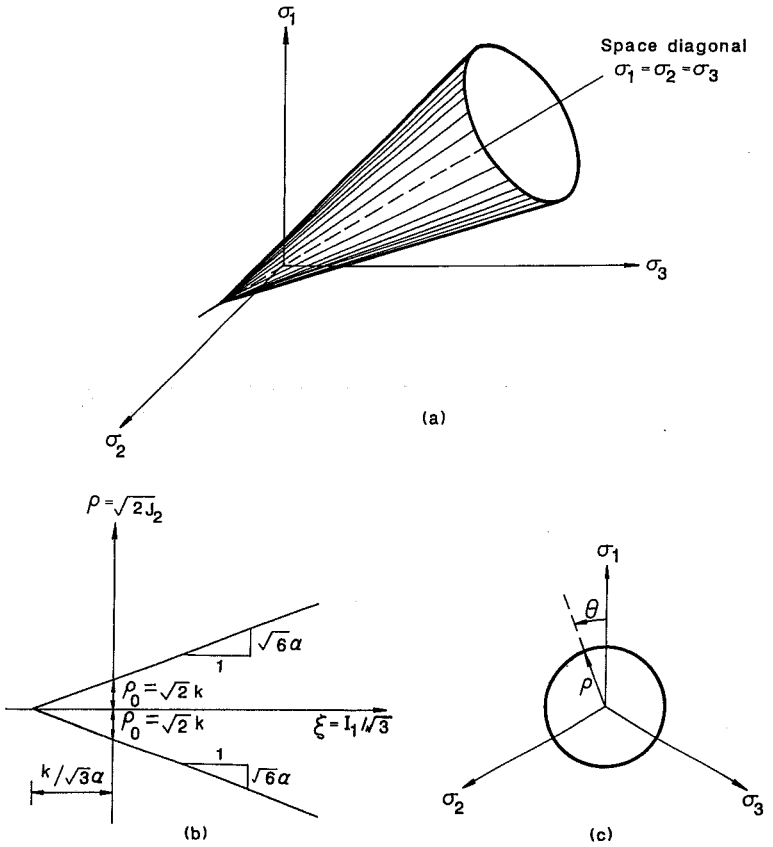

Fig. 3.20. Drucker-Prager failure criterion – Failure surface and traces on the meridian and deviatoric planes. (a) Principal stress space; (b) meridian plane (θ = constant); (c) deviatoric plane.

The cone corresponding to the constant in Eq. (3.22) circumscribes the hexagonal pyramid and represents an outer bound on the Mohr-Coulomb failure surface. On the other hand, the inner cone, which passes through the tensile meridian ($\theta = 60°$) shown as point B in Fig. 3.21 has the constants:

$$\alpha = \frac{2\sin\phi}{\sqrt{3}\,(3 + \sin\phi)}, \qquad k = \frac{6c\cos\phi}{\sqrt{3}\,(3 + \sin\phi)} \tag{3.23}$$

Many such approximations can be easily written but are not really necessary. However, if the extended von Mises and Mohr-Coulomb criteria are expected, for example, to give an identical limit load (Chen, 1975) for load-carrying capacity problems in the case of plane strain, then the following two conditions must be used to determine the constants α and k: (1) the condition of plane strain deformation; (2) the condition of the same rate of dissipation of mechanical energy per unit volume. Based on these conditions, α, k are determined as (Drucker and Prager, 1952):

$$\alpha = \frac{\tan\phi}{(9 + 12\tan^2\phi)^{\frac{1}{2}}}, \qquad k = \frac{3c}{(9 + 12\tan^2\phi)^{\frac{1}{2}}} \tag{3.24}$$

Using Eq. (3.24), it can be shown that the failure function Eq. (3.21) reduces to the Mohr-Coulomb criterion of Eq. (3.17).

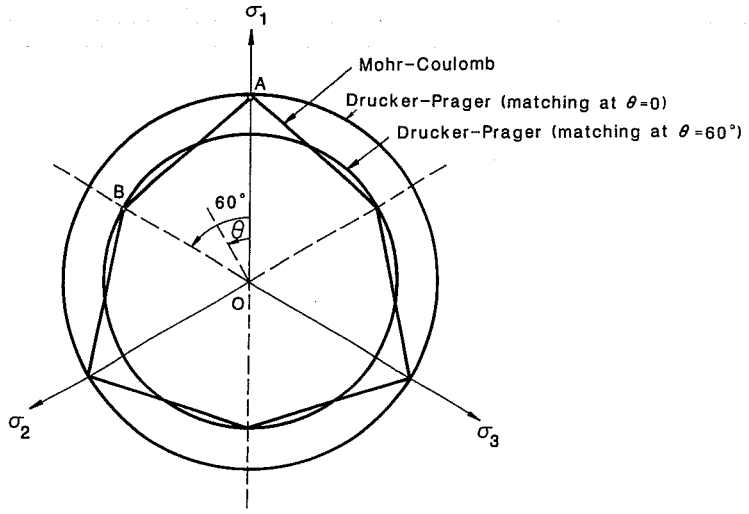

Fig. 3.21. Drucker-Prager and Mohr-Coulomb failure criteria with different matching conditions.

3.4.6 Lade criterion (two-parameter model)

As discussed earlier, experimental results have indicated that the failure envelopes of most soils are curved, particularly over a wide range of confining (or hydrostatic) pressures. The friction angle ϕ decreases with increasing confining pressure, as may be seen in Figs. 3.10, and 3.13. All the failure criteria described previously fail to include such characteristics. Recently Lade (1977) has extended the simple one-parameter model of Eq. (3.13) to take into account the curvature of the failure envelope. This extended failure criterion is expressed in terms of stress invariants, I_1 and I_3, as:

$$f(I_1,I_3) = (I_1^3/I_3 - 27)\,(I_1/p_a)^m - k = 0 \qquad (3.25)$$

where k and m are the two material constants of the model; and p_a is the atmospheric pressure expressed in the same units as I_1. For example, $p_a = 1.033$ kgf/cm^2 ($= 14.7$ psi $= 101.4$ kN/m^2), which is introduced for convenience so that the parameters k and m become dimensionless.

The value of k and m in Eq. (3.25) may easily be obtained from the results of triaxial compression tests, plotting $(I_1^3/I_3 - 27)$ versus (p_a/I_1) at failure in a log-log diagram as shown schematically in Fig. 3.22. On this diagram, k is the intercept with $(p_a/I_1) = 1$ and m is the slope of the straight line fitted to the experimental results.

In the principal stress space, the failure surface of Eq. (3.25) is shaped like an asymmetric bullet with the pointed apex at the origin of the stress space. The apex angle increases with increasing value of k. The deviatoric traces of the failure surface (Fig. 3.23a) have exactly the same shape as those of the one-parameter criterion of Eq. (3.13) (Fig. 3.14). The traces of the failure surface on planes containing the hydrostatic axis are curved (Fig. 3.23b and c), and their curvature increases with increasing m. For $m = 0$, the expression in Eq. (3.25) reduces to that of Eq. (3.13), and the failure surface becomes conical in shape, with straight meridians.

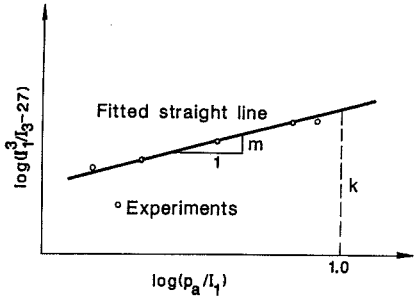

Fig. 3.22. Determination of parameters for Lade's two-parameter failure criterion.

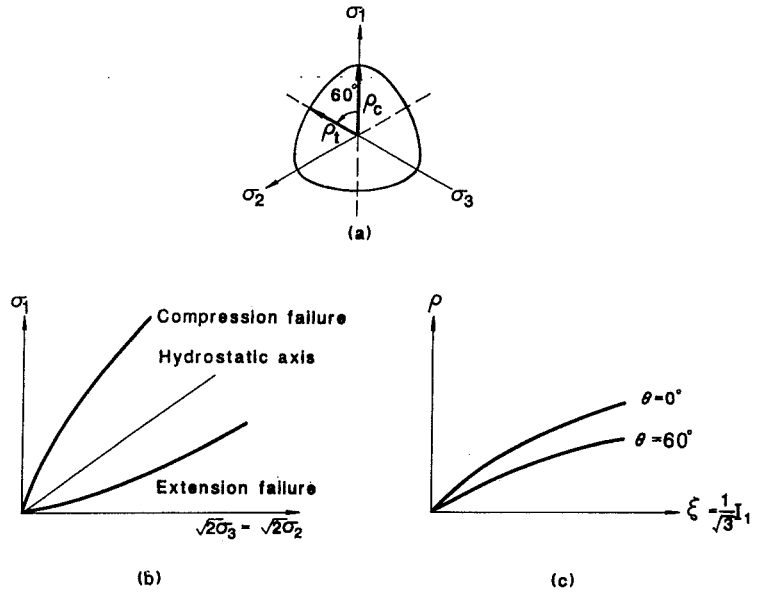

Fig. 3.23. Traces of the failure surface in the deviatoric, triaxial, and meridian planes for Lade's two-parameter failure model. (a) Deviatoric plane; (b) triaxial plane; (c) meridian planes.

The failure surface of Eq. (3.25) is always concave toward the hydrostatic axis (Figs. 3.23b and c). In a Mohr's diagram, this implies that the friction angle is always decreasing with increasing hydrostatic pressure, which has been experimentally verified for a wide range of hydrostatic stresses. However, at very high values of hydrostatic pressure (when crushing of soil grains becomes important), test results indicate that the failure envelopes open up and become straight (Figs. 3.9 and 3.10); that is, the failure surfaces become conical at very high hydrostatic pressures. Therefore, the present failure criterion is valid only in the range of hydrostatic stresses where the failure surface is concave toward the hydrostatic axis. This is the range of stresses that is frequently experienced in most practical applications, and in general this does not represent a serious limitation of the failure model.

The present model has been applied to predict failure stresses in cohesionless soils (Lade, 1977) and normally consolidated clays (Lade and Musante, 1977) under different stress conditions. Reasonably good agreement with experimental results has been obtained in all cases. This may be seen from the comparison of the test (points) and the calculated (solid curves) results in Fig. 3.11.

3.4.7 Summary of soil failure criteria

Based on the discussion presented in the present section for various failure criteria commonly used for soils, the following conclusions may be made:

1. In general, the simple one-parameter models of Tresca and von Mises cannot be applied to soils since they neglect the major effect of the hydrostatic stress component on the strength. They can be used only in problem involving saturated soils under undrained conditions when the analyses are performed in terms of total stresses.
2. For a limited range of hydrostatic pressure, the one-parameter model of Lade and Duncan is very efficient for cohesionless soils under general three-dimensional stress conditions. The model is simple and it captures many of the essential strength characteristics of soils such as the effect of the hydrostatic pressure, the influence of the intermediate principal stress, and the noncircular shape of the deviatoric trace of the failure surface.
3. Owing to its simplicity, the Mohr-Coulomb criterion is a fair approximation of soil strength in most practical applications. Its material parameters (c and ϕ) have well-defined physical interpretation, and they can easily be determined from standard test data. However, the failure surface has corners (singularities), and therefore it is not mathematically convenient to use, particularly for three-dimensional problems.
4. Because of its mathematical convenience, the Drucker-Prager criterion may be employed, as a smooth generalization of the Mohr-Coulomb failure surface, in three-dimensional analysis. However, it is extremely important to properly identify the conditions that are used to determine the material constant (α and k). For example, when the Drucker-Prager criterion is matched with the Mohr-Coulomb criterion along the compressive meridian ($\theta = 0$), the predicted failure stress states at or near the triaxial extension state ($\theta \rightarrow 60°$) will be much in error, particularly for dense soils (larger ϕ). Therefore, only those stress states simulating the field conditions for the particular problem at hand must be utilized in determining the material constants.
5. For problems involving a wide range of hydrostatic pressures, the two-parameter model of Lade, Eq. 3.25, provides a better approximation than the one-parameter criterion of Eq. 3.13, since it accounts for the curvature of the failure surface along the hydrostatic axis.

3.5 Validity of limit analysis in application to soils

3.5.1 Basic assumptions

The limit theorems on which the limit analysis method is based are established under the three basic assumptions:

1. The changes in geometry of a soil mass of concern at the instant of collapse are small and, thus, the virtual work equation is applicable.
2. The material is perfectly plastic and obeys, for the case of soils, the Mohr-Coulomb yield criterion.
3. The axes of principal plastic strain increments coincide with the principal stress axes during plastic flow and the resultant plastic strain increment vector is normal to the yield surface or the Mohr-Coulomb failure envelope.

This is known as the *associated flow rule* or the *normality condition* in plasticity.

As for Assumption (1), soil material is generally much more compressible than most materials, such as metals to which the theory of plasticity is positively applicable. A measurable amount of deformation is therefore expected to take place in a soil mass before the strength of the soil is fully mobilized at the instant of collapse. However, geotechnical engineering is dealing with structures of much larger scale than that in the field of metals, the small change in geometry assumption is generally acceptable for most problems in soil mechanics.

Assumptions (2) and (3) are interrelated. They are the center of controversy on the validity of the application of limit analysis method to soils based on the widely used Mohr-Coulomb yield criterion.

The Mohr-Coulomb yield criterion although having its weakness as described in the preceding section, is still widely accepted in the field of soil mechanics. The criterion has been shown by Bishop (1966) to predict the yield or failure of soils very well. Treating the Mohr-Coulomb envelope as a two-dimensional yield envelope is fully justified for most problems in soil mechanics. The parameters defining the envelope, c and ϕ, must, of course, be properly selected according to the special features of each particular problem.

The typical stress-strain curves for a normally consolidated soil (Soil I) and an overconsolidated soil (Soil II) upon shearing are shown in Fig. 3.24 as examples.

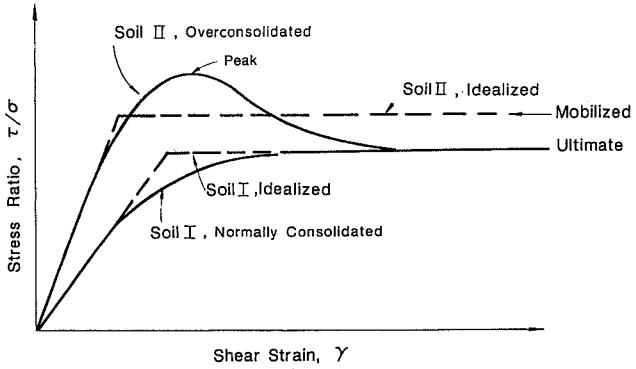

Fig. 3.24. Typical stress-strain curves and perfectly plastic idealizations.

The perfectly plastic idealizations for these materials are shown as dashed lines in the figure. Since during the stage of plastic flow, the plastic strain increment is not affected by the elastic behavior of the material, whether we assume that the material is elastic-perfectly plastic or rigid-perfectly plastic is not of great importance as long as the validity of Assumption (1) is preserved. Hence, for soil I (Fig. 3.24) which exhibits some work hardening, assuming its ultimate behavior as a perfectly plastic one is practically acceptable, if sufficient deformation is allowed for the ultimate state to develop without inducing significant changes in geometry. For soil II (Fig. 3.24) which shows a post-peak strain-softening behavior, the perfectly plastic representation of its ultimate behavior is reasonable only in an average sense, when the progressive failure effect in the whole soil mass is taken into consideration. For this reason, the conventional way of idealizing the ultimate behavior of a soil exhibiting softening behavior by a horizontal line passing through the peak of the actual stress-strain curve (taking $\phi = \phi_{peak}$) is not acceptable. The average mobilized stress level in a soil mass at the instant of collapse should be somewhere between the peak stress and the residual stress. When the progressive failure effect is taken into consideration in the selection of the average mobilized stress level, the perfectly plastic idealization is then acceptable for practical collapse load determination.

It has been experimentally observed that at stress levels close to failure stresses, the directions of the principal strain increments are in consistence with the principal stress axes (Roscoe et al., 1967). For a given stress state, the directions of the components of the plastic strain increments are therefore fixed in any corresponding stress space. Furthermore, based on the *Drucker's stability postulate,* the plastic work increment, dW, which is equal to the plastic strain increment, $d\epsilon_{ij}^p$, multiplied by the corresponding stress increment, $d\sigma_{ij}$, should always be larger than or equal to zero for a *stable material* which work hardens. That is:

$$dW = d\epsilon_{ij}^p \, d\sigma_{ij} \geq 0 \tag{3.26}$$

For a perfectly plastic material, the yield surface is fixed in the stress space and thus the plastic work increment must be equal to zero:

$$d\epsilon_{ij}^p \, d\sigma_{ij} = 0 \tag{3.27}$$

This indicates that $d\epsilon_{ij}^p$ must be perpendicular to the direction of $d\sigma_{ij}$, which is tangential to the yield function. Hence, the consequence of the observed coincidence of principal axes of stress and plastic strain increments near failure and the assumption that the material is perfectly plastic are that the plastic strain increment vector must be normal to the yield function or yield surface for a perfectly plastic material. For two-dimensional problems in soil mechanics, the plastic strain increment vector during plastic flow must therefore be normal to the Mohr-Coulomb failure

envelope, which is taken as the yield surface. The plastic strain increment vector is completely defined in its direction. This implies that the relative magnitude of its components in the corresponding stress space is determined by this normality condition.

3.5.2 Normality condition for 'undrained' purely cohesive soils

In many geotechnical problems, the rate of loading is very rapid in comparison to the permeability or the rate of drainage of a purely cohesive soil so that the cohesive soil behaves essentially in a constant volume and undrained state. The strength of the soil remains practically unchanged upon loading, since there is no possibility of increase in the mean effective stress without any drainage. A typical Mohr-Coulomb envelope for an undrained purely cohesive soil of plane strain problem on a two-dimensional mean effective principal stress, $p = (\sigma_1 + \sigma_3)/2$, versus maximum shear stress, $q = (\sigma_1 - \sigma_3)/2$, plot is shown in Fig. 3.25a. According to the normality condition, the plastic strain increment vector $d\epsilon_{ij}^p$ should be normal to the horizontal Mohr-Coulomb envelope corresponding to $\phi = 0$, if the plastic volumetric strain increment versus the maximum shear strain increment plot, or $dv^p = d\epsilon_1^p + d\epsilon_3^p$ vs. $d\gamma_m^p = d\epsilon_1^p - d\epsilon_3^p$ plot, is super-imposed on the corresponding p vs. q stress plot based on the coincidence of the principal axes. This is also shown in Fig. 3.25a. It is found that the vector $d\epsilon_{ij}^p$ is pointing in a direction parallel to the $d\gamma_m^p$-axis. This indicates that all the plastic strain increment is shear strain increment and there is no plastic volumetric strain increment induced during the plastic flow, which is a property of Tresca material. This is consistent with the actual strain observations. The application of limit analysis to an 'undrained' purely cohesive soil is therefore acceptable.

The power of limit analysis in application to clay stability problems is well demonstrated by an open cut example given by Henkel (1971). This has also been

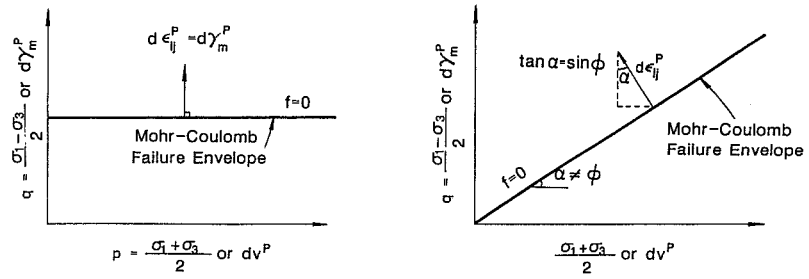

Fig. 3.25. Mohr-Coulomb failure envelopes and normality condition for soils.

described by Wroth (1977). The limit analysis method not only gives the coefficients of active earth pressure, K_A-value, which are very close to the actually observed values in all the sites investigated, but also gives a rational expression for assessing the m-value for the well-known Terzaghi and Peck's pressure distribution for strut load estimation in clays (Terzaghi and Peck, 1967).

3.5.3 Normality condition for cohesionless soils

To investigate the consequence of the normality condition for cohesionless soils, a plot corresponding to Fig. 3.25a is also constructed for this case as shown in Fig. 3.25b. By the normality condition, the relative magnitude of the two plastic strain increment components, $d\nu^p$ and $d\gamma_m^p$ can be expressed as:

$$\frac{d\nu^p}{d\gamma_m^p} = -\tan\alpha = -\sin\phi \tag{3.28}$$

where $d\nu^p = d\epsilon_1^p + d\epsilon_3^p$ and $d\gamma_m^p = d\epsilon_1^p - d\epsilon_3^p$. Noted that α is not equal to ϕ. From Eq. (3.17), we can see that if $c = 0$, $(\sigma_1 - \sigma_3)/(\sigma_1 + \sigma_3) = q/p = \sin\phi$, which is not equal to $\tan\phi$.

Defining the angle of dilatation (Bent Hansen, 1958) as $\nu = \sin^{-1}(-d\nu/d\gamma_m)$, then, during plastic flow, we have:

$$\frac{d\nu^p}{d\gamma_m^p} = -\sin\nu \tag{3.29}$$

Hence, the consequence of applying the normality condition to a cohesionless soil with its angle of internal friction equal to ϕ will be a necessary occurrence of a volume expansion with $\nu = \phi$ during the plastic flow. However, soils are found experimentally to dilate at increments considerably less than those predicted by the normality condition, i.e., $\nu < \phi$. Hence, cohesionless soils must be considered as a non-associated flow rule material with $\nu < \phi$, which is different from the associated flow rule material that obeys the normality condition with $\nu = \phi$. Idealizing a real cohesionless soil to an associated flow rule material is sure to affect the deformation characteristics considerably, and is unrealistic when deformations are of great concern. The normality assumption is therefore the center of dispute on the validity of limit analysis in application to cohesionless soils (Chen and Chang, 1981).

Nevertheless, before discarding an idealized approach based on certain assumptions which do not follow exactly the behavior of the material of concern, it may

be worthwhile to look further on how significant the 'unrealistic' assumption will affect the validity of the approach for solving certain practical problems. It is known that not all the factors presented in a problem predominantly control all types of behavior of concern to us. Firstly, quite often the errors resulting from this idealization on some aspects may be unimportant when compared with those introduced by the variation in soil properties in nature or the inaccuracy of soil parameters induced by experimental limitations. Secondly, as pointed out by Davis (1968), the deformation condition of some problems may not be sufficiently restrictive for the material deformation properties, such as the angle of dilation ν, to affect the collapse load seriously all the time. These two points at least give us some indications here that limit analysis method, as in limit equilibrium method, can be a useful tool for certain stability problems in cohesionless soils, even though the normality condition is not actually observed in the soil. Further discussion on this from stress-dilatancy and energy considerations will be given in the following section.

3.6 Friction-dilatation and related energy in cohesionless soils

3.6.1 Friction and dilatation

Most cohesionless soils can be considered as frictional-dilating materials in general. The shearing resistance of a cohesionless soil is contributed by two actions: (1) the frictional action, which is controlled by the mineral and surface characteristics of soil particles; and (2) the dilating action, which is dependent on the particle packing conditions. The frictional action dissipates external energy by generating heat through relative particle sliding and rolling. The dilating action changes external work into potential energy through the adjustment of relative positions of particles. Hence, the coefficient of internal friction of a cohesionless soil, $\tan\phi$, or the stress ratio on the failure plane, τ_{ff}/σ_{ff}, can be assumed to be composed of two parts, corresponding to the two different forms of energy response. A typical representation of the physical components of the strength of a cohesionless soil for the direct shear condition is given by Bishop (1950) as:

$$\tan\phi = \tan\phi_f + \left(\frac{\partial v}{\partial s}\right)_f \tag{3.30}$$

where $\tan\phi_f$ represents the component contributed by interparticle friction and $(\partial v/\partial s)_f = \tan\nu$, which is the ratio of change in a soil specimen's thickness to increment of horizontal displacement at failure in a direct shear test, represents the component contributed by particle interlocking. A similar expression for plane strain or triaxial compression conditions can be derived from *Rowe's dilatancy equation* (Rowe, 1962) as:

$$\sin\phi = \frac{\sin\phi_f}{1 + \sin\phi_f \sin\nu} + \frac{\sin\nu}{1 + \sin\phi_f \sin\nu} \tag{3.31}$$

where ϕ_f represents the frictional component of ϕ, which is bounded by the intrinsic mineral-to-mineral friction angle, ϕ_μ, and the critical state friction angle, ϕ_{cv}, and ν is the angle of dilatation which is defined by Bent Hansen as mentioned earlier.

It is interesting to note from the two similar expressions, Eqs. (3.30) and (3.31), that if the strength of a soil is contributed predominantly by friction so that $\phi = \phi_f$, then there is practically no volume change, since $(\partial v/\partial s)_f = \tan\nu = 0$ from the expressions. On the contrary, if a soil is assumed to be a purely dilating or perfectly plastic material with zero friction ($\phi_f = 0$), then the shearing process should always be accompanied by a volume expansion, $(\partial v/\partial s)_f > 0$, and $\phi = \nu$ is the direct consequence of this assumption.

3.6.2 Energy considerations

While a purely frictional or purely dilating material as assumed in limit analysis seldom exists in reality, most cohesionless soils can be considered as partially frictional and partially dilating materials with their relative degree depending on the mineral types, the surface properties, and the packings of the constitutive particles. Once a loading is applied to a cohesionless soil mass, the external work will be dissipated essentially by heat through particle-to-particle sliding and rolling, and by the change in potential energy through sliding, rolling and volume expansion. This can be clearly seen from the virtual work equation proposed by Davis (1968) for a non-associated flow rule material with $c = 0$:

$$W_{ext} = \Sigma \int W_D \mathrm{d}l + \int\int D\mathrm{d}x\mathrm{d}z - \int\int E_\gamma \mathrm{d}x\mathrm{d}z \tag{3.32}$$

where W_{ext} is the net rate of external work contributed by the external loads, including that due to the movement along the loading boundary or soil–structure interface. The first term on the right-hand side of Eq. (3.32), $\Sigma \int W_D \mathrm{d}l = W_f$, represents the rate of energy dissipation along the discontinuities. It results from the existence of the friction action. The second term, $\int\int D\mathrm{d}x\mathrm{d}z = W_s$ represents the rate of plastic work due to volume distortion in the plastically deformed regions, which is also induced by friction. The last term, $\int\int E_\gamma \mathrm{d}x\mathrm{d}z = W_\gamma$ represents the rate of change in potential energy due to the tendency of the body forces to resist sliding and the existence of volume expansion contributed by the dilating component. In W_f, the expression of W_D for the case of $c = 0$, i.e., the cohesionless soil is given as:

$$W_D = \frac{\sigma_k \Delta u}{1 - \sin\phi \sin\nu} \sec\nu \, (\sin\phi - \sin\nu) \tag{3.33}$$

in which Δu is the tangential velocity of plastic flow along velocity discontinuities and σ_k is the normal stress acting on the discontinuities. In W_s, the expression for D is given as:

$$D = (\Delta\epsilon_1 - \Delta\epsilon_3) p (\sin\phi - \sin\nu) \tag{3.34}$$

where $\Delta\epsilon_1$ and $\Delta\epsilon_3$ are the principal plastic strain increments and p is the mean normal stress in the plastically deformed region.

From Eqs. (3.33) and (3.34), it is obvious that if the material is an associated flow rule material with $\nu = \phi$, then both W_D and D vanish and $W_f = W_s = 0$ if the interface dissipation or work is included in W_{ext}. This can also be seen physically. If a material is purely plastic there is no friction ($\tan\phi_f = 0$), and consequently no surface traction to cause the soil mass to distortion. The energy dissipation by sliding or rolling (W_D) and by volume distortion (D) should therefore be equal to

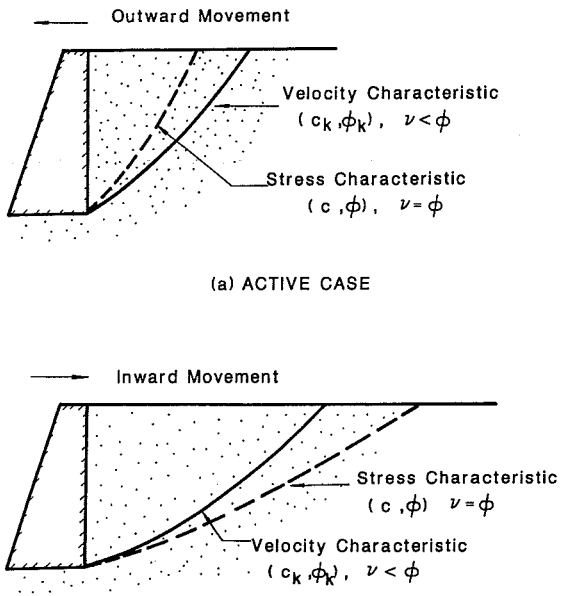

Fig. 3.26. Non-coincidence of stress and velocity characteristics in retaining wall problems.

zero if the material is cohesionless. The consequence of this is that the problem is greatly simplified, since the values of σ_k and p, which are generally unknown, become irrelevant to the problem. If the interface dissipation or work is included in W_{ext}, then the equation is reduced to:

$$[W_{ext}]_\phi = -[W_\gamma]_\phi \tag{3.35}$$

However, it is believed that failure surfaces in a soil mass with $\nu < \phi$ should follow the velocity characteristics rather than the stress characteristics (Davis, 1968). The stress characteristics are the same as the velocity characteristics only when the soil is purely plastic. The introduction of friction in a real soil not only changes the term W_f and adds the term W_s in the internal energy of the virtual work equation, but also shifts the discontinuities (Figs. 3.26a and 3.26b). Consequently, the term W_γ is also different from that when $\nu = \phi$. The virtual work equation for the case of $\nu < \phi$ can be restated as:

$$[W_{ext}]_\nu = [W_f]_\nu + [W_s]_\nu - [W_\gamma]_\nu \tag{3.36}$$

The possible difference in $[W_{ext}]_\phi$ and $[W_{ext}]_\nu$, which will result in the difference in the corresponding collapse loads, p_c^ϕ and p_c^ν, can be expressed as:

$$[W_{ext}]_\nu - [W_{ext}]_\phi = ([W_f]_\nu + [W_s]_\nu) - ([W_\gamma]_\nu - [W_\gamma]_\phi) \tag{3.37}$$

or

$$\Delta W_{ext} = \Delta W_{in} - \Delta W_\gamma \tag{3.38}$$

where ΔW_{ext} represents the difference in external works for the real material and for the idealized material. The term ΔW_{in} represents the difference in the energy dissipation, while ΔW_γ is the difference in potential energy. Both ΔW_{in} and ΔW_γ are non-zero terms and both are the direct or indirect consequence of the existence of friction in the shearing action of the real cohesionless soil. Hence if friction vanishes, both ΔW_{in} and ΔW_γ are zero and the collapse load obtained will be unique. However, with finite friction in real soils, its effect on ΔW_{in} and ΔW_γ, although reflected in different forms, one through sliding and volume distortion, the other through change in potential of body forces, can be of the same order since they are the two and the only two forms of energy in response to external work. Hence, there is a good possibility that the collapse loads determined by both models may be practically the same. It can be a convincing argument if we can further prove that the way of proportionating the frictional and the dilating components in tan ϕ, which is believed to be of great importance in a deformational analysis, is essentially irrelevant to the collapse load analysis in soil stability problems.

3.6.3 A descriptive example of a c-ϕ soil following non-associated flow rule

Let us examine a simple vertical cut in a c-ϕ soil. A planar failure mechanism as shown in Fig. 3.27 is assumed. Since real soils are non-associated flow rule materials, the strength parameters along the failure surfaces or velocity discontinuities, c_k and ϕ_k, are different from the Mohr-Coulomb strength parameter c, ϕ existed on the stress characteristics. The relations between, c_k, ϕ_k, and c, ϕ were given by Davis (1968) as:

$$c_k = \frac{c \cos\phi \cos\nu}{1 - \sin\phi \sin\nu} \tag{3.39a}$$

$$\tan\phi_k = \frac{\sin\phi \cos\nu}{1 - \sin\phi \sin\nu} \tag{3.39b}$$

They are the same as the Mohr-Coulomb c and ϕ only when $\nu = \phi$, i.e. when the material is a perfectly plastic, associated flow rule material. For purely frictional materials, $\nu = 0$, and $c_k = c\cos\phi$, $\tan\phi_k = \sin\phi$.

For energy evaluation, the frictional and dilating components of the overall frictional angle along the velocity discontinuities should be separated. As pointed out by Davis (1968), the velocity discontinuity corresponds to the observed failure plane in the direct shear condition. Equation (3.30) as proposed by Bishop (1950) provides a way of separating these two physical components for the direct shear case with $\tan\phi_f$ representing the frictional component and $(\partial v/\partial s)_f = \tan\nu$ representing the dilating component. Substituting Eq. (3.39b) into Eq. (3.30), we obtain:

$$\tan\phi_f = \frac{\sin\phi - \sin\nu}{(1 - \sin\phi \sin\nu)\cos\nu} \tag{3.40}$$

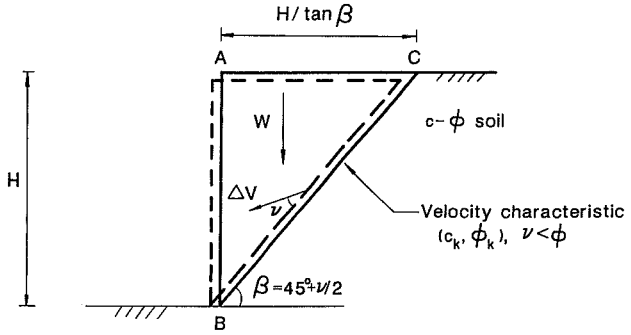

Fig. 3.27. A vertical cut in cohesive-frictional soils.

Consider a vertical cut with the translational outward movement as shown in Fig. 3.27. By the theory of perfect plasticity, the rigid block ABC will slide down with a velocity, ΔV, making an angle of ν with the discontinuity line BC. If the most critical failure plane with $\beta = 45° + \nu/2$ is investigated directly, then the work done by the weight of the soil wedge ABC or the change in potential energy is:

$$W_\gamma = W\Delta V \sin(\beta - \nu) = \tfrac{1}{2}\gamma H^2 \Delta V \tan(45° - \tfrac{1}{2}\nu) \sin(45° - \tfrac{1}{2}\nu) \qquad (3.41)$$

By frictional theory, the total internal energy dissipation along the discontinuity line BC is:

$$\begin{aligned} W_{in} &= W \cos\beta \tan\phi_f \Delta V \cos\nu + c_k \Delta V \cos\nu H \csc\beta \\ &= \tfrac{1}{2}\gamma H^2 \Delta V \tan(45° - \tfrac{1}{2}\nu) \sin(45° - \tfrac{1}{2}\nu) \cos\nu \tan\phi_f \\ &\quad + c_k H \Delta V \cos\nu / \cos(45° - \tfrac{1}{2}\nu) \end{aligned} \qquad (3.42)$$

Substituting c_k from Eq. (3.39a) and $\tan\phi_f$ from Eq. (3.40) into W_{in} and equating W_γ to W_{in}, we obtain the critical height or the real non-associated flow rule material by the principle of virtual work, as:

$$H_c = (4c/\gamma) \tan(45° + \tfrac{1}{2}\nu) \left[\frac{\cos\nu \cos\phi}{1 - \sin\phi + \sin\nu - \sin\phi \sin\nu} \right] \qquad (3.43)$$

Further arrangement reduces Eq. (3.43) to:

$$H_c = (4c/\gamma) \tan(45° + \tfrac{1}{2}\phi) \qquad (3.44)$$

which is independent of ν.

The fact that H_c so derived without making any idealization of the soil is independent of ν is of particular importance. It indicates that at least for this particular vertical cut stability problem for which there are no boundary restrictions and the failure mechanism involves essentially a rigid-to-rigid body sliding, the deformation property, ν, does not affect the collapse load determination. More importantly, it indicates that whether we assume the material to be purely dilating ($\nu = \phi$), or purely frictional ($\nu = 0$), or partially frictional and partially dilating ($\nu < \phi$) as that shown in Fig. 3.28 is immaterial to the collapse load evaluation, at least for this particular case, in which it involves essentially a rigid block sliding. This confirms our hypothesis that the way of proportionating the physical component in tan ϕ is irrelevant to the collapse load analysis and ΔW_{in} and ΔW_γ in Eq. 3.38 can be of the same order of magnitude, so that the collapse load is unaffected

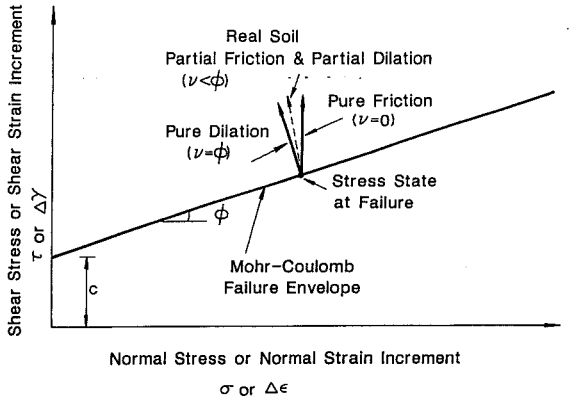

Fig. 3.28. Pure friction and pure dilation idealizations and flow rule for a real soil.

by the idealization. For those soil stability problems in which the boundaries are not very restrictive, the applicability of limit analysis to soil medium is therefore expected to be satisfactory as also pointed out by Davis (1968).

3.7 Effect of friction on the applicability of limit analysis to soils

While the power of limit analysis in application to purely cohesive soils under undrained conditions has been well recognized, its applicability to soils possessing ϕ is still a matter of dispute. This is mainly because the normality condition as assumed in the analysis is not experimentally observed. The energy consideration as discussed in the preceding section, however, shows that the application of limit analysis to stability problems in frictional-dilating soils is quite optimistic, although the excessive volume expansion as predicted by the perfect plasticity idealization as used in limit analysis is unrealistic. This argument can be further justified by investigating how the introduction of $\phi \neq 0$ affects the accuracy of collapse load as obtained by the limit analysis based on the perfect plasticity idealization. An existing example reported by Chen, Giger, and Fang (1969) is investigated for this purpose.

In Chen, Giger and Fang's paper, the slope stability of a homogeneous c-ϕ soil is analyzed by limit analysis using logarithmic spiral failure mechanism. For the special case of a vertical cut, they obtained the N_s-values for soils possessing different ϕ-angles as shown in Table 3-1, with N_s representing the so-called *stability factor*. The critical height, in terms of this dimensionless factor N_s, can be expressed as:

$$H_c = N_s \, c/\gamma \qquad (3.45a)$$

or

$$N_s = \gamma H_c / c \tag{3.45b}$$

where c is the Mohr-Coulomb cohesion and γ is the unit weight of soil. The N_s-values obtained by the ϕ-circle method of Taylor (1937) are also given for ϕ-values up to 25°. Analysis of Taylor's N_s-values shows that the N_s-value is generally expressed as:

$$N_s = 3.83 \tan(45° + \tfrac{1}{2}\phi) \tag{3.46a}$$

Hence, to eliminate the direct influence of ϕ, the N_s-values obtained by the limit analysis are normalized to give:

$$N_s^* = \frac{N_s}{\tan(45° + \tfrac{1}{2}\phi)} = \frac{\gamma H_c}{c \tan(45° + \tfrac{1}{2}\phi)} \tag{3.46b}$$

The values of N_s^* are shown under N_s in Table 3-1. If the logarithmic spiral mechanism assumed is close to the reality, the N_s^*-value for the case of $\phi = 0$, $N_{so}^* = 3.83$, can be considered as a 'close-to-exact' solution. Hence the error involved in the limit analysis as the results of the perfect plasticity idealization and the introduction of ϕ can be evaluated by calculating the values of $(N_s^* - N_{so}^*)/N_{so}^*$ corresponding to each soil with different ϕ-values. The results are as shown in Table 3-1.

It is found from Table 3-1 that the error induced by the perfect plasticity idealization is less than 1% for most $c - \phi$ soils of which the ϕ-value is seldom larger than 30°. Therefore, the introduction of ϕ has essentially no effect on the applicability

TABLE 3-1
Effect of introducing ϕ on limit analysis of the stability of vertical cuts in cohesive-frictional soils

N_s or N_s^*	ϕ								
	0°	5°	10°	15°	20°	25°	30°	35°	40°
By ϕ-circle method	3.83	4.18	4.59	5.03	5.50	6.02	–	–	–
By limit analysis method	3.83	4.19	4.59	5.02	5.51	6.06	6.69	7.43	8.30
$N_s^* = \frac{N_s}{\tan\left(45° + \frac{\phi}{2}\right)}$	3.830	3.839	3.851	3.852	3.858	3.861	3.863	3.868	3.870
$\frac{N_s^* - N_{so}^*}{N_{so}^*}$, % +	0	0.24	0.55	0.57	0.73	0.81	0.86	0.99	1.04

+ N_{so}^* is the N_s-value corresponding to $\phi = 0$ case and has an 'exact' value of 3.83.

of limit analysis method to soils possessing ϕ at least for this particular problem. This further confirms the statement made by Davis (1968) that the upper-bound solution obtained by the limit analysis method may be close to exact if the boundary conditions are not so restrictive as to affect the collapse load seriously.

3.8 Some aspects of retaining wall problems and the associated phenomena at failure

It has been found that the application of limit analysis to soil stability problems with little or no boundary deformation restriction is practically acceptable. The use of it for solving retaining wall problems, however, faces another challenge due to the particular features presented in this kind of problems. The determination of the lateral earth pressure of a fill on a retaining wall, when frictional forces act on the back of the wall, can also be solved conveniently by the limit analysis method.

Before we attempt to find the pressure in the rear face of a retaining wall, we note that the lateral earth pressure problem can be divided into the *active earth pressure* and the *passive earth pressure* as illustrated in Fig. 3.29a, which shows a particular apparatus consisting of a large bin with a movable end section. By filling the bin

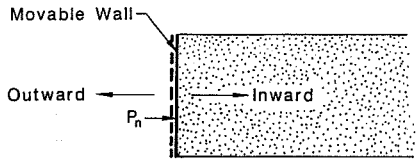

(a) Vertical Section Through Bin

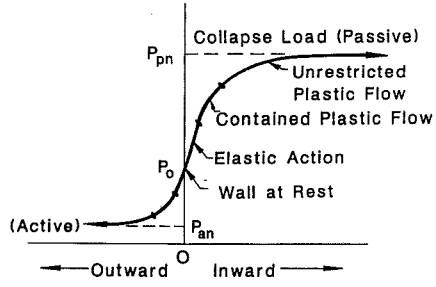

(b) Load Displacement Relationship

Fig. 3.29. Results of retaining wall tests.

with sand, a lateral pressure is developed against the end section which simulates the wall. This wall is constructed so that it can be held in a fixed position or moved inward or outward. A horizontal force P_n normal to the wall must be applied to this wall in order to keep the apparatus in equilibrium in its initial position. Since the wall can have two directions of motion, into the bank or away from the bank, passive and active earth pressures are developed.

If the wall is initially at rest and held by a force $P = P_o$, it is apparent that for a cohesionless soil, as the force P is reduced, the wall will be forced to move outward due to the weight of the soil. As P is gradually reduced, the soil undergoes first elastic deformation, then elastic-plastic deformation and finally, uncontained plastic flow and thus defines the *active collapse load,* P_{an}. Similarly, the *passive collapse load,* P_{pn}, can be defined by forcing the wall to move inward. Figure 3.29b shows a load displacement curve depicting the behavior of the soil under active and passive earth pressures. The points marked P_o, P_{pn} and P_{an} represent the wall force at rest, at passive collapse, and at active collapse, respectively. The subscripts p, a, and n indicate passive, active, and normal components of the force P, respectively. Actually, the active and passive definitions are derived from the role the backfill material plays in the two cases. In the active earth pressure case, the failure is due to the soil's weight overcoming the internal friction and pressure on the wall, that is, the soil is playing an active role. In the passive earth pressure case the failure is due to the pressure on the wall overcoming the soil's weight and internal friction, hence, the soil plays a passive role.

In a recent work reported by Potts and Fourie (1986), the finite-element method has been used to investigate the effects of different modes of wall movements on the generation of earth pressures. Both smooth and rough walls were considered. Referring to Fig. 3.29, the development of active and passive pressure coefficients for both smooth and rough walls is shown in Figs. 3.30a, b. It can be seen that the equivalent coefficient $K = 2P/(\gamma H^2)$ and the amount of displacement necessary to generate fully active or passive failure conditions depends on the mode of wall displacement. The rotation about the toe requires a far more displacement to reach the failure condition than do the other modes of displacement. The final K values for rough walls in the passive case are significantly larger than the corresponding smooth wall case.

In a cohesionless soil, volume change comprises the major part of deformation when there is a change of the state of stress. Certain volume change or volume flow is, therefore, required before the strength of the soil can be fully mobilized along the failure surfaces. As reported by Ladanyi (1958), the volume flow can be neglected for the active pressure case in which the mean normal stress is decreasing during deformation. In the case of passive earth pressure, however, the mean normal stress can increase considerably during deformation. The neglection of the volume flow can be allowed only if the soil adjoining the wall is in a dense or compacted state. Ladanyi also pointed out that the magnitude of dilatation is of great importance for the passive pressure case and it has little influence on the active pressure case as far as wall movement is concerned, although it can also have certain influence on the mobilization of wall friction for both cases. Hence, it can be expected that the perfectly plastic idealization of the backfill material is generally ac-

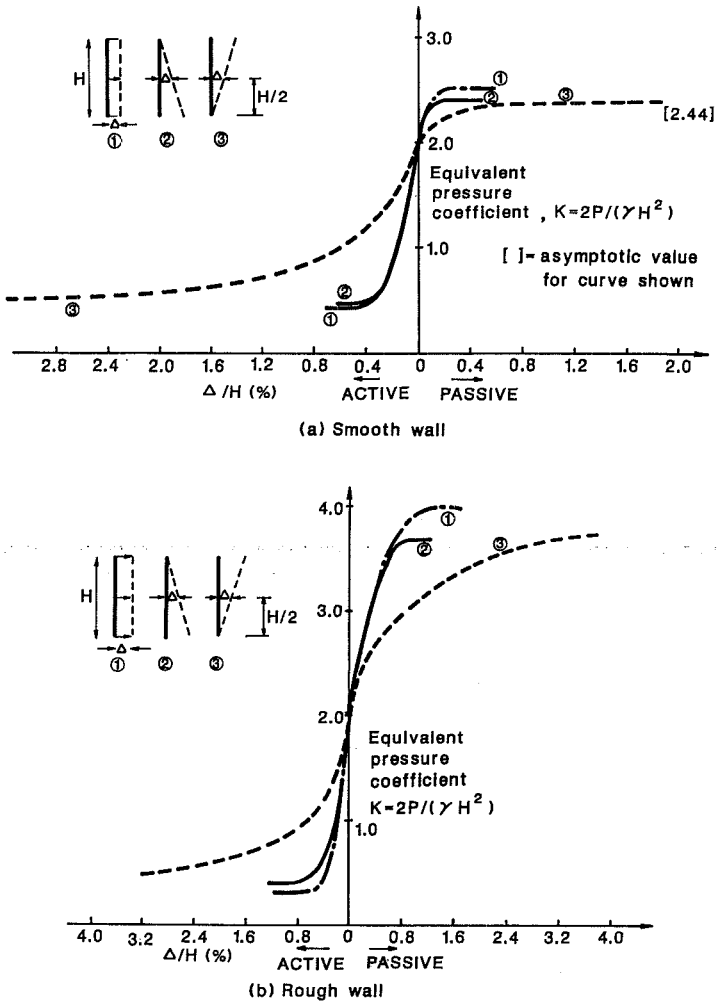

Fig. 3.30. The development of active and passive pressure coefficients for London clay ($c' = 0$, $\phi' = 25°$) by the finite element method (Potts and Fourie, 1986).

ceptable for the active pressure case in which the boundary deformation restriction is not serious. The idealization for the passive pressure case in which the boundary deformation condition is rather restrictive seems not very well justified even though we are only concerned with the collapse load. However, as pointed out by Meyerhof (1971), the use of the customary incomplete stability analyses based on stress characteristics (or perfect plasticity idealization) and the average Mohr-Coulomb shear strength value for the determination of collapse load is optimistic in many geotechnical problems.

It is well recognized that the lateral wall movement required for the development of the passive state of limiting equilibrium is rather large in comparison to that required for the active state of limiting equilibrium. This is believed to be closely related to the points discussed by Ladanyi (1958) and the fact that the boundary deformation conditions are different in the two cases. The direct consequence of this is that the failure of a soil mass in the passive pressure case involves more serious progressive effect than that in the active pressure case. Hence, in the perfectly plastic idealization, progressive failure effect, although generally not of great concern to the active pressure case, should always be considered in the passive pressure case for the collapse load determination. Once the progressive failure effect is properly taken care of in the selection of the average mobilized shear strength parameter, ϕ_m, for analysis, the boundary deformation conditions, which affect the deformation behavior and the extent of progressive failure in the soil mass, will practically have no direct influence on the collapse load determination. Hence, the limit analysis method may be applied to the passive pressure determination if the idealization is based on the average mobilized shear strength represented by ϕ_m, even though the boundary deformation condition is relatively restrictive in this case. For the active pressure case, the progressive failure effect, although it is not as significant as that in the passive pressure case, should also be considered in the idealization for most cases in which the soil – wall interface is generally not perfectly smooth.

References

Bishop, A.W., 1950. Discussion on measurement of the shear strength of soils. Geotechnique, 2(1): 113 – 116.

Bishop, A.W. and Blight, G.E., 1963. Some aspects of effective stress in saturated and partly-saturated soils. Geotechnique, 13: 177 – 197.

Bishop, A.W., 1966. The strength of soils as engineering materials, Sixth Rankine Lecture. Geotechnique, 16(2): 91 – 128.

Bishop, A.W., 1972. Shear strength parameters for undisturbed and remolded soil specimens. In: R.H.G. Parry (Editor), Proceedings of the Roscoe Memorial Symposium: Stress-Strain Behavior of Soils. Foulis, Henley-on-the-Thames, pp. 3 – 58.

Chen, W.F., 1975. Limit Analysis and Soil Plasticity. Elsevier, Amsterdam, 638 pp.

Chen, W.F. and Chang, M.F., 1981. Limit analysis in soil mechanics and its applications to lateral earth pressure problems. Solid Mechanics Archive, Vol. 6, No. 3, Sijthoff & Noordhoff International Publishers, Alphen aan den Rijn, The Netherlands, pp. 331 – 399.

Chen, W.F. and Saleeb, A.F., 1982. Constitutive Equations for Engineering Materials, Vol. 1: Elasticity and Modeling, Wiley-Interscience, New York, NY. 580 pp.

Chen, W.F., Giger, M.W. and Fang, H.Y., 1969. On the limit analysis of stability of slopes. Soil Found. 9(4): 23 – 32.

Cornforth, D.H., 1964. Some experiments on the influence of strain conditions on the strength of sand. Geotechnique, 14(2): 143 – 167.

Davis, E.H., 1968. Theories of plasticity and the failure of soil masses. In: I.K. Lee (Editor), Soil Mechanics: Selected Topics. Butterworth, London, pp. 341 – 380.

Drucker, D.C. and Prager, W., 1952. Soil mechanics and plastic analysis or limit design. Q. Appl. Math., 10(2): 157 – 165.

Drucker, D.C., 1953. Limit analysis of two- and three-dimensional soil mechanics problems. J. Mech. Phys. Solids, 1: 217 – 226.

Finn, W.D., 1967. Applications of limit analysis in soil mechanics. J. Soil Mech. Found. Div., ASCE, 93(SM5): 101 – 120.

Hansen, B., 1958. Line ruptures regarded as narrow rupture zones; basic equations based on kinematic conditions. Proc. Conf. on Earth Pressure Problems, Brussels, Vol. 1, pp. 38 – 47.

Harr, M.E., 1977. Mechanics of Particulate Media – A Probabilistic Approach. McGraw-Hill, New York, NY.

Henkel, D.J., 1971. The calculation of earth pressure in open cuts in soft clays. The Arup Journal, 6, No. 4.

Hvorslev, M.J., 1937. Über die Festigkeitseigenschaften Gestörter Bindiger Böden, Ingridensk, Skr. A, No. 45, (English Translation No. 69-5, Waterways Experiment Station, Vicksburg, Miss., 1969).

Ladanyi, C.E., 1958. The mobilization of shear strength in the active Rankine case of earth pressure. Proc. of Conf. on Earth Pressure Problems, Brussels, Vol. 1, pp. 133 – 147.

Lade, P.V. and Duncan, J.M., 1975. Elastoplastic stress-strain theory for cohesionless soil. J. Geotech. Eng. Divs., ASCE, 101(GT10): 1037 – 1053.

Lade, P.V., 1977. Elasto-plastic stress-strain theory for cohesionless soil with curved yield surfaces. J. Solids Struct., 13: 1019 – 1035.

Lade, P.V., 1979. Stress-strain theory for normally consolidated clay. Proc. 3rd Int. Conf. on Numerical Methods in Geomechanics, Aachen, Germany, Vol. 4, pp. 1325 – 1337.

Lade, P.V. and Musante, H.M., 1977. Failure conditions in sand and remolded clay. Proc. 9th Int. Conf. on Soil Mechanics and Foundation Engineering, Tokyo, Vol. 1, pp. 181 – 186.

Lee, K.L. and Seed, H.B., 1967. Drained strength characteristics of sands. J. Soil Mech. Found. Div., ASCE, 93(SM6): 117 – 141.

Makhlouf, H.M. and Stewart, I.J., 1965. Factors influencing the modulus of elasticity of dry sand. Proc. 6th Int. Conf. Soil Mech. and Foundation Eng., Montreal, Vol. 1, pp. 298 – 302.

Marachi, D.M. et al., 1969. Strength and deformation characteristics of rockfill material. Dep. Civ. Eng., University of California, Rep. TE-69-5.

Meyerhof, G.G., 1971. Discussion on experimental and theoretical investigations of a passive earth pressure problem. Geotechnique, 21: 173.

Potts, D.M. and Fourie, A.B., 1986. A numerical study of the effects of wall deformation on earth pressures. Int. J. Numer. Anal., Methods in Geomech., 10: 383 – 405.

Roscoe, K.H., Bassett, R.H. and Cole, E.R.L., 1967. Principal axes observed during simple shear of a sand. Proc. Geotechnical Conference, Oslo, Vol. 1, pp. 231 – 237.

Rowe, P.W., 1962. The stress-dilatancy relation for static equilibrium of an assembly of particles in contact. Proc. R. Soc. London, Ser. A, 269: 500 – 527.

Taylor, D.W., 1937. Stability of earth slopes. J. Boston Soc. Civ. Eng., 24(3): 197 – 246.

Terzaghi, K., 1943. Theoretical Soil Mechanics. John Wiley & Sons, New York, NY., 510 pp.
Terzaghi, K. and Peck, R.B., 1967. Soil Mechanics in Engineering Practice, 2nd ed. John Wiley & Sons, New York, NY, pp. 394–413.
Wroth, C.P., 1977. The geotechnical aspect of large excavations in urban areas. Twelfth Henry M. Shaw Lecture Series in Civil Engineering, North Carolina State University, Raleigh, NC.

Chapter 4

LATERAL EARTH PRESSURE PROBLEMS

4.1 Introduction

In this chapter, the upper-bound techniques of limit analysis are applied to obtain lateral earth pressures of rigid retaining walls subjected to static forces. The earth pressure problems as the result of an earthquake are presented in Chapter 5. Some practical considerations in the design of rigid retaining structures are given in Chapter 6.

The upper-bound limit analysis method, as in all methods of stability analysis dealing with overall equilibrium, is highly dependent on the failure mechanism chosen for a particular problem. The selection of a proper failure mechanism is therefore of great importance for assessing a reasonable collapse (or limit) load. In this chapter, the translational horizontal wall movement is assumed and the log-sandwich mechanism reported by Chen (1975) is adopted. A ξ log-spiral, with $\xi \leq \phi$ (friction angle), rather than the common ϕ log-spiral is considered in the present formulation and its effect on the limit load is investigated. Furthermore, a non-associated flow rule (or the partial friction – partial dilatation model) rather than the pure friction model as adopted by Chen in 1975, is applied here to the soil – wall interface material. Results of analysis with and without these modifications are presented and discussed.

Some coefficients of the active and passive lateral earth pressures obtained by the upper-bound limit analysis method reported by Chen and Chang (1981) are presented and compared with those obtained by some well-known theoretical methods of analysis. Discrepancies among them are discussed and possible explanations are given.

Finally, some practical aspects in regard to analyses for actual design work are considered. Suggestions are given for actual practice. A tentative conclusion is also included.

4.2 Failure mechanisms

In 1967, Finn suggested that the reliability of the limit analysis may be increased by observing the nature of the slip surface in simple model tests, although, at that time, it was not well-known that the actual sliding surface is a *velocity characteristic*

rather than a *stress characteristic* for a real soil with the angle of dilatation $\nu < \phi$. Generally, different failure mechanisms are associated with different types of wall movement in retaining wall problems. This is clearly reflected by the experimental observations made by James and Bransby (1970) for the passive earth pressure problem.

In this chapter, outward and inward translational wall movements are assumed for the active and passive earth pressure investigations, respectively. Failure mechanisms as generalized from James and Bransby (1970) are adopted for both the passive and the active cases. They are shown in Fig. 4.1. The failure surfaces are assumed to follow the stress characteristics which are also the velocity characteristics for a perfectly plastic material. The mechanism consists of three zones. The first zone, Zone I, is the Rankine zone. The stress condition in this zone is not influenced by the characteristics of the soil – wall interface. The second zone, Zone II, is the mixed zone which is subjected to the influence of the interface characteristics. According to Hettiaratchi and Reece (1975), this zone should be of triangular shape if the angle of wall friction, δ, is uniformly distributed along the interface as generally assumed. The third zone, Zone III, which is a transition zone, is formed by a logarithmic spiral of angle ϕ and the two adjacent boundaries. This kind of combination was reported by Chen and Rosenfarb (1973) to give the best upper bound in the several mechanisms investigated.

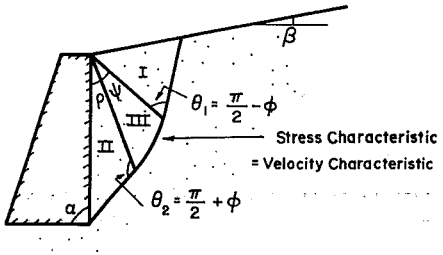

(a) ACTIVE CASE

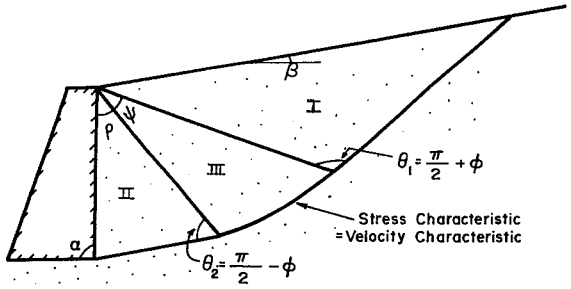

(b) PASSIVE CASE

Fig. 4.1. Assumed failure mechanisms for lateral earth pressure analysis.

Since the upper-bound method of limit analysis is based on energy equilibrium rather than on force equilibrium as employed in the limit equilibrium method, the particular benefit of adopting logarithmic spiral surface with a frictional angle of ϕ is no longer relevant to the upper bound technique. Furthermore, James and Bransby (1970) found that the actual observed failure surfaces follow closely the velocity characteristics and in the Rankine zone $\theta_1 = \pi/2 + \nu$ for the passive pressure case, where the angle of dilatation ν is much smaller than ϕ. This mechanism has recently been adopted by Habibagahi and Ghahramani (1977) who solved the earth pressure problems by the limit equilibrium technique based on a so-called *zero extension line theory*. Much experimental evidence, such as that discussed by Scott (1963), also shows that the actual failure takes place on planes with smaller angles than those predicted by the Mohr-Coulomb criterion which gives the stress characteristics with $\theta_1 = \pi/2 \pm \phi$.

One possible explanation for the difference in the stress characteristics and the velocity characteristics for most soils is that the introduction of the friction in real soils causes the velocity characteristics, which are originally consistent with the stress characteristics for a perfectly plastic material, to shift in such a way as that shown in Fig. 3.26. Consequently, $\theta_1 = \pi/2 \pm \xi$, with an equivalent friction angle ξ being smaller than ϕ and no less than ν. Hence it is justified to adopt a logarithmic spiral with a ξ, with $\nu \leq \xi \leq \phi$, if the solution can be improved. However, it should be noted that when $\xi < \phi$ the solution is, strictly speaking, only an equilibrium solution and not necessarily an upper bound. For the upper-bound theorem of limit analysis to be applicable, the material must be perfectly plastic so that $\xi = \phi$ in the Rankine zone.

Two sets of results by using both ϕ and ξ logarithmic spirals for both the active and passive pressure cases of Fig. 4.1 are shown in Table 4.1. It is found that the active pressure coefficient K_A-values are not altered and K_P-values are somewhat lowered by the use of ξ-spiral rather than ϕ-spiral, especially when the values of the angle of repose of the wall, α, the backfill slope angle, β, and the ϕ-angle are high. This tends to indicate that the conventionally adopted ϕ-spiral failure surface is not necessarily the best mechanism that gives the 'close-to-exact' solution for a given problem. One possible explanation for Table 4.1 in which the use of ξ-spiral results in essentially no improvement for K_A-values but some improvement for K_P-values is that the prefailure volume flow, which is believed to have certain effects on the stress characteristics, is negligible in the active case but of considerable amount in the passive case. To account for this fact, ξ-spiral may be adopted for analysis in the passive case. However, considering the fact that the solution so obtained is not

strictly an upper bound and the fact that the improvement is very limited, ϕ-spiral is suggested for practical application for both the passive and the active cases.

The chosen mechanisms of failure as shown in Fig. 4.1 have the flexibility of being able to be reduced to a simple Coulomb planar failure mechanism when $\psi = 0$, or a logarithmic Rankine mechanism when $\varrho = 0$ or a logarithmic spiral mechanism when $\varrho = 0$ and $\psi = \alpha + \beta$. For the special case of $\phi = 0$, the failure mechanism becomes a circular arc, which seems to agree with the actual observation of sliding in undrained cohesive soil masses. The general mechanism can be optimized so that the most critical failure mechanism is obtained.

TABLE 4.1

a. Effect of assumed failure mechanism on K_A-values*

Assumed mechanisms	$\alpha = 90°, \beta = 10°, \delta = \phi/2$			$\alpha = 90°, \phi = 35°, \delta = \phi/2$		$\beta = 10°, \phi = 35°, \delta = \phi/2$		$\alpha = 90°, \beta = 20°, \phi = 40°$	
	$\phi = 30°$	35°	40°	$\beta = 0°$	20°	$\alpha = 70°$	110°	$\delta = 20°$	40°
Coulomb's planar	0.34	0.28	0.22	0.25	0.32	0.49	0.14	0.25	0.27
ϕ-log -sandwich	0.34	0.28	0.22	0.25	0.32	0.49	0.15	0.25	0.27
ξ-log -sandwich	0.34	0.28	0.22	0.25	0.32	0.49	0.15	0.25	0.27

* K_A is defined as $P_A/\frac{1}{2}\gamma H^2$

b. Effect of assumed failure mechanism on K_P-values*

Assumed mechanisms	$\alpha = 90°, \beta = 10°, \delta = \phi/2$			$\alpha = 90°, \phi = 35°, \delta = \phi/2$		$\beta = 10°, \phi = 35°, \delta = \phi/2$		$\alpha = 90°, \beta = 20°, \phi = 40°$	
	$\phi = 30°$	35°	40°	$\beta = 0°$	20°	$\alpha = 70°$	110°	$\delta = 20°$	40°
Coulomb's planar	8.14	13.65	26.73	7.36	31.94	6.22	148.77	101.61	+
ϕ-log -sandwich	6.75	10.16	16.26	6.71	14.96	6.00	22.52	25.64	56.82
ξ-log -sandwich	6.67	10.00	15.92	6.71	14.48	5.99	21.53	24.62	53.67

* K_P is defined as $P_P/\frac{1}{2}\gamma H^2$

+ No possibility of failure for the given δ-value

4.3 Energy dissipation

4.3.1 Internal energy dissipation

In the upper-bound limit analysis, the evaluation of internal energy dissipation forms the major part of the analysis. The incremental energy dissipation per unit volume in a plastically deformed region of a frictional-dilating material in a two-dimensional plane strain problem has the value (Chen, 1975):

$$\Delta D_v = c \cos \phi \, \Delta\gamma_{max} \tag{4.1}$$

where c is the cohesion parameter, ϕ is the internal friction angle of the material, and $\Delta\gamma_{max} = \Delta\epsilon_1 - \Delta\epsilon_3$ is the maximum incremental shear strain or the maximum incremental deviatorial strain during plastic flow. By using Eq. (4.1), the incremental energy dissipation per unit length along a velocity discontinuity or a narrow transition zone can be derived as (Chen, 1975):

$$\Delta D_L = c \cos \phi \, \Delta V \tag{4.2}$$

where ΔV is the incremental displacement which makes an angle of ϕ with respect to the velocity discontinuity according to the associated flow rule in perfect plasticity.

For simple stability problems involving sliding and/or homogeneous deforming mechanisms, the internal energy dissipation can be evaluated with Eqs. (4.1) and (4.2). By equating the incremental external work (or the external rate of work) to the incremental dissipation (or the interal rate of energy dissipation), the collapse load can be determined. However, for those problems involving soil – structure interaction, such as the retaining wall problems, the evaluation of energy dissipation along the soil – structure interface presents an uncertainity due to the complicated mechanism involved in the interface sliding. This problem will be carefully investigated as follows before a detailed mathematical formulation is developed.

4.3.2 Interface energy dissipation

Since soil – wall interface is an actual slip surface and can be considered as a velocity discontinuity rather than a stress characteristic, perfectly plastic model is not applicable to the interface material. The relative movement between soil and wall, which is dependent on the interface characteristics and the property of the adjacent soil, needs not always be of purely frictional sliding. We should therefore allow the interface material to be considered as a partially frictional and partially dilating non-associated flow rule material and evaluate their effects separately.

However, Chen (1975) suggested that the energy dissipation along soil – wall interface can be evaluated as a purely frictional dissipation. To investigate how this idealization affects the collapse load, Fig. 4.2 is considered. For retaining wall problems, the normal force acting on the soil – wall interface is either the same as the unknown or is the component of the unknown to be determined. Idealization of the material to be a pure dilatation material or a pure friction material is not required for work and energy evaluations. Therefore, the net change in external work that will result in change of passive earth pressure, P_P, due to the introduction of wall friction (the angle of wall friction $\delta > 0$) can be derived as follows:

According to Eq. (3.30), we have:

$$\tan\delta_f = \tan\delta - \tan\nu_w \tag{4.3}$$

where δ_f and ν_w are the frictional and dilating components of δ, respectively. Usually, we expect $\nu_w < \delta$. From Fig. 4.2, the net change in external work can be expressed: When $\nu_w < \delta$:

$$[\Delta W]_{\nu_w < \delta} = \Delta W_E - \Delta W_I \tag{4.4}$$

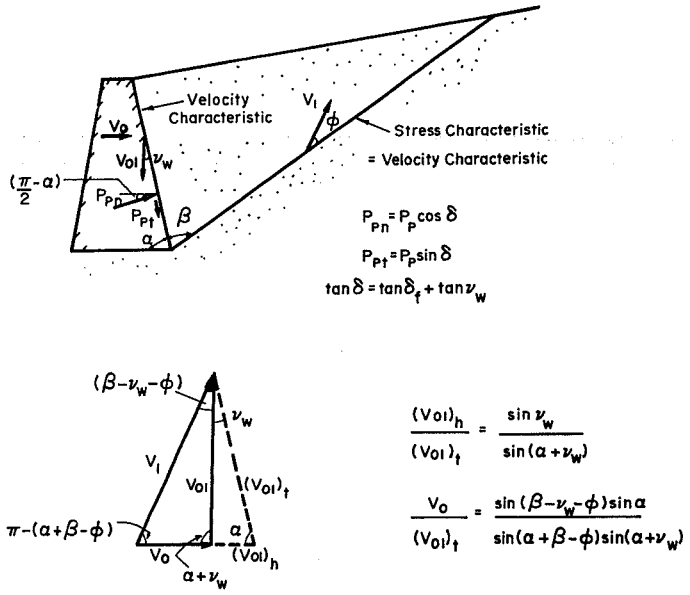

Fig. 4.2. Velocity characteristic along soil-wall interface and incremental displacement diagram for energy dissipation analysis (passive pressure case).

where ΔW_E is the increment of external work without considering the wall friction, ΔW_I is the energy dissipated by sliding friction on the interface between the wall and the soil adjacent to the wall. According to Fig. 4.2, we have:

$$\Delta W_E = (P_{Pn} \tan\delta \cos\alpha)(V_0) - \left[P_{Pn} \cos\left(\frac{\pi}{2} - \alpha\right)\right](V_{01})_h \tag{4.5}$$

where P_{Pn} denotes the normal component of the passive earth pressure P_P acting on the wall. The vector $\vec{V}_0$ is the horizontal inward translating velocity of the wall. The vector $\vec{V}_{01}$ is the relative velocity between the wall and the soil adjacent to the wall, which makes an angle of ν_w with respect to the soil – wall interface. Note that $\vec{V}_{01}$ is not vertical here. From Fig. 4.2, we can also find that:

$$\Delta W_I = P_{Pn} \tan\delta_f (V_{01})_t \tag{4.6}$$

Using Eqs. (4.3), (4.5) and (4.6) and Fig. 4.2, the expression in Eq. 4.4 becomes:

$$[\Delta W]_{\nu_w < \delta} = P_P \cos\delta \left\{\frac{\sin\alpha}{\sin(\alpha + \nu_w)}\left[\tan\delta \cos\alpha \frac{\sin(\beta - \nu_w - \phi)}{\sin(\alpha + \beta - \phi)} - \sin\nu_w\right] - [\tan\delta - \tan\nu_w]\right\}(V_{01})_t \tag{4.7}$$

Note that if we take $\nu_w = 0$, i.e., the interface sliding is of purely frictional characteristics, then we have:

$$[\Delta W]_{\nu_w = 0} = - P_P \sin\delta \left[\frac{\sin\alpha \cos(\beta - \phi)}{\sin(\alpha + \beta - \phi)}\right](V_{01})_t \tag{4.8}$$

If we take $\nu_w = \delta$, i.e, the interface material is perfectly plastic, then we have:

$$[\Delta W]_{\nu_w = \delta} = - P_P \cos\delta \frac{\sin\alpha \sin\delta}{\sin(\alpha + \delta}\left[1 - \frac{\cos\alpha}{\cos\delta}\frac{\sin(\beta - \delta - \phi)}{\sin(\alpha + \beta - \phi)}\right](V_{01})_t \tag{4.9}$$

When $\alpha = \pi/2$, Eqs. (4.7) to (4.9) give the same expression:

$$[\Delta W]_{\nu_w} = - P_P \sin\delta (V_{01})_t \tag{4.10}$$

Therefore, for vertical walls, whether the soil – wall interface material idealized as purely frictional or purely dilating material or not will not affect the result of limit analysis, if the failure mechanism remains the same. However, since Eq. (4.7) cannot be reduced to Eq. (4.8) when $\nu_w > 0$ and $\alpha \neq \pi/2$, the idealization of the inter-

face material as a purely frictional material ($\nu_w = 0$) will, in most cases, introduce certain error in the passive earth pressure analysis.

The same conclusion can also be reached for the active earth pressure case. For proper evaluation of the interface energy dissipation and the change in external work due to the introduction of the wall friction, the partial friction – partial dilation model should be applied to the soil – wall interface.

4.4 Passive earth pressure analysis

In the formulation, a ξ-log-sandwich mechanism is adopted for a greater flexibility. Figure 4.3 shows the ξ-log-sandwich mechanism adopted for the passive pressure analysis. Also shown is the related incremental displacement diagram. The vector $\vec{V}_0$ is the horizontal inward translational velocity of the wall. The vector $\vec{V}_1$ is the velocity of the mixed zone ABO, which is pointing upward at an angle ϕ away from

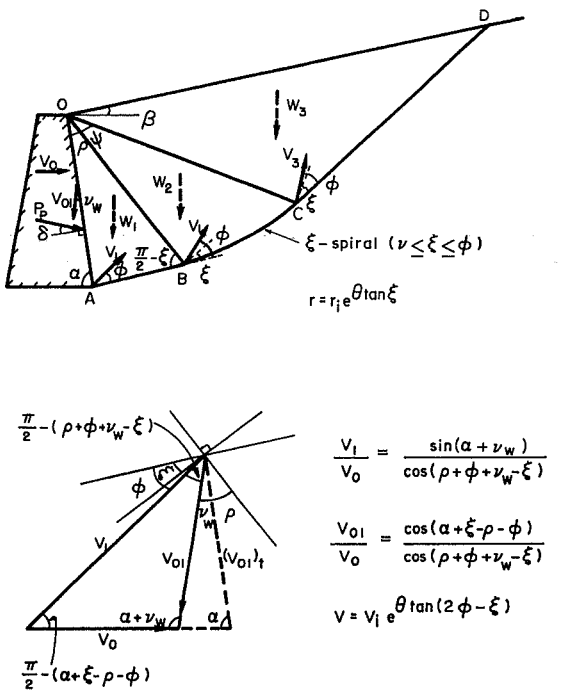

$$\frac{V_1}{V_0} = \frac{\sin(\alpha + \nu_w)}{\cos(\rho + \phi + \nu_w - \xi)}$$

$$\frac{V_{01}}{V_0} = \frac{\cos(\alpha + \xi - \rho - \phi)}{\cos(\rho + \phi + \nu_w - \xi)}$$

$$V = V_i e^{\theta \tan(2\phi - \xi)}$$

Fig. 4.3. Log-sandwich failure mechanism and incremental displacement diagram for passive earth pressure analysis.

the stress characteristics or the assumed failure surface AB. The vector $\vec{V}_{01}$ is the relative velocity between the wall and the soil adjacent to the wall, which makes an angle of ν_w with respect to the soil – wall interface according to the non-associated flow rule.

Shown in Fig. 4.4 are the property of a ξ-spiral and the relationship of the increment displacements on the spiral. The two adjacent incremental displacement along the ξ-spiral, V_j and V_{j+1}, can be related as:

$$\frac{V_{j+1}}{V_j} = \frac{\cos(2\phi - \xi - \Delta\theta/2)}{\cos(2\phi - \xi + \Delta\theta/2)} \tag{4.11}$$

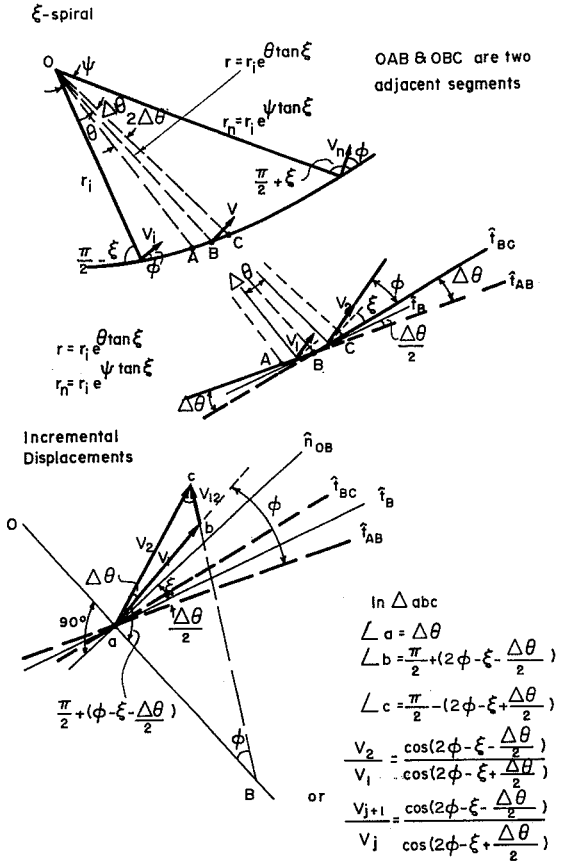

Fig. 4.4. Property of ξ-spiral and relationship between the associated incremental displacements.

Consequently, we have:

$$\frac{V_n}{V_i} = \left\{\frac{\cos(2\phi - \xi - \psi/2n)}{\cos(2\phi - \xi + \psi/2n)}\right\}^n = \left\{1 + \frac{2\tan(2\phi - \xi)\tan(\psi/2n)}{1 - \tan(2\phi - \xi)\tan(\psi/2n)}\right\}^n \tag{4.12}$$

where V_i is the initial incremental displacement at $r = r_i$ and $\theta = 0$, and V_n is the final incremental displacement at $r = r_n$ and $\theta = \psi$. As n approaches infinity, we have:

$$\frac{V_n}{V_i} = \lim_{n\to\infty}\left\{1 + \frac{2\tan(2\phi - \xi)\tan(\psi/2n)}{1 - \tan(2\phi - \xi)\tan(\psi/2n)}\right\}^n$$

$$= \lim_{n\to\infty}\left\{1 + \frac{\psi\tan(2\phi - \xi)}{n}\right\}^n = e^{\psi\tan(2\phi - \xi)} \tag{4.13}$$

In general, the incremental displacement at any location θ along the spiral can be expressed as:

$$V = V_i\, e^{\theta\tan(2\phi - \xi)} \tag{4.14}$$

The relationships between $\vec{V}_0$ and $\vec{V}_1$, $\vec{V}_{01}$ are shown in Fig. 4.3.

The incremental external work due to self-weight of the soil (or the potential energy change) in each zone can be calculated by multiplying the vertical component of the incremental displacement in that zone with the corresponding weight of the soil.

The incremental external work for the triangular zone OAB in Fig. 4.3 is:

$$\Delta W_{OAB} = -W_1 V_{1y}$$

$$= -\frac{\gamma H^2}{2} V_0 \frac{\sin\varrho\cos(\varrho - \xi)\cos(\alpha + \xi - \varrho - \phi)\sin(\alpha + \nu_w)}{\sin^2\alpha\cos\xi\cos(\varrho + \phi + \nu_w - \xi)} \tag{4.15}$$

For the ξ-log-spiral zone OBC:

$$\Delta W_{OBC} = -\int_V \gamma V_y\, dV$$

$$= -\frac{\gamma H^2}{2} V_0 \frac{\cos^2(\varrho - \xi)\sin(\alpha + \nu_w)}{\sin^2\alpha\cos^2\xi\cos(\varrho + \phi + \nu_w - \xi)} \frac{1}{(a^2 + 1)} \times$$

$$\{\cos(\alpha + \xi - \varrho - \phi)[e^{a\psi}(a\cos\psi + \sin\psi) - a] +$$

$$\sin(\alpha + \xi - \varrho - \phi)[e^{a\psi}(a\sin\psi - \cos\psi) + 1]\} \tag{4.16}$$

where $a = 2\tan\xi + \tan(2\phi - \xi)$. And for the triangular Rankine zone OCD:

$$\Delta W_{OCD} = -W_3 V_{3y}$$

$$= -\frac{\gamma H^2}{2} V_0 \frac{e^{a\psi}\cos^2(\varrho - \xi)\sin(\alpha + \beta - \varrho - \psi) \times \cos(\alpha + \xi - \varrho - \psi - \phi)\sin(\alpha + \nu_w)}{\sin^2\alpha\cos\xi\cos(\varrho + \phi + \nu_w - \xi)\cos(\alpha + \beta + \xi - \varrho - \psi)} \tag{4.17}$$

where a is the same as in Eq. (4.16). The incremental external work contributed by the passive earth pressure is:

$$\Delta W_{P_P} = P_{Pn} V_0 (\sin\alpha + \tan\delta\cos\alpha) = P_P V_0 \sin(\alpha + \delta) \tag{4.18}$$

The internal energy dissipation incremental is only that contributed by the soil–wall interface friction since $c = 0$ for cohesionless soils:

$$\Delta D_{OA} = P_{Pn}\tan\delta_f (V_{01}\cos\nu_w)$$

$$= P_P\cos\delta(\tan\delta - \tan\nu_w)\frac{\cos(\alpha + \xi - \varrho - \phi)}{\cos(\varrho + \phi + \nu_w - \xi)} V_0\cos\nu_w \tag{4.19}$$

By equating the total increment of external work to the total internal energy dissipation, we have:

$$\Sigma\Delta W = \Sigma\Delta D \tag{4.20}$$

or

$$\Delta W_{OAB} + \Delta W_{OBC} + \Delta W_{OCD} + \Delta W_{P_P} = \Delta D_{OA} \tag{4.21}$$

Substituting Eqs. (4.15)–(4.19) into Eq. (4.21) and making rearrangements, we have:

$$P_P = \tfrac{1}{2}\gamma H^2 K_P \tag{4.22}$$

where K_P is the *coefficient of passive earth pressure* and is given as:

$$K_P = \frac{\cos(\varrho - \xi)\sin(\alpha + \nu_w)}{\sin^2\alpha\cos\xi[\sin(\alpha + \delta)\cos(\varrho + \phi + \nu_w - \xi) - \cos\delta(\tan\delta - \tan\nu_w)\cos(\alpha + \xi - \varrho - \phi)\cos\nu_w]} \times$$

$$\left[\sin\varrho\cos(\alpha+\xi-\varrho-\phi)+\right.$$

$$\frac{\cos(\varrho-\xi)}{(a^2+1)\cos\xi}\left(\cos(\alpha+\xi-\varrho-\phi)\,[e^{a\psi}(a\cos\psi+\sin\psi)-a]\right.$$

$$\left.+\sin(\alpha+\xi-\varrho-\phi)\,[e^{a\psi}(a\sin\psi-\cos\psi)+1]\right)$$

$$\left.+\frac{\cos(\varrho-\xi)\sin(\alpha+\beta-\varrho-\psi)\cos(\alpha+\xi-\varrho-\psi-\phi)}{\cos(\alpha+\beta+\xi-\varrho-\psi)}e^{a\psi}\right] \quad (4.23)$$

where a is the same as defined in Eq. (4.16).

For practical purpose, the ϕ log-spiral mechanism is suggested to ensure that the solution is strictly an upper bound to the exact solution. Also, by adopting the ϕ log-spiral, the analysis is simplified and the cost is reduced. This can be done by assigning $\xi = \phi$ in Eq. (4.23). The expression for K_P after this simplification is:

$$K_P = \frac{\cos(\varrho-\phi)\sin(\alpha+\nu_w)}{\sin^2\alpha\cos\phi\,[\sin(\alpha+\delta)\cos(\varrho+\nu_w)-\cos\delta\,(\tan\delta-\tan\nu_w)\cos(\alpha-\varrho)\cos\nu_w]}$$

$$\left[\sin\varrho\cos(\alpha-\varrho)+\frac{\cos(\varrho-\phi)}{(b^2+1)\cos\phi}\left(\cos(\alpha-\varrho)[e^{b\psi}(b\cos\psi+\sin\psi)-b]\right.\right.$$

$$\left.+\sin(\alpha-\varrho)[e^{b\psi}(b\sin\psi-\cos\psi)+1]\right)$$

$$\left.+\frac{\cos(\varrho-\phi)\sin(\alpha+\beta-\varrho-\psi)\cos(\alpha-\varrho-\psi)e^{b\psi}}{\cos(\alpha+\beta+\phi-\varrho-\psi)}\right] \quad (4.24)$$

where $b = 3\tan\phi$.

4.5 Active earth pressure analysis

The ξ log-sandwich mechanism considered in the formulation for active earth pressure analysis is shown in Fig. 4.5. The incremental displacement are also shown in the figure. They are very similar to those in the passive pressure analysis except that the wall movement, V_0, is now translationally outward and V_1 and V_3 have downward components rather than upward components. Similar to the formulation for the passive earth pressure, the active earth pressure can be derived as:

$$P_A = \tfrac{1}{2}\gamma H^2 K_A \quad (4.25)$$

where K_A is the *coefficient of active earth pressure* and is given as:

$$K_A = \frac{\cos(\varrho+\xi)\sin(\alpha-\nu_w)}{\left[\sin^2\alpha\cos\xi\,[\sin(\alpha-\delta)\cos(\varrho-\phi-\nu_w+\xi)+\cos\delta\,(\tan\delta-\tan\nu_w)\cos(\alpha-\varrho+\phi-\xi)\cos\nu_w\right]}\times$$

$$\left[\sin\varrho\cos(\alpha-\varrho+\phi-\xi)+\frac{\cos(\varrho+\xi)}{\cos\xi\,(a^2+1)}\left(\cos(\alpha-\varrho+\phi-\xi)\right.\right.$$

$$[e^{-a\psi}(-a\cos\psi+\sin\psi)+a]+\sin(\alpha-\varrho+\phi-\xi)[e^{-a\psi}(-a\sin\psi-$$

$$\left.\cos\psi+1]\right)$$

$$\left.+\frac{\cos(\varrho+\xi)\sin(\alpha+\beta-\varrho-\psi)\cos(\alpha-\varrho-\psi+\phi-\xi)e^{-a\psi}}{\cos(\alpha+\beta-\varrho-\psi-\xi)}\right] \quad (4.26)$$

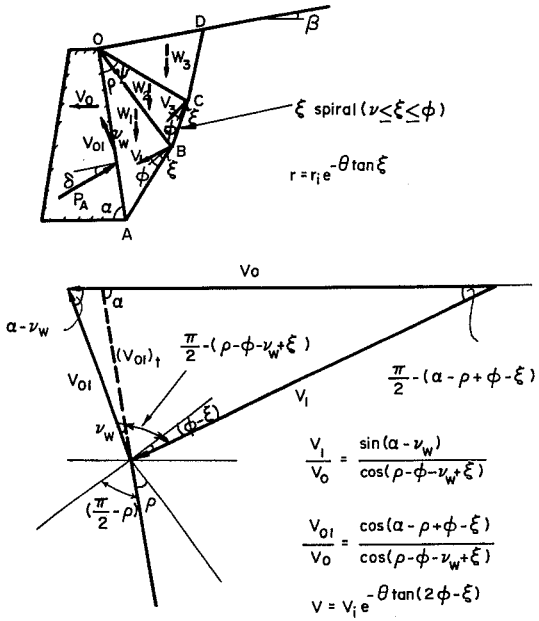

Fig. 4.5. Log-sandwich failure mechanism and incremental displacement diagram for active earth pressure analysis.

where $a = 2\tan\xi + \tan(2\phi - \xi)$ is the same as defined in Eq. (4.16).

Similar to the passive case, Eq. (4.26) can be simplified to that corresponding to the ϕ-log-sandwich mechanism for obtaining strictly upper-bound solution by setting $\xi = \phi$ in the equation. After this simplification, the expression becomes:

$$K_A = \frac{\cos(\varrho + \phi)\sin(\alpha - \nu_w)}{\left[\sin^2\alpha\cos\phi\,[\sin(\alpha - \delta)\cos(\varrho - \nu_w) + \cos\delta\,(\tan\delta - \tan\nu_w)\cos(\alpha - \varrho)\cos\nu_w]\right]} \times$$

$$\left[\sin\varrho\cos(\alpha - \varrho) + \frac{\cos(\varrho + \phi)}{\cos\phi\,(b^2 + 1)}\left(\cos(\alpha - \varrho)[e^{-b\psi}(-b\cos\psi + \sin\psi) + b] + \sin(\alpha - \varrho)\,[e^{-b\psi}(-b\sin\psi - \cos\psi) + 1]\right)\right.$$

$$\left. + \frac{\cos(\varrho + \phi)\sin(\alpha + \beta - \varrho - \psi)\cos(\alpha - \varrho - \psi)\,e^{-b\psi}}{\cos(\alpha + \beta - \varrho - \psi - \phi)}\right] \qquad (4.27)$$

where $b = 3\tan\phi$.

Note that in special cases in which $\nu_w = 0$, Eqs. (4.24) and (4.26) reduce to those obtained previously by Chen and Rosenfarb (1973), as also given in Chen (1975).

There is one point worth mentioning. The K_P (or K_A) obtained by the pure friction assumption, $\nu_w = 0$, and by the partial-friction partial-dilation assumption, $\nu_w < \delta$, will not necessarily be identical, even as $\alpha = \pi/2$ in which $[\Delta W]_{\nu_w = 0} = [\Delta W]_{\nu_w}$. This is because the most critical failure mechanism may be different somewhat in both cases. Nevertheless, the difference in the K_P (or K_A) values obtained in both cases may be small.

4.6 Comparisons and discussions

When the validity of the theoretical analysis is investigated, it is generally required to compare results of the analysis with actual observations and measurements from field or from model tests. Unfortunately, complicated boundary and loading conditions in the field and uncertain scale effect in the model tests often make the direct comparison impossible. Investigation of theoretical results relies highly on the comparison with solutions from currently accepted theoretical analyses.

4.6.1 Comparison with slip-line, zero-extension line, and Coulomb limit equilibrium solutions

Tables 4.2a and 4.2b show some comparisons of K_A and K_P values obtained by the proposed limit analysis method with those well-known Sokolovskii's slip-line solutions (Sokolovskii, 1965) and the recently developed zero-extension line theory presented by Habibagahi and Ghahramani (1977). Results from the classical Coulomb's theory are also included. It is found that for the active case, limit analysis method gives results equal or close to Sokolovskii's solution. It is also

TABLE 4.2

a. Comparison of K_A-values by various methods ($\beta = 0°$)

Analytical methods	$\alpha = 90°$						$\phi = 30°$			
	$\phi = 20°$		$\phi = 30°$		$\phi = 40°$		$\alpha = 70°$		$\alpha = 110°$	
	$\delta = 0°$	$10°$	$\delta = 0°$	$15°$	$\delta = 0°$	$20°$	$\delta = 0°$	$15°$	$\delta = 0°$	$15°$
Coulomb	0.49	0.45	0.33	0.30	0.22	0.20	0.47	0.48	0.20	0.19
Zero-extension	0.49	0.41	0.33	0.27	0.22	0.17	–	–	–	–
Slip-line	0.49	0.45	0.33	0.30	0.22	0.20	0.52	0.49	0.23	0.21
Limit analysis	0.49	0.45	0.33	0.30	0.22	0.20	0.50	0.48	0.22	0.19

* $K_A = P_A/\frac{1}{2}\gamma H^2$

b. Comparison of K_P-values by various methods ($\beta = 0°$)

Analytical methods	$\alpha = 90°$						$\phi = 30°$			
	$\phi = 20°$		$\phi = 30°$		$\phi = 40°$		$\alpha = 70°$		$\alpha = 110°$	
	$\delta = 0°$	$10°$	$\delta = 0°$	$15°$	$\delta = 0°$	$20°$	$\delta = 0°$	$15°$	$\delta = 0°$	$15°$
Coulomb	2.04	2.64	3.00	4.98	4.60	11.81	2.14	3.26	5.02	10.95
Zero-extension	2.04	2.55	3.00	4.65	4.60	9.95	–	–	–	–
Slip-line	2.04	2.55	3.00	4.62	4.60	9.69	2.16	2.16	5.06	8.45
Limit analysis	2.04	2.58	3.00	4.70	4.60	10.07	2.27	3.16	5.09	8.92

* $K_P = P_P/\frac{1}{2}\gamma H^2$

found that when the wall is not perfectly smooth ($\delta > 0$), the limit analysis tends to give higher K_A-values than the zero-extension line theory does. The Coulomb's solution only seems to agree quite well with the Sokolovskii's solution for the active case when the wall friction is low and the wall is vertical.

For the passive case, limit analysis solution tends to slightly overestimate the K_P-value when compared with the Sokolovskii's solution, if the Sokolovskii's solution is considered to be 'close-to-exact'. The zero-extension line theory gives 'better' results than the limit analysis does in this case. As is well recognized, the Coulomb's results show overestimation of the K_P-values in most cases, especially when the wall friction is high and the interface is not vertical. This can readily be seen from Fig. 4.6 which shows the typical critical failure surfaces reflected in the limit analysis and in the Coulomb's analysis of active and passive earth pressures. It is found that in the passive case, the critical failure surface of Coulomb is much more extended than that of limit analysis. The Coulomb's approach therefore gives higher K_P-values than the limit analysis does. The fact that Coulomb solution is a reasonable approx-

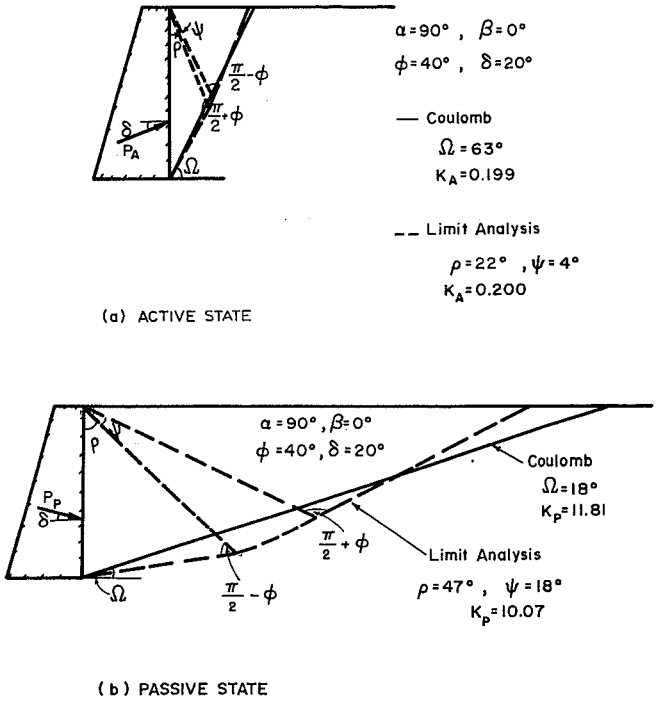

Fig. 4.6. Typical critical slip surfaces for active and passive states of failure.

imation for the active case is obvious since the critical surfaces for both analyses are almost identical.

It should be pointed out here that the critical failure surfaces reflected in the limit analysis or the limit equilibrium method for collapse load estimation are not representative of the actual failure surface. The critical failure surfaces reflected in these analyses are stress characteristics. They are the same as velocity characteristics or the actual failure surfaces only when the soil mass is perfectly plastic and observes the associted flow rule during plastic deformation. Soils are non-associated flow rule material and the stress characteristics are different from the velocity characteristics along which actual failure occurs (Fig. 3.26). Hence, the critical surfaces reflected in the collapse load analyses are fictitious ones. When prediction of the failure surface is of importance, model observation is preferred. Attention should also be paid to backcalculating the mobilized strength of a failed soil mass based on the actually observed failure surfaces and the classical stability analysis techniques. Even if the stability analysis takes into account the non-associated flow

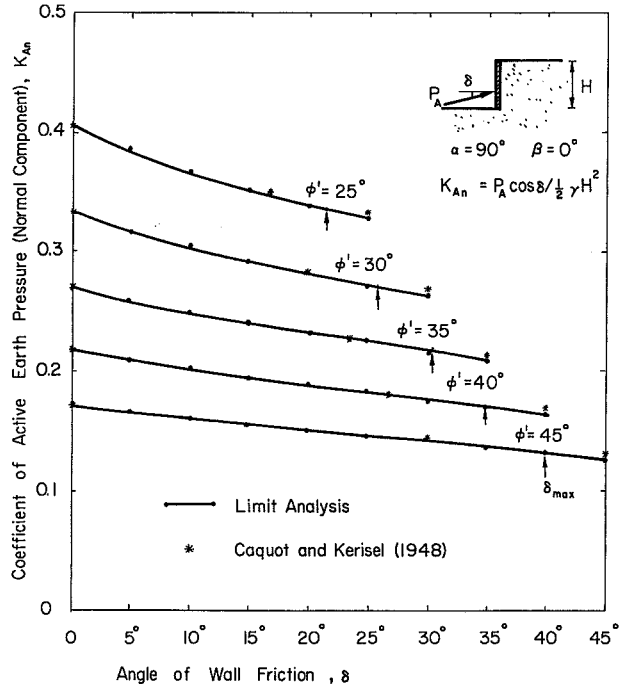

Fig. 4.7. Comparison of K_{An}-values by limit analysis with Caquot and Kerisel's results ($\alpha = 90°$, $\beta = 0°$).

characteristics of the soils, back calculation based on the actual failure surface will give strength parameters c_k and ϕ_k rather than the Mohr-Coulomb's c and ϕ as discussed earlier in Chapter 3. This should be carefully considered in evaluating the field behavior of the stability of a soil mass.

4.6.2 Comparison with Caquot & Kerisel's method (vertical wall and horizontal backfill)

Some comparisons of K_{An} (K_{An} corresponding to the normal component of P_A) and K_P values with the well-known earth pressure tables of Caquot and Kerisel (1948) are shown in Figs. 4.7 and 4.8. The agreement is quite good for this particular case in which the wall is vertical and the backfill is horizontal. The $K_{Pn} - \tan\delta$ relations for a vertical wall with a horizontal backfill by several well-known theoretical methods are compared with that obtained by the limit analysis (Fig. 4.9). The limit analysis tends to give a little too high of K_P-values when the wall is fairly

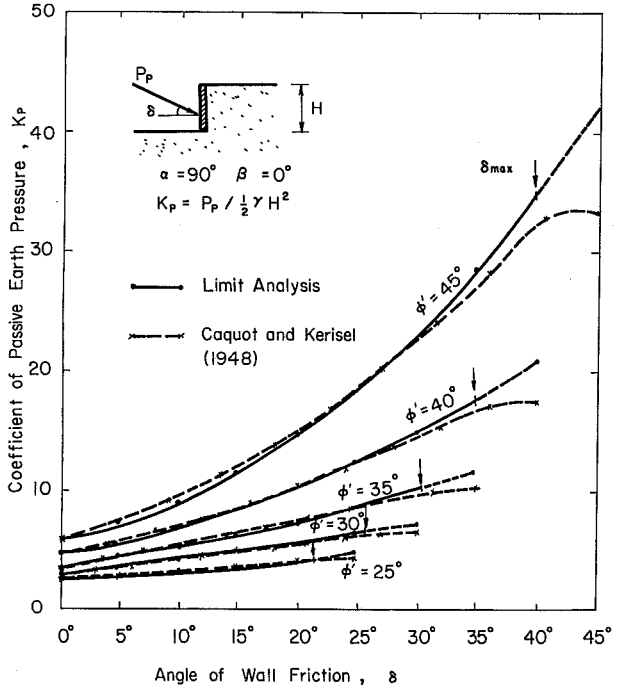

Fig. 4.8. Comparison of K_P-values by limit analysis with Caquot and Kerisel's results ($\alpha = 90°$, $\beta = 0°$).

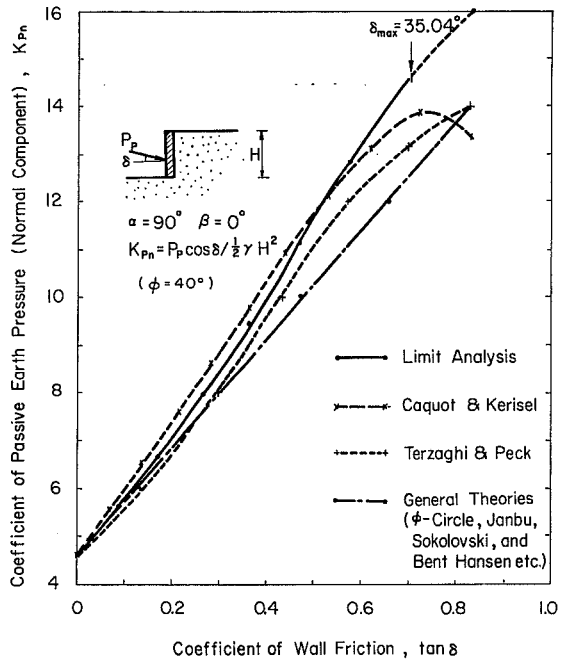

Fig. 4.9. Comparison of K_{Pn}-values by limit analysis and some available theoretical methods.

rough. However, the results are, in general, acceptable for this particular case of vertical wall and the horizontal backfill from the practical point of view.

4.6.3 Comparison with Caquot and Kerisel's and Lee and Herington's methods (general soil-wall system)

In many cases, the retaining wall may not be vertical and the backfill is possibly inclined. To see if the limit analysis is acceptable for solving general retaining wall problems, comparisons of results for the passive pressure case, which is more critical than the active case, are made with some results obtained by Lee and Herington (1972) in which the angle of repose of the wall, α, is 70° and the inclination of the backfill, β, ranges from 0° to −20° as shown in Fig. 4.10. Some Sokolovskii's and Terzaghi's (Terzaghi, 1943) logarithmic spiral solutions are also included. The agreement among them, although they may not be as good when $\alpha > 90°$ and β is high, is remarkably close in the present case with $\phi = 30°$ and $\alpha = 70°$.

Some comparisons of results of limit analysis for $\phi = 45°$, $\delta = (\frac{2}{3})\phi$ and

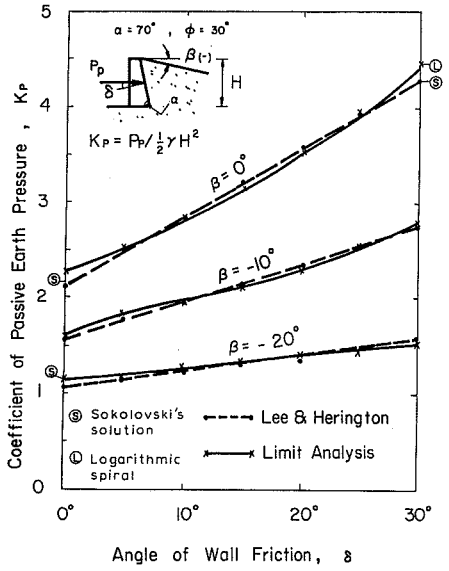

Fig. 4.10. Comparison of results of limit analysis with plasticity solutions by Lee and Herington (1972).

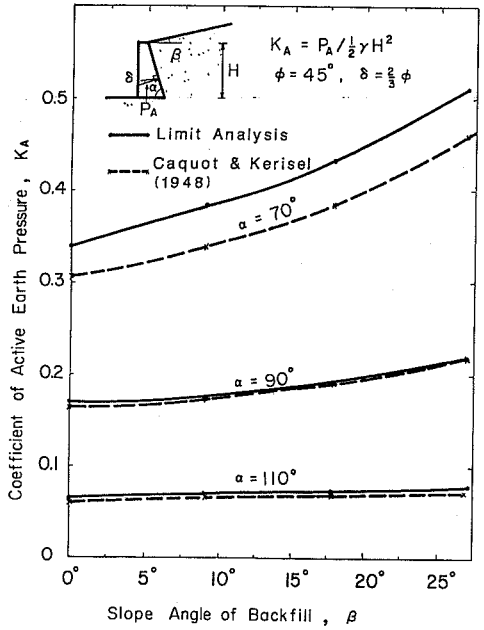

Fig. 4.11. Comparison of K_A-values by limit analysis with Caquot and Kerisel's results ($\beta > 0°$).

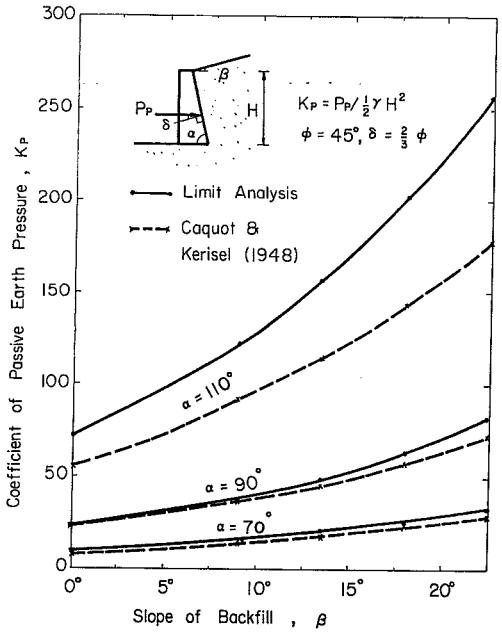

Fig. 4.12. Comparison of K_P-values by limit analysis with Caquot and Kerisel's results ($\beta > 0°$).

$\alpha \neq 90°$, $\beta \neq 0°$ with those given by Caquot and Kerisel (1948) are shown in Figs. 4.11 and 4.12. It is found that the limit analysis gives higher K_A- and K_P-values than Caquot and Kerisel (1948) does. The difference, however, is very small in most cases except when the wall is inclined toward the backfill ($\alpha = 110°$) for the passive case and away from the backfill ($\alpha = 70°$) for the active case.

The fact that the K_P-values obtained by the upper-bound limit analysis are higher than those obtained by Caquot and Kerisel (1948) is reasonable. This is because the solution of Caquot and Kerisel based on the equation of equilibrium may be considered as a lower bound. The exact solution is probably somewhere in between. The reason why the K_A-value obtained by Caquot and Kerisel is lower than that given by the limit analysis is, however, not clear. In the active case, the Caquot and Kerisel's approach should give higher K_A-values. The fact that the higher the K_A-value the closer the value is to the exact solution suggests that the limit analysis method gives better results than Caquot and Kerisel does in the active earth pressure determination.

In the passive pressure case, the exact K_P-value is probably somewhere in between those determined by the limit analysis method and by the Caquot and

Kerisel's method. The difference between them, however, is small even when the wall is not vertical. For practical applications, the results of limit analysis is acceptable.

4.6.4 Effect of pure-friction idealization of interface material

Analyzing the K_A and K_P values for the general retaining wall problems shows that even when ν_w is as high as 15° for a soil – concrete interface, the solutions obtained with and without pure friction idealization are almost the same. The values obtained by the partial friction and partial dilatation model, are higher than those obtained by the idealized models for the passive case and lower for the active case. Nevertheless, it should not be misinterpreted as that the idealized models give 'better' upper bounds. The values obtained by assuming $\nu_w = 0$ are not, strictly speaking, upper bounds, because these models did not follow the normality condition.

Tables 4.3a and 4.3b show the errors introduced by the pure friction idealization of the interface material. The maximum errors are approximately 2.5% and 0.9% for the passive case and the active case, respectively. Practically, they are within the

TABLE 4.3
Error on K_A-values introduced by pure-friction idealization of interface material

$\phi = 45°$, $\nu_w = 15°$, $\delta = \phi_k = 39.9°$	$\alpha = 70°$		$\alpha = 90°$		$\alpha = 110°$	
	K_A	Error (%)	K_A	Error (%)	K_A	Error (%)
$\beta = 0°$	0.372	0.81	0.171	0.50	0.065	0.31
$\beta = 9°$	0.421	0.71	0.186	0.43	0.069	0.15
$\beta = 18°$	0.484	0.83	0.205	0.44	0.073	0.14
$\beta = 27°$	0.571	0.88	0.233	0.39	0.081	0.25

b. Error on K_P-values introduced by pure-friction idealization of interface material

$\phi = 45°$, $\nu_w = 15°$, $\delta = \phi_k = 39.9°$	$\alpha = 70°$		$\alpha = 90°$		$\alpha = 110°$	
	K_P	Error (%)	K_P	Error (%)	K_P	Error (%)
$\beta = 0°$	14.38	−2.23	35.41	−1.81	111.81	−0.56
$\beta = 9°$	24.41	−2.41	60.28	−1.68	191.31	−0.56
$\beta = 13.5°$	31.45	−2.48	77.78	−1.57	247.25	−0.49
$\beta = 18°$	40.24	−2.48	99.69	−1.53	317.14	−0.41
$\beta = 22.5°$	51.17	−2.10	126.93	−1.63	404.01	−0.52

acceptable ranges. It is therefore suggested that the pure friction idealization which gives a 'safe' estimation of the upper bound, can be adopted for practical purposes.

4.7 Some practical aspects

For an actual design work, at least four practical aspects must be considered. They are the loading and strain conditions, the soil – structure interface friction, the progressive failure and scale effect, and the cohesion and surcharge effects.

4.7.1 Loading and strain conditions

The soil parameters for analysis and design are generally obtained by testing in laboratories soil samples taken from the ground. For the results from a test to be useful, not only the initial stress condition of the sample representing an element in the ground of interest should be recognized but also the loading and strain conditions (or the stress paths) should be carefully simulated to those to be expected in the field.

Lateral earth pressures acting on long retaining walls are generally considered as plane strain problems. For lateral earth pressure analyses, the strength parameters should therefore be obtained from plane strain compression (active case) or plane strain extension (passive case) test. However, in many cases, only triaxial compresion test or *direct shear test* results rather than *plane strain test* results are available. Modification of the strength parameters is therefore frequently required before they can be entered into calculation.

A relationship between the triaxial ϕ-value, ϕ_{tx}, and the plane strain ϕ-value, ϕ_{ps}, can be derived from the corresponding stress-dilatancy relations proposed by Rowe (1969a).

From Rowe (1962), the stress-dilatancy relation for the triaxial and plane strain loading cases can be expressed as:

$$\sigma_1'/\sigma_3' = D \tan^2(45° + \tfrac{1}{2}\phi_f) \tag{4.28}$$

where σ_1' and σ_3' are the principal stresses, D represents the dilatancy and is equal to $(1 - d\nu/d\epsilon_a)$, in which $d\nu$ is the volume decrease per unit volume and $d\epsilon_a$ is the axial strain due to particle slips, and ϕ_f is the frictional component of ϕ with its value varies from ϕ_μ, the angle of mineral-to-mineral friction, to ϕ_{cv}, the angle of internal friction at the critical state.

In Eq. (4.28), Rowe (1969a) suggested that D can be taken as 2 and ϕ_f can be taken as ϕ_μ in a triaxial compression test if the sand tested is at its densest state. The upper limit of the stress ratio corresponding to the densest state can then be expressed as:

$$\sigma_1'/\sigma_3' = 2\tan^2(45° + \tfrac{1}{2}\phi_\mu) \tag{4.29}$$

Also, by taking $D = 1$ and $\phi_f = \phi_{cv}$ for the case that the sand is at its loosest state, the lower limit of the stress ratio corresponding to this state can be taken as:

$$\sigma_1'/\sigma_3' = \tan^2(45° + \tfrac{1}{2}\phi_{cv}) \tag{4.30}$$

For the plane strain compression case, Rowe (1969a) suggested that D can be taken as 2 for the densest state and 1 for the loosest state as in the triaxial compression case. He also suggested that ϕ_f can be taken as ϕ_{cv} for sand at any relative density. Hence, the upper and the lower limits of the stress ratio for the plane strain case can be expressed respectively as:

$$\sigma_1'/\sigma_3' = 2\tan^2(45° + \tfrac{1}{2}\phi_{cv}) \tag{4.31}$$

and

$$\sigma_1'/\sigma_3' = \tan^2(45° + \tfrac{1}{2}\phi_{cv}) \tag{4.32}$$

The stress ratios corresponding to the intermediate densities can be obtained by interpolation.

In the general stress-dilatancy equation, Eq. (4.28), D can be expressed in terms of the angle of dilation, ν, as:

$$D = \tan^2(45° + \tfrac{1}{2}\nu) \tag{4.33}$$

Here, ν, or consequently, D, is dependent on the *relative density* (RD), the stress path, and the strain condition. Analysis of the data obtained by Cornforth (1964) for medium-to-fine, well-graded blasted sand reflects that D for both the plane strain compression and the triaxial compression situations can be approximated by:

$$D = 0.64(RD)^2 + 0.36(RD) + 1.0 \tag{4.34}$$

The value of ϕ_f presented in Eq. (4.28) is also dependent on the relative density, the stress path, and the strain condition, in general, although ϕ_f was found independent of the relative density and equal to ϕ_{cv} in the plane strain compression and extension cases. According to the results obtained by Rowe (1962) for a medium-to-fine sand, the value of ϕ_f for the triaxial compression case can be approximated by:

$$\phi_f = \phi_\mu + [1 - 0.463(RD) - 0.537(RD)^2](\phi_{cv} - \phi_\mu) \tag{4.35}$$

Noticing that $\sigma_1'/\sigma_3' = \tan^2(45° + \frac{1}{2}\phi)$ and by combining Eqs. (4.28) to (4.33), the general expressions for the peak triaxial compression and the peak plane strain compression ϕ-values can be expressed, respectively, as:

$$\phi_{tx} = \sin^{-1}\left(\frac{D\tan^2(45° + \tfrac{1}{2}\phi_f) - 1}{D\tan^2(45° + \tfrac{1}{2}\phi_f) + 1}\right) \tag{4.36}$$

and

$$\phi_{ps} = \sin^{-1}\left(\frac{D\tan^2(45° + \tfrac{1}{2}\phi_{cv}) - 1}{D\tan^2(45° + \tfrac{1}{2}\phi_{cv}) + 1}\right) \tag{4.37}$$

where D is given by Eq. (4.34) and ϕ_f is given by Eq. (4.35). Hence, ϕ_{tx} and ϕ_{ps} can be related as:

$$\phi_{ps} = \eta\,\phi_{tx}$$

where

$$\eta = \frac{\sin^{-1}\left(\dfrac{D\tan^2(45° + \tfrac{1}{2}\phi_{cv}) - 1}{D\tan^2(45° + \tfrac{1}{2}\phi_{cv}) + 1}\right)}{\sin^{-1}\left(\dfrac{D\tan^2(45° + \tfrac{1}{2}\phi_f) - 1}{D\tan^2(45° + \tfrac{1}{2}\phi_f) + 1}\right)} \geq 1.0 \tag{4.38}$$

They can also be related by $\tan\phi_{ps} = \eta_t \tan\phi_{tx}$. Some results plotted as η and η_t vs. (RD) for $\phi_\mu = 15°$ to $35°$ are shown in Fig. 4.13 for reference. A linear approximation between ϕ_{cv} and ϕ_μ will be given later in Eq. (4.41).

Since it has been reported (Rowe, 1969a) that in both plane strain compression and extension, $\phi_f = \phi_{cv}$, Eq. (4.38) originally derived for the compression case, is also valid for the extension case, although the values of ϕ_f and D may be different from those given by Eqs. (4.34) and (4.35). Analysis of Cornforth's results (Cornforth, 1964) shows that for the triaxial extension test, D can be approximated by:

$$D = 1.23(RD)^3 - 0.79(RD)^2 + 0.49(RD) + 1.0 \leq 1.93 \tag{4.39}$$

This gives D-values somewhat lower than those estimated by Eq. (4.34) for given relative densities. This tends to indicate that there is more dilatation in the compres-

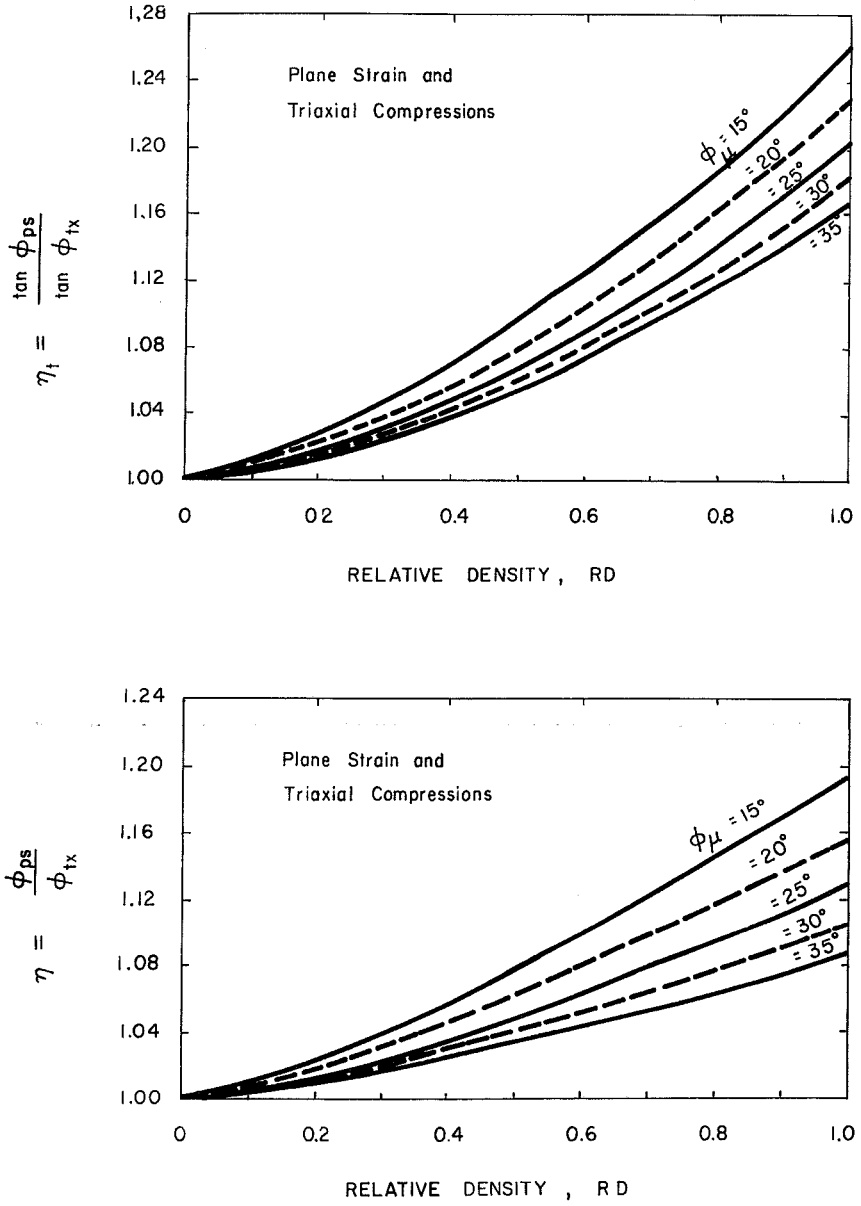

Fig. 4.13. Variation of ϕ_{ps}/ϕ_{tx} and $\tan\phi_{ps}/\tan\phi_{tx}$ with ϕ_μ and relative density of sand.

sion test than in the extension test. The angle of dilatation, ν, of a given soil is therefore expected to be larger if sheared under triaxial compression condition than if sheared under triaxial extension condition. Although, there is no information available on the plane strain extension D-value, it is practically accepted that Eq. (4.39) is also valid for this case in lieu of the fact that Eq. (4.34) is reported to be equally valid for both triaxial and plane strain compressions (Rowe, 1969a).

As far as ϕ_f is concerned, it has also been reported that for both the triaxial compression and triaxial extension cases, $\phi_f = \phi_\mu$, when the soil is in the densest state, and, $\phi_f = \phi_{cv}$, when the soil is in the loosest state. However, there is no adequate information so that a relation similar to Eq. (4.35) can be developed for soils at intermediate density for the extension case. Since D or ν for the triaxial extension case is different from that for the triaxial compression case, it is expected that ϕ_f is also different for the two cases. Equation (4.38) is therefore not strictly applicable to the extension case, since ϕ_f is an indeterminate value.

Another fact worth noting is that in the active earth pressure case, failure is induced by lateral unloading (or plane strain compression), whereas in the passive pressure case, failure is induced by lateral loading (or plane strain extension). As has just discussed, Eq. (4.38) seems not strictly applicable to the passive case. This is because under unloading shear, the sample generally has more 'brittle' behavior. Consequently, both ϕ_f and D may be different from those given by Eqs. (4.34) and (4.35) as developed for the loading case. Fortunately, the variations of both ϕ_f and D are expected to follow quite similar trends for given loading and strain conditions. Unless complete information can be obtained, Eq. (4.38) with D and ϕ_f given by Eqs. (4.34) and (4.35) is suggested for estimating the corresponding factor for the ϕ-value to be used in the analysis of active and passive earth pressures.

In case that only the direct shear ϕ-value, ϕ_{ds}, is available, the correction can be made based on the equation developed by Rowe (1969a):

$$\tan\phi_{ds} = \tan\phi_{ps}\cos\phi_{cv} \tag{4.40}$$

For $\phi_\mu = 15°$ to $40°$, which covers all non-metal materials, the experimental data reported by Horne (1969) reflect that the relation between ϕ_{cv} and ϕ_μ can be fairly approximated by:

$$\phi_{cv} = 22.5° + 0.9(\phi_\mu - 15°) \tag{4.41}$$

For most earth materials, $\phi_\mu \simeq 25°$ to $30°$, the value of ϕ_{cv} ranges approximately from $31.5°$ to $36°$. Hence, once the type of minerals forming the soil and the relative density of the material is known, both ϕ_{tx} and ϕ_{ds} can be properly corrected to give ϕ_{ps} that can be adopted for the theoretical analyses.

4.7.2 Soil–structure interface friction

As pointed out by Davis (1968), the strength parameter ϕ on the velocity characteristics in a soil mass is different from the Mohr-Coulomb ϕ-parameter. If the Mohr-Coulomb value for the plane strain case is ϕ_{ps} and the angle of dilatation is ν for a soil mass, the corresponding ϕ-value on the velocity characteristics in the soil mass is given as Eq. (3.39b), i.e.:

$$\phi_k = \tan^{-1}\left(\frac{\sin\phi_{ps}\cos\nu}{1 - \sin\phi_{ps}\sin\nu}\right) \tag{4.42}$$

It is noted from the expression that $\phi_k \leq \phi_{ps}$. On the soil-structure interface, which is a velocity characteristic if the wall friction is fully mobilized, the maximum δ-value corresponding to the perfectly rough, soil-to-soil sliding situation is $\delta_{max} = \phi_k$. Hence, the angle of wall friction, δ, is always smaller than the Mohr-Coulomb ϕ-value, ϕ_{ps}, unless when $\nu = \phi_{ps}$, in which case the velocity characteristics is the same as the stress characteristics. The value of ν, if not measured, can be calculated from Eqs. (4.28) and (4.33), since ϕ_f can be estimated from Eq. (4.35) if the relative density of the material is known, and according to Eq. (4.33), the ν can be written as:

$$\nu = \sin^{-1}[(D - 1)/(D + 1)] \tag{4.43}$$

In general, the value of δ can be evaluated by a direct shear testing with the soil to be used as the backfill sliding over the wall material. The angle of dilatation for the interface material, ν_w, can also be measured in this manner. For obtaining strict upper bounds by the limit analysis method, both δ and ν_w are required, since a non-associated flow rule should be applied to the interface material. However, the value of ν_w is quite often not given, the following rules are suggested for estimating ν_w.

(a) For 'sand – smooth steel' interface, $\delta \leq \phi_\mu$ is probably the case. Purely frictional soil-wall sliding predominates the interface movement. In this case, ν_w can be taken as zero.

(b) For 'sand – rough steel' interface, $\phi_\mu \leq \delta \leq \phi_{cv}$ is the possible situation. A linear interpolation between $\nu_w = 0$, corresponding to $\delta = \phi_\mu$, and the ν_w-value corresponding to $\delta = \phi_{cv}$ is suggested. Similar to Eq. (4.40) as proposed by Rowe (1969a), the relation between δ, the angle of wall friction in a direct shear test, and the corresponding plane strain value, δ_{ps}, can be approximated by:

$$\tan\delta = \tan\delta_{ps}\cos\delta_{cv} \tag{4.44}$$

where δ_{cv} is the δ-value corresponding to $\nu_w = 0$ case. Note that for the constant volume test, $\nu_w = 0$ and $\delta_{ps} = \delta_{cv}$. Equation (4.44) reduces to $\tan\delta = \sin\delta_{ps} = \sin\delta_{cv}$. But since $\delta = \phi_\mu$ is assumed as $\nu_w = 0$, we have $\tan\phi_\mu = \sin\delta_{cv}$. Consequently, Eq. (4.44) becomes:

$$\tan\delta = \tan\delta_{ps}\sqrt{1 - \tan^2\phi_\mu} \tag{4.45}$$

Furthermore, similar to Eq. (4.42), δ, δ_{ps} and ν_w can be related as:

$$\delta = \tan^{-1}\left(\frac{\sin\delta_{ps}\cos\nu_w}{1 - \sin\delta_{ps}\sin\nu_w}\right) \tag{4.46}$$

By assuming $\delta = \phi_{cv}$ and solving Eqs. (4.45) and (4.46) simultaneously, the ν_w-value corresponding to $\delta = \phi_{cv}$, denoted by ν_{wo}, can be obtained. The ν_w-value for a given δ can then be estimated by:

$$\nu_w = \nu_{wo}\frac{(\delta - \phi_\mu)}{(\phi_{cv} - \phi_\mu)} \tag{4.47}$$

(c) For 'sand – smooth concrete' interface with $\phi_{cv} \leq \delta \leq \phi_k$, the movement is approaching from soil-wall sliding to soil-soil sliding. In this case, $\nu_w \leq \nu$. Also, the δ_{cv}-value is controlled practically by the sand grain-to-sand grain sliding and $\delta_{cv} = \phi_{cv}$ can be assumed. By solving Eqs. (4.44) and (4.46), considering $\delta_{cv} = \phi_{cv}$, the ν_w-value can be reasonably estimated.

(d) For 'sand – rough concrete' interface, δ can be assumed as equal to ϕ_k, although Brumund and Leonards (1973) reported that δ was as high as the triaxial ϕ-value for the same kind of interface. The movement is practically a soil-to-soil sliding and the ν_w-value can be taken as ν.

4.7.3 Progressive failure and scale effect

In a direct application of the Mohr-Coulomb ϕ-parameter, ϕ_{ps}, to plane strain stability problems, we implicitly assume that the strength of the soil along the failure surface is fully mobilized everywhere along the surface. This is probably the case in most laboratory tests in which the tested specimen is assumed representative of a soil element in the soil mass. This is because the specimen is generally so small that the strain is practically considered uniform along the failure surface, although boundary restrains do exist in almost all tests. In a soil mass, the strains along the failure surface are seldom uniform and failure of the soil mass is generally of progressive nature. At the instant of failure, the maximum shearing resistance available

on the failure surface must be, on average, somewhere between the peak state and the ultimate state as explained before (see Fig. 3.24). In most stability analyses, such as the limit analysis and the limit equilibrium method, the overall equilibrium of the soil mass involving deformation is considered. An average mobilized ϕ-value, ϕ_m, rather than the peak ϕ-value, ϕ_{ps}, should be adopted in the analysis.

The selection of ϕ_m should be based on the progressive failure consideration so that the ϕ-value so chosen is corresponding to the average strain or the average stress level in the soil along the failure surface. This can only be obtained from the comparison of the theoretical analysis with the model test results. However, it involves another uncertainty, the *scale effect*, when applying the model test results to the field. This is because different soil masses involved in models of different size will result in a different extent of the progressive effect. Consequently, the ϕ_m-value that fits the theories will be different if the models are of different scale. Furthermore, both the failure mechanism involved and the interface roughness have a great influence on the extent of the progressive failure in a soil mass. Therefore, in the selection of proper ϕ_m-value for design purpose, problem characteristics (e.g., active or passive case in lateral earth pressure problems) and interface roughness as well as the size of the structure (e.g., wall height in lateral earth pressure problems) should be considered.

Rowe (1969b) recommended a method of considering the progressive failure effect in the selection of ϕ_m-value for the stability analysis of granular soils. With the assumption that when the wall is perfectly rough $\delta = \phi_{ps}$ and $\phi_m = \phi_{mo}$, where ϕ_{mo} is the maximum ϕ-value to fit the current failure theory. He introduced a so-called *'progressive index'* μ_p. It is defined as:

$$\mu_p = \frac{\phi_{ps} - \phi_{mo}}{\phi_{ps} - \phi_{cv}} \tag{4.48}$$

He suggested, based on model studies on dense sands, that μ_p at field scales can be taken as 0.4 for active pressure and 0.8 for passive pressure for practical design based on classical failure theories. He also claimed that these values are applicable to sands at intermediate densities.

In order to look more closely at the effect of wall height, H, on the μ_p-value, which has a great influence on the result of stability analysis, especially for the passive pressure case in which the progressive failure effect is great, some test results on models of different size are analyzed. Very limited data from Rowe and Peaker (1965), Rowe (1969b), and Kerisel (1972) are available for this purpose for the passive pressure case. As discussed previously, the maximum possible δ-value for a perfectly rough wall corresponding to a soil-to-soil sliding condition should be equal to ϕ_k. It is therefore proper to redefine ϕ_{mo} as the ϕ_m-value corresponding to

$\delta_{max} = \phi_k$ situation, which is a perfectly rough situation for the case of concrete walls and sand backfills. For the case of steel walls and sand backfills, the maximum possible value of δ may be taken as the ϕ_k-value corresponding to the pure friction case ($\nu = 0$) since the movement is essentially soil-to-wall slippage. In this case, $\delta_{max} = \tan^{-1}(\sin\phi_{cv})$ from Eq. (4.42). The ϕ_m-value corresponding to this situation is taken as ϕ_{mo} for the steel wall case. The results of analysis based on these redefined ϕ_{mo}-values are plotted as μ_p versus H as shown in Fig. 4.14 for the cases of steel wall and concrete wall. A similar relation can be developed from model tests for the active earth pressure case, although the progressive effect is less significant in this case.

It should be noted that the ϕ_m-value backcalculated from the observed failure surface is only an approximation, since the surface is not necessary the most critical one. Also, even if the non-associated characteristics of soils are considered, the ϕ-value backcalculated should be equal to ϕ_k, which is a value not larger than ϕ.

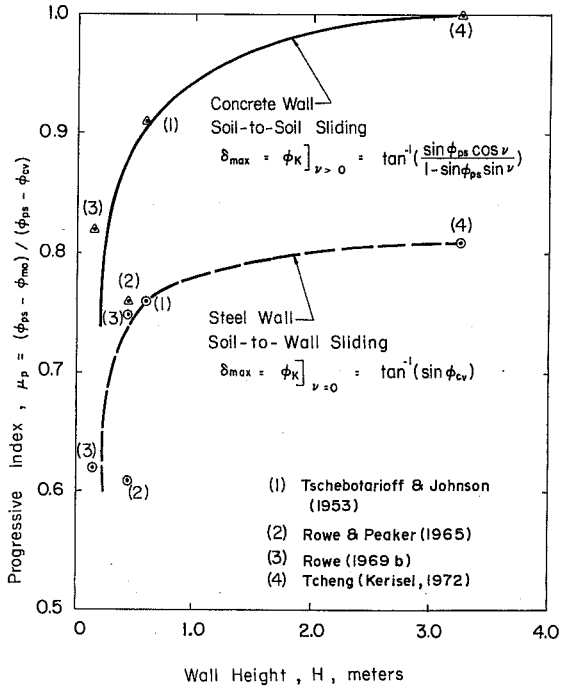

Fig. 4.14. Progressive index as function of wall height for passive translational wall movement case.

Hence, this discrepancy should be recognized in interpreting the information on the progressive index as function of wall height from model test results.

It was found by Rowe (1969b) that the ϕ_m-value of a soil mass subjected to active pressure or passive pressure is approximately equal to its corresponding triaxial ϕ-value, ϕ_{tx}, if the wall is perfectly smooth, i.e., $\delta = 0$. Furthermore, it was found that the ϕ-value decreases linearly as the friction component, tan δ, increases, with its ultimate value equal to ϕ_{mo}. Based on these two findings, the ϕ_m-value corresponding to an arbitrary wall friction, δ, can be approximated by:

$$\phi_m = \phi_{tx} - \frac{\tan \delta}{\tan \delta_{max}} (\phi_{tx} - \phi_{mo}) \tag{4.49}$$

where ϕ_{mo} can be estimated from Fig. 4.14 or similar relations and from Eq. (4.48). In practice, the δ-value, which is a function of the wall movement, may not

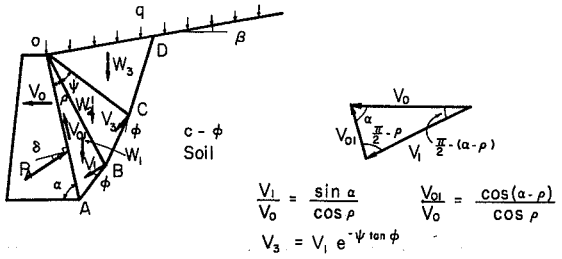

a. Active Case

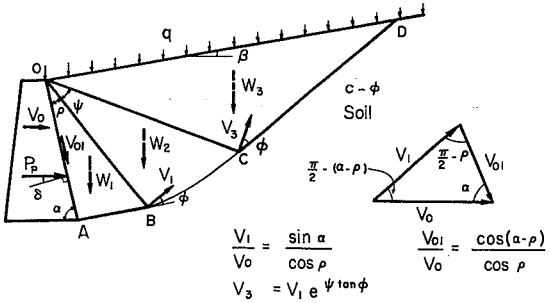

b. Passive Case

Fig. 4.15. Log-sandwich failure mechanisms for lateral earth pressure analyses in c-ϕ soils subjected to uniform surcharge.

be always full mobilized. By Eq. (4.49), a proper ϕ_m-value corresponding to the given δ-value can be selected for analysis and the lateral pressures can then be properly estimated.

4.7.4 Cohesion and surcharge effects

In many cases, the backfill may possess cohesion although free-draining material is generally preferred. Presence of surcharge on the slope of the backfill is not uncommon either. Both cohesion and surcharge have certain influence on the lateral earth pressures. Their effects can be included in the lateral earth pressure evaluations.

The versatility of the upper-bound limit analysis enables the effect of cohesion and surcharge being included in the calculations with rather little difficulty. For practical purposes, the soil-wall systems and their associated mechanisms of failure with pure frictional interface idealization as shown in Fig. 4.15 are considered. By including the internal energy dissipations along AB, BC, CD and in the radial shear zone OBC as contributed by the cohesion component, represented by the c-parameter, the dissipation along the interface OA as contributed by the *adhesion* c_a, and the potential energy change or external work induced by the *surcharge, q*, acting on OD in the analysis for cohesionless soils as stated in Section 4.4, the lateral earth pressures for the generalized case can be evaluated. Detailed derivation for the case of $c_a = 0$ can be found in the book by Chen (1975). If the adhesion is expressed as a ratio of c, e.g. $c_a = \lambda c$, the lateral earth pressures for a mixed soil backfill with uniform surcharge can be expressed as:

$$P_A = \tfrac{1}{2}\gamma H^2 (N_{A\gamma}) + qH(N_{Aq}) + cH(N_{Ac}) \tag{4.50}$$

$$P_P = \tfrac{1}{2}\gamma H^2 (N_{P\gamma}) + qH(N_{Pq}) + cH(N_{Pc}) \tag{4.51}$$

where

$$N_{A\gamma} = \frac{\cos(\varrho + \phi)}{\sin^2\alpha \cos(\varrho - \delta)\cos\phi}\left[\sin\varrho \cos(\alpha - \varrho) + \frac{\cos(\varrho + \phi)}{\cos\phi(1 + 9\tan^2\phi)}\right.$$

$$[\cos(\alpha - \varrho)\{3\tan\phi + e^{-3\psi\tan\phi}(-3\tan\phi\cos\psi + \sin\psi)\}$$

$$+ \sin(\alpha - \varrho)\{1 + e^{-3\psi\tan\phi}(-3\tan\phi\sin\psi - \cos\psi)\}]$$

$$\left. + \frac{\cos(\varrho + \phi)\cos(\alpha - \varrho - \psi)\sin(\alpha + \beta - \varrho - \psi)e^{-3\psi\tan\phi}}{\cos(\alpha + \beta - \phi - \varrho - \psi)}\right] \tag{4.52}$$

$$N_{Aq} = \frac{\cos(\varrho + \phi)\cos(\alpha - \varrho - \psi)e^{-2\psi\tan\phi}}{\sin\alpha\cos(\varrho - \delta)\cos(\alpha + \beta - \phi - \varrho - \psi)} \tag{4.53}$$

$$N_{Ac} = \frac{-1}{\sin\alpha\cos(\varrho - \delta)}\left[\frac{\lambda\cos(\alpha - \varrho)}{\sin\alpha} + \sin\varrho + \frac{\cos(\varrho + \phi)\sin(\alpha + \beta - \varrho - \psi)e^{-2\psi\tan\phi}}{\cos(\alpha + \beta - \phi - \varrho - \psi)} - \frac{\cos(\varrho + \phi)(e^{-2\psi\tan\phi} - 1)}{\sin\phi}\right] \tag{4.54}$$

$$N_{P\gamma} = \frac{\cos(\varrho - \phi)}{\sin^2\alpha\cos(\varrho + \delta)\cos\phi}\left[\sin\varrho\cos(\alpha - \varrho) + \frac{\cos(\varrho - \phi)}{\cos\phi(1 + 9\tan^2\phi)}\right.$$
$$[\cos(\alpha - \varrho)\{-3\tan\phi + e^{3\psi\tan\phi}(3\tan\phi\cos\psi + \sin\psi)\}$$
$$+ \sin(\alpha - \varrho)\{1 + e^{3\psi\tan\phi}(3\tan\phi\sin\psi - \cos\psi)\}]$$
$$\left. + \frac{\cos(\varrho - \phi)\cos(\alpha - \varrho - \psi)\sin(\alpha + \beta - \varrho - \psi)e^{3\psi\tan\phi}}{\cos(\alpha + \beta + \phi - \varrho - \psi)}\right] \tag{4.55}$$

$$N_{Pq} = \frac{\cos(\varrho - \phi)\cos(\alpha - \varrho - \psi)e^{2\psi\tan\phi}}{\sin\alpha\cos(\varrho + \delta)\cos(\alpha + \beta + \phi - \varrho - \psi)} \tag{4.56}$$

$$N_{Pc} = \frac{1}{\sin\alpha\cos(\varrho + \delta)}\left[\frac{\lambda\cos(\alpha - \varrho)}{\sin\alpha} + \sin\varrho + \frac{\cos(\varrho - \phi)\sin(\alpha + \beta - \varrho - \psi)e^{2\psi\tan\phi}}{\cos(\alpha + \beta + \phi - \varrho - \psi)} + \frac{\cos(\varrho - \phi)(e^{2\psi\tan\phi} - 1)}{\sin\phi}\right] \tag{4.57}$$

It should be noted that the value of the soil – wall adhesion, c_a, is a function of both soil properties and characteristics of wall face in contact with the backfill. The maximum possible adhesion is c_k as given in Eq. (3.39a), when there is a soil-to-soil interface sliding. For an idealized purely frictional soil – wall interface, $\nu = \nu_w = 0$, the adhesion can be defined, according to Eq. (3.39a), as:

$$c_a \leq [c_k]_{\nu=0} = c\cos\phi_{cv} \tag{4.58}$$

or

$$\lambda = \frac{c_a}{c} \leq \cos\phi_{cv} \tag{4.59}$$

The actual value of c_a or λ should be carefully evaluated by a direct shear test with the backfill material placed over the wall material.

If the progressive failure effect is taken into consideration, the c-parameter should be modified. However, little is known on this aspect. Assuming that the c-parameter varies in the same manner as the coefficient of internal friction $\tan\phi$ does, the average mobilized c-value, c_m, can be estimated as:

$$c_m = \frac{\tan\phi_m}{\tan\phi_{ps}} c_{ps} \tag{4.60}$$

where c_{ps} is the c-parameter corresponding to the plane strain condition. For practical purposes, the c_{ps}-value can also be taken as the triaxial c-value, c_{tx}, since the cohesion characteristics of a soil, like pure friction, is almost independent of loading and strain conditions. If only the direct shear c-value, c_{ds}, is available, c_{ps} can be estimated by Eq. (3.39a) with ϕ replaced by ϕ_{ps}, c replaced by c_{ps}, and c_k replaced by c_{ds}, if ν is known.

To obtain the most critical values of P_A and P_P, maximization and minimization, respectively, are required. The optimization should be performed with respect to the entire equation rather than to the individual terms in Eqs. (4.50) and (4.51). That is:

$$(P_A)_{max} = \text{Max}\left[\tfrac{1}{2}\gamma H^2(N_{A\gamma}) + qH(N_{Aq}) + cH(N_{Ac})\right] \tag{4.61}$$

$$(P_P)_{min} = \text{Min}\left[\tfrac{1}{2}\gamma H^2(N_{P\gamma}) + qH(N_{Pq}) + cH(N_{Pc})\right] \tag{4.62}$$

In this chapter, we have showed why the upper-bound limit analysis method can be applied to cohesionless soils for obtaining reasonably accurate estimates of the lateral earth pressures despite the fact that the normality condition required in the limit analysis is not actually observed in cohesionless soils during plastic flow. Both theoretical justifications and actual comparisons of the results of analysis confirm this applicability. By properly taking into account the four practical aspects discussed in this section, the upper-bound limit analysis method can be adopted for the analysis and actual design of rigid retaining structures (Chen and Chang, 1981).

By the same principle, the analysis can also be extended to include the earthquake

forces by introducing a seismic coefficient and by using the pseudostatic analysis concept. This will be presented in Chapter 5.

References

Brumund, W.F. and Leonards, G.A., 1973. Experimental study of static and dynamic friction between sand and typical construction materials. J. Test. Eval., 1(2): 162–165.

Caquot, A. and Kerisel, J., 1948. Tables for the Calculation of Passive Pressure, Active Pressure, and Bearing Capacity of Foundations. Gauthier-Villars, Paris.

Chen, W.F., 1975. Limit Analysis and Soil Plasticity. Elsevier, Amsterdam, 638 pp.

Chen, W.F. and Chang, M.F., 1981. Limit Analysis in Soil Mechanics and Its Applications to Lateral Earth Pressure Problems, Solid Mechanics Archives, Vol. 6, No. 3, Sijthoff & Noordhoff International Publishers, Alphen aan den Rijn, The Netherlands, pp. 331–399.

Chen, W.F. and Rosenfarb, J.L., 1973. Limit analysis solutions of earth pressure problems. Soils Found., 13(4): 45–60.

Conforth, D.H., 1964. Some experiments on the influence of strain conditions on the strength of sand. Geotechnique, 14(2): 143–167.

Davis, E.H., 1968. Theories of plasticity and the failure of soil masses. In: I.K. Lee (Editor) Soil Mechanics: Selected Topics. Butterworth & Co., U.K., pp. 341–380.

Finn, W.D., 1967. Applications of limit analysis in soil mechanics. Proc. J. Soil Mech. Found. Div., ASCE, 93(SM5): 101–120.

Habibagahi, K. and Ghahramani, A., 1977. Zero extension theory of earth pressure. J. Geotech. Div., ASCE, 105(GT7): 881–896.

Hettiaratchi, R.P. and Reece, A.R., 1975. Boundary wedges in two-dimensional passive soil failure. Geotechnique, 25(2): 197–220.

Horne, M.R., 1969. The behavior of an assembly of rotund, rigid, cohesionless particles, III. Proc. R. Soc. London, Ser. A, 310: 21–34.

James, R.G. and Bransby, P.L., 1970. Experimental and theoretical investigations of a passive earth pressure problem, Geotechnique, 20(1): 17–37.

Kerisel, J., 1972. The language of models in soil mechanics (translated). Proc. 5th European Conf. on Soil Mech. and Found. Eng., Madrid, Vol. 2, pp. 3–30.

Lee, I.K. and Herington, J.R., 1972. A theoretical study of the pressures acting on a rigid wall by a sloping earth or rockfill. Geotechnique 22(1): 1–26.

Rowe, P.W., 1962. The stress-dilatancy relation for static equilibrium of an assembly of particles in contact. Proc. R. Soc. London, Ser. A, 269: 500–527.

Rowe, P.W., 1969a. The relation between the shear strength of sands in triaxial compression, plane strain, and direct shear. Geotechnique, 19(1): 75–86.

Rowe, P.W., 1969b. Progressive failure and strength of a sand mass. Proc. 7th Int. Conf. on Soil Mech. and Found. Eng., Mexico, Vol. 1, pp. 34–349.

Rowe, P.W. and Peaker, K., 1965. Passive earth pressure measurements. Geotechnique, 15(1): 57–78.

Scott, R.F., 1963. Principles of Soil Mechanics. Addison-Wesley, Reading, MA, 523 pp.

Sokolovskii, V.V., 1965. Static of Granular Media. Pergamon Press, New York, NY, 232 pp.

Terzaghi, K., 1943. Theoretical Soil Mechanics. John Wiley & Sons, New York, NY, 510 pp.

Tschebotarioff, G.P. and Johnson, S.C., 1953. The Effects of Retaining Boundaries on the Passive Resistance of Sand. Princeton University, Princeton, NJ.

Chapter 5

RIGID RETAINING WALLS SUBJECTED TO EARTHQUAKE FORCES*

5.1 Introduction

Although seldom reported and documented, numerous failures of rigid retaining walls in areas of intensive seismic activity have been attributed to earthquake effects.

Earthquake can endanger the stability of a soil–wall system by either increasing the driving forces acting on the wall or by reducing the resistance of the backfill and/or the foundation soils. For most moderate earthquakes in which the seismic acceleration is no more than 0.3 g, the mechanical properties of most soils will probably not change considerably (Okamoto, 1956). It can be practically assumed that there is no strength reduction in the foundation soils that controls the movement of the wall and in the backfill that influences the magnitude of lateral earth pressures, unless that the soil is cohesionless, not very permeable, and submerged under water. Hence, the assessment of seismic lateral earth pressures or changes in lateral earth pressures as the result of an earthquake is of more practical significance in most aseismic designs of retaining walls.

Since the earthquake motion is of an oscillatory nature, dynamic analysis of lateral earth pressures is certainly more realistic. However, dynamic analysis involves many uncertainties, e.g. the extent of soil mass effectively participating in vibrations, that are not yet wholly understood. Furthermore, providing the necessary information for a dynamic analysis and performing such an analysis are relatively expensive. Quasi-static analysis using the seismic coefficient concept is therefore of greater practical value in many cases, although the assessment of the seismic coefficients still relies highly on past experience.

The well-known Mononobe-Okabe analysis of seismic lateral earth pressures proposed by Mononobe and Matsuo (1929) and Okabe (1926) is generally adopted in current practice for aseismic design of retaining walls. The analysis is a direct modification of the Coulomb wedge analysis. In the analysis, the earthquake effects are replaced by a quasi-static inertia force whose magnitude is computed on the basis of the *seismic coefficient concept.*

---

* This chapter is based on the Ph.D. thesis by M.F. Chang (1981) and the paper by Chang and Chen (1982).

As in the Coulomb analysis, the failure surface is assumed planar in the Mononobe-Okabe method, regardless of the fact that the most critical sliding surface may be curved. Similar to Coulomb's, the Mononobe-Okabe analysis may underestimate the active earth pressure and overestimate the passive earth pressure. In the passive earth pressure case in which the most critical sliding surface is usually curved, the overestimation may be very serious, especially when the soil – wall interface is rough and the backfill surface is steeply sloped.

The Mononobe-Okabe analysis has been further modified by Prakash and Saran (1966) for assessing seismic active earth pressure for walls retaining horizontal c-ϕ soils. Uniform surcharge and tension cracks at top of the back fill are included in their formulation. However, the seismic acceleration is assumed to act in the horizontal direction and the failure surface is assumed planar as in the Coulomb or Mononobe-Okabe analysis.

In this chapter, the upper-bound method of limit analysis applied previously to lateral earth pressure calculations is extended to include the earthquake effects. Translational wall movement and log-sandwich mechanism of failure as suggested by Chen and Rosenfarb (1973) are assumed in the formulation. Quasi-static representation of earthquake effects using the seismic coefficient concept is adopted. The direction of seismic acceleration is taken as arbitrary and the most critical direction is found by iteration.

Earthquakes have unfavorable effects of increasing active and decreasing passive lateral earth pressures. To investigate how the lateral earth pressures are affected, extensive numerical results based on the limit analysis method reported by Chang and Chen (1982) are presented in dimensionless forms. For the active earth pressure case, the coefficient of seismic active pressure, K_{AE}, is adopted. For the passive earth pressure case, the coefficient of seismic passive earth pressure, K_{PE}, is used.

In order to see the validity of the limit analysis method, some K_{AE}-values and K_{PE}-values for various soil – wall conditions and seismic accelerations are calculated and compared with solutions by the well-known Mononobe-Okabe analysis. The difference between them is discussed.

Some parametric studies have been conducted to investigate the effects of the parameters involved in the analysis of the calculated K_{AE}- and K_{PE}-values. The variations of K_{AE}- and K_{PE}-values with the ϕ-parameter for different levels of earthquake, or for different seismic coefficients, are presented. The increase in the K_{AE}-value and the decrease in the K_{PE}-value as the result of an earthquake is noted. The effect of the angle of wall friction on the K_{AE}- and K_{PE}-values is also given. The influence of the geometrical factors on the K_{AE}- and K_{PE}-values is mentioned. The effect of the direction of seismic acceleration on the results is carefully discussed.

Afterwards, the effects of possible presence of uniform surcharge and cohesion in the backfill on the K_{AE}-values and the K_{PE}-values, as well as the effect of seismic

forces on the most critical sliding surface are carefully studied and discussed. Their importance in geotechnical engineering is also described.

Finally, the earth pressure tables that provide both static and seismic active and passive earth pressures are presented in terms of dimensionless coefficients (Chang, 1981).

5.2 General considerations

In the theoretical formulation for seismic lateral earth pressure analyses, the upper bound limit analysis method is adopted. A general soil – wall system with translational wall movement and a ϕ-spiral log-sandwich mechanism of failure proposed by Chen and Rosenfarb (1973), as shown in Figs. 5.1 and 5.2 are assumed.

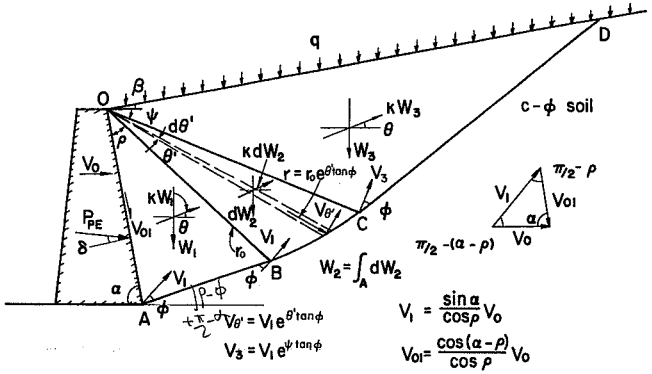

Fig. 5.1. Log-sandwich mechanism for seismic passive earth pressure analysis.

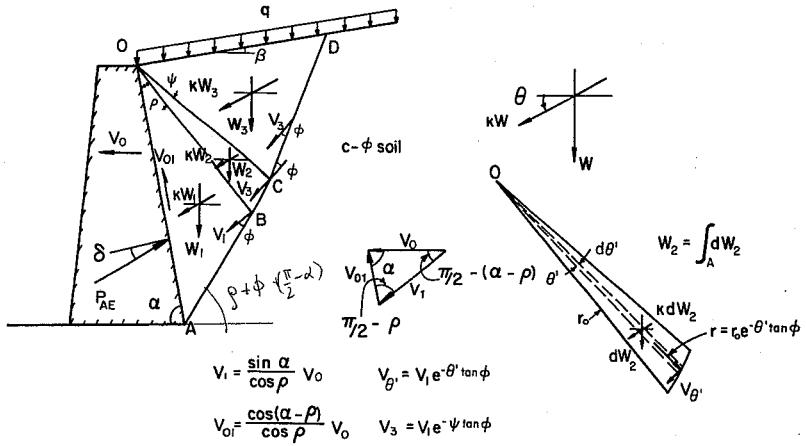

Fig. 5.2. Log-sandwich mechanism for seismic active earth pressure analysis.

The backfill material is assumed to possess some cohesion ($c > 0$). A uniform surcharge q is assumed to act on the surface of the backfill sloped at an angle β. The soil – wall interface is assumed inclined with its repose angle equal to α.

An earthquake has two possible effects on a soil – wall system. One is to increase the driving force. The other is to decrease the shearing resistance of the soil. The reduction in the shearing resistance of a soil during an earthquake is in effect only when the magnitude of the earthquake exceeds a certain limit and the ground conditions are favorable for such a reduction. The evaluation of such a reduction requires considerable knowledge in earthquake engineering and soil dynamics.

Research conducted by Okamoto (1956) indicated that when the average ground acceleration is larger than 0.3 g, there is a considerable reduction in strength for most soils. However, he claimed that in many cases, the ground acceleration is less than 0.3 g and the mechanical properties of most soils do not change significantly in these cases. In this chapter, only the increase in driving force is to be considered. The shear strength of the soil is assumed unaffected as the result of the seismic loading.

In the quasi-static analysis of seismic lateral earth pressures, a constant seismic coefficient, k, is assumed for the entire soil mass involved. A seismic force, which is equal to k times the weight of a soil mass, is assumed to act at the center of gravity of the sliding soil mass. The seismic force is assumed to act in a direction at an angle θ from the horizontal as shown in Figs. 5.1 and 5.2. Quite often, the direction of the seismic acceleration may be essentially horizontal. In some situations, however, the vertical component can be very large, for example, at locations near the epicenter of an earthquake. In general, the relative magnitude of the horizontal and vertical acceleration components varies from one case to another. A general direction of the seismic force is therefore assumed in the present formulation.

In case that the magnitudes of the horizontal and vertical seismic coefficients, k_h and k_v, respectively, are known for a given earthquake, the direction $\theta = \tan^{-1}(k_v/k_h)$ is then fixed. The seismic lateral earth pressure due to that particular earthquake can then be evaluated. In most analysis for design purposes, however, θ is generally unknown. The θ-value should be optimized to give the most critical condition.

5.3 Seismic passive earth pressure analysis

In the passive case, the decrease in the passive earth pressure as the result of an earthquake is of major concern. In this case, the possible critical direction of the seismic force, kW (k = resultant seismic coefficient) is pointing away from the wall, as shown in Fig. 5.1. Herein, as in the lateral earth pressure analyses for the static cases, Chen and Rosenfarb (1973), the seismic passive earth pressure can be easily derived by considering the equilibrium of external work and internal energy dissipation.

5.3.1 Calculations of incremental external work

The incremental external work due to an external force is the external force multiplied by the corresponding incremental displacement or velocity. The incremental external work due to self-weight in a region is the vertical component of the velocity in that region multiplied by the weight of the region. The seismic force which is assumed constant in each region, can be divided into a vertical component and a horizontal component. The incremental external work contributed by this force in a region can be obtained by the muliplication of the force components and the corresponding velocity components in that region. They should be added to those due to self-weight.

In the following derivatives, the variables involved are defined as the following:

γ = unit weight of the backfill material
ϕ = angle of internal friction of the backfill material
δ = angle of soil – wall interface friction
k = seismic coefficient
θ = inclination of the seismic coefficient with the horizontal
H = vertical height of wall.

All the others such as the geometrical factors, α, β, ϱ, ψ, θ', and the incremental displacements or velocities, v_0, v_1, v_3, $v_{\theta'}$ etc. are as defined in Figs. 5.1 and 5.2.

In zone OAB, we have:

$$\Delta W_{OAB} = -(W_1 - kW_1 \sin\theta)\, v_{1y} + kW_1 \cos\theta\, v_{1x}$$

$$= -\frac{\gamma H^2}{2} \frac{\cos(\varrho - \phi)\tan\varrho}{\sin\alpha \cos\phi} \Big[(1 - k\sin\theta)\cos(\alpha - \varrho) - k\cos\theta \sin(\alpha - \varrho)\Big] v_0 \tag{5.1}$$

Note that Eq. (5.1) is similar to Eq. (4.15) except that $k = 0$, $v_w = 0$, and $\xi = \phi$. In Zone OBC, we have:

$$\Delta W_{OBC} = \int_A [-(dW_2 - k\, dW_2 \sin\theta) v_{\theta' y} + k\, dW_2 \cos\theta\, v_{\theta' x}]\, dA$$

$$= -\frac{\gamma H^2}{2} \frac{\cos^2(\varrho - \phi)}{(1 + a^2)\sin\alpha \cos^2\phi \cos\varrho} \Big[(1 - k\sin\theta)[\cos(\alpha - \varrho) \{e^{a\psi}(a\cos\psi + \sin\psi) - a\} + \sin(\alpha - \varrho)\{e^{a\psi}(a\sin\psi - \cos\psi) + 1\}]$$

$$- k\cos\theta [\sin(\alpha - \varrho)\{e^{a\psi}(a\cos\psi + \sin\psi) - a\} - \cos(\alpha - \varrho)\{e^{a\psi}(a\sin\psi - \cos\psi) + 1\}]\Big] v_0 \tag{5.2}$$

where $a = 3\tan\phi$.

In Zone OCD, we have:

$$\Delta W_{OCD} = -(W_3 - kW_3\sin\theta)\,v_{3y} + kW_3\cos\theta\,v_{3x} - q\,(OD)\,(1 - k\sin\theta)\,v_{3y} - q\,(OD)\,k\cos\theta\,v_{3x}$$

$$= -\left[\frac{\gamma H^2}{2}\frac{\cos(\varrho - \phi)\,e^{3\psi\tan\phi}\sin(\alpha + \beta - \varrho - \psi)}{\sin\alpha\cos\phi} + qH\,e^{2\psi\tan\phi}\right]$$

$$\frac{\cos(\varrho - \phi)\,[(1 - k\sin\theta)\cos(\alpha - \varrho - \psi) - k\cos\theta\,\sin(\alpha - \varrho - \psi)]}{\cos\varrho\cos(\alpha + \beta + \phi - \varrho - \psi)}\,v_0 \qquad (5.3)$$

Due to the seismic passive earth pressure P_{PE}, using Eq. (4.18), we have:

$$\Delta W_{P_{PE}} = P_{PE}\sin(\alpha + \delta)v_0 \qquad (5.4)$$

The total incremental external work is the summation of these four parts of contributions, Eqs. (5.1) to (5.4). That is:

$$\Sigma\,[\Delta W]_{ext} = \Delta W_{OAB} + \Delta W_{OBC} + \Delta W_{OCD} + \Delta W_{P_{PE}} \qquad (5.5)$$

5.3.2 Calculations of incremental internal energy dissipation

According to Finn (1967) or Chen (1975), the incremental energy dissipation per unit length along a velocity discontinuity, or a narrow transition zone, can be expressed as:

$$\Delta D_L = c\,\Delta v\cos\phi \qquad (5.6)$$

Where Δv is the incremental displacement or velocity which makes an angle ϕ with the velocity discontinuity according to the associated flow rule of perfect plasticity, and c is the cohesion parameter. On an idealized soil – wall interface, where adhesion and pure friction present, the following equation, which is modified from Eq. (5.6) can be adopted:

$$\Delta D_L = s_f\,\Delta v_L \qquad (5.7)$$

where s_f is cohesion parameter, c, adhesion parameter, c_a, or pure friction component of a unit interface force, and Δv_L is the tangential component of the incremental displacement along the velocity discontinuity.

With this background, the incremental energy dissipation along a velocity discontinuity is simply ΔD_L multiplied by the length of the discontinuity or the total frictional force multiplied by the incremental displacement for the pure friction energy dissipation along the soil – wall interface. It should also be noted that for the case that there is a radial shear zone, such as zone OBC in Fig. 5.1, the energy dissipation in the radial shear zone is the same as that along the spiral arc BC (Chen, 1975). It is noted that the internal dissipation is totally independent of the seismic coefficient.

Along OA, there is:

$$\Delta D_{OA} = P_{PE}\sin\delta\,v_{01} + c_a\,(OA)\,v_{01} = \left(P_{PE}\sin\delta + c_a\frac{H}{\sin\alpha}\right)\frac{\cos(\alpha - \varrho)}{\cos\varrho}\,v_0 \qquad (5.8)$$

Along AB, there is:

$$\Delta D_{AB} = c\,(AB)\,v_1\cos\phi = c\,H\tan\varrho\,v_0 \qquad (5.9)$$

Along BC, there is:

$$\Delta D_{BC} = \int_L [c\,v_{\theta'}\cos\phi]\,dL = \tfrac{1}{2}\frac{c\,H\cos(\varrho - \phi)\,(e^{2\psi\tan\phi} - 1)}{\sin\phi\cos\varrho}\,v_0 \qquad (5.10)$$

Along CD, there is:

$$\Delta D_{CD} = c\,(CD)\,v_3\cos\phi = \frac{c\,H\cos(\varrho - \phi)\sin(\alpha + \beta - \varrho - \psi)\,e^{2\psi\tan\phi}}{\cos\varrho\cos(\alpha + \beta + \phi - \varrho - \psi)}\,v_0 \qquad (5.11)$$

From Zone OBC, we have:

$$\Delta D_{OBC} = \Delta D_{BC} = \frac{c\,H\cos(\varrho - \phi)\,(e^{2\psi\tan\phi} - 1)}{2\sin\phi\cos\varrho}\,v_0 \qquad (5.12)$$

The total incremental energy dissipation is the summation of the five parts given above, Eqs. (5.8) to (5.12). That is:

$$\Sigma[\Delta D] = \Delta D_{OA} + \Delta D_{AB} + \Delta D_{BC} + \Delta D_{CD} + \Delta D_{OBC} \qquad (5.13)$$

By equating $\Sigma[W]_{ext}$ in Eq. (5.5) to $\Sigma[\Delta D]$ in Eq. (5.13), we have:

$$P_{PE} = \frac{\gamma H^2}{2} N_{P\gamma} + qH\, N_{Pq} + cH\, N_{Pc} \tag{5.14}$$

where $N_{P\gamma}$, N_{Pq} and N_{Pc} are passive earth pressure factors. They are given as:

$$\begin{aligned} N_{P\gamma} = {} & \frac{\cos(\varrho - \phi)}{\sin^2\alpha \cos(\varrho + \delta)\cos\phi}\Bigg(\sin\varrho\Big[(1 - k\sin\theta)\cos(\alpha - \varrho) - k\cos\theta \\ & \sin(\alpha - \varrho)\Big] + \frac{\cos(\varrho - \phi)}{(1 + a^2)\cos\phi}\Big[\{e^{a\psi}(a\cos\psi + \sin\psi) - a\}\{(1 - k\sin\theta) \\ & \cos(\alpha - \varrho) - k\cos\theta\sin(\alpha - \varrho)\} + \{e^{a\psi}(a\sin\psi - \cos\psi) + 1\} \\ & \{(1 - k\sin\theta)\sin(\alpha - \varrho) + k\cos\theta\cos(\alpha - \varrho)\}\Big] \\ & + \frac{\cos(\varrho - \phi)\sin(\alpha + \beta - \varrho - \psi)e^{a\psi}}{\cos(\alpha + \beta + \phi - \varrho - \psi)}\Big[(1 - k\sin\theta) \\ & \cos(\alpha - \varrho - \psi) - k\cos\theta\sin(\alpha - \varrho - \psi)\Big]\Bigg) \end{aligned} \tag{5.15}$$

where $a = 3\tan\phi$.

$$N_{Pq} = \frac{\Big[\cos(\varrho - \phi)\, e^{2\psi\tan\phi}\,[(1 - k\sin\theta)\cos(\alpha - \varrho - \psi) - k\cos\theta\sin(\alpha - \varrho - \psi)]\Big]}{\cos(\alpha + \beta + \phi - \varrho - \psi)\sin\alpha\cos(\varrho + \delta)} \tag{5.16}$$

$$\begin{aligned} N_{Pc} = {} & \frac{1}{\sin\alpha\cos(\varrho + \delta)}\Big[\frac{\lambda\cos(\alpha - \varrho)}{\sin\alpha} + \sin\varrho \\ & + \frac{\cos(\varrho - \phi)\sin(\alpha + \beta - \varrho - \psi)e^{2\psi\tan\phi}}{\cos(\alpha + \beta + \phi - \varrho - \psi)} \\ & + \frac{\cos(\varrho - \phi)\,(e^{2\psi\tan\phi} - 1)}{\sin\phi}\Big] \end{aligned} \tag{5.17}$$

where $\lambda = c_a/c$.

The seismic passive earth pressure can also be expressed in terms of an 'equivalent' coefficient of seismic passive earth pressure, K_{PE}, as:

$$P_{PE} = \tfrac{1}{2}\,\gamma\, H^2\, K_{PE} \tag{5.18}$$

in which

$$K_{PE} = N_{P\gamma} + \frac{2q}{\gamma H} N_{Pq} + \frac{2c}{\gamma H} N_{Pc} \tag{5.19}$$

The most critical K_{PE}-value can be obtained by minimization with respect to ϱ and ψ angles in Fig. 5.1. The most critical failure surface is then defined by the ϱ and ψ which give minimum K_{PE}.

5.4 Seismic active earth pressure analysis

In the active case, an increase in the active earth pressure as the result of earthquake is of major concern. The possible critical direction of a seismic acceleration is therefore pointing toward the wall, as assumed in Fig. 5.2. The θ-value is considered positive when the seismic force has a downward vertical component. This is different from that assumed in the passive case, in which the θ-angle is positive when the seismic force has an upward component.

Similar to the formulation for the seismic passive earth pressure, the seismic active earth pressure can be derived as:

$$P_{AE} = \frac{\gamma H^2}{2} N_{A\gamma} + q\, H\, N_{Aq} + c\, H\, N_{Ac} \tag{5.20}$$

where $N_{A\gamma}$, N_{Aq}, and N_{Ac} are active earth pressure factors. They are given as:

$$\begin{aligned} N_{A\gamma} = {} & \frac{\cos(\varrho + \phi)}{\sin^2\alpha\cos(\varrho - \delta)\cos\phi}\Bigg(\sin\varrho[(1 + k\sin\theta)\cos(\alpha - \varrho) \\ & + k\cos\theta\sin(\alpha - \varrho)] + \frac{\cos(\varrho + \phi)}{(1 + a^2)\cos\phi}\Big[\{e^{-a\psi}(-a\cos\psi + \sin\psi) + a\} \\ & \{(1 + k\sin\theta)\cos(\alpha - \varrho) + k\cos\theta\sin(\alpha - \varrho)\} \\ & + \{e^{-a\psi}(-a\sin\psi - \cos\psi) + 1\}\{(1 + k\sin\theta)\sin(\alpha - \varrho) \\ & - k\cos\theta\cos(\alpha - \varrho)\}\Big] + \frac{\cos(\varrho + \phi)\sin(\alpha + \beta - \varrho - \psi)\, e^{-a\psi}}{\cos(\alpha + \beta - \phi - \varrho - \psi)} \\ & \Big[(1 + k\sin\theta)\cos(\alpha - \varrho - \psi) + k\cos\theta\sin(\alpha - \varrho - \psi)\Big]\Bigg) \end{aligned} \tag{5.21}$$

where $a = 3\tan\phi$ is the same as in Eq. (5.15).

$$N_{Aq} = \frac{\cos(\varrho + \phi)\, e^{-2\psi\tan\phi}\,\Big[(1 + k\sin\theta)\cos(\alpha - \varrho - \psi) + k\cos\theta\sin(\alpha - \varrho - \psi)\Big]}{\cos(\alpha + \beta - \phi - \varrho - \psi)\sin\alpha\cos(\varrho - \delta)} \tag{5.22}$$

$$N_{Ac} = \frac{-1}{\sin\alpha \cos(\varrho - \delta)}\left[\frac{\lambda \cos(\alpha - \varrho)}{\sin\alpha} + \sin\varrho + \frac{\cos(\varrho + \phi)\sin(\alpha + \beta - \varrho - \psi)\, e^{-2\psi\tan\phi}}{\cos(\alpha + \beta - \phi - \varrho - \psi)} - \frac{\cos(\varrho + \phi)(e^{-2\psi\tan\phi} - 1)}{\sin\phi}\right] \quad (5.23)$$

where $\lambda = c_a/c$ is the same as in Eq. (5.17).

If expressed in terms of 'equivalent' coefficient of seismic active earth pressure, K_{AE}, Eq. (5.18) becomes:

$$P_{AE} = \tfrac{1}{2}\gamma H^2 K_{AE} \quad (5.24)$$

in which:

$$K_{AE} = N_{A\gamma} + \frac{2q}{\gamma H} N_{Aq} + \frac{2c}{\gamma H} N_{Ac} \quad (5.25)$$

The most critical K_{AE}-value can be obtained by maximization with respect to ϱ and ψ-angles in Fig. 5.2. The ϱ and ψ at which the K_{AE}-value is maximum determine the most critical sliding surface.

Two computer programs for assessing seismic lateral earth pressures have been developed based on Eqs. (5.14) to (5.25). Details of the program documentation can be found in the thesis by Chang (1981).

5.5 Numerical results and discussions

In the presentation of the results of seismic active and passive earth pressure analyses, dimensionless coefficients K_{AE} and K_{PE} are adopted.

As mentioned previously, the present limit analysis solutions are valid when there is no reduction in soil strength due to an earthquake. The results presented are meaningful generally only when the seismic acceleration $a \leq 0.3\ g$, since most soils will either liquify or seriously weaken if $a > 0.3\ g$ (Okamoto, 1956). It is only for purely theoretical interest that, in some cases, results are presented for seismic coefficients up to 0.4. However, only when $k \leq 0.3$ are the results recommended for practical use.

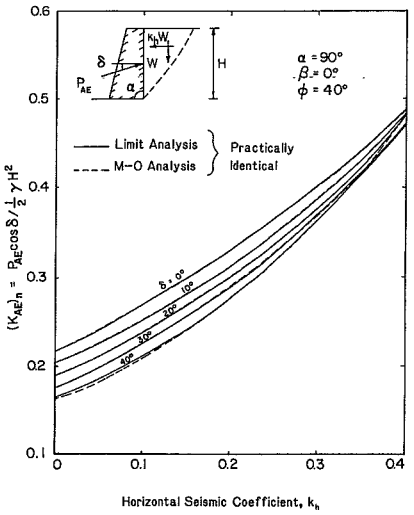

Fig. 5.3. Some $(K_{AE})_n$-values by limit analysis and Mononobe-Okabe analysis (vertical wall and horizontal backfill).

5.5.1 Comparison with Mononobe-Okabe solution

The Mononobe-Okabe analysis, which is an extension of the Coulomb's analysis, has been experimentally proved by Mononobe and Matsuo (1929) and Ishii et al. (1960) to be effective in assessing the seismic active earth pressure. It is generally adopted in the current aseismic design of rigid retaining walls. The Mononobe-Okabe solution is therefore practically acceptable at least for the active pressure case, although its applicability to the passive pressure case is somewhat in doubt.

Some results on seismic active and passive earth pressures as obtained by the present limit analysis method are compared with the Mononobe-Okabe (M-O) solutions. They are shown in Figs. 5.3 to 5.6.

For the active case, the K_{AE}-values obtained by the two methods are practically identical for most cases (Figs. 5.3 and 5.5). This is true even when the wall is inclined and the slope angle of the backfill is larger than zero, as shown in Fig. 5.5. The fact that the most critical, or potential sliding surface for the active case is practically planar, as shown in Fig. 5.7, is responsible for this consequence.

For the passive case, the most critical sliding surface is much different from a planar surface as is assumed in the M-O analysis (Fig. 5.8). The K_{PE}-values are seriously overestimated by the M-O method. They are, in most cases, higher than

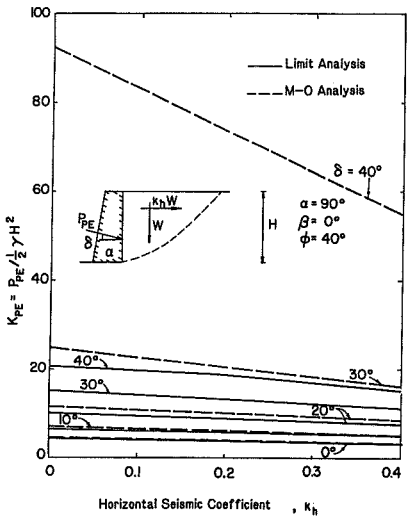

Fig. 5.4. Some K_{PE}-values by limit analysis and Mononobe-Okabe analysis (vertical wall and horizontal backfill).

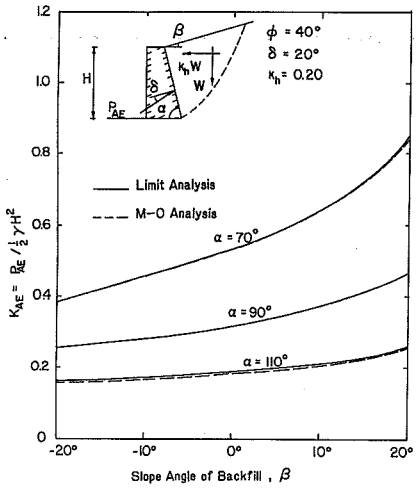

Fig. 5.5. Comparison of K_{AE}-values by limit analysis and Mononobe-Okabe analysis (general soil-wall system).

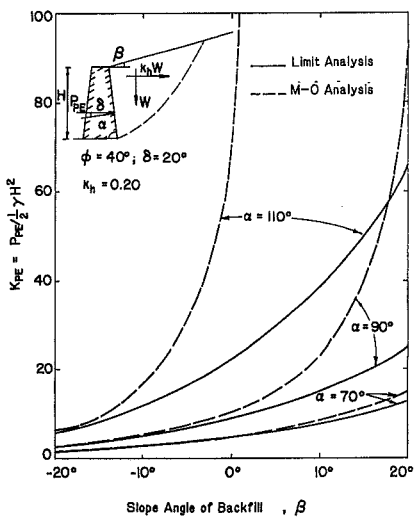

Fig. 5.6. Comparison of K_{PE}-values by limit analysis and Mononobe-Okabe analysis (general soil-wall system).

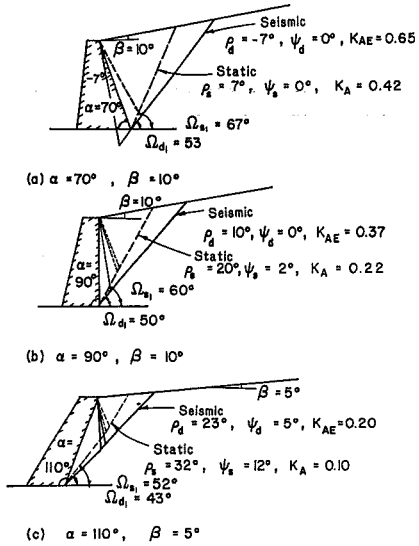

Fig. 5.7. Effect of seismic forces on failure mechanism in active pressure analysis ($\phi = 40°$, $\delta = 20°$, $k_h = 0.20$).

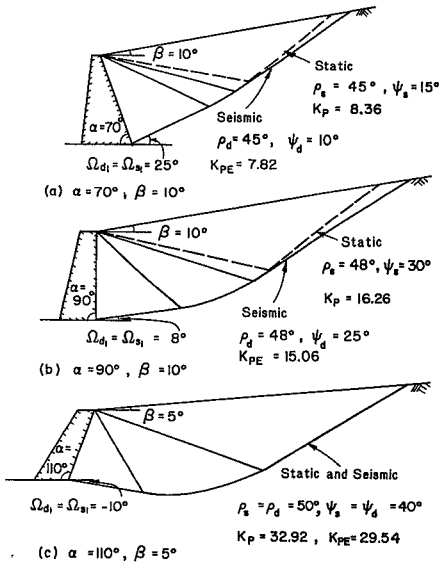

Fig. 5.8. Effect of seismic forces on failure mechanism in passive earth pressure analysis ($\phi = 40°$, $\delta = 20°$, $k_h = 0.20$).

those obtained by the limit analysis. This is especially the case when the wall is rough (Fig. 5.4) and the angle of wall repose is large (Fig. 5.6). For smooth walls, the potential sliding surface is practically planar and the two methods give almost identical results.

5.5.2 Some parametric studies

In the analysis of seismic lateral earth pressures on rigid walls retaining cohesionless soil, the parameters involved include the unit weight of soil, γ, the angle of internal friction, ϕ, the angle of soil – wall interface friction, δ, the slope angle of the backfill, β, the angle of wall repose, α, the height of the wall, H, the seismic coefficient, k, and the direction of the seismic acceleration, θ, if there is no uniform surcharge presented. Since the dimensionless lateral earth pressure coefficients K_{AE} and K_{PE} are generally selected to represent the lateral earth pressure, γ and H are irrelevant to the problem for the case of cohesionless backfill ($c = 0$) and zero surcharge ($q = 0$).

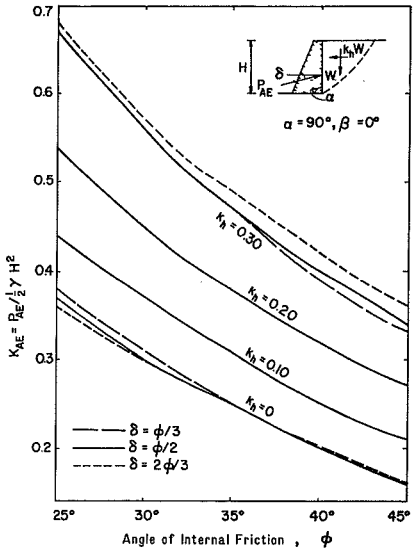

Fig. 5.9. Variation of K_{AE}-values with ϕ-angle for earthquakes of different level.

Parameters ϕ and k – internal friction angle and seismic coefficient

Figures 5.9 and 5.10 show the variation of K_{AE}- and K_{PE}-values with parameter ϕ for different horizontal seismic coefficients, k_h. The K_{AE}-value decreases as ϕ increases for a given k_h-value. On the contrary, the K_{PE}-value increases as ϕ increases for a given k_h-value. When there is an earthquake, the K_{AE}-value increases and the K_{PE}-value decreases. As the magnitude of an earthquake becomes larger, the K_{AE}-value increases and the K_{PE}-value decreases furthermore.

When Figs. 5.9 and 5.10 are replotted as shown in Figs. 5.11 and 5.12, where the increases of pressures due to an earthquake are normalized by the corresponding static pressures, the percentage of increase in the K_{AE}-value and decrease in the K_{PE}-value as the result of increase in the magnitude of an earthquake, or k_h-value, is much more clear. It is found that for the active case, the increase in K_{AE} is more obvious for denser soils with higher ϕ-values than for looser soils with lower ϕ-values. While, the decrease in K_{PE} is more obvious for looser soils than for denser soils in the passive case.

Parameter δ – interface friction

Figures 5.9 to 5.14 also show the parameter δ affects the K_{AE} and K_{PE} values. For the active case, the K_{AE}-value may become smaller or larger when the δ-value increases, depending on the ϕ-angle and the k_h-value as shown in Figs. 5.9 and

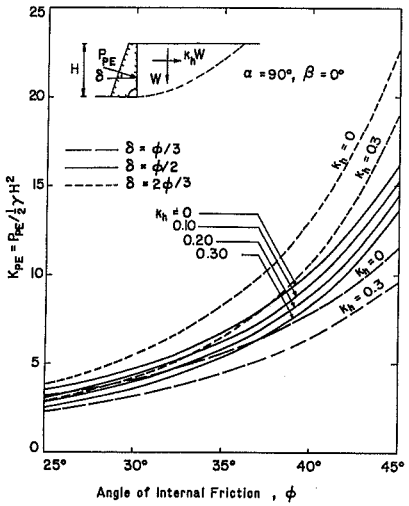

Fig. 5.10. Variation of K_{PE}-values with ϕ-angle for earthquakes of different level.

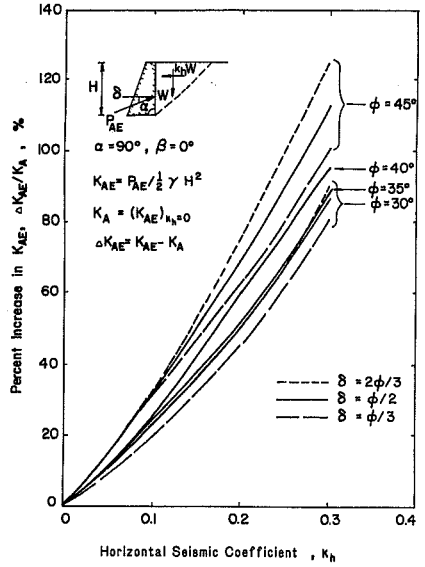

Fig. 5.11. Increase in K_{AE}-values as the result of seismic forces.

5.13. However, as shown in Fig. 5.11, when the δ-value is increased the percentage of change in K_{AE}-value as the result of an earthquake is seen also to increase. It is

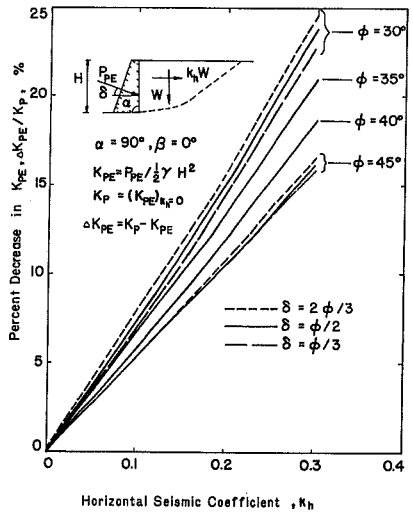

Fig. 5.12. Decrease in K_{PE}-values as the result of seismic forces.

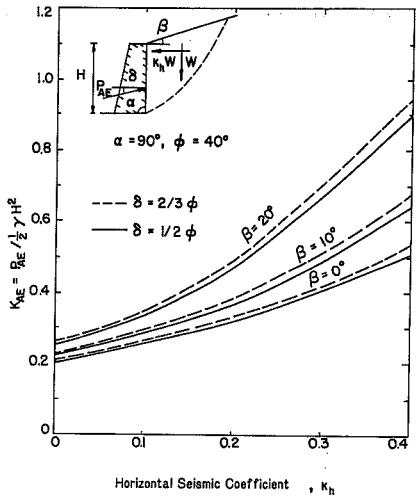

Fig. 5.13. Effect of slope angle on K_{AE}-values for $\delta = \frac{2}{3}\phi$ and $\delta = \phi/2$ cases.

therefore expected that, in most cases when $k_h > 0$, the K_{AE}-value is larger when δ is high than when δ is low. However, it should be noted that if the normal component $(K_{AE})_n$ is considered, the value decreases as δ increases, unless the k_h-value is very high (Fig. 5.3).

For the passive case, the K_{PE}-values increase as the δ-value increases, whether there is an earthquake or not. This is true even when the magnitude of earthquake is high. This is because that the percentages of decreases in the K_{PE}-value as the result of an earthquake, although larger for larger δ-values, are not much different for the cases of lower δ-values and for the cases of high δ-values as shown in Fig. 5.12. The general trend that K_{PE} increases with increasing δ values can also be seen clearly from Fig. 5.4 and Fig. 5.14.

More results on the effects of parameter δ on the K_{AE} and K_{PE} value are given in Figs. 5.15 and 5.18.

Parameters α and β – wall geometry and backfill shape

The geometry of the wall and backfill as reflected by the angles α and β in Fig. 5.1 or 5.2 have considerable effects on the magnitude of the lateral earth pressures. Figure 5.5 shows that for a given k_h-value and soil condition, the K_{AE}-value increases as the slope angle, β, increases and the angle of wall response, α, decreases. The β-effect is larger as the k_h-value becomes higher as shown in Fig. 5.13.

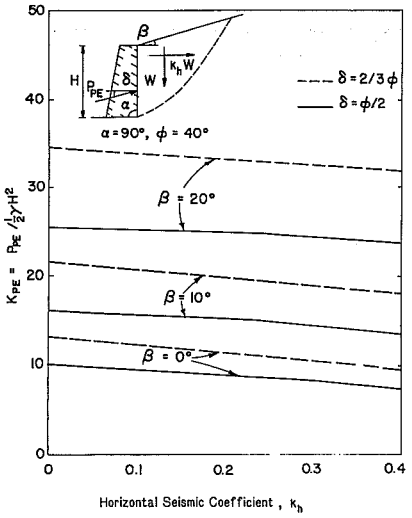

Fig. 5.14. Effect of slope angle on K_{PE}-values for $\delta = \phi/2$ and $\delta = \frac{2}{3}\phi$ cases.

For the passive case, the K_{PE}-value increases as the β-value and the α-angle increases as shown in Fig. 5.6. The β-effect is practically unaffected by the variation in k_h (Fig. 5.14).

Parameter θ – direction of earthquake force

As mentioned previously, the direction of the resultant seismic acceleration varies from one earthquake to another. Although Housner (1974) claimed that $k_v \simeq (\frac{1}{2} - \frac{2}{3})\, k_h$ for most earthquakes, current practice tends to assume that the seismic acceleration is essentially horizontal ($\theta = 0°$). The effect of this assumption on the results of analyses depends on how much the most critical direction differs from the horizontal one, how the actual seismic acceleration differs from the horizontal and what is the magnitude of the earthquake.

Figure 5.15 shows that for the active case, the K_{AE}-value obtained based on the assumption $\theta = 0°$ is not much different from the optimized K_{AE}-value obtained when the seismic acceleration assumes the most critical direction, i.e. $\theta = \theta_{cr}$. This is probably because the θ_{cr}-values are found to be essentially equal to zero, especially if the α-angle is high, as shown in the figures. It may therefore be concluded that

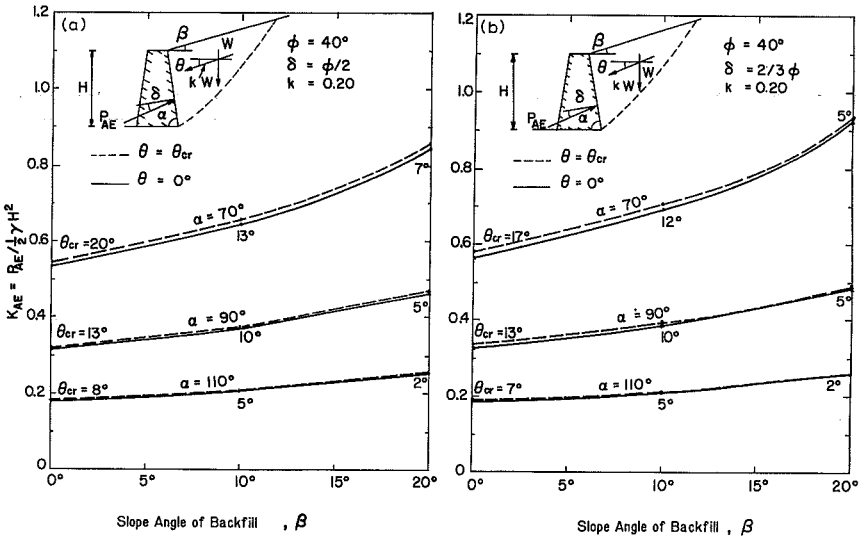

Fig. 5.15. Effect of direction of seismic acceleration on K_{AE}-values for general soil-wall system: (a) $\delta = \phi/2$; (b) $\delta = \frac{2}{3}\phi$.

in a given earthquake, even though its vertical seismic acceleration, $a_v = k_v g$, may be significant compared to its horizontal acceleration, $a_h = k_h g$, its effect on the K_{AE}-value may be neglected for practical applications.

The effect of k_v on the K_{AE}-value is also shown in Fig. 5.16. It can be seen that the K_{AE}-value is increased only in the order of 7% even when the k_v is as high as 2/3 k_h. For this reason, Seed and Whitman (1970) recommended that the influence of k_v can be neglected in practical designs of retaining walls.

Figure 5.16 shows also the following points. First, the effect of k_v is a maximum when k_h is around 0.2 and decreases as k_h further increases. Second, the k_v-effect is smaller when the backfill is sloped than when it is horizontal. Third, the

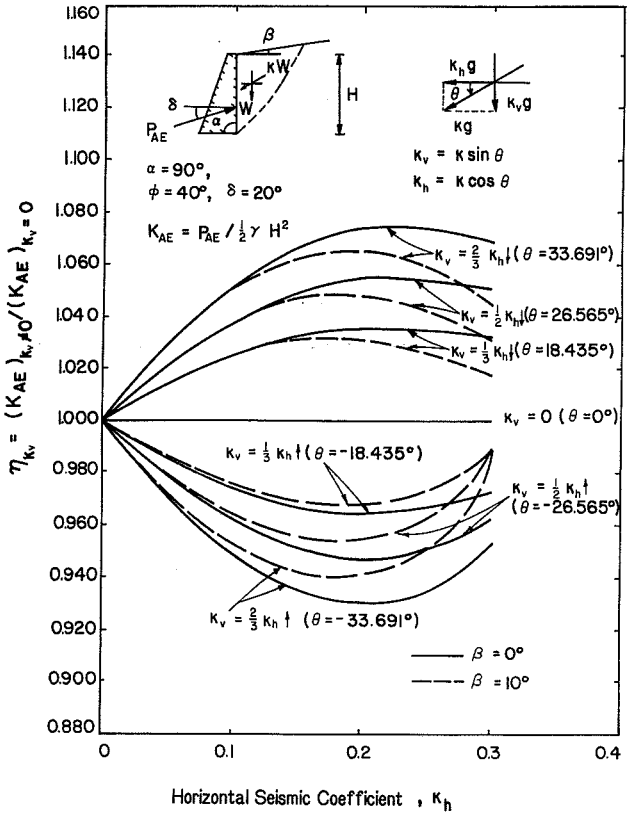

Fig. 5.16. Effect of vertical seismic acceleration component on normalized K_{AE}-values.

downward inertia force a_v ($k_v > 0$) tends to increase the K_{AE}-value while the upward action a_v ($k_v < 0$) tends to decrease the K_{AE}-value.

It is of interest to note that if the resultant seismic acceleration, $a = (a_v^2 + a_h^2)^{\frac{1}{2}}$, is considered and is assumed to act horizontally, the difference between the K_{AE}-value so obtained and that obtained by optimization with respect to $\theta = \tan^{-1}(k_v/k_h)$ will even have a less value than that shown in Fig. 5.16. This is due partly to the fact that the most critical surfaces are practically the same for both cases. Also, there is no change in the magnitude of the resultant acceleration.

Figure 5.17 shows how the normalized K_{AE}-value, and $\hat{\eta}_\theta$ vary with θ for an earthquake of different magnitude. Here $\hat{\eta}_\theta$ is defined as:

$$\hat{\eta}_\theta = \frac{(K_{AE})_{\theta \neq 0}}{(K_{AE})_{\theta = 0}} \tag{5.26}$$

The $\hat{\eta}_\theta$ has a unique maximum in the whole range of θ. It was found that as k increases, the $\hat{\eta}_\theta$-value becomes smaller. The difference between $(K_{AE})_{\theta \neq 0}$ and $(K_{AE})_{\theta = 0}$ becomes larger. However, the maximum $\hat{\eta}_\theta$-values, $(\hat{\eta}_\theta)_{cr}$, which are of primary interest, are not much different from each other. They are all very close to one. Also they all occur at nearly the same θ-angle for a given soil – wall system. In most cases, $(K_{AE})_{\theta = \theta_{cr}}$ can be taken as $(K_{AE})_{\theta=0}$.

For practical purposes, the vertical acceleration, a_v, can be neglected if the actual acceleration is nearly horizontal. Otherwise, the resultant acceleration can be used

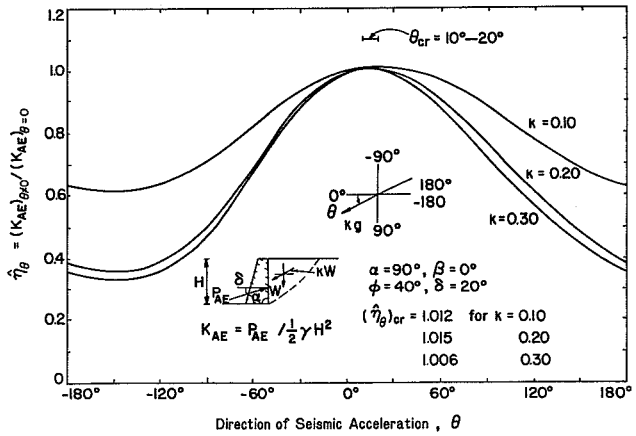

Fig. 5.17. Variation of normalized K_{AE}-values with direction of seismic acceleration for earthquakes of different magnitude.

and assumed to act horizontally ($\theta = 0$) without much sacrifice in the accuracy of the determination of K_{AE}-values.

For the passive case, the effect of the direction of seismic acceleration on the K_{PE}-values are partly shown in Figs. 5.18. Unlike the active case, the K_{PE}-value corresponding to the optimized θ-angle, θ_{cr}, is considerably smaller than that corresponding to $\theta = 0$. This is due to the fact that the θ_{cr}-values are much larger than zero in all the cases investigated. In fact, θ_{cr} is close to 90° when the β-value is high. In this case, the vertical acceleration, a_v, may play even a more important role than the horizontal component, a_h, does.

Figure 5.19 shows the effect of a_v on the K_{PE}-values. It is clear that the effect becomes larger as both the k_h and k_v values become higher. For the case of $k_h = 0.3$ and $k_v = \frac{2}{3} k_h$, the effect is in the order of 25%. The k_v-effect therefore cannot be simply neglected for the passive case.

Figure 5.19 also shows that the η'_{k_v}-value becomes smaller as β becomes larger, where the η'_{k_v} is defined as:

$$\eta'_{k_v} = \frac{(K_{PE})_{k_v \neq 0}}{(K_{PE})_{k_v = 0}} \tag{5.27}$$

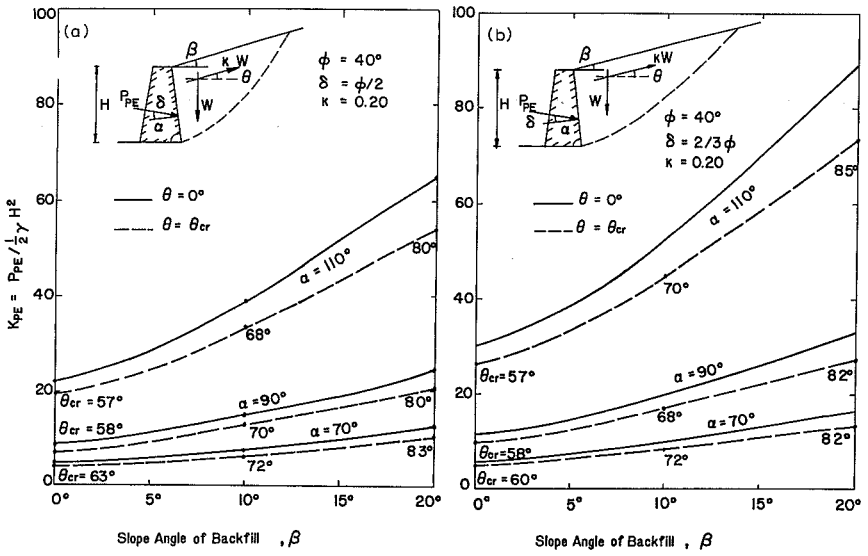

Fig. 5.18. Effect of direction of seismic acceleration on K_{PE}-values for general soil-wall systems: (a) $\delta = \phi/2$, (b) $\delta = \frac{2}{3}\phi$.

This is probably because, as β increases, the $(K_{PE})_{k_v = 0}$ increases in a faster rate than the $(K_{PE})_{k_v \neq 0}$ does, even though θ_{cr} becomes larger as those shown in Fig. 5.18.

Similar to the active case, if the resultant seismic acceleration is adopted and assumed to act horizontally, the difference between $(K_{PE})_{\theta = 0}$ and $(K_{PE})_{\theta = \theta_{cr}}$ becomes smaller. However, the difference is still too significant to be neglected in practice.

Figure 5.20 shows the variation of the normalized K_{PE}-value, and $\hat{\eta}'_\theta$ with θ for different levels of earthquake. Here $\hat{\eta}'_\theta$ is defined as:

$$\hat{\eta}'_\theta = \frac{(K_{PE})_{\theta \neq 0}}{(K_{PE})_{\theta = 0}} \tag{5.28}$$

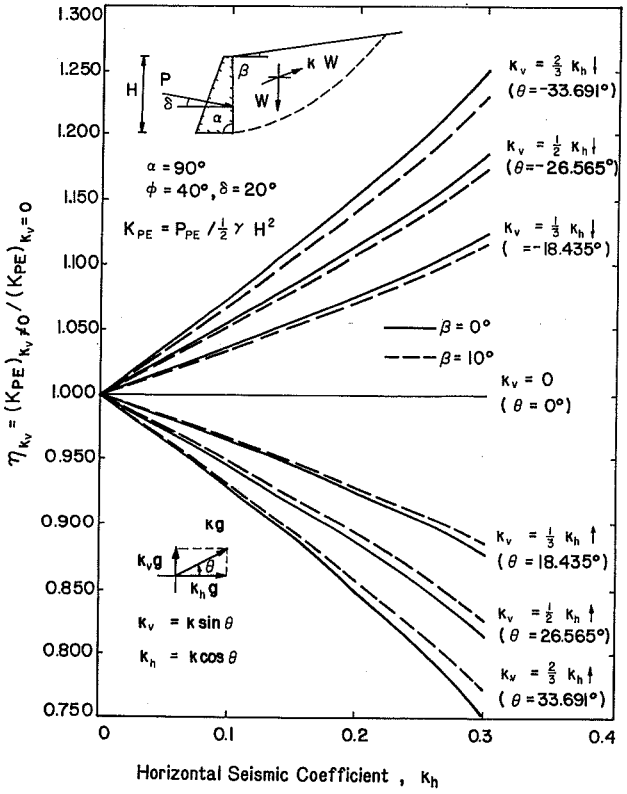

Fig. 5.19. Effect of vertical seismic acceleration component on normalized K_{PE}-values.

It is found that, similar to the active case, there are unique minimum $\hat{\eta}'_\theta$ values, $(\hat{\eta}'_\theta)_{cr}$ for different k-values for a given soil – wall system. They all occur at nearly the same θ-angle. However, the $(\hat{\eta}'_\theta)_{cr}$ values are quite different from one another and are all less than one. That is, in all cases, $(K_{PE})_{\theta = \theta_{cr}}$ is less than $(K_{PE})_{\theta = 0}$.

In actual practice, unless the seismic acceleration is nearly horizontal, the K_{PE}-value should be assessed by optimization with respect to θ. This is of great importance especially when the retaining structures of concern are located close to potential epicenters where the vertical component of the seismic acceleration may be larger than the horizontal component. If this fact is not taken into consideration, use of $(K_{PE})_{\theta = 0}$ will give unsafe designs.

It is noted from Figs. 5.15 and 5.18 that the θ_{cr}-value are almost unaffected by the change in δ-values for both the active and the passive cases.

5.5.3 Surcharge and cohesion effects

Quite often, a soil – wall system is subjected to a surcharge and the backfill may be cohesive. The presence of surcharge and/or cohesion may influence the lateral earth pressures considerably. It is therefore worthwhile to investigate how the lateral earth pressures are affected by the surcharge and the cohesion in the backfill.

We shall first check the surcharge effect in the active earth pressure case.

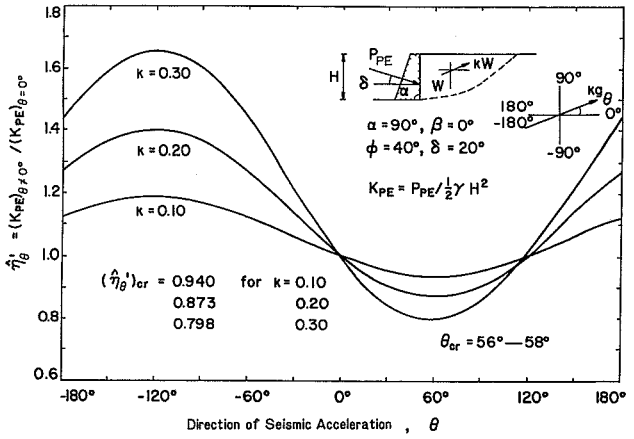

Fig. 5.20. Variation of normalized K_{PE}-values with direction of seismic acceleration for earthquakes of different magnitude.

Active case – surcharge effect

The K_{AE}-value for the case when there is a surcharge q, $(K_{AE})_{q \neq 0}$, is given by Eq. (5.25) as:

$$(K_{AE})_{q \neq 0} = \frac{(P_{AE})_{q \neq 0}}{\frac{1}{2}\gamma H^2} = \left[N_{A\gamma} + \frac{2q}{\gamma H} N_{Aq} \right]_{\varrho = \varrho_{cr},\ \psi = \psi_{cr}} \tag{5.29}$$

and

$$(K_{AE})_{q = 0} = [N_{A\gamma}]_{\varrho = \varrho_{cr},\ \psi = \psi_{cr}} \tag{5.30}$$

If $(K_{AE})_{q \neq 0}$ is normalized with respect to $(K_{AE})_{q = 0}$, we have:

$$\eta_q = \frac{[K_{AE}]_{q \neq 0}}{[K_{AE}]_{q = 0}} = \frac{\left[N_{A\gamma} + \frac{2q}{\gamma H} N_{Aq} \right]_{\varrho = \varrho_{cr},\ \psi = \psi_{cr}}}{[N_{A\gamma}]_{\varrho = \varrho_{cr},\ \psi = \psi_{cr}}}$$

$$= \left[1 + \frac{2q}{\gamma H} \frac{N_{Aq}}{N_{A\gamma}} \right]_{\varrho = \varrho_{cr},\ \psi = \psi_{cr}} \tag{5.31}$$

Note that if $N_{A\gamma}$ and N_{Aq} as given in Eqs. (5.21) and (5.22) are substituted into Eq. (5.31), the resulting equation for η_q is independent of δ, if we use the same critical sliding surface for both $N_{A\gamma}$ and N_{Aq} calculations. In general, η_q is a function of ϕ, α, β, k, and $q/\gamma H$.

The effect of surcharge on the normalized $(K_{AE})_{q \neq 0}$ value is shown in Fig. 5.21. In general, η_q increases linearly with $q/\gamma H$. The rate of increase is larger as α and β get higher.

Figure 5.22 shows that the η_q is totally independent of δ for the case ($\alpha = 90°$, $\beta = \phi/2$) investigated. The unique critical surface as found is responsible for this finding. The η_q-value, although it increases slightly as ϕ increases, can be considered as independent of the ϕ-angle for practical purposes.

Figure 5.23 indicates that the magnitude of an earthquake has no effect on the η_q for the particular case ($\alpha = 90°$, $\beta = 20°$, $\phi = 40°$, $\delta = 20°$) investigated. This is because that when the critical sliding surface is planar, $N_{Aq}/N_{A\gamma} = \sin\alpha/\sin(\alpha + \beta)$ and Eq. (5.31) becomes:

$$\eta_q = 1 + \frac{2q}{\gamma H} \frac{\sin\alpha}{\sin(\alpha + \beta)} \neq f(k_h) \tag{5.32}$$

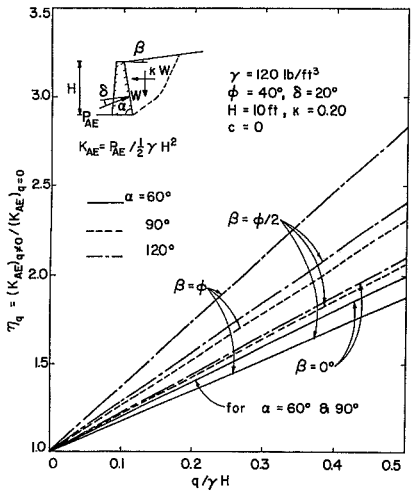

Fig. 5.21. Effect of surcharge on normalized K_{AE}-values for soil-wall systems of different geometry.

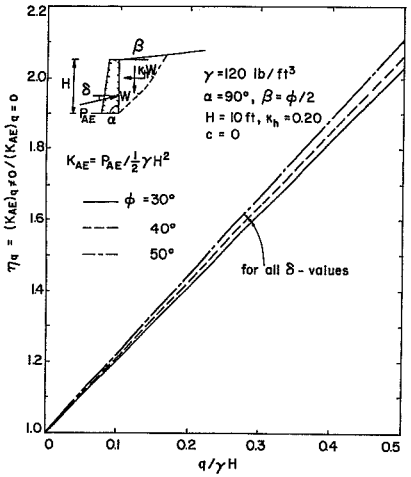

Fig. 5.22. Effect of surcharge on normalized K_{AE}-values for soils of different compaction and interfaces of different roughness.

In general, it may vary slightly with the k_h-value when the critical surface is not exactly planar.

Summarizing Fig. 5.21 through Fig. 5.23, it is interesting to note that η_q is essentially a function of α and β only. This is consistent with Eq. (5.32), since for the active earth pressure case, the most critical sliding surface is often almost planar.

We shall now check the cohesion effect in the active earth pressure case.

Active case – cohesion effect

From Eq. (5.25), the K_{AE}-value for the case when there is a cohesive c in the backfill, $(K_{AE})_{c \neq 0}$, can be expressed as:

$$(K_{AE})_{c \neq 0} = \left[N_{A\gamma} + \frac{2c}{\gamma H} N_{Ac} \right]_{\varrho = \varrho_{cr},\ \psi = \psi_{cr}} \tag{5.33}$$

and

$$(K_{AE})_{c = 0} = [N_{A\gamma}]_{\varrho = \varrho_{cr},\ \psi = \psi_{cr}} \tag{5.34}$$

The normalized $(K_{AE})_{c \neq 0}$-value, η_c, can be expressed as:

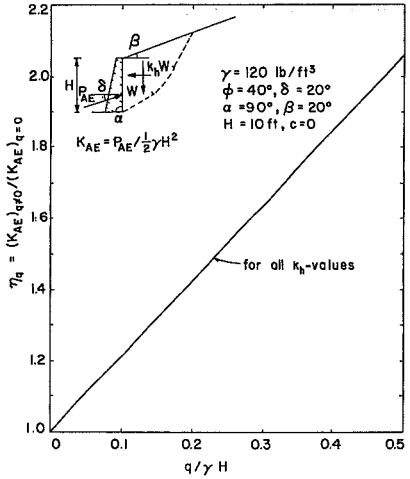

Fig. 5.23. Effect of surcharge on normalized K_{AE}-values for soil-wall systems subjected to earthquakes of different magnitude.

$$\eta_c = \frac{(K_{AE})_{c \neq 0}}{(K_{AE})_{c=0}} = \frac{\left[N_{A\gamma} + \dfrac{2c}{\gamma H} N_{Ac}\right]_{\varrho = \varrho_{cr},\ \psi = \psi_{cr}}}{[N_{A\gamma}]_{\varrho = \varrho_{cr},\ \psi = \psi_{cr}}}$$

$$\approx \left[1 + \frac{2c}{\gamma H} \frac{N_{Ac}}{N_{A\gamma}}\right]_{\varrho = \varrho_{cr},\ \psi = \psi_{cr}} \tag{5.35}$$

Note that N_{Ac} is independent of the seismic coefficient, k, as shown in Eq. (5.23). The λ-value in N_{Ac} can be taken as $\lambda = \cos \phi_{cv}$, if $\phi \geq \phi_{cv}$ or as $\lambda = \cos \phi$, if $\phi < \phi_{cv}$. A typical value of λ is 0.836. This corresponds to a ϕ-angle at critical state, $\phi_{cv} = 33.3°$, which is typical for most siliceous sands.

Figure 5.24 shows that η_c decreases as $c/\gamma H$ increases, since the cohesion has a negative effect on the active earth pressure. The rate of decrease in η_c becomes larger as α increases. However, as $\beta = \phi$, the cohesion effect is practically constant when $c/\gamma H \geq 0.10$. This is probably because as $\beta = \phi$, the ϕ-angle rather than the c-parameter predominantly controls the active earth pressure.

Figure 5.25 shows that η_c is essentially independent of δ and is slightly affected by the ϕ-angle. However, for practical purposes, the η_c-value can be treated as independent of both δ and ϕ.

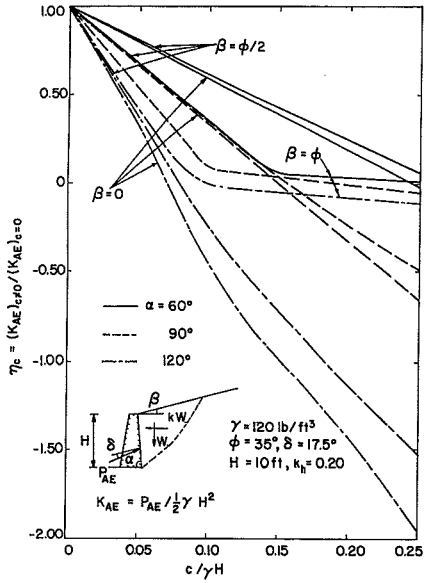

Fig. 5.24. Effect of cohesion on normalized K_{AE}-values for soil-wall systems of different geometry.

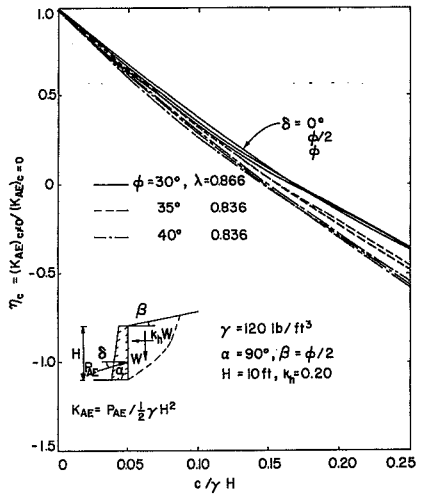

Fig. 5.25. Effect of cohesion on normalized K_{AE}-values for soils of different compaction and interfaces of different roughness.

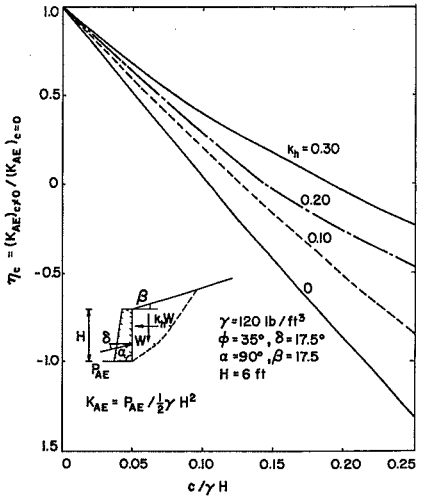

Fig. 5.26. Effect of cohesion on normalized K_{AE}-values for soil-wall systems subjected to earthquakes of different magnitude.

The η_c versus $c/\gamma H$ curves for different k_h-values as shown in Fig. 5.26 reflect that the η_c-value is seriously affected by the earthquake magnitude. This is because in Eq. (5.35), N_{Ac} is totally independent of k, while $N_{A\gamma}$ is dependent on k. It seems that the cohesion has a larger effect on the K_{AE}-value when there is no earthquake ($k = 0$) than when there is an earthquake ($k > 0$). The larger the earthquake is, the less the cohesion affects the active earth pressure for a given $c/\gamma H$ value.

In summary, the η_c-value can be considered as practically independent of the ϕ- and δ-angles only.

We shall now examine the surcharge effect in the passive earth pressure case.

Passive case – surcharge effect

Similar to the active case, the normalized $(K_{PE})_{q \neq 0}$ values, or η_q'-value, can be expressed as:

$$\eta_q' = \frac{(K_{PE})_{q \neq 0}}{(K_{PE})_{q = 0}} = \frac{\left[N_{P\gamma} + \dfrac{2q}{\gamma H} N_{Pq}\right]_{\varrho = \varrho_{cr},\ \psi = \psi_{cr}}}{[N_{P\gamma}]_{\varrho = \varrho_{cr},\ \psi = \psi_{cr}}} \tag{5.36}$$

In general η_q' is dependent on ϕ, α, β, k and $q/\gamma H$ as well as δ, since the most critical sliding surface is seldom the same for the cases $(K_{PE})_{q \neq 0}$ and $(K_{PE})_{q = 0}$ unique in the passive case.

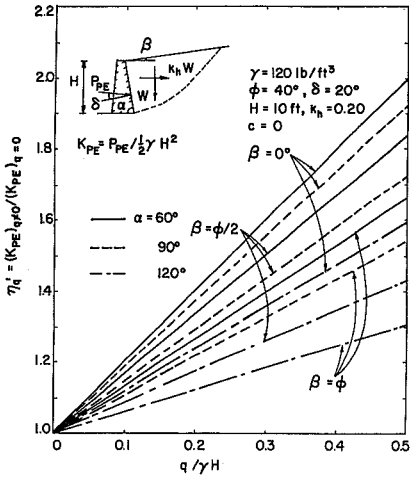

Fig. 5.27. Effect of surcharge on normalized K_{PE}-values for soil-wall systems of different geometry.

Figure 5.27 shows that η_q' increases linearly with $q/\gamma H$. The rate of increase is larger as α and β becomes smaller. This is contrary to the active case.

The effect of surcharge on the η_q'-values for soils of different compaction and interfaces of different roughness is shown in Fig. 5.28. It seems that the η_q'-value is dependent on both ϕ and δ. The rate of increase in η_q' with $q/\gamma H$, or the effect of surcharge on the η_q'-value, is larger as ϕ and δ get smaller. The surcharge therefore has larger effect on the K_{PE}-value for the case of looser soil and smaller δ-value than for the case of denser soil and larger δ-value.

Figure 5.29 shows that the k_h-value, or the magnitude of an earthquake, has little effect on the η_q'-value. This is because the most critical sliding surface, in contrast to the active case, is generally far from being planar. However, the difference in η_q' for different k_h-values is practically negligible.

Passive case – cohesion effect

Finally, for the passive case, the cohesion effect can be investigated by calculating the normalized $(K_{PE})_{c \neq 0}$ or η_c', for different soil – wall conditions and earthquake conditions. Note that, similar to the active case, η_c' can be expressed as:

$$\eta_c' = \frac{(K_{PE})_{c \neq 0}}{(K_{PE})_{c = 0}} = \frac{\left[N_{P\gamma} + \dfrac{2c}{\gamma H} N_{Pc}\right]_{\varrho = \varrho_{cr},\ \psi = \psi_{cr}}}{[N_{P\gamma}]_{\varrho = \varrho_{cr},\ \psi = \psi_{cr}}} \tag{5.37}$$

The effect of cohesion on the η_c'-values for different soil – wall conditions is shown in Figs. 5.30 and 5.31. It is obvious that the η_c'-value depends on the geometry of the wall and backfill, or the angles α and β. It also depends on the strength factors ϕ and δ. In general, the η_c'-value increases linearly as $c/\gamma H$ increases for a given soil – wall system. As α and β decrease, the η_c'-value increases. For given α and β values, the η_c'-value increases as ϕ and δ decrease. The cohesion effect is more obvious in the looser soil than in the denser soil.

Figures 5.32 shows the effect of cohesion on the η_c'-value for earthquake of different magnitude. It is clear that the η_c'-values, although affected by the k_h-value, can be considered as practically independent of the k_h-value, which is different from that for the active case.

5.5.4 Seismic effects on potential sliding surface

The seismic acceleration generated by earthquakes not only imposes extra loading to a soil mass but also shifts the sliding surface to less favorable positions. Consequently, in addition to the change in the lateral earth pressures, the most critical or potential sliding surface is also altered.

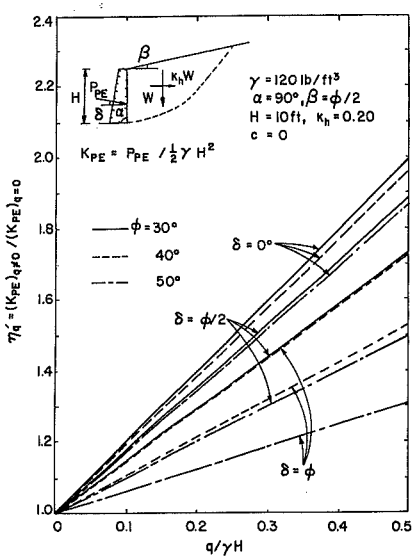

Fig. 5.28. Effect of surcharge on normalized K_{PE}-values for soils of different compaction and interfaces of different roughness.

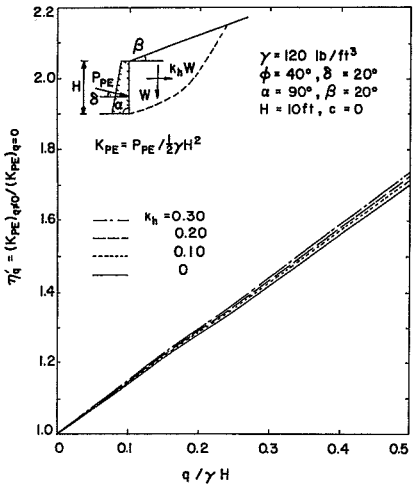

Fig. 5.29. Effect of surcharge on normalized K_{PE}-values for soil-wall systems subjected to earthquakes of different magnitude.

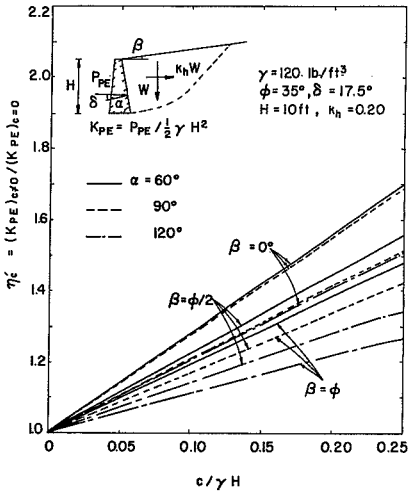

Fig. 5.30. Effect of cohesion on normalized K_{PE}-values for soil-wall systems of different geometry.

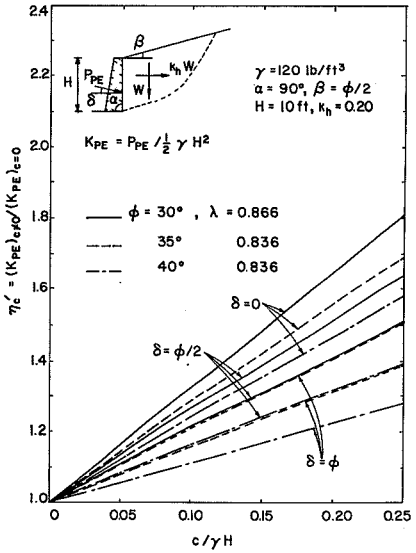

Fig. 5.31. Effect of cohesion on normalized K_{PE}-values for soils of different compaction and interfaces of different roughness.

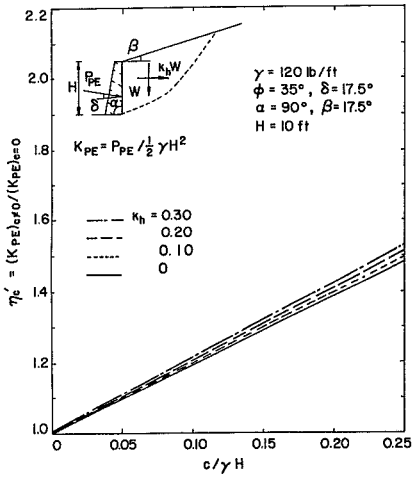

Fig. 5.32. Effect of cohesion on normalized K_{PE}-values for soil-wall systems subjected to earthquakes of different magnitude.

Figures 5.7 and 5.8 show some typical changes in the potential sliding surface as the result of an earthquake with $k = 0.20$. It is interesting to note that the potential sliding surface becomes more extended when earthquake presents, especially in the active case. This conforms with the experimental results of Murphy (1960). For the passive case, it seems that the change in the potential sliding surface is not as much as that in the active case, although it is also found more extended in the earthquake case. The change in the potential sliding surface as the result of earthquake has also been noted by Sabzevari and Ghahramani (1974).

The prediction of the potential sliding surface is of importance when it is necessary to back calculate strength parameters from field test or actual failures. It is also influential in some geotechnical designs, such as in the design of bulkhead anchorages and earth anchors. Although, as was pointed out by Chang and Chen (1982), the potential sliding surface as reflected by the limit analysis is not representative of the actual failure surface, the results as shown in Fig. 5.7, especially deserve special attention. In aseismatic design of most anchorage systems, not only the change in the lateral earth pressures has to be aware, but also the change in the potential sliding surface has to be carefully considered. The retaining structures have to be anchored well outside the potential sliding surface, which is more extended in the case of earthquake, for the safe design of these structures.

5.5.5 General remarks

The upper-bound technique of limit analysis of perfect plasticity is applied to determine the seismic lateral earth pressures in a quasi-static manner. Here, as with most limit equilibrium methods, the present analysis gives no information on the point of action of the resultant seismic lateral pressures. This point will be further discussed in the following chapter. The magnitude of the lateral pressures as calculated by the present method is, however, fairly reasonable for the case of translation wall movement.

5.6 Earth pressure tables for practical use

While earth pressure tables and charts suitable for the static design of retaining walls are generally available, tables or charts for seismic lateral earth pressures are scarce. Seismic active and passive earth pressures are required in a seismic design of retaining walls subjected to earthquake forces. Development of seismic earth pressure tables is of practical value for retaining wall design in earthquake environments.

The upper-bound limit analysis of active and passive earth pressures as developed in this chapter is used to generate earth pressure tables that provide both static and seismic active and passive earth pressures. The effect of earthquake forces is taken into account in a quasi-static manner using the seismic coefficient concept. Dimensionless coefficients of active and passive earth pressures are presented in the forthcoming.

To reduce the number of tables and charts, we generate this information under the following conditions:

1. The seismic acceleration acts in the horizontal direction ($\theta = 0°$).
2. There is no surcharge acting on the surface of the backfill ($q = 0$).
3. There is no cohesion in the backfill material ($c = 0$).

The coefficients of the generated active and passive earth pressures are obtained for the following cases:

1. ϕ-parameter, $\phi = 20°, 25°, 30°, 35°, 40°, 45°, 50°$.
2. Seismic coefficient (acts horizontally). $k = 0, 0.05, 0.10, 0.15, 0.20, 0.25, 0.30$.
3. Angle of wall repose, $\alpha = 60°, 75°, 90°, 105°, 120°$.
4. Slope of backfill (normalized with respect to ϕ). $\beta/\phi = 0, \frac{1}{6}, \frac{1}{3}, \frac{1}{2}, \frac{2}{3}, \frac{5}{6}, 1$.
5. Angle of wall friction (normalized with respect to ϕ). $\delta/\phi = 0, \frac{1}{3}, \frac{1}{2}, \frac{2}{3}, 1$.

The tables generated are listed in Appendix A developed originally by Chang (1981).

For the tables to be of practical value, procedures were developed for extending the present listed earth pressure coefficients to cases other than those specified before. They are given in the following subsections, following the work of Chang (1981).

5.6.1 Correction for direction of seismic acceleration

In general, the direction of the resultant seismic acceleration during a given earthquake is not necessarily horizontal. The seismic acceleration may assume any direction depending on the characteristic of an earthquake and the distance of the structure from the epicenter.

For this reason, it should be assumed that the seismic acceleration in an actual lateral pressure analysis for design purposes can act in any direction. The lateral earth pressures corresponding to the most critical direction of seismic acceleration are then used for actual design.

To develop a way of correlating the seismic active and passive earth pressure coefficients for the special case of horizontal acceleration ($\theta = 0$), $(K_{AE})_{\theta = 0}$ and $(K_{PE})_{\theta = 0}$, to those corresponding to the optimized acceleration direction ($\theta = \theta_{cr}$), $(K_{AE})_{\theta = \theta_{cr}}$ and $(K_{PE})_{\theta = \theta_{cr}}$, some sensitivity analyses were performed. The ratio of $(K_{AE})_{\theta = \theta_{cr}}$ to $(K_{AE})_{\theta = 0}$ is denoted as η_θ, and that of $(K_{PE})_{\theta = \theta_{cr}}$ to $(K_{PE})_{\theta = 0}$ as η_θ.

Some typical results of sensitivity analyses for the active earth pressure case are shown in Figs. 5.33 and 5.34. It is clear that the η_θ-value is sensitive not only to the geometrical factors α and β, but also to the strength factors ϕ and δ. Further, as pointed out previously, the η_θ-value is also a function of the seismic coefficient k. Development of simple correction factors for this case is therefore of great difficulty. Fortunately, the η_θ-value is generally in the order of no more than 1.015. In many cases, the η_θ-values are very close to unity. This is because the critical acceleration angle θ_{cr} does not deviate much from zero, as shown in Fig. 5.15. Furthermore, there is a general tendency that the η_θ-value increases slightly as α, β and δ decrease. For practical purposes it is recommended that no correction is required ($\eta_\theta = 1$) unless $\alpha < 90°$, $\beta \leq \phi/2$, and $\delta \leq \phi/2$, then $\eta_\theta = 1.01$ can be used (Fig. 5.33).

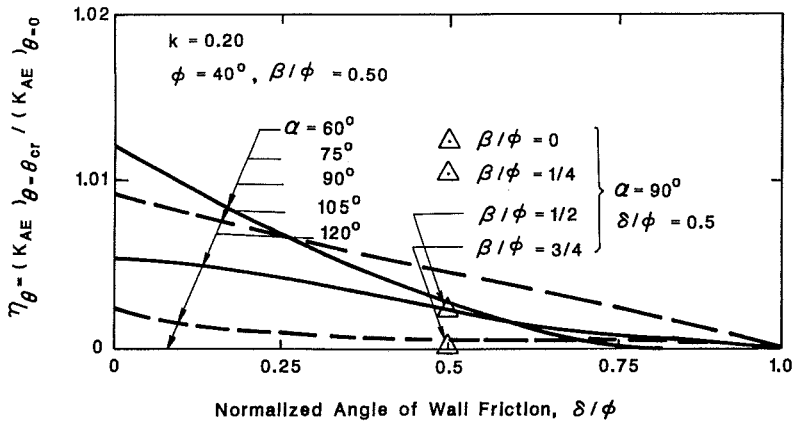

Fig. 5.33. Sensitivity of η_θ to changes in α, β and δ.

In reality, the angle of wall friction, δ, is seldom less than $\phi/2$, the active earth pressure coefficients as listed in the tables can be used for practical purposes without corrections in most cases.

The results of sensitivity analyses for the passive earth pressure case are presented

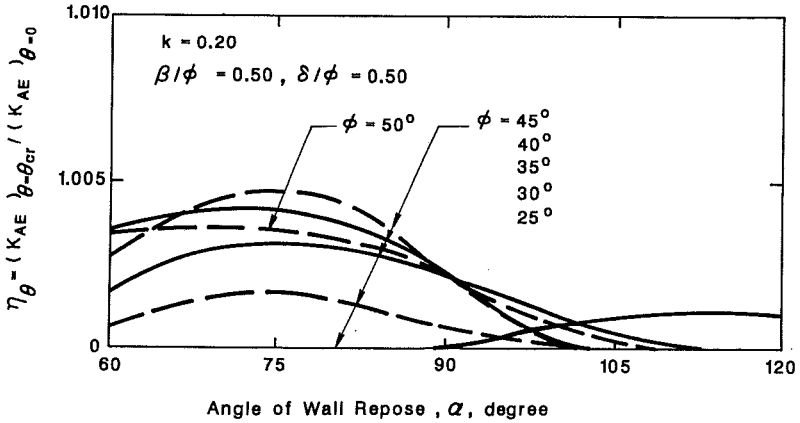

Fig. 5.34. Sensitivity of η_θ to changes in α and ϕ.

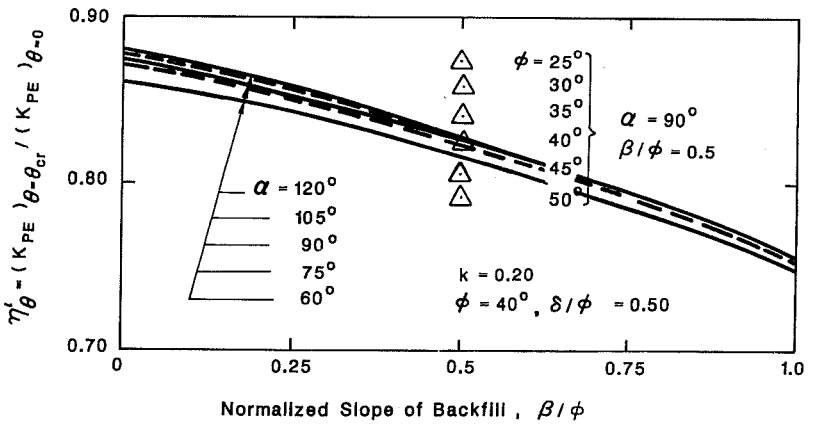

Fig. 5.35. Sensitivity of η'_θ to changes in α and β.

in Figs. 5.35 and 5.36. It is found that the η_θ'-value decreases as β and ϕ increase. In general, η_θ' is not very sensitive to the variation in α and δ/ϕ as long as $\delta/\phi > \frac{2}{3}$ or and $\alpha \geq 90°$ as shown in the figures. Hence, for developing the correlation factors, α and δ/ϕ can be kept constant. The fact that the η_θ'-value varies with α and δ/ϕ when $\delta \leq \frac{2}{3}$ and $\alpha < 90°$ can then be taken care by a modification factor.

Based on the facts that the η_θ'-value decreases as the seismic coefficient k increases, and that η_θ' varies with β/ϕ and α as shown in Fig. 5.35, the correction factors for estimating $(K_{PE})_{\theta = \theta_{cr}}$ from $(K_{PE})_{\theta = 0}$ have been developed. They are summarized in Figs. B5.1 to B5.6 in Appendix B for practical use. To take care of the variation when $\alpha < 90°$ and $\delta/\phi \leq \frac{2}{3}$, a modification factor

$$\mu_\theta' = [\eta_\theta']_{\text{modified}}/\eta_\theta'$$

as shown in Fig. B5.7, Appendix B, is provided.

With this information, the K_{PE}-value corresponding to $\theta = \theta_{cr}$, $(K_{PE})_{\theta = \theta_{cr}}$ can be estimated from the K_{PE}-values listed in the earth pressure tables, $(K_{PE})_{\theta = 0}$, by the following relation:

$$(K_{PE})_{\theta = \theta_{cr}} = \mu_\theta' \eta_\theta' (K_{PE})_{\theta = 0} \tag{5.38}$$

where η_θ' is obtained from Figs. B5.1 to B5.6 and μ_θ' is given in Fig. B5.7. In fact, as it can be seen from Fig. B5.7, μ_θ' is generally greater than 0.97, unless $\alpha < 75°$

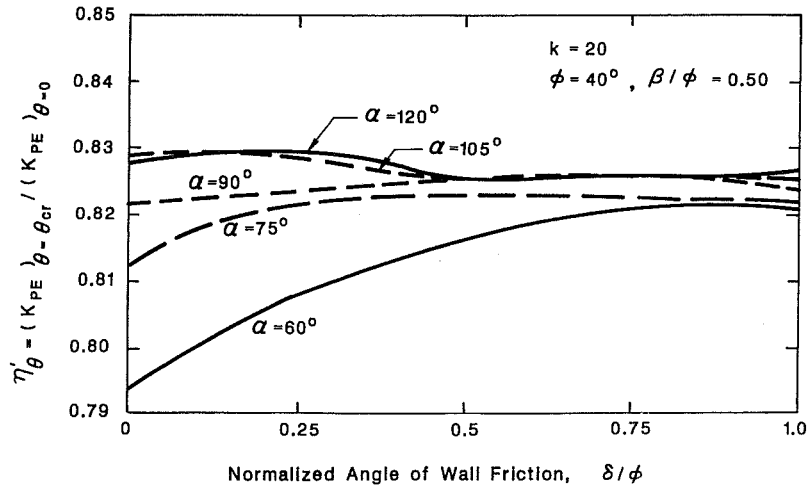

Fig. 5.36. Sensitivity of η_θ' to changes in α and δ.

or the soil – wall interface is fairly smooth ($\delta < \phi/2$). For practical purpose, μ_θ' can be taken as 0.97 if $\alpha < 90°$ and $\delta \leq \frac{2}{3}\phi$, and 1.0 for other cases.

The fact that the critical acceleration angle θ_{cr} for passive earth pressure cases is much different from zero on the horizontal direction, and in many cases close to 90°, is probably the reason for the large difference between $(K_{PE})_{\theta = \theta_{cr}}$ and $(K_{PE})_{\theta = 0}$. The η_θ'-value can be as low as 0.60 when the ϕ-angle and the seismic coefficient are high. The correction factors as shown in Figs. B5.1 to B5.7 should, therefore, be applied when the seismic acceleration of an earthquake force may assume any direction other than the horizontal.

5.6.2 Correction for the presence of surcharge

A uniform surcharge q acting on the surface of the backfill of a soil – wall system will induce additional loading on the wall. The consequence of its presence is to cause both the active and the passive earth pressures to increase. The coefficients of lateral earth pressures should therefore be corrected if $q \neq 0$.

An attempt has been made to find a correlation between the K_{AE} and K_{PE} corresponding to $q = 0$ case, $(K_{AE})_{q=0}$ and $(K_{PE})_{q=0}$, and those corresponding to $q \neq 0$ case, $(K_{AE})_{q\neq 0}$ and $(K_{PE})_{q\neq 0}$, based on an optimization with respect to the whole expressions for the lateral earth pressures as shown below:

$$K_{AE} = \text{Max} \left\{ N_{A\gamma} + \frac{2q}{\gamma H} N_{Aq} + \frac{2c}{\gamma H} N_{Ac} \right\} \tag{5.39}$$

$$K_{PE} = \text{Min} \left\{ N_{P\gamma} + \frac{2q}{\gamma H} N_{Pq} + \frac{2c}{\gamma H} N_{Pc} \right\} \tag{5.40}$$

where $N_{A\gamma}$, N_{Aq}, N_{Ac}, $N_{P\gamma}$, N_{Pq}, and N_{Pc} are earth pressure factors, γ, is the unit weight of the backfill, and H is the height of the retaining wall.

It was found that there is no simple general correlation between $(K_{AE})_{q=0}$ and $(K_{AE})_{q\neq 0}$ and between $(K_{PE})_{q=0}$ and $(K_{PE})_{q\neq 0}$. This is probably because the ratio $\eta_q = (K_{AE})_{q\neq 0}/(K_{AE})_{q=0}$ and $\eta_q' = (K_{PE})_{q\neq 0}/(K_{PE})_{q=0}$ are functions of all variables involved, although it was found practically independent of the seismic coefficient k.

A study has been conducted to see if the K_{AE} and K_{PE} can be practically approximated by an optimization with respect to each individual term in the expressions for K_{AE} and K_{PE}. The corresponding approximate values can be expressed as:

$$\hat{K}_{AE} = \text{Max}\{N_{A\gamma}\} + \frac{2q}{\gamma H} \text{Max}\{N_{Aq}\} + \frac{2c}{\gamma H} \text{Max}\{N_{Ac}\} \tag{5.41}$$

$$\hat{K}_{PE} = \text{Min}\,\{N_{P\gamma}\} + \frac{2q}{\gamma H}\,\text{Min}\,\{N_{Pq}\} + \frac{2c}{\gamma H}\,\text{Min}\,\{N_{Pc}\} \tag{5.42}$$

The results of this study are shown in Figs. 5.37 and 5.38 for the case of zero cohesion ($c = 0$). It is interesting to see that for both the active and the passive cases, the η_q-value and η_q'-value as obtained by Eqs. (5.39) to (5.42) differ only slightly. For the active case, the approximation gives higher K_{AE}-values, i.e. $\hat{K}_{AE} > K_{AE}$. This is because individual optimization will allow each component to take its most critical failure surface while overall optimization will require every component to assume a compromised failure surface.

For the same reasoning as the active case, individual optimization gives lower

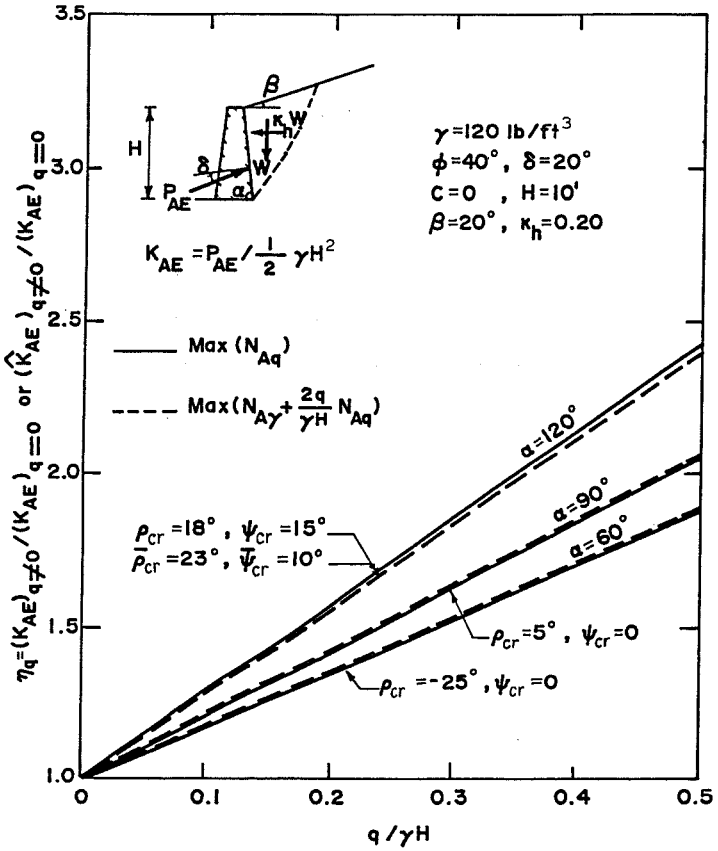

Fig. 5.37. Difference in η_q by optimization with respect to N_{Aq} and $N_{A\gamma} + (2q/\gamma H)N_{Aq}$.

K_{PE}-value than overall optimization does. This is clearly shown in Fig. 5.38. Fortunately, the difference between K_{AE} and $\hat{K}_{AE}$ and between K_{PE} and $\hat{K}_{PE}$ is very small. The zero or slight change in the most critical sliding surface between the two cases of optimization, as noted in Figs. 5.37 and 5.38 is mainly responsible for this consequence. Furthermore, use of $\hat{K}_{AE}$ and $\hat{K}_{PE}$ instead of K_{AE} and K_{PE} for design purpose is on the safe side. Therefore, the active and passive earth pressures obtained based on optimization with respect to the individual components are practically acceptable at least for the case of $c = 0$.

Based on these findings, correlations between earth pressure factors N_{Aq}, N_{Pq}, and $N_{A\gamma}$, $N_{P\gamma}$ are of interest. In fact, the earth pressure tables give directly the $N_{A\gamma}$ and $N_{P\gamma}$-values, since from Eqs. (5.39) and (5.40), $K_{AE} = N_{A\gamma}$ and $K_{PE} = N_{P\gamma}$

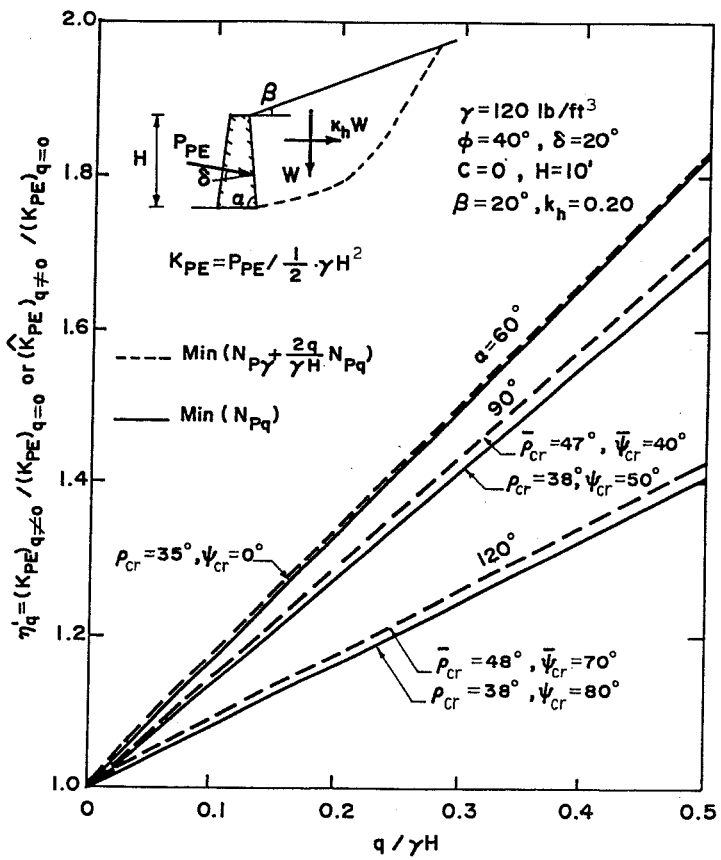

Fig. 5.38. Difference in η_q' by optimization with respect to N_{Pq} and $N_{P\gamma} + (2q/\gamma H)N_{Pq}$.

for the case of $q = c = 0$. Hence if the correlations between $N_{A\gamma}$ and N_{Aq} and between $N_{P\gamma}$ and N_{Pq} can be established, K_{AE} and K_{PE} can be estimated based on Eqs. (5.41) and (5.42) with $N_{A\gamma}$ and $N_{P\gamma}$ obtainable from the earth pressure tables.

The correlations between $N_{A\gamma}$ and N_{Aq}, and $N_{P\gamma}$ and N_{Pq} are completely independent of the $q/\gamma H$-value. In the special case when the most critical sliding surface is planar, it can be proved that the ratios $\alpha_q = N_{Aq}/N_{A\gamma}$ and $\alpha_q' = N_{Pq}/N_{P\gamma}$ can be expressed in the simple form:

$$\alpha_q = \alpha_q' = \frac{\sin\alpha}{\sin(\alpha + \beta)} \tag{5.43}$$

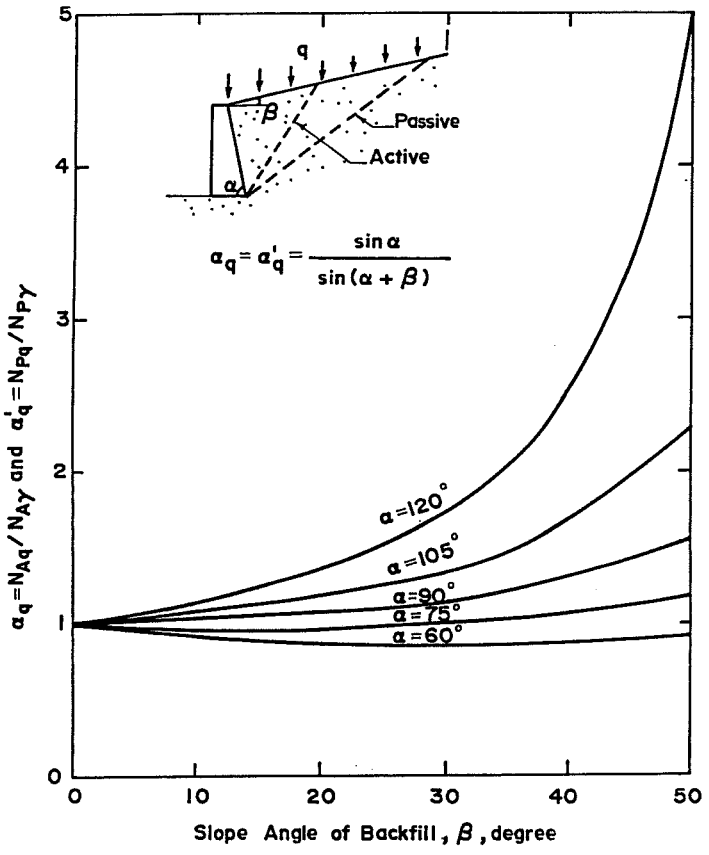

Fig. 5.39. Correlation factor $\alpha_q = \alpha_q'$ for active and passive planar failures.

where α is the angle of wall repose and β is the slope angle of the backfill. The α_q- and α_q'-values are dependent on the geometry of the soil – wall system only. Hence, if the most critical sliding surface is practically planar, Fig. 5.39 as developed based on Eq. (5.43) can then be used for obtaining the correlation factors α_q and α_q' for the active and passive cases, respectively.

In general, the sliding surface is not planar, especially for the passive case, the α_q- and α_q'-values will no longer depend only on α and β. Some sensitivity studies have been conducted to investigate the effect of several variables involved. The results are shown in Figs. 5.40 to 5.45. It is found the α_q is practically independent of the seismic coefficient k and so does the α_q'-value (Figs. 5.40 and 5.41). For α

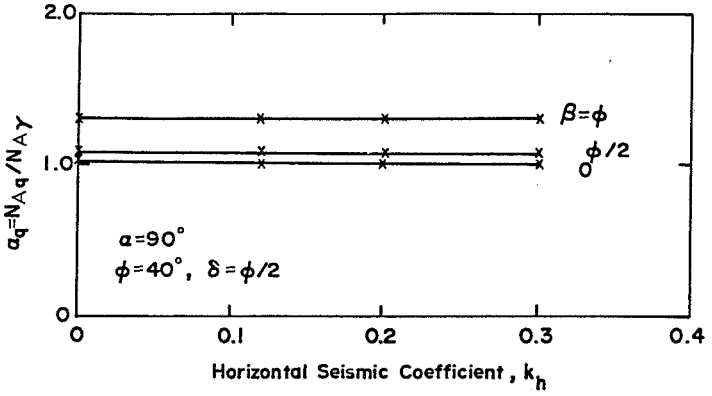

Fig. 5.40. Sensitivity of α_q to changes in k_h.

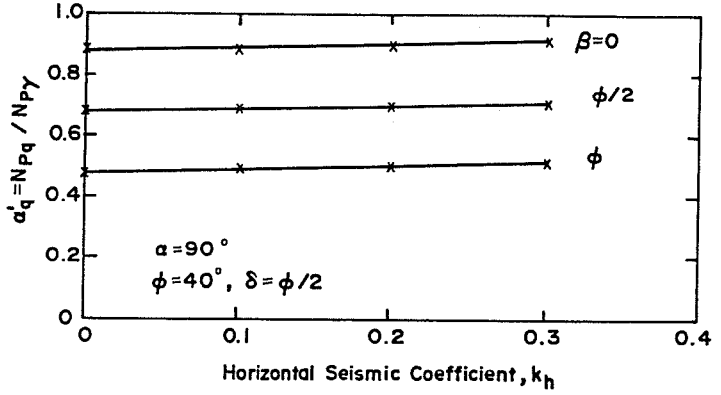

Fig. 5.41. Sensitivity of α_q' to changes in k_h.

essentially independent of the strength parameter, ϕ, and the soil – wall interface friction angle, δ. For the passive case, the α_q'-value is, in general, dependent on α, β, ϕ and δ.

Based on these sensitivity studies, charts for the correlation factor α_q similar to that shown in Fig. 5.42 have been developed. They are shown in Figs. B5.8 – B5.13 in Appendix B for practical use. The α_q'-value is found varying erratically with β. They were plotted in the form shown in Figs. B5.14 – B5.19 for design purposes.

With the availability of these charts for the correlation factors α_q and α_q', the active and passive earth pressure coefficients for the case of $q \neq 0$ and $c = 0$ can be

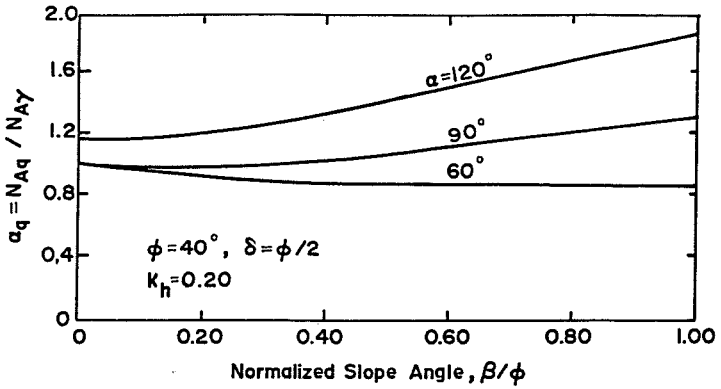

Fig. 5.42. Sensitivity of α_q to changes in α and β.

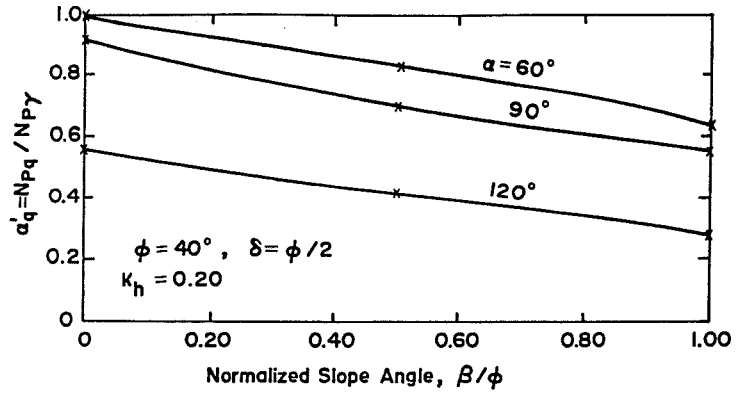

Fig. 5.43. Sensitivity of α_q' to changes in α and β.

easily calculated using the following equations modified from Eqs. (5.41) and (5.42):

$$(K_{AE})_{q \neq 0} \simeq N_{A\gamma}\left(1 + \frac{2q}{\gamma H}\alpha_q\right) \tag{5.44}$$

$$(K_{PE})_{q \neq 0} \simeq N_{P\gamma}\left(1 + \frac{2q}{\gamma H}\alpha_q'\right) \tag{5.45}$$

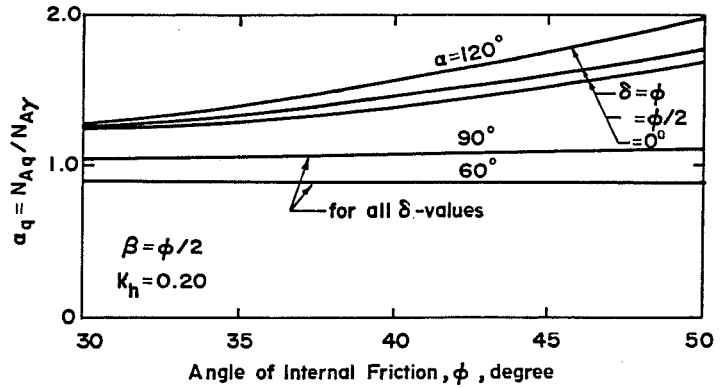

Fig. 5.44. Sensitivity of α_q to changes in ϕ, α and δ.

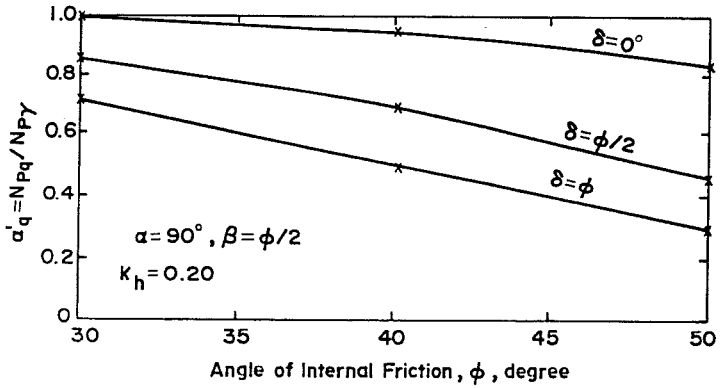

Fig. 5.45. Sensitivity of α_q to changes in ϕ and δ.

where $N_{A\gamma} = (K_{AE})_{q=0}$ and $N_{P\gamma} = (K_{PE})_{q=0}$ can be directly obtained from the earth pressure tables in Appendix A.

5.6.3 *Correction for presence of cohesion*

As noted previously, the contribution of cohesion to the lateral earth pressure is not gravity-related and is therefore independent of the earthquake forces. Thus, any attempt to correct the K_{AE}- and K_{PE}-values as the result of the presence of cohesion by considering the relations between $(K_{AE})_{c\neq 0}$ and $(K_{AE})_{c=0}$ and between $(K_{PE})_{c\neq 0}$ and $(K_{PE})_{c=0}$ will not be practical. Development of N_{Ac} and N_{Pc} for various soil – wall conditions may be more useful, if, as in the case of $q \neq 0$, Eqs. (5.39) and (5.40) are approximated by Eqs. (5.41) and (5.42) for the case of $c \neq 0$. For this approximation to be valid, superposition must hold.

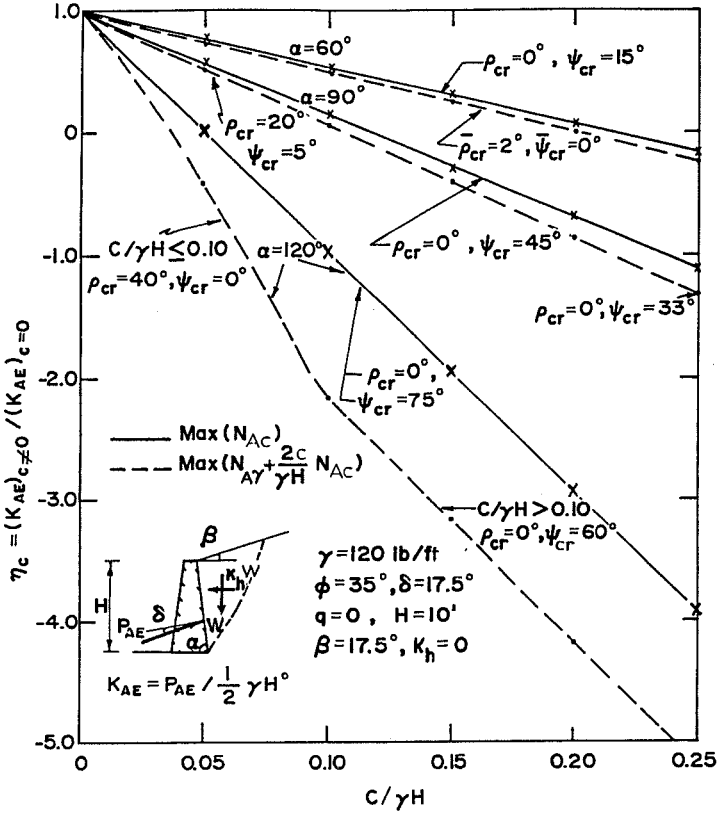

Fig. 5.46. Difference in η_c by optimization with respect to N_{Ac} and $N_{A\gamma} + (2c/\gamma H)\, N_{Ac}$.

In developing earth pressure theories, most investigators tend to take for granted that superposition holds, regardless of the fact that the potential sliding surface in an overall optimization may be quite different from those in an individual optimization (Prakash and Saran, 1966). Figures 5.46 and 5.47 show the difference in both the magnitude of K_{AE} and K_{PE} and the potential sliding surfaces, represented by ϱ_{cr} and ψ_{cr}, between the two optimizations. It is found that for the passive case, both the magnitude in K_{PE} and the mechanism of failure, denoted by $\bar{\varrho}_{cr}$ and $\bar{\psi}_{cr}$ if an average is taken, do not differ considerably between the two cases. This is probably because the rather curved potential sliding surface as detected in the case of cohesionless backfill is not much different from that would be detected if the backfill were purely cohesive. The compromised sliding surface is therefore not much different from either one of the above two cases.

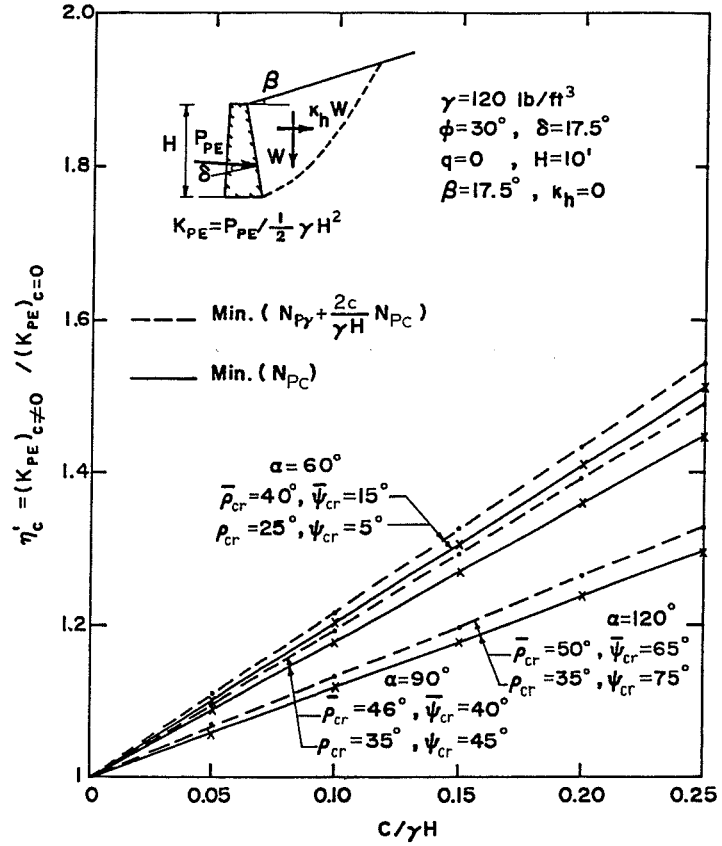

Fig. 5.47. Difference in η_c' by optimization with respect to N_{Pc} and $N_{P\gamma} + (2c/\gamma H)\, N_{Pc}$.

For the active case, it is clear from Fig. 5.46 that the compromised mechanism of failure for the case of an overall optimization differs considerably from that for the case of optimization with respect to the cohesion component, N_{Ac}, alone. The compromised potential sliding surface, as in the case of $c = 0$, is practically planar. Only when both the α-angle and the $c/\gamma H$-value are so high that the cohesion has a predominant influence on the resultant K_{AE}-value, then the sliding surface changes to essentially the logarithmic spiral shape. The most critical sliding surface is found to be the logarithmic spiral shape in the case of optimization with respect to N_{Ac}. The difference in $\eta_c = (K_{AE})_{c \neq 0}/(K_{AE})_{c = 0}$ for the two cases of optimization can be considered in some situations.

The findings as shown in Figs. 5.46 and 5.47 reflect that superposition is not always valid. That is, K_{AE} and K_{PE} as given by Eqs. (5.39) and (5.40), are not always equal to $\hat{K}_{AE}$ and $\hat{K}_{PE}$ as given by Eqs. (5.41) and (5.42) for the case of $c \neq 0$. For the approximation of Eqs. (5.41) and (5.42) to be practically valid, the N_{Ac}-value as obtained by individual optimization should be modified at least for $\alpha \geq 90°$ in the active earth pressure case.

Since the N_{Ac}- and N_{Pc}-values are totally independent of the seismic coefficient and the $c/\gamma H$-value, development of N_{Ac} and N_{Pc} tables or charts is much simplified. Furthermore, the ratios $\alpha_c = N_{Ac}/N_{A\gamma}$ and $\alpha_c' = N_{Pc}/N_{P\gamma}$ are found dependent not only on the seismic coefficient, but also on the geometry of the soil – wall system and the strength parameters ϕ and δ. The direct development of tables or charts for N_{Ac} and N_{Pc} factors, instead of α_c- and α_c'-values is therefore easier and of more practical value.

Based on these considerations, tables showing the N_{Ac}- and N_{Pc}-values for various soil – wall conditions have been developed. In retaining wall design, materials as close to cohesionless as possible are generally selected for the backfill. Although the backfill can be slightly cohesive, the ϕ-angle is generally high. For this reason, the N_{Ac} and N_{Pc} values for $\phi = 25°$ to $45°$ have been calculated. However, to include the case when c-value is appreciably high, the N_{Ac}- and N_{Pc}-values for $\phi = 20°$ have also been generated. They are given in Appendix B for practical use. In preparing these tables, the ratio of soil – wall adhesion c_a to c-parameter, $\lambda = c_a/c$, is take as cos ϕ for $\phi < 33.3°$ and as 0.836 for $\phi \geq 33.3°$. To account for the discrepancy in the N_{Ac}-value resulting from an individual optimization of N_{Ac} alone, a modification factor $\mu_c = [N_{Ac}]_{Max\,[K_A]}/[N_{Ac}]_{Max\,[N_{Ac}]}$ is recommended. It is presented in a graphical form as shown in Fig. B5.20 in Appendix B. In practice, however, α is seldom larger than 90° when the wall is built for retaining purpose. This modification is, therefore, not necessary in most cases.

Against the background of this information, the seismic lateral earth pressures for the case of $c \neq 0$ and $q = 0$ are approximated by the following equations modified from Eqs. (5.41) and (5.42):

$$(K_{AE})_{c \neq 0} \simeq N_{A\gamma} + \frac{2c}{\gamma H}(\mu_c N_{Ac}) \tag{5.46}$$

$$(K_{PE})_{c \neq 0} \simeq N_{P\gamma} + \frac{2c}{\gamma H} N_{Pc} \tag{5.47}$$

where $N_{A\gamma} = (K_{AE})_{c = 0}$ and $N_{P\gamma} = (K_{PE})_{c = 0}$ are obtained from the earth pressure tables in Appendix A.

5.6.4 Correlation for mixed effects from acceleration direction, surcharge and cohesion

In a general situation in which a given earthquake force of unknown direction of acceleration ($\theta \neq 0$) is presented and, in addition, there are uniform surcharge and cohesion on a soil – wall system, a correlation for the mixed effect from these three components has to be considered.

As far as the cohesion component is concerned, since it is independent of the magnitude of an earthquake, the superposition as shown in Eqs. (5.46) and (5.47) is unaffected by the direction of the seismic acceleration. Also, the cohesion component, which is not gravity-related, is not to be significantly affected by the presence of surcharge either. Hence, for the case of $q \neq 0$ and $c \neq 0$, the following equations, combined from Eqs. (5.44) and (5.45), and Eqs. (5.46) and (5.47) are valid:

$$(K_{AE})_{q \neq 0,\, c \neq 0} \simeq N_{A\gamma}\left(1 + \frac{2q}{\gamma H}\alpha_q\right) + \frac{2c}{\gamma H}(\mu_c N_{Ac}) \tag{5.48}$$

$$(K_{PE})_{q \neq 0,\, c \neq 0} \simeq N_{P\gamma}\left(1 + \frac{2q}{\gamma H}\alpha_q'\right) + \frac{2c}{\gamma H} N_{Pc} \tag{5.49}$$

To account for the effect of $\theta \neq 0$ on the seismic lateral pressures when a uniform surcharge is presented, an investigation on how the presence of surcharge affects the correction factors η_θ and η_θ' has been conducted. It is found that for the sample case investigated, $\phi = 40°$, $\delta = 20°$, $k = 0.20$, $q/\gamma H = 0.10$, the average η_θ-value is 1.012, 1.007, and 1.001 respectively for $\alpha = 75°$, 90° and 120° when $\beta \leq \phi/2$. As β increases, the η_θ-value becomes close to one. The η_θ-values show practically no difference from the recommended values as given earlier. Hence, the correction factor η_θ is practically unaffected by the presence of a surcharge.

For the passive case, the η_θ'-values obtained based on $q/\gamma H = 0.10$ are compared with the recommended $\mu_\theta'\eta_\theta'$-values, which are based on $q/\gamma H = 0$, as shown in Fig. 5.48. It is interesting to note that, here, as in the case of $q = 0$, the η_θ'-value is practically the same for walls with different values of α-angle. The calculated η_θ'-values for $q/\gamma H = 0$ are practically identical with the recommended $\mu_\phi'\eta_\theta'$-values shown

earlier. It can therefore be concluded that the η_θ'- and $\mu_\theta'\eta_\theta'$-values as recommended for $q = 0$ case are equally valid for the case of $q \neq 0$.

Based on these findings, the following general equations are suggested for practical use for the case of $\theta = \theta_{cr}$, $q \neq 0$, and $c \neq 0$:

$$(K_{AE})_{\theta,\,q,\,c} \simeq \eta_\theta N_{A\gamma}\left(1 + \frac{2q}{\gamma H}\alpha_q\right) + \frac{2c}{\gamma H}(\mu_c N_{Ac}) \tag{5.50}$$

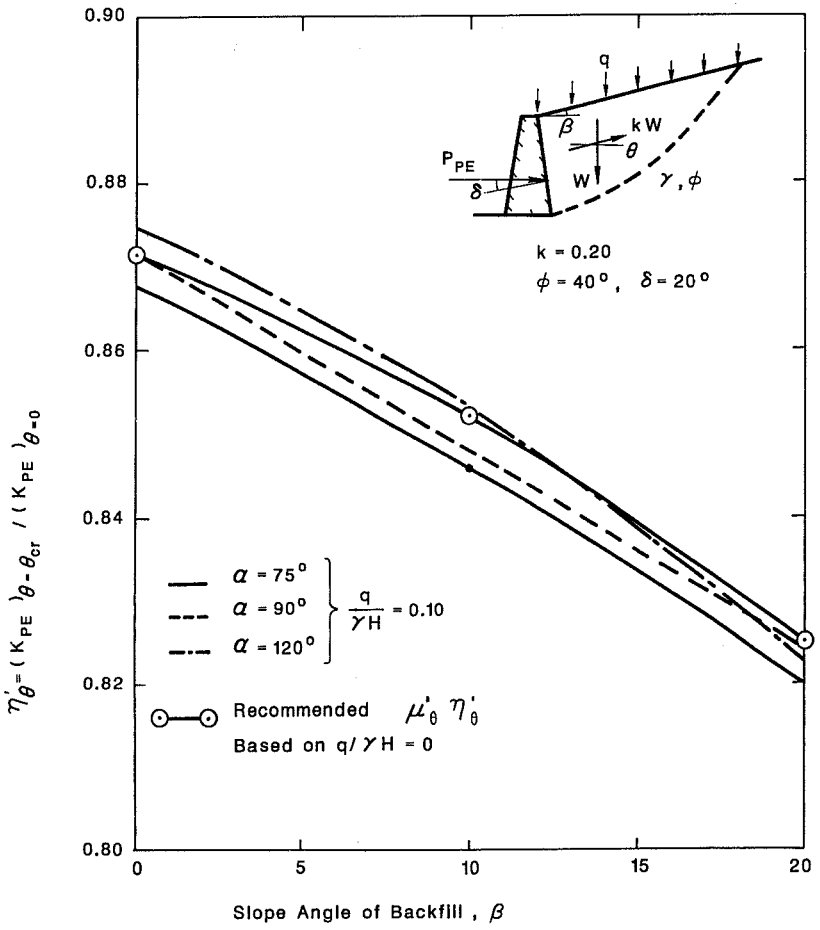

Fig. 5.48. Recommended correlation factor $\mu_\theta'\,\eta_\theta'$ as compared with calculated η_θ'-values based on $q/\gamma H = 0.10$.

$$(K_{PE})_{\theta,\,q,\,c} \simeq \mu_\theta'\,\eta_\theta'\,N_{P\gamma}\left(1 + \frac{2q}{\gamma H}\alpha_q'\right) + \frac{2c}{\gamma H}(N_{Pc}) \tag{5.51}$$

Note that: (a) η_θ can be taken as 1.0 for most cases, or as 1.01 if $\alpha \leq 90°$, $\beta \leq \phi/2$ and $\delta \leq \phi/2$; (b) η_θ' can be obtained from Figs. B5.1 to B5.6 and μ_θ' is given in Fig. B5.7; (c) α_q and α_q' can be obtained from Figs. B5.8 to B5.19; (d) μ_c can be obtained from Fig. B5.20 and N_{Ac} and N_{Pc} are given in Appendix B and (e) $N_{A\gamma}$ and $N_{P\gamma}$ are given in Appendix A.

For special cases in which the c-value is appreciably high, the ϕ-value may be low. N_{Ac} and N_{Pc}-values for $\phi = 20°$ are given in Appendix B. Since backfills with c-values are seldom acceptable in most retaining wall design, correction factors needed in Eqs. (5.50) and (5.51) were not developed for the $\phi = 20°$ case. It is recommended that they can be estimated by extrapolation, or can be taken as those corresponding to $\phi = 25°$ for a slightly conservative design.

References

Chang, M.F., 1981. Static and seismic lateral earth pressures on rigid retaining structures. Ph.D. Thesis, School of Civil Engineering, Purdue University, West Lafayette, IN, 465 pp.

Chang, M.F. and Chen, W.F., 1982. Lateral earth pressures on rigid retaining walls subjected to earthquake forces. Solid Mechanics Archives, Vol. 7, Martinus Nijhoff Publishers, The Hague, The Netherlands, pp. 315–362.

Chen, W.F., 1975. Limit Analysis and Soil Plasticity. Elsevier, Amsterdam, 630 pp.

Chen, W.F. and Rosenfarb, J.L., 1973. Limit analysis solutions of earth pressure problems. Soils Found., 13(4): 45–60.

Finn, W.D., 1967. Application of limit analysis in soil mechanics. Proc. J. Soil Mech. Found. Div., ASCE, 93(SM5): 101–120.

Housner, G.W., 1974. Strong ground motion. In: R.L. Wiegel (Editor), Earthquake Engineering. Prentice-Hall, New York, NY, pp. 75–91.

Ishii, Y., Arai, H. and Tsuchida, H., 1960. Lateral earth pressure in an earthquake. Proc. 2nd World Conference on Earthquake Engineering, Tokyo, Vol. 1, p. 211.

Mononobe, N. and Matsuo, H., 1929. On the determination of earth pressures during earthquakes. Proc. World Engineering Conference, Vol. 9, p. 176.

Murphy, V.A., 1960. The effect of ground characteristics on the aseismic design of structures. Proc. 2nd World Conf. on Earthquake Engineering, Tokyo, pp. 231–247.

Okabe, S., 1926. General theory of earth pressure. J. Jpn. Soc. Civ. Eng., Vol. 12, No. 1.

Okamoto, S., 1956. Bearing capacity of sandy soil and lateral earth pressure during earthquakes. Proc. 1st World Conf. on Earthquake Engineering, California, pp. 27–1 through 27–26.

Prakash, S. and Saran, S., 1966. Static and dynamic earth pressures behind retaining walls. Proc. 3rd. Symp. on Earthquake Engineering, Roorkee, India, pp. 277–288.

Sabzevari, A. and Ghahramani, A., 1974. Dynamic passive earth-pressure problem. J. Geotech. Eng. Div., ASCE, 100(GT1): 15–30.

Seed, H.B. and Whitman, R.V., 1970. Design of earth retaining structures for dynamic loads. Proc. ASCE Specialty Conf. on Lateral Stresses in the Ground and Design of Earth Retaining Structures, Ithaca, NY, pp. 103–147.

APPENDIX A: SEISMIC EARTH PRESSURE TABLES FOR K_A AND K_P (Chang, 1981)

Coefficients for active earth pressure K_A for $\phi = 20°$ and $k = 0$, 0.05, 0.1 and 0.15

* ϕ = 20.00 k = 0 *

β/φ	=	0	1/6	1/3	1/2	2/3	5/6	1
δ/φ	α	--- K_A-VALUES ---						
0	60.00	.77	.81	.86	.93	1.01	1.12	1.48
	75.00	.60	.63	.66	.71	.76	.84	1.09
	90.00	.49	.51	.54	.57	.61	.67	.88
	105.00	.41	.43	.44	.47	.50	.56	.74
	120.00	.34	.35	.37	.39	.41	.46	.63
.3333	60.00	.75	.80	.85	.92	1.01	1.15	1.60
	75.00	.57	.60	.64	.69	.75	.84	1.13
	90.00	.46	.48	.51	.54	.59	.65	.88
	105.00	.38	.39	.41	.44	.47	.53	.72
	120.00	.31	.32	.33	.35	.38	.42	.59
.5000	60.00	.74	.79	.86	.93	1.03	1.18	1.67
	75.00	.56	.60	.64	.68	.75	.84	1.16
	90.00	.45	.47	.50	.53	.58	.65	.88
	105.00	.37	.38	.40	.43	.46	.51	.71
	120.00	.29	.31	.32	.34	.37	.41	.58
.6667	60.00	.74	.80	.86	.94	1.05	1.21	1.75
	75.00	.56	.59	.63	.68	.75	.85	1.20
	90.00	.44	.46	.49	.52	.57	.65	.90
	105.00	.36	.37	.39	.42	.45	.51	.71
	120.00	.28	.30	.31	.33	.36	.40	.57
1.0000	60.00	.76	.82	.89	.98	1.11	1.30	1.98
	75.00	.56	.59	.64	.69	.77	.88	1.28
	90.00	.43	.46	.49	.52	.57	.65	.93
	105.00	.34	.36	.38	.41	.44	.50	.71
	120.00	.27	.28	.30	.31	.34	.39	.55

* ϕ = 20.00 k = .05 *

β/φ	=	0	1/6	1/3	1/2	2/3	5/6	1
δ/φ	α	--- K_A-VALUES ---						
0	60.00	.80	.85	.92	1.00	1.11	1.35	5.73
	75.00	.64	.67	.71	.77	.84	1.01	4.23
	90.00	.53	.55	.59	.63	.69	.82	3.39
	105.00	.45	.47	.49	.53	.58	.70	2.86
	120.00	.39	.40	.42	.45	.49	.61	2.43
.3333	60.00	.79	.85	.92	1.01	1.14	1.44	6.17
	75.00	.61	.65	.70	.76	.84	1.04	4.39
	90.00	.50	.52	.56	.60	.67	.82	3.41
	105.00	.42	.44	.46	.50	.55	.68	2.78
	120.00	.35	.37	.39	.41	.46	.57	2.43
.5000	60.00	.79	.85	.93	1.02	1.17	1.50	6.45
	75.00	.61	.64	.69	.76	.85	1.06	4.49
	90.00	.49	.51	.55	.60	.67	.82	3.43
	105.00	.40	.42	.45	.49	.54	.67	2.76
	120.00	.34	.35	.37	.40	.44	.56	2.45
.6667	60.00	.79	.86	.94	1.05	1.20	1.56	6.78
	75.00	.60	.64	.69	.76	.86	1.09	4.62
	90.00	.48	.51	.54	.59	.66	.83	3.47
	105.00	.40	.42	.44	.48	.53	.67	2.77
	120.00	.33	.34	.36	.39	.43	.55	2.48
1.0000	60.00	.82	.89	.99	1.11	1.30	1.75	7.64
	75.00	.61	.65	.71	.78	.89	1.16	4.95
	90.00	.47	.50	.54	.59	.67	.85	3.59
	105.00	.38	.41	.43	.47	.53	.67	2.87
	120.00	.31	.33	.35	.38	.42	.53	2.57

* ϕ = 20.00 k = .10 *

β/φ	=	0	1/6	1/3	1/2	2/3	5/6	1
δ/φ	α	--- K_A-VALUES ---						
0	60.00	.84	.91	.98	1.09	1.30	2.16	9.98
	75.00	.68	.72	.77	.85	.98	1.62	7.36
	90.00	.57	.60	.64	.70	.82	1.55	5.90
	105.00	.49	.52	.56	.61	.71	6.23	4.97
	120.00	.44	.46	.49	.53	.63	5.73	4.32
.3333	60.00	.84	.91	1.00	1.13	1.38	2.32	10.74
	75.00	.66	.70	.76	.85	1.02	1.68	7.64
	90.00	.54	.58	.62	.69	.81	1.56	5.93
	105.00	.46	.49	.52	.58	.69	6.24	4.84
	120.00	.40	.42	.45	.49	.59	5.75	4.35
.5000	60.00	.84	.92	1.02	1.16	1.44	2.42	11.23
	75.00	.65	.70	.77	.86	1.04	1.72	7.82
	90.00	.53	.57	.61	.68	.82	1.57	5.98
	105.00	.45	.48	.51	.57	.68	6.28	4.81
	120.00	.38	.41	.44	.48	.58	5.78	4.39
.6667	60.00	.85	.94	1.04	1.20	1.51	2.54	11.81
	75.00	.65	.70	.77	.87	1.06	1.76	8.04
	90.00	.53	.56	.61	.68	.83	1.59	6.04
	105.00	.44	.47	.50	.56	.68	6.35	4.85
	120.00	.37	.40	.42	.47	.57	5.84	4.44
1.0000	60.00	.89	.99	1.11	1.30	1.69	2.66	13.30
	75.00	.66	.72	.79	.91	1.13	1.89	8.62
	90.00	.52	.56	.61	.69	.85	1.65	6.24
	105.00	.43	.46	.50	.55	.68	6.54	5.02
	120.00	.36	.38	.41	.46	.56	6.02	4.60

* ϕ = 20.00 k = .15 *

β/φ	=	0	1/6	1/3	1/2	2/3	5/6	1
δ/φ	α	--- K_A-VALUES ---						
0	60.00	.89	.97	1.08	1.26	1.85	3.00	14.23
	75.00	.72	.78	.85	.98	1.41	2.25	10.50
	90.00	.62	.68	.72	.82	1.18	2.32	8.42
	105.00	.55	.59	.63	.72	3.19	12.79	7.09
	120.00	.49	.52	.57	.66	2.54	11.88	6.22
.3333	60.00	.90	.99	1.12	1.34	2.00	3.22	15.31
	75.00	.71	.77	.85	1.00	1.46	2.33	10.88
	90.00	.59	.64	.70	.82	1.19	2.34	8.46
	105.00	.51	.55	.60	.70	3.16	12.83	6.91
	120.00	.45	.48	.53	.62	2.62	11.91	6.27
.5000	60.00	.91	1.01	1.15	1.40	2.09	3.36	16.01
	75.00	.71	.77	.86	1.02	1.50	2.38	11.15
	90.00	.58	.63	.70	.82	1.20	2.36	8.52
	105.00	.50	.54	.59	.69	3.17	12.91	6.85
	120.00	.44	.47	.52	.61	2.78	11.99	6.32
.6667	60.00	.93	1.04	1.19	1.47	2.20	3.53	16.83
	75.00	.71	.78	.88	1.05	1.54	2.45	11.47
	90.00	.58	.63	.70	.83	1.21	2.39	8.61
	105.00	.49	.53	.58	.69	3.18	13.04	6.93
	120.00	.43	.46	.51	.60	2.75	12.11	6.40
1.0000	60.00	.99	1.12	1.30	1.66	2.49	3.97	18.96
	75.00	.73	.81	.92	1.12	1.66	2.62	12.29
	90.00	.58	.63	.71	.85	1.26	2.47	8.90
	105.00	.48	.52	.58	.69	3.23	13.44	7.17
	120.00	.41	.45	.49	.59	2.71	12.48	6.62

Coefficients for active earth pressure K_A for $\phi = 20°$ and $k = 0.20$, 0.25, 0.30, and $\phi = 25°$ and $k = 0$

* ϕ = 20.00 k = .20 *

β/φ	=	0	1/6	1/3	1/2	2/3	5/6	1
δ/φ	α	--- K_A-VALUES ---						
0	60.00	.96	1.06	1.23	1.61	2.45	3.83	18.47
	75.00	.78	.85	.97	1.25	1.86	2.87	13.63
	90.00	.67	.73	.82	1.07	1.58	3.10	10.93
	105.00	.61	.66	.74	2.05	6.76	19.36	9.21
	120.00	.56	.61	.69	1.95	6.23	18.03	8.13
.3333	60.00	.98	1.10	1.31	1.74	2.64	4.12	19.85
	75.00	.77	.86	.98	1.29	1.93	2.98	14.14
	90.00	.65	.72	.82	1.07	1.59	3.12	10.98
	105.00	.57	.63	.72	2.05	6.69	19.41	8.97
	120.00	.52	.57	.65	1.88	5.97	18.08	8.19
.5000	60.00	1.00	1.14	1.37	1.81	2.76	4.30	20.79
	75.00	.78	.87	1.01	1.32	1.98	3.04	14.48
	90.00	.65	.71	.83	1.08	1.60	3.14	11.07
	105.00	.56	.62	.71	2.06	6.69	19.53	8.90
	120.00	.51	.55	.64	1.86	5.88	18.20	8.26
.6667	60.00	1.03	1.18	1.43	1.91	2.91	4.52	21.86
	75.00	.79	.88	1.04	1.36	2.04	3.13	14.89
	90.00	.65	.72	.83	1.10	1.62	3.18	11.19
	105.00	.55	.61	.71	2.07	6.72	19.73	9.01
	120.00	.49	.54	.63	1.84	5.81	18.38	8.36
1.0000	60.00	1.12	1.30	1.61	2.15	3.29	5.07	24.63
	75.00	.82	.93	1.12	1.46	2.19	3.35	15.96
	90.00	.65	.73	.86	1.13	1.68	3.30	11.56
	105.00	.55	.61	.71	2.12	6.84	20.34	9.33
	120.00	.48	.53	.62	1.83	5.74	18.85	8.65

* ϕ = 20.00 k = .25 *

β/φ	=	0	1/6	1/3	1/2	2/3	5/6	1
δ/φ	α	--- K_A-VALUES ---						
0	60.00	1.04	1.19	1.48	1.98	3.04	4.67	22.72
	75.00	.85	.96	1.17	1.53	2.31	3.50	16.77
	90.00	.74	.83	1.01	1.33	1.97	3.87	13.44
	105.00	.68	.76	2.94	4.53	10.32	25.92	11.32
	120.00	.64	.72	2.86	4.29	9.51	24.18	10.04
.3333	60.00	1.08	1.28	1.59	2.13	3.28	5.02	24.46
	75.00	.86	.98	1.21	1.59	2.40	3.62	17.39
	90.00	.73	.83	1.02	1.34	1.98	3.90	13.51
	105.00	.65	.73	2.96	4.52	10.22	25.99	11.03
	120.00	.60	.68	2.79	4.14	9.12	24.24	10.10
.5000	60.00	1.12	1.34	1.66	2.23	3.43	5.24	25.57
	75.00	.87	1.01	1.24	1.63	2.46	3.71	17.81
	90.00	.73	.83	1.03	1.35	2.00	3.93	13.61
	105.00	.64	.73	2.98	4.53	10.22	26.16	10.95
	120.00	.59	.67	2.76	4.10	8.99	24.40	10.19
.6667	60.00	1.17	1.41	1.75	2.35	3.61	5.50	26.82
	75.00	.89	1.04	1.27	1.68	2.54	3.81	18.32
	90.00	.73	.84	1.04	1.37	2.02	3.98	13.76
	105.00	.64	.73	3.01	4.56	10.26	26.42	11.09
	120.00	.58	.66	2.75	4.06	8.88	24.65	10.31
1.0000	60.00	1.30	1.59	1.96	2.64	4.08	6.18	30.29
	75.00	.94	1.11	1.36	1.80	2.72	4.08	19.63
	90.00	.75	.87	1.08	1.42	2.10	4.12	14.22
	105.00	.63	.73	3.11	4.67	10.44	27.24	11.48
	120.00	.57	.65	2.76	4.03	8.77	25.41	10.68

* ϕ = 20.00 k= .30 *

β/φ	=	0	1/6	1/3	1/2	2/3	5/6	1
δ/φ	α	--- K_A -VALUES ---						
0	60.00	1.16	1.41	1.75	2.35	3.64	5.50	26.97
	75.00	.95	1.13	1.38	1.82	2.77	4.13	19.90
	90.00	.83	.98	1.21	1.60	2.36	4.64	15.86
	105.00	.77	1.02	10.64	7.01	13.88	32.48	13.44
	120.00	.75	1.04	10.35	6.64	12.80	30.33	11.94
.3333	60.00	1.24	1.53	1.88	2.53	3.92	5.91	29.03
	75.00	.97	1.17	1.42	1.89	2.87	4.27	20.64
	90.00	.83	.99	1.22	1.61	2.38	4.68	16.03
	105.00	.75	1.02	10.69	6.98	13.75	32.57	13.05
	120.00	.71	1.02	10.09	6.41	12.27	30.41	12.02
.5000	60.00	1.30	1.60	1.96	2.65	4.10	6.18	30.35
	75.00	1.00	1.20	1.46	1.93	2.95	4.37	21.14
	90.00	.84	1.00	1.23	1.62	2.40	4.72	16.15
	105.00	.75	1.03	10.77	7.01	13.75	32.76	13.01
	120.00	.70	1.01	10.01	6.33	12.09	30.61	12.13
.6667	60.00	1.37	1.68	2.06	2.78	4.32	6.49	31.91
	75.00	1.03	1.24	1.50	1.99	3.03	4.49	21.74
	90.00	.85	1.01	1.25	1.64	2.43	4.77	16.33
	105.00	.74	1.05	10.89	7.05	13.80	33.11	13.17
	120.00	.69	1.01	9.96	6.28	11.95	30.91	12.27
1.0000	60.00	1.54	1.90	2.32	3.14	4.88	7.29	35.95
	75.00	1.10	1.33	1.60	2.13	3.25	4.81	23.29
	90.00	.88	1.04	1.29	1.70	2.51	4.94	16.88
	105.00	.75	1.08	11.25	7.23	14.05	34.13	13.63
	120.00	.68	1.02	9.98	6.24	11.80	31.87	12.71

* ϕ = 25.00 k= 0 *

β/φ	=	0	1/6	1/3	1/2	2/3	5/6	1
δ/φ	α	--- K_A -VALUES ---						
0	60.00	.69	.74	.79	.85	.95	1.08	1.51
	75.00	.52	.55	.59	.63	.69	.77	1.07
	90.00	.41	.43	.45	.48	.52	.58	.81
	105.00	.32	.33	.35	.37	.40	.45	.64
	120.00	.24	.25	.26	.28	.30	.34	.50
.3333	60.00	.67	.72	.79	.86	.96	1.12	1.67
	75.00	.50	.53	.56	.61	.68	.77	1.12
	90.00	.38	.40	.42	.45	.50	.57	.82
	105.00	.29	.30	.32	.34	.37	.42	.63
	120.00	.21	.22	.23	.25	.27	.31	.46
.5000	60.00	.67	.73	.79	.87	.98	1.16	1.77
	75.00	.48	.52	.56	.61	.68	.78	1.16
	90.00	.37	.39	.41	.45	.49	.56	.83
	105.00	.28	.29	.31	.33	.36	.41	.62
	120.00	.21	.21	.22	.24	.26	.30	.46
.6667	60.00	.68	.74	.81	.89	1.01	1.20	1.95
	75.00	.48	.52	.56	.61	.68	.80	1.20
	90.00	.36	.38	.41	.44	.49	.56	.85
	105.00	.27	.29	.30	.33	.36	.41	.67
	120.00	.20	.21	.22	.23	.25	.29	.44
1.0000	60.00	.71	.77	.86	.96	1.10	1.34	2.15
	75.00	.49	.53	.57	.63	.71	.84	1.33
	90.00	.36	.38	.41	.45	.49	.58	.85
	105.00	.27	.28	.30	.32	.35	.41	.65
	120.00	.19	.20	.21	.22	.24	.28	.43

Coefficients of active earth pressure K_A for $\phi = 25°$ and $k = 0.05$, 0.10, 0.15 and 0.20

* ϕ = 25.00 k = .05 *

β/φ	=	0	1/6	1/3	1/2	2/3	5/6	1
δ/φ	α			--- K_A -VALUES ---				
0	60.00	.72	.78	.84	.93	1.04	1.27	5.65
	75.00	.55	.59	.63	.69	.76	.92	4.13
	90.00	.44	.46	.49	.53	.59	.71	3.15
	105.00	.35	.37	.39	.42	.47	.57	2.48
	120.00	.28	.29	.31	.33	.36	.44	1.93
.3333	60.00	.71	.77	.85	.94	1.08	1.36	6.44
	75.00	.53	.57	.62	.69	.76	.94	4.35
	90.00	.41	.44	.47	.51	.57	.70	3.17
	105.00	.32	.34	.36	.39	.44	.54	2.42
	120.00	.25	.26	.28	.30	.33	.41	1.90
.5000	60.00	.72	.78	.86	.97	1.12	1.43	6.84
	75.00	.53	.57	.61	.68	.77	.96	4.47
	90.00	.40	.43	.46	.50	.57	.71	3.21
	105.00	.31	.33	.35	.38	.43	.53	2.41
	120.00	.24	.25	.27	.29	.32	.39	1.83
.6667	60.00	.73	.80	.88	1.00	1.16	1.51	7.32
	75.00	.53	.57	.62	.69	.79	.99	4.66
	90.00	.40	.42	.46	.50	.57	.71	3.27
	105.00	.31	.32	.35	.38	.42	.53	2.40
	120.00	.23	.24	.26	.29	.31	.39	1.97
1.0000	60.00	.77	.85	.95	1.09	1.30	1.76	8.71
	75.00	.54	.58	.64	.72	.83	1.08	5.15
	90.00	.40	.43	.46	.51	.59	.74	3.45
	105.00	.30	.32	.34	.37	.42	.53	2.54
	120.00	.22	.23	.25	.27	.30	.38	2.08

* ϕ = 25.00 k = .10 *

β/φ	=	0	1/6	1/3	1/2	2/3	5/6	1
δ/φ	α			--- K_A -VALUES ---				
0	60.00	.76	.83	.91	1.01	1.19	1.98	10.19
	75.00	.59	.63	.68	.76	.87	1.42	7.19
	90.00	.48	.51	.54	.60	.69	1.17	5.42
	105.00	.39	.41	.44	.48	.56	6.94	4.34
	120.00	.32	.33	.36	.39	.45	5.90	3.38
.3333	60.00	.76	.83	.92	1.05	1.27	2.17	11.21
	75.00	.57	.62	.68	.76	.90	1.49	7.54
	90.00	.45	.48	.52	.58	.68	1.16	5.52
	105.00	.36	.38	.41	.46	.54	7.01	4.21
	120.00	.29	.30	.32	.36	.42	5.96	3.43
.5000	60.00	.77	.85	.95	1.09	1.33	2.31	11.9
	75.00	.57	.62	.68	.77	.92	1.54	7.71
	90.00	.44	.47	.52	.58	.68	1.19	5.55
	105.00	.35	.37	.40	.45	.53	7.11	4.18
	120.00	.28	.29	.31	.35	.41	6.04	3.47
.6667	60.00	.78	.87	.98	1.13	1.41	2.48	12.76
	75.00	.57	.62	.69	.78	.94	1.60	8.11
	90.00	.44	.47	.51	.58	.69	1.22	5.69
	105.00	.34	.37	.40	.44	.52	7.24	4.21
	120.00	.27	.29	.31	.34	.40	6.16	3.54
1.0000	60.00	.84	.94	1.08	1.27	1.64	2.95	15.17
	75.00	.59	.65	.72	.83	1.02	1.78	8.97
	90.00	.44	.48	.52	.59	.72	1.29	6.06
	105.00	.34	.36	.39	.44	.53	7.66	4.45
	120.00	.26	.27	.30	.33	.39	6.51	3.74

* ϕ = 25.00 k = .15 *

β/φ	=	0	1/6	1/3	1/2	2/3	5/6	1
δ/φ	α			--- K_A -VALUES ---				
0	60.00	.81	.88	.98	1.14	1.53	2.64	14.83
	75.00	.63	.68	.75	.85	1.12	2.04	10.24
	90.00	.52	.55	.60	.68	.90	1.75	7.82
	105.00	.43	.46	.50	.57	1.21	18.51	6.18
	120.00	.36	.39	.42	.47	.97	15.89	4.90
.3333	60.00	.81	.90	1.02	1.21	1.69	3.12	15.55
	75.00	.62	.67	.75	.87	1.18	2.14	10.75
	90.00	.49	.53	.58	.67	.91	1.77	7.85
	105.00	.40	.43	.47	.54	1.22	18.70	6.00
	120.00	.33	.35	.38	.44	.98	16.06	4.95
.5000	60.00	.83	.93	1.06	1.27	1.79	3.38	16.97
	75.00	.62	.68	.76	.89	1.22	2.21	11.11
	90.00	.49	.53	.58	.67	.92	1.79	7.87
	105.00	.39	.42	.46	.53	1.23	18.96	5.96
	120.00	.32	.34	.37	.43	.99	16.27	5.02
.6667	60.00	.85	.96	1.11	1.34	1.92	3.56	18.19
	75.00	.63	.69	.78	.91	1.27	2.30	11.56
	90.00	.48	.53	.59	.68	.94	1.83	8.17
	105.00	.39	.42	.46	.53	1.25	19.32	6.02
	120.00	.31	.33	.36	.42	1.00	16.59	5.11
1.0000	60.00	.93	1.07	1.25	1.56	2.29	4.25	21.03
	75.00	.65	.73	.83	.99	1.41	2.55	12.77
	90.00	.49	.54	.60	.71	.99	1.93	8.55
	105.00	.38	.42	.46	.53	1.31	20.42	6.36
	120.00	.30	.32	.36	.41	1.05	17.53	5.41

* ϕ = 25.00 k = .20 *

β/φ	=	0	1/6	1/3	1/2	2/3	5/6	1
δ/φ	α			--- K_A -VALUES ---				
0	60.00	.85	.93	1.09	1.35	2.01	3.70	18.87
	75.00	.68	.74	.83	1.01	1.47	2.66	13.30
	90.00	.55	.61	.68	.82	1.20	2.20	10.15
	105.00	.48	.52	.58	.70	7.65	30.07	8.03
	120.00	.42	.45	.50	.61	6.54	25.68	6.41
.3333	60.00	.86	.93	1.16	1.49	2.21	4.07	20.76
	75.00	.67	.74	.85	1.06	1.54	2.78	13.55
	90.00	.54	.59	.67	.83	1.21	2.30	10.20
	105.00	.45	.49	.55	.68	7.69	30.38	7.79
	120.00	.38	.41	.46	.57	6.57	26.16	6.47
.5000	60.00	.91	1.03	1.21	1.53	2.36	4.35	22.04
	75.00	.68	.75	.87	1.10	1.66	2.83	14.47
	90.00	.54	.59	.67	.84	1.25	2.35	10.26
	105.00	.44	.48	.54	.68	7.77	30.80	7.73
	120.00	.37	.40	.45	.56	6.64	26.51	6.56
.6667	60.00	.94	1.08	1.29	1.70	2.52	4.64	23.61
	75.00	.69	.77	.89	1.14	1.66	3.00	15.01
	90.00	.54	.59	.68	.85	1.25	2.43	10.51
	105.00	.44	.48	.54	.68	7.90	31.39	7.83
	120.00	.36	.38	.44	.55	6.75	27.01	6.69
1.0000	60.00	1.05	1.23	1.51	2.03	3.00	5.58	28.73
	75.00	.73	.83	.97	1.27	1.84	3.32	16.61
	90.00	.55	.61	.71	.90	1.36	2.57	11.11
	105.00	.44	.48	.55	.70	8.30	33.16	8.27
	120.00	.35	.38	.43	.55	7.10	28.56	7.07

Coefficients for active earth pressure K_A for $\phi = 25°$, $k = 0.25$ and 0.30, and $\phi = 30°$ and $k = 0$ and 0.05

* ϕ = 25.00 k = .25 *

β/φ	=	0	1/6	1/3	1/2	2/3	5/6	1
δ/φ	α			--- K_A -VALUES ---				
0	60.00	.92	1.05	1.25	1.68	2.48	4.56	23.21
	75.00	.73	.82	.95	1.25	1.82	3.28	16.36
	90.00	.62	.68	.79	1.02	1.50	2.91	12.42
	105.00	.54	.59	.68	3.53	14.09	41.64	9.88
	120.00	.48	.52	.61	3.17	12.10	35.87	7.91
.3333	60.00	.96	1.11	1.37	1.85	2.73	5.02	25.52
	75.00	.74	.83	1.00	1.31	1.91	3.44	17.18
	90.00	.60	.67	.79	1.03	1.51	2.95	12.52
	105.00	.51	.56	.66	3.54	14.16	42.09	9.58
	120.00	.44	.48	.57	3.06	12.17	36.25	8.00
.5000	60.00	1.00	1.17	1.46	1.96	2.90	5.32	27.11
	75.00	.75	.85	1.03	1.35	1.97	3.56	17.74
	90.00	.60	.67	.80	1.05	1.53	2.99	12.74
	105.00	.50	.55	.65	3.57	14.32	42.65	9.51
	120.00	.43	.47	.56	3.03	12.30	36.74	8.11
.6667	60.00	1.05	1.24	1.57	2.11	3.11	5.72	29.01
	75.00	.77	.88	1.07	1.42	2.05	3.78	18.46
	90.00	.60	.68	.82	1.07	1.56	3.04	12.85
	105.00	.50	.55	.65	3.63	14.55	43.47	9.63
	120.00	.42	.46	.55	3.02	12.50	37.44	8.26
1.0000	60.00	1.21	1.47	1.87	2.51	3.71	6.81	34.54
	75.00	.82	.96	1.19	1.57	2.28	4.10	20.43
	90.00	.62	.71	.86	1.13	1.65	3.22	13.67
	105.00	.50	.56	.67	3.60	15.29	45.95	10.18
	120.00	.41	.46	.55	3.04	13.14	39.58	8.73

* ϕ = 25.00 k = .30 *

β/φ	=	0	1/6	1/3	1/2	2/3	5/6	1
δ/φ	α			--- K_A -VALUES ---				
0	60.00	1.00	1.17	1.49	2.00	2.96	5.43	27.55
	75.00	.80	.91	1.13	1.49	2.16	3.90	19.42
	90.00	.66	.77	.94	1.23	1.80	3.50	14.82
	105.00	.60	.68	.85	8.24	20.52	53.21	11.72
	120.00	.55	.62	.91	7.41	17.67	45.86	9.42
.3333	60.00	1.07	1.29	1.64	2.20	3.26	5.97	30.31
	75.00	.82	.95	1.19	1.57	2.27	4.09	20.37
	90.00	.67	.77	.95	1.24	1.82	3.53	14.94
	105.00	.58	.66	.96	8.26	20.64	53.78	11.37
	120.00	.51	.58	.89	7.15	17.77	46.35	9.52
.5000	60.00	1.12	1.37	1.74	2.34	3.46	6.34	32.16
	75.00	.84	.99	1.23	1.62	2.35	4.23	21.06
	90.00	.67	.78	.96	1.26	1.84	3.58	15.12
	105.00	.57	.65	.97	8.34	20.86	54.50	11.29
	120.00	.50	.57	.89	7.08	17.96	46.97	9.65
.6667	60.00	1.20	1.47	1.87	2.51	3.71	6.80	34.48
	75.00	.86	1.03	1.28	1.69	2.45	4.40	21.91
	90.00	.68	.80	.98	1.28	1.88	3.65	15.35
	105.00	.57	.66	.99	8.47	21.20	55.54	11.44
	120.00	.49	.56	.09	7.05	18.25	47.87	9.83
1.0000	60.00	1.41	1.75	2.23	3.00	4.42	8.09	41.00
	75.00	.95	1.14	1.42	1.87	2.71	4.87	24.25
	90.00	.71	.84	1.03	1.35	1.88	3.86	16.22
	105.00	.58	.67	1.05	8.87	22.28	58.71	12.09
	120.00	.48	.56	.91	7.10	19.18	50.60	10.40

* ϕ = 30.00 k = 0 *

β/φ	=	0	1/6	1/3	1/2	2/3	5/6	1
δ/φ	α			--- K_A -VALUES ---				
0	60.00	.62	.67	.72	.79	.88	1.03	1.52
	75.00	.45	.48	.51	.55	.61	.70	1.02
	90.00	.33	.35	.37	.40	.44	.50	.74
	105.00	.24	.25	.27	.29	.31	.36	.54
	120.00	.17	.17	.18	.19	.21	.24	.35
.3333	60.00	.61	.66	.72	.80	.91	1.08	1.72
	75.00	.42	.46	.49	.54	.60	.71	1.01
	90.00	.31	.33	.35	.38	.42	.48	.75
	105.00	.22	.23	.25	.26	.29	.33	.52
	120.00	.15	.15	.16	.17	.18	.21	.35
.5000	60.00	.61	.67	.73	.82	.94	1.12	1.89
	75.00	.42	.45	.49	.54	.61	.72	1.14
	90.00	.30	.32	.34	.37	.41	.48	.77
	105.00	.21	.23	.24	.26	.28	.33	.53
	120.00	.14	.14	.15	.16	.18	.20	.34
.6667	60.00	.62	.68	.75	.85	.98	1.18	2.03
	75.00	.42	.46	.50	.55	.62	.74	1.20
	90.00	.30	.32	.34	.37	.41	.49	.78
	105.00	.21	.22	.23	.25	.28	.32	.53
	120.00	.13	.14	.15	.16	.17	.20	.33
1.0000	60.00	.67	.74	.83	.94	1.11	1.38	2.55
	75.00	.44	.48	.52	.58	.66	.80	1.38
	90.00	.30	.32	.35	.38	.43	.51	.85
	105.00	.21	.22	.23	.25	.28	.33	.57
	120.00	.13	.13	.14	.15	.17	.19	.33

* ϕ = 30.00 k = .05 *

β/φ	=	0	1/6	1/3	1/2	2/3	5/6	1
δ/φ	α			--- K_A -VALUES ---				
0	60.00	.65	.71	.77	.86	.98	1.20	5.88
	75.00	.48	.51	.55	.61	.68	.83	3.95
	90.00	.36	.39	.41	.45	.50	.61	2.87
	105.00	.27	.29	.31	.33	.37	.45	2.11
	120.00	.20	.20	.21	.23	.26	.31	1.59
.3333	60.00	.64	.71	.78	.88	1.02	1.30	6.63
	75.00	.46	.50	.54	.60	.69	.85	4.21
	90.00	.34	.36	.39	.43	.48	.60	2.90
	105.00	.25	.26	.28	.30	.34	.43	2.05
	120.00	.17	.18	.19	.21	.23	.28	1.51
.5000	60.00	.65	.72	.80	.91	1.07	1.38	7.16
	75.00	.46	.50	.54	.60	.70	.88	4.40
	90.00	.33	.36	.38	.42	.48	.60	2.98
	105.00	.24	.26	.27	.30	.34	.42	2.04
	120.00	.17	.17	.18	.20	.22	.28	1.53
.6667	60.00	.67	.74	.83	.95	1.13	1.48	7.85
	75.00	.46	.50	.55	.62	.72	.91	4.64
	90.00	.33	.35	.38	.42	.48	.61	3.03
	105.00	.24	.25	.27	.29	.33	.42	2.07
	120.00	.16	.17	.18	.19	.22	.27	1.53
1.0000	60.00	.73	.82	.93	1.08	1.32	1.82	10.00
	75.00	.48	.53	.58	.66	.78	1.03	5.35
	90.00	.34	.36	.39	.44	.50	.65	3.88
	105.00	.24	.25	.27	.29	.34	.43	2.21
	120.00	.15	.16	.17	.19	.21	.27	1.61

Coefficients of active earth pressure K_A for $\phi = 30°$ and $k = 0.1$, 0.15, 0.20 and 0.25

$\phi = 30.00$ $k = .10$

β/φ	=	0	1/6	1/3	1/2	2/3	5/6	1
δ/φ	α			--- K_A -VALUES ---				
0	60.00	.69	.75	.83	.94	1.10	1.66	10.26
	75.00	.51	.55	.60	.67	.76	1.15	6.90
	90.00	.40	.42	.46	.50	.58	.90	5.04
	105.00	.31	.32	.35	.38	.44	1.09	3.69
	120.00	.23	.24	.25	.28	.32	.82	2.82
.3333	60.00	.69	.76	.85	.99	1.19	1.85	11.5
	75.00	.50	.54	.60	.67	.80	1.21	7.32
	90.00	.37	.40	.44	.49	.57	.91	5.06
	105.00	.28	.30	.32	.36	.42	1.07	3.58
	120.00	.20	.21	.23	.25	.29	.78	2.75
.5000	60.00	.70	.78	.88	1.02	1.26	2.01	12.47
	75.00	.50	.54	.60	.68	.82	1.26	7.69
	90.00	.37	.40	.43	.49	.58	.93	5.15
	105.00	.27	.29	.31	.35	.41	1.07	3.59
	120.00	.20	.21	.22	.24	.28	.77	2.76
.6667	60.00	.72	.81	.92	1.08	1.35	2.15	13.67
	75.00	.50	.55	.61	.70	.85	1.30	8.00
	90.00	.37	.40	.43	.49	.58	.86	5.21
	105.00	.27	.29	.31	.35	.41	1.08	3.63
	120.00	.19	.20	.22	.24	.28	.78	2.78
1.0000	60.00	.81	.92	1.06	1.27	1.65	2.77	17.42
	75.00	.53	.59	.66	.77	.95	1.53	9.31
	90.00	.37	.41	.45	.51	.62	1.04	5.71
	105.00	.27	.29	.31	.35	.42	1.14	2.18
	120.00	.18	.20	.21	.23	.28	.80	2.95

$\phi = 30.00$ $k = .15$

β/φ	=	0	1/6	1/3	1/2	2/3	5/6	1
δ/φ	α			--- K_A -VALUES ---				
0	60.00	.73	.80	.90	1.04	1.32	2.22	14.62
	75.00	.55	.60	.68	.75	.93	1.57	9.84
	90.00	.43	.47	.51	.57	.71	1.35	7.12
	105.00	.34	.37	.40	.45	.56	2.88	5.25
	120.00	.26	.28	.30	.34	.43	2.25	4.10
.3333	60.00	.74	.83	.94	1.11	1.48	2.55	16.45
	75.00	.54	.59	.66	.77	.99	1.66	10.45
	90.00	.41	.45	.49	.56	.72	1.37	7.21
	105.00	.32	.34	.37	.42	.54	2.84	5.11
	120.00	.24	.25	.27	.31	.40	2.18	3.97
.5000	60.00	.76	.85	.98	1.18	1.60	2.75	17.75
	75.00	.54	.60	.67	.79	1.03	1.73	10.52
	90.00	.41	.44	.49	.56	.73	1.40	7.34
	105.00	.31	.33	.36	.42	.54	2.84	5.10
	120.00	.23	.24	.27	.30	.39	2.17	3.98
.6667	60.00	.79	.90	1.04	1.26	1.76	3.01	19.49
	75.00	.55	.61	.69	.82	1.09	1.82	11.52
	90.00	.41	.44	.49	.57	.75	1.44	7.50
	105.00	.30	.33	.36	.41	.54	2.87	5.19
	120.00	.22	.24	.26	.30	.38	2.20	4.02
1.0000	60.00	.90	1.04	1.24	1.55	2.24	3.80	24.03
	75.00	.59	.66	.76	.91	1.25	2.09	13.27
	90.00	.42	.46	.52	.61	.81	1.56	8.14
	105.00	.31	.33	.37	.42	.56	1.83	3.00
	120.00	.22	.23	.26	.29	.39	2.34	4.30

$\phi = 30.00$ $k = .20$

β/φ	=	0	1/6	1/3	1/2	2/3	5/6	1
δ/φ	α			--- K_A-VALUES ---				
0	60.00	.78	.87	.99	1.19	1.71	2.90	18.99
	75.00	.59	.65	.73	.86	1.21	2.00	12.78
	90.00	.47	.51	.57	.67	.94	1.80	9.25
	105.00	.38	.41	.46	.53	1.68	4.69	6.82
	120.00	.31	.33	.36	.42	1.36	3.70	5.35
.3333	60.00	.80	.91	1.06	1.31	1.82	3.26	21.27
	75.00	.59	.65	.74	.90	1.26	2.11	13.57
	90.00	.45	.50	.56	.67	.95	1.83	9.39
	105.00	.36	.39	.43	.51	1.68	4.61	6.64
	120.00	.28	.30	.33	.39	1.31	3.59	5.20
.5000	60.00	.83	.95	1.12	1.41	2.06	3.56	23.05
	75.00	.60	.67	.76	.93	1.34	2.20	14.18
	90.00	.45	.50	.56	.68	.97	1.86	9.53
	105.00	.35	.38	.43	.51	1.69	4.60	6.63
	120.00	.27	.29	.32	.38	1.30	3.60	5.21
.6667	60.00	.87	1.01	1.20	1.54	2.28	3.82	25.31
	75.00	.61	.69	.78	.98	1.41	2.32	14.95
	90.00	.45	.50	.57	.69	1.00	1.92	9.78
	105.00	.35	.38	.42	.51	1.72	4.68	6.75
	120.00	.26	.28	.32	.38	1.31	3.64	5.27
1.0000	60.00	1.02	1.20	1.48	1.85	2.90	4.83	32.25
	75.00	.66	.75	.89	1.13	1.63	2.66	17.25
	90.00	.47	.53	.60	.75	1.08	2.08	10.52
	105.00	.35	.38	.43	.53	1.29	2.79	3.83
	120.00	.26	.28	.31	.38	1.38	3.89	2.96

$\phi = 30.00$ $k = .25$

β/φ	=	0	1/6	1/3	1/2	2/3	5/6	1
δ/φ	α			--- K_A-VALUES ---				
0	60.00	.83	.94	1.10	1.42	2.10	3.51	23.36
	75.00	.64	.71	.82	1.02	1.48	2.42	15.72
	90.00	.52	.57	.65	.81	1.17	2.25	11.35
	105.00	.43	.47	.53	.67	3.70	6.50	8.32
	120.00	.35	.38	.43	.56	3.02	5.15	6.61
.3333	60.00	.87	1.01	1.21	1.59	2.37	3.54	26.28
	75.00	.64	.73	.85	1.08	1.57	2.56	16.65
	90.00	.50	.55	.64	.82	1.19	2.29	11.52
	105.00	.40	.44	.51	.66	3.69	6.38	8.17
	120.00	.32	.35	.40	.53	2.92	5.01	6.42
.5000	60.00	.91	1.05	1.30	1.71	2.56	4.24	25.40
	75.00	.66	.75	.88	1.13	1.64	2.67	17.43
	90.00	.50	.56	.65	.84	1.21	2.33	11.72
	105.00	.40	.44	.50	.67	3.73	6.37	8.16
	120.00	.31	.34	.39	.52	2.93	5.02	6.44
.6667	60.00	.97	1.15	1.42	1.87	2.80	4.64	31.14
	75.00	.68	.77	.93	1.19	1.74	2.81	18.28
	90.00	.51	.57	.67	.86	1.25	2.40	12.00
	105.00	.39	.44	.50	.66	3.80	6.48	8.30
	120.00	.31	.34	.39	.52	2.96	5.08	6.52
1.0000	60.00	1.18	1.43	1.81	2.37	3.57	5.85	35.68
	75.00	.75	.87	1.06	1.35	2.00	3.22	21.26
	90.00	.53	.61	.72	.93	1.35	2.50	13.01
	105.00	.40	.45	.52	.72	2.38	3.74	4.65
	120.00	.30	.34	.39	.53	3.16	2.90	3.62

Coefficients of active earth pressure K_A for $\phi = 30°$ and $k = 0.30$, and for $\phi = 35°$ and $k = 0$, 0.05 and 0.10

$\phi = 30.00$ $k = .30$

β/φ	=	0	1/6	1/3	1/2	2/3	5/6	1
δ/φ	α			--- K_A -VALUES ---				
0	60.00	.90	1.04	1.27	1.67	2.50	4.13	27.72
	75.00	.70	.79	.94	1.20	1.76	2.85	18.65
	90.00	.57	.63	.75	.97	1.41	2.70	13.50
	105.00	.48	.53	.63	2.22	5.72	8.30	9.88
	120.00	.40	.45	.53	1.91	4.68	6.60	7.85
.3333	60.00	.96	1.13	1.45	1.87	2.81	4.63	31.20
	75.00	.71	.82	1.00	1.27	1.87	3.01	19.81
	90.00	.55	.63	.76	.98	1.43	2.74	13.67
	105.00	.45	.51	.61	2.25	5.71	8.15	9.70
	120.00	.37	.41	.50	1.86	4.54	6.42	7.64
.5000	60.00	1.01	1.22	1.54	2.01	3.04	4.99	33.71
	75.00	.73	.85	1.04	1.33	1.95	3.14	20.69
	90.00	.56	.64	.77	1.00	1.46	2.80	13.91
	105.00	.45	.51	.61	2.30	5.76	8.14	9.69
	120.00	.36	.41	.49	1.88	4.55	6.43	7.66
.6667	60.00	1.09	1.33	1.69	2.20	3.33	5.45	36.96
	75.00	.76	.89	1.10	1.40	2.06	3.31	21.83
	90.00	.57	.65	.80	1.03	1.50	2.88	14.28
	105.00	.45	.51	.62	2.36	5.87	8.28	9.86
	120.00	.36	.40	.48	1.85	4.61	6.52	7.77
1.0000	60.00	1.38	1.68	2.15	2.78	4.24	6.88	47.08
	75.00	.86	1.02	1.26	1.69	2.37	3.78	25.16
	90.00	.61	.71	.86	1.12	1.62	3.12	15.44
	105.00	.46	.53	.65	2.56	3.48	4.69	5.47
	120.00	.36	.40	.49	1.91	2.71	3.67	4.29

$\phi = 35.00$ $k = 0$

β/φ	=	0	1/6	1/3	1/2	2/3	5/6	1
δ/φ	α			--- K_A -VALUES ---				
0	60.00	.55	.60	.66	.73	.82	.96	1.51
	75.00	.39	.41	.44	.48	.54	.63	.97
	90.00	.27	.29	.31	.33	.37	.42	.66
	105.00	.18	.19	.20	.22	.24	.28	.45
	120.00	.11	.11	.12	.12	.13	.16	.27
.3333	60.00	.54	.60	.66	.74	.85	1.02	1.74
	75.00	.37	.40	.43	.47	.53	.63	1.04
	90.00	.25	.27	.29	.31	.35	.41	.67
	105.00	.17	.17	.18	.20	.22	.25	.43
	120.00	.09	.10	.10	.11	.12	.14	.24
.5000	60.00	.55	.61	.68	.76	.88	1.06	1.92
	75.00	.37	.40	.43	.48	.54	.65	1.10
	90.00	.25	.26	.28	.31	.35	.41	.65
	105.00	.16	.17	.18	.19	.21	.25	.42
	120.00	.09	.09	.10	.10	.11	.13	.24
.6667	60.00	.57	.63	.71	.80	.94	1.16	2.16
	75.00	.37	.40	.44	.49	.56	.67	1.10
	90.00	.25	.26	.28	.31	.35	.41	.72
	105.00	.16	.17	.18	.19	.21	.25	.44
	120.00	.09	.09	.10	.10	.11	.13	.25
1.0000	60.00	.64	.72	.81	.94	1.12	1.44	3.01
	75.00	.40	.43	.47	.53	.62	.76	1.42
	90.00	.25	.27	.29	.32	.37	.44	.80
	105.00	.16	.17	.18	.19	.22	.28	.48
	120.00	.08	.09	.09	.10	.11	.13	.27

$\phi = 35.00$ $k = .05$

β/φ	=	0	1/6	1/3	1/2	2/3	5/6	1
δ/φ	α			--- K_A-VALUES ---				
0	60.00	.58	.64	.70	.79	.90	1.12	5.64
	75.00	.41	.45	.48	.53	.69	.74	3.74
	90.00	.30	.32	.34	.37	.42	.51	2.56
	105.00	.21	.22	.23	.25	.28	.35	1.74
	120.00	.13	.14	.14	.15	.17	.21	1.03
.3333	60.00	.58	.64	.72	.82	.96	1.24	6.73
	75.00	.40	.43	.47	.53	.61	.77	4.03
	90.00	.28	.30	.32	.35	.40	.51	2.61
	105.00	.19	.20	.21	.23	.26	.33	1.68
	120.00	.12	.12	.13	.14	.15	.19	1.04
.5000	60.00	.60	.66	.74	.85	1.01	1.33	7.42
	75.00	.40	.44	.48	.54	.62	.80	4.26
	90.00	.27	.29	.32	.35	.40	.51	2.67
	105.00	.18	.20	.21	.23	.26	.32	1.68
	120.00	.11	.12	.12	.13	.15	.19	1.07
.6667	60.00	.62	.69	.78	.90	1.09	1.46	8.35
	75.00	.41	.44	.49	.55	.65	.84	4.57
	90.00	.27	.29	.32	.35	.41	.52	2.77
	105.00	.18	.19	.21	.23	.26	.32	1.70
	120.00	.11	.11	.12	.13	.15	.18	1.11
1.0000	60.00	.71	.80	.92	1.09	1.35	1.91	11.65
	75.00	.44	.48	.54	.61	.73	.98	5.54
	90.00	.29	.31	.34	.37	.44	.57	3.05
	105.00	.18	.20	.21	.23	.26	.33	1.89
	120.00	.10	.11	.12	.13	.14	.18	1.24

$\phi = 35.00$ $k = .10$

β/φ	=	0	1/6	1/3	1/2	2/3	5/6	1
δ/φ	α			--- K_A-VALUES ---				
0	60.00	.62	.69	.76	.88	1.02	1.49	10.15
	75.00	.45	.48	.53	.59	.69	.99	6.52
	90.00	.33	.35	.38	.42	.49	.70	4.46
	105.00	.24	.25	.27	.30	.34	.51	3.04
	120.00	.16	.17	.18	.19	.22	.34	1.87
.3333	60.00	.63	.70	.78	.91	1.11	1.72	11.72
	75.00	.43	.47	.52	.59	.71	1.06	7.02
	90.00	.31	.33	.36	.41	.48	.72	4.54
	105.00	.22	.23	.25	.27	.32	.48	2.93
	120.00	.14	.15	.16	.17	.20	.27	1.91
.5000	60.00	.64	.72	.82	.96	1.19	1.90	12.91
	75.00	.44	.48	.53	.61	.73	1.12	7.42
	90.00	.31	.33	.36	.41	.48	.74	4.62
	105.00	.21	.22	.24	.27	.32	.49	2.98
	120.00	.13	.14	.15	.17	.19	.27	1.96
.6667	60.00	.67	.76	.87	1.03	1.30	2.13	14.55
	75.00	.45	.49	.55	.63	.77	1.20	7.91
	90.00	.31	.33	.36	.41	.49	.77	4.82
	105.00	.21	.22	.24	.27	.32	.51	2.99
	120.00	.13	.14	.15	.16	.19	.28	2.04
1.0000	60.00	.79	.91	1.06	1.29	1.70	2.97	20.26
	75.00	.49	.54	.61	.72	.89	1.45	9.64
	90.00	.32	.35	.39	.44	.53	.86	5.35
	105.00	.21	.23	.25	.28	.33	.55	3.32
	120.00	.13	.14	.15	.16	.19	.30	2.28

Coefficients of active earth pressure K_A for $\phi = 35°$ and $k = 0.15$, 0.20, 0.25 and 0.30

$\phi = 35.00$ $k = .15$

β/φ	=	0	1/6	1/3	1/2	2/3	5/6	1
δ/φ	α			--- K_A -VALUES ---				
0	60.00	.66	.73	.82	.95	1.19	2.11	14.49
	75.00	.48	.52	.59	.66	.81	1.39	9.34
	90.00	.36	.39	.42	.48	.58	1.06	6.33
	105.00	.27	.28	.31	.35	.42	1.31	4.22
	120.00	.19	.20	.21	.24	.29	.91	2.72
.3333	60.00	.67	.76	.87	1.03	1.34	2.44	16.71
	75.00	.47	.52	.58	.68	.85	1.50	10.01
	90.00	.34	.37	.41	.47	.58	1.08	6.47
	105.00	.25	.26	.25	.33	.41	1.30	4.17
	120.00	.17	.18	.19	.21	.27	.90	2.78
.5000	60.00	.70	.79	.92	1.10	1.47	2.66	18.41
	75.00	.48	.53	.60	.70	.90	1.59	10.55
	90.00	.34	.37	.41	.47	.60	1.11	6.81
	105.00	.24	.26	.28	.32	.40	1.32	4.16
	120.00	.16	.17	.19	.21	.26	.88	2.85
.6667	60.00	.74	.85	.99	1.21	1.65	3.02	20.74
	75.00	.49	.55	.62	.73	.95	1.70	11.31
	90.00	.34	.37	.42	.48	.62	1.15	6.87
	105.00	.24	.26	.28	.32	.41	1.36	4.23
	120.00	.16	.17	.18	.21	.26	.90	2.96
1.0000	60.00	.89	1.04	1.25	1.59	2.28	4.20	28.91
	75.00	.55	.61	.71	.85	1.15	2.06	13.75
	90.00	.36	.40	.45	.52	.68	1.29	7.67
	105.00	.25	.26	.29	.34	.43	2.63	4.75
	120.00	.16	.17	.18	.21	.26	1.80	3.32

$\phi = 35.00$ $k = .20$

β/φ	=	0	1/6	1/3	1/2	2/3	5/6	1
δ/φ	α			--- K_A -VALUES ---				
0	60.00	.70	.79	.90	1.07	1.49	2.74	18.82
	75.00	.52	.57	.64	.75	1.01	1.80	12.07
	90.00	.40	.43	.48	.55	.74	1.41	8.28
	105.00	.30	.32	.36	.41	.58	2.13	5.62
	120.00	.22	.23	.26	.29	.43	1.53	3.57
.3333	60.00	.73	.83	.97	1.20	1.71	3.15	21.70
	75.00	.52	.57	.65	.78	1.08	1.94	13.00
	90.00	.36	.42	.47	.55	.76	1.44	8.46
	105.00	.28	.30	.34	.39	.58	2.13	5.42
	120.00	.20	.21	.23	.27	.41	1.51	3.65
.5000	60.00	.76	.88	1.04	1.30	1.89	3.47	22.91
	75.00	.53	.59	.68	.82	1.15	2.05	13.74
	90.00	.38	.42	.47	.56	.76	1.46	8.61
	105.00	.27	.30	.33	.39	.59	2.16	5.40
	120.00	.19	.21	.23	.26	.40	1.49	3.75
.6667	60.00	.82	.95	1.14	1.45	2.12	3.51	28.91
	75.00	.55	.61	.71	.87	1.23	2.20	14.72
	90.00	.38	.42	.48	.58	.81	1.53	8.52
	105.00	.27	.30	.33	.39	.59	2.22	5.51
	120.00	.19	.20	.22	.26	.40	1.53	3.89
1.0000	60.00	1.02	1.22	1.52	2.01	2.94	5.43	37.97
	75.00	.61	.70	.83	1.04	1.48	2.66	17.61
	90.00	.41	.46	.52	.64	.91	1.72	9.51
	105.00	.28	.31	.35	.41	.65	4.74	6.17
	120.00	.19	.20	.23	.27	.40	3.33	4.36

$\phi = 35.00$ $k = .25$

β/φ	=	0	1/6	1/3	1/2	2/3	5/6	1
δ/φ	α			--- K_A -VALUES ---				
0	60.00	.75	.85	1.00	1.25	1.82	3.36	23.14
	75.00	.56	.62	.71	.87	1.23	2.21	14.65
	90.00	.43	.48	.54	.65	.93	1.76	10.15
	105.00	.34	.37	.41	.50	3.04	2.85	6.91
	120.00	.26	.28	.31	.37	.92	2.16	4.43
.3333	60.00	.79	.92	1.10	1.44	2.10	3.87	26.65
	75.00	.57	.64	.74	.93	1.33	2.28	15.92
	90.00	.42	.47	.54	.65	.95	1.80	10.20
	105.00	.32	.35	.39	.49	3.07	2.95	6.66
	120.00	.23	.25	.28	.35	.87	2.07	4.52
.5000	60.00	.84	.98	1.20	1.58	2.31	4.66	28.40
	75.00	.58	.66	.77	.99	1.40	2.52	16.90
	90.00	.42	.47	.54	.68	.98	1.84	10.59
	105.00	.31	.34	.39	.49	3.14	3.00	6.65
	120.00	.23	.25	.28	.34	.88	2.11	4.64
.6667	60.00	.91	1.06	1.34	1.77	2.60	4.79	33.12
	75.00	.61	.69	.82	1.06	1.50	2.70	18.12
	90.00	.43	.49	.56	.71	1.01	1.92	10.90
	105.00	.31	.34	.39	.50	3.24	3.07	6.78
	120.00	.22	.24	.27	.34	.88	2.16	4.82
1.0000	60.00	1.19	1.46	1.85	2.46	3.60	6.67	48.17
	75.00	.70	.81	.99	1.28	1.82	3.27	21.86
	90.00	.47	.53	.62	.79	1.14	2.15	12.27
	105.00	.33	.36	.42	.53	1.86	6.85	7.60
	120.00	.22	.25	.28	.35	1.28	4.87	5.40

$\phi = 35.00$ $k = .30$

β/φ	=	0	1/6	1/3	1/2	2/3	5/6	1
δ/φ	α			--- K_A -VALUES ---				
0	60.00	.81	.93	1.12	1.47	2.16	3.98	27.47
	75.00	.61	.68	.80	1.03	1.46	2.62	17.62
	90.00	.48	.53	.61	.78	1.12	2.11	12.05
	105.00	.38	.42	.48	.65	5.78	3.77	8.20
	120.00	.30	.33	.37	.51	1.41	2.78	5.28
.3333	60.00	.87	1.03	1.28	1.70	2.48	4.58	31.67
	75.00	.62	.71	.85	1.10	1.57	2.82	18.97
	90.00	.47	.53	.62	.80	1.14	2.16	12.22
	105.00	.38	.40	.47	.65	5.84	3.77	7.91
	120.00	.27	.30	.35	.49	1.38	2.68	5.39
.5000	60.00	.93	1.12	1.40	1.86	2.73	5.05	34.90
	75.00	.64	.74	.90	1.16	1.65	2.58	20.06
	90.00	.47	.54	.64	.82	1.17	2.21	12.57
	105.00	.36	.40	.47	.66	5.96	3.83	7.89
	120.00	.27	.29	.34	.48	1.37	2.72	5.54
.6667	60.00	1.03	1.25	1.58	2.10	3.07	5.66	39.32
	75.00	.68	.79	.98	1.25	1.70	3.20	21.51
	90.00	.48	.55	.66	.85	1.22	2.36	13.03
	105.00	.36	.40	.47	.68	6.15	8.13	8.06
	120.00	.26	.29	.34	.49	1.40	2.79	5.75
1.0000	60.00	1.40	1.72	2.18	2.90	4.26	7.90	54.60
	75.00	.80	.95	1.16	1.51	2.15	3.87	26.07
	90.00	.53	.61	.74	.95	1.36	2.58	14.56
	105.00	.38	.42	.51	.75	3.13	8.97	9.03
	120.00	.27	.30	.35	.51	2.21	6.40	6.45

Coefficients of active earth pressure K_A for $\phi = 40°$ and $k = 0$, 0.05, 0.10 and 0.15

$\phi = 40.00$ $k = 0$

β/φ	=	0	1/6	1/3	1/2	2/3	5/6	1
δ/φ	α			--- K_A -VALUES ---				
0	60.00	.49	.54	.59	.66	.75	.89	1.47
	75.00	.33	.35	.38	.42	.47	.55	.80
	90.00	.22	.23	.25	.27	.30	.35	.53
	105.00	.13	.14	.15	.16	.17	.20	.35
	120.00	.07	.07	.07	.07	.08	.09	.17
.3333	60.00	.49	.54	.60	.68	.78	.96	1.74
	75.00	.32	.34	.37	.41	.47	.56	.82
	90.00	.20	.21	.23	.25	.28	.34	.52
	105.00	.12	.13	.13	.14	.16	.19	.34
	120.00	.06	.06	.06	.07	.07	.08	.16
.5000	60.00	.50	.56	.62	.71	.83	1.03	1.96
	75.00	.32	.34	.38	.42	.48	.58	1.05
	90.00	.20	.21	.23	.25	.28	.34	.61
	105.00	.12	.12	.13	.14	.16	.19	.34
	120.00	.05	.06	.06	.06	.07	.08	.15
.6667	60.00	.53	.59	.66	.76	.89	1.13	2.29
	75.00	.32	.35	.39	.43	.50	.61	1.15
	90.00	.20	.21	.23	.25	.29	.35	.64
	105.00	.12	.12	.13	.14	.16	.19	.35
	120.00	.05	.05	.06	.06	.07	.08	.15
1.0000	60.00	.62	.71	.81	.94	1.15	1.52	3.69
	75.00	.36	.39	.44	.49	.57	.72	1.49
	90.00	.21	.23	.25	.27	.31	.38	.74
	105.00	.12	.13	.13	.15	.16	.20	.38
	120.00	.05	.05	.06	.06	.07	.08	.15

$\phi = 40.00$ $k = .05$

β/φ	=	0	1/6	1/3	1/2	2/3	5/6	1
δ/φ	α			--- K_A -VALUES ---				
0	60.00	.52	.57	.64	.72	.83	1.04	5.70
	75.00	.36	.38	.42	.46	.53	.65	3.48
	90.00	.24	.26	.28	.30	.34	.42	2.23
	105.00	.16	.16	.17	.19	.21	.26	1.38
	120.00	.08	.09	.09	.10	.11	.13	.88
.3333	60.00	.53	.59	.66	.75	.89	1.16	6.74
	75.00	.35	.38	.41	.46	.54	.68	3.80
	90.00	.23	.24	.26	.29	.33	.42	2.26
	105.00	.14	.15	.16	.17	.20	.25	1.32
	120.00	.07	.08	.08	.09	.10	.12	.70
.5000	60.00	.54	.61	.69	.78	.95	1.27	7.55
	75.00	.35	.38	.42	.47	.55	.71	4.07
	90.00	.22	.24	.26	.29	.33	.43	2.36
	105.00	.14	.15	.16	.17	.19	.24	1.34
	120.00	.07	.07	.08	.08	.09	.12	.73
.6667	60.00	.57	.65	.74	.86	1.05	1.43	8.83
	75.00	.36	.39	.44	.49	.58	.76	4.45
	90.00	.23	.24	.26	.29	.34	.44	2.48
	105.00	.14	.15	.16	.17	.19	.24	1.35
	120.00	.07	.07	.08	.08	.09	.11	.77
1.0000	60.00	.70	.80	.93	1.12	1.41	2.06	13.90
	75.00	.40	.44	.50	.57	.69	.84	5.74
	90.00	.24	.26	.29	.32	.38	.49	2.80
	105.00	.14	.15	.16	.18	.20	.26	1.57
	120.00	.07	.07	.08	.08	.09	.12	.89

$\phi = 40.00$ $k = .10$

β/φ	=	0	1/6	1/3	1/2	2/3	5/6	1
δ/φ	α			--- K_A -VALUES ---				
0	60.00	.56	.62	.69	.79	.94	1.32	9.82
	75.00	.39	.42	.46	.51	.60	.83	6.05
	90.00	.27	.29	.31	.35	.40	.56	3.65
	105.00	.18	.19	.20	.22	.26	.36	2.41
	120.00	.10	.11	.12	.13	.14	.21	1.29
.3333	60.00	.57	.64	.72	.84	1.03	1.55	11.72
	75.00	.38	.41	.46	.52	.62	.90	6.61
	90.00	.25	.27	.30	.33	.40	.57	3.92
	105.00	.16	.17	.19	.21	.24	.35	2.32
	120.00	.09	.10	.10	.11	.13	.19	1.32
.5000	60.00	.59	.67	.77	.90	1.12	1.76	13.21
	75.00	.38	.42	.47	.54	.65	.97	7.05
	90.00	.25	.27	.30	.34	.40	.59	4.11
	105.00	.16	.17	.18	.20	.24	.25	2.33
	120.00	.09	.09	.10	.11	.13	.19	1.37
.6667	60.00	.63	.72	.83	.99	1.25	2.05	15.37
	75.00	.40	.44	.49	.57	.69	1.06	7.75
	90.00	.26	.28	.30	.35	.41	.62	4.33
	105.00	.16	.17	.18	.20	.24	.36	2.57
	120.00	.09	.09	.10	.11	.12	.15	1.44
1.0000	60.00	.78	.92	1.09	1.35	1.80	3.27	24.26
	75.00	.45	.50	.57	.67	.85	1.38	9.92
	90.00	.28	.30	.33	.38	.46	.72	5.01
	105.00	.17	.18	.19	.22	.26	.38	2.76
	120.00	.09	.09	.10	.11	.13	.19	1.68

$\phi = 40.00$ $k = .15$

β/φ	=	0	1/6	1/3	1/2	2/3	5/6	1
δ/φ	α			--- K_A -VALUES ---				
0	60.00	.59	.66	.75	.87	1.08	1.53	14.14
	75.00	.42	.46	.50	.58	.70	1.22	8.62
	90.00	.30	.32	.35	.40	.48	.83	5.55
	105.00	.20	.22	.24	.27	.32	.75	3.43
	120.00	.13	.13	.14	.16	.18	.47	1.88
.3333	60.00	.61	.70	.80	.95	1.23	2.29	16.73
	75.00	.41	.46	.51	.59	.75	1.33	9.42
	90.00	.26	.31	.34	.39	.48	.65	5.62
	105.00	.19	.20	.22	.25	.31	.75	3.30
	120.00	.11	.12	.13	.14	.17	.44	1.94
.5000	60.00	.65	.74	.86	1.04	1.37	2.55	18.85
	75.00	.42	.47	.53	.62	.78	1.43	10.10
	90.00	.28	.31	.34	.39	.49	.88	5.87
	105.00	.19	.20	.22	.25	.31	.76	3.31
	120.00	.11	.12	.13	.14	.17	.44	2.01
.6667	60.00	.70	.80	.95	1.16	1.57	3.02	21.62
	75.00	.44	.49	.56	.66	.85	1.57	11.04
	90.00	.28	.32	.35	.41	.51	.93	6.15
	105.00	.19	.20	.22	.25	.31	.79	3.38
	120.00	.11	.12	.12	.14	.17	.45	2.11
1.0000	60.00	.91	1.08	1.32	1.69	2.44	4.62	34.51
	75.00	.51	.58	.67	.81	1.09	2.03	14.25
	90.00	.32	.35	.39	.46	.59	1.08	7.14
	105.00	.20	.21	.23	.27	.33	1.15	3.96
	120.00	.11	.12	.13	.14	.18	.50	2.46

Coefficients of active earth pressure K_A for $\phi = 40°$ and $k = 0.20$, 0.25 and 0.30, and for $\phi = 45°$ and $k = 0$

* ϕ = 40.00 k = .20 *

β/φ	=	0	1/6	1/3	1/2	2/3	5/6	1
δ/φ	α			--- K_A -VALUES ---				
0	60.00	.63	.71	.82	.97	1.31	2.55	18.22
	75.00	.45	.50	.56	.65	.85	1.61	11.21
	90.00	.33	.36	.40	.46	.59	1.10	7.20
	105.00	.23	.25	.28	.32	.42	1.22	4.46
	120.00	.15	.16	.18	.20	.26	.77	2.49
.3333	60.00	.67	.76	.90	1.10	1.54	3.02	21.72
	75.00	.45	.51	.58	.69	.92	1.76	12.2
	90.00	.32	.35	.39	.46	.61	1.13	7.37
	105.00	.22	.23	.25	.30	.41	1.22	4.29
	120.00	.14	.15	.16	.18	.25	.76	2.56
.5000	60.00	.71	.82	.97	1.22	1.73	3.42	24.45
	75.00	.47	.52	.60	.72	.93	1.85	13.15
	90.00	.32	.35	.39	.47	.63	1.17	7.65
	105.00	.21	.23	.25	.30	.41	1.25	4.29
	120.00	.13	.14	.16	.18	.24	.75	2.65
.6667	60.00	.77	.91	1.09	1.39	2.01	3.98	28.47
	75.00	.49	.55	.64	.78	1.08	2.07	14.34
	90.00	.33	.36	.41	.48	.66	1.23	7.97
	105.00	.22	.23	.26	.30	.42	1.30	4.42
	120.00	.13	.14	.16	.18	.24	.78	2.78
1.0000	60.00	1.07	1.30	1.64	2.18	3.12	6.36	44.61
	75.00	.58	.67	.79	.99	1.39	2.69	18.50
	90.00	.36	.40	.46	.56	.77	1.44	9.26
	105.00	.23	.25	.28	.33	.46	2.09	5.15
	120.00	.14	.15	.16	.18	.25	1.28	3.25

* ϕ = 40.00 k = .25 *

β/φ	=	0	1/6	1/3	1/2	2/3	5/6	1
δ/φ	α			--- K_A -VALUES ---				
0	60.00	.68	.77	.90	1.11	1.60	3.16	22.59
	75.00	.49	.54	.62	.75	1.04	2.00	13.79
	90.00	.35	.40	.45	.53	.74	1.36	8.86
	105.00	.27	.29	.32	.38	1.91	1.69	5.48
	120.00	.18	.20	.22	.25	1.18	1.10	3.09
.3333	60.00	.73	.85	1.01	1.30	1.86	3.76	25.72
	75.00	.50	.56	.65	.81	1.13	2.19	15.06
	90.00	.35	.39	.45	.54	.76	1.42	9.67
	105.00	.25	.27	.31	.37	1.84	1.70	5.27
	120.00	.17	.18	.20	.23	1.21	1.08	3.17
.5000	60.00	.78	.92	1.12	1.47	2.11	4.25	30.16
	75.00	.52	.59	.69	.86	1.21	2.35	16.14
	90.00	.35	.40	.46	.56	.79	1.47	9.37
	105.00	.25	.27	.31	.37	2.00	1.73	5.28
	120.00	.16	.17	.19	.23	1.25	1.07	3.29
.6667	60.00	.87	1.03	1.28	1.71	2.45	4.86	35.02
	75.00	.55	.63	.74	.94	1.32	2.57	17.64
	90.00	.37	.41	.47	.59	.83	1.54	9.83
	105.00	.25	.27	.31	.38	2.10	1.80	5.44
	120.00	.16	.17	.19	.23	1.30	1.11	3.46
1.0000	60.00	1.29	1.58	2.04	2.69	3.81	7.91	55.11
	75.00	.66	.78	.94	1.22	1.69	3.34	22.76
	90.00	.41	.46	.54	.69	.97	1.80	11.49
	105.00	.27	.29	.34	.41	2.42	3.03	6.35
	120.00	.17	.18	.20	.24	1.50	1.89	4.03

* ϕ = 40.00 k = .30 *

β/φ	=	0	1/6	1/3	1/2	2/3	5/6	1
δ/φ	α			--- K_A -VALUES ---				
0	60.00	.73	.84	1.00	1.31	1.88	3.78	26.80
	75.00	.53	.60	.69	.83	1.23	2.38	16.36
	90.00	.40	.44	.51	.63	.89	1.65	10.52
	105.00	.30	.33	.37	.47	6.89	2.16	6.50
	120.00	.21	.23	.26	.33	4.41	1.43	3.69
.3333	60.00	.80	.94	1.16	1.54	2.22	4.49	31.71
	75.00	.55	.63	.74	.96	1.33	2.61	17.67
	90.00	.39	.44	.51	.65	.92	1.70	10.76
	105.00	.28	.31	.36	.46	7.03	2.17	6.26
	120.00	.20	.21	.24	.31	4.49	1.40	3.79
.5000	60.00	.87	1.04	1.31	1.74	2.45	5.05	33.73
	75.00	.57	.66	.79	1.03	1.43	2.81	19.15
	90.00	.40	.45	.53	.67	.95	1.75	11.12
	105.00	.28	.31	.36	.47	7.24	2.22	6.27
	120.00	.19	.21	.24	.31	4.63	1.40	3.93
.6667	60.00	.98	1.20	1.53	2.02	2.89	5.93	41.56
	75.00	.61	.71	.87	1.12	1.55	3.07	20.92
	90.00	.42	.47	.56	.71	1.00	1.85	11.67
	105.00	.28	.32	.37	.48	7.58	2.30	6.47
	120.00	.19	.21	.24	.31	4.85	1.45	4.13
1.0000	60.00	1.53	1.86	2.44	3.19	4.49	9.40	65.41
	75.00	.77	.91	1.13	1.45	2.00	3.99	27.01
	90.00	.47	.54	.65	.82	1.10	2.16	13.59
	105.00	.31	.35	.41	.54	8.74	3.97	7.55
	120.00	.20	.22	.25	.33	5.59	2.51	4.82

* ϕ = 45.00 k = 0 *

β/φ	=	0	1/6	1/3	1/2	2/3	5/6	1
δ/φ	α			--- K_A -VALUES ---				
0	60.00	.44	.48	.53	.59	.67	.81	1.42
	75.00	.28	.30	.32	.35	.40	.48	.82
	90.00	.17	.18	.19	.21	.23	.28	.49
	105.00	.10	.10	.10	.11	.12	.14	.27
	120.00	.03	.04	.04	.04	.04	.05	.10
.3333	60.00	.44	.48	.55	.62	.72	.90	1.72
	75.00	.27	.29	.32	.35	.40	.48	.91
	90.00	.16	.17	.18	.20	.22	.27	.51
	105.00	.09	.09	.09	.10	.11	.13	.26
	120.00	.03	.03	.03	.03	.04	.04	.09
.5000	60.00	.46	.51	.57	.66	.77	.98	1.89
	75.00	.27	.30	.33	.36	.42	.51	.99
	90.00	.16	.17	.18	.20	.23	.27	.53
	105.00	.08	.09	.09	.10	.11	.13	.25
	120.00	.03	.03	.03	.03	.04	.04	.09
.6667	60.00	.49	.55	.62	.72	.85	1.10	2.40
	75.00	.28	.31	.34	.38	.44	.55	1.11
	90.00	.16	.17	.19	.20	.23	.28	.56
	105.00	.08	.09	.09	.10	.11	.13	.26
	120.00	.03	.03	.03	.03	.04	.04	.09
1.0000	60.00	.62	.71	.82	.97	1.20	1.64	4.49
	75.00	.33	.36	.40	.46	.54	.69	1.54
	90.00	.18	.19	.21	.23	.26	.32	.68
	105.00	.09	.09	.10	.11	.12	.14	.30
	120.00	.03	.03	.03	.03	.04	.04	.09

Coefficients of active earth pressure K_A for $\phi = 45°$ and $k = 0.05$, 0.10, 0.15 and 0.20

* ϕ = 45.00 k = .05 *

β/φ	=	0	1/6	1/3	1/2	2/3	5/6	1
δ/φ	α			---K_A -VALUES ---				
0	60.00	.46	.51	.57	.65	.75	.95	5.47
	75.00	.30	.33	.36	.40	.45	.57	3.17
	90.00	.19	.21	.22	.24	.28	.34	1.90
	105.00	.11	.12	.12	.13	.15	.19	1.04
	120.00	.05	.05	.05	.06	.06	.08	.52
.3333	60.00	.48	.53	.60	.69	.82	1.08	6.65
	75.00	.30	.32	.36	.40	.47	.60	3.52
	90.00	.18	.20	.21	.23	.27	.34	1.96
	105.00	.10	.11	.11	.12	.14	.18	1.01
	120.00	.04	.04	.05	.05	.05	.07	.49
.5000	60.00	.50	.56	.64	.74	.89	1.21	7.69
	75.00	.30	.33	.37	.41	.49	.63	3.82
	90.00	.18	.20	.21	.24	.27	.35	2.04
	105.00	.10	.11	.11	.12	.14	.17	1.03
	120.00	.04	.04	.04	.05	.05	.07	.51
.6667	60.00	.54	.61	.70	.82	1.01	1.40	9.29
	75.00	.32	.35	.39	.44	.52	.69	4.27
	90.00	.19	.20	.22	.24	.28	.36	2.17
	105.00	.10	.11	.11	.12	.14	.18	1.07
	120.00	.04	.04	.04	.05	.05	.07	.52
1.0000	60.00	.71	.83	.97	1.18	1.52	2.30	17.36
	75.00	.37	.41	.47	.54	.65	.90	5.97
	90.00	.21	.22	.24	.27	.32	.43	2.64
	105.00	.11	.11	.12	.13	.15	.20	1.26
	120.00	.04	.04	.05	.05	.05	.07	.58

* ϕ = 45.00 k = .10 *

β/φ	=	0	1/6	1/3	1/2	2/3	5/6	1
δ/φ	α			--- K_A -VALUES ---				
0	60.00	.50	.55	.62	.71	.85	1.18	9.52
	75.00	.33	.36	.39	.44	.52	.71	5.52
	90.00	.22	.23	.25	.28	.32	.44	3.31
	105.00	.13	.14	.15	.16	.19	.26	1.81
	120.00	.06	.07	.07	.08	.09	.12	.98
.3333	60.00	.52	.58	.66	.77	.95	1.41	11.58
	75.00	.33	.36	.40	.45	.54	.76	6.12
	90.00	.21	.22	.24	.27	.32	.45	3.41
	105.00	.12	.13	.14	.15	.18	.25	1.78
	120.00	.06	.06	.06	.07	.08	.11	.94
.5000	60.00	.54	.62	.71	.84	1.06	1.62	13.36
	75.00	.34	.37	.41	.48	.58	.84	6.06
	90.00	.21	.22	.25	.28	.33	.47	3.55
	105.00	.12	.13	.14	.15	.18	.25	1.81
	120.00	.06	.06	.06	.07	.08	.11	.94
.6667	60.00	.59	.68	.79	.95	1.22	1.88	16.17
	75.00	.35	.39	.44	.51	.62	.94	7.44
	90.00	.21	.23	.25	.29	.34	.50	3.76
	105.00	.12	.13	.14	.15	.18	.26	1.88
	120.00	.06	.06	.06	.07	.08	.11	.97
1.0000	60.00	.83	.97	1.17	1.47	2.02	3.00	30.22
	75.00	.42	.48	.54	.64	.81	1.30	10.39
	90.00	.24	.26	.29	.33	.40	.61	4.60
	105.00	.13	.14	.15	.17	.20	.29	2.23
	120.00	.06	.06	.06	.07	.08	.11	1.13

* ϕ = 45.00 k = .15 *

β/φ	=	0	1/6	1/3	1/2	2/3	5/6	1
δ/φ	α			--- K_A -VALUES ---				
0	60.00	.53	.60	.68	.79	.98	1.62	13.58
	75.00	.36	.39	.44	.50	.61	.98	7.87
	90.00	.24	.26	.29	.32	.39	.64	4.71
	105.00	.15	.16	.18	.20	.24	1.13	2.58
	120.00	.08	.08	.09	.10	.12	.58	1.43
.3333	60.00	.56	.64	.74	.88	1.13	1.97	16.51
	75.00	.36	.40	.45	.52	.65	1.08	8.73
	90.00	.23	.25	.28	.32	.39	.67	4.85
	105.00	.14	.15	.16	.18	.23	1.16	2.54
	120.00	.07	.08	.08	.09	.11	.59	1.37
.5000	60.00	.60	.69	.80	.97	1.28	2.27	19.08
	75.00	.37	.41	.47	.55	.70	1.17	9.50
	90.00	.24	.26	.28	.33	.40	.70	5.06
	105.00	.14	.15	.16	.18	.23	1.71	2.57
	120.00	.07	.08	.08	.09	.11	.62	1.41
.6667	60.00	.66	.77	.91	1.12	1.52	2.73	23.06
	75.00	.39	.44	.50	.59	.77	1.31	10.61
	90.00	.24	.26	.29	.34	.43	.74	5.39
	105.00	.14	.15	.17	.19	.23	1.28	2.69
	120.00	.07	.07	.08	.09	.11	.65	1.46
1.0000	60.00	.90	1.18	1.47	1.94	2.76	5.02	43.09
	75.00	.49	.55	.64	.78	1.05	1.82	14.82
	90.00	.26	.30	.34	.40	.51	.91	6.55
	105.00	.16	.17	.18	.21	.26	1.55	1.71
	120.00	.07	.08	.08	.09	.11	.79	1.72

* ϕ = 45.00 k = .20 *

β/φ	=	0	1/6	1/3	1/2	2/3	5/6	1
δ/φ	α			---K_A -VALUES ---				
0	60.00	.57	.65	.74	.88	1.16	2.08	17.63
	75.00	.39	.43	.48	.56	.72	1.26	10.22
	90.00	.27	.29	.32	.37	.47	.86	6.12
	105.00	.18	.19	.21	.24	.30	3.23	3.36
	120.00	.10	.11	.12	.13	.16	1.78	1.88
.3333	60.00	.61	.70	.83	1.01	1.40	2.53	21.44
	75.00	.40	.44	.50	.60	.80	1.39	11.33
	90.00	.26	.29	.32	.37	.48	.89	6.31
	105.00	.17	.18	.20	.23	.29	3.31	3.31
	120.00	.09	.10	.11	.12	.15	1.82	1.83
.5000	60.00	.66	.77	.91	1.14	1.61	2.91	24.78
	75.00	.41	.46	.53	.64	.87	1.51	12.33
	90.00	.27	.29	.33	.39	.51	.93	6.58
	105.00	.17	.18	.20	.23	.30	3.44	3.34
	120.00	.09	.10	.10	.12	.15	1.90	1.87
.6667	60.00	.74	.87	1.06	1.35	1.93	3.51	28.85
	75.00	.44	.50	.58	.70	.96	1.68	13.78
	90.00	.28	.30	.34	.41	.55	.99	7.00
	105.00	.17	.18	.20	.23	.31	3.65	3.51
	120.00	.09	.10	.10	.12	.15	2.01	1.93
1.0000	60.00	1.21	1.49	1.90	2.55	3.50	6.45	55.95
	75.00	.56	.64	.76	.96	1.33	2.34	19.24
	90.00	.32	.35	.40	.49	.67	1.22	8.51
	105.00	.18	.20	.22	.26	.35	4.42	2.18
	120.00	.09	.10	.11	.12	.16	2.43	2.27

Coefficients of active earth pressure K_A for $\phi = 45°$ and $k = 0.25$ and 0.30, and for $\phi = 50°$ and $k = 0$ and 0.05

* ϕ = 45.00 k= .25 *

β/φ	=	0	1/6	1/3	1/2	2/3	5/6	1
δ/φ	α			--- K_A-VALUES ---				
0	60.00	.61	.70	.82	1.00	1.41	2.55	21.69
	75.00	.43	.47	.54	.64	.88	1.53	12.56
	90.00	.30	.33	.37	.43	.59	1.07	7.53
	105.00	.20	.22	.25	.29	.42	5.32	4.14
	120.00	.13	.13	.15	.17	.25	2.98	2.33
.3333	60.00	.67	.78	.93	1.19	1.70	3.08	26.37
	75.00	.44	.49	.57	.70	.97	1.70	13.94
	90.00	.30	.33	.37	.44	.61	1.11	7.76
	105.00	.19	.21	.23	.28	.42	5.46	4.00
	120.00	.11	.12	.13	.15	.23	3.06	2.26
.5000	60.00	.73	.86	1.05	1.37	1.85	3.55	30.47
	75.00	.46	.52	.61	.76	1.05	1.84	15.17
	90.00	.30	.33	.38	.46	.64	1.16	8.09
	105.00	.19	.21	.24	.28	.41	5.68	4.12
	120.00	.11	.12	.13	.15	.23	3.18	2.32
.6667	60.00	.84	1.00	1.25	1.66	2.34	4.28	36.83
	75.00	.50	.57	.67	.85	1.17	2.05	16.55
	90.00	.31	.35	.40	.49	.68	1.24	8.61
	105.00	.20	.21	.24	.28	.44	6.03	4.32
	120.00	.11	.12	.13	.15	.24	3.37	2.40
1.0000	60.00	1.47	1.82	2.33	3.16	4.25	7.88	68.82
	75.00	.65	.76	.93	1.19	1.61	2.85	23.67
	90.00	.37	.42	.48	.60	.84	1.52	10.47
	105.00	.22	.24	.27	.33	.53	7.28	2.66
	120.00	.12	.13	.14	.17	.26	4.07	2.85

* ϕ = 45.00 k = .30 *

β/φ	=	0	1/6	1/3	1/2	2/3	5/6	1
δ/φ	α			--- K_A-VALUES ---				
0	60.00	.66	.76	.91	1.16	1.65	3.01	25.74
	75.00	.46	.52	.60	.75	1.03	1.81	14.91
	90.00	.33	.37	.42	.51	.71	1.29	8.93
	105.00	.23	.26	.29	.35	1.48	7.42	4.91
	120.00	.15	.16	.18	.22	.95	4.10	2.77
.3333	60.00	.73	.87	1.07	1.41	2.00	3.64	31.30
	75.00	.48	.55	.65	.83	1.14	2.00	16.54
	90.00	.33	.37	.43	.53	.73	1.33	9.21
	105.00	.22	.24	.28	.34	1.53	7.61	4.75
	120.00	.14	.15	.17	.20	.91	4.29	2.72
.5000	60.00	.81	.98	1.23	1.63	2.29	4.20	36.17
	75.00	.51	.59	.70	.91	1.23	2.18	18.00
	90.00	.34	.38	.44	.55	.77	1.40	9.60
	105.00	.22	.25	.28	.35	1.59	7.92	4.89
	120.00	.14	.15	.16	.20	.93	4.46	2.77
.6667	60.00	.95	1.17	1.49	1.98	2.75	5.06	43.72
	75.00	.56	.65	.79	1.01	1.37	2.43	20.12
	90.00	.36	.40	.47	.59	.82	1.49	10.21
	105.00	.23	.25	.29	.37	1.70	8.40	5.14
	120.00	.14	.15	.17	.20	.96	4.73	2.88
1.0000	60.00	1.73	2.15	2.77	3.77	4.89	9.38	81.69
	75.00	.76	.90	1.10	1.43	1.90	3.37	28.10
	90.00	.43	.49	.58	.72	1.00	1.82	12.42
	105.00	.26	.28	.33	.42	1.36	10.15	3.13
	120.00	.15	.16	.18	.22	1.12	5.72	3.42

* ϕ = 50.00 k = 0 *

β/φ	=	0	1/6	1/3	1/2	2/3	5/6	1
δ/φ	α			--- K_A-VALUES ---				
0	60.00	.38	.42	.47	.52	.60	.73	1.34
	75.00	.23	.25	.27	.30	.34	.40	.73
	90.00	.13	.14	.15	.16	.18	.22	.40
	105.00	.06	.07	.07	.07	.08	.09	.19
	120.00	.01	.01	.01	.02	.02	.02	.04
.3333	60.00	.39	.44	.49	.56	.65	.82	1.67
	75.00	.23	.25	.27	.30	.34	.42	.83
	90.00	.13	.13	.14	.15	.17	.21	.42
	105.00	.06	.06	.06	.07	.07	.09	.18
	120.00	.01	.01	.01	.01	.02	.02	.04
.5000	60.00	.42	.47	.53	.60	.71	.91	1.99
	75.00	.23	.26	.28	.31	.36	.44	.91
	90.00	.13	.13	.14	.16	.18	.22	.44
	105.00	.06	.06	.06	.07	.07	.09	.19
	120.00	.01	.01	.01	.01	.02	.02	.04
.6667	60.00	.46	.51	.58	.68	.81	1.06	2.52
	75.00	.25	.27	.30	.33	.39	.49	1.05
	90.00	.13	.14	.15	.16	.18	.23	.48
	105.00	.06	.06	.06	.07	.08	.09	.19
	120.00	.01	.01	.01	.01	.02	.02	.04
1.0000	60.00	.65	.75	.87	1.04	1.31	1.84	6.13
	75.00	.31	.34	.37	.43	.50	.65	1.62
	90.00	.15	.16	.17	.18	.22	.27	.62
	105.00	.06	.07	.07	.08	.08	.10	.22
	120.00	.01	.01	.01	.01	.02	.02	.04

* ϕ = 50.00 k = .05 *

β/φ	=	0	1/6	1/3	1/2	2/3	5/6	1
δ/φ	α			--- K_A-VALUES ---				
0	60.00	.41	.46	.51	.58	.67	.86	5.17
	75.00	.25	.28	.30	.33	.38	.48	2.83
	90.00	.15	.16	.17	.19	.22	.27	1.56
	105.00	.08	.08	.09	.09	.10	.13	.74
	120.00	.02	.03	.03	.03	.03	.04	.22
.3333	60.00	.43	.48	.54	.63	.75	1.00	6.47
	75.00	.25	.28	.30	.34	.40	.52	3.19
	90.00	.14	.15	.17	.18	.21	.27	1.62
	105.00	.07	.08	.08	.09	.10	.12	.71
	120.00	.02	.02	.02	.02	.03	.03	.23
.5000	60.00	.46	.52	.59	.69	.83	1.14	7.65
	75.00	.26	.29	.32	.36	.42	.56	3.53
	90.00	.15	.16	.17	.19	.22	.28	1.71
	105.00	.07	.07	.08	.09	.10	.12	.72
	120.00	.02	.02	.02	.02	.03	.03	.25
.6667	60.00	.51	.58	.66	.78	.97	1.36	9.74
	75.00	.28	.31	.34	.39	.46	.62	4.08
	90.00	.15	.16	.18	.19	.23	.29	1.95
	105.00	.07	.08	.08	.09	.10	.12	.75
	120.00	.02	.02	.02	.02	.03	.03	.27
1.0000	60.00	.76	.89	1.07	1.31	1.74	2.78	23.69
	75.00	.35	.39	.44	.51	.62	.87	6.26
	90.00	.18	.19	.21	.23	.27	.36	2.38
	105.00	.08	.08	.09	.10	.11	.14	.57
	120.00	.02	.02	.02	.02	.03	.03	.35

Coefficients of active earth pressure K_A for $\phi = 50°$ and $k = 0.10$, 0.15, 0.20 and 0.25

* ϕ = 50.00 k = .10 *

β/φ	=	0	1/6	1/3	1/2	2/3	5/6	1
δ/φ	α			---K_A-VALUES ---				
0	60.00	.44	.49	.56	.64	.76	1.06	9.00
	75.00	.28	.30	.34	.38	.44	.60	4.93
	90.00	.17	.18	.20	.22	.26	.35	2.72
	105.00	.09	.10	.11	.11	.13	.18	1.29
	120.00	.04	.04	.04	.04	.05	.06	.47
.3333	60.00	.47	.53	.60	.71	.87	1.29	11.26
	75.00	.28	.31	.34	.39	.47	.67	5.56
	90.00	.17	.18	.19	.22	.26	.36	2.83
	105.00	.09	.09	.10	.11	.12	.17	1.24
	120.00	.03	.03	.03	.04	.04	.06	.49
.5000	60.00	.50	.57	.66	.79	.99	1.51	13.39
	75.00	.29	.32	.36	.41	.50	.73	6.15
	90.00	.17	.18	.20	.22	.26	.35	2.93
	105.00	.09	.09	.10	.11	.12	.17	1.26
	120.00	.03	.03	.03	.04	.04	.06	.52
.6667	60.00	.56	.65	.76	.92	1.18	1.90	16.55
	75.00	.31	.35	.39	.45	.56	.83	7.05
	90.00	.18	.19	.21	.23	.28	.40	3.22
	105.00	.09	.09	.10	.11	.13	.18	1.33
	120.00	.03	.03	.03	.04	.04	.06	.57
1.0000	60.00	.93	1.11	1.37	1.76	2.52	4.71	41.25
	75.00	.41	.46	.52	.62	.75	1.28	10.90
	90.00	.21	.23	.25	.28	.34	.52	4.15
	105.00	.10	.11	.11	.13	.15	.21	1.73
	120.00	.03	.03	.04	.04	.04	.06	.74

* ϕ = 50.00 k = .15 *

β/φ	=	0	1/6	1/3	1/2	2/3	5/6	1
δ/φ	α			--- K_A-VALUES ---				
0	60.00	.48	.53	.61	.71	.88	1.45	12.83
	75.00	.31	.34	.37	.43	.52	.83	7.02
	90.00	.18	.21	.23	.26	.31	.50	3.88
	105.00	.11	.12	.13	.14	.17	.48	1.84
	120.00	.05	.05	.05	.06	.07	.17	.72
.3333	60.00	.51	.58	.68	.81	1.04	1.82	16.05
	75.00	.31	.35	.39	.45	.56	.84	7.92
	90.00	.19	.21	.23	.26	.31	.52	4.03
	105.00	.10	.11	.12	.13	.16	.49	1.77
	120.00	.04	.05	.05	.05	.06	.18	.75
.5000	60.00	.56	.64	.75	.91	1.20	2.16	19.09
	75.00	.33	.36	.41	.48	.61	1.04	8.77
	90.00	.19	.21	.23	.27	.33	.55	4.25
	105.00	.11	.11	.12	.13	.16	.52	1.79
	120.00	.04	.04	.05	.05	.06	.19	.79
.6667	60.00	.63	.74	.88	1.09	1.49	2.75	24.17
	75.00	.35	.40	.45	.53	.69	1.19	10.05
	90.00	.20	.22	.24	.28	.35	.59	4.59
	105.00	.11	.11	.12	.14	.17	.56	1.91
	120.00	.04	.04	.05	.05	.06	.20	.86
1.0000	60.00	1.22	1.49	1.86	2.41	3.71	6.82	58.81
	75.00	.47	.54	.63	.77	1.03	1.85	15.54
	90.00	.24	.27	.30	.35	.44	.77	5.92
	105.00	.12	.13	.14	.16	.20	.71	2.49
	120.00	.05	.05	.05	.06	.07	.26	1.12

* ϕ = 50.00 k = .20 *

β/φ	=	0	1/6	1/3	1/2	2/3	5/6	1
δ/φ	α			---K_A -VALUES ---				
0	60.00	.51	.58	.67	.79	1.03	1.80	15.66
	75.00	.34	.37	.42	.48	.61	1.09	9.12
	90.00	.22	.24	.26	.30	.38	.66	5.04
	105.00	.13	.14	.15	.17	.22	3.05	2.39
	120.00	.06	.07	.07	.08	.10	1.43	.97
.3333	60.00	.56	.65	.76	.93	1.27	2.38	20.85
	75.00	.35	.39	.44	.52	.69	1.23	10.29
	90.00	.22	.24	.26	.30	.39	.69	5.23
	105.00	.12	.13	.15	.17	.21	3.13	2.30
	120.00	.06	.06	.07	.07	.09	1.48	1.01
.5000	60.00	.62	.72	.86	1.07	1.52	2.83	24.79
	75.00	.37	.41	.47	.57	.76	1.36	11.39
	90.00	.22	.24	.27	.32	.41	.73	5.52
	105.00	.13	.13	.15	.17	.22	3.25	2.32
	120.00	.06	.06	.06	.07	.09	1.55	1.07
.6667	60.00	.72	.85	1.03	1.33	1.94	3.60	31.36
	75.00	.40	.45	.52	.64	.87	1.56	13.06
	90.00	.23	.26	.29	.34	.45	.79	5.95
	105.00	.13	.14	.15	.17	.22	3.55	2.50
	120.00	.06	.06	.07	.07	.09	1.67	1.16
1.0000	60.00	1.58	1.92	2.38	3.06	4.90	8.93	76.37
	75.00	.55	.64	.76	.96	1.37	2.43	20.18
	90.00	.28	.32	.36	.43	.56	1.03	7.68
	105.00	.15	.16	.18	.20	.27	4.53	3.24
	120.00	.06	.07	.07	.08	.10	2.13	1.51

* ϕ = 50.00 k = .25 *

β/φ	=	0	1/6	1/3	1/2	2/3	5/6	1
δ/φ	α			---K_A -VALUES ---				
0	60.00	.55	.63	.74	.90	1.26	2.34	20.49
	75.00	.37	.41	.47	.55	.75	1.34	11.22
	90.00	.25	.27	.30	.35	.47	.83	6.20
	105.00	.15	.17	.18	.21	.29	5.52	2.94
	120.00	.08	.09	.09	.11	.14	2.69	1.22
.3333	60.00	.61	.72	.86	1.09	1.58	2.94	25.65
	75.00	.38	.43	.50	.61	.85	1.52	12.65
	90.00	.24	.27	.30	.36	.49	.86	6.44
	105.00	.15	.16	.18	.21	.28	5.77	2.82
	120.00	.07	.08	.09	.10	.13	2.78	1.27
.5000	60.00	.69	.81	.99	1.28	1.89	3.56	30.49
	75.00	.41	.47	.54	.67	.94	1.68	14.00
	90.00	.25	.28	.32	.38	.52	.91	6.78
	105.00	.15	.16	.18	.21	.30	6.07	2.86
	120.00	.07	.08	.08	.10	.14	2.92	1.34
.6667	60.00	.82	.98	1.24	1.61	2.41	4.45	38.60
	75.00	.45	.52	.61	.77	1.09	1.93	16.06
	90.00	.27	.30	.34	.41	.56	.99	7.34
	105.00	.15	.17	.18	.22	.31	6.54	3.08
	120.00	.07	.08	.09	.10	.14	3.14	1.45
1.0000	60.00	1.94	2.35	2.90	3.72	6.09	11.04	93.53
	75.00	.66	.77	.93	1.16	1.70	3.00	24.63
	90.00	.33	.38	.44	.54	.73	1.29	9.45
	105.00	.18	.19	.22	.26	.30	6.35	4.00
	120.00	.08	.09	.10	.11	.16	4.01	1.89

Coefficients of active earth pressure K_A

$\phi = 50.00$ $k = .30$

β/φ	=	0	1/6	1/3	1/2	2/3	5/6	1
δ/φ	α			--- K_A -VALUES ---				
0	60.00	.60	.69	.82	1.03	1.50	2.79	24.32
	75.00	.40	.45	.52	.64	.90	1.60	13.31
	90.00	.28	.30	.34	.41	.56	.99	7.36
	105.00	.18	.19	.22	.26	.49	8.14	3.49
	120.00	.10	.11	.12	.14	.28	3.94	1.46
.3333	60.00	.69	.80	.98	1.28	1.89	3.50	30.44
	75.00	.43	.49	.57	.72	1.02	1.81	15.02
	90.00	.28	.31	.35	.43	.59	1.04	7.64
	105.00	.17	.19	.21	.26	.51	8.41	3.35
	120.00	.09	.10	.11	.13	.29	4.07	1.53
.5000	60.00	.77	.93	1.16	1.51	2.26	4.17	36.19
	75.00	.46	.53	.63	.79	1.13	2.00	16.62
	90.00	.29	.32	.37	.46	.62	1.10	8.05
	105.00	.17	.19	.22	.26	.54	8.84	3.39
	120.00	.09	.10	.11	.13	.29	4.28	1.61
.6667	60.00	.85	1.17	1.46	1.89	2.85	5.30	45.82
	75.00	.51	.60	.72	.90	1.30	2.30	19.06
	90.00	.31	.35	.40	.49	.67	1.19	8.71
	105.00	.18	.20	.23	.28	.58	9.53	3.66
	120.00	.09	.10	.11	.13	.30	4.61	1.75
1.0000	60.00	2.31	2.78	3.42	4.37	7.28	13.15	111.49
	75.00	.78	.92	1.10	1.37	2.03	3.58	28.47
	90.00	.39	.45	.52	.64	.87	1.55	11.22
	105.00	.21	.23	.27	.33	.76	12.16	4.76
	120.00	.10	.11	.13	.15	.36	5.89	2.28

Coefficients of passive earth pressure K_P

$\phi = 20.00$ $k = 0$

β/φ	=	0	1/6	1/3	1/2	2/3	5/6	1
δ/φ	α			--- K_P -VALUES ---				
0	60.00	1.74	1.88	2.02	2.17	2.32	2.47	2.61
	75.00	1.78	1.93	2.07	2.22	2.37	2.53	2.68
	90.00	2.04	2.21	2.38	2.55	2.73	2.91	3.08
	105.00	2.61	2.83	3.06	3.29	3.53	3.77	4.01
	120.00	3.79	4.13	4.49	4.85	5.22	5.60	5.98
.3333	60.00	1.91	2.10	2.30	2.50	2.70	2.91	3.11
	75.00	2.02	2.22	2.42	2.63	2.84	3.04	3.25
	90.00	2.40	2.62	2.86	3.10	3.35	3.60	3.85
	105.00	3.16	3.47	3.79	4.11	4.45	4.80	5.14
	120.00	4.75	5.24	5.75	6.27	6.81	7.37	7.93
.5000	60.00	2.00	2.22	2.44	2.67	2.90	3.14	3.37
	75.00	2.16	2.38	2.61	2.84	3.08	3.32	3.56
	90.00	2.58	2.85	3.12	3.39	3.68	3.96	4.26
	105.00	3.45	3.81	4.18	4.56	4.96	5.35	5.76
	120.00	5.27	5.85	6.44	7.05	7.69	8.34	9.00
.6667	60.00	2.09	2.34	2.59	2.84	3.10	3.37	3.63
	75.00	2.29	2.54	2.80	3.06	3.33	3.60	3.88
	90.00	2.78	3.07	3.38	3.69	4.02	4.35	4.68
	105.00	3.76	4.17	4.59	5.03	5.48	5.94	6.41
	120.00	5.82	6.48	7.16	7.87	8.60	9.36	10.12
1.0000	60.00	2.29	2.58	2.88	3.19	3.50	3.83	4.15
	75.00	2.56	2.86	3.17	3.49	3.82	4.16	4.51
	90.00	3.17	3.54	3.91	4.30	4.71	5.12	5.55
	105.00	4.39	4.90	5.43	5.99	6.55	7.14	7.73
	120.00	6.96	7.80	8.67	9.57	10.50	11.46	12.44

Coefficients of passive earth pressure K_P for $\phi = 20°$ and $k = 0.05$ and 0.10

$\phi = 20.00$ $k = .05$

β/φ	=	0	1/6	1/3	1/2	2/3	5/6	1
δ/φ	α			--- K_P -VALUES ---				
0	60.00	1.70	1.85	2.00	2.15	2.30	2.46	2.62
	75.00	1.74	1.88	2.03	2.19	2.35	2.50	2.66
	90.00	1.97	2.14	2.32	2.50	2.68	2.86	3.05
	105.00	2.50	2.73	2.96	3.20	3.44	3.69	3.94
	120.00	3.59	3.95	4.31	4.68	5.06	5.45	5.86
.3333	60.00	1.85	2.05	2.25	2.46	2.67	2.89	3.10
	75.00	1.95	2.16	2.36	2.57	2.79	3.01	3.23
	90.00	2.30	2.53	2.77	3.02	3.27	3.53	3.80
	105.00	3.01	3.33	3.65	3.99	4.33	4.69	5.05
	120.00	4.50	5.00	5.51	6.05	6.60	7.18	7.76
.5000	60.00	1.93	2.16	2.39	2.62	2.86	3.11	3.35
	75.00	2.07	2.30	2.54	2.78	3.02	3.27	3.53
	90.00	2.47	2.74	3.02	3.30	3.59	3.89	4.20
	105.00	3.29	3.65	4.03	4.42	4.82	5.23	5.66
	120.00	4.99	5.57	6.17	6.80	7.45	8.12	8.81
.6667	60.00	2.02	2.27	2.53	2.79	3.06	3.33	3.61
	75.00	2.20	2.45	2.72	2.99	3.26	3.54	3.83
	90.00	2.65	2.96	3.27	3.59	3.92	4.26	4.61
	105.00	3.57	3.99	4.42	4.87	5.33	5.80	6.29
	120.00	5.51	6.17	6.87	7.59	8.34	9.12	9.91
1.0000	60.00	2.20	2.49	2.80	3.12	3.44	3.78	4.12
	75.00	2.45	2.76	3.07	3.40	3.74	4.09	4.45
	90.00	3.02	3.39	3.78	4.18	4.59	5.02	5.46
	105.00	4.17	4.69	5.23	5.79	6.37	6.98	7.60
	120.00	6.57	7.42	8.30	9.22	10.18	11.17	12.19

$\phi = 20.00$ $k = .10$

β/φ	=	0	1/6	1/3	1/2	2/3	5/6	1
δ/φ	α			--- K_P -VALUES ---				
0	60.00	1.66	1.82	1.97	2.13	2.29	2.45	2.61
	75.00	1.68	1.83	1.99	2.15	2.31	2.47	2.64
	90.00	1.89	2.07	2.25	2.44	2.62	2.81	3.01
	105.00	2.38	2.61	2.85	3.10	3.35	3.60	3.87
	120.00	3.39	3.76	4.13	4.51	4.90	5.30	5.72
.3333	60.00	1.79	2.00	2.20	2.42	2.64	2.86	3.08
	75.00	1.88	2.08	2.30	2.52	2.74	2.96	3.19
	90.00	2.19	2.43	2.68	2.94	3.20	3.46	3.74
	105.00	2.85	3.18	3.51	3.86	4.21	4.58	4.95
	120.00	4.22	4.74	5.27	5.82	6.38	6.98	7.58
.5000	60.00	1.86	2.09	2.33	2.57	2.82	3.07	3.33
	75.00	1.98	2.22	2.46	2.71	2.96	3.22	3.48
	90.00	2.35	2.63	2.91	3.20	3.50	3.81	4.13
	105.00	3.11	3.48	3.87	4.27	4.68	5.11	5.54
	120.00	4.68	5.28	5.90	6.54	7.21	7.90	8.60
.6667	60.00	1.94	2.19	2.46	2.73	3.01	3.29	3.58
	75.00	2.10	2.36	2.63	2.91	3.19	3.49	3.78
	90.00	2.52	2.83	3.15	3.48	3.82	4.17	4.54
	105.00	3.37	3.80	4.24	4.70	5.17	5.66	6.16
	120.00	5.16	5.85	6.56	7.30	8.07	8.86	9.68
1.0000	60.00	2.10	2.40	2.72	3.04	3.37	3.72	4.07
	75.00	2.33	2.64	2.97	3.31	3.66	4.02	4.39
	90.00	2.86	3.24	3.64	4.05	4.47	4.91	5.37
	105.00	3.92	4.46	5.01	5.58	6.18	6.80	7.44
	120.00	6.16	7.02	7.93	8.87	9.85	10.86	11.92

Coefficients of passive earth pressure K_P for $\phi = 20°$ and $k = 0.15$, 0.20, 0.25 and 0.30

$\phi = 20.00$ $k = .15$

β/φ	=	0	1/6	1/3	1/2	2/3	5/6	1
δ/φ	α			--- K_P -VALUES ---				
0	60.00	1.62	1.78	1.94	2.11	2.27	2.44	2.61
	75.00	1.62	1.78	1.94	2.11	2.27	2.44	2.62
	90.00	1.80	1.99	2.18	2.37	2.57	2.76	2.96
	105.00	2.25	2.50	2.75	3.00	3.25	3.52	3.79
	120.00	3.18	3.56	3.94	4.33	4.73	5.15	5.57
.3333	60.00	1.73	1.94	2.15	2.37	2.60	2.83	3.06
	75.00	1.79	2.01	2.23	2.45	2.68	2.92	3.15
	90.00	2.09	2.33	2.59	2.85	3.12	3.39	3.67
	105.00	2.68	3.02	3.37	3.72	4.08	4.46	4.84
	120.00	3.94	4.47	5.02	5.58	6.16	6.77	7.39
.5000	60.00	1.79	2.02	2.26	2.52	2.77	3.03	3.30
	75.00	1.89	2.13	2.38	2.64	2.90	3.16	3.44
	90.00	2.23	2.51	2.80	3.10	3.41	3.73	4.06
	105.00	2.92	3.30	3.70	4.11	4.54	4.97	5.42
	120.00	4.36	4.98	5.61	6.26	6.95	7.66	8.39
.6667	60.00	1.85	2.11	2.39	2.66	2.95	3.24	3.54
	75.00	1.99	2.26	2.54	2.83	3.12	3.42	3.73
	90.00	2.38	2.70	3.03	3.37	3.72	4.08	4.45
	105.00	3.16	3.60	4.06	4.52	5.01	5.51	6.03
	120.00	4.80	5.51	6.23	6.99	7.77	8.59	9.44
1.0000	60.00	1.99	2.30	2.63	2.96	3.30	3.66	4.02
	75.00	2.20	2.53	2.86	3.21	3.56	3.94	4.32
	90.00	2.69	3.08	3.49	3.91	4.34	4.80	5.26
	105.00	3.67	4.21	4.78	5.37	5.98	6.62	7.28
	120.00	5.72	6.61	7.53	8.49	9.49	10.54	11.62

$\phi = 20.00$ $k = .20$

β/φ	=	0	1/6	1/3	1/2	2/3	5/6	1
δ/φ	α			--- K_P -VALUES ---				
0	60.00	1.56	1.74	1.91	2.08	2.25	2.42	2.60
	75.00	1.56	1.72	1.89	2.06	2.23	2.41	2.59
	90.00	1.71	1.91	2.10	2.30	2.50	2.71	2.92
	105.00	2.11	2.37	2.63	2.89	3.16	3.43	3.70
	120.00	2.95	3.35	3.74	4.14	4.55	4.98	5.42
.3333	60.00	1.65	1.87	2.09	2.32	2.55	2.78	3.04
	75.00	1.70	1.92	2.15	2.39	2.62	2.86	3.11
	90.00	1.95	2.22	2.48	2.75	3.03	3.31	3.60
	105.00	2.50	2.85	3.21	3.57	3.95	4.34	4.73
	120.00	3.63	4.18	4.75	5.32	5.92	6.54	7.18
.5000	60.00	1.70	1.94	2.19	2.45	2.72	2.99	3.27
	75.00	1.78	2.04	2.30	2.56	2.83	3.10	3.38
	90.00	2.08	2.38	2.69	2.99	3.31	3.64	3.98
	105.00	2.71	3.11	3.52	3.95	4.38	4.83	5.30
	120.00	4.01	4.65	5.30	5.98	6.68	7.41	8.16
.6667	60.00	1.75	2.02	2.30	2.59	2.89	3.19	3.50
	75.00	1.87	2.16	2.44	2.74	3.04	3.35	3.67
	90.00	2.22	2.56	2.90	3.25	3.61	3.98	4.36
	105.00	2.93	3.39	3.85	4.34	4.83	5.35	5.89
	120.00	4.41	5.14	5.89	6.66	7.48	8.32	9.19
1.0000	60.00	1.87	2.20	2.53	2.87	3.22	3.59	3.97
	75.00	2.06	2.40	2.74	3.10	3.47	3.85	4.24
	90.00	2.50	2.91	3.32	3.76	4.20	4.67	5.15
	105.00	3.38	3.85	4.53	5.14	5.77	6.42	7.10
	120.00	5.24	6.16	7.11	8.10	9.13	10.20	11.32

$\phi = 20.00$ $k = .25$

β/φ	=	0	1/6	1/3	1/2	2/3	5/6	1
δ/φ	α			--- K_P -VALUES ---				
0	60.00	1.49	1.68	1.86	2.04	2.22	2.40	2.58
	75.00	1.48	1.66	1.83	2.01	2.19	2.37	2.56
	90.00	1.61	1.81	2.02	2.23	2.44	2.65	2.86
	105.00	1.95	2.23	2.50	2.77	3.05	3.33	3.62
	120.00	2.70	3.12	3.53	3.95	4.37	4.81	5.26
.3333	60.00	1.55	1.79	2.03	2.26	2.50	2.75	3.00
	75.00	1.59	1.83	2.07	2.31	2.56	2.81	3.06
	90.00	1.81	2.09	2.37	2.65	2.94	3.23	3.53
	105.00	2.30	2.67	3.04	3.42	3.81	4.20	4.61
	120.00	3.30	3.88	4.46	5.06	5.67	6.31	6.97
.5000	60.00	1.59	1.86	2.12	2.38	2.66	2.94	3.23
	75.00	1.66	1.93	2.20	2.47	2.75	3.04	3.33
	90.00	1.92	2.25	2.56	2.89	3.21	3.54	3.89
	105.00	2.48	2.91	3.34	3.77	4.22	4.68	5.16
	120.00	3.63	4.31	4.98	5.67	6.39	7.14	7.92
.6667	60.00	1.63	1.92	2.21	2.51	2.82	3.13	3.45
	75.00	1.73	2.04	2.34	2.64	2.95	3.27	3.60
	90.00	2.05	2.40	2.76	3.12	3.49	3.87	4.27
	105.00	2.68	3.16	3.64	4.14	4.65	5.18	5.73
	120.00	3.98	4.75	5.53	6.33	7.15	8.02	8.91
1.0000	60.00	1.73	2.08	2.42	2.77	3.14	3.51	3.90
	75.00	1.90	2.28	2.61	2.98	3.36	3.76	4.16
	90.00	2.29	2.72	3.15	3.60	4.06	4.54	5.04
	105.00	3.08	3.68	4.28	4.90	5.54	6.22	6.92
	120.00	4.71	5.69	6.66	7.68	8.73	9.84	10.99

$\phi = 20.00$ $k = .30$

β/φ	=	0	1/6	1/3	1/2	2/3	5/6	1
δ/φ	α			--- K_P -VALUES ---				
0	60.00	1.39	1.61	1.81	2.00	2.19	2.37	2.56
	75.00	1.37	1.58	1.77	1.95	2.14	2.33	2.52
	90.00	1.48	1.71	1.93	2.15	2.37	2.59	2.81
	105.00	1.77	2.08	2.37	2.65	2.94	3.23	3.52
	120.00	2.40	2.87	3.31	3.74	4.18	4.63	5.10
.3333	60.00	1.43	1.70	1.95	2.20	2.45	2.70	2.97
	75.00	1.46	1.73	1.98	2.23	2.48	2.74	3.01
	90.00	1.64	1.95	2.25	2.54	2.84	3.14	3.45
	105.00	2.05	2.47	2.86	3.25	3.65	4.06	4.49
	120.00	2.90	3.55	4.16	4.78	5.41	6.07	6.75
.5000	60.00	1.46	1.75	2.03	2.31	2.59	2.88	3.18
	75.00	1.51	1.81	2.10	2.38	2.67	2.96	3.27
	90.00	1.73	2.08	2.42	2.75	3.09	3.44	3.80
	105.00	2.21	2.68	3.13	3.58	4.04	4.52	5.02
	120.00	3.19	3.92	4.64	5.36	6.10	6.87	7.67
.6667	60.00	1.49	1.81	2.11	2.43	2.74	3.07	3.40
	75.00	1.57	1.90	2.22	2.54	2.86	3.19	3.53
	90.00	1.83	2.23	2.60	2.98	3.36	3.75	4.16
	105.00	2.37	2.90	3.41	3.93	4.45	5.00	5.57
	120.00	3.46	4.32	5.14	5.97	6.82	7.71	8.63
1.0000	60.00	1.56	1.94	2.30	-2.67	3.05	3.43	3.83
	75.00	1.71	2.10	2.47	2.85	3.25	3.65	4.07
	90.00	2.04	2.51	2.97	3.43	3.90	4.40	4.91
	105.00	2.71	3.37	4.00	4.64	5.31	6.00	6.72
	120.00	4.10	5.16	6.19	7.24	8.33	9.46	10.64

Coefficients of passive earth pressure K_P for $\phi = 25°$ and $k = 0$, 0.05, 0.10 and 0.15

* ϕ = 25.00 k = 0 *

β/φ	=	0	1/6	1/3	1/2	2/3	5/6	1
δ/φ	α				K_p-VALUES			
0	60.00	1.93	2.14	2.37	2.59	2.84	3.08	3.35
	75.00	2.05	2.28	2.52	2.78	3.05	3.32	3.61
	90.00	2.45	2.75	3.06	3.38	3.71	4.07	4.43
	105.00	3.34	3.76	4.19	4.66	5.16	5.68	6.22
	120.00	5.23	5.93	6.67	7.48	8.33	9.24	10.20
.3333	60.00	2.20	2.50	2.83	3.17	3.53	3.91	4.29
	75.00	2.45	2.79	3.14	3.52	3.92	4.34	4.77
	90.00	3.06	3.51	3.96	4.44	4.96	5.50	6.07
	105.00	4.37	4.99	5.67	6.38	7.16	7.98	8.84
	120.00	7.16	8.25	9.42	10.68	12.05	13.50	15.02
.5000	60.00	2.36	2.71	3.09	3.49	3.91	4.36	4.82
	75.00	2.69	3.08	3.49	3.94	4.41	4.91	5.43
	90.00	3.43	3.94	4.48	5.06	5.67	6.33	7.01
	105.00	4.95	5.71	6.52	7.39	8.33	9.32	10.36
	120.00	8.30	9.61	11.02	12.57	14.22	15.99	17.85
.6667	60.00	2.52	2.93	3.37	3.83	4.32	4.84	5.38
	75.00	2.93	3.38	3.87	4.39	4.94	5.53	6.14
	90.00	3.81	4.40	5.03	5.71	6.44	7.22	8.03
	105.00	5.60	6.49	7.44	8.48	9.58	10.77	12.02
	120.00	9.53	11.08	12.78	14.62	16.58	18.70	20.92
1.0000	60.00	2.83	3.40	3.95	4.54	5.17	5.85	6.55
	75.00	3.45	4.03	4.65	5.33	6.05	6.82	7.64
	90.00	4.62	5.39	6.21	7.11	8.06	9.11	10.19
	105.00	6.98	8.15	9.42	10.80	12.28	13.87	15.54
	120.00	12.17	14.26	16.52	18.99	21.64	24.48	27.47

* REMARK: THE KP-VALUE IS OVER 1000 WHEN 999.99 APPEARS

* ϕ = 25.00 k = .05 *

β/φ	=	0	1/6	1/3	1/2	2/3	5/6	1
δ/φ	α				K_p-VALUES			
0	60.00	1.90	2.12	2.34	2.58	2.83	3.09	3.36
	75.00	2.01	2.24	2.48	2.74	3.02	3.30	3.59
	90.00	2.38	2.68	2.99	3.31	3.66	4.02	4.40
	105.00	3.21	3.63	4.08	4.55	5.05	5.59	6.16
	120.00	4.99	5.70	6.45	7.27	8.14	9.08	10.07
.3333	60.00	2.15	2.45	2.78	3.13	3.50	3.89	4.30
	75.00	2.37	2.72	3.08	3.46	3.87	4.30	4.75
	90.00	2.97	3.40	3.86	4.35	4.88	5.43	6.02
	105.00	4.18	4.81	5.49	6.23	7.02	7.86	8.75
	120.00	6.82	7.91	9.10	10.39	11.78	13.27	14.84
.5000	60.00	2.29	2.64	3.03	3.44	3.88	4.33	4.82
	75.00	2.59	2.99	3.41	3.87	4.35	4.86	5.40
	90.00	3.30	3.81	4.35	4.94	5.57	6.25	6.96
	105.00	4.74	5.50	6.32	7.20	8.16	9.19	10.26
	120.00	7.89	9.21	10.66	12.22	13.91	15.72	17.66
.6667	60.00	2.44	2.86	3.30	3.77	4.27	4.81	5.37
	75.00	2.83	3.28	3.77	4.30	4.87	5.47	6.11
	90.00	3.66	4.25	4.89	5.58	6.33	7.12	7.97
	105.00	5.35	6.24	7.21	8.28	9.38	10.61	11.98
	120.00	9.06	10.64	12.35	14.20	16.23	18.39	20.69
1.0000	60.00	2.79	3.30	3.85	4.46	5.10	5.80	6.52
	75.00	3.32	3.90	4.53	5.22	5.96	6.75	7.59
	90.00	4.42	5.19	6.03	6.95	7.93	8.99	10.11
	105.00	6.67	7.84	9.12	10.52	12.04	13.66	15.40
	120.00	11.58	13.67	15.98	18.47	21.18	24.09	27.20

* REMARK: THE KP-VALUE IS OVER 1000 WHEN 999.99 APPEARS

* ϕ = 25.00 k = .10 *

β/φ	=	0	1/6	1/3	1/2	2/3	5/6	1
δ/φ	α				K_p-VALUES			
0	60.00	1.86	2.09	2.32	2.55	2.82	3.09	3.37
	75.00	1.96	2.19	2.44	2.71	2.99	3.28	3.58
	90.00	2.30	2.60	2.92	3.25	3.60	3.98	4.37
	105.00	3.08	3.51	3.96	4.44	4.96	5.51	6.09
	120.00	4.75	5.46	6.23	7.06	7.95	8.90	9.93
.3333	60.00	2.09	2.40	2.73	3.09	3.47	3.87	4.29
	75.00	2.29	2.64	3.01	3.40	3.82	4.26	4.72
	90.00	2.85	3.28	3.75	4.25	4.79	5.36	5.97
	105.00	3.99	4.63	5.32	6.06	6.87	7.73	8.65
	120.00	6.47	7.57	8.77	10.08	11.50	13.02	14.65
.5000	60.00	2.21	2.57	2.97	3.39	3.83	4.31	4.81
	75.00	2.50	2.90	3.33	3.79	4.29	4.81	5.37
	90.00	3.16	3.67	4.23	4.83	5.47	6.16	6.88
	105.00	4.52	5.28	6.11	7.01	7.98	9.03	10.15
	120.00	7.48	8.81	10.26	11.86	13.57	15.44	17.43
.6667	60.00	2.36	2.77	3.22	3.71	4.22	4.77	5.35
	75.00	2.71	3.17	3.67	4.21	4.79	5.41	6.07
	90.00	3.50	4.09	4.75	5.45	6.20	7.02	7.89
	105.00	5.09	5.99	6.97	8.03	9.19	10.44	11.77
	120.00	8.58	10.16	11.90	13.79	15.84	18.07	20.44
1.0000	60.00	2.67	3.19	3.76	4.37	5.03	5.74	6.50
	75.00	3.17	3.76	4.40	5.10	5.85	6.67	7.53
	90.00	4.22	4.99	5.84	6.77	7.78	8.86	10.02
	105.00	6.32	7.51	8.82	10.23	11.78	13.45	15.23
	120.00	10.96	13.07	15.39	17.94	20.70	23.69	26.89

* REMARK: THE KP-VALUE IS OVER 1000 WHEN 999.99 APPEARS

* ϕ = 25.00 k = .15 *

β/φ	=	0	1/6	1/3	1/2	2/3	5/6	1
δ/φ	α				K_p-VALUES			
0	60.00	1.82	2.06	2.29	2.54	2.81	3.08	3.36
	75.00	1.90	2.14	2.39	2.66	2.95	3.25	3.58
	90.00	2.21	2.52	2.84	3.18	3.54	3.93	4.33
	105.00	2.94	3.37	3.83	4.32	4.85	5.41	6.02
	120.00	4.50	5.22	6.00	6.84	7.74	8.73	9.78
.3333	60.00	2.02	2.34	2.68	3.04	3.43	3.85	4.28
	75.00	2.20	2.55	2.93	3.33	3.76	4.21	4.69
	90.00	2.72	3.16	3.64	4.14	4.70	5.28	5.91
	105.00	3.79	4.43	5.13	5.89	6.71	7.59	8.54
	120.00	6.10	7.22	8.43	9.75	11.21	12.77	14.43
.5000	60.00	2.13	2.50	2.90	3.33	3.79	4.27	4.78
	75.00	2.39	2.80	3.24	3.71	4.21	4.76	5.33
	90.00	3.01	3.53	4.09	4.70	5.36	6.07	6.82
	105.00	4.28	5.05	5.89	6.81	7.80	8.87	10.02
	120.00	7.05	8.40	9.86	11.47	13.23	15.13	17.19
.6667	60.00	2.26	2.69	3.14	3.63	4.16	4.72	5.33
	75.00	2.59	3.06	3.57	4.11	4.70	5.34	6.02
	90.00	3.33	3.93	4.58	5.30	6.08	6.91	7.81
	105.00	4.82	5.73	6.72	7.80	8.97	10.26	11.62
	120.00	8.08	9.68	11.43	13.35	15.45	17.71	20.17
1.0000	60.00	2.56	3.08	3.65	4.28	4.95	5.69	6.46
	75.00	3.02	3.62	4.27	4.98	5.74	6.58	7.47
	90.00	4.00	4.79	5.65	6.58	7.61	8.72	9.91
	105.00	5.98	7.18	8.49	9.93	11.51	13.21	15.05
	120.00	10.31	12.45	14.80	17.37	20.19	23.24	26.54

* REMARK: THE KP-VALUE IS OVER 1000 WHEN 999.99 APPEARS

Coefficients of passive earth pressure K_P for $\phi = 25°$ and $k = 0.20$, 0.25 and 0.30, and for $\phi = 30°$ and $k = 0$

* ϕ = 25.00 k = .20 *

β/φ	=	0	1/6	1/3	1/2	2/3	5/6	1
δ/φ	α				K_p-VALUES			
0	60.00	1.77	2.02	2.28	2.52	2.79	3.08	3.38
	75.00	1.83	2.08	2.34	2.62	2.92	3.23	3.56
	90.00	2.12	2.43	2.76	3.11	3.48	3.87	4.29
	105.00	2.79	3.23	3.70	4.20	4.74	5.32	5.93
	120.00	4.23	4.96	5.75	6.61	7.54	8.53	9.62
.3333	60.00	1.95	2.27	2.62	2.99	3.39	3.82	4.27
	75.00	2.11	2.46	2.85	3.26	3.70	4.16	4.66
	90.00	2.58	3.03	3.52	4.04	4.60	5.20	5.84
	105.00	3.57	4.23	4.94	5.71	6.55	7.45	8.42
	120.00	5.71	6.84	8.08	9.43	10.89	12.48	14.21
.5000	60.00	2.05	2.42	2.83	3.27	3.74	4.23	4.76
	75.00	2.28	2.70	3.14	3.63	4.14	4.69	5.29
	90.00	2.85	3.38	3.95	4.57	5.24	5.97	6.74
	105.00	4.03	4.81	5.67	6.59	7.61	8.70	9.88
	120.00	6.59	7.96	9.45	11.09	12.87	14.82	16.92
.6667	60.00	2.16	2.59	3.06	3.56	4.10	4.69	5.29
	75.00	2.46	2.94	3.46	4.01	4.62	5.26	5.96
	90.00	3.15	3.76	4.43	5.15	5.94	6.80	7.72
	105.00	4.53	5.45	6.45	7.55	8.75	10.05	11.46
	120.00	7.55	9.17	10.95	12.89	15.02	17.35	19.86
1.0000	60.00	2.43	2.86	3.34	4.17	4.86	5.61	6.41
	75.00	2.86	3.47	4.12	4.84	5.63	6.48	7.40
	90.00	3.77	4.57	5.44	6.40	7.44	8.57	9.80
	105.00	5.61	6.82	8.15	9.62	11.22	12.96	14.85
	120.00	9.63	11.78	14.17	16.80	19.65	22.78	26.16

* REMARK: THE KP-VALUE IS OVER 1000 WHEN 999.99 APPEARS

* ϕ = 25.00 k = .25 *

β/φ	=	0	1/6	1/3	1/2	2/3	5/6	1
δ/φ	α				K_p-VALUES			
0	60.00	1.72	1.97	2.23	2.49	2.77	3.07	3.38
	75.00	1.76	2.02	2.29	2.57	2.88	3.20	3.54
	90.00	2.02	2.34	2.68	3.03	3.41	3.82	4.25
	105.00	2.63	3.08	3.56	4.07	4.62	5.21	5.85
	120.00	3.85	4.70	5.50	6.37	7.31	8.34	9.45
.3333	60.00	1.87	2.20	2.56	2.94	3.35	3.78	4.25
	75.00	2.01	2.37	2.77	3.18	3.63	4.11	4.62
	90.00	2.44	2.90	3.40	3.93	4.50	5.11	5.77
	105.00	3.35	4.02	4.74	5.52	6.37	7.30	8.30
	120.00	5.31	6.46	7.70	9.07	10.58	12.20	13.96
.5000	60.00	1.95	2.34	2.75	3.20	3.68	4.19	4.74
	75.00	2.16	2.59	3.04	3.53	4.06	4.63	5.24
	90.00	2.69	3.23	3.81	4.44	5.12	5.86	6.66
	105.00	3.77	4.57	5.43	6.37	7.40	8.52	9.73
	120.00	6.12	7.50	9.01	10.67	12.50	14.48	16.64
.6667	60.00	2.05	2.49	2.97	3.48	4.03	4.62	5.26
	75.00	2.33	2.82	3.34	3.91	4.52	5.19	5.90
	90.00	2.95	3.58	4.26	5.00	5.80	6.67	7.62
	105.00	4.22	5.17	6.18	7.30	8.51	9.85	11.29
	120.00	7.00	8.64	10.44	12.43	14.59	16.95	19.55
1.0000	60.00	2.30	2.84	3.42	4.07	4.77	5.53	6.35
	75.00	2.70	3.30	3.97	4.71	5.50	6.37	7.32
	90.00	3.53	4.33	5.22	6.19	7.25	8.41	9.67
	105.00	5.21	6.45	7.80	9.28	10.91	12.70	14.64
	120.00	8.91	11.12	13.52	16.17	19.10	22.28	25.75

* REMARK: THE KP-VALUE IS OVER 1000 WHEN 999.99 APPEARS

* ϕ = 25.00 k = .30 *

β/φ	=	0	1/6	1/3	1/2	2/3	5/6	1
δ/φ	α				K_p-VALUES			
0	60.00	1.65	1.92	2.19	2.46	2.75	3.05	3.38
	75.00	1.69	1.95	2.23	2.52	2.83	3.16	3.52
	90.00	1.91	2.24	2.59	2.95	3.34	3.76	4.20
	105.00	2.45	2.92	3.42	3.94	4.50	5.10	5.76
	120.00	3.65	4.42	5.24	6.12	7.09	8.13	9.27
.3333	60.00	1.77	2.13	2.49	2.88	3.30	3.75	4.22
	75.00	1.90	2.27	2.67	3.10	3.56	4.05	4.57
	90.00	2.28	2.76	3.26	3.80	4.39	5.02	5.70
	105.00	3.10	3.79	4.53	5.33	6.20	7.14	8.16
	120.00	4.87	6.05	7.33	8.71	10.24	11.90	13.71
.5000	60.00	1.85	2.25	2.67	3.12	3.62	4.14	4.70
	75.00	2.02	2.46	2.93	3.43	3.97	4.56	5.19
	90.00	2.50	3.06	3.65	4.30	4.99	5.75	6.57
	105.00	3.48	4.30	5.18	6.15	7.19	8.33	9.57
	120.00	5.59	7.02	8.57	10.25	12.10	14.13	16.34
.6667	60.00	1.93	2.38	2.87	3.39	3.96	4.56	5.22
	75.00	2.17	2.68	3.22	3.79	4.42	5.10	5.84
	90.00	2.74	3.39	4.08	4.83	5.65	6.54	7.51
	105.00	3.89	4.85	5.90	7.03	8.27	9.63	11.11
	120.00	6.39	8.10	9.91	11.92	14.14	16.58	19.19
1.0000	60.00	2.14	2.70	3.30	3.96	4.67	5.45	6.30
	75.00	2.50	3.13	3.82	4.56	5.37	6.26	7.23
	90.00	3.26	4.09	4.99	5.98	7.06	8.24	9.53
	105.00	4.79	6.05	7.43	8.94	10.61	12.42	14.40
	120.00	8.13	10.38	12.85	15.53	18.51	21.77	25.32

* REMARK: THE KP-VALUE IS OVER 1000 WHEN 999.99 APPEARS

* ϕ = 30.00 k = 0 *

β/φ	=	0	1/6	1/3	1/2	2/3	5/6	1
δ/φ	α				K_p-VALUES			
0	60.00	2.15	2.46	2.79	3.14	3.54	3.96	4.42
	75.00	2.38	2.73	3.11	3.54	4.01	4.52	5.07
	90.00	3.00	3.48	4.01	4.60	5.24	5.96	6.73
	105.00	4.35	5.10	5.94	6.88	7.93	9.09	10.35
	120.00	7.38	8.78	10.34	12.14	14.14	16.37	18.82
.3333	60.00	2.57	3.03	3.55	4.14	4.78	5.47	6.22
	75.00	3.02	3.58	4.20	4.90	5.67	6.52	7.45
	90.00	4.06	4.83	5.71	6.69	7.79	9.01	10.33
	105.00	6.24	7.49	8.92	10.53	12.35	14.38	16.62
	120.00	11.24	13.62	16.38	19.50	23.06	26.98	31.30
.5000	60.00	2.82	3.38	4.02	4.73	5.52	6.38	7.32
	75.00	3.42	4.16	4.97	5.73	6.69	7.76	8.92
	90.00	4.71	5.67	6.75	7.98	9.37	10.91	12.59
	105.00	7.42	8.99	10.78	12.84	15.15	17.71	20.53
	120.00	13.67	16.70	20.19	24.16	28.65	33.67	39.17
.6667	60.00	3.11	3.78	4.54	5.40	6.35	7.40	8.54
	75.00	3.87	4.68	5.61	6.66	7.84	9.14	10.57
	90.00	5.45	6.61	7.94	9.45	11.16	13.05	15.14
	105.00	8.77	10.69	12.92	15.44	18.30	21.47	24.96
	120.00	16.45	20.21	24.50	29.44	35.01	41.24	48.07
1.0000	60.00	3.77	4.67	5.70	6.87	8.18	9.65	11.25
	75.00	4.87	5.95	7.28	8.74	10.39	12.23	14.28
	90.00	7.10	8.74	10.60	12.74	15.15	17.85	20.83
	105.00	11.79	14.52	17.67	21.26	25.33	29.86	34.84
	120.00	22.70	28.01	34.18	41.20	49.17	58.04	67.77

* REMARK: THE KP-VALUE IS OVER 1000 WHEN 999.99 APPEARS

Coefficients for passive earth pressure K_p for $\phi = 30°$ and $k = 0.05, 0.10, 0.15$ and 0.20

$\phi = 30.00$ $k = .05$

β/φ	=	0	1/6	1/3	1/2	2/3	5/6	1
δ/φ	α			--- K_p-VALUES ---				
0	60.00	2.12	2.44	2.77	3.14	3.54	3.98	4.45
	75.00	2.33	2.68	3.07	3.51	3.99	4.51	5.08
	90.00	2.91	3.39	3.93	4.53	5.19	5.92	6.73
	105.00	4.20	4.95	5.79	6.75	7.82	9.01	10.34
	120.00	7.08	8.48	10.06	11.89	13.93	16.21	18.75
.3333	60.00	2.51	2.98	3.51	4.10	4.76	5.47	6.25
	75.00	2.93	3.49	4.13	4.84	5.63	6.50	7.46
	90.00	3.92	4.70	5.57	6.58	7.69	8.95	10.33
	105.00	5.99	7.25	8.69	10.33	12.19	14.26	16.57
	120.00	10.76	13.16	15.92	19.10	22.71	26.75	31.22
.5000	60.00	2.74	3.31	3.96	4.68	5.48	6.37	7.35
	75.00	3.31	4.00	4.77	5.64	6.63	7.72	8.93
	90.00	4.54	5.50	6.60	7.85	9.26	10.84	12.58
	105.00	7.12	8.71	10.51	12.59	14.94	17.58	20.50
	120.00	13.10	16.14	19.65	23.66	28.26	33.39	39.10
.6667	60.00	3.02	3.70	4.46	5.33	6.30	7.38	8.57
	75.00	3.74	4.56	5.49	6.56	7.75	9.10	10.58
	90.00	5.24	6.41	7.76	9.28	11.02	12.97	15.13
	105.00	8.41	10.34	12.57	15.14	18.05	21.32	24.93
	120.00	15.75	19.51	23.85	28.84	34.52	40.91	48.00
1.0000	60.00	3.65	4.55	5.59	6.77	8.11	9.61	11.28
	75.00	4.70	5.82	7.11	8.60	10.27	12.17	14.26
	90.00	6.83	8.46	10.35	12.51	14.98	17.74	20.80
	105.00	11.32	14.05	17.22	20.85	25.00	29.65	34.83
	120.00	21.72	27.09	33.27	40.40	48.49	57.61	67.72

* REMARK: THE KP-VALUE IS OVER 1000 WHEN 999.99 APPEARS

$\phi = 30.00$ $k = .10$

β/φ	=	0	1/6	1/3	1/2	2/3	5/6	1
δ/φ	α			--- K_p-VALUES ---				
0	60.00	2.09	2.41	2.75	3.13	3.54	3.99	4.49
	75.00	2.28	2.63	3.03	3.48	3.96	4.50	5.09
	90.00	2.82	3.31	3.85	4.46	5.13	5.89	6.72
	105.00	4.04	4.75	5.65	6.62	7.71	8.93	10.30
	120.00	6.77	8.18	9.78	11.62	13.69	16.04	18.66
.3333	60.00	2.45	2.92	3.45	4.06	4.73	5.47	6.28
	75.00	2.84	3.41	4.05	4.76	5.57	6.47	7.46
	90.00	3.78	4.56	5.44	6.46	7.60	8.89	10.31
	105.00	5.75	7.01	8.46	10.12	12.01	14.14	16.52
	120.00	10.27	12.69	15.46	18.69	22.35	26.49	31.11
.5000	60.00	2.67	3.24	3.89	4.63	5.44	6.36	7.37
	75.00	3.20	3.89	4.67	5.55	6.56	7.68	8.93
	90.00	4.37	5.33	6.43	7.70	9.14	10.75	12.56
	105.00	6.82	8.41	10.24	12.32	14.72	17.42	20.44
	120.00	12.51	15.55	19.07	23.16	27.81	33.09	38.99
.6667	60.00	2.92	3.60	4.38	5.26	6.25	7.36	8.58
	75.00	3.60	4.43	5.37	6.45	7.67	9.04	10.57
	90.00	5.03	6.20	7.56	9.11	10.87	12.87	15.11
	105.00	8.04	10.00	12.23	14.83	17.80	21.13	24.87
	120.00	15.03	18.79	23.15	28.21	34.02	40.55	47.87
1.0000	60.00	3.52	4.42	5.47	6.67	8.03	9.57	11.29
	75.00	4.52	5.64	6.94	8.44	10.16	12.09	14.25
	90.00	6.55	8.18	10.08	12.28	14.77	17.61	20.78
	105.00	10.81	13.57	16.75	20.44	24.64	29.43	34.77
	120.00	20.74	26.11	32.34	39.54	47.79	57.12	67.56

* REMARK: THE KP-VALUE IS OVER 1000 WHEN 999.99 APPEARS

$\phi = 30.00$ $k = .15$

β/φ	=	0	1/6	1/3	1/2	2/3	5/6	1
δ/φ	α			--- K_p-VALUES ---				
0	60.00	2.05	2.38	2.73	3.11	3.52	4.00	4.51
	75.00	2.22	2.58	2.98	3.44	3.94	4.49	5.10
	90.00	2.73	3.22	3.77	4.39	5.08	5.84	6.70
	105.00	3.88	4.64	5.50	6.48	7.59	8.84	10.25
	120.00	6.47	7.87	9.48	11.35	13.45	15.85	18.55
.3333	60.00	2.38	2.86	3.40	4.01	4.70	5.45	6.28
	75.00	2.74	3.32	3.97	4.69	5.51	6.43	7.46
	90.00	3.63	4.42	5.31	6.34	7.49	8.81	10.32
	105.00	5.50	6.76	8.22	9.90	11.82	14.00	16.45
	120.00	9.78	12.19	15.00	18.24	21.97	26.20	30.97
.5000	60.00	2.58	3.16	3.82	4.57	5.40	6.34	7.38
	75.00	3.08	3.78	4.57	5.46	6.48	7.63	8.91
	90.00	4.19	5.16	6.27	7.55	9.01	10.66	12.53
	105.00	6.51	8.09	9.93	12.06	14.49	17.26	20.36
	120.00	11.88	14.84	18.49	22.61	27.35	32.74	38.80
.6667	60.00	2.82	3.51	4.29	5.18	6.19	7.32	8.59
	75.00	3.47	4.29	5.24	6.33	7.57	8.99	10.56
	90.00	4.82	6.00	7.36	8.93	10.72	12.76	15.06
	105.00	7.68	9.62	11.89	14.50	17.51	20.93	24.79
	120.00	14.29	18.07	22.46	27.58	33.45	40.14	47.70
1.0000	60.00	3.39	4.29	5.35	6.56	7.94	9.52	11.29
	75.00	4.33	5.46	6.77	8.29	10.03	12.01	14.23
	90.00	6.26	7.90	9.81	12.02	14.56	17.47	20.72
	105.00	10.31	13.06	16.27	19.99	24.28	29.16	34.65
	120.00	19.74	25.09	31.38	38.66	47.04	56.58	67.36

* REMARK: THE KP-VALUE IS OVER 1000 WHEN 999.99 APPEARS

$\phi = 30.00$ $k = .20$

β/φ	=	0	1/6	1/3	1/2	2/3	5/6	1
δ/φ	α			--- K_p-VALUES ---				
0	60.00	2.01	2.35	2.71	3.10	3.53	4.01	4.54
	75.00	2.16	2.53	2.93	3.39	3.91	4.48	5.10
	90.00	2.63	3.13	3.68	4.31	5.02	5.80	6.69
	105.00	3.71	4.48	5.35	6.34	7.47	8.75	10.19
	120.00	6.15	7.55	9.17	11.06	13.21	15.65	18.43
.3333	60.00	2.31	2.80	3.34	3.97	4.66	5.44	6.30
	75.00	2.64	3.22	3.87	4.62	5.45	6.39	7.44
	90.00	3.47	4.27	5.18	6.21	7.39	8.73	10.24
	105.00	5.23	6.51	7.97	9.67	11.63	13.84	16.37
	120.00	9.27	11.67	14.50	17.79	21.57	25.91	30.79
.5000	60.00	2.49	3.07	3.74	4.50	5.36	6.31	7.38
	75.00	2.96	3.66	4.46	5.37	6.41	7.57	8.90
	90.00	4.00	4.98	6.10	7.39	8.88	10.57	12.47
	105.00	6.20	7.78	9.63	11.78	14.25	17.07	20.27
	120.00	11.24	14.31	17.92	22.05	26.89	32.36	38.62
.6667	60.00	2.71	3.41	4.20	5.10	6.13	7.28	8.59
	75.00	3.32	4.15	5.12	6.21	7.47	8.91	10.53
	90.00	4.60	5.78	7.15	8.73	10.57	12.64	15.01
	105.00	7.29	9.23	11.52	14.17	17.22	20.73	24.68
	120.00	13.52	17.32	21.73	26.92	32.66	39.13	47.46
1.0000	60.00	3.24	4.15	5.21	6.44	7.86	9.46	11.28
	75.00	4.13	5.26	6.59	8.12	9.89	11.91	14.20
	90.00	5.95	7.60	9.52	11.76	14.36	17.30	20.65
	105.00	9.78	12.53	15.77	19.53	23.69	28.87	34.52
	120.00	18.66	24.06	30.38	37.75	46.25	56.02	67.00

* REMARK: THE KP-VALUE IS OVER 1000 WHEN 999.99 APPEARS

Coefficients of passive earth pressure K_p for $\phi = 30°$ and $k = 0.25$ and 0.30, and for $\phi = 35°$ and $k = 0$ and 0.05

$\phi = 30.00$ $k = .25$

β/φ	=	0	1/6	1/3	1/2	2/3	5/6	1
δ/φ	α			--- K_p-VALUES ---				
0	60.00	1.96	2.31	2.69	3.08	3.52	4.01	4.56
	75.00	2.10	2.47	2.88	3.35	3.87	4.46	5.10
	90.00	2.53	3.03	3.59	4.23	4.95	5.75	6.65
	105.00	3.53	4.30	5.19	6.20	7.35	8.64	10.13
	120.00	5.80	7.23	8.87	10.76	12.94	15.44	18.29
.3333	60.00	2.23	2.73	3.28	3.91	4.62	5.42	6.31
	75.00	2.54	3.12	3.78	4.53	5.38	6.35	7.43
	90.00	3.31	4.11	5.02	6.08	7.28	8.65	10.19
	105.00	4.95	6.23	7.72	9.44	11.41	13.69	16.27
	120.00	8.72	11.16	13.99	17.33	21.16	25.56	30.59
.5000	60.00	2.40	2.99	3.66	4.43	5.30	6.28	7.38
	75.00	2.83	3.53	4.34	5.26	6.32	7.52	8.87
	90.00	3.80	4.78	5.92	7.23	8.74	10.46	12.42
	105.00	5.85	7.46	9.32	11.48	14.00	16.87	20.16
	120.00	10.60	13.67	17.27	21.48	26.36	31.99	38.37
.6667	60.00	2.60	3.30	4.10	5.01	6.05	7.25	8.58
	75.00	3.16	4.00	4.97	6.09	7.38	8.84	10.50
	90.00	4.36	5.55	6.94	8.54	10.39	12.52	14.94
	105.00	6.88	8.85	11.13	13.82	16.83	20.48	24.55
	120.00	12.72	16.52	21.01	26.20	32.28	39.24	47.20
1.0000	60.00	3.09	4.02	5.08	6.32	7.75	9.40	11.26
	75.00	3.92	5.08	6.40	7.95	9.75	11.81	14.16
	90.00	5.63	7.30	9.23	11.49	14.11	17.13	20.57
	105.00	9.24	12.00	15.24	19.07	23.46	28.56	34.36
	120.00	17.55	23.01	29.33	36.78	45.43	55.37	66.72

* REMARK: THE KP-VALUE IS OVER 1000 WHEN 999.99 APPEARS

$\phi = 30.00$ $k = .30$

β/φ	=	0	1/6	1/3	1/2	2/3	5/6	1
δ/φ	α			--- K_p-VALUES ---				
0	60.00	1.81	2.27	2.65	3.06	3.51	4.01	4.57
	75.00	2.02	2.41	2.82	3.30	3.83	4.44	5.10
	90.00	2.42	2.92	3.50	4.15	4.88	5.70	6.62
	105.00	3.34	4.13	5.02	6.04	7.21	8.54	10.06
	120.00	5.45	6.88	8.54	10.46	12.67	15.23	18.13
.3333	60.00	2.15	2.65	3.21	3.85	4.58	5.40	6.31
	75.00	2.42	3.01	3.68	4.45	5.31	6.29	7.41
	90.00	3.14	3.95	4.87	5.93	7.16	8.55	10.14
	105.00	4.66	5.96	7.45	9.20	11.20	13.51	16.16
	120.00	8.16	10.62	13.47	16.83	20.74	25.21	30.38
.5000	60.00	2.30	2.89	3.57	4.36	5.24	6.25	7.38
	75.00	2.69	3.40	4.22	5.16	6.23	7.46	8.84
	90.00	3.53	4.58	5.73	7.05	8.59	10.34	12.36
	105.00	5.50	7.11	8.99	11.18	13.73	16.68	20.02
	120.00	9.89	13.00	16.61	20.80	25.83	31.56	38.11
.6667	60.00	2.48	3.18	3.99	4.92	5.98	7.19	8.57
	75.00	3.00	3.85	4.83	5.96	7.25	8.76	10.46
	90.00	4.11	5.31	6.71	8.34	10.21	12.38	14.86
	105.00	6.45	8.44	10.75	13.45	16.61	20.23	24.41
	120.00	11.89	15.71	20.22	25.48	31.64	38.74	46.89
1.0000	60.00	2.94	3.86	4.94	6.19	7.64	9.32	11.24
	75.00	3.71	4.86	6.20	7.77	9.59	11.69	14.10
	90.00	5.30	6.96	8.92	11.21	13.86	16.95	20.47
	105.00	8.64	11.44	14.71	18.56	23.04	28.22	34.17
	120.00	16.41	21.85	28.28	35.79	44.58	54.69	66.36

* REMARK: THE KP-VALUE IS OVER 1000 WHEN 999.99 APPEARS

$\phi = 35.00$ $k = 0$

β/φ	=	0	1/6	1/3	1/2	2/3	5/6	1
δ/φ	α			--- K_p-VALUES ---				
0	60.00	2.41	2.84	3.32	3.88	4.52	5.25	6.05
	75.00	2.78	3.30	3.91	4.64	5.48	6.44	7.53
	90.00	3.69	4.48	5.41	6.50	7.79	9.28	11.00
	105.00	5.75	7.12	8.74	10.71	13.01	15.73	18.85
	120.00	10.72	13.51	16.92	21.03	25.87	31.77	38.47
.3333	60.00	3.03	3.74	4.59	5.60	6.76	8.11	9.65
	75.00	3.79	4.72	5.84	7.16	8.73	10.55	12.65
	90.00	5.49	6.93	8.65	10.74	13.21	16.11	19.45
	105.00	9.26	11.84	14.98	18.77	23.33	28.69	34.87
	120.00	18.53	24.03	30.70	38.87	48.68	60.15	73.47
.5000	60.00	3.44	4.35	5.44	6.72	8.24	10.01	12.03
	75.00	4.48	5.68	7.12	8.86	10.92	13.34	16.12
	90.00	6.72	8.58	10.86	13.62	16.91	20.76	25.25
	105.00	11.67	15.08	19.26	24.35	30.43	37.61	45.87
	120.00	24.00	31.26	40.27	51.14	64.23	79.66	97.46
.6667	60.00	3.84	5.07	6.43	8.05	9.99	12.25	14.85
	75.00	5.30	6.81	8.65	10.88	13.53	16.65	20.23
	90.00	8.17	10.56	13.51	17.05	21.31	26.34	32.12
	105.00	14.56	18.97	24.39	30.96	38.86	48.17	58.90
	120.00	30.44	39.96	51.56	65.74	82.78	102.85	126.00
1.0000	60.00	5.16	6.80	8.80	11.24	14.15	17.57	21.53
	75.00	7.27	9.53	12.31	15.67	19.73	24.49	29.99
	90.00	11.68	15.33	19.79	25.24	31.77	39.47	48.36
	105.00	21.47	28.21	36.53	46.66	58.75	73.05	89.56
	120.00	45.88	60.38	78.31	100.14	126.21	157.06	192.65

* REMARK: THE KP-VALUE IS OVER 1000 WHEN 999.99 APPEARS

$\phi = 35.00$ $k = .05$

β/φ	=	0	1/6	1/3	1/2	2/3	5/6	1
δ/φ	α			--- K_p-VALUES ---				
0	60.00	2.38	2.82	3.32	3.88	4.53	5.29	6.14
	75.00	2.73	3.25	3.87	4.61	5.47	6.46	7.59
	90.00	3.59	4.38	5.32	6.43	7.74	9.28	11.06
	105.00	5.57	6.93	8.58	10.55	12.92	15.71	18.95
	120.00	10.32	13.14	16.54	20.73	25.74	31.70	38.69
.3333	60.00	2.97	3.68	4.54	5.56	6.76	8.14	9.74
	75.00	3.69	4.63	5.75	7.10	8.69	10.56	12.75
	90.00	5.32	6.75	8.50	10.60	13.13	16.11	19.58
	105.00	8.94	11.52	14.66	18.52	23.15	28.66	35.10
	120.00	17.85	23.32	30.05	38.35	48.30	60.13	73.94
.5000	60.00	3.36	4.27	5.36	6.67	8.22	10.04	12.14
	75.00	4.35	5.55	7.01	8.76	10.87	13.35	16.24
	90.00	6.50	8.38	10.65	13.46	16.80	20.78	25.42
	105.00	11.27	14.67	19.89	24.90	30.21	37.60	46.18
	120.00	23.09	30.37	39.41	50.44	63.81	79.63	98.14
.6667	60.00	3.83	4.97	6.34	7.98	9.95	12.28	14.98
	75.00	5.14	6.66	8.50	10.75	13.45	16.57	20.39
	90.00	7.90	10.29	13.25	16.84	21.19	25.35	32.36
	105.00	14.04	18.47	23.88	30.57	38.59	48.15	59.34
	120.00	29.35	38.80	50.49	64.90	82.19	102.81	126.93
1.0000	60.00	5.00	6.64	8.66	11.12	14.09	17.61	21.73
	75.00	7.04	9.29	12.08	15.50	19.62	24.51	30.24
	90.00	11.28	14.92	19.41	24.93	31.58	39.49	48.72
	105.00	20.72	27.45	35.81	46.02	58.36	73.07	90.24
	120.00	44.22	58.70	76.79	98.74	125.37	157.03	194.09

* REMARK: THE KP-VALUE IS OVER 1000 WHEN 999.99 APPEARS

Coefficients of passive earth pressure K_P for $\phi = 35°$ and $k = 0.10$, 0.15, 0.20 and 0.25

* ϕ = 35.00 k = .10 *

β/φ	=	0	1/6	1/3	1/2	2/3	5/6	1
δ/φ	α			--- K_p-VALUES ---				
0	60.00	2.35	2.80	3.30	3.88	4.55	5.33	6.21
	75.00	2.67	3.20	3.83	4.58	5.45	6.47	7.65
	90.00	3.49	4.29	5.23	6.36	7.70	9.28	11.12
	105.00	5.39	6.74	8.40	10.40	12.80	15.66	19.02
	120.00	9.92	12.74	16.17	20.39	25.49	31.62	38.84
.3333	60.00	2.91	3.62	4.49	5.52	6.74	8.17	9.82
	75.00	3.58	4.52	5.66	7.02	8.65	10.57	12.83
	90.00	5.15	6.58	8.33	10.46	13.03	16.08	19.59
	105.00	8.61	11.19	14.35	18.27	22.96	28.61	35.28
	120.00	17.17	22.60	29.40	37.75	47.89	60.04	74.34
.5000	60.00	3.27	4.18	5.29	6.61	8.20	10.06	12.23
	75.00	4.21	5.42	6.88	8.67	10.80	13.35	16.35
	90.00	6.27	8.14	10.45	13.27	16.69	20.76	25.57
	105.00	10.86	14.25	18.47	23.65	29.99	37.53	46.43
	120.00	22.17	29.48	38.54	48.74	63.24	79.50	98.68
.6667	60.00	3.72	4.86	6.24	7.91	9.91	12.31	15.10
	75.00	4.97	6.48	8.35	10.62	13.38	16.66	20.53
	90.00	7.62	10.01	12.98	16.63	21.03	26.32	32.55
	105.00	13.52	17.91	23.38	30.12	38.28	48.10	59.68
	120.00	28.24	37.62	49.43	63.93	81.53	102.71	127.66
1.0000	60.00	4.85	6.48	8.51	10.99	14.02	17.63	21.89
	75.00	6.80	9.05	11.85	15.31	19.49	24.52	30.45
	90.00	10.88	14.50	19.03	24.59	31.37	39.48	49.07
	105.00	19.96	26.66	35.06	45.38	57.98	73.05	90.83
	120.00	42.47	57.03	75.11	97.34	124.52	157.02	195.35

* REMARK: THE KP-VALUE IS OVER 1000 WHEN 999.99 APPEARS

* ϕ = 35.00 k = .15 *

β/φ	=	0	1/6	1/3	1/2	2/3	5/6	1
δ/φ	α			--- K_p-VALUES ---				
0	60.00	2.32	2.78	3.29	3.87	4.55	5.36	6.28
	75.00	2.62	3.15	3.78	4.55	5.44	6.49	7.70
	90.00	3.39	4.19	5.15	6.28	7.65	9.26	11.17
	105.00	5.20	6.55	8.22	10.25	12.68	15.62	19.08
	120.00	9.53	12.33	15.79	20.04	25.24	31.53	38.97
.3333	60.00	2.84	3.56	4.43	5.48	6.73	8.19	9.90
	75.00	3.47	4.42	5.56	6.94	8.60	10.56	12.90
	90.00	4.97	6.40	8.16	10.32	12.92	16.06	19.76
	105.00	8.28	10.85	14.04	17.97	22.76	28.56	35.43
	120.00	16.48	21.86	28.74	37.13	47.47	59.86	74.63
.5000	60.00	3.18	4.05	5.21	6.55	8.16	10.08	12.32
	75.00	4.08	5.28	6.75	8.56	10.73	13.35	16.44
	90.00	6.04	7.91	10.24	13.08	16.55	20.72	25.65
	105.00	10.41	13.82	18.05	23.31	29.73	37.47	46.66
	120.00	21.24	28.55	37.66	48.92	62.68	78.36	98.17
.6667	60.00	3.61	4.74	6.13	7.82	9.86	12.31	15.24
	75.00	4.79	6.31	8.20	10.49	13.28	16.66	20.65
	90.00	7.33	9.74	12.70	16.38	20.86	26.29	32.72
	105.00	12.97	17.35	22.87	29.65	37.96	48.05	59.56
	120.00	27.02	36.44	48.34	62.91	80.87	102.55	129.30
1.0000	60.00	4.67	6.33	8.35	10.87	13.93	17.64	22.04
	75.00	6.54	8.61	11.62	15.11	19.36	24.52	30.63
	90.00	10.45	14.07	18.64	24.24	31.14	39.43	49.32
	105.00	19.12	25.65	34.27	44.73	57.52	72.92	91.28
	120.00	40.72	55.28	73.38	95.94	123.51	156.71	196.20

* REMARK: THE KP-VALUE IS OVER 1000 WHEN 999.99 APPEARS

* ϕ = 35.00 k = .20 *

β/φ	=	0	1/6	1/3	1/2	2/3	5/6	1
δ/φ	α			--- K_p-VALUES ---				
0	60.00	2.28	2.75	3.27	3.86	4.56	5.39	6.34
	75.00	2.56	3.10	3.74	4.51	5.42	6.49	7.73
	90.00	3.29	4.09	5.05	6.20	7.59	9.24	11.21
	105.00	5.00	6.37	8.03	10.10	12.57	15.57	19.13
	120.00	9.13	11.92	15.41	19.69	24.99	31.37	39.05
.3333	60.00	2.77	3.49	4.37	5.43	6.70	8.20	9.97
	75.00	3.36	4.31	5.46	6.86	8.55	10.56	12.96
	90.00	4.79	6.22	7.99	10.18	12.82	16.03	19.84
	105.00	7.94	10.51	13.73	17.67	22.56	28.46	35.54
	120.00	15.71	21.16	27.99	36.50	46.97	59.67	74.91
.5000	60.00	3.09	4.00	5.13	6.49	8.12	10.08	12.40
	75.00	3.94	5.15	6.63	8.45	10.66	13.33	16.52
	90.00	5.81	7.67	10.00	12.88	16.40	20.67	25.86
	105.00	9.96	13.37	17.62	22.96	29.44	37.37	46.82
	120.00	20.32	27.58	36.74	48.08	62.11	79.16	99.51
.6667	60.00	3.48	4.63	6.03	7.73	9.82	12.32	15.29
	75.00	4.62	6.13	8.02	10.35	13.18	16.64	20.74
	90.00	7.03	9.43	12.42	16.12	20.69	26.24	32.85
	105.00	12.41	16.79	22.34	29.18	37.67	47.90	60.21
	120.00	25.79	35.26	47.12	61.90	80.16	102.27	128.80
1.0000	60.00	4.50	6.14	8.19	10.74	13.85	17.64	22.16
	75.00	6.28	8.54	11.37	14.89	19.24	24.48	30.78
	90.00	10.01	13.64	18.21	23.88	30.87	39.37	49.57
	105.00	18.28	25.03	33.47	44.05	56.99	72.78	91.72
	120.00	38.94	53.43	71.65	94.50	122.35	156.39	197.24

* REMARK: THE KP-VALUE IS OVER 1000 WHEN 999.99 APPEARS

* ϕ = 35.00 k = .25 *

β/φ	=	0	1/6	1/3	1/2	2/3	5/6	1
δ/φ	α			--- K_p-VALUES ---				
0	60.00	2.24	2.71	3.25	3.86	4.57	5.42	6.40
	75.00	2.49	3.04	3.68	4.47	5.40	6.49	7.79
	90.00	3.18	3.99	4.96	6.12	7.53	9.22	11.24
	105.00	4.80	6.18	7.65	9.92	12.45	15.49	19.17
	120.00	8.71	11.50	14.99	19.34	24.68	31.22	39.13
.3333	60.00	2.69	3.42	4.31	5.39	6.68	8.21	10.03
	75.00	3.25	4.21	5.36	6.77	8.49	10.55	13.02
	90.00	4.60	6.03	7.81	10.01	12.72	15.97	19.81
	105.00	7.59	10.14	13.37	17.37	22.32	28.35	35.65
	120.00	14.94	20.43	27.24	35.88	46.47	59.48	75.10
.5000	60.00	2.99	3.91	5.04	6.42	8.08	10.08	12.47
	75.00	3.79	5.00	6.50	8.33	10.59	13.30	16.58
	90.00	5.57	7.44	9.77	12.69	16.25	20.63	25.82
	105.00	9.50	12.91	17.19	22.54	29.15	37.22	46.95
	120.00	19.35	26.57	35.78	47.24	61.55	78.83	99.81
.6667	60.00	3.36	4.51	5.91	7.64	9.75	12.31	15.37
	75.00	4.44	5.96	7.84	10.20	13.08	16.60	20.82
	90.00	6.73	9.11	12.13	15.87	20.53	26.16	32.98
	105.00	11.83	16.23	21.77	28.71	37.28	47.75	60.43
	120.00	24.55	34.04	45.89	60.88	79.36	101.93	129.27
1.0000	60.00	4.32	5.96	8.02	10.59	13.75	17.61	22.28
	75.00	6.02	8.27	11.12	14.66	19.07	24.43	30.92
	90.00	9.55	13.19	17.76	23.51	30.59	39.28	49.75
	105.00	17.44	24.22	32.67	43.31	56.46	72.65	92.04
	120.00	37.10	51.52	69.91	92.63	121.19	156.08	197.91

* REMARK: THE KP-VALUE IS OVER 1000 WHEN 999.99 APPEARS

Coefficients of passive earth pressure K_P for $\phi = 35°$ and $k = 0.30$, and for $\phi = 40°$ and $k = 0$, 0.05 and 0.10

* ϕ = 35.00 k = .30 *

β/φ	=	0	1/6	1/3	1/2	2/3	5/6	1
δ/φ	α			--- K_p-VALUES ---				
0	60.00	2.19	2.68	3.22	3.85	4.57	5.44	6.45
	75.00	2.42	2.98	3.63	4.43	5.37	6.49	7.83
	90.00	3.06	3.87	4.86	6.04	7.47	9.19	11.27
	105.00	4.59	5.96	7.67	9.74	12.30	15.42	19.20
	120.00	8.26	11.07	14.56	18.98	24.37	31.07	39.16
.3333	60.00	2.61	3.35	4.24	5.34	6.65	8.21	10.09
	75.00	3.13	4.09	5.26	6.68	8.42	10.52	13.06
	90.00	4.39	5.85	7.63	9.84	12.58	15.91	19.96
	105.00	7.21	9.78	13.01	17.07	22.06	28.24	35.74
	120.00	14.17	19.61	26.49	35.19	45.97	59.20	75.23
.5000	60.00	2.88	3.80	4.96	6.35	8.04	10.08	12.52
	75.00	3.63	4.86	6.36	8.21	10.49	13.27	16.64
	90.00	5.31	7.19	9.53	12.47	16.10	20.55	25.94
	105.00	9.05	12.44	16.76	22.12	28.86	37.07	47.09
	120.00	18.29	25.57	34.78	46.41	60.81	78.51	100.11
.6667	60.00	3.23	4.38	5.80	7.55	9.68	12.30	15.43
	75.00	4.25	5.77	7.67	10.04	12.97	16.55	20.90
	90.00	6.42	8.80	11.83	15.61	20.30	26.07	33.08
	105.00	11.24	15.65	21.18	28.23	36.87	47.59	60.61
	120.00	23.30	32.70	44.65	59.77	78.48	101.60	129.57
1.0000	60.00	4.14	5.78	7.84	10.43	13.65	17.59	22.38
	75.00	5.74	7.99	10.88	14.44	18.89	24.38	31.03
	90.00	9.10	12.72	17.32	23.10	30.31	39.17	49.80
	105.00	16.57	23.27	31.82	42.53	55.84	72.37	92.30
	120.00	35.25	49.60	68.08	91.13	120.04	155.48	198.44

* REMARK: THE KP-VALUE IS OVER 1000 WHEN 999.99 APPEARS

* ϕ = 40.00 k = 0 *

β/φ	=	0	1/6	1/3	1/2	2/3	5/6	1
δ/φ	α			--- K_p-VALUES ---				
0	60.00	2.71	3.31	4.02	4.88	5.96	7.25	8.80
	75.00	3.26	4.04	5.04	6.29	7.84	9.77	12.07
	90.00	4.60	5.80	7.57	9.69	12.37	15.72	19.82
	105.00	7.80	10.32	13.58	17.64	23.32	30.18	38.57
	120.00	16.15	21.85	28.70	39.78	52.76	69.17	89.34
.3333	60.00	3.63	4.73	6.15	7.93	10.18	12.96	16.35
	75.00	4.87	6.47	8.52	11.18	14.57	18.81	24.00
	90.00	7.73	10.46	14.07	18.73	24.76	32.35	41.65
	105.00	14.51	20.04	27.38	37.02	49.45	65.13	84.40
	120.00	32.78	45.90	63.51	86.70	116.54	154.22	200.50
.5000	60.00	4.29	5.78	7.70	10.16	13.30	17.21	21.95
	75.00	6.08	8.26	11.13	14.86	19.65	25.68	33.05
	90.00	10.08	13.91	18.98	25.65	34.19	45.00	58.28
	105.00	19.67	27.58	37.98	51.65	69.35	91.74	119.25
	120.00	45.47	64.32	89.52	122.39	164.94	218.79	284.93
.6667	60.00	5.17	7.12	9.68	13.00	17.26	22.59	29.14
	75.00	7.62	10.55	14.45	19.53	26.08	34.36	44.51
	90.00	13.09	18.32	25.31	34.42	46.20	61.06	79.32
	105.00	26.19	37.02	51.35	70.23	94.62	125.40	163.24
	120.00	61.83	87.67	122.13	167.54	226.18	300.20	391.16
1.0000	60.00	7.45	10.62	14.81	20.33	27.42	36.40	47.42
	75.00	11.67	16.54	23.06	31.58	42.60	56.55	73.67
	90.00	20.91	29.72	41.43	56.83	76.72	101.83	132.69
	105.00	43.09	61.33	85.54	117.45	158.65	210.66	274.60
	120.00	103.18	146.99	205.19	281.93	381.00	506.07	659.81

* REMARK: THE KP-VALUE IS OVER 1000 WHEN 999.99 APPEARS

* ϕ = 40.00 k = .05 *

β/φ	=	0	1/6	1/3	1/2	2/3	5/6	1
δ/φ	α			--- K_p-VALUES ---				
0	60.00	2.69	3.30	4.02	4.89	6.00	7.34	8.96
	75.00	3.21	3.99	5.00	6.27	7.86	9.84	12.25
	90.00	4.45	5.79	7.47	9.62	12.35	15.81	20.09
	105.00	7.59	10.10	13.38	17.70	23.26	30.34	39.09
	120.00	15.65	21.42	29.24	39.41	52.65	69.55	90.60
.3333	60.00	3.57	4.66	6.10	7.91	10.20	13.07	16.61
	75.00	4.75	6.35	8.43	11.11	14.57	18.95	24.35
	90.00	7.51	10.25	13.86	18.60	24.75	32.54	42.26
	105.00	14.07	19.57	26.96	36.73	48.36	63.52	82.66
	120.00	31.69	44.82	62.57	86.02	116.40	155.28	203.53
.5000	60.00	4.20	5.70	7.63	10.12	13.33	17.35	22.34
	75.00	5.92	8.11	10.99	14.77	19.63	25.85	33.55
	90.00	9.79	13.60	18.72	25.45	34.17	45.29	59.16
	105.00	19.04	26.89	37.37	51.22	69.29	92.34	121.07
	120.00	44.03	62.91	88.06	121.38	164.82	220.25	289.32
.6667	60.00	5.04	6.99	9.57	12.93	17.26	22.76	29.60
	75.00	7.41	10.34	14.26	19.39	26.07	34.60	45.20
	90.00	12.70	17.94	24.91	34.15	46.20	61.50	80.54
	105.00	25.38	36.15	50.58	69.74	94.63	126.32	165.76
	120.00	59.90	85.60	120.30	166.36	226.21	302.43	397.25
1.0000	60.00	7.25	10.40	14.63	20.20	27.44	36.68	48.19
	75.00	11.32	16.19	22.73	31.36	42.61	56.97	74.84
	90.00	20.29	29.10	40.84	56.41	76.71	102.60	134.78
	105.00	41.77	59.91	84.29	116.61	158.65	212.27	278.90
	120.00	99.98	143.55	202.19	279.95	381.04	509.92	670.14

* REMARK: THE KP-VALUE IS OVER 1000 WHEN 999.99 APPEARS

* ϕ = 40.00 k = .10 *

β/φ	=	0	1/6	1/3	1/2	2/3	5/6	1
δ/φ	α			--- K_p-VALUES ---				
0	60.00	2.66	3.28	4.01	4.91	6.04	7.42	9.11
	75.00	3.16	3.95	4.95	6.25	7.88	9.91	12.42
	90.00	4.38	5.69	7.38	9.55	12.34	15.89	20.34
	105.00	7.36	9.87	13.17	17.52	23.20	30.49	39.57
	120.00	15.11	20.90	28.74	39.03	52.55	69.92	91.76
.3333	60.00	3.50	4.60	6.04	7.89	10.22	13.18	16.85
	75.00	4.63	6.23	8.33	11.04	14.57	19.05	24.68
	90.00	7.28	10.02	13.65	18.46	24.70	32.71	42.62
	105.00	13.62	19.10	26.54	36.37	49.26	65.87	86.80
	120.00	30.60	43.74	61.62	85.19	116.18	155.12	206.30
.5000	60.00	4.10	5.60	7.55	10.07	13.33	17.47	22.66
	75.00	5.76	7.95	10.84	14.67	19.61	26.01	34.01
	90.00	9.49	13.29	18.45	25.24	34.14	45.58	59.87
	105.00	18.40	26.26	36.75	50.80	69.23	92.94	122.73
	120.00	42.60	61.38	86.60	120.37	164.70	221.71	293.35
.6667	60.00	4.91	6.86	9.45	12.86	17.26	22.94	30.03
	75.00	7.20	10.12	14.06	19.25	26.07	34.84	45.83
	90.00	12.29	17.52	24.52	33.88	46.11	61.84	81.67
	105.00	24.57	35.29	49.82	68.20	94.43	127.01	168.10
	120.00	57.83	83.53	118.48	165.08	225.76	304.08	402.88
1.0000	60.00	7.04	10.18	14.44	20.07	27.46	36.96	48.90
	75.00	10.97	15.84	22.39	31.13	42.61	57.34	75.93
	90.00	19.66	28.40	40.21	55.99	76.64	103.20	136.72
	105.00	40.44	58.49	83.03	115.70	158.44	213.47	282.96
	120.00	96.72	140.12	199.17	277.75	380.45	512.78	679.73

* REMARK: THE KP-VALUE IS OVER 1000 WHEN 999.99 APPEARS

Coefficients of passive earth pressure K_P for $\phi = 40°$ and $k = 0.15, 0.20, 0.25$ and 0.30

$\phi = 40.00$ $k = .15$

β/φ	=	0	1/6	1/3	1/2	2/3	5/6	1
δ/φ	α			--- K_p -VALUES ---				
0	60.00	2.63	3.28	4.01	4.92	6.07	7.50	9.25
	75.00	3.10	3.89	4.91	6.22	7.69	9.97	12.57
	90.00	4.27	5.58	7.28	9.48	12.32	15.97	20.57
	105.00	7.13	9.63	12.97	17.35	23.13	30.59	40.02
	120.00	14.57	20.38	28.22	38.65	52.41	70.18	92.84
.3333	60.00	3.43	4.54	5.99	7.85	10.23	13.27	17.09
	75.00	4.50	6.11	8.21	10.87	14.56	19.15	24.69
	90.00	7.05	9.78	13.43	18.28	24.64	32.69	43.35
	105.00	13.15	18.63	26.13	35.02	49.16	66.22	87.89
	120.00	29.50	42.66	60.51	84.35	115.95	156.88	208.90
.5000	60.00	4.00	5.48	7.46	10.02	13.33	17.58	22.93
	75.00	5.58	7.77	10.69	14.54	19.59	26.16	34.44
	90.00	9.17	12.98	18.14	25.02	34.09	45.80	60.72
	105.00	17.76	25.58	36.14	50.37	69.13	93.38	124.29
	120.00	41.16	59.74	85.14	119.35	164.47	222.77	297.11
.6667	60.00	4.77	6.73	9.33	12.77	17.26	23.07	30.43
	75.00	6.97	9.89	13.85	19.11	26.05	35.02	46.42
	90.00	11.88	17.08	24.12	33.61	46.02	62.17	82.70
	105.00	23.72	34.42	49.04	68.52	94.24	127.69	170.22
	120.00	55.74	81.45	116.66	163.45	225.30	305.73	408.01
1.0000	60.00	6.83	9.86	14.23	19.82	27.45	37.18	49.57
	75.00	10.61	15.47	22.05	30.91	42.56	57.68	76.92
	90.00	19.00	27.71	39.58	55.53	76.52	103.78	138.48
	105.00	39.09	57.08	81.68	114.69	158.16	214.67	286.54
	120.00	93.55	136.70	195.93	275.24	379.76	515.65	688.47

* REMARK: THE KP-VALUE IS OVER 1000 WHEN 999.99 APPEARS

$\phi = 40.00$ $k = .20$

β/φ	=	0	1/6	1/3	1/2	2/3	5/6	1
δ/φ	α			--- K_p -VALUES ---				
0	60.00	2.59	3.24	4.00	4.92	6.10	7.57	9.38
	75.00	3.04	3.84	4.86	6.19	7.89	10.03	12.72
	90.00	4.15	5.47	7.18	9.42	12.29	16.04	20.80
	105.00	6.90	9.39	12.74	17.17	23.07	30.69	40.42
	120.00	14.02	19.86	27.69	38.28	52.18	70.40	93.82
.3333	60.00	3.35	4.46	5.92	7.82	10.25	13.36	17.29
	75.00	4.37	5.99	8.09	10.90	14.53	19.26	25.25
	90.00	6.82	9.55	13.22	18.10	24.58	33.05	43.85
	105.00	12.68	18.16	25.66	35.66	49.06	66.54	88.92
	120.00	28.41	41.58	59.37	83.52	115.67	157.51	211.26
.5000	60.00	3.90	5.39	7.37	9.96	13.34	17.69	23.25
	75.00	5.41	7.59	10.53	14.42	19.57	26.28	34.83
	90.00	8.86	12.67	17.83	24.79	33.99	45.99	61.41
	105.00	17.12	24.89	35.52	48.94	68.90	93.77	125.72
	120.00	39.57	58.11	83.68	118.29	163.84	223.74	300.55
.6667	60.00	4.63	6.59	9.20	12.67	17.26	23.19	30.80
	75.00	6.75	9.67	13.63	18.97	25.99	35.18	46.99
	90.00	11.47	16.64	23.73	33.28	45.93	62.50	83.73
	105.00	22.85	33.52	48.20	67.83	94.05	128.37	172.35
	120.00	53.64	79.38	114.60	161.82	224.95	307.36	413.13
1.0000	60.00	6.61	9.74	14.01	19.77	27.41	37.38	50.18
	75.00	10.25	15.12	21.70	30.67	42.49	57.98	77.89
	90.00	18.33	27.00	38.94	55.01	76.39	104.36	140.24
	105.00	37.57	55.60	80.34	113.59	157.88	215.87	290.18
	120.00	89.78	133.19	192.68	272.56	379.08	518.52	697.20

* REMARK: THE KP-VALUE IS OVER 1000 WHEN 999.99 APPEARS

Coefficients of passive earth pressure K_P for $\phi = 45°$ and $k = 0, 0.05, 0.10$ and 0.15

$\phi = 45.00$ $k = 0$

β/φ	=	0	1/6	1/3	1/2	2/3	5/6	1
δ/φ	α			--- K_p -VALUES ---				
0	60.00	3.06	3.90	4.95	6.32	8.15	10.65	13.81
	75.00	3.86	5.04	6.68	8.93	12.00	16.13	21.57
	90.00	5.83	8.03	11.11	15.48	21.54	29.82	40.62
	105.00	10.92	15.71	22.72	32.69	46.80	66.26	92.02
	120.00	25.66	38.42	57.20	84.39	122.78	175.43	245.52
.3333	60.00	4.44	6.16	8.50	12.00	16.66	23.04	31.40
	75.00	6.46	9.28	13.32	19.10	27.16	38.23	52.69
	90.00	11.43	16.96	25.01	36.67	53.05	75.61	105.61
	105.00	24.36	37.18	56.09	83.34	121.83	174.86	245.37
	120.00	53.17	98.07	149.61	223.92	328.95	473.68	666.05
.5000	60.00	5.52	8.05	11.65	16.74	23.85	33.58	46.45
	75.00	8.65	12.88	19.00	27.84	40.27	57.36	80.03
	90.00	15.18	24.66	37.14	55.02	80.33	115.23	161.61
	105.00	36.12	55.97	84.99	127.02	186.51	268.55	377.58
	120.00	96.25	149.99	229.18	343.85	506.16	730.03	999.99
.6667	60.00	7.07	10.66	15.84	23.23	33.76	48.12	67.20
	75.00	11.69	17.85	26.89	39.86	58.21	83.53	117.15
	90.00	22.86	35.37	53.70	80.23	117.79	169.59	238.43
	105.00	52.52	81.71	124.79	187.17	275.46	397.23	559.04
	120.00	141.55	221.26	338.78	508.99	749.89	999.99	999.99
1.0000	60.00	11.63	18.23	27.96	42.02	61.90	89.25	125.60
	75.00	20.64	32.16	49.32	74.13	109.13	157.34	221.43
	90.00	41.95	65.74	100.85	151.51	223.18	321.84	452.99
	105.00	98.33	154.27	236.85	355.80	524.33	756.28	999.99
	120.00	257.81	420.43	645.81	970.25	999.99	999.99	999.99

* REMARK: THE KP-VALUE IS OVER 1000 WHEN 999.99 APPEARS

$\phi = 45.00$ $k = .05$

β/φ	=	0	1/6	1/3	1/2	2/3	5/6	1
δ/φ	α			--- K_p -VALUES ---				
0	60.00	3.04	3.89	4.96	6.36	8.28	10.83	14.14
	75.00	3.81	4.99	6.65	8.93	12.07	16.34	22.05
	90.00	5.71	7.90	11.02	15.43	21.64	30.18	41.73
	105.00	10.64	15.47	22.47	32.58	47.00	67.07	94.10
	120.00	24.96	37.65	56.54	84.11	123.35	177.82	251.21
.3333	60.00	4.36	6.09	8.56	11.99	16.77	23.37	32.13
	75.00	6.32	9.15	13.20	19.06	27.31	38.76	54.11
	90.00	11.14	16.65	24.78	35.60	53.26	76.59	108.07
	105.00	23.70	36.51	55.51	83.02	122.33	177.17	251.18
	120.00	51.46	96.34	149.08	223.13	330.40	480.03	691.91
.5000	60.00	5.41	7.94	11.56	16.73	24.00	34.04	47.58
	75.00	8.45	12.66	18.84	27.75	40.44	58.12	81.92
	90.00	15.76	24.24	35.76	54.98	80.75	116.76	165.48
	105.00	35.16	54.89	84.09	126.70	187.50	272.16	386.68
	120.00	93.60	147.10	226.77	343.02	508.94	738.91	999.99
.6667	60.00	6.91	10.43	15.72	23.24	33.93	48.78	68.82
	75.00	11.40	17.56	26.63	39.77	58.53	84.65	119.98
	90.00	22.26	34.71	53.14	80.04	118.44	171.88	244.19
	105.00	51.06	80.16	123.49	185.73	276.58	402.62	572.59
	120.00	137.65	217.05	335.29	507.84	754.08	999.99	999.99
1.0000	60.00	11.35	17.84	27.72	41.89	62.22	90.50	128.65
	75.00	20.02	31.62	48.87	73.92	109.65	159.51	226.77
	90.00	40.86	64.60	99.89	151.09	224.23	326.25	463.89
	105.00	95.76	151.61	234.58	354.88	528.80	766.63	999.99
	120.00	250.76	413.23	638.79	967.78	999.99	999.99	999.99

* REMARK: THE KP-VALUE IS OVER 1000 WHEN 999.99 APPEARS

$\phi = 40.00$ $k = .25$

β/φ	=	0	1/6	1/3	1/2	2/3	5/6	1
δ/φ	α			--- K_p -VALUES ---				
0	60.00	2.56	3.21	3.99	4.93	6.12	7.64	9.52
	75.00	2.98	3.78	4.82	6.16	7.89	10.08	12.86
	90.00	4.03	5.36	7.07	9.33	12.27	16.08	20.59
	105.00	6.66	9.15	12.50	17.00	23.00	30.78	40.83
	120.00	13.48	19.26	27.14	37.80	51.95	70.63	94.80
.3333	60.00	3.27	4.39	5.85	7.78	10.26	13.44	17.50
	75.00	4.24	5.85	7.98	10.80	14.50	19.35	25.55
	90.00	6.59	9.31	13.00	17.92	24.53	33.14	44.28
	105.00	12.18	17.69	25.16	35.31	48.94	66.74	89.83
	120.00	27.31	40.33	58.23	82.68	115.25	158.14	213.63
.5000	60.00	3.79	5.28	7.27	9.90	13.33	17.80	23.51
	75.00	5.24	7.42	10.37	14.28	19.55	26.40	35.23
	90.00	8.54	12.36	17.51	24.56	33.88	46.18	62.10
	105.00	16.49	24.20	34.91	49.38	68.68	94.16	127.14
	120.00	37.92	56.48	82.22	117.02	163.41	224.70	304.00
.6667	60.00	4.48	6.45	9.08	12.57	17.25	23.32	31.16
	75.00	6.51	9.44	13.40	18.78	25.92	35.34	47.51
	90.00	11.05	16.20	23.34	32.95	45.84	62.80	84.64
	105.00	21.94	32.50	47.27	67.15	93.86	128.99	174.24
	120.00	51.54	77.28	112.38	160.19	224.40	308.89	417.68
1.0000	60.00	6.39	9.51	13.79	19.62	27.36	37.58	50.80
	75.00	9.88	14.70	21.35	30.37	42.39	58.27	78.80
	90.00	17.61	26.28	38.27	54.49	76.23	104.85	141.83
	105.00	36.14	54.09	78.89	112.48	157.58	216.88	293.42
	120.00	86.32	129.54	189.12	269.88	378.37	520.87	704.97

* REMARK: THE KP-VALUE IS OVER 1000 WHEN 999.99 APPEARS

$\phi = 40.00$ $k = .30$

β/φ	=	0	1/6	1/3	1/2	2/3	5/6	1
δ/φ	α			--- K_p -VALUES ---				
0	60.00	2.51	3.18	3.97	4.94	6.15	7.70	9.65
	75.00	2.91	3.73	4.77	6.13	7.88	10.14	13.00
	90.00	3.91	5.24	6.96	9.24	12.24	16.13	21.19
	105.00	6.42	8.90	12.26	16.82	22.88	30.87	41.24
	120.00	12.94	18.66	26.58	37.32	51.71	70.85	95.78
.3333	60.00	3.19	4.32	5.79	7.73	10.25	13.52	17.71
	75.00	4.11	5.72	7.85	10.71	14.47	19.41	25.81
	90.00	6.36	9.07	12.77	17.75	24.47	33.24	44.73
	105.00	11.68	17.16	24.66	34.95	48.71	66.93	90.73
	120.00	26.17	39.08	57.09	81.80	114.84	159.76	215.98
.5000	60.00	3.68	5.17	7.17	9.82	13.31	17.87	23.77
	75.00	5.06	7.24	10.19	14.16	19.48	26.49	35.62
	90.00	8.20	12.01	17.19	24.29	33.77	46.37	62.79
	105.00	15.79	23.52	34.29	48.81	68.45	94.55	128.57
	120.00	36.27	54.84	80.67	115.66	162.88	225.66	307.24
.6667	60.00	4.33	6.28	8.94	12.48	17.21	23.44	31.53
	75.00	6.26	9.19	13.17	18.59	25.85	35.51	47.99
	90.00	10.61	15.76	22.91	32.62	45.72	62.99	85.49
	105.00	21.01	31.58	46.35	66.47	93.67	129.37	175.99
	120.00	49.42	74.98	110.17	158.56	223.95	308.80	421.92
1.0000	60.00	6.16	9.27	13.56	19.44	27.31	37.78	51.37
	75.00	9.50	14.31	20.98	30.06	42.29	58.53	79.62
	90.00	16.97	25.56	37.63	53.96	76.03	105.26	143.29
	105.00	34.61	52.58	77.63	111.38	157.13	217.65	296.44
	120.00	82.68	125.89	186.15	267.21	377.29	522.76	712.20

* REMARK: THE KP-VALUE IS OVER 1000 WHEN 999.99 APPEARS

$\phi = 45.00$ $k = .10$

β/φ	=	0	1/6	1/3	1/2	2/3	5/6	1
δ/φ	α			--- K_p -VALUES ---				
0	60.00	3.02	3.88	4.96	6.40	8.36	10.99	14.46
	75.00	3.76	4.95	6.61	8.93	12.13	16.54	22.50
	90.00	5.59	7.78	10.93	15.38	21.74	30.54	42.57
	105.00	10.36	15.20	22.22	32.46	47.20	67.89	96.10
	120.00	24.21	36.88	55.88	83.83	123.72	178.83	256.69
.3333	60.00	4.29	6.02	8.50	11.98	16.88	23.66	32.83
	75.00	6.17	9.01	13.09	19.02	27.41	39.21	55.27
	90.00	10.83	16.34	24.54	36.45	53.47	77.50	110.42
	105.00	23.03	35.83	54.84	82.69	122.83	179.31	256.65
	120.00	59.74	94.62	146.30	222.31	331.82	485.92	697.05
.5000	60.00	5.30	7.83	11.47	15.71	24.11	34.46	48.63
	75.00	8.24	12.44	18.68	27.66	40.62	58.85	83.67
	90.00	15.33	23.82	36.34	54.74	81.17	118.23	169.02
	105.00	34.20	53.81	83.19	126.37	188.50	275.76	395.03
	120.00	90.79	144.21	224.36	342.19	511.71	749.79	999.99
.6667	60.00	6.75	10.32	15.60	23.18	34.10	48.43	70.30
	75.00	11.10	17.27	26.36	39.69	58.85	85.77	122.57
	90.00	21.67	34.04	52.59	79.86	119.08	174.17	249.48
	105.00	49.54	78.60	122.20	186.29	278.50	408.01	585.03
	120.00	133.55	212.84	331.79	506.68	758.27	999.99	999.99
1.0000	60.00	11.08	17.62	27.46	41.87	62.53	91.65	131.55
	75.00	19.49	31.08	48.37	73.69	110.18	161.52	231.87
	90.00	38.75	63.42	98.79	150.82	225.28	330.35	474.31
	105.00	93.16	148.82	231.90	353.74	529.25	776.24	999.99
	120.00	253.71	405.58	632.21	964.63	999.99	999.99	999.99

* REMARK: THE KP-VALUE IS OVER 1000 WHEN 999.99 APPEARS

$\phi = 45.00$ $k = .15$

β/φ	=	0	1/6	1/3	1/2	2/3	5/6	1
δ/φ	α			--- K_p -VALUES ---				
0	60.00	2.99	3.87	4.97	6.42	8.43	11.15	14.78
	75.00	3.70	4.90	6.57	8.93	12.18	16.73	22.94
	90.00	5.46	7.66	10.82	15.33	21.83	30.89	43.41
	105.00	10.05	14.89	21.97	32.35	47.40	68.65	97.84
	120.00	23.45	36.11	55.22	83.46	124.10	181.81	261.73
.3333	60.00	4.22	5.95	8.45	11.97	16.99	23.85	33.48
	75.00	6.01	8.86	12.97	18.97	27.51	39.55	56.36
	90.00	10.53	16.03	24.25	36.29	53.68	78.41	112.60
	105.00	22.37	35.13	54.16	82.37	123.33	181.45	261.84
	120.00	58.03	92.57	144.51	221.49	333.24	491.81	711.19
.5000	60.00	5.18	7.72	11.38	16.68	24.22	34.83	49.60
	75.00	8.03	12.21	18.47	27.57	40.79	59.55	85.41
	90.00	14.91	23.33	35.90	54.54	81.59	119.76	172.55
	105.00	33.19	52.74	82.28	126.05	189.50	278.24	403.27
	120.00	87.98	141.33	221.95	341.36	514.48	755.33	999.99
.6667	60.00	6.59	10.15	15.44	23.12	34.27	50.07	71.79
	75.00	10.81	16.93	26.06	39.60	59.17	86.26	125.16
	90.00	21.04	33.38	52.04	79.67	119.73	176.28	254.76
	105.00	48.03	77.05	120.90	185.86	280.03	413.22	597.45
	120.00	128.46	208.64	328.29	505.52	762.30	999.99	999.99
1.0000	60.00	10.78	17.30	27.20	41.74	62.84	92.81	134.26
	75.00	18.95	30.50	47.83	73.47	110.70	163.54	235.62
	90.00	38.59	62.21	97.66	150.14	226.33	334.45	483.99
	105.00	90.43	145.82	229.22	352.59	531.69	785.85	999.99
	120.00	246.24	397.24	624.86	961.48	999.99	999.99	999.99

* REMARK: THE KP-VALUE IS OVER 1000 WHEN 999.99 APPEARS

Coefficients of passive earth pressure K_P for $\phi = 45°$ and $k = 0.20$, 0.25 and 0.30, and for $\phi = 50°$ and $k = 0$

* ϕ = 45.00 k = .20 *

β/φ	=	0	1/6	1/3	1/2	2/3	5/6	1
δ/φ	α				--- K_p-VALUES ---			
0	60.00	2.96	3.85	4.98	6.45	8.51	11.30	15.05
	75.00	3.64	4.84	6.53	8.93	12.25	16.93	23.36
	90.00	5.34	7.53	10.70	15.27	21.88	31.18	44.19
	105.00	9.81	14.57	21.72	32.24	47.48	69.34	99.73
	120.00	22.70	35.34	54.57	83.04	124.47	183.79	266.65
.3333	60.00	4.13	5.88	8.40	11.86	17.06	24.23	34.11
	75.00	5.86	8.71	12.85	18.90	27.62	40.09	57.44
	90.00	10.23	15.72	23.95	36.13	53.89	79.31	114.79
	105.00	21.70	34.35	53.49	82.05	123.83	183.59	266.98
	120.00	56.21	90.52	142.73	220.67	334.65	497.70	725.24
.5000	60.00	5.07	7.60	11.28	16.64	24.33	35.30	50.57
	75.00	7.82	11.99	18.25	27.48	40.97	60.22	87.03
	90.00	14.48	22.83	35.47	54.35	81.80	121.00	175.67
	105.00	32.14	51.66	81.38	125.73	190.02	282.17	411.15
	120.00	85.17	138.44	219.54	340.53	515.96	767.38	999.99
.6667	60.00	6.43	9.98	15.28	23.06	34.43	50.60	73.17
	75.00	10.50	16.59	25.77	39.47	59.35	87.78	127.57
	90.00	20.39	32.72	51.48	79.48	120.07	178.25	259.69
	105.00	46.52	75.50	119.61	185.37	280.85	417.61	609.04
	120.00	125.37	204.43	324.79	503.81	764.74	999.99	999.99
1.0000	60.00	10.48	16.98	26.90	41.61	63.16	93.97	136.97
	75.00	18.39	29.92	47.28	73.25	111.23	165.55	241.33
	90.00	37.44	60.93	96.52	149.66	227.38	338.54	493.66
	105.00	87.70	142.85	226.53	351.44	534.14	795.46	999.99
	120.00	238.76	389.19	617.50	959.33	999.99	999.99	999.99

* REMARK: THE KP-VALUE IS OVER 1000 WHEN 999.99 APPEARS

* ϕ = 45.00 k = .25 *

β/φ	=	0	1/6	1/3	1/2	2/3	5/6	1
δ/φ	α				--- K_p-VALUES ---			
0	60.00	2.93	3.84	4.98	6.48	8.58	11.44	15.34
	75.00	3.58	4.79	6.48	8.91	12.31	17.12	23.76
	90.00	5.21	7.41	10.59	15.22	21.93	31.47	44.84
	105.00	9.51	14.26	21.46	32.04	47.57	69.99	101.53
	120.00	21.95	34.56	53.91	82.61	124.84	185.76	271.58
.3333	60.00	4.05	5.80	8.34	11.85	17.13	24.51	34.75
	75.00	5.71	8.55	12.73	18.84	27.72	40.53	58.52
	90.00	9.92	15.41	23.64	35.97	54.10	80.22	116.97
	105.00	21.04	33.58	52.81	81.73	124.33	185.68	272.04
	120.00	54.22	88.46	140.94	219.84	335.93	502.88	738.52
.5000	60.00	4.85	7.48	11.18	16.60	24.43	35.72	51.55
	75.00	7.59	11.77	18.04	27.39	41.14	60.83	88.58
	90.00	14.05	22.34	35.04	54.15	82.02	122.25	179.02
	105.00	31.09	50.58	80.46	125.06	190.54	285.10	418.57
	120.00	82.36	135.56	217.13	338.77	517.42	775.43	999.99
.6667	60.00	6.26	9.80	15.11	23.01	34.59	51.14	74.50
	75.00	10.18	16.24	25.47	39.32	59.52	88.70	128.88
	90.00	19.74	32.05	50.93	79.08	120.41	180.12	264.38
	105.00	45.01	73.94	118.31	184.48	281.66	422.01	620.10
	120.00	121.27	200.22	321.10	501.82	766.97	999.99	999.99
1.0000	60.00	10.14	16.67	26.59	41.47	63.43	95.08	139.67
	75.00	17.82	29.28	46.74	73.03	111.75	167.55	246.08
	90.00	36.26	59.61	95.39	149.18	228.42	342.39	503.23
	105.00	84.78	139.73	223.84	350.30	536.51	804.41	999.99
	120.00	230.69	380.64	610.14	955.18	999.93	999.99	999.99

* REMARK: THE KP-VALUE IS OVER 1000 WHEN 999.99 APPEARS

* ϕ = 45.00 k = .30 *

β/φ	=	0	1/6	1/3	1/2	2/3	5/6	1
δ/φ	α				--- K_p-VALUES ---			
0	60.00	2.90	3.82	4.98	6.51	8.65	11.59	15.64
	75.00	3.52	4.73	6.44	8.90	12.37	17.28	24.16
	90.00	5.07	7.28	10.47	15.17	21.98	31.76	45.62
	105.00	9.21	13.94	21.18	31.84	47.65	70.65	103.33
	120.00	21.20	33.79	53.19	82.18	125.22	187.74	276.51
.3333	60.00	3.97	5.72	8.28	11.94	17.20	24.77	35.39
	75.00	5.56	8.38	12.59	18.77	27.82	40.97	59.48
	90.00	9.61	15.09	23.34	35.81	54.31	80.96	118.91
	105.00	20.29	32.81	52.14	81.41	124.79	187.46	276.68
	120.00	52.24	86.41	139.16	219.02	336.81	508.04	751.59
.5000	60.00	4.82	7.35	11.07	16.55	24.54	36.07	52.41
	75.00	7.35	11.54	17.82	27.30	41.28	61.45	90.13
	90.00	13.58	21.84	34.61	53.87	82.23	123.49	182.17
	105.00	29.98	49.43	79.45	124.38	191.05	288.03	425.95
	120.00	79.55	132.67	214.45	336.96	518.07	783.48	999.99
.6667	60.00	6.08	9.63	14.95	22.95	34.71	51.68	75.82
	75.00	9.87	15.90	25.17	39.12	59.69	89.61	132.18
	90.00	19.06	31.36	50.31	78.66	120.75	181.59	269.05
	105.00	43.49	72.39	116.82	183.51	282.46	426.40	631.15
	120.00	117.18	196.01	316.94	499.22	769.19	999.99	999.99
1.0000	60.00	9.83	16.34	26.28	41.34	63.68	96.08	142.08
	75.00	17.25	28.63	46.20	72.79	112.17	169.21	250.32
	90.00	34.99	58.29	94.25	148.70	229.30	345.99	511.56
	105.00	81.83	136.50	221.15	349.15	538.66	812.87	999.99
	120.00	222.66	372.10	602.79	952.03	999.99	999.99	999.99

* REMARK: THE KP-VALUE IS OVER 1000 WHEN 999.99 APPEARS

* ϕ = 45.00 k = .0 *

β/φ	=	0	1/6	1/3	1/2	2/3	5/6	1
δ/φ	α				--- K_p-VALUES ---			
0	60.00	3.48	4.65	6.22	8.50	11.95	17.03	24.25
	75.00	4.63	6.43	9.23	13.52	20.11	30.16	44.72
	90.00	7.55	11.40	17.50	27.27	42.66	66.09	100.22
	105.00	15.98	25.76	42.10	68.35	110.02	174.07	268.41
	120.00	43.72	74.33	125.44	208.68	340.86	543.61	842.17
.3333	60.00	5.54	8.34	12.82	19.82	30.78	47.39	71.77
	75.00	8.91	14.22	22.94	36.93	58.97	92.92	142.78
	90.00	18.02	30.30	50.52	83.51	136.00	216.75	335.41
	105.00	45.26	78.28	133.48	223.64	367.08	587.78	912.04
	120.00	136.29	243.02	418.13	704.10	999.99	999.99	999.99
.5000	60.00	7.39	11.95	19.26	31.07	49.57	78.05	118.89
	75.00	13.12	22.05	36.68	60.52	98.45	156.82	242.57
	90.00	28.68	49.47	84.20	140.92	230.94	369.56	573.53
	105.00	75.20	131.89	226.70	381.44	627.30	999.99	999.99
	120.00	234.22	414.05	714.80	999.99	999.99	999.99	999.99
.6667	60.00	10.32	17.42	29.22	48.18	78.40	124.91	193.24
	75.00	19.69	34.00	57.84	96.78	158.64	253.82	393.87
	90.00	45.08	78.97	135.65	228.14	375.09	601.53	934.71
	105.00	120.84	213.45	368.32	621.08	999.99	999.99	999.99
	120.00	380.67	674.41	999.99	999.99	999.99	999.99	999.99
1.0000	60.00	20.18	35.65	61.62	104.01	171.35	275.11	427.79
	75.00	41.27	73.10	126.33	213.20	351.22	563.90	876.83
	90.00	98.06	173.77	300.41	507.06	835.42	999.99	999.99
	105.00	267.69	474.61	820.67	999.99	999.99	999.99	999.99
	120.00	848.58	999.99	999.99	999.99	999.99	999.99	999.99

* REMARK: THE KP-VALUE IS OVER 1000 WHEN 999.99 APPEARS

Coefficients of passive earth pressure K_P for $\phi = 50°$ and $k = 0.05$, 0.10, 0.15 and 0.20

* ϕ = 50.00 k = .05 *

β/φ	=	0	1/6	1/3	1/2	2/3	5/6	1
δ/φ	α				--- K_p-VALUES ---			
0	60.00	3.47	4.65	6.25	8.58	12.11	17.38	25.01
	75.00	4.58	6.38	9.21	13.56	20.33	30.74	46.11
	90.00	7.41	11.25	17.41	27.33	43.07	67.41	103.82
	105.00	15.63	25.40	41.78	68.38	111.10	177.63	277.12
	120.00	42.67	73.25	124.48	208.86	344.37	554.64	869.73
.3333	60.00	5.47	8.27	12.78	19.90	31.11	48.37	74.07
	75.00	8.75	14.05	22.82	36.98	59.55	94.78	147.42
	90.00	17.62	29.89	50.18	83.64	137.35	221.16	346.38
	105.00	44.14	77.08	132.60	224.02	370.81	588.84	942.06
	120.00	134.85	239.32	415.44	705.43	999.99	999.99	999.99
.5000	60.00	7.26	11.81	19.18	31.12	50.08	79.63	123.76
	75.00	12.84	21.76	36.45	60.63	99.44	160.01	250.51
	90.00	28.05	48.72	83.65	141.17	233.52	377.03	592.40
	105.00	73.39	130.02	225.48	382.58	634.43	999.99	999.99
	120.00	228.78	408.35	711.11	999.99	999.99	999.99	999.99
.6667	60.00	10.12	17.20	29.04	48.28	78.21	127.47	199.59
	75.00	19.27	33.50	57.48	96.97	160.37	258.97	406.85
	90.00	43.98	77.82	134.87	228.81	378.37	613.78	965.56
	105.00	118.05	210.52	366.44	623.02	999.99	999.99	999.99
	120.00	371.90	665.22	999.99	999.99	999.99	999.99	999.99
1.0000	60.00	19.69	35.20	61.34	104.36	173.35	280.76	441.96
	75.00	40.35	72.13	125.71	213.90	355.29	575.45	905.88
	90.00	95.83	171.44	298.92	508.70	845.07	999.99	999.99
	105.00	261.58	468.21	816.59	999.99	999.99	999.99	999.99
	120.00	829.18	999.99	999.99	999.99	999.99	999.99	999.99

* REMARK: THE KP-VALUE IS OVER 1000 WHEN 999.99 APPEARS

* ϕ = 50.00 k = .10 *

β/φ	=	0	1/6	1/3	1/2	2/3	5/6	1
δ/φ	α				--- K_p-VALUES ---			
0	60.00	3.45	4.65	6.28	8.65	12.27	17.72	25.74
	75.00	4.52	6.34	9.19	13.60	20.55	31.32	47.44
	90.00	7.27	11.13	17.33	27.39	43.44	68.64	106.88
	105.00	15.27	25.03	41.45	68.41	112.08	180.95	285.45
	120.00	41.63	72.02	123.52	209.03	347.55	564.91	896.59
.3333	60.00	5.38	8.20	12.73	19.98	31.42	49.25	76.31
	75.00	8.57	13.88	22.68	37.02	60.13	96.51	151.92
	90.00	17.22	29.41	49.85	83.77	138.70	225.26	357.07
	105.00	43.01	75.87	131.71	224.41	374.54	611.09	971.32
	120.00	131.40	235.62	412.74	706.77	999.99	999.99	999.99
.5000	60.00	7.12	11.66	19.11	31.18	50.58	81.10	127.58
	75.00	12.56	21.43	36.22	60.73	100.44	162.99	258.10
	90.00	27.37	47.88	83.11	141.42	235.87	384.51	610.33
	105.00	71.53	128.02	224.03	383.40	641.51	999.99	999.99
	120.00	223.34	402.65	707.25	999.99	999.99	999.99	999.99
.6667	60.00	9.89	16.99	28.86	48.38	80.02	129.87	205.72
	75.00	18.84	33.01	57.12	97.16	162.00	264.12	419.18
	90.00	42.88	76.64	134.02	229.26	383.51	626.02	994.91
	105.00	115.26	207.57	364.36	624.65	999.99	999.99	999.99
	120.00	363.13	656.04	999.99	999.99	999.99	999.99	999.99
1.0000	60.00	19.25	34.74	61.05	104.72	175.35	286.41	455.45
	75.00	39.42	71.16	125.10	214.69	359.35	587.00	933.47
	90.00	93.61	169.11	297.43	510.26	854.71	999.99	999.99
	105.00	255.47	461.80	812.48	999.99	999.99	999.99	999.99
	120.00	809.77	999.99	999.99	999.99	999.99	999.99	999.99

* REMARK: THE KP-VALUE IS OVER 1000 WHEN 999.99 APPEARS

* ϕ = 50.00 k = .15 *

β/φ	=	0	1/6	1/3	1/2	2/3	5/6	1
δ/φ	α				---K_p-VALUES ---			
0	60.00	3.43	4.65	6.31	8.73	12.42	18.06	25.45
	75.00	4.47	6.29	9.17	13.65	20.77	31.89	48.77
	90.00	7.14	10.98	17.24	27.46	43.81	69.50	109.53
	105.00	14.89	24.67	41.13	68.44	113.06	184.08	283.75
	120.00	40.55	70.79	122.55	209.20	350.73	575.19	921.84
.3333	60.00	5.30	8.12	12.69	20.06	31.72	50.15	78.42
	75.00	8.38	13.71	22.54	37.06	60.71	98.25	156.16
	90.00	16.82	28.94	49.51	83.89	140.05	229.36	357.13
	105.00	41.89	74.67	130.83	224.79	378.26	622.33	999.99
	120.00	127.95	231.93	413.05	708.11	999.99	999.99	999.99
.5000	60.00	6.99	11.52	19.03	31.24	51.09	82.50	131.16
	75.00	12.28	21.11	35.99	60.84	101.43	165.97	255.45
	90.00	26.67	47.23	82.56	141.68	238.23	391.79	627.82
	105.00	69.67	126.03	222.57	384.13	647.93	999.99	999.99
	120.00	217.74	396.51	702.74	999.99	999.99	999.99	999.99
.6667	60.00	9.67	16.78	28.67	48.49	80.83	132.26	211.59
	75.00	18.36	32.51	56.76	97.35	163.63	269.05	431.20
	90.00	41.78	75.46	133.16	229.71	387.40	638.17	999.99
	105.00	112.33	204.38	362.05	625.91	999.99	999.99	999.99
	120.00	354.35	646.31	999.99	999.99	999.99	999.99	999.99
1.0000	60.00	18.78	34.23	60.70	104.98	177.31	292.05	468.60
	75.00	38.50	70.18	124.42	215.19	362.92	598.41	960.36
	90.00	91.38	168.77	295.84	511.79	863.07	999.99	999.99
	105.00	248.36	455.40	808.19	999.99	999.99	999.99	999.99
	120.00	790.37	999.99	999.99	999.99	999.99	999.99	999.99

* REMARK: THE KP-VALUE IS OVER 1000 WHEN 999.99 APPEARS

* ϕ = 50.00 k = .20 *

β/φ	=	0	1/6	1/3	1/2	2/3	5/6	1
δ/φ	α				--- K_p-VALUES ---			
0	60.00	3.40	4.64	6.33	8.79	12.58	18.40	27.16
	75.00	4.41	6.25	9.14	13.69	20.96	32.43	49.99
	90.00	7.00	10.82	17.15	27.49	44.18	70.96	112.72
	105.00	14.51	24.30	40.81	68.48	114.05	187.21	301.34
	120.00	39.41	69.56	121.60	209.37	353.92	585.46	946.42
.3333	60.00	5.21	8.05	12.64	20.12	32.03	51.01	80.47
	75.00	8.19	13.52	22.39	37.11	61.28	99.58	160.28
	90.00	16.41	28.47	49.17	84.02	141.40	233.46	376.52
	105.00	40.77	73.47	129.94	225.18	381.89	633.58	999.99
	120.00	124.51	228.23	407.35	709.45	999.99	999.99	999.92
.5000	60.00	6.85	11.37	18.85	31.28	51.59	84.05	134.64
	75.00	12.01	20.78	35.76	60.95	102.42	168.95	272.63
	90.00	25.95	46.49	82.01	141.93	240.59	398.89	645.31
	105.00	67.81	124.03	221.12	384.87	654.47	999.99	999.99
	120.00	211.94	390.28	698.23	999.99	999.99	999.99	999.99
.6667	60.00	9.45	16.55	28.49	48.59	81.64	134.65	217.28
	75.00	17.88	32.01	56.40	97.54	165.26	273.92	443.22
	90.00	40.68	74.28	132.31	230.16	391.28	645.78	999.99
	105.00	109.36	201.18	359.74	627.17	999.99	999.99	999.99
	120.00	344.99	636.25	999.99	999.99	999.99	999.99	999.99
1.0000	60.00	18.32	33.73	60.34	105.23	178.87	297.24	481.75
	75.00	37.52	69.11	123.66	215.66	366.41	609.03	987.30
	90.00	89.09	164.24	294.00	512.87	871.35	999.99	999.99
	105.00	243.13	448.50	803.13	999.99	999.99	999.99	999.99
	120.00	770.63	999.99	999.99	999.99	999.99	999.99	999.99

* REMARK: THE KP-VALUE IS OVER 1000 WHEN 999.99 APPEARS

Coefficients of passive earth pressure K_p for $\phi = 50°$ and $k = 0.25$ and 0.30

• ϕ = 50.00 k= .25 •

β/φ	=	0	1/6	1/3	1/2	2/3	5/6	1
δ/φ	α				---K_p -VALUES ---			
0	60.00	3.38	4.63	6.35	8.85	12.73	18.73	27.86
	75.00	4.35	6.20	9.12	13.74	21.14	32.95	51.21
	90.00	6.85	10.67	17.04	27.48	44.55	72.11	115.51
	105.00	14.13	23.94	40.48	68.51	115.03	190.37	308.94
	120.00	38.27	68.33	120.64	209.54	357.10	595.74	971.03
.3333	60.00	5.13	7.96	12.60	20.15	32.33	51.87	82.53
	75.00	8.00	13.33	22.25	37.15	61.86	101.72	164.41
	90.00	16.00	28.00	48.83	84.15	142.75	237.56	386.71
	105.00	39.65	72.87	129.05	225.57	385.72	644.82	999.99
	120.00	121.06	224.54	404.65	710.79	999.99	999.99	999.99
.5000	60.00	6.71	11.22	18.64	31.35	52.10	85.53	138.12
	75.00	11.72	20.45	35.53	61.06	103.41	171.93	278.72
	90.00	25.23	45.74	81.47	142.19	242.89	405.65	662.35
	105.00	65.95	122.04	219.67	385.60	660.18	999.99	999.99
	120.00	206.14	384.05	693.73	999.99	999.99	999.99	999.99
.6667	60.00	9.22	16.31	28.31	48.70	82.44	137.04	222.93
	75.00	17.40	31.52	56.04	97.73	166.50	278.68	454.85
	90.00	39.59	73.11	131.45	230.62	394.81	660.68	999.99
	105.00	106.38	197.99	357.43	628.33	999.99	999.99	999.99
	120.00	335.62	626.18	999.99	999.99	999.99	999.99	999.99
1.0000	60.00	17.85	33.22	59.98	105.32	180.58	302.41	494.32
	75.00	36.53	68.04	122.90	215.63	369.90	619.65	999.99
	90.00	86.71	161.67	292.16	512.63	879.63	999.99	999.99
	105.00	236.58	441.46	798.07	999.99	999.99	999.99	999.99
	120.00	749.84	999.99	999.99	999.99	999.99	999.99	999.99

• REMARK: THE KP-VALUE IS OVER 1000 WHEN 999.99 APPEARS

• ϕ = 50.00 k= .30 •

β/φ	=	0	1/6	1/3	1/2	2/3	5/6	1
δ/φ	α				---K_p-VALUES ---			
0	60.00	3.35	4.63	6.37	8.91	12.88	19.07	28.51
	75.00	4.29	6.15	9.08	13.78	21.31	33.45	52.43
	90.00	6.69	10.52	16.91	27.48	44.93	73.27	118.30
	105.00	13.75	23.52	40.16	68.54	116.01	193.48	316.53
	120.00	37.13	67.10	119.68	209.71	360.28	606.02	999.99
.3333	60.00	5.04	7.88	12.55	20.18	32.64	52.74	84.58
	75.00	7.81	13.14	22.10	37.19	62.44	103.45	168.54
	90.00	15.57	27.52	48.50	84.28	144.10	241.67	396.51
	105.00	38.52	71.07	128.17	225.95	389.44	656.07	999.99
	120.00	117.61	220.84	401.96	712.13	999.99	999.99	999.99
.5000	60.00	6.56	11.08	18.71	31.40	52.60	87.00	141.60
	75.00	11.42	20.12	35.30	61.16	104.40	174.78	285.63
	90.00	24.51	45.00	80.92	142.44	244.85	412.10	678.15
	105.00	64.09	120.05	218.22	385.71	655.59	999.99	999.99
	120.00	200.35	377.83	689.06	999.99	999.99	999.99	999.99
.6667	60.00	9.00	16.06	28.13	48.80	83.25	139.40	228.54
	75.00	16.92	31.02	55.68	97.92	168.29	283.13	465.84
	90.00	38.49	71.93	130.59	230.77	398.06	671.26	999.99
	105.00	103.41	194.79	355.12	628.50	999.99	999.99	999.99
	120.00	326.25	616.11	999.99	999.99	999.99	999.99	999.99
1.0000	60.00	17.53	32.72	59.58	105.44	182.10	307.29	506.47
	75.00	35.54	66.98	121.85	215.85	373.08	629.68	999.99
	90.00	84.32	159.11	289.51	513.42	887.25	999.99	999.99
	105.00	230.04	434.42	790.65	999.99	999.99	999.99	999.99
	120.00	729.04	999.99	999.99	999.99	999.99	999.99	999.99

• REMARK: THE KP-VALUE IS OVER 1000 WHEN 999.99 APPEARS

APPENDIX B: EARTH PRESSURE TABLES FOR N_{Ac} AND N_{Pc} (Chang, 1981)

Active earth pressure factor N_{Ac} for $\phi = 20°$, $25°$, $30°$ and $35°$

• ϕ = 20.00 •

β/φ	=	0	1/6	1/3	1/2	2/3	5/6	1
δ/φ	α				---N_{Ac} -VALUES ---			
0	60.00	-1.84	-1.92	-2.00	-2.07	-2.15	-2.21	-2.28
	75.00	-1.65	-1.71	-1.77	-1.83	-1.88	-1.93	-1.98
	90.00	-1.59	-1.64	-1.68	-1.73	-1.77	-1.81	-1.85
	105.00	-1.59	-1.63	-1.67	-1.72	-1.81	-1.78	-1.81
	120.00	-1.71	-1.81	-1.89	-1.97	-2.08	-1.81	-1.84
.3333	60.00	-1.85	-1.93	-2.01	-2.09	-2.16	-2.23	-2.30
	75.00	-1.66	-1.73	-1.78	-1.84	-1.89	-1.94	-1.99
	90.00	-1.60	-1.65	-1.69	-1.74	-1.78	-1.82	-1.86
	105.00	-1.60	-1.64	-1.68	-1.73	-1.80	-1.79	-1.83
	120.00	-1.70	-1.78	-1.85	-1.92	-2.01	-1.82	-1.85
.5000	60.00	-1.87	-1.95	-2.03	-2.11	-2.18	-2.25	-2.31
	75.00	-1.68	-1.74	-1.80	-1.85	-1.91	-1.96	-2.01
	90.00	-1.61	-1.66	-1.71	-1.75	-1.80	-1.84	-1.88
	105.00	-1.62	-1.66	-1.70	-1.74	-1.81	-1.81	-1.84
	120.00	-1.71	-1.78	-1.84	-1.91	-1.98	-1.83	-1.87
.6667	60.00	-1.89	-1.97	-2.05	-2.13	-2.20	-2.27	-2.34
	75.00	-1.70	-1.76	-1.82	-1.88	-1.93	-1.98	-2.03
	90.00	-1.63	-1.68	-1.73	-1.77	-1.82	-1.86	-1.90
	105.00	-1.64	-1.68	-1.72	-1.76	-1.82	-1.83	-1.86
	120.00	-1.72	-1.78	-1.84	-1.90	-1.97	-1.86	-1.89
1.0000	60.00	-1.92	-1.99	-2.06	-2.13	-2.20	-2.27	-2.34
	75.00	-1.72	-1.79	-1.85	-1.91	-1.96	-2.02	-2.07
	90.00	-1.68	-1.73	-1.78	-1.83	-1.87	-1.92	-1.96
	105.00	-1.69	-1.74	-1.78	-1.82	-1.86	-1.90	-1.93
	120.00	-1.75	-1.81	-1.85	-1.90	-1.95	-1.92	-1.96

• ϕ = 25.00 •

β/φ	=	0	1/6	1/3	1/2	2/3	5/6	1
δ/φ	α				---N_{Ac} -VALUES ---			
0	60.00	-1.70	-1.80	-1.88	-1.96	-2.03	-2.10	-2.17
	75.00	-1.51	-1.57	-1.63	-1.68	-1.74	-1.78	-1.83
	90.00	-1.42	-1.46	-1.51	-1.55	-1.59	-1.62	-1.66
	105.00	-1.38	-1.42	-1.45	-1.49	-1.52	-1.55	-1.57
	120.00	-1.36	-1.39	-1.42	-1.45	-1.48	-1.50	-1.53
.3333	60.00	-1.73	-1.82	-1.90	-1.98	-2.06	-2.12	-2.19
	75.00	-1.53	-1.59	-1.65	-1.70	-1.76	-1.80	-1.85
	90.00	-1.43	-1.48	-1.52	-1.57	-1.61	-1.64	-1.68
	105.00	-1.39	-1.43	-1.47	-1.50	-1.53	-1.56	-1.59
	120.00	-1.37	-1.40	-1.44	-1.47	-1.49	-1.52	-1.54
.5000	60.00	-1.75	-1.84	-1.93	-2.01	-2.08	-2.15	-2.22
	75.00	-1.55	-1.61	-1.67	-1.73	-1.78	-1.83	-1.87
	90.00	-1.45	-1.50	-1.54	-1.59	-1.63	-1.66	-1.70
	105.00	-1.41	-1.45	-1.49	-1.52	-1.55	-1.58	-1.61
	120.00	-1.39	-1.42	-1.46	-1.49	-1.51	-1.54	-1.57
.6667	60.00	-1.78	-1.87	-1.95	-2.04	-2.12	-2.19	-2.26
	75.00	-1.57	-1.64	-1.70	-1.76	-1.81	-1.86	-1.91
	90.00	-1.48	-1.53	-1.57	-1.62	-1.66	-1.70	-1.73
	105.00	-1.44	-1.48	-1.52	-1.55	-1.58	-1.62	-1.64
	120.00	-1.42	-1.45	-1.48	-1.51	-1.54	-1.57	-1.59
1.0000	60.00	-1.84	-1.92	-1.99	-2.06	-2.13	-2.19	-2.26
	75.00	-1.61	-1.68	-1.74	-1.80	-1.85	-1.91	-1.95
	90.00	-1.54	-1.59	-1.64	-1.69	-1.73	-1.77	-1.81
	105.00	-1.52	-1.56	-1.60	-1.64	-1.67	-1.71	-1.74
	120.00	-1.50	-1.53	-1.57	-1.60	-1.63	-1.66	-1.69

• ϕ = 30.00 •

β/φ	=	0	1/6	1/3	1/2	2/3	5/6	1
δ/φ	α				---N_{Ac}-VALUES ---			
0	60.00	-1.55	-1.67	-1.76	-1.84	-1.91	-1.97	-2.03
	75.00	-1.37	-1.43	-1.49	-1.54	-1.59	-1.63	-1.67
	90.00	-1.26	-1.30	-1.35	-1.38	-1.42	-1.45	-1.47
	105.00	-1.19	-1.23	-1.26	-1.29	-1.31	-1.33	-1.36
	120.00	-1.12	-1.15	-1.18	-1.20	-1.22	-1.24	-1.26
.3333	60.00	-1.60	-1.70	-1.79	-1.87	-1.94	-2.00	-2.06
	75.00	-1.39	-1.46	-1.51	-1.57	-1.62	-1.66	-1.70
	90.00	-1.28	-1.32	-1.37	-1.40	-1.44	-1.47	-1.50
	105.00	-1.21	-1.24	-1.28	-1.31	-1.33	-1.35	-1.38
	120.00	-1.14	-1.17	-1.20	-1.22	-1.24	-1.26	-1.28
.5000	60.00	-1.63	-1.73	-1.82	-1.90	-1.98	-2.04	-2.10
	75.00	-1.42	-1.48	-1.54	-1.60	-1.65	-1.69	-1.73
	90.00	-1.30	-1.35	-1.39	-1.43	-1.47	-1.50	-1.53
	105.00	-1.23	-1.27	-1.30	-1.33	-1.36	-1.38	-1.40
	120.00	-1.16	-1.19	-1.22	-1.24	-1.27	-1.29	-1.30
.6667	60.00	-1.67	-1.77	-1.85	-1.94	-2.02	-2.09	-2.15
	75.00	-1.46	-1.53	-1.59	-1.64	-1.69	-1.74	-1.78
	90.00	-1.34	-1.39	-1.43	-1.47	-1.51	-1.54	-1.57
	105.00	-1.27	-1.30	-1.34	-1.37	-1.40	-1.42	-1.44
	120.00	-1.20	-1.23	-1.25	-1.28	-1.30	-1.32	-1.34
1.0000	60.00	-1.77	-1.84	-1.91	-1.98	-2.04	-2.10	-2.15
	75.00	-1.51	-1.57	-1.63	-1.69	-1.74	-1.79	-1.83
	90.00	-1.42	-1.47	-1.52	-1.56	-1.60	-1.63	-1.66
	105.00	-1.38	-1.42	-1.45	-1.48	-1.51	-1.54	-1.56
	120.00	-1.30	-1.33	-1.36	-1.39	-1.41	-1.43	-1.45

• ϕ = 35.00 •

β/φ	=	0	1/6	1/3	1/2	2/3	5/6	1
δ/φ	α				---N_{Ac} -VALUES ---			
0	60.00	-1.40	-1.54	-1.64	-1.72	-1.78	-1.84	-1.89
	75.00	-1.25	-1.31	-1.36	-1.41	-1.45	-1.48	-1.51
	90.00	-1.12	-1.16	-1.19	-1.23	-1.25	-1.28	-1.30
	105.00	-1.02	-1.05	-1.08	-1.10	-1.12	-1.14	-1.15
	120.00	-.92	-.94	-.96	-.98	-.99	-1.01	-1.02
.3333	60.00	-1.48	-1.59	-1.68	-1.76	-1.82	-1.88	-1.93
	75.00	-1.27	-1.34	-1.39	-1.44	-1.48	-1.51	-1.54
	90.00	-1.14	-1.18	-1.22	-1.25	-1.28	-1.30	-1.32
	105.00	-1.05	-1.08	-1.10	-1.12	-1.14	-1.16	-1.18
	120.00	-.94	-.96	-.98	-1.00	-1.02	-1.03	-1.04
.5000	60.00	-1.53	-1.63	-1.72	-1.80	-1.87	-1.93	-1.98
	75.00	-1.31	-1.37	-1.43	-1.48	-1.52	-1.55	-1.59
	90.00	-1.17	-1.21	-1.25	-1.28	-1.31	-1.34	-1.36
	105.00	-1.07	-1.10	-1.13	-1.15	-1.17	-1.19	-1.21
	120.00	-.96	-.99	-1.01	-1.03	-1.04	-1.06	-1.07
.6667	60.00	-1.59	-1.68	-1.77	-1.85	-1.92	-1.99	-2.04
	75.00	-1.36	-1.42	-1.48	-1.53	-1.58	-1.61	-1.65
	90.00	-1.22	-1.26	-1.30	-1.33	-1.36	-1.39	-1.41
	105.00	-1.12	-1.15	-1.18	-1.20	-1.22	-1.24	-1.25
	120.00	-1.00	-1.03	-1.05	-1.07	-1.08	-1.10	-1.11
1.0000	60.00	-1.72	-1.79	-1.85	-1.91	-1.96	-2.01	-2.05
	75.00	-1.43	-1.49	-1.55	-1.59	-1.64	-1.67	-1.70
	90.00	-1.32	-1.37	-1.41	-1.44	-1.47	-1.50	-1.52
	105.00	-1.25	-1.29	-1.32	-1.34	-1.37	-1.39	-1.41
	120.00	-1.12	-1.15	-1.17	-1.20	-1.21	-1.23	-1.24

Active earth pressure factor N_{Ac} for $\phi = 40°$ and 45°

$\phi = 40.00$

β/φ	=	0	1/6	1/3	1/2	2/3	5/6	1
δ/φ	α				--- N_{Ac}-VALUES ---			
0	60.00	-1.27	-1.42	-1.55	-1.62	-1.67	-1.72	-1.76
	75.00	-1.14	-1.20	-1.24	-1.28	-1.32	-1.34	-1.36
	90.00	-.99	-1.02	-1.05	-1.08	-1.10	-1.11	-1.13
	105.00	-.87	-.89	-.91	-.93	-.94	-.95	-.96
	120.00	-.72	-.74	-.75	-.76	-.77	-.78	-.79
.3333	60.00	-1.38	-1.50	-1.59	-1.66	-1.72	-1.77	-1.81
	75.00	-1.17	-1.23	-1.28	-1.32	-1.35	-1.38	-1.40
	90.00	-1.01	-1.05	-1.08	-1.11	-1.13	-1.15	-1.16
	105.00	-.89	-.91	-.93	-.95	-.97	-.98	-.99
	120.00	-.74	-.76	-.77	-.79	-.80	-.80	-.81
.5000	60.00	-1.45	-1.56	-1.65	-1.72	-1.78	-1.83	-1.87
	75.00	-1.21	-1.27	-1.32	-1.36	-1.40	-1.43	-1.45
	90.00	-1.05	-1.09	-1.12	-1.15	-1.17	-1.19	-1.20
	105.00	-.92	-.95	-.97	-.99	-1.00	-1.01	-1.02
	120.00	-.77	-.79	-.80	-.81	-.82	-.83	-.84
.6667	60.00	-1.54	-1.63	-1.71	-1.79	-1.85	-1.91	-1.95
	75.00	-1.27	-1.34	-1.39	-1.44	-1.47	-1.50	-1.53
	90.00	-1.10	-1.15	-1.18	-1.21	-1.23	-1.25	-1.26
	105.00	-.97	-1.00	-1.02	-1.04	-1.05	-1.06	-1.07
	120.00	-.81	-.83	-.84	-.86	-.87	-.87	-.88
1.0000	60.00	-1.72	-1.78	-1.83	-1.88	-1.92	-1.95	-1.97
	75.00	-1.39	-1.44	-1.49	-1.53	-1.56	-1.59	-1.60
	90.00	-1.24	-1.28	-1.32	-1.35	-1.37	-1.39	-1.40
	105.00	-1.13	-1.16	-1.19	-1.21	-1.23	-1.24	-1.25
	120.00	-.94	-.96	-.98	-1.00	-1.01	-1.02	-1.03

$\phi = 45.00$

β/φ	=	0	1/6	1/3	1/2	2/3	5/6	1
δ/φ	α				--- N_{Ac}-VALUES ---			
0	60.00	-1.12	-1.28	-1.43	-1.51	-1.56	-1.59	-1.62
	75.00	-1.02	-1.09	-1.13	-1.16	-1.19	-1.20	-1.22
	90.00	-.87	-.90	-.92	-.94	-.95	-.96	-.97
	105.00	-.72	-.74	-.76	-.77	-.77	-.78	-.79
	120.00	-.54	-.56	-.57	-.57	-.58	-.58	-.59
.3333	60.00	-1.28	-1.40	-1.50	-1.57	-1.61	-1.65	-1.68
	75.00	-1.07	-1.13	-1.17	-1.20	-1.23	-1.25	-1.26
	90.00	-.90	-.93	-.95	-.97	-.99	-1.00	-1.01
	105.00	-.75	-.77	-.78	-.79	-.80	-.81	-.81
	120.00	-.56	-.58	-.59	-.59	-.60	-.60	-.61
.5000	60.00	-1.38	-1.49	-1.57	-1.64	-1.69	-1.72	-1.75
	75.00	-1.12	-1.18	-1.22	-1.26	-1.28	-1.30	-1.32
	90.00	-.94	-.97	-1.00	-1.02	-1.03	-1.04	-1.05
	105.00	-.78	-.80	-.82	-.83	-.84	-.85	-.85
	120.00	-.59	-.60	-.61	-.62	-.63	-.63	-.63
.6667	60.00	-1.49	-1.58	-1.66	-1.72	-1.78	-1.82	-1.86
	75.00	-1.20	-1.26	-1.30	-1.34	-1.37	-1.39	-1.41
	90.00	-1.00	-1.04	-1.06	-1.08	-1.10	-1.11	-1.12
	105.00	-.83	-.85	-.87	-.88	-.89	-.90	-.91
	120.00	-.63	-.64	-.65	-.66	-.67	-.67	-.68
1.0000	60.00	-1.72	-1.77	-1.81	-1.84	-1.87	-1.88	-1.89
	75.00	-1.36	-1.40	-1.44	-1.47	-1.49	-1.50	-1.51
	90.00	-1.17	-1.21	-1.24	-1.26	-1.28	-1.29	-1.29
	105.00	-1.02	-1.05	-1.07	-1.08	-1.10	-1.10	-1.11
	120.00	-.77	-.79	-.80	-.81	-.82	-.82	-.83

Passive earth pressure factor N_{Pc} for $\phi = 20°$ and 25°

$\phi = 20.00$

β/φ	=	0	1/6	1/3	1/2	2/3	5/6	1
δ/φ	α				--- N_{Pc}-VALUES ---			
0	60.00	2.93	3.13	3.34	3.56	3.78	4.03	4.28
	75.00	3.20	3.42	3.65	3.89	4.13	4.39	4.66
	90.00	3.86	4.12	4.38	4.65	4.94	5.24	5.55
	105.00	5.01	5.32	5.64	5.99	6.34	6.71	7.09
	120.00	6.94	7.36	7.80	8.25	8.73	9.22	9.73
.3333	60.00	3.13	3.36	3.60	3.85	4.11	4.38	4.66
	75.00	3.48	3.72	3.98	4.25	4.53	4.82	5.12
	90.00	4.24	4.53	4.82	5.13	5.45	5.79	6.15
	105.00	5.54	5.89	6.26	6.65	7.05	7.48	7.91
	120.00	7.73	8.21	8.71	9.22	9.77	10.33	10.92
.5000	60.00	3.24	3.49	3.73	4.00	4.27	4.55	4.85
	75.00	3.63	3.88	4.15	4.43	4.73	5.03	5.35
	90.00	4.43	4.73	5.04	5.38	5.71	6.07	6.45
	105.00	6.81	6.19	6.58	6.98	7.41	7.86	8.32
	120.00	8.13	8.64	9.17	9.72	10.30	10.89	11.52
.6667	60.00	3.35	3.60	3.86	4.14	4.42	4.72	5.03
	75.00	3.77	4.03	4.32	4.61	4.92	5.24	5.57
	90.00	4.62	4.94	5.27	5.61	5.97	6.35	6.74
	105.00	6.08	6.47	6.89	7.32	7.76	8.24	8.72
	120.00	8.53	9.07	9.62	10.20	10.81	11.44	12.10
1.0000	60.00	3.52	3.78	4.07	4.36	4.66	4.98	5.32
	75.00	4.00	4.30	4.60	4.92	5.25	5.60	5.96
	90.00	4.97	5.31	5.66	6.03	6.42	6.83	7.25
	105.00	6.57	6.99	7.44	7.91	8.39	8.90	9.43
	120.00	9.27	9.84	10.45	11.08	11.73	12.42	13.13

$\phi = 25.00$

β/φ	=	0	1/6	1/3	1/2	2/3	5/6	1
δ/φ	α				--- N_{Pc}-VALUES ---			
0	60.00	3.03	3.30	3.59	3.91	4.25	4.62	5.00
	75.00	3.40	3.71	4.06	4.42	4.80	5.22	5.66
	90.00	4.24	4.63	5.04	5.48	5.95	6.45	6.98
	105.00	5.71	6.21	6.76	7.33	7.94	8.60	9.30
	120.00	8.25	8.97	9.73	10.53	11.40	12.34	13.32
.3333	60.00	3.34	3.68	4.03	4.41	4.82	5.25	5.71
	75.00	3.85	4.23	4.63	5.06	5.52	6.01	6.54
	90.00	4.68	5.34	5.83	6.36	6.92	7.52	8.16
	105.00	6.64	7.24	7.90	8.60	9.33	10.12	10.97
	120.00	9.70	10.56	11.48	12.46	13.52	14.65	15.86
.5000	60.00	3.52	3.88	4.27	4.67	5.11	5.58	6.08
	75.00	4.10	4.50	4.93	5.40	5.90	6.43	7.00
	90.00	5.22	5.72	6.25	6.82	7.43	8.09	8.80
	105.00	7.15	7.79	8.50	9.26	10.06	10.92	11.84
	120.00	10.46	11.40	12.41	13.48	14.62	15.85	17.16
.6667	60.00	3.71	4.09	4.50	4.95	5.41	5.91	6.45
	75.00	4.34	4.77	5.24	5.74	6.28	6.85	7.46
	90.00	5.56	6.10	6.68	7.28	7.94	8.65	9.41
	105.00	7.65	8.35	9.11	9.92	10.79	11.73	12.74
	120.00	11.27	12.25	13.33	14.49	15.73	17.05	18.51
1.0000	60.00	4.02	4.44	4.90	5.39	5.91	6.47	7.07
	75.00	4.79	5.28	5.80	6.36	6.96	7.60	8.28
	90.00	6.21	6.81	7.46	8.15	8.89	9.68	10.52
	105.00	8.59	9.39	10.24	11.17	12.14	13.18	14.30
	120.00	12.70	13.85	15.06	16.36	17.75	19.23	20.83

Passive earth pressure factor N_{Pc} for $\phi = 30°$, 35°, 40° and 45°

$\phi = 30.00$

β/φ	=	0	1/6	1/3	1/2	2/3	5/6	1
δ/φ	α				--- N_{Pc}-VALUES ---			
0	60.00	3.12	3.47	3.86	4.31	4.81	5.36	5.96
	75.00	3.59	4.04	4.53	5.07	5.66	6.31	7.03
	90.00	4.66	5.23	5.86	6.56	7.33	8.17	9.10
	105.00	6.55	7.35	8.22	9.18	10.24	11.40	12.69
	120.00	9.93	11.11	12.41	13.84	15.43	17.19	19.14
.3333	60.00	3.57	4.04	4.56	5.13	5.77	6.47	7.24
	75.00	4.28	4.85	5.48	6.17	6.92	7.76	8.66
	90.00	5.69	6.41	7.22	8.11	9.09	10.19	11.39
	105.00	8.11	9.13	10.26	11.51	12.89	14.42	16.11
	120.00	12.47	14.01	15.71	17.59	19.67	21.97	24.52
.5000	60.00	3.85	4.38	4.96	5.59	6.30	7.07	7.93
	75.00	4.67	5.30	6.00	6.77	7.62	8.56	9.60
	90.00	6.26	7.08	7.98	8.99	10.08	11.30	12.65
	105.00	8.99	10.13	11.39	12.79	14.34	16.05	17.94
	120.00	13.87	15.60	17.50	19.61	21.95	24.53	27.38
.6667	60.00	4.15	4.73	5.37	6.07	6.85	7.71	8.67
	75.00	5.10	5.80	6.56	7.40	8.34	9.38	10.53
	90.00	6.85	7.76	8.77	9.87	11.10	12.46	13.96
	105.00	9.92	11.19	12.59	14.15	15.86	17.76	19.86
	120.00	15.37	17.29	19.41	21.75	24.34	27.21	30.38
1.0000	60.00	4.70	5.37	6.11	6.94	7.85	8.85	9.96
	75.00	5.90	6.71	7.62	8.61	9.72	10.94	12.29
	90.00	8.05	9.12	10.30	11.60	13.05	14.64	16.41
	105.00	11.73	13.23	14.88	16.70	18.72	20.96	23.43
	120.00	18.23	20.48	23.02	25.77	28.82	32.19	35.92

$\phi = 35.00$

β/φ	=	0	1/6	1/3	1/2	2/3	5/6	1
δ/φ	α				--- N_{Pc}-VALUES ---			
0	60.00	3.22	3.67	4.20	4.82	5.55	6.38	7.33
	75.00	3.80	4.42	5.13	5.93	6.84	7.90	9.10
	90.00	5.15	5.99	6.95	8.05	9.32	10.76	12.43
	105.00	7.61	8.80	10.25	11.88	13.76	15.90	18.37
	120.00	12.12	14.09	16.36	18.98	21.95	25.33	29.43
.3333	60.00	3.85	4.52	5.28	6.16	7.15	8.30	9.64
	75.00	4.83	5.68	6.65	7.76	9.05	10.52	12.22
	90.00	6.76	7.91	9.26	10.80	12.59	14.63	16.98
	105.00	10.16	11.89	13.90	16.19	18.85	21.93	25.45
	120.00	16.54	19.32	22.52	26.21	30.48	35.43	41.14
.5000	60.00	4.28	5.05	5.92	6.93	8.09	9.43	10.96
	75.00	5.46	6.43	7.56	8.85	10.34	12.07	14.06
	90.00	7.70	9.06	10.61	12.40	14.48	16.87	19.69
	105.00	11.73	13.73	16.05	18.73	21.83	25.38	29.49
	120.00	19.14	22.40	26.17	30.48	35.43	41.15	47.77
.6667	60.00	4.77	5.62	6.62	7.77	9.10	10.63	12.41
	75.00	6.15	7.27	8.55	10.04	11.75	13.71	16.06
	90.00	8.78	10.30	12.09	14.15	16.54	19.29	22.44
	105.00	13.36	15.68	18.37	21.48	25.03	29.12	33.83
	120.00	21.96	25.69	30.00	34.95	40.75	47.32	54.89
1.0000	60.00	5.69	6.75	7.99	9.42	11.07	12.97	15.16
	75.00	7.55	8.94	10.54	12.39	14.53	16.98	19.82
	90.00	10.69	12.63	15.06	17.65	20.61	24.03	27.99
	105.00	16.77	19.69	23.02	26.88	31.29	36.41	42.31
	120.00	27.66	32.31	37.71	43.92	51.02	59.25	68.76

$\phi = 40.00$

β/φ	=	0	1/6	1/3	1/2	2/3	5/6	1
δ/φ	α				--- N_{Pc}-VALUES ---			
0	60.00	3.37	3.94	4.65	5.53	6.61	7.90	9.46
	75.00	4.08	4.92	5.93	7.15	8.60	10.36	12.47
	90.00	5.77	6.99	8.47	10.25	12.42	15.03	18.20
	105.00	8.97	10.91	13.26	16.08	19.50	23.69	28.80
	120.00	15.20	18.51	22.55	27.46	33.36	40.52	49.31
.3333	60.00	4.25	5.18	6.31	7.66	9.29	11.27	13.68
	75.00	5.59	6.85	8.39	10.26	12.53	15.27	18.57
	90.00	8.23	10.13	12.42	15.17	18.56	22.67	27.64
	105.00	13.19	16.22	19.90	24.33	29.72	36.34	44.36
	120.00	22.92	28.11	34.48	42.21	51.49	62.93	76.87
.5000	60.00	4.88	6.00	7.36	9.00	11.01	13.43	16.34
	75.00	6.57	8.12	9.99	12.24	14.99	18.36	22.45
	90.00	9.82	12.11	14.92	18.33	22.44	27.42	33.58
	105.00	15.94	19.61	24.06	29.57	36.16	44.16	53.98
	120.00	27.88	34.21	41.92	51.37	62.85	76.70	93.66
.6667	60.00	5.63	6.96	8.58	10.53	12.91	15.81	19.34
	75.00	7.70	9.53	11.78	14.51	17.81	21.80	26.75
	90.00	11.66	14.41	17.74	21.87	26.79	32.78	40.09
	105.00	18.99	23.44	28.80	35.32	43.34	52.95	64.67
	120.00	33.33	41.06	50.33	61.60	75.49	92.14	112.39
1.0000	60.00	7.15	8.93	11.09	13.71	16.90	20.77	25.48
	75.00	10.14	12.61	15.61	19.25	23.69	29.08	35.63
	90.00	15.61	19.29	23.78	29.25	35.90	43.99	53.80
	105.00	25.65	31.57	38.80	47.57	58.25	71.25	87.00
	120.00	45.18	55.43	67.93	83.11	101.60	124.09	151.36

$\phi = 45.00$

β/φ	=	0	1/6	1/3	1/2	2/3	5/6	1
δ/φ	α				--- N_{Pc}-VALUES ---			
0	60.00	3.52	4.25	5.19	6.46	8.09	10.17	12.84
	75.00	4.39	5.52	6.99	8.85	11.24	14.35	18.36
	90.00	6.52	8.32	10.63	13.64	17.51	22.48	29.02
	105.00	10.78	13.89	17.89	23.04	29.81	38.49	49.79
	120.00	19.66	25.40	32.95	42.63	55.24	71.72	92.86
.3333	60.00	4.72	6.05	7.74	9.93	12.78	16.41	21.13
	75.00	6.57	8.53	11.09	14.33	18.56	24.10	31.18
	90.00	10.41	13.53	17.60	22.95	29.79	38.81	50.36
	105.00	17.88	23.43	30.50	39.82	51.80	67.47	87.75
	120.00	33.58	43.96	57.33	74.80	97.43	126.85	165.13
.5000	60.00	5.68	7.36	9.55	12.35	15.98	20.74	26.82
	75.00	8.17	10.65	13.91	18.18	23.62	30.76	40.01
	90.00	13.07	17.21	22.45	29.34	38.29	49.87	65.01
	105.00	22.87	29.99	39.26	51.24	66.93	87.12	113.64
	120.00	43.32	56.66	74.18	96.67	126.27	164.22	214.21
.6667	60.00	6.84	8.95	11.74	15.26	19.84	25.89	33.58
	75.00	10.04	13.25	17.34	22.70	29.66	38.68	50.47
	90.00	16.38	21.54	28.28	36.98	48.38	63.04	82.30
	105.00	28.89	37.88	49.70	64.86	84.92	110.40	144.10
	120.00	54.93	71.82	94.10	122.62	160.23	208.37	271.85
1.0000	60.00	9.50	12.57	16.60	21.79	28.59	37.37	48.84
	75.00	14.49	19.16	25.24	33.13	43.39	56.70	74.03
	90.00	24.06	31.67	41.59	54.45	71.18	92.89	121.14
	105.00	42.71	56.08	73.35	95.83	125.08	163.01	212.39
	120.00	81.37	106.55	138.07	181.38	236.45	307.88	400.84

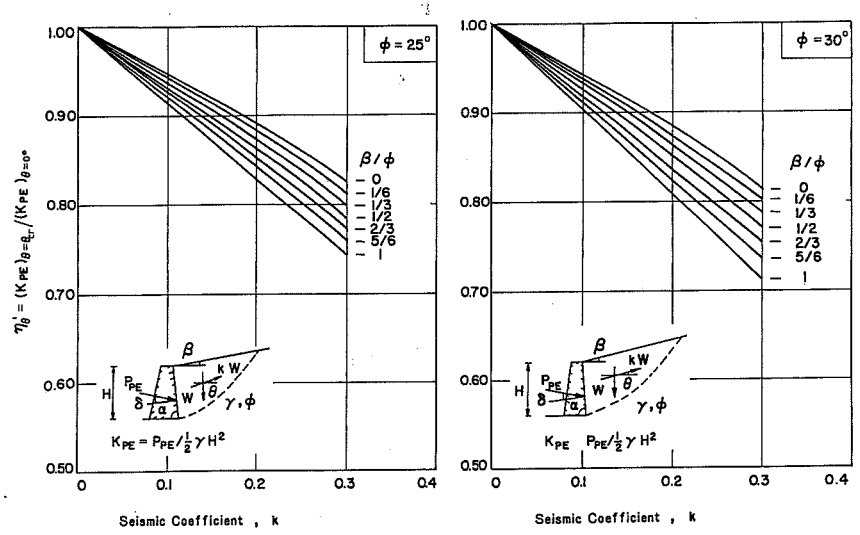

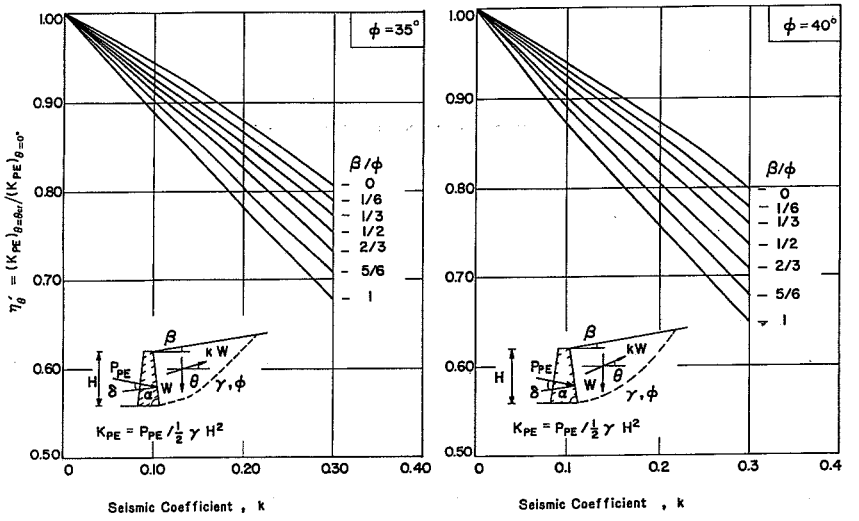

Figs. B5.1 to B5.4. Correction factor η'_θ for estimating $(K_{PE})_{\theta = \theta_{cr}}$ from $(K_{PE})_{\theta = 0°}$, ϕ = 25°, 30°, 35° and 40°.

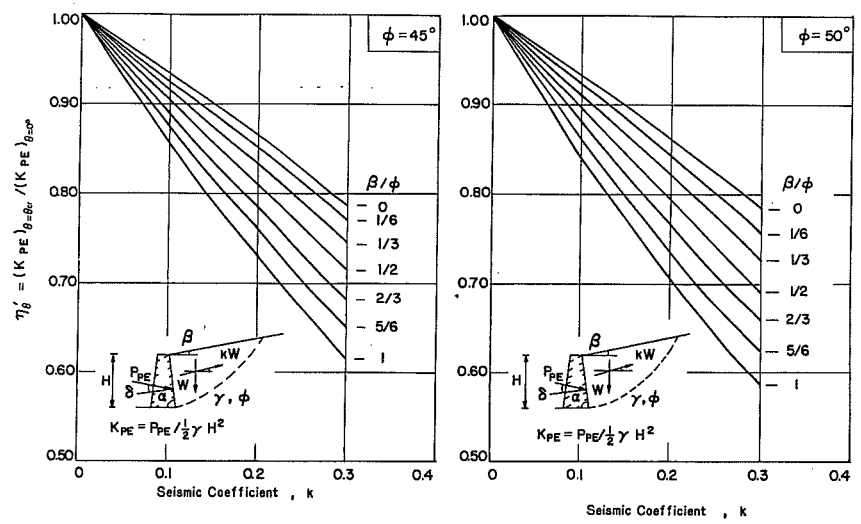

Figs. B5.5 and B5.6. Correction factor η'_θ for estimating $(K_{PE})_{\theta = \theta_{cr}}$ from $(K_{PE})_{\theta = 0°}$, ϕ = 45° and 50°.

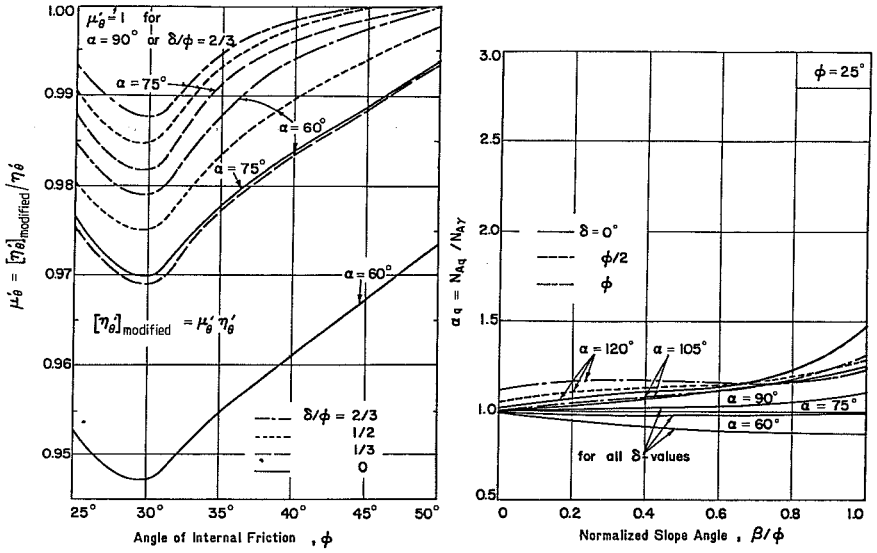

Fig. B5.7. Modification factor for η'_θ when $\alpha < 90°$ and $\delta \leq \frac{2}{3}\phi$.

Fig. B5.8. Correlation factor α_q (ϕ = 25°).

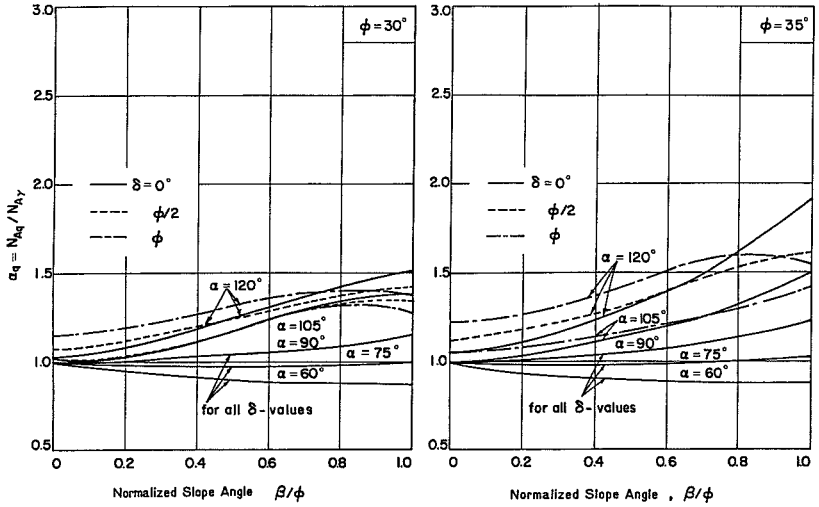

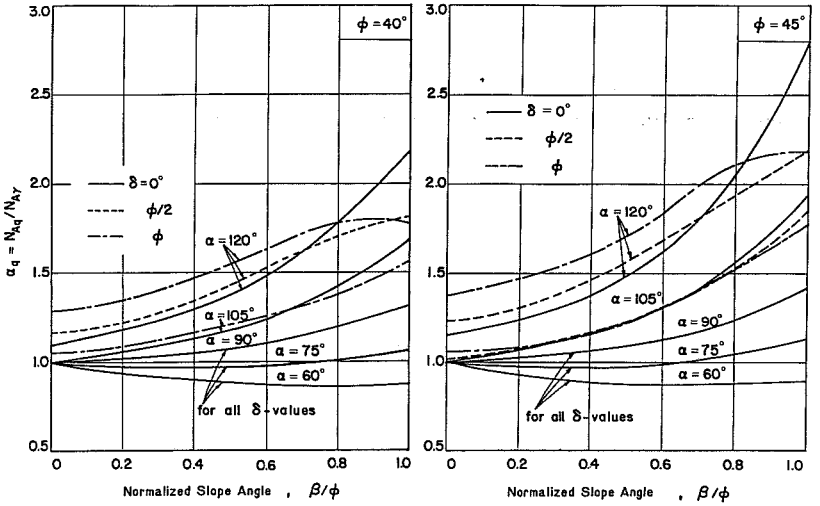

Figs. B5.9 to B5.12. Correlation factor α_q: ϕ = 30°, 35°, 40° and 45°.

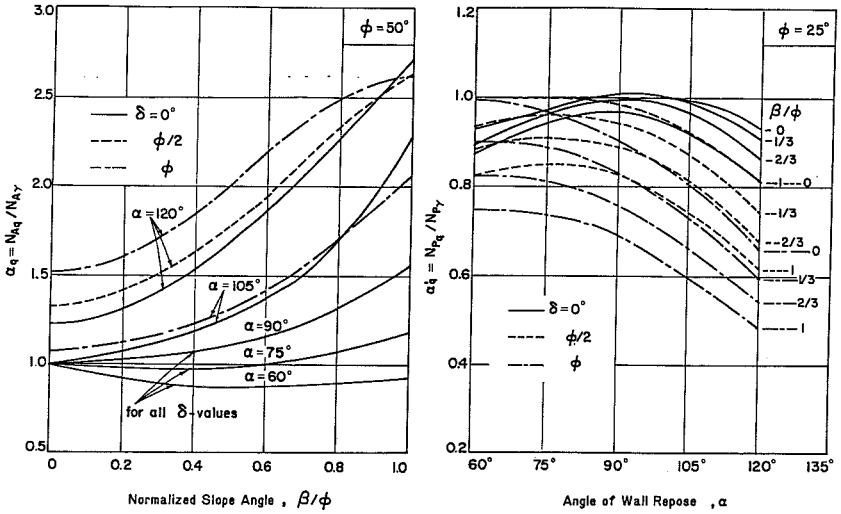

Fig. B5.13. Correlation factor α_q (ϕ = 50°).

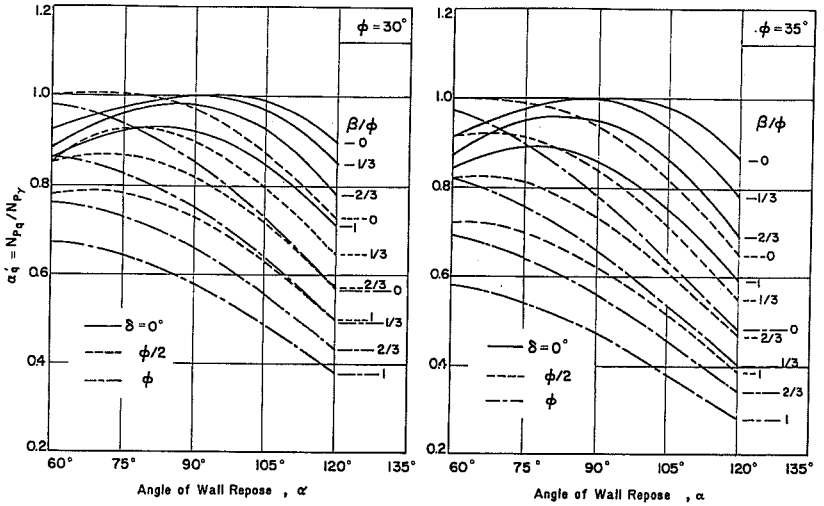

Figs. B5.14 to B5.16. Correlation factor α'_q : ϕ = 25°, 30° and 35°.

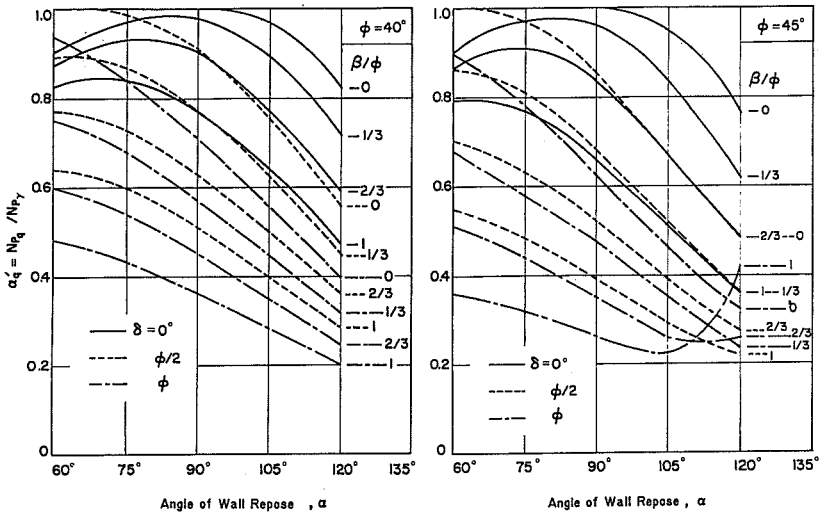

Figs. B5.17 to B5.19. Correlation factor α'_q : ϕ = 40°, 45° and 50°.

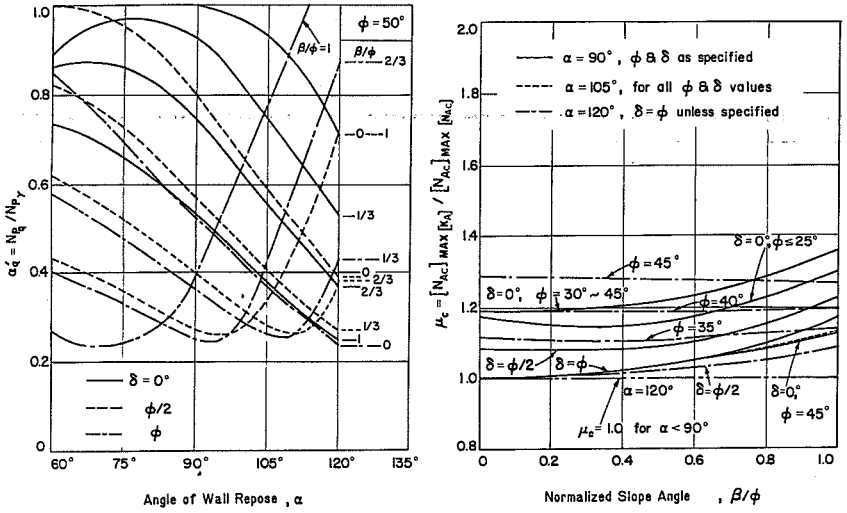

Fig. B5.20. Recommended modification factor μ_c for $\alpha \geq 90°$.

Chapter 6

SOME PRACTICAL CONSIDERATIONS IN DESIGN OF RIGID RETAINING STRUCTURES

By M. F. Chang and W. F. Chen

6.1 Introduction

In the design of retaining structures, either ultimate-load-based or displacement-based, both the magnitude and the distribution of lateral earth pressure acting on the structure is of great importance. There are numerous methods available for assessing the resultant lateral earth pressures. Some of them have been extended to include the earthquake effects. However, most of the methods are developed based on translational wall movements and may not be suitable for assessing the lateral pressures corresponding to other modes of wall movement. At present, there is still a lack of well-developed theoretical methods for determining the distribution of lateral earth pressure, or the point of action of resultant lateral pressure. A method for assessing the distribution of lateral pressures, taking into consideration the mode of wall movement, is therefore urgently needed. Furthermore, the effect of wall movement on the magnitude of lateral earth pressures also deserves attention.

In an attempt to assess the point of action of resultant lateral earth pressures and to investigate the effect of wall movement on lateral earth pressures, a so-called modified Dubrova method proposed by Chang (1981) is developed here based on the philosophy of Dubrova (1963) as described in the book by Harr (1966). In order that the method can be applied to general soil-wall systems subjected to earthquake forces, the well-known Mononobe-Okabe formula (Okabe, 1926; Mononobe and Matsuo, 1929) is used as the framework in the modified formulation. Dependence of strength mobilization on wall movement is carefully studied. Proper distributions for strength parameters ϕ and δ, which completely control the results of the modified Dubrova analysis, are suggested for three basic modes of wall movement based on the consideration of change in state of stress in the backfill during wall yielding.

This chapter presents the *modified Dubrova method* and its numerical results. The effect of assumed distributions of mobilized ϕ and δ is discussed. Changes in pressure distribution behind rigid walls, as the result of gradual wall yielding are included. Points of action for both static and earthquake cases as suggested and

adopted by previous investigators are reviewed. They are compared with those obtained by the modified Dubrova method. Effects of earthquake magnitude, strength parameters, and geometry of soil-wall systems on the point of action based on the modified Dubrova method are included. The validity of the developed method is carefully evaluated.

It is well-recognized that not only the point of action but also the magnitude of resultant lateral earth pressure is highly dependent on the mode of wall movement. Some numerical results based on the modified Dubrova method are presented and compared with other theoretical or numerical solutions available for three different types of wall movement. Discrepancies are noted.

Finally, problems are considered for some earth pressure theories for practical applications. Several analytical methods for assessing seismic lateral earth pressures and points of action of resultant forces are compared both qualitatively and numerically. Suggestions for selecting the analytical method for design of rigid retaining structures in seismic environments are also given.

6.2 Theoretical considerations of the modified Dubrova method

In retaining structure design, not only the magnitude but also the point of action of the resultant lateral earth pressure has to be known.

Most earth pressure theories are based on the *limiting state concept.* The backfill material which controls the lateral pressures acting on a retaining wall is generally assumed to behave as a rigid-plastic material. However, lateral pressure distribution is displacement related. In spite of this, most earth pressure theories give no information about the point of action of the resultant pressure.

The distribution of lateral earth pressure highly depends on the mode of wall movement. Its assessment generally requires a complicated step-by-step load deformation analysis (Potts and Fourie, 1986). Common practice still tends to assume that the distribution of the lateral earth pressure acting on a rigid wall is generally quasi-hydrostatic and consider the resultant force to act at the lower one-third point of the wall section, irrespective of the type of wall movement. It has been proved that this is not always true as described by Tschaebotarioff (1962). In many cases, the distribution is more parabolic-like.

The distribution of lateral earth pressure is further complicated by the presence of earthquake. As in Coulomb's analysis, a quasi-hydrostatic distribution is assumed in the widely accepted Mononoke-Okabe method for the seismic lateral earth pressure determination. However, several researchers such as Matsuo (1941), Matsuo and Ohara (1960), and Ishii et al. (1960) showed experimentally that the distribution of seismic lateral earth pressure is not hydrostatic. Theoretical works of Prakash and Basavanna (1969) and Basavanna (1970) also showed that the point of application is higher than the lower one-third point for the active pressure case. These works, although provide ways of determining the point of action, do not take

into consideration the mode of wall movement and its effect on the degree of mobilization of soil strength.

Based on the assumption that the static-active failure Coulomb wedge holds for the dynamic condition, Nandakumaran and Joshi (1973) suggested a way of assessing the point of action of dynamic increment of active earth pressure. Unfortunately, the method is based on an unrealistic assumption. In general, the failure surface or the most critical sliding surface is flatter for the earthquake case than that for the static case as found by Murphy (1960) and as already shown in Chapter 5.

It is clear that, at present, there exists no theoretically sound and yet simple procedure for assessing the point of action of resultant active pressure. Here, the upper-bound limit analysis method, as in most earth pressure theories, gives no information on the lateral earth pressure distribution. The current practice of assuming the dynamic increment of earth pressure to act at the upper third point or the middle point of a rigid wall is not wholly justified.

As far as the point of application of resultant passive pressure is concerned, Sabzevari and Ghahramani (1974) have developed a rigorous method of solving the problem using the method of associated fields of stress and displacement. They found that the point of action of dynamic forces differs from that for the corresponding static ones. They also claimed that the location of these points depends on the form of the wall displacement. The method has not been used extensively due to its dependence on large computers.

The distribution of dynamic passive pressure has also been briefly treated by Ghahramani and Clemence (1980). It seems that the problem about the assessment of point of action still deserves more attention.

The Dubrova method of redistribution of pressure (Dubrova, 1963) as described by Harr (1966) provides a way of assessing the earth pressure distribution for a specified wall movement. The method, which was originally developed for the case of vertical wall retaining cohesionless horizontal backfill, considers the degree of mobilization of strength as the result of the specified wall movement. It is an extension of the Coulomb's wedge theory with the effect of wall movement included. Detailed description of the method can also be found in Harr (1977).

An attempt has been made by Saran and Prakash (1977) to extend the Dubrova method for assessing the distribution of seismic lateral earth pressures. However, no actual formulation of the pressure distribution was given. The work described here tends to generalize the Dubrova method using a similar idea as mentioned by them and assuming that the Mononobe-Okabe concept is valid for assessing seismic lateral earth pressures.

The same idea is equally applicable if one makes use of the more rigorous formula as developed by the upper-bound limit analysis in which log-sandwich mechanism of failure rather than planar mechanism is assumed. However, since the most critical surface, which involves two variables, is also a function of the degree of mobilization of strength, the formulation becomes much more complicated. For

practical purposes, especially for the active case in which the most critical surface is almost planar, the Mononobe-Okabe formula is adequate. The Mononobe-Okabe formula is therefore adopted here as the basis for the formulation of the modified Dubrova equation.

The theoretical consideration of the modified Dubrova method can be introduced as follows.

6.2.1 Dependence of strength mobilization on wall movement

In the derivation of Coulomb's formula and the Mononobe-Okabe formula, no wall movement was specified, regardless of the fact that the distribution of earth pressure is highly dependent on the mode of this movement. To take into account the effect of wall movement on the lateral earth pressures, Dubrova (1963) assumed that the backfill material mobilizes its strength to an extent in proportion to the corresponding wall movement. He hypothesized that the mobilized strength of the backfill, represented by ψ, where $|\psi| \leq \phi$, should vary along the height of the wall. However, he assumed that the angle of wall friction δ is constant and related to ϕ.

The fact that ψ should vary with depth according to the mode of wall movement can be clearly seen from the works of James and Bransby (1970, 1971) for the static case. The velocity fields they predicted and observed clearly show the dependence of shear strain in the backfill on the wall movement. The theoretical work of Sabzevari and Ghahramani (1974) also showed that for the dynamic passive pressure case in which the wall rotates about the toe, the shear strain in the backfill is the largest at the top and decreases as depth increases.

It is well accepted that the angle of soil–wall interface friction δ, although generally assumed constant with depth, is also dependent on the wall movement. The extensive experimental work of James and Bransby (1970) remarkably showed that the angle of wall friction is maximum and close to the ϕ-angle at the top and decreases to a very small value near the toe for the passive case and rotation about the toe. For this reason, it seems reasonable to assume that both ψ and δ vary with depth in a same manner.

6.2.2 Formulation of the modified Dubrova method

Based on Fig. 6.1, the Mononobe-Okabe formula for the resultant active earth pressure, P_{AE}, can be obtained by the equilibrium consideration (Okabe, 1926; and Mononobe and Matsuo, 1929), such as:

$$P_{AE} = \frac{\gamma H^2}{2} \frac{(1 + k_v)\cos^2(\phi - i - \theta_k)}{\cos\theta_k \cos^2 i \cos(\delta + i + \theta_k)\left[1 + \left\{\frac{\sin(\phi + \delta)\sin(\phi - \beta - \theta_k)}{\cos(\beta - i)\cos(\delta + i + \theta_k)}\right\}^{\frac{1}{2}}\right]^2} \quad (6.1)$$

where

γ = unit weight of soil backfill
ϕ = angle of internal friction of backfill
δ = angle of wall friction
k_v = vertical seismic coefficient
θ_k = $\tan^{-1}[k_h/(1 + k_v)]$, k_h is the horizontal seismic coefficient as shown in Fig. 6.1
i, β, H = geometrical factors as defined in Fig. 6.1.

Equation (6.1) is derived by the conventional limit equilibrium approach.

By replacing H with z, ϕ with $\psi(z)$ and δ with $\delta_w(z)$, the accumulative resultant active pressure at depth z is:

$$P_{AE} = \frac{\gamma z^2}{2} \frac{(1 + k_v)\cos^2(\psi - i - \theta_k)}{\cos\theta_k \cos^2 i \cos(\delta_w + i + \theta_k)(1 + \xi_A)^2} \quad (6.2)$$

where

$$\xi_A = \left[\frac{\sin(\psi + \delta_w)\sin(\psi - \beta - \theta_k)}{\cos(\beta - i)\cos(\delta_w + i + \theta_k)}\right]^{\frac{1}{2}}$$

ψ = mobilized angle of internal friction which varies along the height of the wall depending on the wall movement with its maximum value equal to ϕ.
δ_w = mobilized angle of wall friction which also varies along the height of the wall and can be taken as $m\psi$, with $m = d\delta_w/d\psi \leq 1$.
z = depth below the top of the wall.

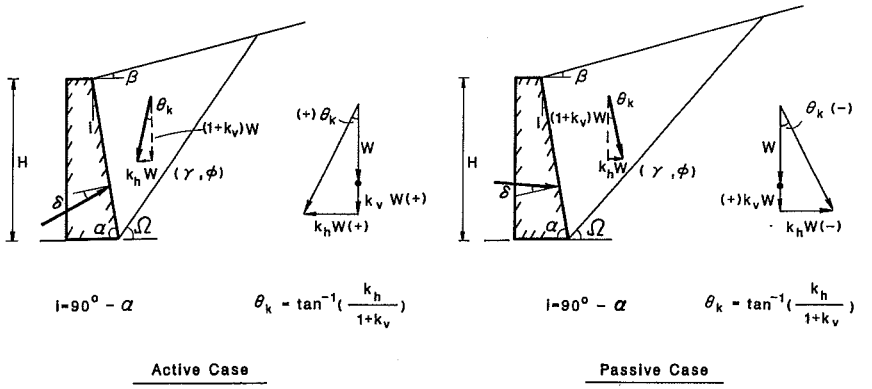

Fig. 6.1. Failure mechanisms assumed in modified Coulomb's analysis of seismic lateral earth pressures.

The unit active pressure at depth z can be obtained by taking derivative with respect to z using the following equation:

$$p_{AE}(z) = \frac{dP_{AE}}{dz} = \frac{\partial P_{AE}}{\partial z} + \frac{\partial P_{AE}}{\partial \psi}\frac{d\psi}{dz} \tag{6.3}$$

The result can be expressed as:

$$p_{AE}(z) = \frac{\gamma z(1 + k_v)\cos(\psi - i - \theta_k)}{\cos\theta_k \cos^2 i \cos(\delta_w + i + \theta_k)(1 + \xi_A)^2}\left\{\cos(\psi - i - \theta_k) - z\left(\frac{d\psi}{dz}\right)\left(\sin(\psi - i - \theta_k) + \frac{\cos(\psi - i - \theta_k)}{2(1 + \xi_A)}[(1 + m)\xi_A \cos(\psi + \delta_w) + \xi_A \cos(\psi - \beta - \theta_k) - m\tan(\delta_w + i + \theta_k)]\right)\right\} \tag{6.4}$$

where

$$\xi_A = \left[\frac{\sin(\psi + \delta_w)\sin(\psi - \beta - \theta_k)}{\cos(\beta - i)\cos(\delta_w + i + \theta_k)}\right]^{\frac{1}{2}}$$

$$m = d\delta_w/d\psi = \delta/\psi$$

$\theta_k = \tan^{-1}[k_h/(1 + k_v)]$; with $k_v > 0$ if acting downward and $k_h > 0$ if pointing toward the wall.

Similarly, in the passive case, if we define $k_v > 0$ when acting downward and $k_h > 0$ if pointing toward a wall, as those assumed in the active case, the resultant passive earth pressure on the wall with height of H can be expressed as:

$$P_{PE} = \frac{\gamma H^2}{2}\frac{(1 + k_v)\cos^2(\phi + i + \theta_k)}{\cos\theta_k \cos^2 i \cos(\delta - i - \theta_k)\left\{1 - \left[\frac{\sin(\phi + \delta)\sin(\phi + \beta + \theta_k)}{\cos(\beta - i)\cos(\delta - i - \theta_k)}\right]^{\frac{1}{2}}\right\}^2} \tag{6.5}$$

By replacing H with z, ϕ with $-\psi(z)$, and δ with $-\delta_w(z)$, we have:

$$P_{PE} = \frac{\gamma z^2}{2}\frac{(1 + k_v)\cos^2(\psi - i - \theta_k)}{\cos\theta_k \cos^2 i \cos(\delta_w + i + \theta_k)(1 - \xi_P)^2} \tag{6.6}$$

where

$$\xi_P = \left[\frac{\sin\{-(\psi + \delta_w)\}\sin\{-(\psi - \beta - \theta_k)\}}{\cos(\beta - i)\cos(\delta_w + i + \theta_k)}\right]^{\frac{1}{2}}$$

After differentiation, the unit passive pressure at depth z can be obtained as:

$$p_{PE}(z) = \frac{\gamma z(1 + k_v)\cos(\psi - i - \theta_k)}{\cos\theta_k \cos^2 i \cos(\delta_w + i + \theta_k)(1 - \xi_P)^2}\left\{\cos(\psi - i - \theta_k) - z\left(\frac{d\psi}{dz}\right)\left(\sin(\psi - i - \theta_k) + \frac{\cos(\psi - i - \theta_k)}{2(1 - \xi_P)}\left[-(1 + m)\xi_P \cos(\psi + \delta_w) - \xi_P \cos(\psi - \beta - \theta_k) - m\tan(\delta_w + i + \theta_k)\right]\right)\right\} \tag{6.7}$$

where

$$\xi_P = \left[\frac{\sin\{-(\psi + \delta_w)\}\sin\{-(\psi - \beta - \theta_k)\}}{\cos(\beta - i)\cos(\delta_w + i + \theta_k)}\right]^{\frac{1}{2}}$$

It is noted that in the active case $\psi \geq 0$, $\delta_w \geq 0$ and in the passive case $\psi \leq 0$ and $\delta_w \leq 0$. Consequently:

$$\xi_A = \xi_P = \left[\frac{\sin|\psi + \delta_w|\sin|\psi - \beta - \theta_k|}{\cos(\beta - i)\cos(\delta_w + i + \theta_k)}\right]^{\frac{1}{2}} \geq 0 \tag{6.8}$$

With this consideration, Eqs. (6.4) and (6.7) can be combined into one equation of $\xi_A = \xi_k$ and $\xi_P = -\xi_k$ are substituted into the two equations. The resulting equation is:

$$p(z) = \frac{\gamma z(1 + k_v)\cos(\psi - i - \theta_k)}{\cos\theta_k \cos^2 i \cos(\delta_w + i + \theta_k)(1 + \xi_k)^2}\left\{\cos(\psi - i - \theta_k) - z\left(\frac{d\psi}{dz}\right)\left[\sin(\psi - i - \theta_k) + \frac{\cos(\psi - i - \theta_k)}{2(1 + \xi_k)}\left((1 + m)\xi_k \cos(\psi + \delta_w) + \xi_k \cos(\psi - \beta - \theta_k) - m\tan(\delta_w + i + \theta_k)\right)\right]\right\} \tag{6.9}$$

where

$$\xi_k = \pm\left[\frac{\sin|\psi + \delta_w|\sin|\psi - \beta - \theta_k|}{\cos(\beta - i)\cos(\delta_w + i + \theta_k)}\right]^{\frac{1}{2}}$$

the upper sign is for the active case and the lower sign is for the passive case;
$m = d\delta_w/d\psi = \delta/\psi$
$\theta_k = \tan^{-1}[k_h/(1 + k_v)]$; $k_v > 0$ if acting downward, $k_h > 0$ if pointing toward the wall; for active case, $\theta_k \geq 0$ is critical and for passive case, $\theta_k \leq 0$ is critical.

6.2.3 Distribution of mobilized strength parameters

As pointed out in Section 6.2.1, the degree of mobilization of the strength parameters ϕ and δ is highly dependent on wall movements. Both experimental investigations (James and Bransby, 1970) and theoretical works (James and Bransby, 1971; Sabzevari and Ghahramani, 1974) suggest that the mobilized ϕ- and δ-values, denoted as ψ and δ_w respectively, vary with depth in a manner depending on the mode of wall movement (Potts and Fourie, 1986).

James and Bransby (1970), based on their observed failure patterns as shown in Fig. 6.2 and stress measurements along the interface, found that for the case of rotation about the toe into the backfill, both ψ and δ_w decrease as depth increases. They also found that for the passive case, rotation about the top, the degree of strength mobilization is the highest near the toe. Based on the rupture patterns postulated for the active case (Fig. 6.2), the variations of ψ and δ_w with depth for the active case may be similar to the passive case. It is therefore expected that both ψ and δ_w increase as depth increases in both active and passive cases for rotation about the top of the wall.

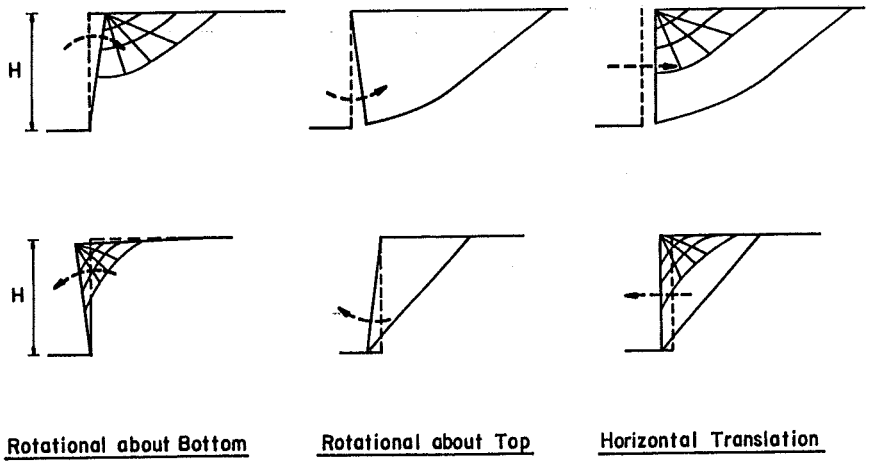

Fig. 6.2. Typical passive rupture patterns reported by James and Bransby (1970) and postulated active rupture patterns.

Although the Dubrova method (Dubrova, 1963) does provide a way of including the important wall movement effect into earth pressure analyses, their results depend highly on the assumed distribution for ψ and δ_w. Selection of proper distributions of ψ and δ_w is of prime importance. The fact that the ψ- and δ_w- values at a given depth are closely related to the wall displacement and the corresponding stress condition in the backfill at that depth should be carefully considered.

Dubrova's and Saran and Prakash's distributions of $\psi(z)$ and $\delta_w(z)$

Recognizing the fact that the mobilized strength in the backfill should vary with depth, Dubrova (1963) assumed a linear distribution for $\psi(z)$, with the ψ-value at the point of rotation, taken as $\psi_a = 0$, and the ψ-value at the moving end, $\psi_b = \phi$ for the case of active rotation of vertical wall away from horizontal backfill. He further assumed the $\delta_w(z)$ is related to ϕ and equals to the maximum δ_w-value, or the angle of wall friction δ. For the passive pressure case, the same $\psi(z)$-distribution was adopted by Dubrova (1963) except that the ψ-value is taken as negative in this case.

The linear distribution of $\psi(z)$ as adopted by Dubrova (1963) was modified by Saran and Prakash (1977) for soil-wall system subjected to earthquake forces. They suggested that ψ can be assumed to vary linearly from $\psi_b = \phi$ at the moving end of an active rotating wall to $\psi_a = \beta + \theta_k$ at the point of rotation, where β and θ_k are the slope angle of the backfill and the direction of the resultant gravity force, respectively (Fig. 6.1). Instead of assuming $\delta_w = \delta$ all the way along the soil – wall interface, they recommended that $\delta_w(z)$ be taken as $m\psi(z)$ with $m \leq 1$. They believed that the mobilized δ-value should be less than the mobilized ϕ-value. This is a reasonable assumption since the mobilization of δ is also dependent on the wall movement. The δ_w-value should be expected to vary in a similar way as the ψ-value.

Although the distribution of $\psi(z)$ as assumed by Saran and Prakash (1977) is much more generalized and the distribution of $\delta_w(z)$ seems more reasonable than those assumed by Dubrova (1963), they gave no explanation to their assumed $\psi(z)$-distribution. The $\psi(z)$-distribution was probably selected by them on the basis that the term inside the square root in ξ_A of Eq. (6.2) should be positive so that its solution would be determinate. In spite of its simplicity, taking $\psi_a = \beta + \theta_k$ simply for the sake of avoiding numerical difficulties without any physical reasoning may result in an improper $\psi(z)$-distribution. Both Dubrova's and Saran and Prakash's distributions of $\psi(z)$ require further stronger physical grounds.

Recommended distributions of $\psi(z)$ and $\delta_w(z)$ – Static case, horizontal backfill

For a $\psi(z)$-distribution to be reasonable, it is better to select it based on the considerations of the changes of stress condition in the backfill as the result of a specified wall movement.

Take the case of a vertical wall rotating about its toe away from a horizontal

backfill as an example. Before the wall starts tilting, it is reasonable to assume that the backfill is everywhere under the at-rest K_0-condition, if a naturally deposited soil mass is considered. As the wall starts yielding, the lateral displacement in the soil will be the largest near the top if the wall is rigid. It decreases as depth increases and reaches zero at the point of rotation. The consequence of this lateral yielding is to bring the backfill material from a K_0-condition to an active limiting equilibrium K_A-condition or somewhat in between at locations where the shear strain is not high enough.

In actuality, the average mobilized ψ-value depends on the shear strain within the soil mass, rather than the displacement of the wall, although the shear strain is related to the wall displacement. However, Dubrova (1963) assumed that the ψ-value is directly related to the wall displacement. Therefore, it seems reasonable, for the case of rotation about the toe, to take the ψ_a-value at the ϕ-parameter corresponding to the K_0-condition, denoted by ϕ_0. That is, assuming $\psi_a = \phi_0$ rather than $\psi_a = 0$, as was done by Dubrova (1963), seems more reasonable. Taking $\psi_b = \phi$ at the top, however, is well accepted in this case.

For the case of active rotation about the top, it can be assumed that the backfill behind the wall is under K_0-condition near the top and K_A-condition near the toe. Similar to the case of rotation about the toe, the ψ-values can be taken as $\psi_a = \phi_0$ at the top and $\psi_b = \phi$ at the toe.

The ψ_a- and ψ_b-values similar to those selected for the active rotation cases are recommended for the passive rotation cases, except those values are taken as negatives in these cases.

The reason for selecting $\phi_0 \leq \psi \leq \phi$ for the case of $\beta = 0$ can also be readily seen from (a) in Fig. 6.3. The stress state everywhere in the backfill at any stage of wall movement should be in the dotted region for the case of outward active movement.

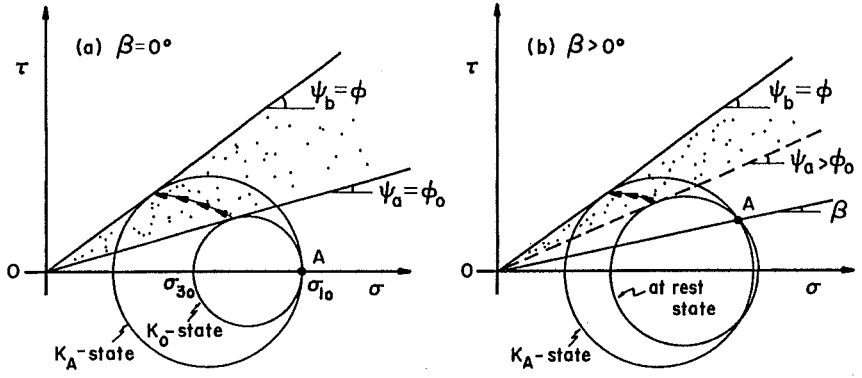

Fig. 6.3. State of stress and mobilized ϕ-parameter behind a rigid wall rotating outward about the toe.

According to Jaky (1948), the K_0-value for cohesionless soil can be related to the ϕ-parameter as:

$$K_0 = 1 - \sin\phi \tag{6.10}$$

Based on Fig. 6.3, the following equation can be obtained:

$$\sin\phi_0 = \frac{(\sigma_1)'_0 - (\sigma_3)'_0}{(\sigma_1)'_0 + (\sigma_3)'_0} \tag{6.11}$$

where $(\sigma_1)'_0$ and $(\sigma_3)'_0$ are major and minor principal stresses corresponding to K_0-condition. By definition, $K_0 = (\sigma_h)'_0/(\sigma_v)'_0 = (\sigma_3)'_0/(\sigma_1)'_0$. In general, $K_0 < 1$ for cohesionless soil. Consequently, Eq. (6.11) can then be reduced to:

$$\phi_0 = \sin^{-1}\left(\frac{1 - K_0}{1 + K_0}\right) \tag{6.12}$$

By combining Eqs. (6.10) and (6.12), the ϕ_0-value can be estimated from the following expression:

$$\phi_0 = \sin^{-1}\left(\frac{\sin\phi}{2 - \sin\phi}\right) \tag{6.13}$$

For example, the K_0-value for sand with $\phi = 40°$ is 0.36 and the corresponding ϕ_0-value is 28.3°, which is about 0.7ϕ.

Since the stress-strain behavior of soils is nonlinear, theoretically, the $\psi(z)$-distribution in the soil behind the rigid wall rotating either about the top or the toe should not be linear. Nevertheless, the difference in the two extreme ψ-values, ψ_a and ψ_b, is in the order of 30%. Furthermore, the strain field observed by James and Bransby (1970) and predicted by James and Bransby (1971) and Sabzevari and Ghahramani (1974) show, for the case of rotating about the toe into the backfill, that the shear strain varies nonlinearly with depth in a manner very similar to the variation of shear stress with shear strain. This somewhat indicates that the variation in the stress level or the mobilized ϕ-angle may be essentially linearly with depth. The measurement of James and Bransby (1970) also shows that δ_w, which is believed to vary with depth in a similar manner as ψ does, is linear with depth along large portions of wall height. For practical purposes, it is recommended that linear variation between ψ_a and ψ_b can be assumed.

Although, in general, the displacement required for a complete mobilization of soil-wall interface friction δ is lower than that required for a complete mobilization of shear strength, or ϕ-angle, experimental results of James and Bransby (1970) does

show that δ_w decreases essentially linearly with depth for the case of passive, rotation about the toe. However, the mobilized δ-angle, δ_w, in no cases can be larger than the ϕ-angle based on the stress-dilatancy reported by Davis (1968) and Lee and Herington (1972). It is therefore reasonable to assume that here $\delta_w(z)$, as in $\psi(z)$, is linearly distributed and the magnitude is equal to $m\psi$, with $m \leq 1$.

The value of $m = d\delta_w/d\psi$ can be taken as δ/ϕ since both $\delta_w(z)$ and $\psi(z)$ are assumed to be linear with z. The δ-value can be either measured in laboratories or estimated from the following equation proposed by Lee and Herington (1972), if ν is known:

$$\tan\delta = \frac{\sin\phi \cos\nu}{1 - \sin\delta \sin\nu} \tag{6.14}$$

where ν is the angle of dilatation of the interface material. This equation has recently been confirmed by Potts and Fourie (1986).

Recommended distributions of $\psi(z)$ and $\delta_w(z)$ – Earthquake case, inclined backfill

Earthquakes have two possible effects on a soil–wall system. They can either reduce the shearing resistance of soil or induce an additional driving force to the system. However, it has been generally recognized that the shear strength of a cohesionless soil is practically unaffected by the presence of most earthquakes unless the developed seismic acceleration is large, say larger than 0.3 g, and both the water table condition and soil characteristics favor the occurrence of liquefaction. The distributions of $\psi(z)$ and $\delta_w(z)$ should, therefore, remain the same for both the static and the earthquake cases. This partly explains why the distribution of $\psi(z)$ proposed by Saran and Prakash (1977) is improper.

When the ground surface of the backfill is inclined ($\beta > 0$), the state of stress in the backfill and its change upon wall movement is more complicated than when the backfill is horizontal. The Mohr circles for both cases of $\beta = 0$ and $0 < \beta < \phi$ are shown in Fig. 6.3. Point A in the figure represents the state of stress on a plane parallel to the ground surface at a given depth. Every Mohr circle representing the state of stress at different strain condition at the given depth should pass through point A. It is clear from the Mohr diagram that for the case of $\beta = 0$, the minimum mobilized ϕ-angle, or ψ_a, is ϕ_0 as mentioned earlier. The possible state of stress in the backfill is located in the dotted region as shown in Fig. 6.3. That is, $\psi_0 \leq \psi \leq \phi$ in this case.

As $\phi > \beta > 0$, the minimum ψ-parameter, ψ_a, or the ψ-parameter before the wall starts yielding, is believed to be higher than the ψ_0-value, which representing the ψ-value corresponding to the at rest K_0-condition for the case of $\beta = 0$. This is because the deviatoric stress level is higher for the case of $\beta > 0$ than that for the case of $\beta = 0$.

In order to assess the value of ψ_a, the other extreme case in which $\beta = \phi$ is considered. It is clear that for this case the mobilized ϕ-angle is equal to ϕ under at rest condition, before the wall starts moving. That is $\psi_a = \phi$ in this particular case. Based on these considerations, it seems that as β changes from 0 to ϕ, the ψ-value corresponding to the at-rest condition, ψ_a, changes from ϕ_0 to ϕ. The ψ_a-value for a given β-value should therefore be somewhere in between ϕ_0 and ϕ. It is obvious that the variation is dependent on the level of β with respect to ϕ. For practical purposes, the following relation based on a linear interpolation is suggested for estimating the ψ_a-value for a backfill with slope angle of β:

$$\psi_a = \phi_0 + (\phi - \phi_0)\frac{\tan\beta}{\tan\phi} \tag{6.15}$$

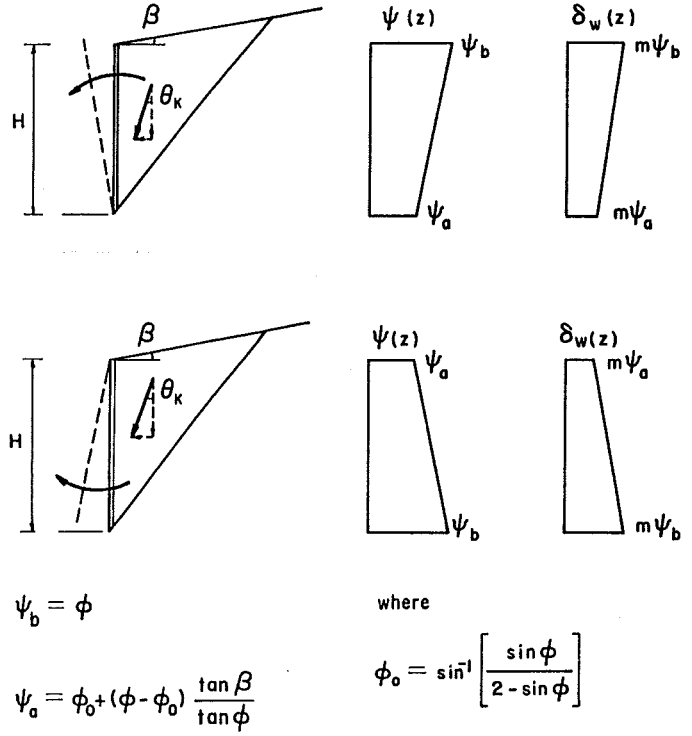

Fig. 6.4. Assumed distributions of $\psi(z)$ and $\delta_w(z)$ for seismic active earth pressure analysis.

The maximum possible ψ-value, ψ_b, is again equal to ϕ, which is independent of the slope angle. Hence the ψ-value at any stage of wall yielding should be in the range between ψ_a, as given by Eq. (6.15), and ϕ. That is, the state of stress should be in the dotted region as shown in Fig. 6.3b.

For the passive case, negatives of those ψ_a- and ψ_b-values as recommended for the active pressure case are taken. As in the case of $\beta = 0$, a linear variation is again assumed between the two extremes for the case of $\beta > 0$.

The distributions of $\psi(z)$ for active and passive rotations developed based on above-mentioned considerations are summarized in Figs. 6.4 and 6.5.

It should be noted here that the ψ-value at any depth z at any stage of wall movement can be generally expressed as:

$$\psi = \psi_a + (\psi_b - \psi_a)\, z/H \tag{6.16}$$

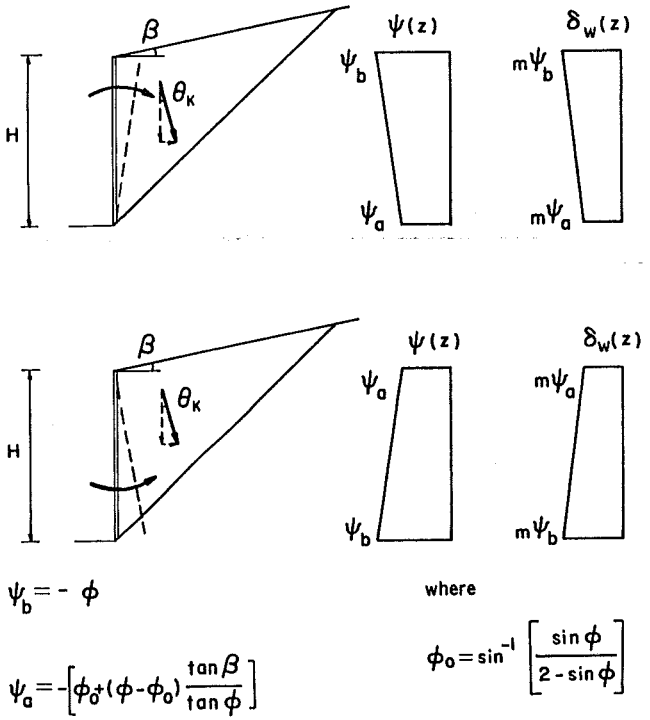

Fig. 6.5. Assumed distributions of $\psi(z)$ and $\delta_w(z)$ for seismic passive earth pressure analysis.

where H is the height of the wall, $\psi_b \cong \phi$, and ψ_a is given in Eq. (6.15). The minimum possible ψ-value is ψ_a and the maximum possible ψ-value is ϕ.

In order to satisfy the condition that the term inside the square root of ξ_A in Eq. (6.4) should be positive for the solution to be real, it requires for the active rotation case, that:

$$\theta_k \leq \psi_a - \beta \tag{6.17}$$

Similarly, for the passive rotation case, the following condition is needed:

$$|\theta_k| \leq |\psi_a| + \beta \tag{6.18}$$

The condition required for the passive solution to be real, as given by Eq. (6.18), is generally easy to be satisfied. This is because $|\psi_a|_{min} = \phi_0$ and is positive in most cases. However, the condition as required for a real active solution as shown in Eq. (6.17), may be critical to some soil–wall systems with steep backfill slopes. Although $(\psi_a - \beta)$ is positive, in general, the value may become very small or negative as β approaches ϕ, since $\tan\beta/\tan\phi \leq \beta/\phi$. The acceptable θ_k-value (or the magnitude of earthquake a soil-wall system can be tolerated) may be very limited if the slope angle is high. The presence of earthquakes, therefore, can be very critical for a soil–wall system with a steep backfill slope.

6.2.4 Resultant lateral pressure and point of action

For purely rotational wall movements, the resultant lateral pressure is simply a direct integration of the pressure distribution calculated from the modified Dubrova equation, Eq. (6.9). The trapezoidal approximation of areas is adopted in the integration. To avoid serious error in the approximation, reasonably small segmental heights are used. The trapezoidal rule is adopted in calculating the resultant pressure and its point of action for each segment. The point of action of the total resultant lateral pressure is obtained on the basis that the summation of first moments of each individual trapezoid about the toe equals to the first moment of the corresponding resultant pressure about the toe.

For a translational movement, ψ and δ_w depend on the amount of translation. At the ultimate state, however, $\psi = \phi$ and $\delta_w = \delta$, as commonly adopted, are reasonable. By differentiating $p_{AE}(z)$ in Eq. (6.3) with respect to z, it can be found that the pressure distribution is theoretically linear as was assumed by Coulomb. However, Dubrova (1963) recommended that the translational wall movement can be considered as a combination of rotation about the top and the bottom. He suggested that the pressure distribution in a translational movement can be taken as the average of the distributions resulting from rotating about the top and rotating about the bottom.

Based on Dubrova's suggestion, the total resultant lateral earth pressure for the translational case can then be taken as the average of those for the two rotational cases, disregarding whether the backfill material is in an active state or in a passive state. Experimental results of Narain et al. (1969) on passive earth pressure for different wall movements coincidentally tend to support Dubrova's suggestion. On the other hand, the experimental and theoretical works of James and Bransby (1970, 1971) clearly show that the failure pattern for wall translation is a combination of that for rotation about the top and that for rotation about the toe (Fig. 6.2). They argued that the passive translational force should be greater than those sustained by walls which rotate either about the top or the toe.

There are at least two reasons indicating that Dubrova's suggestion for combining rotational lateral pressures into translational lateral pressure is not justified. Firstly, the principle of superposition which may be good when strain is small so that the material still behaves elastically, is not necessarily applicable to the limiting equilibrium case. Secondly, unlike the passive earth pressure which increases as ϕ increases, the active earth pressure decreases as ϕ increases. Direct combination of the rotational active earth pressures for obtaining the translational active pressure is obviously not correct. Simply taking the average of the rotational pressure is not necessarily justified even for the passive case either.

Based on these considerations, it is suggested that the unit translational active earth pressure can be obtained directly from Eq. (6.4) based on $\psi = \phi$ and $\delta_w = \delta$. The unit translational passive earth pressure can be obtained from Eq. (6.7), by assuming $\psi = -\phi$ and $\delta_w = -\delta$. Consequently, for the translational wall movement, the lateral pressure distribution is linear based on the modified Dubrova method for both static and earthquake cases. The resultant lateral pressure is equal to that of Coulomb's for both active and passive cases.

6.3 Some numerical results and discussions of the modified Dubrova method

6.3.1 Effects of distribution of mobilized strength parameter on calculated lateral earth pressure

Dubrova's concept of pressure redistribution on which the present modified Dubrova method is based is versatile in that the effect of wall movement on lateral earth pressure can be taken into account. This is done by assuming a distribution of mobilized strength according to the mode of wall movement. Unfortunately, the stress-strain behavior of soils is generally nonlinear. Even if the wall displacement is well known, the resulting distribution of mobilized strength, which controls the lateral pressure distribution, varies from one soil–wall system to another.

Perhaps, an ideal way of obtaining the distribution of mobilized strength, which

can be represented by the mobilized ϕ-parameter for cohesionless soils, is to backcalculate from stress measurements on model tests of different scale. However, this is expensive and generally not feasible. Another possible way is to assume the distribution based on the consideration of change of stress state upon wall yielding as described in Section 6.2.

In order to see how the assumed distribution of ϕ-parameter, $\psi(z)$ affects the calculated lateral pressure distributions, results obtained based on the recommended distributions, as shown in Figs. 6.4 and 6.5 and the distributions suggested by Dubrova (1963) and Saran and Prakash (1977) are compared. Figures 6.6 and 6.7 show the comparisons of static active and passive earth pressures based on

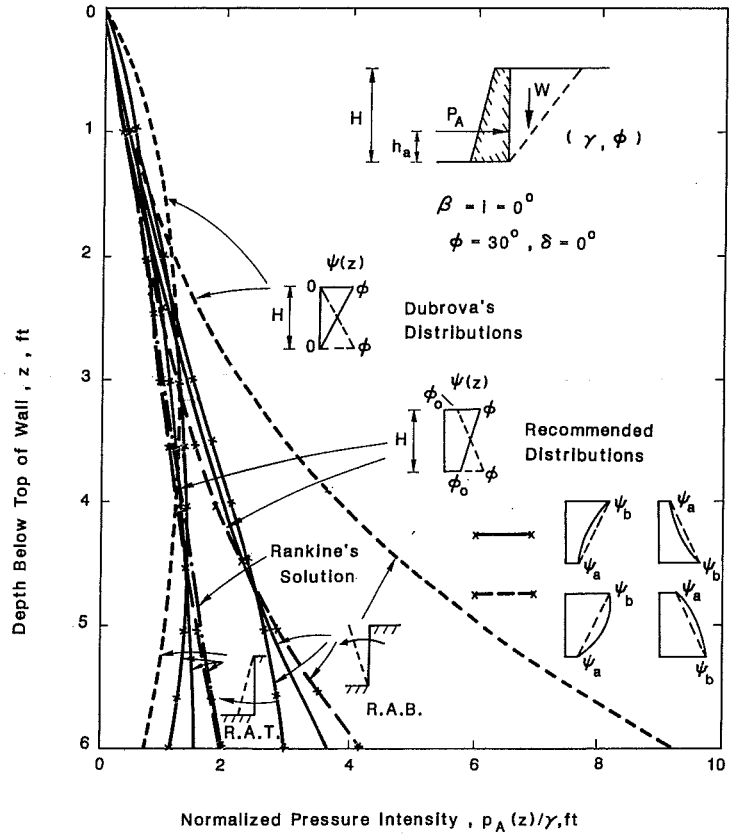

Fig. 6.6. Distributions of static active earth pressure based on different distributions of mobilized strength.

Dubrova's distribution and the recommended distribution of $\psi(z)$. Also shown in the figures are the Rankine solutions which also represent the solutions of modified Dubrova's method for translation wall movement. It is found that the calculated lateral pressure distribution is significantly influenced by the assumed $\psi(z)$-distribution.

The K_A- and K_P-values and the corresponding points of action, h_a and h_p, for those distributions shown in Figs. 6.6 and 6.7 are summarized in Tables 6.1 and 6.2.

For the case of rotation about the top, although the distributions of active and passive earth pressures are influenced by the assumed $\psi(z)$-distribution, it seems that the resultant pressures are almost unaffected as shown in Tables 6.1 and 6.2. They

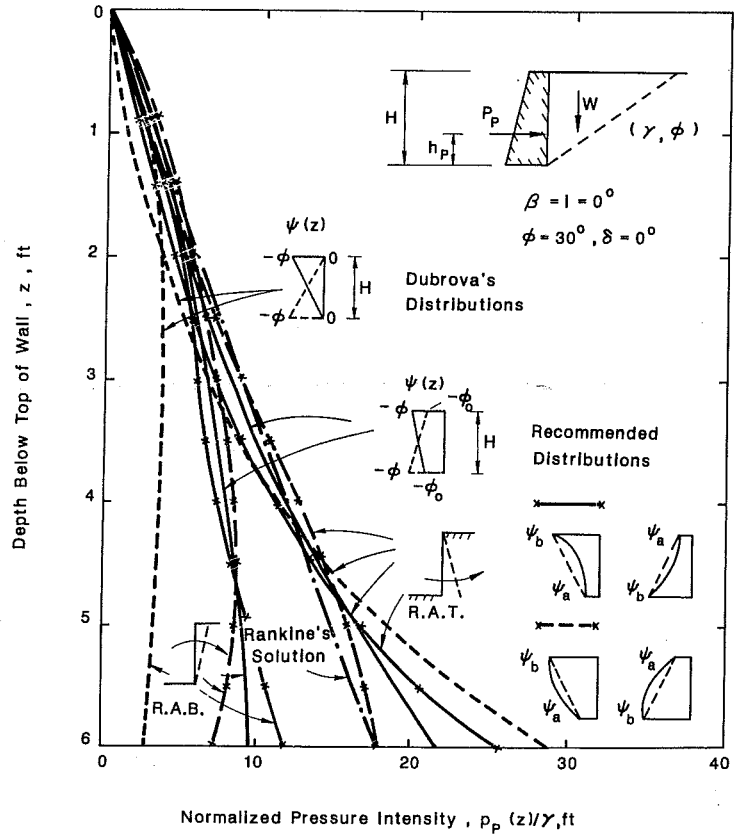

Fig. 6.7. Distributions of static passive earth pressure based on different distributions of mobilized strength.

are practically the same as the Rankine solutions. However, for the case of rotation about the bottom or toe, the Dubrova distribution results in a K_A-value two times the Rankine solution and a K_P-value one-half that of Rankine. This tends to suggest that the distribution of $\psi(z)$ assumed is improper. Assuming $\psi = 0$ at the toe, which means no mobilization of strength at all at the point of rotation, seriously underestimates the soil resistance. This is mostly responsible for the too high K_A- and too low K_P-values obtained based on Dubrova's distributions. It is clearly shown in Figs. 6.6 and 6.7 that the lateral pressure distribution obtained based on the recommended distribution of $\psi(z)$ is much more reasonable. It should be noted that the difference between the two solutions may even be larger if $\delta > 0$ is considered. This is because the $\delta_w(z)$-distribution recommended, $\delta_w(z) = m\,\psi(z)$, is much different from that assumed by Dubrova (1963), that is $\delta_w(z) = \delta$ = constant.

Even if two extreme values of ψ are fixed, the shape of the $\psi(z)$-distribution in-

TABLE 6.1

K_A-values and corresponding h_a-values based on different distributions of mobilized strength ($\phi = 30°$, $\delta = 0°$, $\beta = i = 0°$)

Wall movement	Distribution of mobilized strength	K_A	h_a/H
Rotation about the bottom	Dubrova's	1.001	0.261
	Recommended	0.500*	0.303
Rotation about the top	Dubrova's	0.333	0.456
	Recommended	0.333	0.371

* $K_A \simeq K_o = 1 - \sin\phi = (1 - \sin\phi_o)/(1 + \sin\phi_o)$

TABLE 6.2

K_P-values and corresponding h_p-values based on different distributions of mobilized strength ($\phi = 30°$, $\delta = 0°$, $\beta = i = 0°$)

Wall movement	Distribution of mobilized strength	K_P	h_p/H
Rotation about the bottom	Dubrova's	0.999	0.444
	Recommended	2.000*	0.369
Rotation about the top	Dubrova's	3.002	0.256
	Recommended	3.001	0.301

* $K_P \simeq K_{Po} = (1 + \sin\phi_o)/(1 - \sin\phi_o)$

fluences the calculated lateral pressure distribution too. In Fig. 6.6, active pressure distributions based on two different shapes of ψ-distribution as shown are plotted together with results based on the recommended linear ψ-distribution. In one case, the ψ-value at mid-height, ψ_m, is assumed $\frac{1}{4}(\psi_b - \psi_a)$ smaller than that corresponding to a linear distribution of which $\psi_m = \frac{1}{2}(\psi_b + \psi_a)$. That is, $\psi_m = \frac{1}{4}(\psi_b + 3\psi_a)$ is taken. In the other case, ψ_m of $\frac{1}{4}(\psi_b - \psi_a)$ larger than that corresponding to a linear distribution is assumed. That is $\psi_m = \frac{1}{4}(3\psi_b + \psi_a)$ is taken.

As expected, it is noted that the shape of calculated pressure distribution is different for each different shape of ψ-distribution. Consequently, the point of action of resultant lateral pressure is different for each distribution. However, it is interesting to note that the area enclosed by each pressure distribution curve, which represents the magnitude of the resultant force, is the same for these three cases.

TABLE 6.3
Effect of shape of ψ-distribution on h_a- and K_A-values

Mode of movement	ψ_m	h_a/H	K_A
Rotation about bottom	$\frac{1}{4}(\psi_b + 3\psi_a)$	0.321	0.500
	$\frac{1}{2}(\psi_b + \psi_a)$	0.303	0.500
	$\frac{1}{4}(3\psi_b + \psi_a)$	0.286	0.500
Rotation about top	$\frac{1}{4}(\psi_b + 3\psi_a)$	0.396	0.333
	$\frac{1}{2}(\psi_b + \psi_a)$	0.371	0.333
	$\frac{1}{4}(3\psi_b + \psi_a)$	0.348	0.333

TABLE 6.4
Effect of shape of ψ-distribution on h_p- and K_P-values

Mode of movement	ψ_m	h_p/H	K_P
Rotation about bottom	$\frac{1}{4}(\psi_b + 3\psi_a)$	0.347	2.000
	$\frac{1}{2}(\psi_b + \psi_a)$	0.369	2.000
	$\frac{1}{4}(3\psi_b + \psi_a)$	0.393	1.999
Rotation about top	$\frac{1}{4}(\psi_b + 3\psi_a)$	0.284	3.002
	$\frac{1}{2}(\psi_b + \psi_a)$	0.301	3.000
	$\frac{1}{4}(3\psi_b + \psi_a)$	0.320	3.000

It is apparent that the shape of the ψ-distribution seems to influence only the shape of the calculated pressure distribution, based on the modified Dubrova method.

Effect of the shape of ψ-distribution on passive pressure distribution is also shown in Fig. 6.7. Results similar to the active case are found.

The points of action and the K_A- and K_P-values corresponding to the pressure distributions shown in Figs. 6.6 and 6.7 for three different shapes of ψ-distribution are summarized in Tables 6.3 and 6.4. It is apparent that the h_a- and h_p-values obtained based on a nonlinear ψ-distribution differ from those based on a linear ψ-distribution only by an order of 6%.

For the seismic case, Saran and Prakash's distribution, which is a direct extension

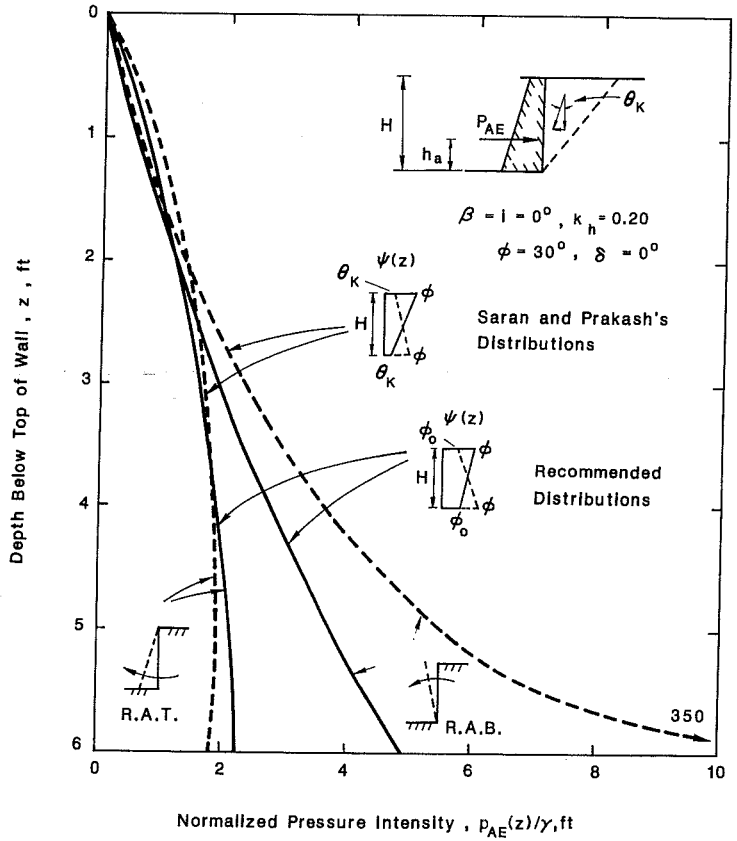

Fig. 6.8. Distributions of seismic active earth pressure based on different distributions of mobilized strength.

of Dubrova's distribution, is compared with the recommended distribution. Some results are shown in Figs. 6.8 and 6.9 for $k_h = 0.2$. They show that the pressure distribution based on Saran and Prakash's $\psi(z)$-distribution is different from that based on the recommended $\psi(z)$-distribution, especially for the case of rotation about the toe. However, it seems that the difference is less than that in static case, in general. This is because a non-zero ψ-value is assumed at the point of rotation by Saran and Prakash (1977) for the seismic case. This allows consideration of some degree of mobilization of strength at the point of rotation.

The K_{AE}- and K_{PE}-values and corresponding h_a- and h_p-values for those lateral pressure distributions shown in Figs. 6.8 and 6.9 are summarized in Tables 6.5 and

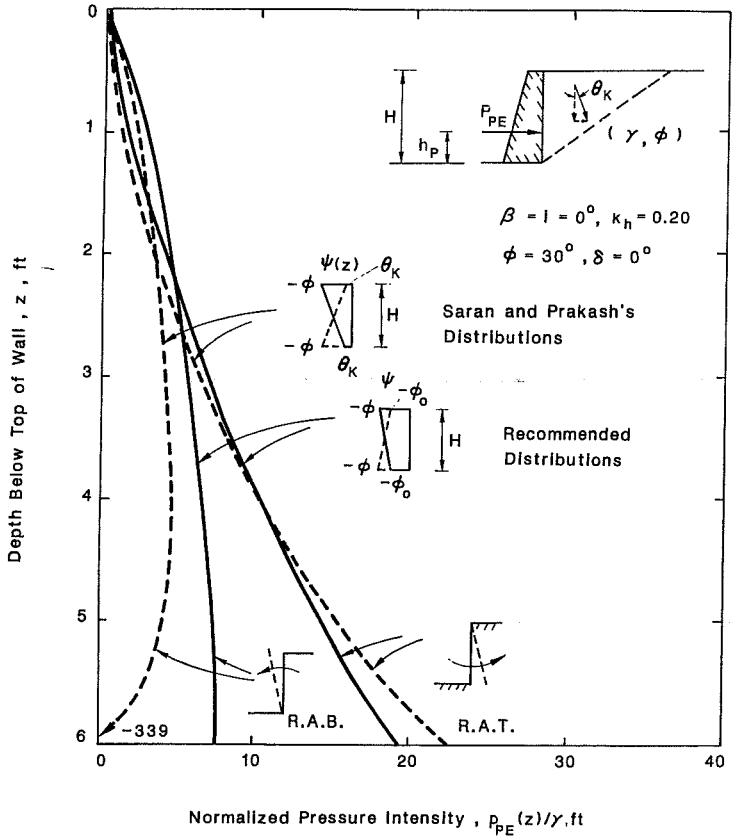

Fig. 6.9. Distributions of seismic passive earth pressure based on different distributions of mobilized strength.

6.6. Again, the K_{AE}-values obtained by the two different distributions of $\psi(z)$ are the same for the case of rotation about the top, although the corresponding h_a-values are different. The differences in both the resultant pressure and the points of action, similar to the active case, are larger for the case of rotation about the toe.

6.3.2 Pressure distributions at different stages of wall yielding

The Dubrova method enables lateral earth pressure distributions at different stages of wall yielding to be obtained. For developing such a kind of lateral pressure distribution, the change in state of stress as described in Section 6.2 is referred to.

Before walls start yielding, the soil mass is everywhere under an at-rest condition. A uniform $\psi(z)$-distribution, with $\psi = \psi_a$ might be appropriate. As the strength of the soil near the moving end is fully mobilized, $\psi_b = \phi$, is assumed for the moving end. At the point of rotation, however, the at-rest ψ-value, ψ_a, as given in Eq. (6.15) is considered. For the special case of $\beta = 0$, the at-rest condition corresponds

TABLE 6.5
K_{AE}-values and corresponding h_a-values based on different distributions of mobilized strength ($\phi = 30°$, $\delta = 0°$, $\beta = i = 0°$, $k_h = 0.20$)

Wall movement	Distribution of mobilized strength	K_{AE}	h_a/H
Rotation about the bottom	Saran and Prakash's	1.041	0.256
	Recommended	0.685	0.305
Rotation about the top	Saran and Prakash's	0.473	0.396
	Recommended	0.473	0.367

TABLE 6.6
K_{PE}-values and corresponding h_p-values based on different distributions of mobilized strength ($\phi = 30°$, $\delta = 0°$, $\beta = i = 0°$, $k_h = 0.20$)

Wall movement	Distribution of mobilized strength	K_{PE}	h_p/H
Rotation about the bottom	Saran and Prakash's	1.039	0.461
	Recommended	1.673	0.375
Rotation about the top	Saran and Prakash's	2.630	0.276
	Recommended	2.630	0.299

to the K_0-condition, and $\psi_a = \phi_0$. On the basis of this consideration, the ψ_b-value at any stage of wall yielding may be expressed as:

$$\psi_b = \psi_a + \alpha_m (\phi - \psi_a) \tag{6.19}$$

The at-rest condition, which existed before any wall yielding, corresponds to $\alpha_m = 0$. The state at which the soil strength is fully mobilized at the moving end corresponds to $\alpha_m = 1$.

Using Eq. (6.19) as the basis of assuming the distribution of $\psi(z)$ for different stages of wall yielding, typical lateral pressure distributions corresponding to $\alpha_m = 0, \frac{1}{3}, \frac{2}{3}$, and 1 have been generated for both the static active and the static passive

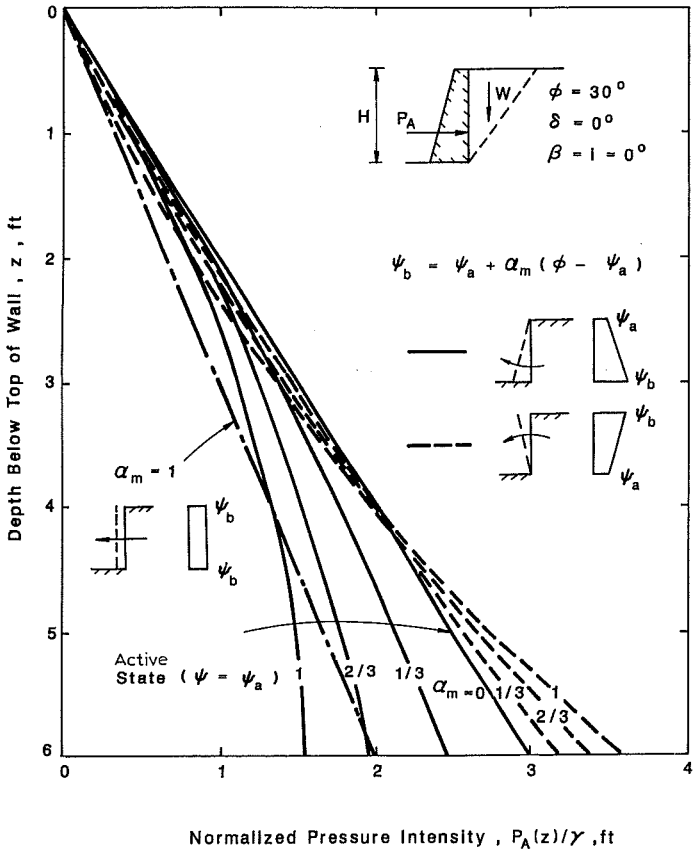

Fig. 6.10. Change in distribution of static active earth pressure as the result of gradual wall yielding.

cases. They are shown in Figs. 6.10 and 6.11. The gradual change in the pressure distribution as the result of gradual wall yielding is clearly illustrated in the figures. For reference, the translational pressure distribution for $\alpha_m = 1$, which corresponds to the ultimate state of all types of wall movement is also shown in the same figures.

It is interesting to note from both Figs. 6.10 and 6.11 that the lateral pressure distribution for the case of rotation about the toe only changes locally from the original at-rest line as the wall continuously yields until the strength in the backfill is fully mobilized near the top, although it is believed that the pressure distribution may eventually approach the ultimate state if further movement is allowed. This can

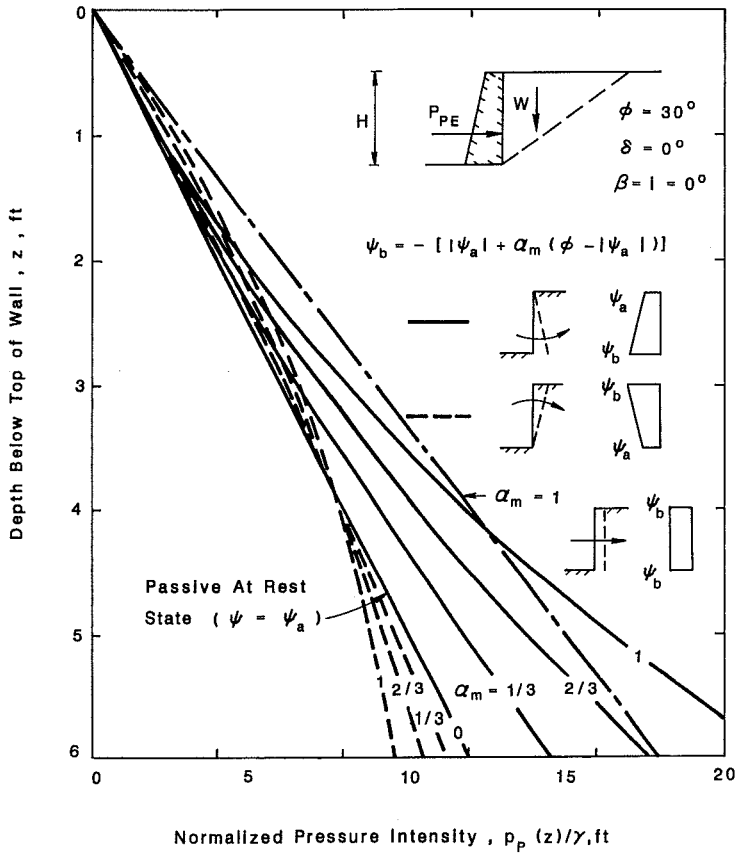

Fig. 6.11. Change in distribution of static passive earth pressure as the result of gradual wall yielding.

be seen from the finite-element results shown in Figs. 6.12 and 6.13 (Potts and Fourie, 1986). The lateral pressure distribution changes considerably from the at-rest distribution as the wall displacement increases, until the strength of the backfill is fully mobilized at the moving end for the case of rotation about the top.

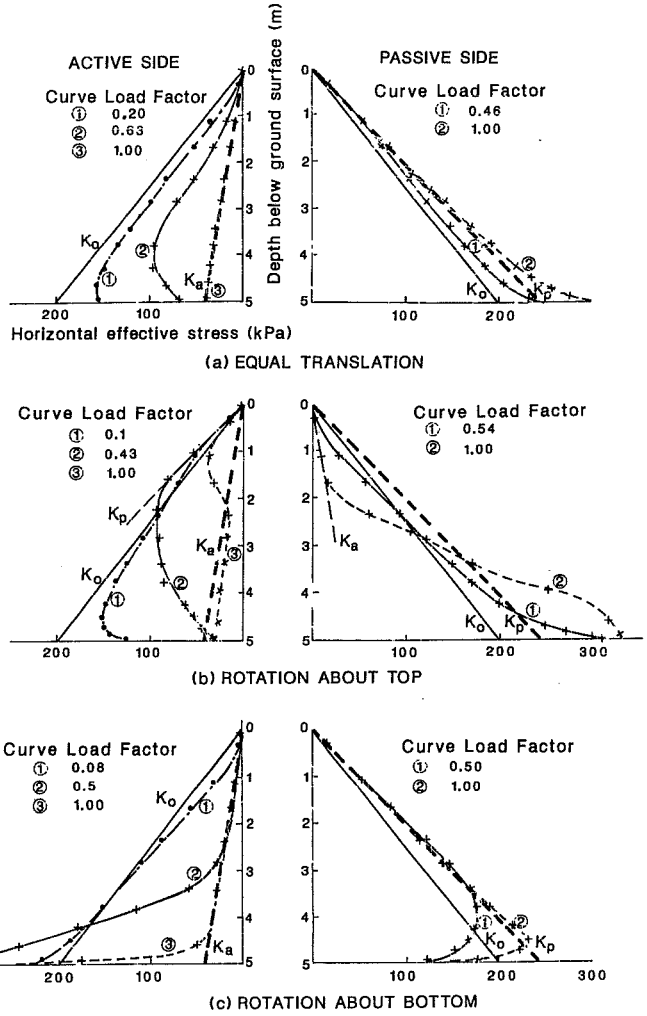

Fig. 6.12. Finite-element solutions of active and passive pressure distributions for smooth wall ($\phi' = 25°$, $\delta = 0$, $\beta = i = 0$) (Potts and Fourie, 1986).

Thereafter, it is expected that the lateral pressure distribution will gradually approach the straight line representing the translational wall movement case if the wall is allowed to move further. This is because the limiting state will propagate upward as the result of pressure redistribution. Consequently, the soil near the point of rota-

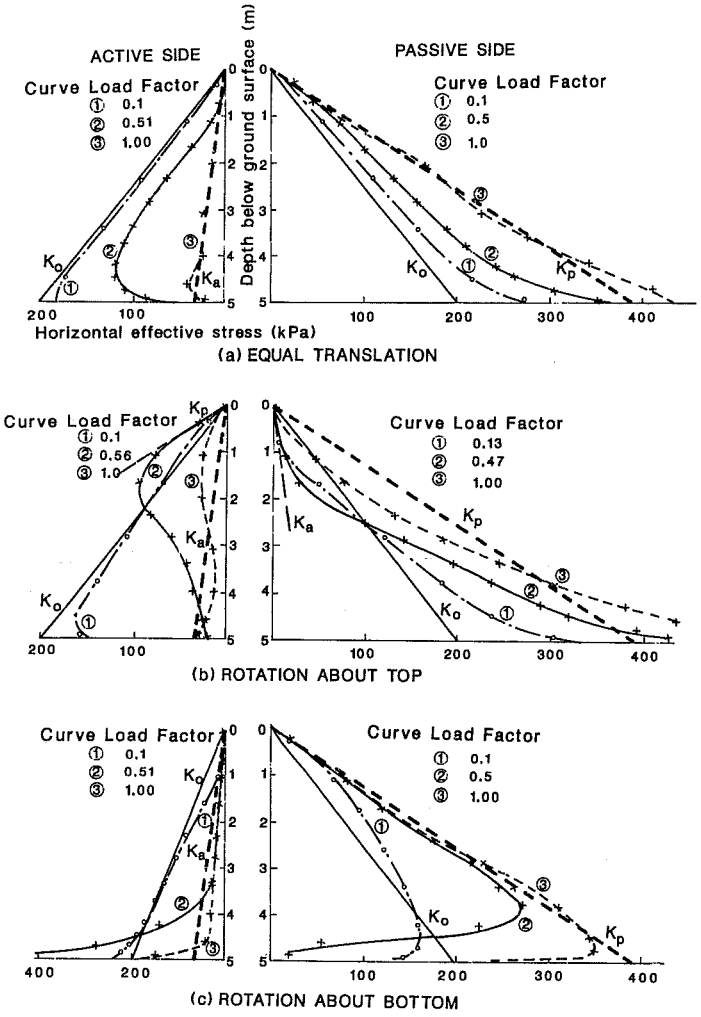

Fig. 6.13. Finite-element solutions of active and passive pressure distributions for rough wall ($\phi' = 25°$, $\delta = \phi'$, $\beta = i = 0$) (Potts and Fourie, 1986).

tion will be brought to the ultimate state of $\psi = \phi$ and result in a uniform distribution of $\psi(z)$, if the soil is considered perfectly plastic, as is done in all limiting equilibrium methods of analysis, including limit equilibrium and limit analysis.

The lateral pressure distributions as shown in Figs. 6.10 to 6.13 lead to a very interesting finding. Note that at the stage of full mobilization of strength at the moving end, the pressure distribution for the case of rotation about the top approaches the ultimate translational line with its corresponding resultant pressure the same as that for the translational case. On the other hand, the pressure distributions at the end of wall yielding for the rotation about the toe are not very different from the at-rest lines with their corresponding resultant pressures the same as the active and passive at-rest pressures in the active and passive cases, respectively. These tend to indicate that the resultant lateral pressure is dependent only on the mobilized ϕ-value at the toe, although the shape of the pressure distribution is surely affected by the assumed distribution of $\psi(z)$ as shown earlier.

This finding explains why the lateral pressure distribution for the case of the rotation about the toe, in which the ψ-value at the toe, $\psi = \psi_a$, remains unchanged upon wall yielding, does not change as much as that for the case of rotation about the top in which the ψ value, or ψ_b-value, changes with the amount of wall displacement. Also, this helps to explain why rotation about the bottom gives higher K_A-values and lower K_P-values than rotation about the top and translation do.

The above also explains why the differences in pressure distributions for the rotation about the top, based on the Dubrova and the recommended distributions, do not differ as much as those for the rotation about the toe. This is illustrated in Figs. 6.6 and 6.7. In fact, the consequence of $K_A = K_P = 1.0$ for the case of rotation about the toe based on the Dubrova distribution can be explained by the above-mentioned finding. The ψ-value is assumed by Dubrova as zero at the toe, and consequently the backfill behaves like a liquid or undrained clay with $\phi = 0$ and $K = 1$, although the pressure distribution is not linear.

The importance of the above-mentioned finding is particularly important when the shape of the assumed distribution of $\psi(z)$ is considered. After the two extremes of a $\psi(z)$-distribution, ψ_a and ψ_b, are selected based on consideration of the state of stress at different stages of wall movement, the only problem remains to be solved is how to vary the ψ-values between the two extremes. Perhaps, it has to be relied mainly on experimental observations. The linear distribution of $\psi(z)$ adopted in this chapter is based on limited experimental results available. Fortunately, the above suggests that the assumption of a linear variation of $\psi(z)$ between the two extremes, ψ_a and ψ_b, is justified.

Based on Figs. 6.6 and 6.7, it appears that although the magnitude of resultant lateral pressure is essentially controlled by the ψ-value at the toe, ψ_l, the shape of the pressure distribution is greatly influenced by the ψ-value at the top, ψ_u, or the difference between ψ_l and ψ_u. The shape of the ψ-distribution assumed seems to influence the pressure distribution to a much smaller extent than that of the assumed ψ_u-value. Hence, once the two extreme values of ψ-distribution, ψ_u and ψ_l, are properly selected, the shape of pressure distribution, or the point of action will be influenced by the assumed shape of ψ-distribution to a relatively minor extent. As discussed before, the magnitude of resultant force is practically unaffected by the shape of the ψ-distribution when ψ_u and ψ_l are specified. Therefore, the suitability of selecting a linear ψ-distribution is greatly enhanced.

The conclusion made from the study of changes in lateral pressure distribution as the result of wall yielding as shown here by the modified Dubrova method appears reasonably justified. Nevertheless, the general validity of the finding may need further justification.

Terzaghi (1936), interpreting from his experimental observations, indicated that for rotation about the toe, the total resultant pressure drops off immediately after wall starts yielding, even long before the actual slip in the backfill is observed. The close-to-at-rest pressure as obtained, based on the modified Dubrova method and the recommended distribution of ψ and δ_w, is not consistent with the actual observations of free standing retaining walls. The validity of the modification of the Dubrova method for actual application therefore needs further justification at least for the case of rotation about the toe.

For translation and rotation about the top, the preliminary results obtained so far based on the modified Dubrova method seems reasonable, although it has been observed that rotation about top gives higher resultant pressure (Terzaghi, 1941). For rotation about the toe, it is apparent that the pressure so obtained is not representative of the limiting active or passive pressure. However, the lateral earth pressure so obtained using the recommended ψ-distribution corresponds reasonably to that when the soil near the top of the wall has just reached the limiting active or passive state while the soil below remains essentially at rest. Hence, the pressure distribution so obtained is at least representative of this particular state, which may resemble the behavior of basement walls during an earthquake or the behavior of rigid retaining structure fixed at the bottom and somewhat restrained at the top. Hence it is still worthwhile to present some numerical results for all three modes of wall movement before giving an overall evaluation of the modified Dubrova method.

6.3.3 Point of action for static conditions

It is generally considered that Rankine's theory is applicable for lateral earth pressure assessments when the wall is rigid, vertical, and perfectly smooth, and the backfill is horizontal. The theory gives a linearly distributed lateral pressure behind a perfectly smooth rigid wall for both outward and inward translational wall movements. The points of action, expressed in terms of the height from the bottom

of the wall, h_a for the active case and h_p for the passive case, can be taken as $H/3$(H = wall height) above its base, according to the theory.

Some results of the modified Dubrova method are first compared with those of Rankine for $i = \beta = \delta = 0$. Figures at 6.14 and 6.15 show the lateral pressure distributions as obtained from the proposed method for the two rotational modes of wall movement. The translational lateral pressure which is linearly distributed with its magnitude equal to the Coulomb's solution, or Rankine's solution for this special case in which $\delta = 0$, according to the modified Dubrova method is also shown in the same figures. It is found that the pressure distribution for the three different modes of wall movement differs from one another. For both rotational cases, the distribution is not linear, in general. The same results can be found in the finite-element solutions shown in Figs. 6.12 and 6.13.

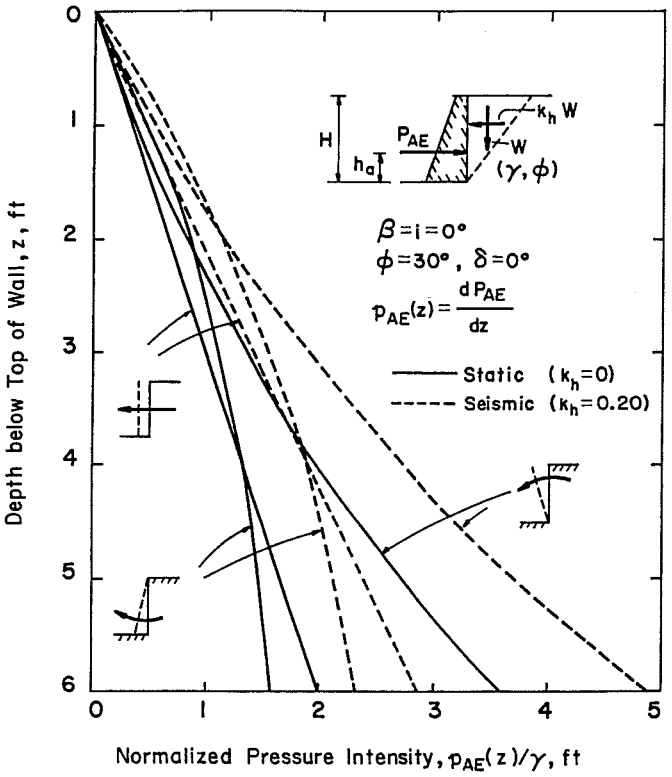

Fig. 6.14. Distributions of static and seismic active earth pressures for a perfectly smooth wall.

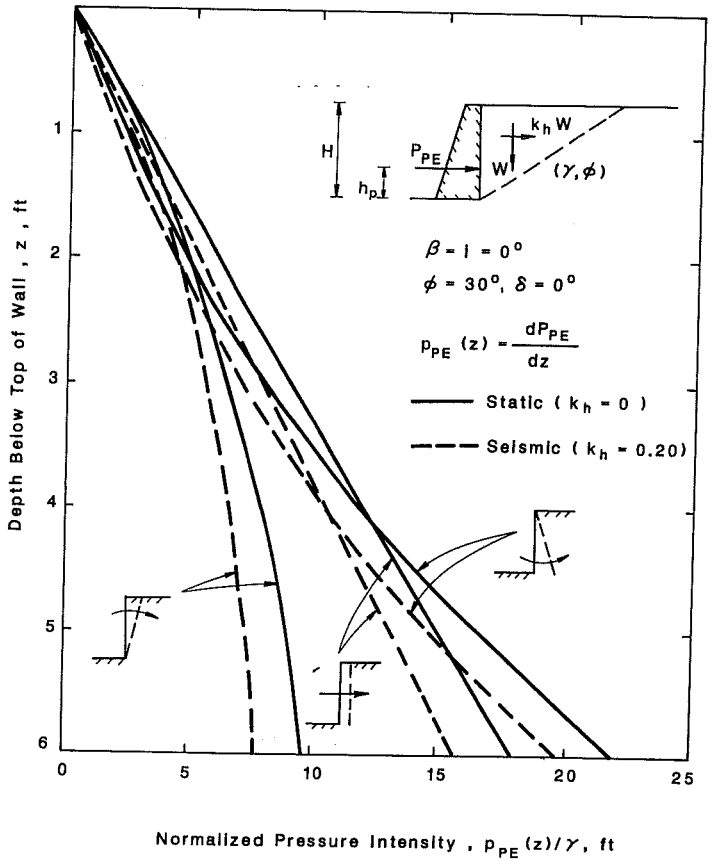

Fig. 6.15. Distributions of static and seismic passive earth pressures for a perfectly smooth wall.

The points of action h_a and h_p, corresponding to each pressure distribution in Figs. 6.14 and 6.15 are listed in Tables 6.1 and 6.2, except for translation in which $h_a = h_p = \frac{1}{3}$ is found. For rotations, they are found to be different from the Rankine value: $h_a = h_p = H/3$. The difference is expected, since in the modified Dubrova method, the ψ-value is allowed to vary along the height of the wall, while $\psi = \phi$ is assumed in the Rankine theory. The h_a- and h_p-values are found to be highly dependent on the mode of wall movement.

For the case of outward rotation about the toe, the state of stress in the soil near the top of the wall is expected to change from the at-rest condition to the active condition while that very close to the toe remains at-rest. The concave upward distribu-

tion curve as obtained by the proposed method is not unreasonable, although Terzaghi (1936), based on his large retaining wall tests (Terzaghi, 1934), claimed that $h_a = H/3$ for this case. It should be noted that the point of rotation in all the tilting tests he conducted was not right at the toe. On the other hand, for rotation about the top, some arching effect is expected near the upper portion of the wall. The parabolic-like distribution as shown in Fig. 6.14 seems reasonable, although it is flatter than that reported by Terzaghi (1941).

The nonlinear distribution of passive pressures for inward rotational cases as shown in Fig. 6.15 are also reasonable, since passive resistance increases as the degree of strength mobilization increases, in general. For the case of inward rotation about the top, the mobilized strength parameter ψ increases as depth increases. The concave upward distribution may therefore be expected. The pressure intensity is supposed to decrease as depth increases for the case of rotation about the bottom

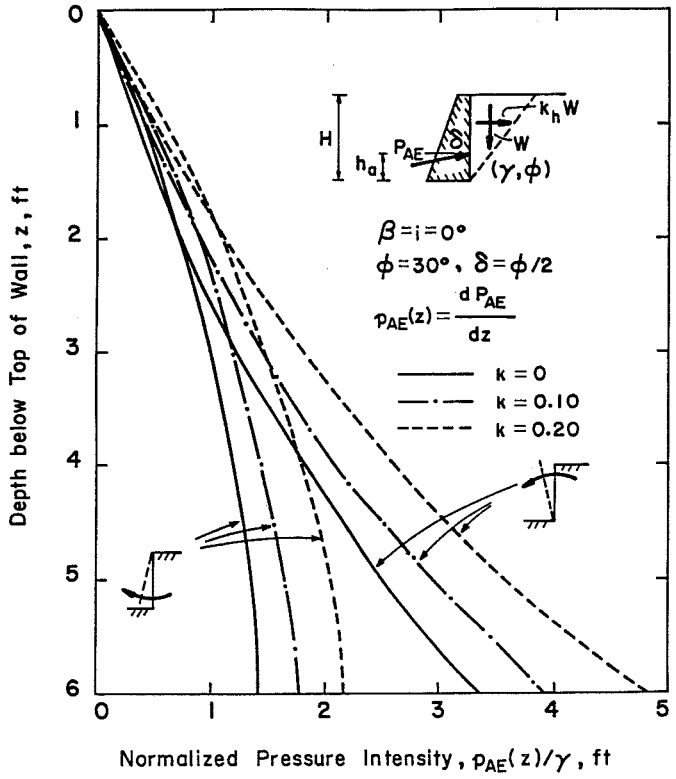

Fig. 6.16. Distributions of active earth pressure for earthquakes of different magnitude.

in which the degree of strength mobilization varies from the highest value at the top to the lowest value at the bottom. However, the effective overburden pressure increases as depth increases. This may compensate partly the effect due to a reduction in ψ-value with depth. As shown in Fig. 6.15, the change in pressure intensity with depth is, therefore, not as sharp as that if a material of less weight is considered.

Some results on active and passive pressure distributions for a fairly rough wall are also obtained based on the modified Dubrova method. They are presented in Figs. 6.16 and 6.17. The distributions are found to be similar to those for perfectly smooth walls. The comparison with available information is presented as follows.

There exists a very limited theoretical work in the open literature that deals with

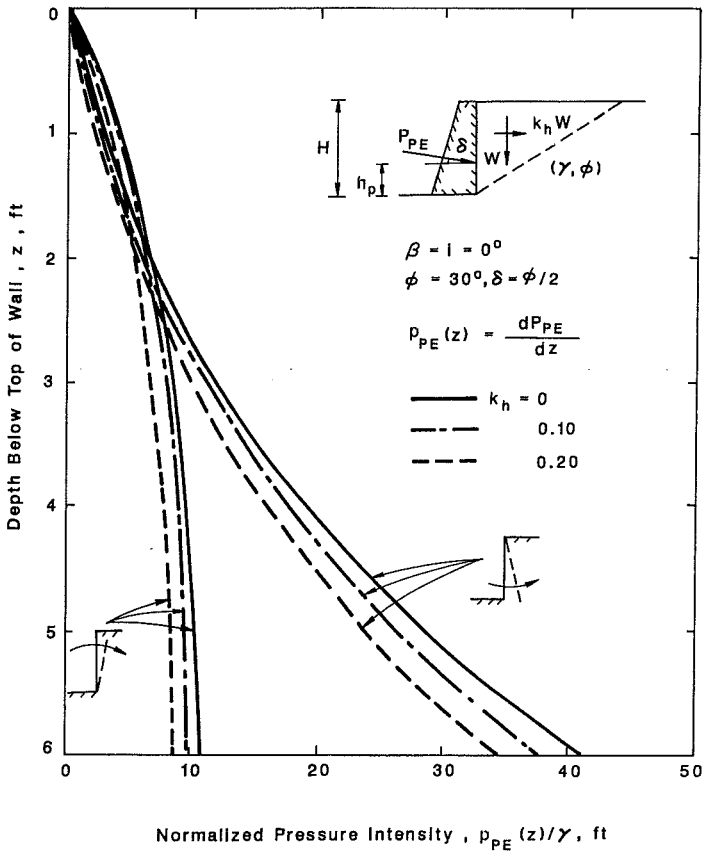

Fig. 6.17. Distributions of passive earth pressure for earthquakes of different magnitude.

lateral earth pressure distributions. Here, the work of Prakash and Basavanna (1969) which makes a distinction between a sliding (translational) wall and a tilting wall, a wall rotates about its toe, is selected for comparison with the modified Dubrova method for the active case. In their method, they take into consideration not only the force equilibrium on the triangular sliding wedge, but also the moment equilibrium of the rotating wedge. By optimizing the overturning moment or the active force for the determination of the most critical sliding surface, they were able to make the distinction between a tilting wall that occurs when the overturning moment is maximum, and a sliding wall that occurs when the active force is a maximum. Basavanna (1970) tried to improve the solution of Prakash and Basavanna (1969) for the sliding case based on the same framework. However, the improvement is very limited.

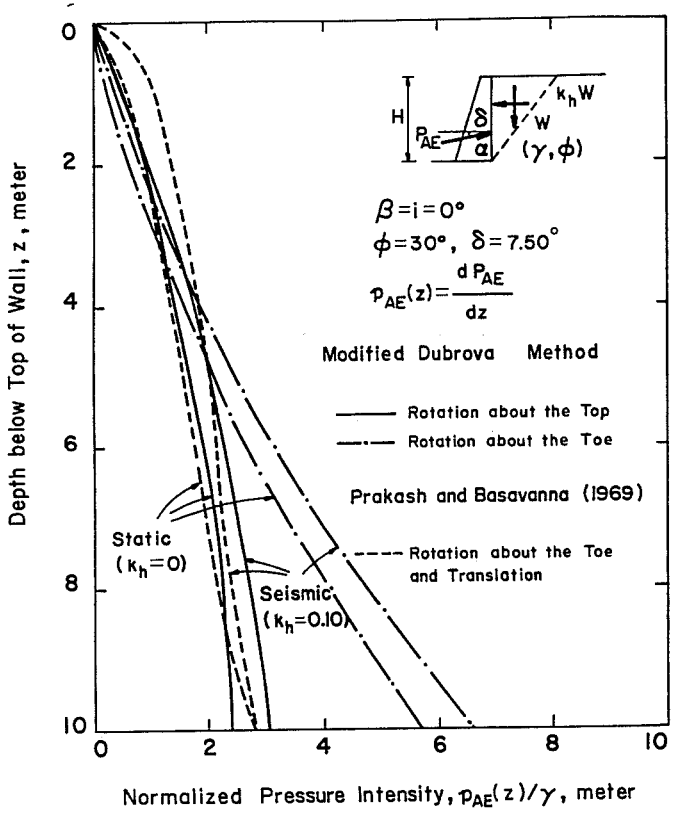

Fig. 6.18. Distributions of static and seismic active earth pressures by the modified Dubrova method and Prakash and Basavanna's solution.

A typical comparison of the result of Prakash and Basavanna (1969) and that of the modified Dubrova method is shown in Fig. 6.18. It is found that although Prakash and Basavanna (1969) tried to differentiate sliding walls from tilting walls, they obtained identical results from the two different wall movements for the static case. The modified Dubrova's method, however, gives a different pressure distribution for a different wall movement.

The distribution of translational pressure obtained by the modified Dubrova method, which is not shown in Fig. 6.18, is linear. It is close to the distribution curve for the rotation about the top, as shown in Fig. 6.14. It is therefore clear that the distribution of translational pressure obtained by Prakash and Basavanna (1969), although not linear, does not deviate much from that obtained by the modified

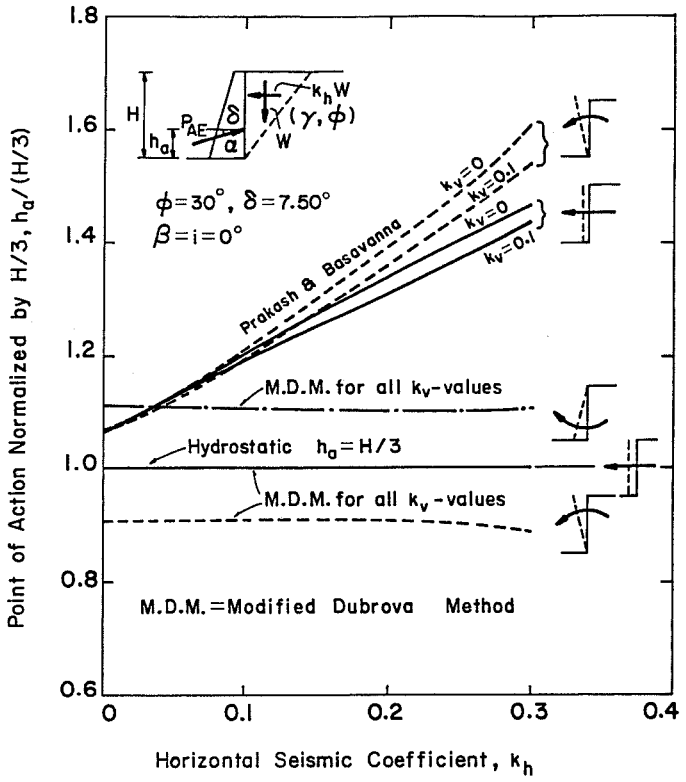

Fig. 6.19. Comparison of h_a-values obtained by the modified Dubrova method with solutions of Prakash and Basavanna (1969).

Dubrova method, which is linear. However, the distribution of active pressure for a tilting wall as obtained by them seems close to that for a wall rotating about the top rather than that for a wall rotating about the toe based on the modified Dubrova method. According to the modified Dubrova method, the distribution of the active earth pressure for a tilting wall about the toe is very close to the at-rest line.

The points of action, h_a, corresponding to those distributions in Fig. 6.18 are shown in Fig. 6.19. It is found that for the static case, the h_a-value obtained by Prakash and Basavanna (1969) for both tilting and sliding walls is higher than those for the translational wall, $h_a = H/3$, and for walls rotating about the toe as obtained by the modified Dubrova method. For the reasons given earlier, it seems that the distribution curve should be concave upward for the case of rotation about the bottom. This tends to suggest that $h_a < H/3$ as obtained by the modified Dubrova method is more reasonable.

It should be noted that both ψ- and δ_w-values are assumed to vary with depth in the modified Dubrova method, while they are assumed constant with depth and equal to their corresponding maximum values, ϕ and δ, in the Prakash and Basavanna's formulation. This is probably partially responsible for the difference in pressure distributions as obtained by the two methods.

In summary, it can be concluded that the distribution of lateral earth pressure, or the resultant pressure and its point of action, is highly dependent on the mode of wall movement. The current practice of assuming $h_a = h_p = H/3$, regardless of the type of wall movement, appears to be very much in error. The distribution of static lateral pressure is found to be nonlinear for rotational wall movements, regardless of the soil–wall interface roughness.

6.3.4 Point of action for earthquake condition

It is generally reported that the point of action of resultant lateral pressure for the seismic case is higher than that for the static case. To see if this is the case, distributions of seismic lateral pressures for different wall movements, as obtained by the modified Dubrova method are shown together with the static pressure distributions in Figs. 6.14 and 6.15 for a perfectly smooth wall. It is found that the translational lateral pressure, which is the same as the Mononobe-Okabe or the modified Coulomb solution, is linearly distributed. The distribution of rotational lateral pressures are nonlinear, however, the shape of the distribution of seismic lateral earth pressure is found to differ from that of the static lateral pressure.

In general, the active pressure intensity increases and the passive pressure intensity decreases when subject to the action of an earthquake. Consequently, K_{AE} increases and K_{PE} decreases. However, since the shape of the distribution is not much altered by the presence of earthquakes, the point of action of the resultant lateral pressure changes only slightly. The changes in K_{AE}, K_{PE} and their corresponding points of action h_a, h_p for the distributions shown in Figs. 6.14 and 6.15 are summarized in Tables 6.5 and 6.6.

Figures 6.16 and 6.17 show the gradual change in lateral pressure distribution for rotational wall movements as the result of a gradual increase in the magnitude of earthquake, which is represented by the seismic coefficient, k or its horizontal component k_h. The corresponding h_a- and h_p-values are plotted against the k_h-value as shown in Fig. 6.20. It is found that the h_a- and h_p-values are practically unaffected or only decreases gradually as the k_h-value increases for the case of rotation about the top. For the case of rotation about the toe the h_a-value gently increases up to $k_h = 0.1$ and decreases thereafter, while the h_p-value increases as the k_h-value increases for this case.

The comparison with available information in active cases is presented as follows.

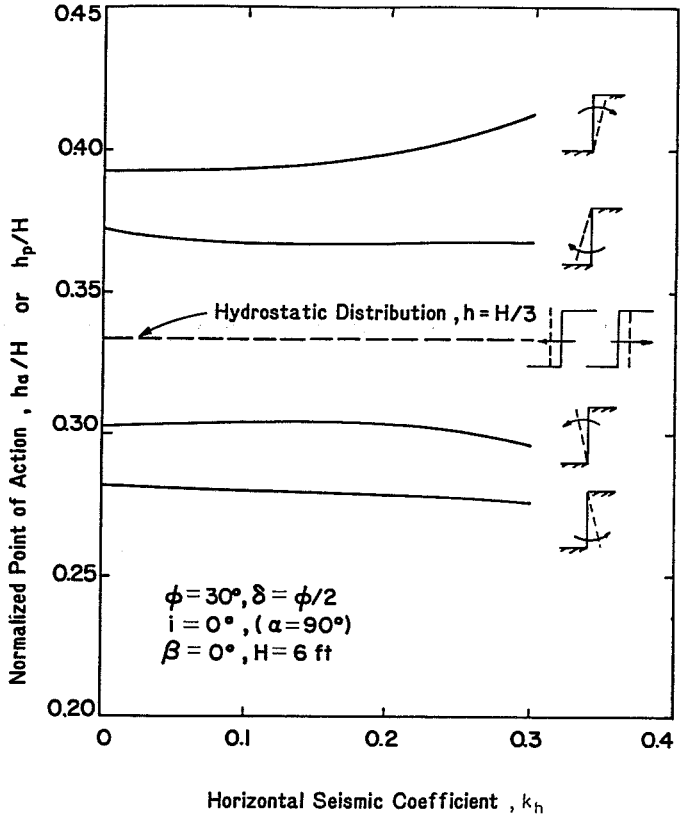

Fig. 6.20. Effect of earthquake forces on point of action for different wall movements.

The point of action of resultant active earth pressure during earthquakes was first extensively investigated by Ishii et al. (1960) experimentally. Their model tests on gravity walls reflect that for the case of translational wall movement, the point of action h_a increases gradually from a value of about $H/3$ at $k_h = 0$ to a value of about $0.4\,H$ when $k_h = 0.4$. For the case of rotation about the toe, they found that the h_a-value is only slightly increased as the k_h-value is increased. Their observations seem to agree with the results of the modified Dubrova method for rotation about the toe, on one hand, and disagree for translation, on the other hand. However, it should always be recognized that all the model tests may distort the actual soil behavior because of scale effect. Results of model test may, therefore, be unreliable.

For comparing the results of the modified Dubrova method with other theoretical solutions, the work of Prakash and Basavanna (1969) as described earlier is referred. A typical result of the active pressure distribution for the case of $k_h = 0.10$ obtained by them is compared with that obtained by the modified Dubrova method as shown in Fig. 6.18. As in the static case, it is found that for the case of $k_h = 0.10$, the pressure distributions for a sliding wall and that for a tilting wall are practically identical. Hence, only the average distribution is shown in the figure. Again, the seismic pressure distribution as obtained by them is close to that for the case of rotation about the top as obtained by the modified Dubrova method. The distribution of seismic active earth pressure for the case of rotation about the toe, as obtained by the modified Dubrova method, is found to be much flatter.

Figure 6.19 shows the variation of h_a with k_h for results obtained by the two different methods. The h_a-values as given by Prakash and Basavanna (1969) are found to increase rapidly as the k_h-value increases. The distinction between the h_a-value for a sliding wall and that for a tilting wall is clear only when the k_h-value is high. They also show the vertical acceleration component, $k_v g$, has some effects on the h_a-values for both the sliding and tilting cases.

The results of the modified Dubrova method, however, indicate that the point of action, h_a, is practically unaffected by the k_h-value for all three modes of wall movement. Also, the h_a-value is found unaffected by the present of k_v. For the case of rotation about the top, $h_a > H/3$ is obtained. For the case of rotation about the toe, $h_a < H/3$ is found. The translational movement, similar to the modified Coulomb solution, gives $h_a = H/3$, which is completely independent of k_h-value. However, based on Prakash and Basavanna (1969), the h_a-value is found always higher than $H/3$ for either sliding or tilting wall. This finding may need further justification at least for the case of tilting wall about the toe for which a concave upward distribution is probably more representative of the actual distribution.

In order to see how the earthquake alone affects the active earth pressure, seismic increments of active pressures on a perfectly smooth wall are calculated for different wall movements. The resulting distributions of the seismic increments are shown in Fig. 6.21. It is found that, based on the modified Dubrova method, the distribution is linear only for the translational case. The point of action corresponding to ΔK_{AE}, $h'_a = H/3$ (h'_a is the h_a-value corresponding to the seismic increment of the active earth pressure) as found by Nandahumaran and Joshi (1973) for the case of $\delta = 0$, is only true for the translational wall movement.

It is interesting to note that the distributions of seismic increments of active earth pressures as shown in Fig. 6.21 are almost identical in shape to their corresponding resulting active pressure distributions for different modes of wall movement. Also it is found that K_{AE} and ΔK_{AE} for the rotation about the top are the same as those for the translation case. The h'_a-value is larger than $H/3$ for the case of rotation about the top, while $h'_a < H/3$ is found for the case of rotation about the toe.

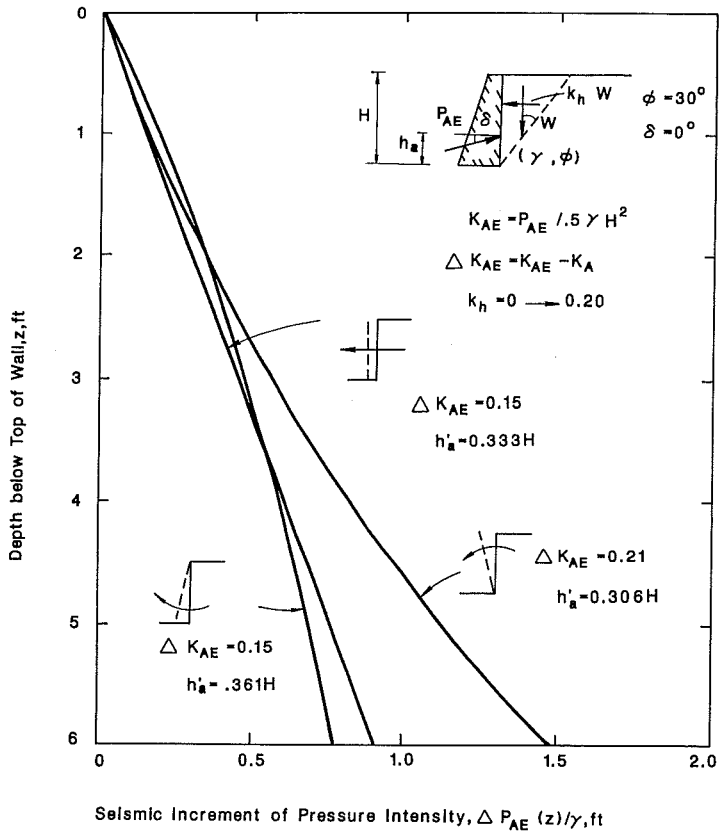

Fig. 6.21. Distributions of seismic increments of active earth pressure for different wall movements.

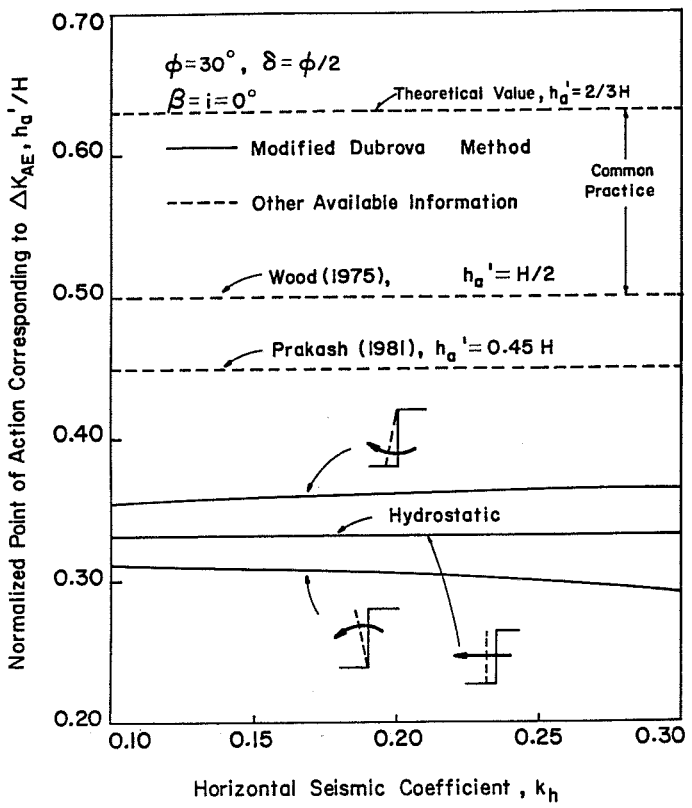

Fig. 6.22. Point of action of seismic increments of active earth pressure.

Figure 6.22 shows the change of h_a'-value with k_h for different modes of wall movements as obtained by the modified Dubrova method for a fairly rough wall. The h_a'-values so obtained are found not much different from the hydrostatic value of $H/3$. They are much lower than the theoretical value of $2H/3$, the value found by Wood (1975), and the value as suggested by Prakash (1981). However, according to the general wedge theory (Terzaghi, 1941), the point of action will rise when the sliding surface becomes curved, if both ϕ and δ are assumed constant. In fact, Prakash and Basavanna (1969) also noted that $h_a' = H/3$ for the case of $\delta = 0$. Hence, it is believed that the high h_a'-value as obtained by many investigators for rough walls is partly the direct consequence of assuming $\psi = \phi$ and $\delta_w = \delta$ all the way along the height of the wall, as is usually done in conventional earth pressure theories.

It is found that the h_a'-value is only slightly affected by the k_h-value. This is also different from that found by Nandahumaran and Joshi (1973) who reported that h_a' increased linearly with the k_h-value. Nevertheless, due to the unreasonable assumption made by them, Nandahumaran and Joshi's findings are not necessarily justified.

The comparison with available information in passive cases is presented as follows.

Since passive earth pressure problems involve extensive interaction and progressive failure phenomena, the problem is more complicated than the active earth pressure case. Furthermore, the most critical sliding surface, unlike the active case, is generally curved for the passive case. For these reasons, studies on the seismic passive earth pressure are more difficult than those of the seismic active pressure.

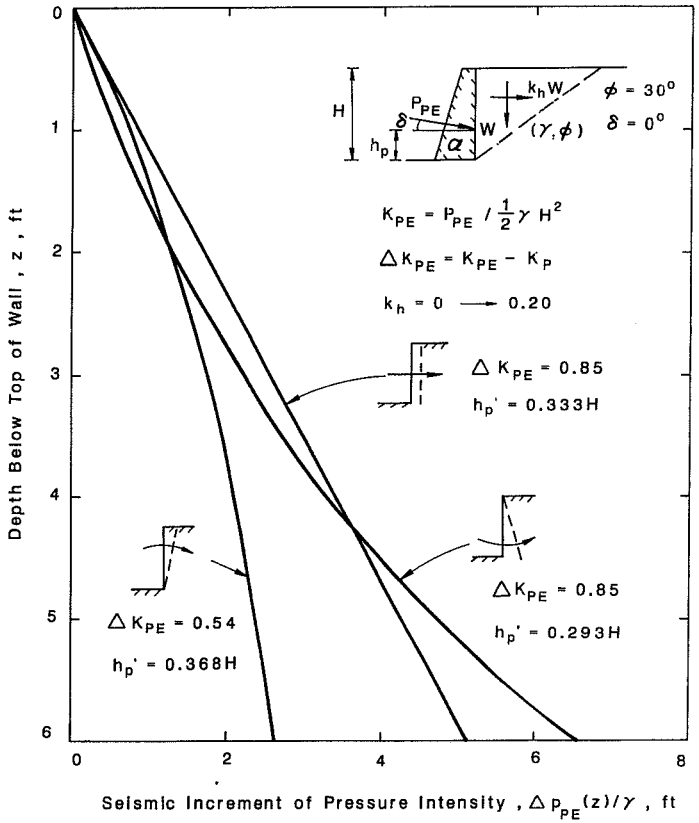

Fig. 6.23. Distributions of seismic increments of passive earth pressure for different wall movements.

There is even less information available on the point of resultant seismic passive earth pressure, h_p.

As shown in Fig. 6.20 the h_p-value for a translational wall movement is $H/3$. The rotation about the top gives $h_p < H/3$, while the case of rotation about the toe gives $h_p > H/3$, which are the reverse of those for the active case. These results are consistent with the finding of Narain et al. (1969) based on model tests in sand. The deviation of h_p from the hydrostatic value $H/3$ is found larger which indicates that the distribution is more curved for the passive pressure case than for the active pressure case.

In order to compare results of the modified Dubrova method with the only available information on the distribution of seismic passive pressure, as given by Ghahramani and Clemence (1980), the seismic increment of passive earth pressure is considered. Figure 6.23 shows the distributions of seismic increments of passive pressure for different wall movements as obtained by the modified Dubrova method. It is found that the shapes of these distributions are almost identical to those of seismic passive pressure.

By using the theory of zero-extension line, Ghahramani and Clemence (1980) developed a method of assessing the coefficient of passive earth pressure for the increment of pressure as the result of a seismic acceleration. Also, based on the work

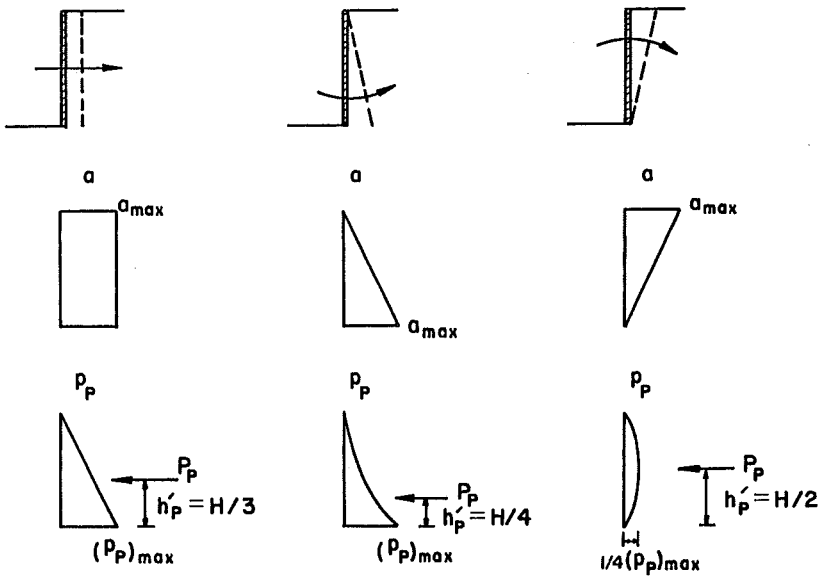

Fig. 6.24. Distributions of acceleration assumed and passive pressure increments obtained by Ghahramani and Clemence (1980) for different wall movements.

of Sabzevari and Ghahramani (1979), in which walls were allowed to move independently at a maximum acceleration $a_{max} = kg$ in an incremental manner, they suggested a distribution of seismic acceleration for each mode of wall movement. These are shown in Fig. 6.24. By incorporating these distributions into their proposed method of analysis, they found that the distributions of passive pressure increments as the result of different wall movements are those shown in Fig. 6.24. Their shapes are independent of a_{max} and δ.

Comparing Fig. 6.23 with Fig. 6.24, it is interesting to note that, although based on completely different concepts, the two methods give identical distribution for seismic increment of passive pressure in the case of translational wall movement. The distributions for the case of wall rotating about the top are practically similar, although the corresponding h_p-value obtained by the modified Dubrova method is

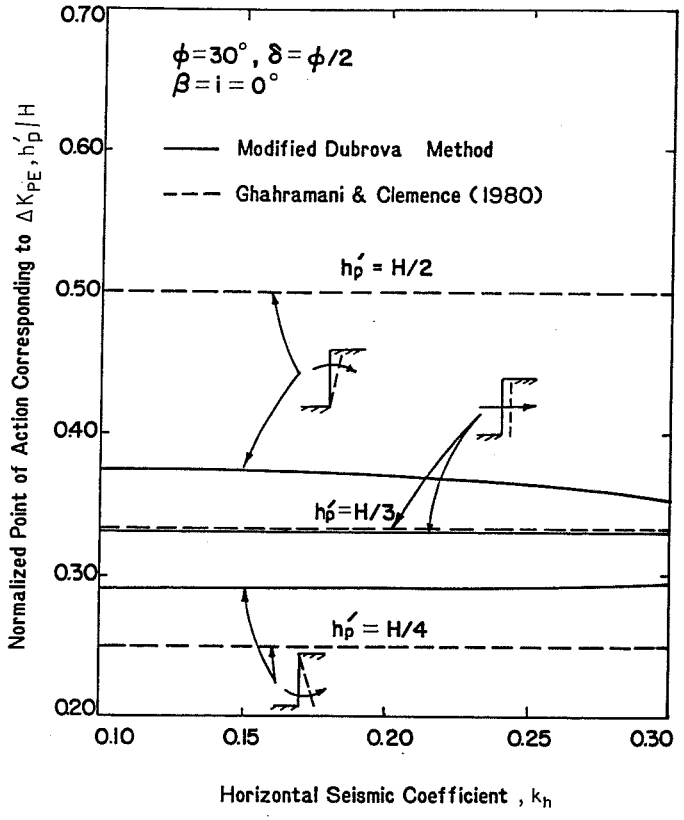

Fig. 6.25. Point of action of seismic increments of passive earth pressure.

a little higher. The distributions for the case of rotating about the bottom, although very different, all indicate that $h_p > H/3$.

The h_p'-values obtained by the modified Dubrova method for different wall movements for a fairly rough wall are shown together with those reported by Ghahramani and Clemence (1980) in Fig. 6.25. It is found that they both follow the same general trend. More importantly, they both indicate that the h_p'-values are practically independent of the seismic coefficient. This is in contrast to the active case in which many investigators found that h_a' increases as the k_h-value increases. Although similar to the active case, the modified Dubrova method also shows that h_p' is practically independent of k or k_h.

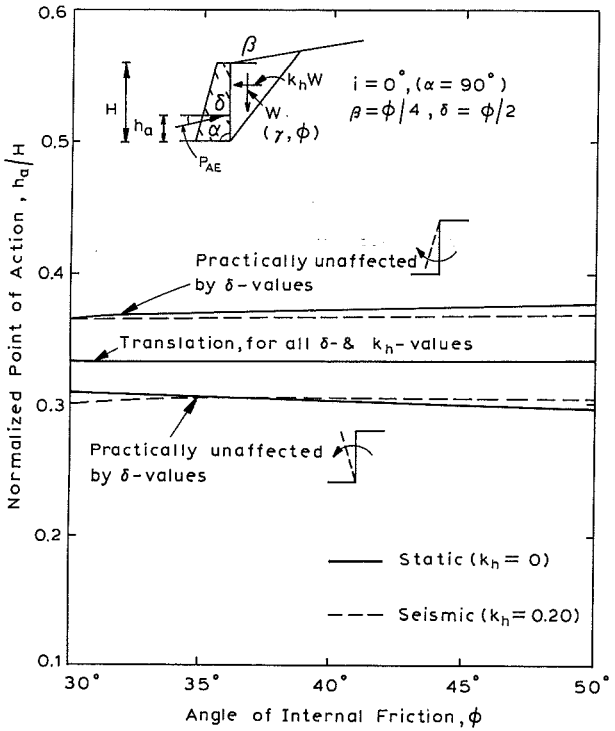

Fig. 6.26. Variation of h_a with ϕ- and δ-parameters for different wall movements.

6.3.5 Effects of strength parameters and geometry of soil-wall system on point of action

In addition to the mode of wall movement that affects the lateral pressure distribution and the point of action of resultant lateral pressure, the h_a- and h_p-values are also dependent on the strength parameters ϕ and δ and the geometry of soil-wall systems, represented by the angle of backfill slope β and the angle of wall repose α or wall tilt angle $i = 90° - \alpha$. The modified Dubrova method is adopted for studying the effects of these factors on the h_a- and h_p-values.

The effects of strength parameters ϕ and δ are first investigated. Figures 6.26 and 6.27 show the variations of h_a and h_p, respectively, with the ϕ- and δ-parameters

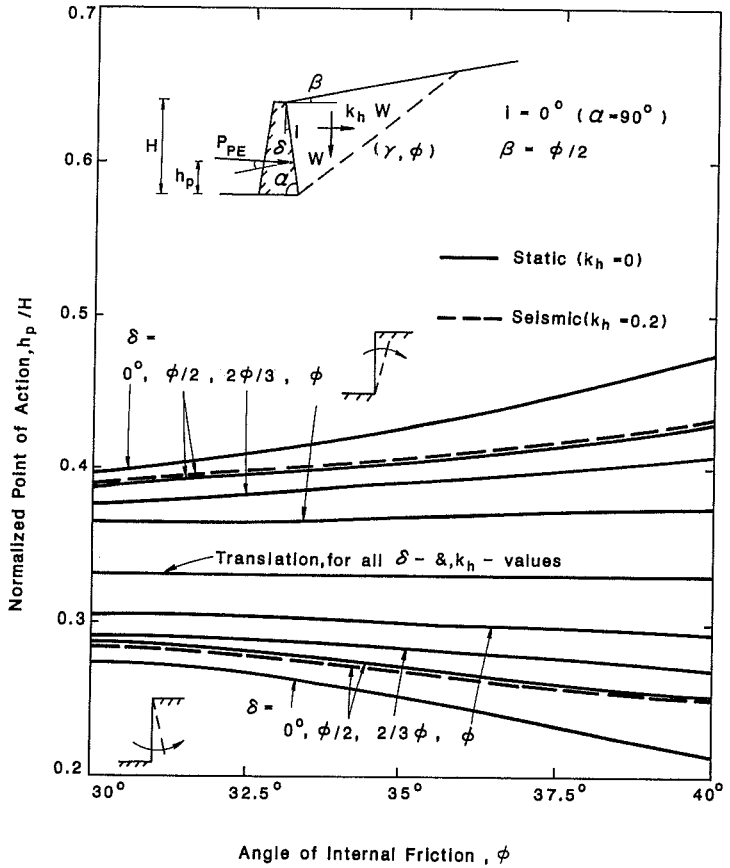

Fig. 6.27. Variation of h_p with ϕ- and δ-parameters for different wall movements.

for different wall movements. It is found that the δ-value has practically no effect on the h_a-values for all modes of wall movement. As found earlier, the h_a-value for the case investigated is also practically unaffected by the presence of earthquakes. Consequently, it can be concluded that the h_a'-value, is also practically unaffected by the δ-value. This is different from that reported by Nandakumaran and Joshi (1973) who found h_a' increases parabolically with increasing δ-value. However, it should be noted that Nandakumaran and Joshi's work is based on a questionable assumption that the static-failure wedge is the same for the seismic condition. Their finding is therefore subjected to question.

In the active case, it is also found that h_a is only slightly affected by the ϕ-parameter for rotational wall movements. For the translation case, $h_a = H/3$ is ob-

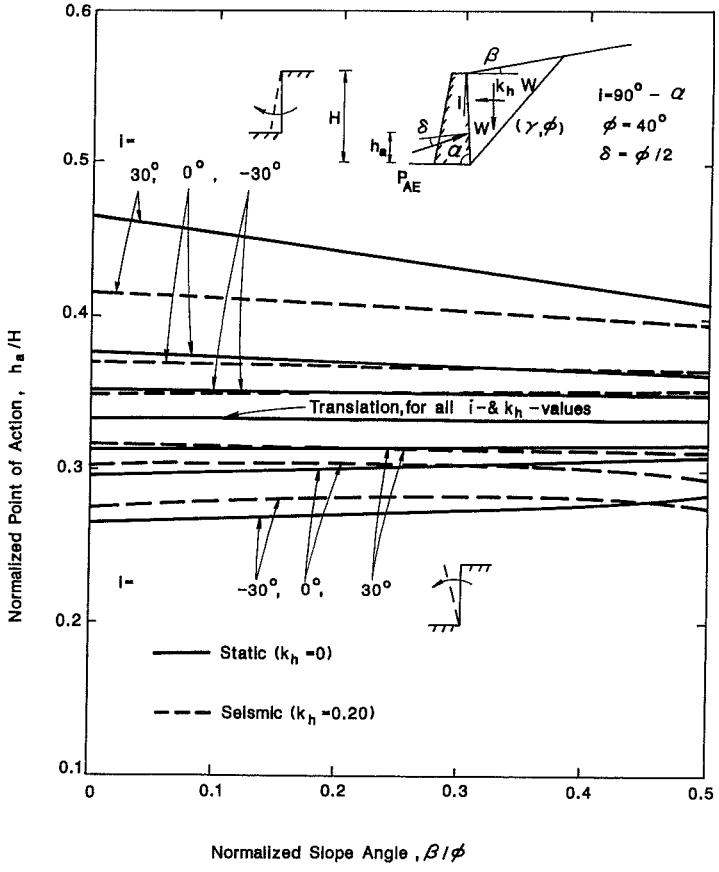

Fig. 6.28. Variation of h_a with geometry of soil-wall system for different wall movements.

tained. It is not only independent of the k_h-value and δ-value, but also independent of ϕ.

In the passive case, although as shown before, h_p-values are practically unaffected by the k_h-value for the cases studied, it does depend on both ϕ and δ except for the translation in which $h_a = H/3$ for all δ- and ϕ-values. As shown in Fig. 6.27, the effects of ϕ and δ on h_p are of the same order for the two basic types of rotational movements. Nevertheless, the effect of ϕ is larger when δ is smaller. In general, h_p increases as ϕ increases for a given δ-value for the rotation about the bottom case. On the other hand, for rotation about the top, h_a decreases as ϕ increases for a given δ-value.

The effects of geometrical factors β and i on the h_a- and h_p-values are presented

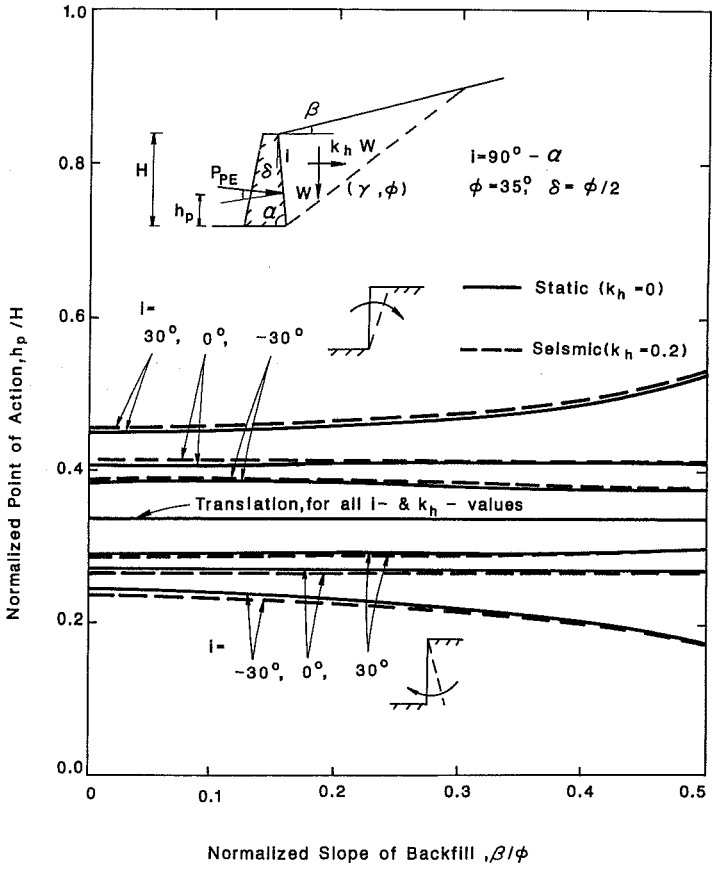

Fig. 6.29. Variation of h_p with geometry of soil-wall system for different wall movements.

in Figs. 6.28 and 6.29. Again, the figures show that for translating walls, the h_a- and h_p-values are equal to $H/3$ and are independent of the geometry.

In the active case, it is interesting to note that the h_a-value is not always independent of the seismic acceleration k_h. When $i = 30°$ in the case of rotation about the top and $i = -30°$, rotation about the bottom, h_a is found to be different for both the static and earthquake cases. This finding is different from that reported earlier based on $i = 0°$. The conclusion that h_a is practically independent of k_h is therefore not always true and it depends on the geometry of soil-wall systems.

Figure 6.28 also shows that h_a decreases as the i-value decreases (or the α-value increases) for both types of rotation. Also, it is found that, in general, the h_a-value for both the static and the earthquake cases, decreases as β increases when the wall rotates about the top. On the other hand, for wall rotating about the toe, it is found that h_a increases slightly as β increases in the static case and h_a has a tendency to decrease with β as $\beta \geq \phi/4$ in the seismic case.

In the passive case, the following points are of interest: (a) h_p is practically independent of k_h for any soil-wall geometry; (b) when $i > 0°$, h_p increases with β for the cases of rotation about the bottom for the rotation about the top; (c) when $i \leq 0°$, h_p decreases very slightly with β for the cases of rotation about the bottom and for the rotation about the top; and (d) the effects of i and β on h_p are of the same order for both types of rotation.

6.4 Evaluation of the modified Dubrova method

The modified Dubrova method developed in this chapter is mainly for the purpose of locating the point of action of the resultant lateral earth pressure. Since it gives a complete pressure distribution for a specified wall movement, the resultant force corresponding to a distribution or a type of wall movement can also be calculated.

In order to study the validity of the method for actual applications, not only the point of action but also the magnitude of the resultant lateral pressure, as obtained by the method, have to be compared with actual field observations.

All the previous results and numerical results for static and seismic cases obtained above based on the modified Dubrova method and the assumed ψ- and δ-distributions for the case of rotation about the toe tend to suggest that the active and passive pressures so obtained are close to the active at-rest and passive at-rest pressures, respectively. However, as pointed out earlier, the full-scale free-standing wall tilting tests conducted by Terzaghi (1934) clearly showed that the total resultant pressure acting on the wall drops off long before an actual slip in the backfill occurs. The validity of the modified Dubrova method for actual applications, therefore, needs a careful evaluation.

6.4.1 Basic assumptions of the modified Dubrova method

The Dubrova method was first developed by Dubrova (1963) for the case of vertical wall and horizontal cohesionless backfill by assuming the validity of the Coulomb solution and the existence of an infinite number of quasi-rupture planes on which the mobilized ϕ-parameter is directly dependent on the amount of wall movement.

The modified Dubrova method developed in this chapter is a direct extension of this method. The Mononobe-Okabe formula, or modified Coulomb's equations, for the seismic active and passive resultant forces are used as the framework for the development of the method. The Dubrova concept of pressure redistribution is used as the basis for taking the wall movement into consideration. The wall friction angle δ is allowed to vary with depth.

Detailed investigation of the methodology proposed by Dubrova (1963) reflects that the basic assumptions of the modified Dubrova method can be summarized as follows.

1. The Mononobe-Okabe solution is assumed to be valid. It assumes that the shear strength is fully mobilized simultaneously along a planar sliding surface passing through the toe of a wall at the instant when the displacement of the wall is just sufficient to bring the soil mass behind the wall to a limiting active or passive state. The soil behind the wall behaves as a rigid body and the seismic accelerations are uniform throughout the entire soil mass so that the effect of earthquake force can be represented by two inertial forces corresponding to the effects of the vertical and horizontal components of the seismic acceleration.
2. There exists an infinite number of quasi-rupture planes on which the average mobilized ϕ-parameter, represented by $\psi(z)$ (where z is the distance from the top of the wall to the point where the assumed quasi-rupture plane of concern intersects the wall), is dependent on, but not proportional to, the amount of wall movement.
3. The mobilized wall friction $\delta_w(z)$ corresponding to each $\psi(z)$ is proportional to $\psi(z)$ such that $\delta_w(z) = m\,\psi(z)$, $m = \delta/\phi \leq 1$.
4. The accumulative resultant active and passive earth pressure at depth z can be obtained by replacing H with z, ϕ with $\psi(z)$, and δ with $\delta_w(z)$ in the Mononobe-Okabe equations, Eqs. 6.1 and 6.5, in which ϕ and δ are assumed constant with depth, even though both $\psi(z)$ and $\delta_w(z)$ may be variables and functions of the depth z.
5. The functions $\psi(z)$ and $\delta_w(z)$ and their derivatives are continuous. It should be noted that this assumption is necessary for avoiding unrealistic jump in the calculated pressure distribution.

6.4.2 Failure mechanisms for free-standing rigid retaining walls

In evaluating the validity of Coulomb's solution, Terzaghi (1936) pointed out that in the case of outward wall movement, the lateral yield of retaining walls is also 'always' sufficient to mobilize at least the major part of the shearing resistance along the sliding plane which separates the sliding wedge from the soil mass. There is no doubt about this for the case of translation and rotation about the top. This is because a distinct sliding surface passing through the toe is always developed at the early stage of tests for these two modes of movement (James and Bransby, 1970), although it should be recognized that the sliding surface is generally curved for the case of rotation about the top, even in the active pressure case.

For the case of passive rotation about the toe, James and Bransby's model test results (James and Bransby, 1970) clearly showed that rupture starts near the top and propagates downward as the amount of rotation increases. A distinct rupture surface is only found after a considerable rotation when the soil mass behind the wall reaches a limiting, impending collapse state. Their results showed that this distinct rupture surface intersected the wall at about mid-height rather than passing through the toe.

The findings of James and Bransby (1970) indicate that rupture surfaces are first observed at the top of the wall, not near the toe, as would be anticipated from conventional earth pressure theories. For this reason, they indicated that the simple failure mechanisms, as adopted in most conventional methods of earth pressure analysis, do not occur for the case of rotation about the toe.

The same mode of wall movement for the active case has been studied by Kezdi (1958). His experimental results on a model wall continuously rotating about the toe clearly show the progress of failure. Among the important findings observed by him are:

1. A continuous surface of sliding develops after a certain amount of rotation only.
2. The distinct sliding surface does not go through the toe and instead it intersects the wall at a height h_0 about the toe, in which h_0 is dependent on soil characteristics and the amount of rotation.
3. Definite slides rather than uniform deformation is found in the sliding mass.

These findings clearly indicate that rupture pattern as observed for the active rotation about the toe case is similar to that postulated based on the passive test results (Fig. 6.2). He has pointed out that it is obviously wrong to consider a surface on which there is no displacement at all, as a surface of sliding. The sliding surface passing through the toe as assumed in conventional limit equilibrium solutions based on wedge theory is, in fact, a surface on which the force of reactions is corresponding to the 'earth pressure at rest' condition.

Based on the above considerations, use of conventional analytical method for determining lateral earth pressures is therefore improper for the case of rotation about the toe. It should be kept in mind that all the limit equilibrium and limit analysis methods are generally subjected to the limitation that the validity of the solution is highly dependent on whether the failure mechanism assumed is proper or not.

6.4.3 Characteristics of the modified Dubrova method

The discussion of the preceding section tends to suggest that the modified Dubrova method, which is based on the assumption that the Mononobe-Okabe equations are valid for determining the resultant active and passive earth pressures, is applicable to the cases of translation and rotation about the top. The implication of this can be clearly seen from Eq. (6.2) or Eq. (6.6), which is the consequence of Assumption (4).

Based on Eq. (6.2), the accumulative resultant pressure at depth z can be obtained by inputting the ψ- and δ_w-values corresponding to that depth into the equation. For both the translation and rotation about the top, the ψ-distributions with $\psi_l = \phi$ are assumed. Also based on Assumption (3), $\delta_w = m\,\psi_l = \delta$ is assumed at the toe in both cases. Consequently, both types of movement give exactly the same expression for the accumulative resultant active force, which is actually the original Mononobe-Okabe equation, Eq. (6.1). This explains why the K_A-values as obtained on the basis of the modified Dubrova method and the recommended ψ-distribution as shown in Section 6.3 are exactly the same for the cases of translation and rotation about the top.

On the other hand, for the cases of rotation about the toe, the ψ-distribution with $\psi_l = \psi_a$, in which $\psi_a = \phi_0$ for the case of $\beta = 0$, is generally assumed. Also $\delta_w = m\,\psi_a$ at the toe. Consequently, at depth $z = H$, for the case of $i = 90°$ and $\beta = \delta_w = \theta_k = k_v = 0$, Eq. (6.2) becomes:

$$P = \frac{\gamma H^2}{2}\left(\frac{\cos\phi_0}{1 + \sin\phi_0}\right)^2 = \frac{\gamma H^2}{2}\left(\frac{1 - \sin\phi_0}{1 + \sin\phi_0}\right) \tag{6.20}$$

This is exactly the active at-rest pressure. Similarly, for the passive case, Eq. (6.6) gives:

$$P = \frac{\gamma H^2}{2}\left(\frac{\cos\phi_0}{1 - \sin\phi_0}\right)^2 = \frac{\gamma H^2}{2}\left(\frac{1 + \sin\phi_0}{1 - \sin\phi_0}\right) \tag{6.21}$$

This is exactly the passive at-rest pressure. The reason why, for rotation about the toe, the resultant lateral force obtained based on the modified Dubrova method and the recommended ψ-distribution equals to the at-rest pressure is therefore apparent.

In fact, the finding in Section 6.3.2 that the resultant lateral force obtained based on the modified Dubrova method depends only on the ψ_l-value is simply the direct consequence of Assumption (4). However, this unique outcome is not actually observed. It is generally recognized that rotation about the top gives slightly higher K_A-value than translation does; whereas, the modified Dubrova method gives the same K_A-values for both cases. Its actual applicability therefore, needs further justification.

6.4.4 Validity of the modified Dubrova method in practical applications

Based on the discussion given above, it appears that the modified Dubrova method is strictly applicable only to the cases of translation and rotation about the top, in which a distinct sliding surface passing through the toe actually develops at the limiting state. The limiting active and passive pressures obtained based on the method and the properly assumed ψ- and δ-distributions are, however, justified only if the actual sliding surface is essentially planar, which is seldom true for rotation about the top (Terzaghi, 1941).

The method does not appear applicable to the case of rotation about the toe for determining the limiting lateral earth pressures, since the assumed failure mechanism is inconsistent with actual observations. Moreover, although a ψ-distribution more realistic than that recommended can be assumed based on the work of Kezdi (1958), Eq. (6.2) tends to indicate that the total resultant pressure as obtained will not be affected once $\psi_l = \psi_a$ is selected. This is also clearly reflected in Figs. 6.6 and 6.7. Changes of the ψ-value at the top, ψ_u, and the shape of the ψ-distribution seem to affect only the shape of the resulting lateral pressure distribution, and consequently the point of action of the resultant force. Hence, it seems that the lateral earth pressure corresponding to the limiting state for the case of rotation about the toe cannot be simply solved by improving the assumed ψ-distribution. The method can therefore be applied to this type of movement only if the actual wall displacement is somewhat restricted at the top.

In general, the point of action for the resultant lateral pressure is only directly influenced by how the ψ-distribution assumed differs from the uniform distribution. If a ψ-distribution is properly assumed based on actual field observations, the point of action as obtained by the modified Dubrova method could be a reasonable estimate.

The work of Kezdi (1958) tends to indicate that for retaining walls tilting about the toe, a ψ-distribution (should be continuous according to Assumption (5) before) with steeper slope at the upper part and gentle slope at the lower part, is more realistic. The results of James and Bransby (1970) also tend to indicate that similar kind of ψ-distribution is more realistic for passive rotation about the toe. Based on Figs. 6.6 and 6.7, the h_a-value obtained by using this kind of distribution is smaller

than that obtained by using a linear ψ-distribution. The reverse is found for the h_p-value. Hence, use of the h_a- and h_p-values as shown in Section 6.3 will result in a slightly larger overturning moment and slightly smaller resisting moment than if a close-to-real ψ-distribution is assumed. These h_a- and h_p-values could be useful if the actual wall displacement is close to what is assumed.

The active and passive earth pressures as obtained by the modified Dubrova method based on the recommended linear ψ-distribution, although not representative of the limiting active state, correspond to the pressure when the outward and inward rotations, respectively, are just enough to bring the soil right near the top of the wall to limiting active and passive states. At shallow depths, where the confining pressures are very small, the shear strength needs only a very small amount of displacement to reach its full mobilization, which can be seen from conventional triaxial test results. This is especially the case for failure due to lateral extension, which represents the mode of active failure. It is therefore expected that major portion of the soil is still essentially under the at-rest condition while the soil right near the top first reaches a limiting state. Assuming that there is a quasi-sliding surface, on which the mobilized ϕ-value is equal to ψ_a, passing through the toe appears reasonable in this case. The results are, therefore, representative of the condition of wall movement just described. Although, the distributions of lateral pressure are different from those corresponding to the completely at-rest states, the resultant lateral pressures, which are exactly the same as the at-rest pressures, also seem reasonable.

In fact, based on the assumption that there is a quasi-sliding surface, on which the mobilized ϕ-value is equal to ψ_a (passing through the toe), the long time unsolved problems of evaluating the increase in at-rest pressure as the result of an earthquake can be easily handled by using the modified Dubrova method. By assuming a uniform ψ-distribution with $\psi = \psi_a$, or ϕ_0 for the case of $\beta = 0$, both the static and the seismic at-rest pressures corresponding to either the active or the passive condition can be calculated. This could be of practical value for the case in which the retaining structures are rigidly connected and they move together with the surrounding soil mass during earthquake.

In short, the modified Dubrova method, if properly used, could be a useful tool in actual design applications. However, its limitations should always be recognized in order to gain benefits from it.

To sum up, the study of the point of action of the resultant lateral pressure shows that the point of action is highly dependent on the mode of wall movement for both static and earthquake cases. Results of analysis based on the proposed modified Dubrova method show that the point of action for both active and passive translational movements is always at $H/3$. The distribution of translation pressure is always linear whether there is an earthquake or not, if the ultimate state is reached.

For the rotation about the top of wall, $h_a > H/3$ and $h_p < H/3$ are found for the active and the passive cases, respectively. On the other hand, for the rotation

about the toe of the wall, $h_a < H/3$ and $h_p > H/3$ are obtained. The h_a-value is found practically independent of the seismic acceleration when $i \leq 0°$ for the rotation about the top and $i \geq 0°$ for the rotation about the toe. The h_p-value, however, is found practically unaffected by the presence of earthquakes.

Comparison of results obtained by the modified Dubrova method with others shows that the h_a- and h_p-values obtained by the proposed method are, in general, closer to the hydrostatic value of $H/3$, than the others for all types of wall movement. This is probably the consequence of the fact that the strength parameters adopted in the proposed method, $\psi(z)$ and $\delta_w(z)$, are allowed to vary with depth according to the nature of the wall movement; whereas, $\psi = \phi$ and $\delta_w = \delta$ are generally assumed by the others.

The modified Dubrova method, which allows the distribution of lateral earth pressure corresponding to each stage of wall yielding to be calculated, shows that the resultant lateral pressure is governed only by the assumed ψ-value at the toe. This special characteristic of the method can be clearly seen from Eqs. (6.2) to (6.5). Of secondary importance are the difference between the two extreme ψ-values and the shape of the ψ-distribution assumed.

For the case of rotation about the toe, in which $\psi = \psi_a$ is assumed at the toe, the active and passive pressure distributions do not shift considerably from the at-rest pressure distribution curve. On the other hand, for the case of rotation about the top, for which $\psi = \phi$ is assumed at the toe, both the active and passive pressure distributions shift gradually from the active and passive at-rest distribution curves, respectively, to those close to the ultimate translational pressure distribution curves. It is therefore concluded that once the two extremes of the ψ-distribution, especially that near the toe, are properly selected based on the consideration of the change in stress state in the backfill during wall yielding, the lateral earth pressure distribution corresponding to the condition of the displacement specified can be reasonably assessed by the modified Dubrova method.

Parametric studies show that

1. h_a is practically unaffected by ϕ and δ;
2. h_a is affected by i and is moderately affected by β only when i is much larger than zero in the case of rotation about the top and when i is much smaller than zero in the case of rotation about the toe;
3. ϕ, δ and i, β all affect the h_p-value for the case of rotation about the toe as much as that for the case of rotation about the top;
4. h_p is practically unaffected by β when $i \leq 0°$ for the case of rotation about the toe and when $i \geq 0°$ for the case of rotation about the top.

Overall evaluation of the modified Dubrova method reflects that the method, although it has its limitations, can be applied to several earth pressure problems. The resultant lateral earth pressure and its point of action for the cases of translation and rotation about the top can be reasonably assessed by the method based on the recommended linear ψ-distribution, if the actual sliding surface is planar. For rotation about the toe, the method is not strictly applicable for determining the lateral earth pressures corresponding to the limiting active and passive states. The method, however, could be used for determining the seismic at-rest pressure acting on a rigidly connected box structures, if there is no relative displacement between the structures and the surrounding soils during earthquake. In actual applications, the limitations of the modified Dubrova method, nevertheless, should always be recognized.

A computer program developed for calculating the lateral earth pressures based on the modified Dubrova method is given in the thesis by Chang (1981).

6.5 Effects of wall movement on lateral earth pressures

Although the mode of wall movement is seldom specified in the development of most classical earth pressure theories, it has been reported that both the magnitude of resultant lateral pressure and its point of action are highly dependent on the wall movement. The effect of wall movement on the point of action of the resultant lateral force has been treated in Sections 6.1 to 6.4. This section intends to explore its effect on the resultant lateral pressures, which are generally expressed as the dimensionless coefficients K_A and K_P for the static case or K_{AE} and K_{PE} for the seismic case.

Results of the limit analysis which represent the resultant lateral pressure for translational wall movement and results obtained by the modified Dubrova method as described in the preceding section are selected for comparison with those obtained by others for which wall movement has been considered. The modified Dubrova method, theoretically, can yield the lateral earth pressure corresponding to any specified mode of wall movement if the distribution of mobilized strength corresponding to the specified wall movement can be reasonably assumed. However, only results for purely active and purely passive translational and rotational wall movements are considered here.

6.5.1 Effects of wall movement on static and seismic active earth pressures

The modified Dubrova method is versatile in that the effect of wall movement, which affects the distribution of lateral earth pressure, can be incorporated into the analysis. However, it should be kept in mind that the method is developed based on the assumption that the Mononobe-Okabe, or the modified Coulomb solution is valid for assessing the resultant seismic lateral forces.

For the solutions of the modified Dubrova method to be justified, the assumed mechanism of failure has to be close to the reality in the first place. For the cases of rotation about the top and translation, it has been experimentally observed that

a distinct failure surface does run through the toe as was assumed by Coulomb. Hence, it is expected that the K_A- and K_{AE}-values obtained by the modified Dubrova method could be practically acceptable, if the actual failure surface is essentially planar, and the distributions of mobilized ϕ- and δ-values, i.e., ψ and δ_w can be reasonably assumed.

For the case of rotation about the toe, it has been reported by Kezdi (1958) that it is obviously wrong to consider that there is a planar failure surface running through the toe. The most critical sliding plane as assumed in Coulomb wedge analysis is actually a plane corresponding to the earth pressure at rest condition since

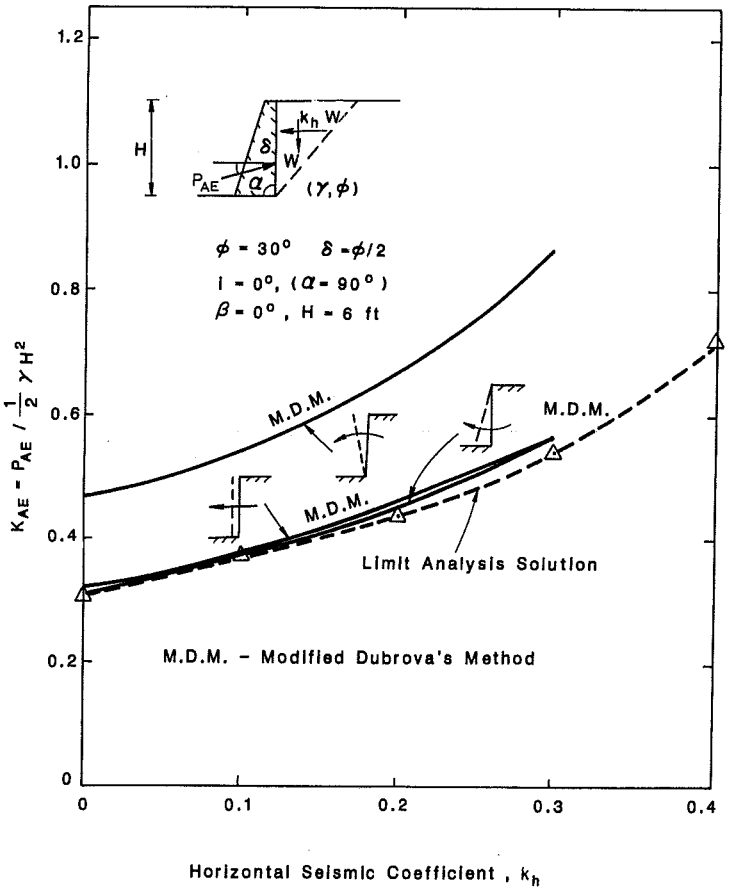

Fig. 6.30. Comparison of K_{AE}-values obtained by the modified Dubrova method with the translational K_{AE}-values obtained by limit analysis.

there is no displacement occurring on this plane at all. He found that even in the ultimate stage of the rotation, the actual sliding plane last developed runs into the wall at certain height h_0 above the toe, in which h_0 is function of soil characteristics and the amount of rotation. Hence, it is expected that the results obtained by the modified Dubrova method and the recommended distributions of ψ and δ_w are only corresponding to the state at which the backfill near the top just reaches limiting equilibrium. The K_A- and K_{AE}-values so obtained are, therefore, close to the at-rest values. This can be seen from Table 6.1, in which $K_A \approx K_0 = 1 - \sin \phi = 0.50$ is shown for this case. They are not representative of the actual active states. Therefore, they should not be used for design purpose, unless the wall movement expected is consistent with that assumed.

The upper bound limit analysis, such as that developed earlier in previous chapters is based on a more flexible log-sandwich mechanism of failure. However, at present, it has been formulated for the case of translation wall movement only. Hence, it is expected that the results are applicable only when the wall movement is predominantly translational, theoretically speaking.

Figure 6.30 shows the results on K_{AE} for three different modes of wall movement as obtained by the modified Dubrova method for earthquakes of different magnitude. The translation K_{AE}-values as obtained by the upper bound limit analysis are also shown in the figure. It is noted that both the translation and the rotation about the top give identical K_{AE}-values based on the modified Dubrova method. The K_{AE} for rotation about the toe, which is more representative of the at-rest condition, is much higher. The translational K_{AE} as obtained by the limit analysis is found practically the same as that based on the modified Dubrova method.

The active earth pressure problem has also been studied by Prakash and Basavanna (1969). Their method of analysis is based on the consideration of equilibrium of both force and moment on an assumed triangular failure wedge. They tried to differentiate sliding wall from tilting wall by optimization with respect to active force and with respect to overturning moment, respectively. Results obtained by them are compared with those by the modified Dubrova method in Fig. 6.31. It is found that for both sliding and tilting walls, Prakash and Basavanna's solution is very close to the solutions of the modified Dubrova method for the rotation about the top and the translation cases. The K_{AE}-values for the rotation about the toe case as obtained by them are found close to the translational K_{AE}-values, which are much more close to the reality than the solution of the modified Dubrova method does.

6.5.2 Effects of wall movement on static and seismic passive earth pressures

In the passive earth pressure case, the actual failure surface is generally curved, especially when the α-angle, and ϕ-, δ-values are high. Hence, similar to Coulomb's,

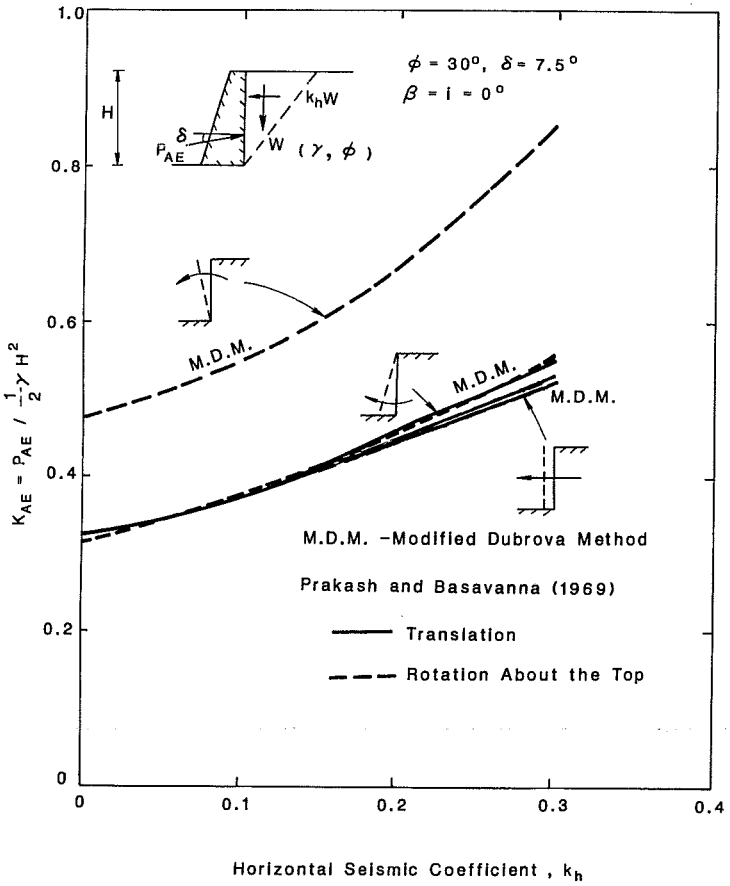

Fig. 6.31. Comparison of K_{AE}-values obtained by the modified Dubrova method with solutions of Prakash and Basavanna (1969).

the K_P- and K_{PE}-values obtained by the modified Dubrova method are generally too high if the most critical sliding surface is far from being planar. For this reason, it is suggested that Dubrova's concept can be more reasonably applied to the passive pressure problem, if the basic framework of the formulation is based on equations developed by assuming a nonplanar sliding mechanism, such as that shown in Chapter 5, rather on the modified Coulomb or the Mononobe-Okabe equation.

Nevertheless, the modified Dubrova method gives K_{PE}-values for three different kinds of wall movement. When ϕ and δ are small and $\alpha \leq 90°$, the overestimation of K_{PE}-values may not be too serious. Comparing these results with the limit

analysis solutions, which are based on a more reasonable log-sandwich failure mechanism, is therefore worthwhile. The comparison is shown in Fig. 6.32.

Similar to the active case, translation wall movement and rotation about the top give practically identical K_{PE}-values based on the modified Dubrova method. The case of rotation about the bottom, however, gives the lowest K_{PE}-values, which as explained before, are more representative of the passive at-rest values (see Table 6.2).

Since planar quasi-sliding surfaces are assumed in the modified Dubrova method, while a more reasonable log-sandwich mechanism of failure is assumed in the limit analysis method, the K_{PE}-value obtained by the limit analysis is therefore, as ex-

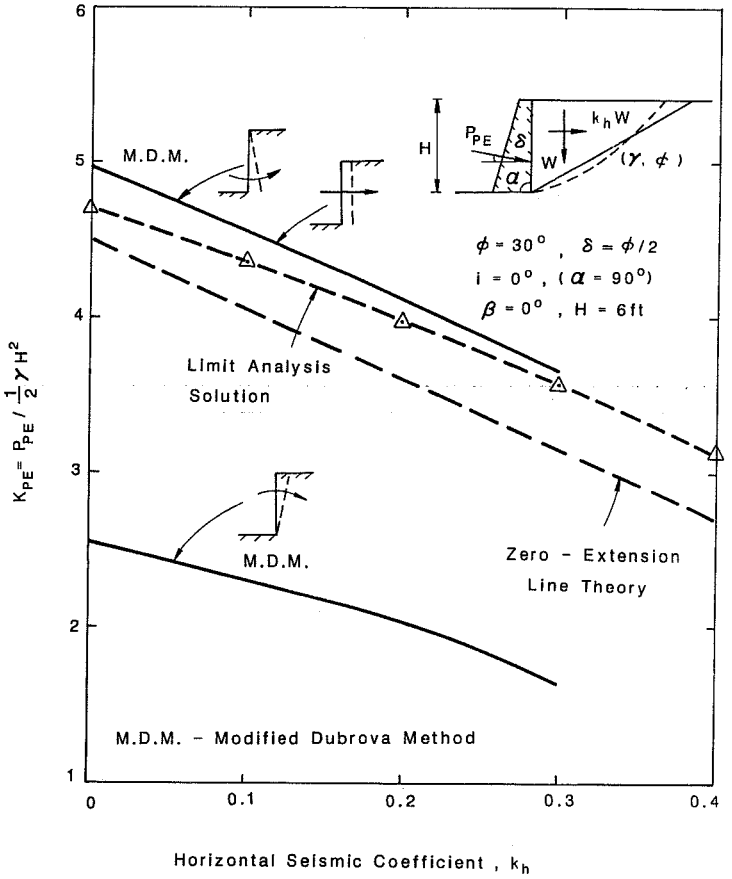

Fig. 6.32. Effect of wall movement on static and seismic passive earth pressures.

pected, lower than that of the modified Dubrova method for the translation case to which the limit analysis method is applicable.

A study of seismic passive earth pressure was recently published by Ghahramani and Clemence (1980). Based on the zero-extension line theory, a method was developed by them for evaluating the seismic increment of passive earth pressure. They suggested that their work can be combined with Habibagahi and Ghahramani (1979) for obtaining the resultant seismic passive earth pressure.

Since in the passive earth pressure case, a reduction rather than an increase in passive resistance of a soil – wall system is of concern to us, instead of adding the seismic increment to the static passive earth pressure as that was done by Ghahramani and Clemence (1980), it is suggested that the seismic increment should be substracted from the static pressure to give the resultant seismic passive pressure. Some results so obtained for the translation case are shown in Fig. 6.32 for comparing with solutions of the modified Dubrova method and the limit analysis method. It is found that the zero-extension line solution is lower than the limit analysis solution as well as the solution of the modified Dubrova method.

The zero-extension line solution is based on a log-sandwich failure mechanism as the limit analysis method does. However, limiting equilibrium of force, rather than equilibrium of energy as adopted in the limit analysis, is considered in both Habibagahi and Ghahramani (1979) and Ghahramani and Clemence (1980). This difference may be somewhat responsible for the discrepancy between the two solutions. However, in general, most stability solutions considering overall limiting equilibrium are still considered as upper bounds to the exact solution. The fact that the zero-extension line solution for the translational mode of wall movement is lower than the limit analysis solution and the solution of the modified Dubrova method for the same mode of wall movement tends to indicate that the zero-extension line theory gives the best result at least for the particular case studied.

By assuming different distributions of seismic acceleration for different modes of wall movement, Ghahramani and Clemence (1980) based on their proposed method found that for the same maximum k_h-value, translation wall movement produces the maximum seismic increment of passive earth pressure. They also found that rotation about the top creates about $\frac{2}{3}$ of the translation force, and rotation about the bottom creates $\frac{1}{3}$ of the translation force. Based on their findings, K_{PE}-values for the case of $\phi = 30°$, $\delta = 15°$, and $\beta = i = 0°$ are calculated. They are shown together with those obtained by the modified Dubrova method in Fig. 6.33. It is found that the ΔK_{PE}-values obtained by both methods are practically the same for translational wall movement. The ΔK_{PE}-values for both rotational wall movements as obtained by the modified Dubrova method are much higher than those based on Ghahramani and Clemence (1980). The fact that the K_{PE}-value obtained by the modified Dubrova method is close to the passive at-rest value, instead of the limiting passive state value, is probably partially responsible for the high ΔK_{PE}-value obtained for the case of rotation about the toe.

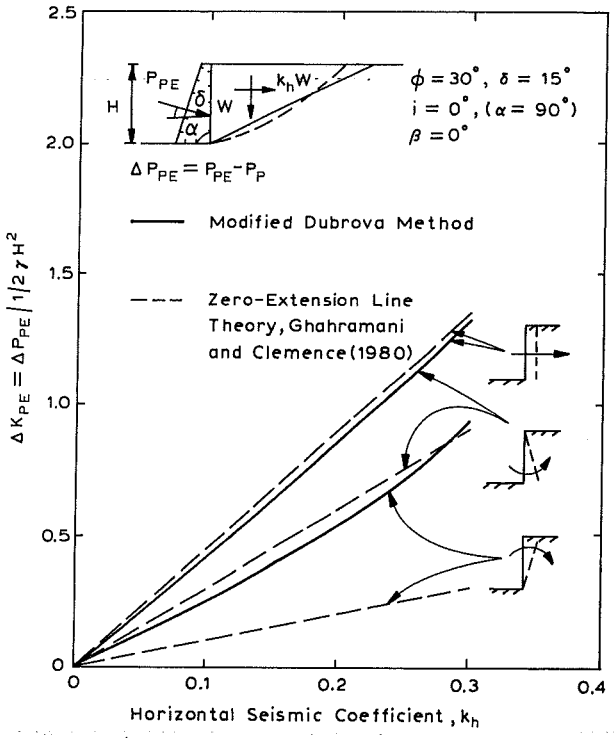

Fig. 6.33. Comparison of ΔK_{PE}-values obtained by the modified Dubrova method and the zero-extension line theory.

In summary, the mode of wall movement affects not only the point of action of resultant lateral earth pressure, but also the magnitude of the lateral pressure. It is found that the K_{AE}- and K_{PE}-values for the case of rotation about the top are practically identical to those for the case of translation. Based on the modified Dubrova method and the recommended distribution of ψ and δ_w, the rotation about the toe case gives the highest K_{AE}-value and the lowest K_{PE}-value, which are in reality close to the active and passive at-rest coefficients of earth pressure, respectively.

Comparison of the results of the modified Dubrova method with other solutions shows that for the case of translation, the K_{AE}-value obtained by the method is practically the same as the limit analysis solution and the solution of Prakash and Basavanna (1969). The translation K_{PE}-value obtained by this method is, however, higher than the limit analysis solution and the solution of Ghahramani and Clemence (1980). It seems clear that the zero-extension line theory gives the best result in this case.

In the active case, the K_{AE}-value for the case of rotation about the toe as found by Prakash and Basavanna (1969), which is close to the solution for the translation case, seems reasonable. The K_{AE}-value for this case as obtained by the modified Dubrova is more representative of the at-rest pressure.

By comparing the ΔK_{PE}-values to different wall movements obtained by the modified Dubrova method and those calculated based on Ghahramani and Clemence (1980), it seems that the values are the same for the translation case. For rotational cases, the ΔK_{PE}-values as obtained by the modified Dubrova method are higher.

6.6 Earth pressure theories for design applications in seismic environments

Since earthquake forces are of oscillatory nature, design of retaining structures in seismic-active zone based on displacement consideration seems to be more realistic. While a step-by-step dynamic analysis seems more rigorous, it requires accurate earthquake data, advanced constitutive models of soils, and sophisticated numerical techniques. A simplified displacement analysis as that described by Richards and Elms (1979) may be more promising. Nevertheless, the conventionally adopted design procedure based on ultimate load and empirical factors of safety still has the advantage of being simple and having high acceptability.

For designing rigid retaining structures in seismic environments, the first step is to obtain required earthquake data. If a quasi-static approach is to be adopted in the analysis of seismic lateral earth pressure, the seismic coefficients can be assessed by methods such as that suggested by the Japanese Society of Civil Engineers (1980), that recommended by Prakash (1981), and that summarized by Emery and Thompson (1976).

Once the input earthquake information is ready, evaluation of seismic lateral earth pressure becomes the primary step to ultimate-load-based design of retaining structures. In displacement-based design, however, assessment of seismic lateral earth pressure is also absolutely necessary. This information is required when evaluating the yield acceleration, which is the acceleration over which the safety factor against the specified failure mechanism is less than one and permanent displacement is bound to occur. Hence, no matter which design method is used, seismic lateral earth pressure should be carefully evaluated.

Most earth pressure theories are developed on the basis of different assumptions. Results of analysis based on different theories usually differ from one another. Furthermore, they are all subjected to certain limitations and may be suitable only for a certain type of wall movement. For these reasons, in selecting earth pressure theories for practical applications, the expected field conditions should be carefully considered. The assumptions behind each earth pressure theory and its limitations should be fully understood. No matter which design method is to be adopted, selection of a proper earth pressure theory or analytical method is of great importance.

This section attempts to compare some well-known earth pressure theories or analytical methods that are suitable for assessment of seismic lateral earth pressures. For practical reasons, only those methods essentially based on the perfect plasticity or the limiting state equilibrium, which are practically applicable to rigid retaining wall problems, are included. Methods based on elastic wave theory and approaches based on elasto-plastic and nonlinear theory are not considered here.

6.6.1 Analytical methods for determining seismic active earth pressure

The first well-known method for seismic earth pressure analysis, the Mononobe-Okabe (M-O) method was developed fifty years ago based on the Coulomb's wedge theory (Okabe, 1926; Mononobe and Matsuo, 1929). The analysis method has been widely used in current practice of retaining wall design. Basic assumptions of the M-O analysis, which is applicable to a soil – wall system with general configuration, dry cohesionless backfill, and zero surcharge, are:

1. The failure surface is planar and passes through the toe.
2. The backfill material is perfectly plastic and the wall displacement is sufficient to produce a limiting equilibrium state so that shear strength along the failure plane is fully mobilized simultaneously.
3. The soil wedge acts as a rigid body so that the vertical and horizontal seismic accelerations in the wedge are uniform and have the same magnitude as the base of the wall.
4. The lateral earth pressure increases hydrostatically with depth.

For the active earth pressure case in which the most critical sliding surface is essentially planar in most cases and the soil – wall interaction effect or/and progressive failure phenomena is not very significant, use of the M-O analysis is practically desirable. The analysis has been shown to be reasonable by several experimental works. Probably for these reasons, the method is commonly used in determining the seismic active earth pressure in ultimate-load-based design of retaining structures.

Although, boundary deformation condition is not considered in the formulation of the M-O method, it seems that the solution is applicable to the cases of translation movement and rotation about the top in which a distinguished failure surface passing through the toe is actually developed as found by James and Bransby (1970) in a passive pressure model study. However, the point of action of the resultant force as suggested by Mononobe and Okabe may need further revision by considering the wall movement effect and the earthquake magnitude.

The M-O method has been modified and simplified by Seed and Whitman (1970). Suggestions have been given by them for actual design applications. They suggested that for practical purpose, K_{AE} can be estimated as $K_A + \frac{3}{4} k_h$. In other words, the seismic active earth pressure can be calculated as:

$$P_{AE} \simeq \tfrac{1}{2}\gamma H^2 (K_A + \tfrac{3}{4} k_h) \qquad (6.22)$$

In particular, they suggested that the value $h_a = (H/3)$ obtained by Prakash and Basavanna (1969) can be used for locating the point of action of the resultant active force. Or for practical purpose, they suggested that the seismic increment of pressure can be assumed to act at $0.6H$ above the bottom and the static active pressure at $h_a = H/3$.

Based on essentially the same concept and assumptions as the M-O analysis, Prakash and Saran (1966) developed dimensionless earth pressure factors for active earth pressure analysis and assumed that the principle of superposition is valid. The earth pressure factors they developed are applicable to cohesive horizontal backfill with tension cracks considered. It seems that the method is a great improvement if the backfill does contain a large amount of cohesive material. However again, the method has the same limitations as the M-O analysis does. The point of action, h_a, is taken as H/3, which is similar to the M-O analysis.

Determination of the point of action, which is the center of dispute of the applicability of the M-O analysis, has been attempted by Prakash and Basavanna (1969). By making an assumption regarding the distribution of vertical pressure on any surface parallel to the ground surface, they were able to consider force and moment equilibrium of a triangular sliding wedge. Again, by making the assumptions similar to the M-O analysis, they developed a method for calculating the active moment, active force, and the point of action, h_a. By optimizing the active moment and the active force, respectively, they were able to make distinction between wall tilting (rotating about the toe) and wall sliding (translating).

The method, which is applicable to the case of cohesionless backfill with zero surcharge, gives a complete information on the distribution of active earth pressure. It is very promising. However, based on this method, the difference in pressure distribution for the two types of wall movement is very small, especially when the seismic coefficient is small ($k \leq 0.15$). In fact, it is understandable that the pressure distribution for wall translating and wall rotating about the toe can give significantly different pressure distributions even in the static case. The validity of differentiating the two different types of wall movement by optimization with respect to different physical components is therefore somewhat in doubt.

The limit analysis method as developed in previous chapters based on the upper-bound technique of perfect plasticity is capable of solving the lateral earth pressure problems for a general soil – wall system in earthquake environments. It has been described in detail in previous chapters.

By using the concept of virtual work, or energy equilibrium, the limit analysis method is theoretically developed based on a translational wall movement. However, the log-sandwich mechanism assumed in the formulation is well representative of the actual failure condition for the case of translation and fairly representative of that for the case of rotation about the top (James and Bransby, 1970). It is suggested that the estimated lateral earth pressure is suitable for the above two types of wall movement.

Similar to most limit equilibrium methods, the limit analysis method gives no information on the point of action. For practical applications, it is suggested that earth pressure tables developed in Chapter 5 based on the limit analysis method can be adopted for determining the K_{AE}-values for both cases of translation and rotation about the top of wall movement, while, the modified Dubrova method as described in this chapter is recommended for assessing the corresponding point of action.

The modified Dubrova method developed based on Dubrova's idea (Dubrova, 1963), which is applicable only to cohesionless soils, is theoretically capable of assessing both the magnitude of lateral earth pressure and the point of action of the resultant force, or the lateral pressure distribution, for different modes of wall movement.

This modified method is based on the framework of the M-O equations. The assumptions are therefore similar to those in the M-O analysis, except that strength in the backfill is assumed to mobilize to that somewhat in proportion to the amount of wall displacement. Detailed formulation and description of the method have been given in Chapter 5.

Comparison of those analytical methods as described above are tabulated in Table 6.7. For comparison of numerical results as obtained by these methods, two examples are given. The results are listed in Tables 6.8a and 6.8b. In the tables, K_A, K_{AE}, and ΔK_{AE} are listed. The corresponding points of action, static h_a, seismic h_a, and increment h_a' are also listed in the tables. Dimensionless normalized overturning moment, $M_o = K_A(h_a/H)$, is also calculated for each analytical method and used as a basis for comparison.

From Tables 6.8a and 6.8b, it seems that for the cases of translation and rotation about the top, all methods given essentially the same K_A- and K_{AE}-values, since in the active case the actual failure surface is practically planar. The major difference among them is on the h_a-value.

Based on the modified Dubrova method, the h_a-value is found higher for the case of rotation about the top than for the translation case. Consequently, as expected, the M_o-value is larger for the case of rotation about the top.

For the translational wall movement, the h_a'-value suggested by Seed and Whitman (1970), $h_a' = 0.6\,H$, and that calculated by Prakash and Basavanna (1969) for the case of $\alpha = 90°$, $\beta = 0°$, $\phi = 30°$, $\delta = 7.5°$ and $k_h = 0.15$, $h_a' = 0.64\,H$, are much larger than those based on other methods that give $h_a' = 0.33\,H$. Consequently, the overturning moments as obtained by them are much larger than the others. However, based on Prakash and Basavanna (1969), the h_a-value for the static translation case, of which the distribution is generally recognized as practically

TABLE 6.7
Comparison of analytical methods for seismic active earth pressure analysis

Methods	Basis	Mode of movement	Failure mechanism	Analytical techniques	Applicable soil-wall conditions	Results given	Remarks
M-O analysis and Seed and Whitman (1970)	Coulomb's wedge theory	Not specified	Planar	Limiting force equilibrium, quasi-static	General soil-wall configuration, ϕ-soils, no surcharge	K_{AE}	$h_a' = 0.6\,H$ is recommended by Seed and Whitman (1970)
Prakash and Saran (1966)	Coulomb's wedge theory	Not specified	Planar	Limiting force equilibrium, quasi-static	General soil-wall system with horizontal backfill	K_{AE}	Considers tension cracks
Prakash and Basavanna (1969)	Couloumb's wedge theory	Translation and rotation about toe	Planar	Force and moment equilibrium, quasi-static	General soil-wall configurations, ϕ- soils, no surcharge	K_{AE}, h_a	
Limit analysis	Upper-bound limit theorem	Translation	Log-sandwich	Energy equilibrium, quasi-static	General soil-wall system	K_{AE}	
Modified Dubrova method (M.D.M.)	Pressure redistribution	Translation and two types of rotation	Planar	Limiting force equilibrium, quasi-static	General soil-wall configurations, ϕ-soils, no surcharge	K_{AE}, h_a	Considers wall movement effects on mobilized strength

TABLE 6.8a
Numerical comparison of solutions of various analytical methods for seismic active earth pressure analysis ($\alpha = 75°$, $\beta = 0°$, $\phi = 40°$, $\delta = (\frac{2}{3})\phi$, $k_h = 0$ and 0.15)

Analytical method		Static		Seismic		Increment		Normalized overturning moment, M_o	Remarks
		K_A	h_a/H	K_{AE}	h_a/H	ΔK_{AE}	h_a'/H		
M-O analysis		0.325	0.333	0.440	0.333	–	–	0.147	
Seed and Whitman (1970)		0.325	0.333	0.438	–	0.113	0.600	0.176	Suggested for $\alpha = 90°$ only
Prakash and Saran (1966)		0.325	0.333	0.442	0.333	–	–	0.147	
Limit analysis	Translation	0.325	0.333	0.440	0.333	–	–	0.147	The h_a-value is based on M.D.M.
	Rotation about top	0.325	0.333	0.440	0.357	–	–	0.157	
Modified Dubrova method (M.D.M.)	Translation	0.325	0.333	0.440	0.333	0.115	0.333	0.147	
	Rotation about top	0.325	0.361	0.440	0.357	0.115	0.344	0.157	
	Rotation about toe	0.445	0.309	0.577	0.311	0.115	0.321	0.179	

TABLE 6.8b
Numerical comparison of solutions of various analytical methods for seismic active earth pressure analysis ($\alpha = 90°$, $\beta = 0°$, $\phi = 30°$, $\delta = 7.5°$, $k_h = 0$ and 0.15)

Analytical methods		Static		Seismic		Increment		Normalized overturning moment, M_o	Remarks
		K_A	h_a/H	K_{AE}	h_a/H	ΔK_{AE}	h_a'/H		
M-O analysis		0.313	0.333	0.415	0.333	–	–	0.138	
Seed and Whitman (1970)		0.313	0.333	0.426	–	0.113	0.600	0.172	
Prakash and Basavanna (1969)	Translation	0.315	0.356	0.415	0.425	–	0.642	0.176	
	Rotation about toe	0.315	0.356	0.410	0.433	–	0.654	0.178	
Limit analysis	Translation	0.313	0.333	0.415	0.333	–	–	0.138	The h_a-value is based on M.D.M.
	Rotation about top	0.313	0.372	0.415	0.369	–	–	0.153	
Modified Dubrova method (M.D.M.)	Translation	0.313	0.333	0.415	0.333	0.102	0.333	0.138	
	Rotation about top	0.313	0.372	0.415	0.369	0.102	0.368	0.153	
	Rotation about toe	0.474	0.302	0.608	0.304	0.134	0.311	0.185	

linear, is found higher than $H/3$. Whether the high h_a-value as obtained by the same method is reasonable or not is difficult to justify. Hence, the high M_o-values obtained by Prakash and Basavanna (1969) and Seed and Whitman (1970), whose recommended $h_a' = 0.6\,H$ was mainly based on the work of Prakash and Basavanna (1969), need further justification. Based on the modified Dubrova method, $h_a = H/3$ is found for all k_h-values for the case of translation movement, which is the same as that assumed in the M-O analysis.

Although the h_a-value for the translation case may need further explorations, it appears that the K_{AE}-value can be obtained by any of the methods as listed in Table 6.7. However, the limit analysis method, which is applicable to general soil – wall systems, is highly recommended, especially when surcharge, q, and cohesion, c, are present. In this case, both the active pressure resulting from the surcharge and the cohesion can be assumed to act at the middle height of the wall. Unless strong evidence showing that $h_a > H/3$ is available, it is reasonable that the active pressure for $q = c = 0$ case be assumed to act at $h_a = H/3$ for practical purposes, if the movement is found essentially translational and the amount of the movement is sufficiently large.

For the case of rotation about the top, it is recommended that the modified Dubrova method which gives both the K_{AE}-value and its corresponding h_a-value can be used for the case of no surcharge ($q = 0$) and zero cohesion ($c = 0$). However, if surcharge and/or cohesion are present, the limit anaysis is highly recommended for determining the K_{AE}-value. The value can be easily estimated from the tables and charts provided in Appendices A and B of Chapter 5. While the active pressure as contributed by the surcharge and cohesion can again assume to act at the mid-height, the h_a-value for the case of $q = c = 0$ is recommended to obtain from the modified Dubrova method.

For the case of rotation about the toe, it is found that the K_A- and K_{AE}-values obtained by the modified Dubrova method, which are close to the at-rest values, are much larger than those based on Prakash and Basavanna (1969) for the same mode of movement. On the other hand, based on Prakash and Basavanna (1969), the h_a-value for the case investigated ($\alpha = 90°$, $\beta = 0°$, $\phi = 30°$, $\delta = 7.5°$, and $k_h = 0.15$) is as high as $0.433\,H$. As explained earlier, the distribution of active pressure for the case of rotation about the toe may be concave upward, and consequently $h_a < H/3$ is expected. The result based on the modified Dubrova method, which gives $h_a < H/3$, is consistent with this reasoning as far as the h_a-value is concerned. However, considering the results from Prakash and Basavanna's method and the absence of results from full-scale tests, further study of this question is justified.

Although both Prakash and Basavanna (1969) and the modified Dubrova method coincidentally give almost the same overturning moments for the case of rotation about the toe, for the reasons just discussed, it seems that both methods are not strictly suitable for assessing the overturning moment M_o corresponding to the

limiting active state. The modified Dubrova method, however, can be used for estimating the seismic overturning moment for the case in which the retaining structure is allowed to rotate outward about the bottom for a very limited amount of rotation, such as the case of basement wall.

If no better theories are available, it is recommended that for the case of rotation about the toe, the K_{AE}-value, which is supposed to be close to the translational K_{AE}-value if the limiting state is allowed to develop, can be taken from that obtained based on the limit analysis method. Due to the assumption inherent in the use of seismic coefficients the actual value of h_a is uncertain. Accordingly, further study of this question is highly recommended.

6.6.2 Analytical methods for determining seismic passive earth pressure

The well-known M-O analysis generally adopted for seismic active earth pressure analysis has also been used for calculating seismic passive earth pressure. However, in the passive case, there are serious interactions between the wall and the backfill material, progressive failure phenomena is of great significance. Consequently, the failure surface is generally curved and the actual average mobilized strength parameter can fall well below the peak value. For these reasons, the method is not highly desirable unless that the actual failure is practically planar and a reasonable assessed average ϕ-parameter is considered.

A completely new approach of solving passive earth pressure problems in static and seismic cases has been presented recently by Habibagahi and Ghahramani (1979) and Ghahramani and Clemence (1980), respectively. In this method, a simple zero-extension line field is first developed based on associated fields of stress and displacement. The limit equilibrium technique is then applied for determining the resultant passive earth pressure. In the static case, it appears that the theory is applicable only for the case of translational wall movement. No point of action has been mentioned by Habibagahi and Ghahramani (1979).

In developing the approach for assessing seismic increments of passive earth pressure, Ghahramani and Clemence (1980) tried to incorporate the seismic acceleration effect in an incremental manner based on the work of Sabzevari and Ghahramani (1974). However, on the basis of the incremental approach, it appears that only the relative acceleration between soil above and soil below the toe is considered. The foundation soil is assumed to remain static. The suitability of this assumption is somewhat questionable.

Nevertheless, based on a simple zero-extension line field, Ghahramani and Clemence (1980) developed a chart for obtaining the 'dynamic' seismic passive earth pressure coefficient for the case of translational wall movement. Also, by assuming different distributions of seismic acceleration, they showed that the ΔK_{PE}-values for the cases of rotation about the top and about the toe are $\frac{2}{3}$ and $\frac{1}{3}$ of the translational ΔK_{PE}-value, respectively. They further showed that the corresponding point of action h_p equals to $H/3$ for the translation case, $H/2$ for the case of rotation about the toe, and $H/4$ for the case of rotation about the top.

Ghahramani and Clemence (1980) based on their study, suggested that the resulting seismic passive earth pressure can be taken as the combination of the static passive pressure obtained based on Habibagahi and Ghahramani (1979) and the 'dynamic' increment as calculated by their suggested method.

The limit analysis method and the modified Dubrova method, which have been briefly described earlier in this chapter, are applicable not only to the active earth pressure case, but also to the passive earth pressure case. Use of the limit analysis method, in which the log-sandwich mechanism of failure is assumed, in the determination of passive earth pressure is extremely beneficial. On the contrary, like the M-O analysis, the application of the modified Dubrova method to this case has to be carefully considered, since the planar failure mechanism as assumed in the method is quite often unrealistic. Consequently, the K_P- and K_{PE}-values may be seriously overestimated by this method.

Nevertheless, due to lack of theoretically sound methods for assessing the point of action of resultant passive pressure, it is suggested that the modified Dubrova method can be used for estimating the h_p-values. The h_p-value so assessed can then be incorporated with the K_{PE}-values calculated based on the limit analysis method for obtaining a reasonable estimation of the normalized resisting moment, $M_r = K_{PE}\,(h_p/H)$.

The above-mentioned analytical methods have been compared and summarized in Table 6.9.

To compare the suitability of these analytical methods for practical design applications, an example has been worked out. Comparison of the solution based on these methods is given in Table 6.10. It should be pointed out here that in presenting the solutions of Ghahramani and Clemence (1980), it is assumed that for all types of wall movement the static K_P-value is the same. Also, negative seismic increments of pressure are considered. The static h_p-value is taken as $H/3$ for all cases of wall movement.

It is clear from Table 6.10 that both the M-O analysis and the modified Dubrova method seriously overestimate the K_P- and K_{PE}-values for the cases of translation and rotation about the top. The solutions of Ghahramani and Clemence (1980) and the limit analysis method, which are both based on the log-sandwich failure mechanism, are more reasonable. The zero-extension line theory appears to give the best result on the assessment of the K_P- and K_{PE}-values.

For the case of rotation about the toe, the modified Dubrova method gives much lower K_P- and K_{PE}-values than the zero-extension line theory does. This is because the K_P- and K_{PE}-values so obtained based on the recommended ψ- and δ-distributions are more representative of the at-rest values.

TABLE 6.9
Comparisons of analytical methods for seismic passive earth pressure analysis

Methods	Basic idea	Mode of movement	Failure mechanism	Analytical techniques	Applicable soil-wall conditions	Information given	Remarks
Mononobe-Okabe analysis	Coulomb's wedge theory	Not specified	Planar	Limiting force equilibrium, quasi-static	General soil-wall configuration, ϕ-soil, no surcharge	k_{PE}	
Ghahramani and Clemence (1980)	Zero-extension line theory	Translation and two types of rotation	Log-sandwich	Limiting force equilibrium, incremental approach, quasi-static	Vertical wall and horizontal cohesionless backfill, no surcharge	K_{PE}, h'_p	Wall movement specified for seismic case only
Limit analysis	Upper-bound limit theorem	Translation	Log-sandwich	Energy equilibrium, quasi-static	General soil-wall system	K_{PE}	
Modified Dubrova method (M.D.M.)	Pressure redistribution	Translation and two types of rotation	Planar	Limiting force equilibrium, quasi-static	General soil-wall configuration, ϕ-soil, no surcharge	K_{PE}, h_p	Consider wall-moment effects of mobilized strength

TABLE 6.10
Numerical comparison of solutions of various analytical methods for seismic passive earth pressure analysis ($\alpha = 90°$, $\beta = 0°$, $\phi = 40°$, $\delta = (\frac{2}{3})\phi$, $k_h = 0$ and 0.15)

Analytical method		Static		Seismic		Increment		Normalized resisting moment, M_r	Remarks
		K_P	h_p/H	K_{PE}	h_p/H	ΔK_{PE}	h'_p/H		
M-O analysis		18.72	0.333	16.42	0.333	–	–	5.47	
Ghahramani Clemence (1980)	Translation	11.90	0.333	10.16	0.333	−1.74	0.333	3.37	Translational K_P and static h_p are used for all cases
	Rotation about top	11.90	0.333	10.74	0.342	−1.16	0.250	3.68	
	Rotation about toe	11.90	0.333	11.32	0.325	−0.58	0.500	3.68	
Limit analysis	Translation	13.09	0.333	11.88	0.333	–	–	3.96	The h_p-value is based on M.D.M.
	Rotation about top	13.09	0.237	11.88	0.236	–	–	3.09	
Modified Dubrova method (M.D.M.)	Translation	18.72	0.333	16.43	0.333	−2.29	0.333	5.47	
	Rotation about top	18.72	0.237	16.43	0.236	−2.29	0.214	3.89	
	Rotation about toe	5.27	0.447	4.53	0.450	−0.74	0.429	2.04	

It is interesting to note that the h'_p-values obtained based on the zero-extension line theory and the modified Dubrova method are the same or very close in all cases of wall movement. However, comparison of h_p corresponding to K_{PE} shows that $h_p > H/3$ for the case of rotation about the top and $h_p < H/3$ for the case of rotation about the toe are obtained based on the zero-extension line theory. This contradicts to the solutions of the modified Dubrova method. This is because $h_p = H/3$ is assumed for the static case in the zero-extension line solution. According to the modified Dubrova method, the relative magnitudes of h_p and h'_p for different wall movements are very close. That is, $h_p < H/3$ for the case of rotation about the top and $h_p > H/3$ for the case of rotation about the toe as found on the basis of the modified Dubrova method seem more reasonable.

As far as the resisting moment is concerned, it appears that for both cases of the translation and the rotation about the top, both the zero-extension line theory and the limit analysis method with h_p-values based on the results of the modified Dubrova method, give very close and reasonable M_r-values. However, it should be noted that the larger M_r-value for the translation case than for the case of rotation about the top as found by the modified Dubrova is more reasonable for the reason just discussed.

In fact, if a distinction between the K_P-value and the h_p-value for different wall movements for the static case is possible based on the zero-extension line theory, the theory will give the best results on M_r. Nevertheless, the zero-extension line theory has so far been applied only to the very special case of vertical wall and horizontal cohesionless backfill with zero surcharge. The actual application of the method is, therefore, very limited. In this regard, it appears that the limit analysis method in combination with the h_p-value based on the modified Dubrova method could probably be a preferable approach for assessing the passive resisting moment for actual design applications in the case that the mode of wall movement is expected to be mainly translational or rotating about the top.

Appendices A and B of Chapter 5 which show K_{PE}-tables and charts required for estimating K_{PE}-values corresponding to the case of $q \neq 0$, $c \neq 0$, $\theta \neq 0$ (nonhorizontal seismic acceleration) are recommended for determining the K_{PE}-value. If surcharge and cohesion are present, they can be assumed to act at the mid-height of the wall.

For the case of rotating about the toe, the resisting moments obtained by the zero-extension line theory and the modified Dubrova method are much different, although the corresponding h'_p-values obtained are fairly close. On the one hand, in the approach of Ghahramani and Clemence (1980), assuming that K_P and h_a are the same for all types of wall movement for the static case is not justified. On the other hand, use of the modified Dubrova method, which is based on a planar failure mechanism, for assessing passive resistance is not necessarily proper either. Furthermore, the results obtained by the modified Dubrova method and the recommended ψ- and δ-distributions are not representative of the limiting passive state, as pointed out previously in Section 6.4. Hence, it appears that further investigation on this mode of wall movement is urgently needed. Perhaps, one of the possible ways of solving this problem is to use the equations developed based on the limit analysis method as the framework for developing the modified Dubrova method. At the same time, the ψ- and δ-distributions have to be assumed based on more extensive field observations. Its feasibility, however, needs further investigation. The difficulty with the modified Dubrova method in regard to the fact that the resultant lateral force may not solely be dependent on the mobilized ϕ-value near the toe should be overcome first. Alternatively, the finite-element method may be used to obtain a more realistic solution (Potts and Fourie, 1986).

Again, if no better theories are available the K_{PE}-value obtained by the limit analysis method, which is representative of the ultimate translation value, could be used. With regard to the point of action, $h_p = H/3$ could be adopted, although it is quite possible that $h_p > H/3$, as given by the modified Dubrova method, may be true for the case of rotation about the toe.

6.7 Design recommendations

Evaluation of seismic lateral earth pressures is important in both ultimate-load-based design and displacement-based design of retaining structures in seismic zones. For reasonable estimation of seismic lateral earth pressures and points of action of the resultant forces, the expected field conditions, especially the type and amount of wall movement, should be considered in the first place. Based on the comparison of some well-known earth pressure theories with the limit analysis method and the modified Dubrova method proposed herein, proper analytical methods can then be selected for reasonable assessment of the magnitude and the point of action of the resultant active and passive earth pressures for actual design applications.

As described by Nazarian and Hadjian (1979), most reported damage of retaining walls by earthquake can be attributed to increased lateral pressures inducing sliding and tilting of the structures. Nandakumaran and Prakash (1970) also reported that outward wall movement and settlement of backfill are generally found on retaining walls damaged by earthquake. It, therefore, appears that tilting and translational wall movements are predominant in most earthquakes for the case of free-standing rigid retaining walls.

The study of this chapter tends to indicate that all the earth pressure theories investigated are applicable to the determination of resultant seismic active earth pressure if the wall movement is essentially translational. However, the limit analysis method, which is applicable to general soil-wall systems, is highly recommended. Appendices A and B of Chapter 5 presenting earth pressure tables and charts for application of the earth pressures have been developed based on the limit analysis method. They can be used for actual design applications. In regard to the point of

action, $h_a > H/3$ should be adopted since there are evidences showing $h_a > H/3$ in the seismic case, although at the ultimate state $h_a = H/3$ as given by the modified Dubrova method may be true.

In case that tilting movement is predominant, the K_{AE}-value estimated from Prakash and Basavanna (1969) or the limit analysis method is recommended if no better theories are available for this mode of movement. At present, the point of action, h_a, should be taken as greater than $H/3$, although, in this case, the distribution curve for the active earth pressure may be concave upward such that $h_a < H/3$.

Quite possibly, most free-standing walls may move in a way combining tilt and translation. Such kind of wall movement, although not treated in this chapter, could be solved by the finite-element approach. It could also be reasonably handled by the modified Dubrova method by considering the point of rotation to locate at certain points below the bottom of the wall. The modified Dubrova method certainly has a great potential for treating problems of such kind. Nevertheless, its limitations should always be recognized.

For the case of bridge abutment, in which lateral movement is restricted at the top, rotation about the top is the most likely mode of movement. In this case, the limit analysis method is recommended for assessing the K_{AE}-value, if surcharge and cohesion are present. For the case of no surcharge and zero cohesion, the modified Dubrova method or the Mononobe-Okabe analysis can also be used for obtaining the K_{AE}-value. However, it is suggested that h_a should be obtained by the modified Dubrova method. According to the modified Dubrova method, the K_{AE}-value as predicted is the same as the Mononobe-Okabe solution. However, based on this method, h_a is found higher than that was assumed in the Mononobe-Okabe analysis, i.e., $h_a = H/3$. Consequently, the resulting driving moment obtained based on the modified Dubrova method is larger than that calculated by using the Mononobe-Okabe method. This may be one cause of the damage to bridge abutment in New Zealand in the 1968 earthquake, which was reported in Richards and Elms (1979).

Foundation or basement walls of structures, although presenting more interesting design and construction problems than free-standing retaining walls, have received less attention in the literature. Estimation of seismic increment of at-rest pressure as the result of earthquake forces generally follows empirical rules. A simple method has recently been proposed by Hall (1978) for evaluating the 'dynamic' at-rest pressure by interpolating between the 'dynamic' active and passive pressures. However, it appears that the modified Dubrova method, which can theoretically be applied to any stage of wall yielding if the movement is essentially translation or rotation about the top, is capable of solving this problem directly. By assuming a uniform ψ-distribution with its magnitude equal to the at-rest ψ-value, ψ_a, the static and seismic at-rest pressures can be easily obtained by the method. The seismic increment of the pressure can also be calculated. It is apparent that both the seismic

at-rest pressure and the increment of the pressure are higher than the actual values.

Although the way retaining structures move under lateral pressures is seldom documented, purely active and virtually no passive states are not always predominant. Also, it has been pointed out by Nazarian and Hadjian (1979) that the center of rotation for the passive case could move up and down the wall depending on the interaction characteristics of the externally applied force, the wall, and the backfill. It appears that a combination of active and passive states, quite often, can occur in reality. If this is the case, the modified Dubrova method could be a useful analytical tool.

In short, the earth pressure theories should be carefully selected in actual design of rigid retaining structures in seismic environments. This must be done by considering not only the assumptions, the limitation, and the applicability of the analytical method but also the actual conditions, such as the type and amount of wall movement, that might be expected in the field. It should also be kept in mind that the construction method, the loading and strain conditions, the soil-structure interface friction, and the progressive failure and scale effect as discussed earlier should always be taken into consideration in actual applications of all earth pressure theories. No earth pressure theories can be blindly applied to actual designs without these considerations.

References

Basavanna, B.M., 1970. Dynamic earth pressure distribution behind retaining walls. Proc. 4th Symp. on Earthquake Eng., Univ. of Roorkee, India, Vol. 1, pp. 311 – 320.

Chang, M.F., 1981. Static and seismic lateral earth pressures on rigid retaining structures. Ph.D. Thesis, School of Civil Engineering, Purdue University, West Lafayette, IN, 466 pp.

Davis, E.H., 1968. Theories of plasticity and the failure of soil masses. In: I.K. Lee (Editor), Soil Mechanics: Selected Topics. Butterworths, London, pp. 341 – 380.

Dubrova, G.A., 1963. Interaction of Soil and Structures. Rehnoy Transport, Moscow, U.S.S.R.

Emery, J.J. and Thompson, C.D., 1976. Seismic design considerations for gravity retaining structures. Can. J. Civ. Eng., 3: 248 – 264.

Ghahramani, A. and Clemence, S.P., 1980. Zero extension line theory of dynamic passive pressure. J. Geotech. Eng. Div., ASCE, 106 (GT6): 631 – 644.

Habibagahi, K., and Ghahramani, A., 1979. Zero extension line theory of earth pressure. J. Geotech. Eng. Div., ASCE, 105 (GT7): 881 – 896.

Hall, J.R., 1978. Comments on Lateral Forces – Active and Passive. ASCE Specialty Conference on Earthquake Engineering and Soil Dynamics, Pasadena, CA, Vol. 3, pp. 1436 – 1441.

Harr, M.E., 1966. Foundation of Theoretical Soil Mechanics. McGraw-Hill, New York, NY, 381 pp.

Harr, M.E., 1977. Mechanics of Particulate Media – A Probabilistic Approach. McGraw-Hill, New York, NY.

Ishii, Y., Arai, H. and Tsuchida, H., 1960. Lateral earth pressure in an earthquake. Proc. 2nd World Conf. on Earthquake Engineering, Tokyo, Vol. 1, pp. 211 – 230.

Jaky, J., 1948. Pressures in soils. Proc. 2nd ICSMFE, 1: 103 – 107.

James, R.G. and Bransby, P.L., 1970. Experimental and theoretical investigations of a passive earth pressure problem. Geotechnique, 20 (1): 17 – 37.

James, R.G. and Bransby, P.L., 1971. A velocity field for some passive earth pressure problems. Geotechnique, 21 (1): 61 – 83.
Kedi, A., 1958. Earth pressure on retaining wall, tilting about the toe. Proc. Brussels Conf. on Earth Pressure Problems, Brussels, Vol. 1, pp. 116 – 132.
Lee, I.K. and Herington, J.R., 1972. A theoretical study of the pressure acting on a rigid wall by a sloping earth or rockfill. Goetechnique, 22 (1): 1 – 26.
Matsuo, H., 1941. Experimental study on the distribution of earth pressure acting on a vertical wall during an earthquake. J. Jpn. Soc. Civ. Eng. 27 (2).
Matsuo, H. and Ohara, S., 1960. Lateral earth pressures and stability of quay walls during earthquakes. Proc. 2nd World Conf. on Earthquake Engineering, Tokyo, Vol. 1, pp. 165 – 181.
Mononobe, N. and Matsuo, H., 1929. On determination of earth pressure during earthquakes. Proc. World Engineering Congress, Tokyo, Vol. 9, pp. 275.
Murphy, V.A., 1960. The effect of ground characteristics on the aseismic design of structures. Proc. 2nd World Conf. on Earthquake Engineering, Tokyo, Vol. 1, pp. 231 – 248.
Nandakumaran, P. and Prakash, S., 1970. The problem of retaining walls in seismic zones. Proc. 4th Symp. on Earthquake Eng., Univ. of Roorkee, India, Vol. 1, pp. 307 – 310.
Nandakumaran, P. and Joshi, V.H., 1973. Static and dynamic active earth pressures behind retaining walls. Paper No. 136, Bull., I.E.S.T., 10 (3): pp. 113 – 123.
Narain, J., Saran, S. and Nandakumaran, P., 1969. Model study of passive pressure in sand. J. Soil Mech. Found. Div., ASCE, 95 (SM4): 969 – 984.
Nazarian, H. and Hadjian, A.H., 1979. Earthquake induced lateral soil pressures on structures. J. Geot. Eng. Div., ASCE, 105 (GT7): 1049 – 1066.
Okabe, S., 1926. General theory on earth pressure and seismic stability of retaining walls and dams. J. Jpn. Soc. Civ. Eng., 12, (1).
Potts, D.M. and Fourie, A.B., 1986. A numerical study of the effects of wall deformation on earth pressures. Int. J. Numer. Anal. Methods, Geomech., 10: 383 – 405.
Prakash, S., 1981. Soil Dynamics. McGraw-Hill, New York, NY, 426 pp.
Prakash, S. and Saran, S., 1966. Static and dynamic earth pressures behind retaining walls. Proc. 3rd Sym. on Earthquake Eng., Univ. of Roorkee, India, pp. 277 – 288.
Prakash, S. and Basavanna, B.M., 1969. Earth pressure distribution behind retaining walls during earthquake. Proc. 4th World Conf. on Earthquake Eng., Chile, pp. 133 – 148.
Richards, R. and Elms, D.G., 1979. Seismic behavior of gravity retaining walls. J. Geotech. Eng. Div., ASCE, 105 (GT4): 449 – 464.
Sabzevari, A. and Ghahramani, A., 1974. Dynamic passive earth pressure problem. J. Geotech. Eng. Div., ASCE, 100 (GT1): 15 – 30.
Saran, S. and Prakash, S., 1977. Effect of wall movement on lateral earth pressure. Proc. 6th World Conf. on Earthquake Engineering, India, pp. 2371 – 2372.
Seed, H.B. and Whitman, R.V., 1970. Design of earth retaining structures for dynamic loads. ASCE Specialty Conf. on Lateral Stresses in the Ground and Design of Earth-Retaining Structures, Cornell Univ., Ithaca, NY, pp. 103 – 147.
Terzaghi, K., 1934. Large retaining-wall tests. Eng. News Rec., Vol. 112, May.
Terzaghi, K., 1936. A fundamental fallacy in earth pressure computation. J. Boston Soc. Civ. Eng., 23 (2): 71 – 88.
Terzaghi, K., 1941. General wedge theory of earth pressure. ASCE Trans., 106: 68 – 80.
The Japanese Society of Civil Engineers, 1980. Earthquake Resistant Design for Civil Engineering Structures, Earth Structures, and Foundations in Japan. Tokyo.
Tschaebotarioff, G.P., 1962. Retaining structures. In: G.A. Leonards (Editor), Foundation Engineering. McGraw-Hill, New York NY, pp. 438 – 524.
Wood, J.H., 1975. Earthquake induced pressures on a rigid wall structure. Bull. N.Z. Soc. Earthquake Eng., 18 (3): 175 – 186.

Chapter 7

BEARING CAPACITY OF STRIP FOOTING ON ANISOTROPIC AND NONHOMOGENEOUS SOILS

7.1 Introduction

The bearing capacity of strip footings on homogeneous and isotropic soils has been extensively studied by several investigators. The fundamental theory and practical applications of strip as well as square, rectangular and circular footings have been described in details in Chen's book (1975). However, it has been recognized that natural soil deposits are nonhomogeneous and anisotropic with respect to shear strength (Casagrande and Carillo, 1944; Lo, 1965; Bishop 1966; Livneh and Komornik 1967). Considerable work has been done with regard to the influence of anisotropy and nonhomogeneity on the bearing capacity of clays, in which $\phi = 0$ (Raymond, 1967; Reddy and Srinivasan, 1967, 1971; Davis and Christian, 1971; Davis and Brooker, 1973; Livneh and Greenstein, 1973; Salencon, 1974a, b). Most of these studies found that the anisotropy and nonhomogeneity have a considerable influence on the bearing capacity of clays. On the other hand, however, very few attempts have been made for studying the effect of anisotropy and nonhomogeneity on the bearing capacity of c-ϕ soils. Reddy and Srinivasan (1970) studied the effect of anisotropy and nonhomogeneity on the bearing capacity of c-ϕ soils including $\phi = 0$ condition of soils. In their study, they used the method of characteristics to obtain the bearing capacity. Meyerhof (1978) obtained the bearing capacity for soils exhibiting anisotropy in friction by the conventional Terzaghi's type approach using two extreme values of ϕ for the outer zones and an equivalent ϕ for the radial shear zone. Shklarsky and Livneh (1961a) found from tests made on asphalt paving mixture that the ratio of strengths with load parallel and perpendicular to the direction of compaction was greater than one. It was shown that such paving mixture has anisotropic cohesion and isotropic angle of friction. Shklarsky and Livneh (1961b) also made an analysis of splitting tests for asphalt mixture and Shklarsky and Livneh (1962) presented equations for slip lines in anisotropic cohesion medium. It is generally believed that for compacted soils it is highly probable that, analogous to asphalt, the cohesion is dependent on the direction of compaction. Salencon (1974b) and Salencon et al. (1976) presented analysis for the bearing capacity of c-ϕ-γ soil taking a linear variation of cohesion with depth.

Limit analysis, particularly the upper bound analysis, has been found to be a convenient tool for solving such complex problems involving anisotropy and

nonhomogeneity of soil. Chen (1975) extensively dealt with the applications of limit analysis to soil engineering problems. He has applied the limit analysis for the bearing capacity of footings on a single layer and two-layered soils, exhibiting both the anisotropy and nonhomogeneity. Chen's analysis was again based on the assumption of a circular failure surface and hence agreed with the solution by Reddy and Srinivasan (1967). However, for soils exhibiting anisotropy and nonhomogeneity, the assumption of a circular failure surface is found to considerably overestimate the bearing capacity (Davis and Brooker, 1973; Salencon, 1974a). The assumption of a circular failure surface by many investigators was due to the fact that for anisotropic and nonhomogeneous soils, solutions become very difficult. Besides, Purushothama et al. (1972) obtained the bearing capacity factors of homogeneous and isotropic soil by treating the boundary wedge angles as variables. In 1982, Reddy and Venkatakrishna, by adopting a Prandtl type of failure mechanism, applied the limit analysis (upper bound) to obtain the bearing capacity of a strip footing on c-ϕ soils exhibiting anisotropy and nonhomogeneity in cohesion.

In this chapter, we shall introduce the Reddy and Venkatakrishna method as an extension and improvement of Chen's work (1975). The results are presented in a nondimensional form of charts for various parameters considered.

7.2 Analysis

The problem is treated here as a two-dimensional problem and is based on Limit Theorem II in Section 2.8 (Drucker and Prager, 1952). The following assumptions are made.

(a) The Prandtl type of failure mechanism is valid (Fig. 7.1). In the experiments reported by Ko and Davidson (1973), it is observed that the Prandtl type of mechanism used in predicting the bearing capacity of rough strip footings is justified. In this failure mechanism, wedge abc is translating vertically as a rigid body with the same initial downward velocity v_1 as the footing. The downward movement of the footing and wedge is accommodated by the lateral movement of the adjacent soils as indicated by the radial shear zone bcd and zone bdef. The

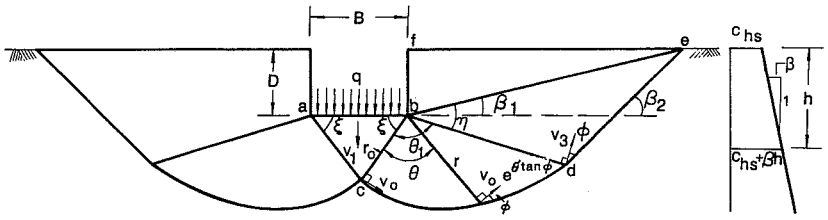

Fig. 7.1. Assumed failure mechanism.

angles ξ and η are as yet unspecified. Since the movement is symmetrical about the footing, it is only necessary to consider the movement on the right-hand side of Fig. 7.1.

(b) Based on earlier studies (Casagrande and Carillo, 1944; Shklarsky and Livneh, 1961a, b, 1962; Lo, 1965; Livneh and Komornik, 1967), the variation of cohesion c_i, with the major principal stress inclined at an angle i with the vertical, is assumed to be given by:

$$c_i = c_h + (c_v - c_h)\cos^2 i \tag{7.1}$$

where c_i is the cohesion corresponding to the inclination i of the major principal stress with the vertical direction. c_h is the cohesion corresponding to the horizontal direction of major principal stress, and c_v is the cohesion corresponding to the vertical direction of the major principal stress (see Fig. 9.1b). The variation of cohesion with depth is assumed to be linear. Thus, the cohesion at depth h from the surface is given by (Salencon, 1974b; Salencon et al., 1976):

$$c_h = c_{hs} + \beta h \tag{7.2}$$

where c_{hs} is the cohesion in the horizontal direction at $h = 0$, and β is the variation of the cohesion with depth. The ratio c_v/c_h is found to be constant for a given soil (Lo, 1965) and is denoted by k.

Referring to Fig. 7.1, the angle β_1 is obtained from the geometry by the expression:

$$e^{\beta_1 \tan\phi} \sin\beta_1 = \frac{2(D/B)\cos\xi \cos(\phi + \eta)}{e^{(\pi - \xi - \eta)\tan\phi}\cos\phi} \tag{7.3}$$

where ϕ is the angle of internal friction of soil. If v_0 is the initial velocity along the line bc, v_1 is the downward velocity of the footing and v_r is the relative velocity inclined at an angle ϕ with the line of velocity discontinuity bc, then v_1 and v_r are given by (Fig. 7.2):

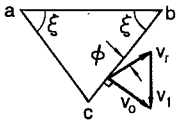

Fig. 7.2. Velocity diagram.

$$v_1 = v_0 \cos\phi/\cos(\xi - \phi) \tag{7.4}$$

$$v_r = v_0 \sin\xi/\cos(\xi - \phi) \tag{7.5}$$

The rate of external work done by the foundation load considering the symmetry is:

$$\dot{W}_q = \tfrac{1}{2} \frac{qBv_0 \cos\phi}{\cos(\xi - \phi)} \tag{7.6}$$

The rate of energy dissipation along the velocity discontinuity bc is:

$$D_{bc} = (\text{average } c_i \text{ along bc}) (\text{length bc}) v_r \cos\phi \tag{7.7}$$

The average c_i along the line bc is taken as the average of c_i at b and c_i at c. At b:

$$c_i = [c_{hs} + \beta D] [1 + (k - 1) \cos^2 i] \tag{7.8}$$

At c:

$$c_i = [c_{hs} + \beta D + \tfrac{1}{2} \beta B \tan\xi] [1 + (k - 1) \cos^2 i] \tag{7.9}$$

where the angle i is given by:

$i = \tfrac{1}{2}\pi - (\xi + \mu)$ and $\mu = \tfrac{1}{4}\pi - \tfrac{1}{2}\phi$

Substituting the values of average c_i, v_r and the length bc into Eq. (7.7), we have:

$$D_{bc} = \left[c_{hs} + \beta D + \frac{\beta B}{4} \tan\xi\right] [1 + (k - 1)\sin^2 (\xi + \mu)] \frac{Bv_0 \tan\xi \cos\phi}{2 \cos(\xi - \phi)} \tag{7.10}$$

The rate of energy dissipation along the log-spiral cd is:

$$D_{cd} = \int_0^{\theta_1} c_i \, r \, v \, d\theta \tag{7.11}$$

where c_i on the log-spiral with an angle θ is given by:

$$c_i = [c_{hs} + \beta D + \beta r \sin(\theta + \xi)] [1 + (k - 1) \cos^2 i] \tag{7.12}$$

where

$$r = r_0 \, e^{\theta \tan\phi} \tag{7.13}$$

$$v = v_0 \, e^{\theta \tan\phi} \tag{7.14}$$

where the angle i is given by:

$$i = \tfrac{1}{2}\pi - [(\tfrac{1}{2}\pi + \phi + \mu - \xi) - \theta] = \tfrac{1}{2}\pi - (\chi - \theta) \tag{7.15}$$

in which $\chi = \tfrac{1}{2}\pi + \phi + \mu - \xi$

and

$$\theta_1 = \pi + \beta_1 - \xi - \eta \tag{7.16}$$

Substituting these values into Eq. (7.11), we obtain:

$$D_{cd} = \int_0^{\theta_1} \left[c_{hs} + \beta D + \tfrac{1}{2} \frac{\beta B}{\cos\xi} e^{\theta \tan\phi} \sin(\theta + \xi)\right] [1 + (k - 1) \sin^2(\chi - \theta)] \left[\frac{Bv_0 \, e^{2\theta \tan\phi}}{2 \cos\xi} d\theta\right] \tag{7.17}$$

After further simplifications, Eq. (7.17) can be reduced to:

$$D_{cd} = \frac{Bv_0}{2 \cos\xi} [c_{hs} + \beta D] [I_1 + (k - 1)I_2] + \frac{\beta B^2 v_0}{4 \cos^2\xi} [I_3 + (k - 1)I_4] \tag{7.18}$$

where I_1, I_2, I_3, and I_4 are integrals given by:

$$I_1 = \int_0^{\theta_1} e^{2\theta \tan\phi} d\theta \tag{7.19}$$

$$I_2 = \int_0^{\theta_1} e^{2\theta \tan\phi} \sin^2(\chi - \theta) \, d\theta \tag{7.20}$$

$$I_3 = \int_0^{\theta_1} e^{3\theta \tan\phi} \sin(\theta + \xi) \, d\theta \tag{7.21}$$

and

$$I_4 = \int_0^{\theta_1} e^{3\theta \tan\phi} \sin^2(\chi - \theta) \sin(\theta + \xi) \, d\theta \tag{7.22}$$

The rate of energy dissipation in the radial shear zone bcd is given by:

$$D_{bcd} = \int_0^{\theta_1} (\text{average } c_{iav} \text{ along any radial line})\, r\, v\, d\theta \tag{7.23}$$

where c_{iav}, the average c_i along any radial line, is taken as the average of c_i at b given by Eq. (7.8) and c_i given by Eq. (7.12), but with $i = \pi/2 - (\theta + \xi + \mu)$. Substituting the values of average c_{iav} and other quantities into Eq. (7.23), we have:

$$D_{bcd} = \int_0^{\theta_1} \left[c_{hs} + \beta D + \frac{\beta B}{4\cos\xi} e^{\theta \tan\phi} \sin(\theta + \xi)\right] [1 + (k-1)\sin^2(\theta + \xi + \mu)] \frac{Bv_0}{2\cos\xi} e^{2\theta\tan\phi}\, d\theta \tag{7.24}$$

After further simplifications, Eq. (7.24) reduces to:

$$D_{bcd} = \frac{Bv_0}{2\cos\xi}[c_{hs} + \beta D][I_a + (k-1) I_b] + \frac{\beta B^2 v_0}{8\cos^2\xi}[I_c + (k-1) I_d] \tag{7.25}$$

where I_a, I_b, I_c and I_d are integrals given by:

$$I_a = \int_0^{\theta_1} e^{2\theta\tan\phi}\, d\theta \tag{7.26}$$

$$I_b = \int_0^{\theta_1} e^{2\theta\tan\phi} \sin^2(\theta + \xi + \mu)\, d\theta \tag{7.27}$$

$$I_c = \int_0^{\theta_1} e^{3\theta\tan\phi} \sin(\theta + \xi)\, d\theta \tag{7.28}$$

and

$$I_d = \int_0^{\theta_1} e^{3\theta\tan\phi} \sin^2(\theta + \xi + \mu) \sin(\theta + \xi)\, d\theta \tag{7.29}$$

The rate of energy dissipation along the discontinuous line de is:

$$D_{de} = (\text{average } c_i \text{ along de})(\text{length de})\, v_3 \cos\phi \tag{7.30}$$

At e:

$$c_i = c_{hs}[1 + (k-1)\cos^2 i] \tag{7.31}$$

At d:

$$c_i = [c_{hs} + \beta(de)\sin\beta_2][1 + (k-1)\cos^2 i] \tag{7.32}$$

where the angle $i = \frac{1}{2}\pi - \beta_2 + \mu$, $v_3 = v_0 e^{\theta_1 \tan\phi}$, β_2 is the angle between the line de with the horizontal and the length de is given by the geometric relation:

$$\overline{de} = \frac{B\, e^{\theta_1 \tan\phi} \sin\eta}{2\cos\xi\cos(\phi + \eta)} \tag{7.33}$$

Substituting these quantities into Eq. (7.30), we obtain:

$$D_{de} = \left[c_{hs} + \frac{\beta B}{4\cos\xi} \frac{e^{\theta_1\tan\phi}\sin\eta\sin\beta_2}{\cos(\phi + \eta)}\right][1 + (k-1)\sin^2(\beta_2 - \mu)] \left[\frac{Bv_0}{2\cos\xi} e^{2\theta_1\tan\phi} \frac{\sin\eta\cos\phi}{\cos(\phi + \eta)}\right] \tag{7.34}$$

Rate of work done by the soil weight in the triangle area abc, taking only one half, is:

$$(\dot{W}_\gamma)_{abc} = \tfrac{1}{8} \frac{\gamma B^2 v_0 \sin\xi\cos\phi}{\cos\xi\cos(\xi - \phi)} \tag{7.35}$$

where γ is the unit weight of soil.

The rate of work done by the weight of soil in the radial shear zone bcd is given by:

$$(\dot{W}_\gamma)_{bcd} = \tfrac{1}{2}\gamma \int_0^{\theta_1} r^2 v \cos(\theta + \xi)\, d\theta \tag{7.36}$$

Equation (7.36) can be integrated and simplified to:

$$(\dot{W}_\gamma)_{bcd} = -\tfrac{1}{8} \frac{\gamma B^2 v_0}{\cos^2\xi\,(1 + 9\tan^2\phi)} \{3\tan\phi\cos\xi + \sin\xi + [3\tan\phi\cos(\beta_1 - \eta) + \sin(\beta_1 - \eta)]\, e^{3(\pi + \beta_1 - \xi - \eta)\tan\phi}\} \tag{7.37}$$

The rate of work done by the weight of soil in the area bdef is given by:

$$(\dot{W}_\gamma)_{\text{bdef}} = -\tfrac{1}{8}\frac{\gamma v_0 B^2}{\cos^2\xi}\left[\frac{\sin\eta\cos\phi}{\cos(\phi+\eta)} + \frac{\sin\beta_1\cos\beta_1\cos^2\phi}{\cos^2(\phi+\eta)}\right]$$

$$\cos(\beta_1 - \eta)\, e^{3(\pi+\beta_1-\xi-\eta)\tan\phi} \tag{7.38}$$

Equations (7.37) and (7.38) are the same as those given previously by Chen (1975).

Equating the rates of external work done by the footing (Eq. 7.6) and by the weight of the soil (Eqs. 7.35, 7.37, and 7.38) to the rates of internal energy dissipation (Eqs. 7.10, 7.18, 7.25, and 7.34), and introducing the nondimensional parameters:

$$d' = D/B \tag{7.39}$$

$$\nu = \beta B/c_{\text{hs}} \tag{7.40}$$

$$q' = q/c_{\text{vs}} \tag{7.41}$$

where c_{vs} is the cohesion in the vertical direction at $h = 0$, and:

$$G = \gamma B/c_{\text{hs}} \tag{7.41}$$

the expression for q' is obtained as:

$$q' = N_c + G\,N_{\gamma q} \tag{7.42}$$

where the bearing capacity factors N_c and $N_{\gamma q}$ are functions of the angles ξ and η for given values of parameters, d', ν, k, G and μ. For the minimum value of q', the angles ξ and η must satisfy the conditions:

$$\partial q'/\partial\xi = 0 \tag{7.43}$$

$$\partial q'/\partial\eta = 0 \tag{7.44}$$

The minimum value of q' can be obtained by any optimization program.

7.3 Results and discussions

Values of the normalized bearing capacity pressure, $q' = q/c_{\text{vs}}$, have been obtained for $\phi = 10$, 20, 30, and 40°, $D/B = 0.0$, and 1.0, $G = \gamma B/c_{\text{hs}} = 0.0$ and 2.0, $k = c_{\text{v}}/c_{\text{h}} = 0.8$, 1.0, 1.2, 1.6, and 2.0, and $\nu = \beta B/c_{\text{hs}} = 0.0$, 0.40, 0.80, and 1.2.

TABLE 7.1
Comparison of values of N_c for $G = \gamma B/c_{\text{hs}} = 0.0$, $k = c_{\text{v}}/c_{\text{h}} = 1$, and $\nu = \beta B/c_{\text{hs}} = 0.0$

ϕ (degrees) (1)	Present analysis (2)	Sokolovskii (1965) (3)	Salencon (1974b) (4)	Chen (1975) (5)	Reddy and Srinivasan (1970) (6)	Terzaghi (1943) (7)	Meyerhof (1978) (8)
10	8.34	8.34	8.35	8.34	9.30	9.30	8.00
20	14.83	14.80	14.84	14.80	16.00	17.00	14.50
30	30.14	30.10	30.15	30.10	32.00	37.00	31.00
40	75.32	75.30	75.34	75.31	82.00	97.50	73.00

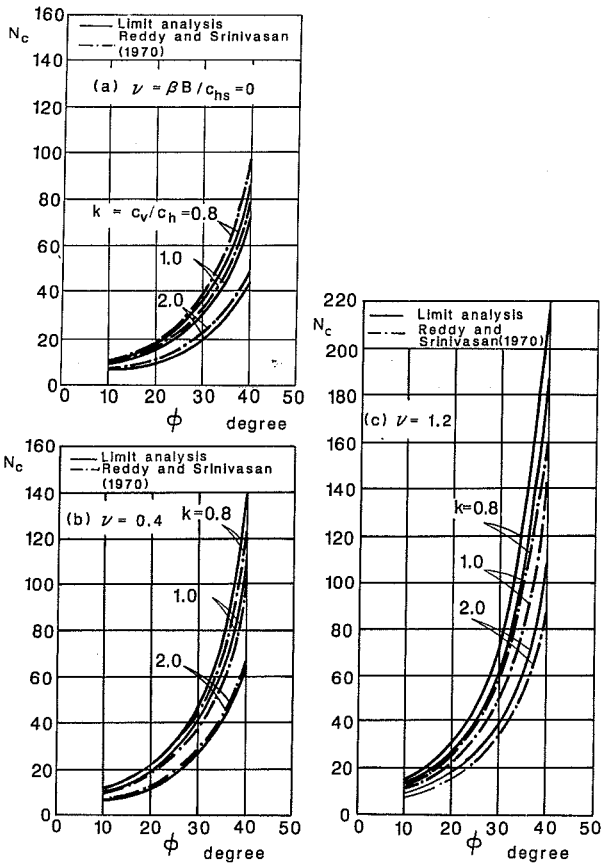

Fig. 7.3. Comparison of N_c values for $G = \gamma B/c_{\text{hs}} = 0.0$.

TABLE 7.2
Comparison of ratios of N_c (nonhomogeneous) to N_c (homogeneous) for $k = c_v/c_h = 1$, $G = \gamma B/c_{hs} = 0.0$, and $\nu = \beta B/c_{hs} = 1.2$

ϕ (degrees) (1)	Present analysis (2)	Salencon (1974b) (3)
10	1.527	1.45
20	1.699	1.60
30	1.965	1.85
40	3.437	3.25

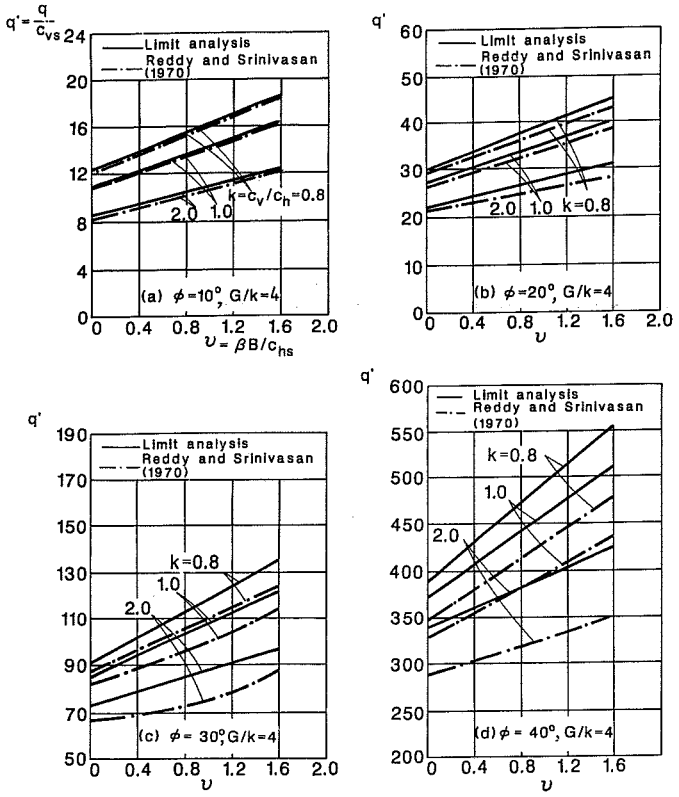

Fig. 7.4. Comparison of q' values.

Table 7.1 compares the values of the bearing capacity factor N_c for an isotropic and homogeneous soil, obtained by the present limit analysis with those of others reported previously. The values of N_c obtained by the present method are seen practically the same as those obtained by Sokolovskii (1965), Salencon (1974b) and Chen (1975).

Table 7.2 compares the ratios of N_c nonhomogeneous to N_c homogeneous, obtained by the present analysis and those of Salencon (1974b). The ratios obtained by the present analysis are slightly higher than those of Salencon. Values of the pre-

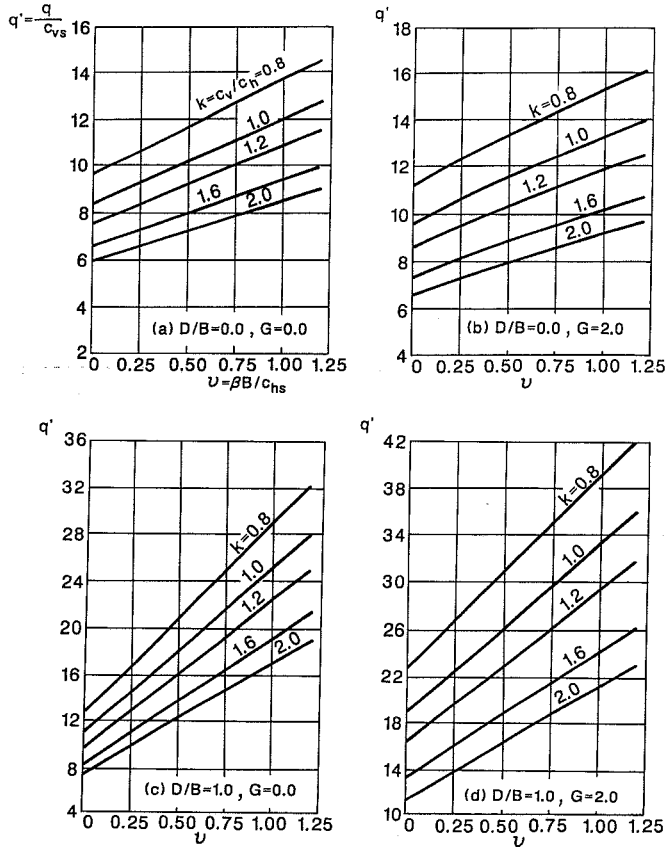

Fig. 7.5. Values of q' for $\phi = 10$ degrees.

sent analysis are about 5.3% higher for $\phi = 10°$ and 8.3% higher for $\phi = 10°$.

Figure 7.3 compares the values of N_c obtained for $G = 0.0$ and $\nu = 0$, 0.4 and 1.2, by the present analysis, with those of Reddy and Srinivasan (1970). It can be seen from these figures that, the values of N_c by the present analysis are slightly lower for $\nu = 0.0$ case and are slightly higher for $\nu \neq 0$ case. Figure 7.4 compares the values of q' obtained by the present analysis with those obtained by Reddy and Srinivasan (1970) for the combination of $\phi = 10°$, 20°, 30° and 40°, and $G/k = 4$. It can be seen from these figures, that the present analysis gives values higher than

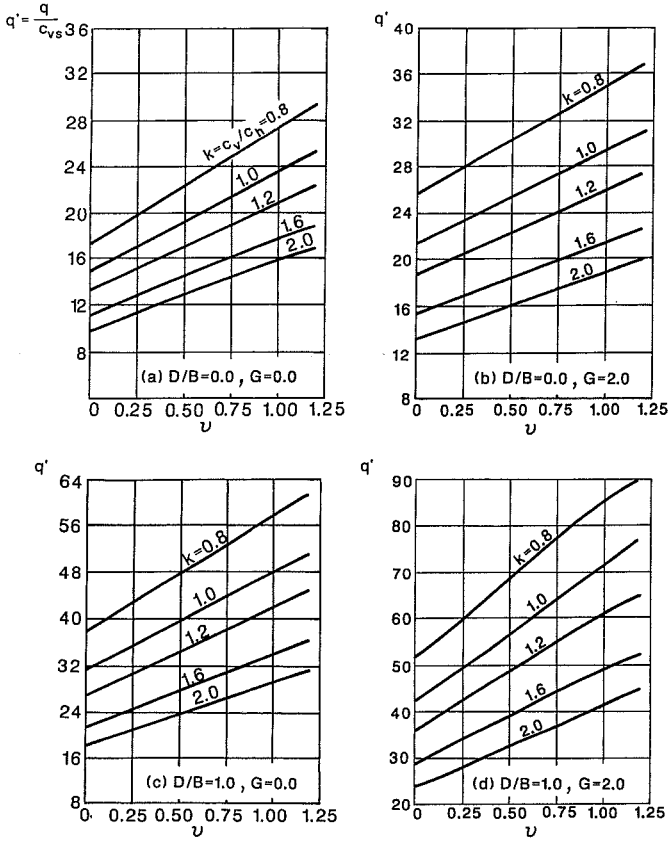

Fig. 7.6. Values of q' for $\phi = 20$ degrees.

those obtained by Reddy and Srinivasan (1970). The difference in the values of q' obtained by the two methods, increases with an increase in the friction angle ϕ.

Figures 7.5 to 7.8 show the q' variation with $\nu = \beta B/c_{hs}$ for several combinations of the parameters ϕ, D/B and G considered. These figures reveal that the variation of q' with ν is almost linear for the range of parameters considered. The values of q' increase with increasing ν, and decreases with increasing k.

Table 7.3 shows the percentage change in the bearing capacity pressure q' with

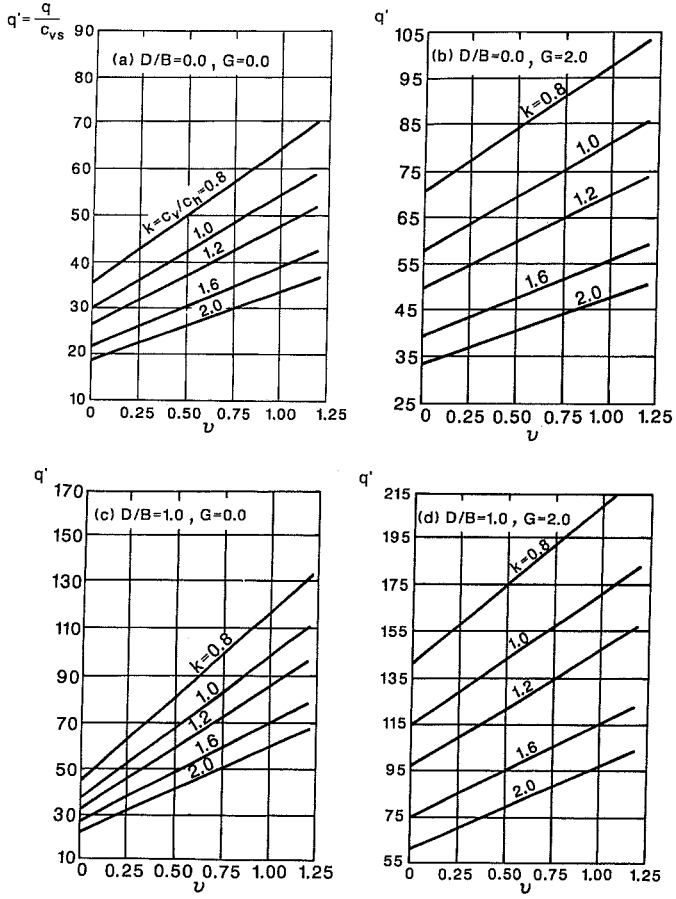

Fig. 7.7. Values of q' for $\phi = 30$ degrees.

respect to the isotropic and homogeneous values for the extreme values of parameters considered. The change in q', when compared to its values for $k = 1$ and $\nu = 0$, is seen to vary from -48% to $+305\%$.

In summary, for the range of parameters considered, numerical values for the bearing capacity of anisotropic and nonhomogeneous soils have been presented in the nondimensional form of charts, which can be used easily in practice. The results clearly show that the anisotropy and nonhomogeneity of soils do have a considerable influence on their load-carrying capacity.

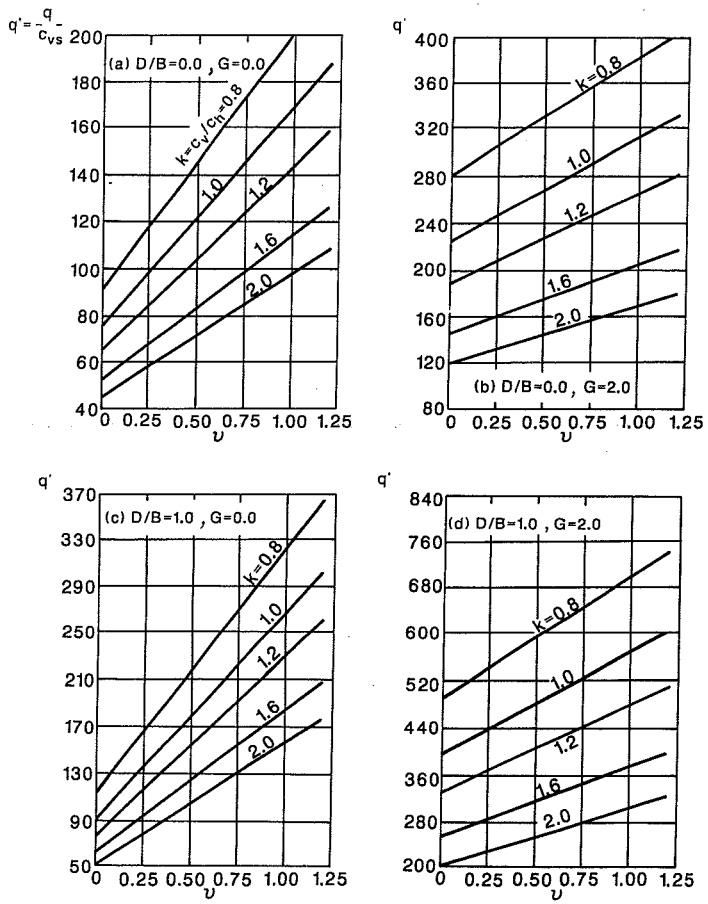

Fig. 7.8. Values of q' for $\phi = 40$ degrees.

TABLE 7.3
Percentage change in values of $q' = q/c_{vs}$ with respect to homogeneous and isotropic values

ϕ (degrees)	$d' = D/B$	$G = \gamma B/c_{hs}$	$k' = c_v/c_h = 0.8$		$k = 2.0$		$k = 1.0$
			$\nu = \beta B/c_{hs} = 0.0$	$\nu = 1.2$	$\nu = 0.0$	$\nu = 1.2$	$\nu = 1.2$
(1)	(2)	(3)	(4)	(5)	(6)	(7)	(8)
10	0.0	0.0	+14.33	+ 74.91	−28.72	+ 8.00	+ 52.69
		2.0	+15.83	+ 65.89	−31.71	− 8.44	+ 43.66
	1.0	0.0	+15.81	+197.00	−32.33	+74.92	+156.80
		2.0	+19.33	+123.50	−39.50	+22.32	+ 90.10
20	0.0	0.0	+16.41	+ 98.02	−32.82	+13.69	+ 69.91
		2.0	+18.93	+ 73.54	−37.89	− 6.52	+ 46.86
	1.0	0.0	+18.08	+183.50	−36.30	+73.60	+169.10
		2.0	+21.91	+110.20	−43.46	+ 5.25	+ 75.22
30	0.0	0.0	+18.41	+132.60	−36.92	+24.15	+ 96.47
		2.0	+23.52	+ 78.60	−43.09	−12.43	+ 48.25
	1.0	0.0	+19.81	+248.40	−39.69	+79.13	+192.00
		2.0	+23.27	+ 99.06	−46.54	− 6.99	+ 63.72
40	0.0	0.0	+20.11	+191.08	−40.58	+46.94	+143.68
		2.0	+23.33	+ 79.08	−46.73	−18.22	+ 46.67
	1.0	0.0	+21.05	+305.20	−42.37	+98.56	+235.50
		2.0	+24.08	+ 88.24	−47.18	−16.29	+ 55.43

References

Bishop, A.W., 1966. The strength of soils as engineering materials. Geotechnique, 16(1): 85–128.

Casagrande, A. and Carillo, N., 1944. Shear failure of anisotropic materials. Boston Soc. Civ. Eng. Reprinted in Contributions to Soil Mechanics, 1941–1953, Boston Society of Civil Engineers, 1953, pp. 122–135.

Chen, W.F., 1975. Limit Analysis and Soil Plasticity. Elsevier, Amsterdam, 638 pp.

Davis, E.H. and Brooker, J.R., 1973. The effect of increasing depth on the bearing capacity of clays. Geotechnique, 23(4): 551–563.

Davis, E.H. and Christian, J.T., 1971. Bearing capacity of anisotropic cohesive soil. J. Soil Mech. Found. Div., ASCE, 97(SM5): 753–769.

Drucker, D.C. and Prager, W., 1952. Soil mechanics and plastic analysis or limit design. Q. Appl. Math., 10(2): 157–164.

Ko, H.Y. and Davidson, L.W., 1973. Bearing capacity of footings in plane strain. J. Soil Mech. Found. Div. ASCE, 99 (SM1): 1–23.

Livneh, M. and Greenstein, J., 1973. The bearing capacity of footings on nonhomogeneous clays. Proc. 8th Int. Conf. on Soil Mechanics and Foundation Engineering, Moscow, USSR, Vol. 1, pp. 151–153.

Livneh, M. and Komornik, A., 1967. Anisotropic strength of compacted clays. Proc., 3rd Asian Regional Conference on Soil Mechanics and Foundation Engineering, Haifa, Israel, Vol. 1, pp. 298 – 304.
Lo, K.Y., 1965. Stability of slopes in anisotropic soils. J. Soil Mech. Found. Div., ASCE, 31(SM4): 85 – 106.
Meyerhof, G.G., 1978. Bearing capacity of anisotropic cohesionless soils. Can. Geotech. J., 15(4): 592 – 595.
Purushothama Raj, P. Ramiah, B.K. and Venkatakrishna Rao, K.N., 1972. Limit analysis on bearing capacity of shallow foundations. Symposium on Strength Deformation Behavior of Soils, Bangalore, India, pp. 191 – 196.
Raymond, G.P., 1967. The bearing capacity of large footings and embankments on clays. Geotechnique, 17: 1 – 10.
Reddy, A.S. and Srinivasan, R.J., 1967. Bearing capacity of footings on layered clays. J. Soil. Mech. Found. Div., ASCE, 93(SM2): 83 – 99.
Reddy, A.S. and Srinivasan, R.J., 1970. Bearing capacity of footings on anisotropic soils. J. Soil Mech. Found. Div., ASCE, 96(SM6): 1967 – 1986.
Reddy, A.S. and Srinivasan, R.J., 1971. Bearing capacity of footings on clays. Soils Found., 11(3): 51 – 64.
Reddy, A.S. and Venkatakrishna Rao, K.N., 1982. Bearing capacity of strip footing on c-ϕ soils exhibiting anisotropy and nonhomogeneity in cohesion. Soils Found., Jpn. Soc. Soil Mech. Found., Eng. 22(1): 49 – 60.
Salencon, J., 1974a. Bearing capacity of a footing on a $\phi = 0$ soil with linearly varying shear strength. Geotechnique, 24(3): 443 – 446.
Salencon, J., 1974b. Discussion on the paper 'The effect of increasing depth on the bearing capacity of clays by Davis and Brooker. Geotechnique, 24(3): 449 – 451.
Salencon, J., Florentin, P. and Gabriel, Y., 1976. Capacité portante globalendune Foundation sur un sol Nonhomogène. Geotechnique, 26(2): 351 – 370.
Shklarsky, E. and Livneh, M., 1961a. The anisotropic strength of asphalt paving mixtures. Bull. Res. Council Israel, 9C(4): 183 – 192.
Shklarsky, E. and Livneh, M., 1961b. Theoretical analysis of the splitting test for asphalt specimens. Bull. Res. Council Israel, 9C(4): 202.
Shklarsky, E. and Livneh, M., 1962. Equations of slip lines in anisotropic cohesive medium. Bull. Res. Council Israel, Vol. C(4): pp. 159 – 170.
Sokolovskii, V.V., 1965. Statics of Granular Media. Pergamon Press, New York, NY, 237 pp.
Terzaghi, K., 1943. Theoretical Soil Mechanics. John Wiley, New York, NY, 510 pp.

Chapter 8

EARTHQUAKE-INDUCED SLOPE FAILURE AND LANDSLIDES*

8.1 Introduction

Slope failures and landslides occur extensively in all parts of the world and frequently result in a tremendous toll of death and destruction of properties. It is therefore of prime importance to devise the means and capability necessary to achieve a satisfactory assessment of the danger of slope failures and landslides. The term *landslide* refers to a sudden rupture of a mass of rock or soil and its movement downslope by the force of gravity. Slides on the slopes of man-made cuts or earth structures are generally referred to as *slope failures.* Slides on natural slopes are commonly referred to as *landslides.* On steep slopes, among the many types of landslides that may occur, falls, slides, and avalanches of rock and soil are most frequent during rainstorm or earthquakes (Chen, 1977). In this chapter, for the sake of convenience of discussion, the term landslide, refers to a sudden slip of a mass of soil along a well-defined slip surface for both natural slopes and slopes of man-made cuts.

It is true that, in many instances, the most severe destructions and greatest number of casualties result from earthquake-induced landslides. Records show that this kind of earthquake-induced landslides occur most frequently on sloping earthmasses. They are observed on the slopes of dams, embankments, and other man-made cuts; on the banks of rivers, lakes, reservoirs, and along coasts as well as on mountain slopes (Koh and Chen, 1978). For simplicity, such sloping earth masses will be referred to as *'earth slopes'* throughout this chapter.

Because of the potential threats associated with these landslides, there is an urgent need to advance the state of the art to develop more effective methods for the assessment of such dangers. Common practice in such analysis involves two points: the first is the neglecting of the more complex soil behaviors and properties; the second is the simplification of the seismic forces as being a constant. This chapter focuses on the improvement of the analysis through the incorporation of nonconstant seismic forces throughout the slope height. In the following chapter this procedure will be extended and incorporates the nonhomogeneity of some soil properties.

* This chapter is based on the M.S. thesis by S.W. Chan (1980) and the paper by Chen, Chan en Koh (1984).

Thus, a more realistic estimation on the earthslope stability can be made with relative ease (Chen and Koh, 1978; Chen, 1980).

The extension of the limit analysis method for the static case to the case of seismic loadings is a logical step forward. The existing approach involves essentially adding to the deadweight of the potential collapse mass a *pseudo-static force* simulating the seismic load. This force acting through the center of gravity of the soil mass is expressed as the product of the soil mass and a *seismic coefficient* as defined previously in Chapter 5. As shown in Fig. 8.1, $m\gamma$ is the soil mass and k_h is the seismic coefficient in the horizontal direction.

The criticisms on this rather crude approach are: Firstly, the seismic coefficient of a slope is not a constant value during any instant of earthquake. Owing to the nonrigidity of the soil layers, the reactive forces developed throughout the height of the slope as a result of the movement of the ground always vary. Secondly, because of the granular nature of the soil, it is reasonable to expect the density and strength properties to vary along the height as the consequence of different degrees of water saturation inside the intergranular voids of the soil.

To get around the first problem, a more recent effort by Chen et al. (1978) was made to incorporate zones of different seismic coefficients along the height to approximate the actual variation (Fig. 8.2). While such approach is a definite improvement over the earlier ones, there are also restrictions to its application. A conceivable difficulty is the case where the variation of the seismic coefficient is so sharp that a large number of thin zones have to be used. In the presence of secon-

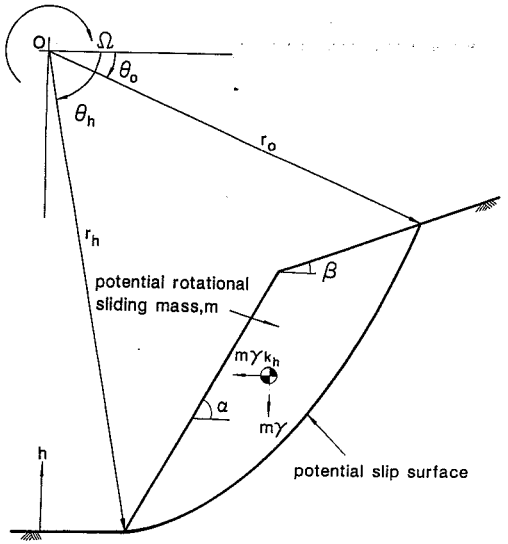

Fig. 8.1. Schematic of a pseudo-static constant seismic profile approach.

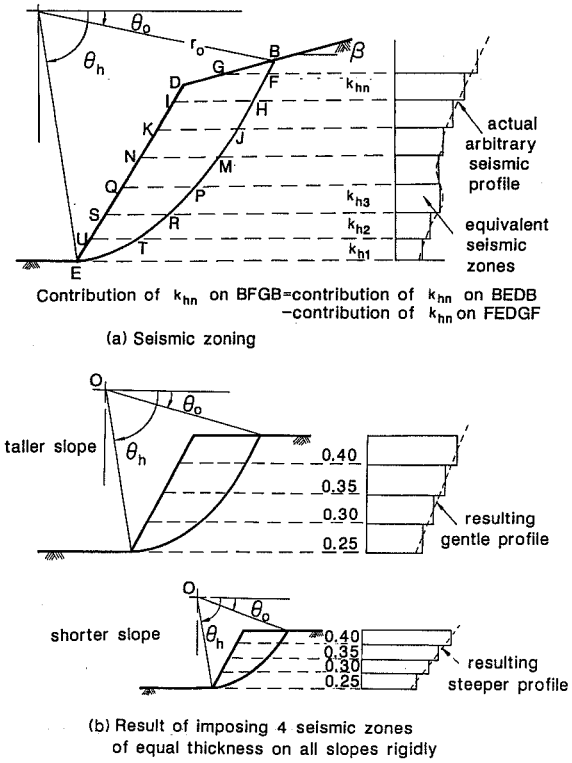

Fig. 8.2. Schematic of the seismic coefficient zoning approach.

dary slope as shown in Fig. 8.2 with $\beta > 0$, the analysis will necessitate the handling of two different slope geometries. In this case, rather than considering the original slope with one knee (section B-E-D-B in Fig. 8.2), one will have to consider a fictitious slope with two knees (F-E-D-G-F). With the need to prepare a map of coefficient zones for each profile of seismic forces at each instant, it would be quite time-consuming when investigating the hazard of the slope at intervals within the duration of the earthquake.

The next logical step towards a better analysis of the earthslope is to develop formulations to account for a more accurate seismic profile. The seismic coefficient as a function of the elevation about the ground level must be recognized. The vertical component of the seismic force, neglected in earlier works, must be included. Through appropriate interpretation, the vertical seismic profile can also be used to represent the variation of density along the height as well. With more rigorous and general formulations, further implications of the possibility of incorporating the

profiles of strength parameters into the model can be made. All these are undertaken in this chapter, following the work of Chen et al. (1984).

Since every mathematical model has its own limitations, it is the wise application of a model to different situations that determines its usefulness and efficiency. The slight changes of the model for the analysis of the location of the most critical slip surface in a given slope are demonstrated. Further directions for the applications of the model, as well as improvement for the future, are also discussed.

8.2 Failure surface

In the analysis of slope stability, the determination of the *critical height* of the slope, the height at which the slope is at the verge of collapse, yields an important criterion. According to the upper-bound theorem, failure can occur if a compatible failure mechanism exists in the body. A convenient way to approach the problem is to assume that a single, well-defined slip surface exists for the slope. For example, in Section 2.10, Chapter 2, the straight and logspiral surfaces were chosen as the translational and rotational mechanisms respectively to determine the critical height of the slope. The arguments were essentially based on the geometric compatibilities. The question that remains is that of these two types of mechanisms, which one would be more critical? That is, which one would be developed with the least input of external work? For the earthslope under the static loads, the ϕ-logspiral has been shown to be the most critical (Chen, 1975). This can be seen in the example problem of Section 2.10, Chapter 2. However, it is still necessary to find out, for more complicated loading situations, whether this type of failure mechanism is still the most likely to occur.

Since different shapes of failure surface will result in earthslopes of different soil masses, the stress state along the slip surface is mechanism-dependent. The process of determining the most critical surface is thus controlled by the consideration of the *shape function* and the *stress-distribution function.* The shape of the mechanism and the resulting stresses along the failure surface must be chosen in such a way that the external loads from the soil mass above this surface will be just balanced by the stresses developed at the surface. At the incipience of any collapse, when the stress state satisfies a certain criterion, the flow of the velocity discontinuity will then carry the block it supports along. Of all the possible shapes that satisfy the above requirement, the one that needs the minimum of applied load would be the most critical. This then is the criterion of optimization.

Using the techniques of variational calculus, the applied load on a potential slip surface can be defined by a function (Fig. 8.3):

$$W = \int_H [(\mathrm{d}F_x)^2 + (\mathrm{d}F_y)^2]^{\frac{1}{2}} \tag{8.1}$$

where $\mathrm{d}F_x$ and $\mathrm{d}F_y$ are the orthogonal force components of an infinitesimal soil layer at an arbitrary elevation. They are defined as:

$$\mathrm{d}F_x = \gamma\, k_x\, l\, \mathrm{d}h \tag{8.2}$$

and

$$\mathrm{d}F_y = \gamma\, k_y\, l\, \mathrm{d}h \tag{8.3}$$

Here, γ is the unit weight of soil; k_x and k_y are the seismic coefficients in x-, y-directions, respectively; l is the length of the infinitesimal soil layer, and $\mathrm{d}h$ is its thickness. For the static case involving the gravitational force only, $k_x = 0$ and $k_y = 1$. For seismic loading, both k_x and k_y are nonzero. The present formulation

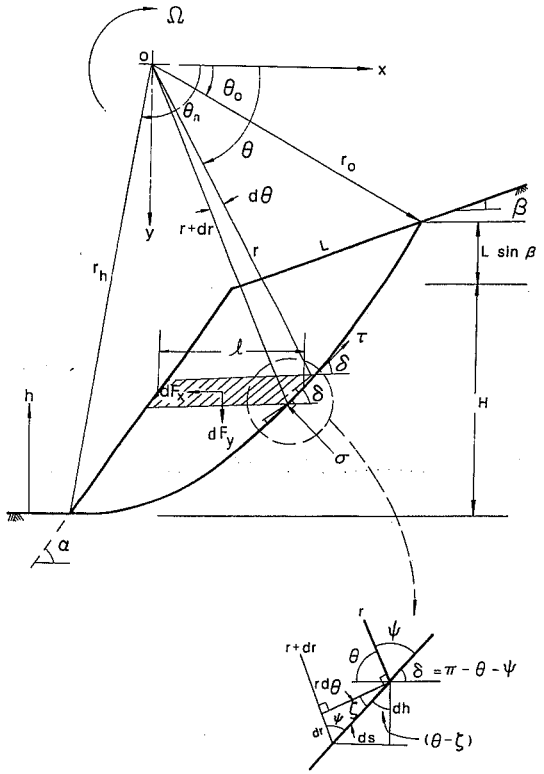

Fig. 8.3. Arbitrary potential failure surface.

permits the consideration of cases where the seismic load has a vertical component; for this case, $k_y \neq 1$.

To account for the variations of loadings along the vertical and horizontal distances from the toe of the slope, k_x and k_y are allowed to be any functions of r and θ, the reference polar coordinates (Fig. 8.3), as:

$$k_x = k_x(r,\theta) \tag{8.4}$$

and

$$k_y = k_y(r,\theta) \tag{8.5}$$

The function l depends on the shape of the slip surface, the geometry of the slope, as well as their relative positions with respect to each other. That is, the l-value depends on the *slip surface* ψ_1 and the *perimeter function* ψ_2 of the slope (Fig. 8.4). Recoursing to the rectangular coordinates for the time being, we have:

$$l = \psi_1(y) - \psi_2(\alpha,\beta,y) = l(\alpha,\beta,y) \tag{8.6}$$

Note that the actual form of ψ_2 is immaterial here. It can be any complicated function or even a Fourier series to account for the kink at the knee. Also notice that

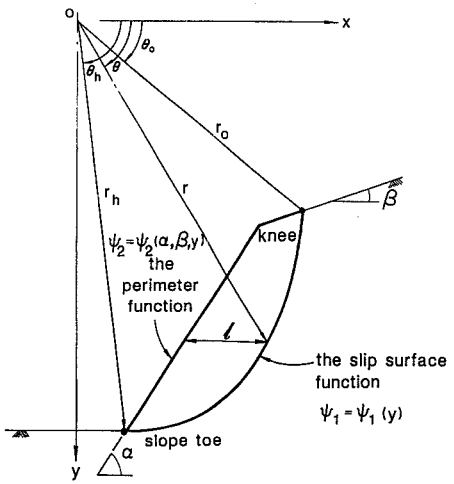

Fig. 8.4. The equivalency of l, the horizontal slice length, for a toe-surface of failure.

Eq. (8.6) is so general that it is true for any other slope-surface combinations (Figs. 8.5 and 8.6). Therefore, by transformation back to polar coordinates, l becomes:

$$l = l(\alpha,\beta,r,\theta) \tag{8.7}$$

From the consideration of the geometry along the slip line (Fig. 8.3):

$$dh = ds\cos(\theta - \zeta) \tag{8.8}$$

where ζ is the angle between the perpendicular to the radius and the surface element ds, which is:

$$ds = \frac{r\,d\theta}{\cos\zeta} \tag{8.9}$$

Therefore:

$$dh = f(r,\theta,\zeta)\,d\theta \tag{8.10}$$

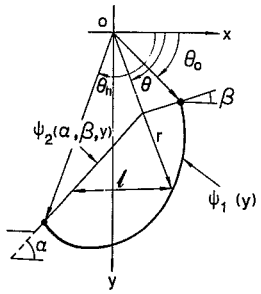

Fig. 8.5. The equivalency of l for a raised sagging slip surface.

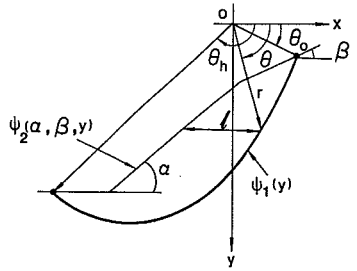

Fig. 8.6. The equivalency of l for a stretched slip surface.

With respect to the polar coordinates, and with θ_0 and θ_h being the initial and final angles of the slip surface, the functional W may be expressed as:

$$W = \int_{\theta_0}^{\theta_h} \gamma\, l(r,\theta,\alpha,\beta)\, [k_x^2(r,\theta) + k_y^2(r,\theta)]^{\frac{1}{2}}\, f(r,\theta,\zeta)\, d\theta \tag{8.11}$$

The additional equations are the equations of equilibrium:

$$\Sigma F_x = 0\,, \quad \int [\tau \cos\delta - \sigma \sin\delta]\, ds - \int \gamma\, k_x\, l\, dh = 0 \tag{8.12}$$

$$\Sigma F_y = 0\,, \quad -\int [\tau \sin\delta + \sigma \cos\delta]\, ds + \int \gamma\, k_y\, l\, dh = 0 \tag{8.13}$$

and

$$\Sigma M_0 = 0\,, \quad \int [r\sigma \sin\zeta - r\tau \cos\zeta]\, ds + \int \gamma\, [k_x r l \sin\theta + k_y l\, (r\cos\theta - \tfrac{1}{2} l)]\, dh = 0 \tag{8.14}$$

where $\delta = \pi - \theta - \psi$. These three equations can be simplified from the geometry. Furthermore, if we assume that the Coulomb's criterion (Eq. 2.32) is satisfied everywhere along the slip surface, then, they become:

$$\Sigma F_x = \int_{\theta_0}^{\theta_h} (R_1 - B_1)\, d\theta = 0 \tag{8.15}$$

$$\Sigma F_y = \int_{\theta_0}^{\theta_h} (R_2 + B_2)\, d\theta = 0 \tag{8.16}$$

$$\Sigma M_0 = \int_{\theta_0}^{\theta_h} (R_3 + B_3)\, d\theta = 0 \tag{8.17}$$

where

$$R_1 = -\sigma\, [(r\cos\theta)' \tan\phi + (r\sin\theta)'] - c(r\cos\theta)' = R_1(\theta,r,r',\phi,c,\sigma) \tag{8.18}$$

$$R_2 = \sigma\, [(r\cos\theta)' - (r\sin\theta)' \tan\phi] - c(r\sin\theta)' = R_2(\theta,r,r',\phi,c,\sigma) \tag{8.19}$$

$$R_3 = \sigma\, (rr' - r^2 \tan\phi) - cr^2 = R_3(r,r',\phi,\sigma) \tag{8.20}$$

$$B_1 = \gamma\, l(\theta,r,\alpha,\beta)\, k_x(\theta,r)\, f(\theta,r,\zeta) = B_1(\theta,r,\zeta,\alpha,\beta,\gamma) \tag{8.21}$$

$$B_2 = \gamma\, l(\theta,r,\alpha,\beta)\, k_y(\theta,r)\, f(\theta,r,\zeta) = B_2(\theta,r,\zeta,\alpha,\beta,\gamma) \tag{8.22}$$

$$B_3 = \gamma\, l(\theta,r,\alpha,\beta)\, \{(r\sin\theta)\, k_x(\theta,r) + [r\cos\theta - \tfrac{1}{2} l(\theta,r,\alpha,\beta)]\, k_y(\theta,r)\} = B_3(\theta,r,\alpha,\beta,\gamma) \tag{8.23}$$

where the R's are the reaction forces from the stress state of the slip surface, and the B's are the applied forces contributed by the soil block supported by the surface.

In minimizing the functional:

$$W = \int_{\theta_0}^{\theta_h} P(\theta,r,\alpha,\beta,\zeta)\, d\theta \tag{8.24}$$

subjected to the three constraints, it is necessary to make use of the Lagrangian multipliers:

$$I = P + \lambda_1(R_1 - B_1) + \lambda_2(R_2 + B_2) + \lambda_3(R_3 + B_3) \tag{8.25}$$

where λ_1, λ_2, and λ_3 are constants. By the Euler-Lagrange differential equation for multi-variable variational calculus, we get:

$$\frac{\partial I}{\partial r} - \frac{\partial^2 I}{\partial r' \partial \theta} - r' \frac{\partial^2 I}{\partial r' \partial r} - r'' \frac{\partial^2 I}{\partial r' \partial r'} = 0 \tag{8.26}$$

and

$$\frac{\partial I}{\partial \sigma} - \frac{\partial^2 I}{\partial \sigma' \partial \theta} - \sigma' \frac{\partial^2 I}{\partial \sigma' \partial \sigma} - \sigma'' \frac{\partial^2 I}{\partial \sigma' \partial \sigma'} = 0 \tag{8.27}$$

From the fact that P, B_1, B_2, and B_3 are independent of σ, it is obvious that:

$$\frac{\partial B_1}{\partial \sigma} = \frac{\partial B_2}{\partial \sigma} = \frac{\partial B_3}{\partial \sigma} = \frac{\partial P}{\partial \sigma} = 0 \tag{8.28}$$

With these, and the condition that:

$$\frac{\partial I}{\partial \sigma'} = 0 \tag{8.29}$$

Equation (8.27) becomes:

$$\lambda_1 \frac{\partial R_1}{\partial \sigma} + \lambda_2 \frac{\partial R_2}{\partial \sigma} + \lambda_3 \frac{\partial R_3}{\partial \sigma} = 0 \tag{8.30}$$

Substituting the expressions of R_1, R_2, and R_3 in Eqs. (8.18), (8.19), and (8.20) into Eq. (8.30), we obtain:

$$\lambda_1 \{- [(r'\cos\theta - r\sin\theta)\tan\phi + (r'\sin\theta + r\cos\theta)]\} + \lambda_2 \{(r'\cos\theta - r\sin\theta) - \tan\phi\,(r'\sin\theta + r\cos\theta)\} + \lambda_3 (rr' - r^2\tan\phi) = 0 \tag{8.31}$$

To convert the coordinates to the cartesian system, the following transformation identities are used:

$$\begin{cases} x = r\cos\theta \\ y = r\sin\theta \end{cases} \tag{8.32}$$

$$\frac{dx}{d\theta} = r'\cos\theta - r\sin\theta \tag{8.33}$$

$$\frac{dy}{d\theta} = r'\sin\theta + r\cos\theta \tag{8.34}$$

$$x\frac{dy}{d\theta} - y\frac{dx}{d\theta} = r^2 \tag{8.35}$$

and

$$x\frac{dx}{d\theta} + y\frac{dy}{d\theta} = rr' \tag{8.36}$$

Equation (8.31) is then reduced to:

$$\lambda_1 \left[-\tan\phi\frac{dx}{d\theta} - \frac{dy}{d\theta}\right] + \lambda_2\left[\frac{dx}{d\theta} - \tan\phi\frac{dy}{d\theta}\right] + \lambda_3\left[x\frac{dx}{d\theta} + y\frac{dy}{d\theta} - \tan\phi\left(x\frac{dy}{d\theta} - y\frac{dx}{d\theta}\right)\right] = 0 \tag{8.37}$$

Knowing that:

$$\frac{dy}{dx} = \left(\frac{dy}{d\theta}\right)\Big/\left(\frac{dx}{d\theta}\right) \tag{8.38}$$

we obtain:

$$\lambda_1\left[-\tan\phi - \frac{dy}{dx}\right] + \lambda_2\left[1 - \tan\phi\frac{dy}{dx}\right] + \lambda_3\left[x + y\frac{dy}{dx} - \tan\phi\left(x\frac{dy}{dx} - y\right)\right] = 0 \tag{8.39}$$

By collecting terms, it becomes:

$$\left(y - \frac{\lambda_1}{\lambda_3}\right)\frac{dy}{dx} + \left(x + \frac{\lambda_2}{\lambda_3}\right) + \tan\phi\left[\left(y - \frac{\lambda_1}{\lambda_3}\right) - \left(x + \frac{\lambda_2}{\lambda_3}\right)\frac{dy}{dx}\right] = 0 \tag{8.40}$$

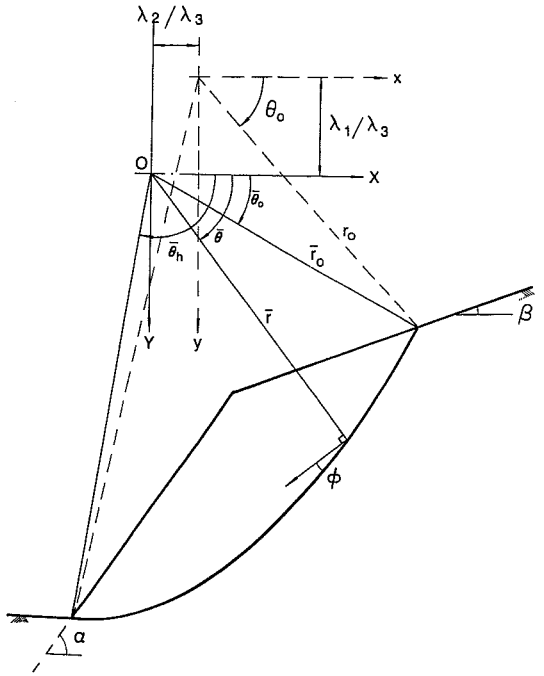

Fig. 8.7. Transformation of the x-y (r-θ) coordinates into the X-Y ($\bar{r}$-$\bar{\theta}$) coordinates.

Translating the origin (0,0) of the x,y-system to $(-\lambda_2/\lambda_3, \lambda_1/\lambda_3)$ of the new X,Y-system (Fig. 8.7), the differential equation evolves into:

$$Y\left(\frac{dY}{dX}\right) + X + \tan\phi\left(Y - X\frac{dY}{dX}\right) = 0 \tag{8.41}$$

or

$$(Y - X\tan\phi)\,dY + (Y\tan\phi + X)\,dX = 0 \tag{8.42}$$

Assuming:

$$Y = v\,X \tag{8.43}$$

where v will be explained later, then we have:

$$dY = v\,dX + X\,dv \tag{8.44}$$

Thus, Eq. (8.41) becomes:

$$(v^2 X + X)\,dX + (v\,X^2 - X^2\tan\phi)\,dv = 0 \tag{8.45}$$

Integrating Eq. (8.45), we obtain:

$$\int\frac{dX}{X} = \tan\phi\int\frac{dv}{1+v^2} - \int\frac{v\,dv}{1+v^2} + c_0 \tag{8.46}$$

where c_0 is a constant. That is:

$$ln\,X = \tan\phi\,[\arctan v] - \tfrac{1}{2}\,ln\,(1+v^2) + c_0 \tag{8.47}$$

Since $v = Y/X$, then from Fig. 8.7 it is obvious:

$$\bar{\theta} = \arctan(v) \tag{8.48}$$

and

$$(\bar{r}/X)^2 = 1 + v^2 \tag{8.49}$$

Therefore:

$$\ln X = \bar{\theta}\,\tan\phi - \tfrac{1}{2}\,ln\,(\bar{r}/X)^2 + c_0 \tag{8.50}$$

or

$$ln\,\bar{r} = \bar{\theta}\,\tan\phi + c_0 \tag{8.51}$$

From the boundary condition, where $\bar{r}_0$ corresponds to $\bar{\theta}_0$ for the initiation of the slip surface curve:

$$ln\,\bar{r}_0 = \bar{\theta}_0\,\tan\phi + c_0 \tag{8.52}$$

or

$$c_0 = ln\,\bar{r}_0 - \bar{\theta}_0\,\tan\phi \tag{8.53}$$

Substituting Eq. (8.53) back into Eq. (8.51), we finally obtain:

$$\bar{r} = \bar{r}_0\exp\left[(\bar{\theta} - \bar{\theta}_0)\tan\phi\right] \tag{8.54}$$

This is the equation for a ϕ-logspiral. The ϕ-logspiral is then the most critical slip surface.

From the solution of Eq. (8.27), it is obvious that the process of solving Eq. (8.26) will be even more tedious. The solution will be very complicated, and will result in the profile of the normal stress distribution along the slip surface. Since the resultant of normal and shear stresses along the entire surface is directed toward the center of rotation, they have no contribution to the internal work for our rotational mechanism. It is sufficient to know from the examination of Eq. (8.26) that the normal stress distribution along the slip surface varies with different loadings.

Note that by means of similar derivations, the following statement can be obtained. For the case where body forces as well as soil nonhomogeneity and anisotropy in cohesion are considered only, the most critical failure surface, if the Coulomb's criterion is used, is still the ϕ-log-spiral.

8.3 Determination of the critical height for seismic stability

As shown in Section 8.2, the ϕ-logspiral surface may be used as the failure mechanism in the stability analysis of an earthslope under seismic loading situations. Following traditional approach in slope stability analysis, we predict the critical height of the slope rather than the critical load itself. Such a prediction is an upper bound on the actual value. It is quite useful in providing insight to the evaluation of the slope stability as well as guidelines for the design of earthprojects.

Pertinent to the analysis of the stability of an earthslope under seismic loads is the development of a suitable representation for the loads. In conventional works

(Prater, 1979), the seismic load is considered constant and in the horizontal direction only. Further studies (Newmark, 1965; Seed, 1966, 1967; Ambraseys and Sarma, 1967) considered the seismic load to increase with height. In addition, studies have taken into consideration the vertical component of seismic load.

More realistically, the seismic profile is nonlinear. A convenient representation is to treat profiles of the vertical and horizontal components as polynomials of the elevation, as follows:

$$k_x(h) = a_0 + a_1 h + a_2 h^2 + \ldots + a_m h^m = \sum_{j=0}^{m} a_j h^j \tag{8.55}$$

and

$$k_y(h) = b_0 + b_1 h + b_2 h^2 + \ldots + b_n h^n = \sum_{j=0}^{n} b_j h^j \tag{8.56}$$

However, to conform to the polar coordinates used to describe the failure spiral surface, these must be expressed in terms of θ and r. If the spiral is to pass through the toe of the slope, then the height of any horizontal layer of soil is (Fig. 8.8):

$$h = \eta - y \tag{8.57}$$

where

$$\eta = r_h \sin\theta_h = r_0 \exp[(\theta_h - \theta_0)\tan\phi]\sin\theta_h \tag{8.58}$$

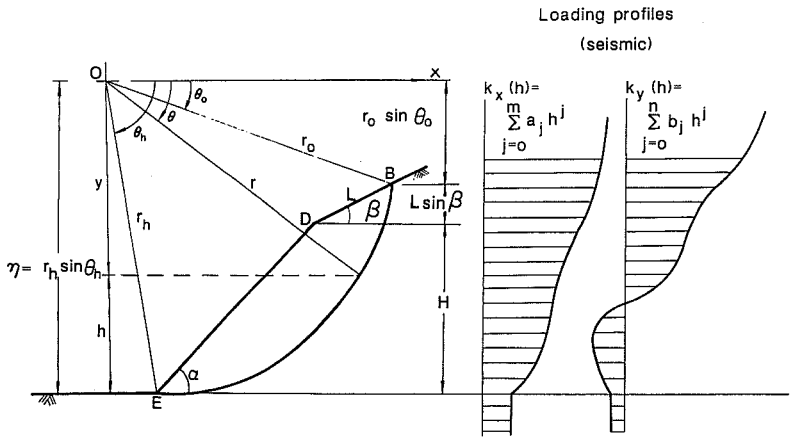

Fig. 8.8. Relation of the loading profiles to the geometry of the slope.

and

$$y = r\sin\theta = r_0 \exp[(\theta - \theta_0)\tan\phi]\sin\theta \tag{8.59}$$

with $\theta_0 \leq \theta \leq \theta_h$.

Substituting Eq. (8.57), into Eq. (8.55) for $k_x(h)$, we obtain:

$$k_x(y) = a_0 + a_1(\eta - y) + a_2(\eta - y)^2 + \ldots + a_m(\eta - y)^m \tag{8.60}$$

which expands to:

$$k_x(y) = a_0 + a_1\eta - a_1 y + a_2\eta^2 - 2a_2\eta y + a_2 y^2 + a_3\eta^3 - 3a_3\eta^2 y + 3a_3\eta y^2 - a_3 y^3 + \ldots + a_m\eta^m + a_m \sum_{k=1}^{m} \binom{m}{k} \eta^{(m-k)} y^k \tag{8.61}$$

Equation (8.61) may be rewritten as:

$$k_x(y) = (a_0 + a_1\eta + a_2\eta^2 + a_3\eta^3 + \ldots + a_m\eta^m) - (a_1 + 2a_2\eta + 3a_3\eta^2 + 4a_4\eta^3 + \ldots + a_m \binom{m}{1} \eta^{m-1}) y + (a_2 + 3a_3\eta + 6a_4\eta^2 + \ldots + a_m \binom{m}{2} \eta^{m-2}) y^2 - (a_3 + 4a_4\eta + \ldots + a_m \binom{m}{3} \eta^{m-3}) y^3 + \ldots + (\ldots + a_m \binom{m}{m} \eta^{m-m}) y^m \tag{8.62}$$

If we set:

$$\nu_j = \sum_{i=j}^{m} \binom{i}{j} a_i \eta^{i-j} (-1)^j \tag{8.63}$$

Equation (8.62) can be expressed as:

$$k_x(y) = \sum_{j=0}^{m} \nu_j y^j = \sum_{j=0}^{m} \nu_j (r\sin\theta)^j = k_x(r,\theta) \tag{8.64}$$

Similarly, for $k_y(y)$ with:

$$\mu_j = \sum_{i=j}^{n} \binom{i}{j} b_i \eta^{i-j} (-1)^j \tag{8.65}$$

we have:

$$k_y(y) = \sum_{j=0}^{n} \mu_j y^j = \sum_{j=0}^{n} \mu_j (r\sin\theta)^j = k_y(r,\theta) \tag{8.66}$$

8.3.1 *The critical height of toe-spiral*

A spiral that begins somewhere in the β-portion and terminates at the base of the α-portion of the slope shall be referred to as a *toe-spiral*. With the toe-spiral prescribed as the failure surface, together with the seismic profiles specified along the slope, the critical height of the slope may be derived.

The critical height of a toe-spiral is the height of the slope at which such a failure mechanism can be developed so that the soil mass resting upon the failure surface will be carried down in the fashion of pure rotation. Yielding impends when the loads from the rotating mass perform external work at a rate equal to the internal rate of energy dissipation in the mechanism. It is then only necessary to impose a virtually small rotational velocity to the rotational block, and require that the energy rate equilibrium be observed. Equating the external work rate to the internal dissipation rate will provide the basis for the calculation of the critical height.

By means of superposition, the rate of external work done contributed by the rotating soil mass D-B-E-D (Fig. 8.9) can be found as the rate of work done by A-B-E-F-A (the gross work rate), minus the work rate by A-B-D-C-A and C-D-E-F-C (the fictitious work rate). Considering the region of A-B-E-F-A first, we have (Fig. 8.10):

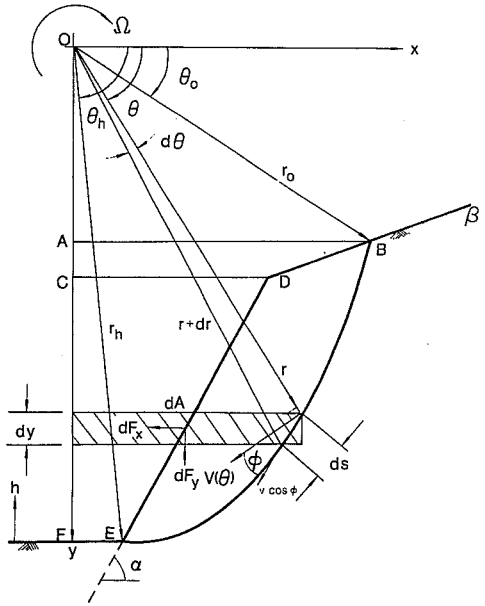

Fig. 8.9. Logspiral slip surface for seismic loading, calculation of the gross external work rate.

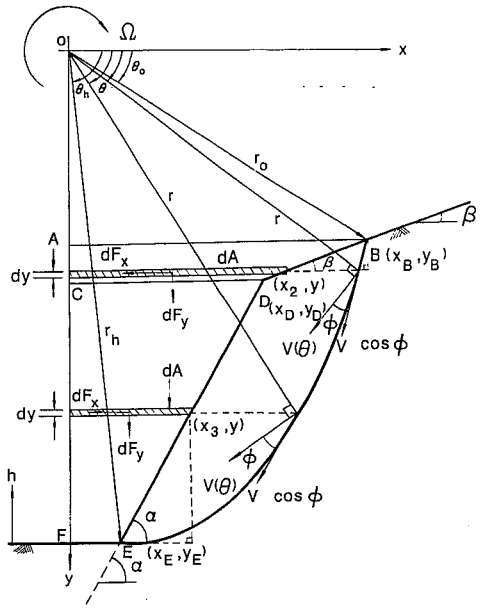

Fig. 8.10. Logspiral slip surface for seismic loading, calculation for the fictitious external work rate.

$$\dot{W}_1 = \int d\dot{W}_{1x} + \int d\dot{W}_{1y} = \int \Omega\, y\, dF_x + \int \tfrac{1}{2}\, \Omega\, x\, dF_y \tag{8.67}$$

with $dF_x = \gamma k_x(y)\, dA$, $dF_y = \gamma k_y(y)\, dA$, $x = r\cos\theta$, and $y = r\sin\theta$.
Noting that:

$$\begin{aligned} dy &= [(dr/d\theta)\sin\theta + r\cos\theta]\, d\theta \\ &= [\sin\theta\, d[r_0 \exp\{(\theta - \theta_0)\tan\phi\}]/d\theta + r\cos\theta]\, d\theta \\ &= (\sin\theta\tan\phi + \cos\theta)\, r\, d\theta \end{aligned} \tag{8.68}$$

and

$$dA = x\, dy = (\sin\theta\cos\theta\tan\phi + \cos^2\theta)\, r^2 d\theta \tag{8.69}$$

we have:

$$\int d\dot{W}_{1x} = \int_{\theta_0}^{\theta_h} \gamma\Omega\, k_x(y)\, r^3[\sin^2\theta\cos\theta\tan\phi + \sin\theta\cos^2\theta]\, d\theta \tag{8.70}$$

and

$$\int d\dot{W}_{1y} = \tfrac{1}{2}\gamma\Omega \int_{\theta_0}^{\theta_h} k_y(y)\, r^3\, [\sin\theta \cos^2\theta \tan\phi + \cos^3\theta]\, d\theta \tag{8.71}$$

For region A-B-D-C-A, we have:

$$\dot{W}_2 = \int d\dot{W}_{2x} + \int d\dot{W}_{2y} = \int_{y_B}^{y_D} \gamma\Omega\, k_x(y)\, [y x_2\, dy] + \int_{y_B}^{y_D} \tfrac{1}{2}\gamma\Omega\, k_y(y)\, [x_2^2 dy] \tag{8.72}$$

From the geometry, the expression of x_2 can be derived from:

$$\tan\beta = (y - y_B)/(x_B - x_2) \tag{8.73}$$

so that, for $y_B \le y \le y_D$:

$$x_2 = (x_B + y_B/\tan\beta) - y/\tan\beta = l_2 - y/\tan\beta \tag{8.74}$$

Thus:

$$\int d\dot{W}_{2x} = \int_{y_B}^{y_D} \gamma\Omega\, k_x(y)\, (l_2 - y/\tan\beta) y\, dy \tag{8.75}$$

and

$$\int d\dot{W}_{2y} = \int_{y_B}^{y_D} (\tfrac{1}{2})\, \gamma\Omega k_y(y)\, (l_2 - y/\tan\beta)^2\, dy \tag{8.76}$$

Similarly, for region C-D-E-F-C:

$$\dot{W}_3 = \int d\dot{W}_{3x} + \int d\dot{W}_{3y} = \int_{y_D}^{y_E} \gamma\Omega k_x(y)\, [y x_3 dy] + \int_{y_D}^{y_E} (\tfrac{1}{2})\, \gamma\Omega k_y(y)\, [x_3^2\, dy] \tag{8.77}$$

where from:

$$\tan\alpha = (y_E - y)/(x_3 - x_E) \tag{8.78}$$

and for $y_D \le y \le y_E$:

$$x_3 = (x_E + y_E/\tan\alpha) - y/\tan\alpha = l_3 - y/\tan\alpha \tag{8.79}$$

Thus:

$$\int d\dot{W}_{3x} = \int_{y_E}^{y_D} \gamma\Omega\, k_x(y)\, (l_3 - y/\tan\alpha) y\, dy \tag{8.80}$$

and

$$\int d\dot{W}_{3y} = \int_{y_E}^{y_D} (\tfrac{1}{2})\, \gamma\Omega\, k_y(y)\, (l_3 - y/\tan\alpha)^2\, dy \tag{8.81}$$

The above six equations Eqs. (8.70), (8.71), (8.75), (8.76), (8.80), and (8.81), can be expanded by substituting the expressions for $k_x(y)$ and $k_y(y)$ into them:

$$\int d\dot{W}_{1x} = \int_{\theta_0}^{\theta_h} \gamma\Omega \sum_{j=0}^{m} [\nu_j r^{j+3} (\sin^{j+1}\theta \cos^2\theta + \sin^{j+2}\theta \cos\theta \tan\phi)]\, d\theta \tag{8.82}$$

$$\int d\dot{W}_{1y} = \tfrac{1}{2}\int_{\theta_0}^{\theta_h} \gamma\Omega \sum_{j=0}^{n} [\mu_j r^{j+3} (\sin^{j}\theta \cos^3\theta + \sin^{j+1}\theta \cos^2\theta \tan\phi)]\, d\theta \tag{8.83}$$

$$\int d\dot{W}_{2x} = \int_{y_B}^{y_D} \gamma\Omega \sum_{j=0}^{m} [\nu_j (l_2\, y^{j+1} - y^{j+2}/\tan\beta)]\, dy \tag{8.84}$$

$$d\dot{W}_{2y} = \tfrac{1}{2}\int_{y_B}^{y_D} \gamma\Omega \sum_{j=0}^{n} [\mu_j (l_2^2\, y^j - 2l_2\, y^{j+1}/\tan\beta + y^{j+2}/\tan^2\beta)]\, dy \tag{8.85}$$

$$\int d\dot{W}_{3x} = \int_{y_D}^{y_E} \gamma\Omega \sum_{j=0}^{m} [\nu_j (l_3\, y^{j+1} - y^{j+2}/\tan\alpha)]\, dy \tag{8.86}$$

and

$$\int d\dot{W}_{3y} = \tfrac{1}{2}\int_{y_D}^{y_E} \gamma\Omega \sum_{j=0}^{n} [\mu_j (l_3^2\, y^j - 2l_3\, y^{j+1}/\tan\alpha + y^{j+2}/\tan^2\alpha)]\, dy \tag{8.87}$$

Equations (8.82) and (8.83) are expressed into more consistent forms with the application of the following identities:

$$\cos^2\theta = 1 - \sin^2\theta \tag{8.88}$$

and

$$r = \varrho \exp(\theta \tan\phi) \tag{8.89}$$

where

$$\varrho = r_0 \exp(-\theta_0 \tan\phi) \tag{8.90}$$

Thus, we have:

$$\int d\dot{W}_{1x} = \gamma\Omega \sum_{j=0}^{m} \left[\nu_j \varrho^{j+3} \int_{\theta_0}^{\theta_h} e^{\theta(j+3)\tan\phi} (\sin^{j+1}\theta - \sin^{j+3}\theta + \cos\theta \sin^{j+2}\theta \tan\phi)\, d\theta \right] \tag{8.91}$$

and

$$\int d\dot{W}_{1y} = \tfrac{1}{2} \gamma\Omega \sum_{j=0}^{n} \left[\mu_j \varrho^{j+3} \int_{\theta_0}^{\theta_h} e^{\theta(j+3)\tan\phi} (\cos\theta \sin^{j}\theta - \cos\theta \sin^{j+2}\theta + \sin^{j+1}\theta \tan\phi - \sin^{j+3}\theta \tan\phi)\, d\theta \right] \tag{8.92}$$

Each of these two equations involves two integral forms, namely $e^{A\theta} \sin^B\theta \cos\theta\, d\theta$, and $e^{A\theta} \sin^B\theta\, d\theta$. Their solutions are:

$$\int e^{A\theta} \sin^B\theta \cos\theta\, d\theta = \frac{e^{A\theta} \sin^B\theta\, [A \cos\theta + (B+1) \sin\theta]}{A^2 + (B+1)^2} - \frac{AB}{A^2 + (B+1)^2} \int e^{A\theta} \sin^{B-1}\theta\, d\theta \tag{8.93}$$

and

$$\int e^{A\theta} \sin^B\theta\, d\theta = \frac{e^{A\theta} \sin^{B-1}\theta\, (A \sin\theta - B \cos\theta)}{A^2 + B^2} + \frac{B\,(B-1)}{A^2 + B^2} \int e^{A\theta} \sin^{B-2}\theta\, d\theta \tag{8.94}$$

We expand Eq. (8.94) iteratively as:

$$\int e^{A\theta} \sin^B\theta\, d\theta = \frac{1}{A^2 + B^2} \left[e^{A\theta} \sin^{B-1}\theta\, (A \sin\theta - B \cos\theta) + B(B-1) \left(\frac{1}{A^2 + (B-2)^2} [e^{A\theta} \sin^{B-3}\theta\, \{A \sin\theta - (B-2)\cos\theta\} + (B-2)(B-3)\, e^{A\theta} \sin^{B-4}\theta\, d\theta] \right) \right]$$

$$= e^{A\theta} \left\{ \frac{\sin^{B-1}\theta\, (A \sin\theta - B \cos\theta)}{A^2 + B^2} + \frac{B\,(B-1) \sin^{B-3}\theta}{A^2 + B^2} \right. \frac{A \sin\theta - (B-2)\cos\theta}{A^2 + (B-2)^2} + \frac{B\,(B-1)\,(B-2)\,(B-3) \sin^{B-5}\theta}{(A^2 + B^2)\,[A^2 + (B-2)^2]} \left. \frac{A \sin\theta - (B-4)\cos\theta}{A^2 + (B-4)^2} + \ldots \right\} + \lambda \tag{8.95}$$

where λ is the last term of the series. The expression for λ depends on whether B is even or odd. If B is even, then $\lambda = \lambda_e$:

$$\lambda_e = k_e \int e^{A\theta}\, d\theta = \begin{cases} k_e \dfrac{e^{A\theta}}{A} & \text{if } A \neq 0 \\ k_e \theta & \text{if } A = 0 \end{cases} \tag{8.96}$$

with:

$$k_e = \frac{B(B-1)(B-2)(B-3) \ldots [B - (B-1)]}{(A^2 + B^2)\,[A^2 + (B-2)^2] \ldots \{A^2 + [B - (B-2)]^2\}} \tag{8.97}$$

or

$$\lambda_e = \begin{cases} e^{A\theta} \left\{ \dfrac{B(B-1) \ldots (1)\, A}{(A^2 + B^2)\,[A^2 + (B-2)^2] \ldots (A^2 + 2^2)\, A^2} \right\} & \text{if } A \neq 0 \\ \dfrac{B(B-1) \ldots (1)}{B^2(B-2)^2 \ldots (2)^2} \theta & \text{if } A = 0 \end{cases} \tag{8.98}$$

If B is odd, then $\lambda = \lambda_0$:

$$\lambda_0 = k_0 \int e^{A\theta} \sin\theta\, d\theta = k_0 \left[\frac{A \sin\theta - \cos\theta}{A^2 + 1} e^{A\theta} \right] \tag{8.99}$$

with:

$$k_0 = \frac{B(B-1) \ldots [B - (B-2)]}{[A^2 + B^2] \ldots \{A^2 + [B - (B-3)]^2\}} \tag{8.100}$$

or

$$\lambda_0 = e^{A\theta}\left[\frac{B(B-1)\ldots(2)\,(A\sin\theta-\cos\theta)}{(A^2+B^2)\ldots(A^2+3^2)\,(A^2+1^2)}\right] \tag{8.101}$$

Now, since:

$$\begin{bmatrix} B \\ 2s \end{bmatrix} = \frac{(B)\,(B-1)\ldots(B-2s+1)}{(2s)!} \tag{8.102}$$

and

$$\begin{bmatrix} B \\ 0 \end{bmatrix} = 1$$

then, Eq. (8.95) can be expressed as:

$$\int e^{A\theta}\sin^B\theta\,d\theta = e^{A\theta}\sum_{s=0}^{\text{int}\left(\frac{B}{2}\right)}\left\{\begin{bmatrix} B \\ 2s \end{bmatrix}(2s)!\,\frac{[A\sin\theta-(B-2s)\cos\theta]\sin^{B-2s-1}\theta}{\prod_{t=0}^{s}[A^2+(B-2t)^2]}\right\} \tag{8.103}$$

where int$(B/2)$ = the integer part of $(B/2)$. Note that the last term, λ_e or λ_0 is included. For, if B is even, then int $(B/2) = B/2$, and the last term in the sum of Eq. (8.103) is:

$$\lambda_e = \frac{B(B-1)\ldots[B-2(B/2)+1]\,(\sin\theta)^{-1}\,(A\sin\theta)}{(A^2+B^2)\ldots\{A^2+[B-(B-2)]^2\}\,[A^2]}\,e^{A\theta} \tag{8.104}$$

If B is odd, then int $(B/2) = (B-1)/2$ and the last term in the sum of Eq. (8.103) is:

$$\lambda_0 = \frac{B(B-1)\ldots[B-2(B-1)/2+1]\,(\sin\theta)^0\,(A\sin\theta-\cos\theta)}{(A^2+B^2)\ldots(A^2+3^2)\,(A^2+1^2)}\,e^{A\theta} \tag{8.105}$$

If Eq. (8.103) is written in the simple form:

$$\int e^{A\theta}\sin^B\theta\,d\theta = I[A, B] \tag{8.106}$$

Then, similarly, after some manipulation, Eq. (8.93) can be expressed as:

$$\int e^{A\theta}\sin^B\theta\cos\theta\,d\theta = \frac{e^{A\theta}\sin^B\theta\,[A\cos\theta+(B+1)\sin\theta]}{A^2+(B+1)^2} - \frac{AB}{A^2+(B+1)^2}I[A, B-1] = J[A, B] \tag{8.107}$$

Ultimately, Eqs. (8.91) and (8.92) can be reduced to the final form:

$$d\dot{W}_{1x} = \gamma\Omega r_0^3 f_{1x}(r_0, \theta_0, \theta_h) \tag{8.108}$$

and

$$d\dot{W}_{1y} = \tfrac{1}{2}\gamma\Omega r_0^3 f_{1y}(r_0, \theta_0, \theta_h) \tag{8.109}$$

where

$$f_{1x}(r_0,\theta_0,\theta_h) = r_0^{-3}\sum_{j=0}^{m}\nu_j\varrho^{j+3}\left\{I\left[(j+3)\tan\phi,\, j+1\right]_{\theta_0}^{\theta_h} - I\left[(j+3)\tan\phi,\, j+3\right]_{\theta_0}^{\theta_h} + \tan\phi\, J\left[(j+3)\tan\phi,\, j+2\right]_{\theta_0}^{\theta_h}\right\} \tag{8.110}$$

and

$$f_{1y}(r_0,\theta_0,\theta_h) = r_0^{-3}\sum_{j=0}^{n}\mu_j\varrho^{j+3}\left\{J\left[(j+3)\tan\phi,\, j\right]_{\theta_0}^{\theta_h} - J\left[(j+3)\tan\phi,\, j+2\right]_{\theta_0}^{\theta_h} + \tan\phi\, I\left[(j+3)\tan\phi,\, j+1\right]_{\theta_0}^{\theta_h} - \tan\phi\, I\left[(j+3)\tan\phi,\, j+3\right]_{\theta_0}^{\theta_h}\right\} \tag{8.111}$$

Next, the coordinates of the points B, D, and E of the soil mass D-B-E-D are seen to be (Fig. 8.10):

$$y_B = r_0\sin\theta_0 \tag{8.112}$$

$$y_D = r_0\sin\theta_0 + L\sin\beta \tag{8.113}$$

and

$$y_E = r_h \sin\theta_h = r_0 \exp[(\theta_h - \theta_0)\tan\phi] \sin\theta_h \tag{8.114}$$

Therefore, from Eqs. (8.74) and (8.79):

$$l_2 = x_B + y_B/\tan\beta = r_0(\cos\theta_0 + \sin\theta_0/\tan\beta) \tag{8.115}$$

and

$$l_3 = x_E + y_E/\tan\alpha = r_0 \exp[(\theta_h - \theta_0)\tan\phi] (\cos\theta_h + \sin\theta_h/\tan\alpha) \tag{8.116}$$

The variables L, like H, is the geometric parameter describing the rotating soil mass D-B-E-D. From the geometrical configuration of the slope shown in Fig. 8.8, we have the following relations:

$$r_0 \cos\theta_0 - r_h \cos\theta_h - H/\tan\alpha - L\cos\beta = 0 \tag{8.117}$$

and

$$r_h \sin\theta_h - r_0 \sin\theta_0 - H - L\sin\beta = 0 \tag{8.118}$$

The solution of these two simultaneous equations gives explicit expressions for both L and H:

$$L = [r_0 \sin(\theta_0 + \alpha) - r_h \sin(\theta_h + \alpha)]/\sin(\alpha - \beta) \tag{8.119}$$

and

$$H = [r_h \sin(\theta_h + \beta) - r_0 \sin(\theta_0 + \beta)] \sin\alpha/\sin(\alpha - \beta) \tag{8.120}$$

Equations (8.84) to (8.87) are all in integrable forms, and can be expressed formally as:

$$\int d\dot{W}_{2x} = \gamma\Omega r_0^3 f_{2x}(r_0, \theta_0, \theta_h) \tag{8.121}$$

$$\int d\dot{W}_{2y} = \tfrac{1}{2}\gamma\Omega r_0^3 f_{2y}(r_0, \theta_0, \theta_h) \tag{8.122}$$

$$\int d\dot{W}_{3x} = \gamma\Omega r_0^3 f_{3x}(r_0, \theta_0, \theta_h) \tag{8.123}$$

and

$$\int d\dot{W}_{3y} = \tfrac{1}{2}\gamma\Omega r_0^3 f_{3y}(r_0, \theta_0, \theta_h) \tag{8.124}$$

where

$$f_{2x}(r_0, \theta_0, \theta_h) = r_0^{-3} \sum_{j=0}^{m} \nu_j \left[\frac{l_2 y^{j+2}}{j+2} - \frac{y^{j+3}}{(j+3)\tan\beta}\right]\Bigg|_{y_B}^{y_D} \tag{8.125}$$

$$f_{2y}(r_0, \theta_0, \theta_h) = r_0^{-3} \sum_{j=0}^{n} \mu_j \left[\frac{l_2^2 y^{j+1}}{j+1} - \frac{2l_2 y^{j+2}}{(j+2)\tan\beta} + \frac{y^{j+3}}{(j+3)\tan^2\beta}\right]\Bigg|_{y_B}^{y_D} \tag{8.126}$$

$$f_{3x}(r_0, \theta_0, \theta_h) = r_0^{-3} \sum_{j=0}^{m} \nu_j \left[\frac{l_3 y^{j+2}}{j+2} - \frac{y^{j+3}}{(j+3)\tan\alpha}\right]\Bigg|_{y_D}^{y_E} \tag{8.127}$$

$$f_{3y}(r_0, \theta_0, \theta_h) = r_0^{-3} \sum_{j=0}^{n} \mu_j \left[\frac{l_3^2 y^{j+1}}{j+1} - \frac{2l_3 y^{j+2}}{(j+2)\tan\alpha} + \frac{y^{j+3}}{(j+3)\tan^2\alpha}\right]\Bigg|_{y_D}^{y_E} \tag{8.128}$$

The total rate of external work done is now expressed as:

$$\dot{W}_E = \dot{W}_1 - \dot{W}_2 - \dot{W}_3 = \int d\dot{W}_{1x} + \int d\dot{W}_{1y} - \int d\dot{W}_{2x} - \int d\dot{W}_{2y} - \int d\dot{W}_{3x} - \int d\dot{W}_{3y} \tag{8.129}$$

or

$$\dot{W}_E = \gamma\Omega r_0^3 [f_{1x} + \tfrac{1}{2} f_{1y} - f_{2x} - \tfrac{1}{2} f_{2y} - f_{3x} - \tfrac{1}{2} f_{3y}] \tag{8.130}$$

The next step is to calculate the rate of internal energy dissipation along the velocity discontinuity surface BE, where yielding occurs. Similar as Eq. (2.33) (Fig. 2.14), this dissipation rate for an infinitesimal surface element is:

$$dD = (\tau - \sigma\tan\phi)\,\dot{\gamma}\,dv \tag{8.131}$$

where

$$\dot{\gamma} = r\Omega\cos\phi/t \tag{8.132}$$

in which t is the extremely small thickness of the velocity transition zone resulting from the dilatation. The negative sign for the second terms is necessary because σ represents the compressive normal stress while $\dot{\gamma}\tan\phi$ stands for the outwards dilatation. Since the Coulomb's criterion (Eq. 2.32) must be satisfied, we have $-\sigma\tan\phi = c - \tau$. Substituting it into Eq. (8.131) and integrating over the entire region of the mechanism results in:

$$\int_v \mathrm{d}D = \int_v (\tau - \sigma \tan\phi)\,\dot{\gamma}\,\mathrm{d}v = \int_s \int_0^t \left(cr\,\Omega\,\frac{\cos\phi}{t}\right)\mathrm{d}\Delta\,\mathrm{d}s$$
$$= \frac{c\Omega\cos\phi}{t}\int_s r \int_0^t \mathrm{d}\Delta\,\mathrm{d}s \tag{8.133}$$

Here, $\mathrm{d}\Delta$ is the differential thickness of an element. The extremely small thickness of the transition zone is constant throughout. Noting that $\mathrm{d}s = r\,\mathrm{d}\theta/\cos\phi$, we have for the total internal rate of work (or the total energy dissipation rate) expression:

$$\dot{W}_\mathrm{I} = D = \frac{c\Omega}{t}\int_{\theta_0}^{\theta_\mathrm{h}} r^2\,t\,\mathrm{d}\theta = c\Omega\int_{\theta_0}^{\theta_\mathrm{h}} \{r_0 \exp[(\theta - \theta_0)\tan\phi]\}^2\,\mathrm{d}\theta$$
$$= c\Omega r_0^2\,\{\exp[2(\theta_\mathrm{h} - \theta_0)\tan\phi] - 1\}/(2\tan\phi) \tag{8.134}$$

Equating the external work rate to the internal rate of dissipation:

$$\dot{W}_\mathrm{E} = \dot{W}_\mathrm{I} = D \tag{8.135}$$

we have:

$$r_0 = \frac{c}{\gamma}\,\frac{\exp[2(\theta_\mathrm{h} - \theta_0)\tan\phi] - 1}{2\tan\phi\,[(f_{1x} - f_{2x} - f_{3x}) + \frac{1}{2}(f_{1y} - f_{2y} - f_{3y})]} \tag{8.136}$$

By the upper-bound theorem, this means that any toe-spiral satisfying the above equation will be a surface along which yielding impends. Substitution of Eq. (8.136) into Eq. (8.120) gives an expanded expression for H, the vertical distance of the knee D above the ground, or the height of the slope:

$$H = \frac{c}{\gamma}\,F(r_0,\theta_0,\theta_\mathrm{h}) \tag{8.137}$$

where

$$F(r_0,\theta_0,\theta_\mathrm{h}) =$$
$$\frac{\sin\alpha[\mathrm{e}^{(\theta_\mathrm{h} - \theta_0)\tan\phi}\sin(\theta_\mathrm{h} + \beta) - \sin(\theta_0 + \beta)]\,[\mathrm{e}^{2(\theta_\mathrm{h} - \theta_0)\tan\phi} - 1]}{2\tan\phi\,\sin(\alpha - \beta)\,[f_{1x} - f_{2x} - f_{3x} + \frac{1}{2}(f_{1y} - f_{2y} - f_{3y})]} \tag{8.138}$$

The critical height of instability is then the minimum value of H attainable for a combination of ϕ, α, and β, as well as $k_x(y)$ and $k_y(y)$. It may be written as:

$$H^* \leq \frac{c}{\gamma}\,N^* \tag{8.139}$$

with

$$N^* = \min\,[F(r_0,\theta_0,\theta_\mathrm{h})] = F(r_0^*,\theta_0^*,\theta_\mathrm{h}^*) \tag{8.140}$$

such that r_0^*, θ_0^* and θ_h^* satisfy the conditions of:

$$\frac{\partial F}{\partial r_0} = 0, \qquad \frac{\partial F}{\partial \theta_0} = 0, \qquad \frac{\partial F}{\partial \theta_\mathrm{h}} = 0 \tag{8.141}$$

The dimensionless number N^* is the *seismic stability factor* of the earthslope. The value of N^* is a pure number, and is dependent on ϕ, α, β, $k_x(y)$ and $k_y(y)$.

Note that when the loading force is a constant (i.e. zero-th degree polynomial in y), the function F becomes dependent on θ_0 and θ_h only, and:

$$F(k_x = \text{constant},\ k_y = \text{constant}) = F(\theta_0,\theta_\mathrm{h}) \tag{8.142}$$

8.3.2 Earthslopes of purely cohesive soil

A purely cohesive soil is one in which there is no internal friction ($\phi = 0$). It is also called the *Tresca material.*

It is observed from Eq. (8.138) that:

$$F = \frac{g(\phi)}{q(\phi)} \tag{8.143}$$

where

$$g(\phi) = \sin\alpha\,[\mathrm{e}^{(\theta_\mathrm{h} - \theta_0)\tan\phi}\sin(\theta_\mathrm{h} + \beta) - \sin(\theta_0 + \beta)]\,[\mathrm{e}^{2(\theta_\mathrm{h} - \theta_0)\tan\phi} - 1] \tag{8.144}$$

and

$$q(\phi) = 2\tan\phi\,\sin(\alpha - \beta)\,[f_{1x} - f_{2x} - f_{3x} + \tfrac{1}{2}(f_{1y} - f_{2y} - f_{3y})] \tag{8.145}$$

For $\phi = 0$, function F becomes:

$$F(\phi = 0) = \frac{g(\phi = 0)}{q(\phi = 0)} = \frac{0}{0} \tag{8.146}$$

By the L'Hopital rule, we have:

$$F(\phi = 0) = \lim_{\phi \to 0} \frac{g(\phi)}{q(\phi)} = \frac{g'(0)}{q'(0)} \tag{8.147}$$

Differentiating functions $g(\phi)$ and $q(\phi)$ from Eqs. (8.144) and (8.145) with respect to ϕ, collecting terms, and evaluating at $\phi = 0$, we have:

$$g'(0) = 2(\theta_h - \theta_0)\,[\sin(\theta_h + \beta) - \sin(\theta_0 + \beta)]\sin\alpha \tag{8.148}$$

$$q'(0) = 2\sin(\alpha - \beta)\,[(f_{1x} - f_{2x} - f_{3x}) + \tfrac{1}{2}(f_{1y} - f_{2y} - f_{3y})]\,|_{\phi = 0} \tag{8.149}$$

Accordingly:

$$F(r_0, \theta_0, \theta_h)\,|_{\phi = 0} = \frac{(\theta_h - \theta_0)\,[\sin(\theta_h + \beta) - \sin(\theta_0 + \beta)]\,\sin\alpha}{\sin(\alpha - \beta)\,[f_{1x} - f_{2x} - f_{3x} + \frac{1}{2}(f_{1y} - f_{2y} - f_{3y})]|_{\phi = 0}} \tag{8.150}$$

8.3.3 Physical ranges and constraints

Since the problem concerned has been associated with certain geometries, it is necessary to identify the physical constraints corresponding to the geometrical restrictions. Applicability of the analysis to physical situations is discussed in this section.

A total of eleven constraints, stemming from physical considerations, can be identified. These are:

$$\text{(a) } r_0 - \frac{c}{\gamma}\,\frac{\exp[2(\theta_h - \theta_0)\tan\phi] - 1}{2\tan\phi\,[(f_{1x} - f_{2x} - f_{3x}) + \frac{1}{2}(f_{1y} - f_{2y} - f_{3y})]} = 0 \tag{8.151}$$

This is the only equality constraint. It is the same as Eq. (8.136), which must be satisfied for spiral failure mechanism.

$$\text{(b) } r_h \sin\theta_h - r_0 \sin\theta_0 - L\sin\beta > 0 \tag{8.152}$$

This is similar to the second of the two simultaneous equations for the slope geometry, Eq. (8.118). Its inclusion in this list imposes the restriction that the spiral must terminate in the α-portion of the slope.

$$\text{(c) } L > 0 \tag{8.153}$$

This requires that the spiral be started out in the β-zone of the slope. Thus, the second and third constraints assure the condition that the spiral traverses both zones of the slope under investigation.

$$\text{(d) } f_{1x} - f_{2x} - f_{3x} + \tfrac{1}{2}(f_{1y} - f_{2y} - f_{3y}) > 0 \tag{8.154}$$

and

$$\{\exp[(\theta_h - \theta_0)\tan\phi]\,\sin(\theta_h + \beta) - \sin(\theta_0 + \beta)\}\,\sin\alpha/\sin(\alpha - \beta) > 0 \tag{8.155}$$

A close examination of the equation for the critical height as formally stated in Eq. (8.138) reveals that the value for the critical height can still be illusively positive yet physically unrealistic. This is the case when both the numerator and the denominator expressions are negative-valued. In order to rule out such a possibility, the constraint (d) is introduced. As it may seen quite redundant to use both expressions as constraints instead of just either one of these, it must be pointed out that using both can safeguard the function from assuming negative values. This is extremely important as far as the optimization process is concerned.

$$\text{(e) } L/H > 0.1 \tag{8.156}$$

This essentially requires that the spiral not be skewed towards and along the height of the slope. The most part of it lies in the α-zone (Fig. 8.11).

$$\text{(f) } H/L > 0.1 \tag{8.157}$$

It specifies that a spiral skewing out of proportions towards and along the top of the slope, i.e., the most part of it lies in the β-zone (Fig. 8.11), is not acceptable.

Such skewing tendencies are observable when the slope angle β is equal or close to the internal friction angle ϕ, in addition to a small α angle. The presence of these skewness usually results in critical height values that are very low. Two reasons are given to dispel such skewing spirals. The first being that for such spirals, the geometry is quite different from the ideal picture on which the derivations are based. So, results obtained may be questionable. Secondly, even if these skewed spirals are perfectly all right, the degree of hazard associated with them may not be as great as the less-skewed ones. Based on these considerations, the ratios are set as shown. Of course, they are subjected to relaxations or further restrictions, according to the judgements of the investigators.

$$\text{(g) } \theta_h > \theta_0 \tag{8.158}$$

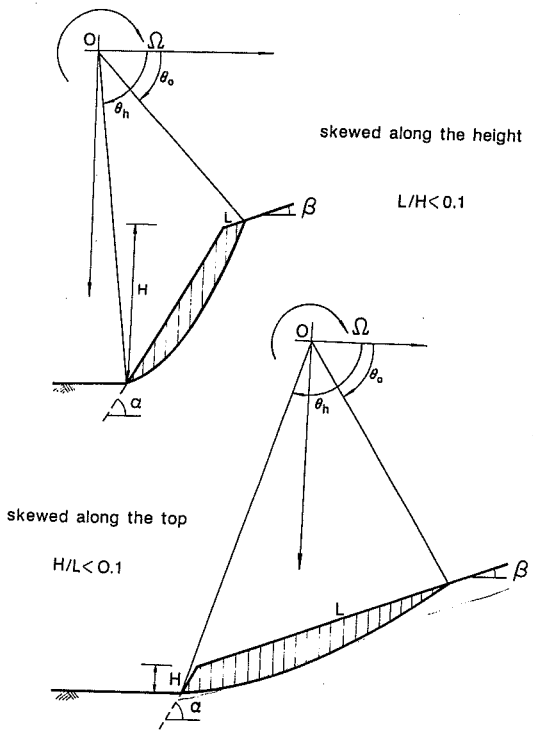

Fig. 8.11. Skewed spirals.

This assures that the spiral does not go backward.

(h) $H_s > H$ (8.159)

This constraint is for the determination of the location of the most critical spiral for a slope of given height only.

(i) $\theta_0 > \pi - 2\alpha - \theta_h$
$\theta_0 < \pi - 2\beta - \theta_h$, for purely cohesive soil only (8.160)

This constraint is related to the physical ranges of the spiral angles θ_0 and θ_h. The first of these two is more general. It is derived from a consideration of the expression for the length L, Eq. (8.119). For the length to be greater than zero, the following must be true:

$$\sin(\theta_0 + \alpha) - \exp[(\theta_h - \theta_0)\tan\phi]\sin(\theta_h + \alpha) > 0 \tag{8.161}$$

Since:

$$\exp[(\theta_h - \theta_0)\tan\phi] = 1 \tag{8.162}$$

then:

$$\sin(\theta_0 + \alpha) - \sin(\theta_h + \alpha) > 0 \tag{8.163}$$

This can only be satisfied if $\theta_h > \frac{1}{2}\pi - \alpha$ and $\theta_0 + \alpha > \frac{1}{2}\pi$ or $\theta_0 + \alpha < \frac{1}{2}\pi$. The result is then for the first case: $\theta_h > \theta_0$ which is reflected in the constraint (g). For the second case, it is $\theta_0 + \alpha > \pi - (\theta_h + \alpha)$ which is constraint (i). Constraint (h), the expression for the slope height H, Eq. (8.120) is used. In order that it is positive, the following must be true:

$$\exp[(\theta_h - \theta_0)\tan\phi]\sin(\theta_h + \beta) - \sin(\theta_0 + \beta) > 0 \tag{8.164}$$

If the slope under investigation is composed of purely cohesive soil, then, Eq. (8.164) becomes:

$$\sin(\theta_h + \beta) > \sin(\theta_0 + \beta) \tag{8.165}$$

or

$$|\theta_h + \beta - \tfrac{1}{2}\pi| < \tfrac{1}{2}\pi - (\theta_0 + \beta) \tag{8.166}$$

This gives $\theta_0 < \pi - 2\beta - \theta_h$ and $\theta_0 < \theta_h$, which are constraints (i) and (g).

While much have been said of the constraints, the importance of the ranges of the independent variables r_0, θ_0 and θ_h must not be overlooked. Although no specific statement has been made in the derivations, the validity of these formulations can be easily seen to rest on the following implied variable ranges:

$$0 < r_0 < \infty \tag{8.167}$$

$$\theta_0 > 0 \tag{8.168}$$

and

$$\theta_h < \pi \tag{8.169}$$

However, to provide greater insight into the applicability of these formulations as well as to expedite the optimization process, better refining of these ranges is necessary. These narrowing down of the ranges can be achieved by geometric and algebraic considerations. The geometry of the model requires that the spiral be confined within the slope by the perimeter of the slope. This results in the upper and lower limit for θ_0 and θ_h, respectively (Fig. 8.12):

$$\theta_0 < \tfrac{1}{2}\pi + \phi - \beta \tag{8.170}$$

$$\theta_h > \tfrac{1}{2}\pi + \phi - \alpha \tag{8.171}$$

The upper limit for θ_h can be further refined by next considering the expression for the slope height again, Eq. (8.120). To satisfy the fact that H is positive, the expression is reduced to:

$$\sin(\theta_h + \beta) > (r_0/r_h)\sin(\theta_0 + \beta) \tag{8.172}$$

with:

$$0 < r_0/r_h < 1, \tag{8.173}$$

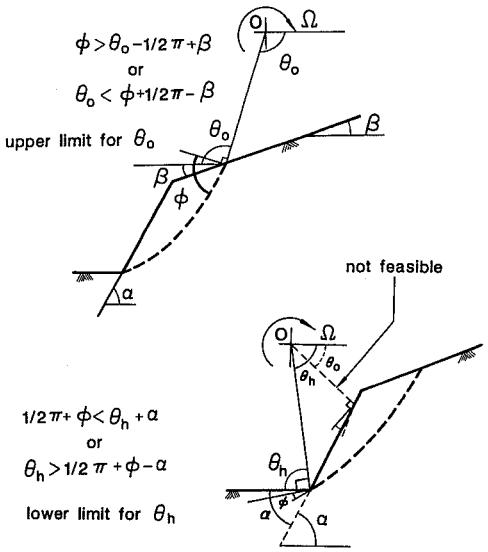

Fig. 8.12. Partial limits for θ_0 and θ_h.

and the implied and established limits for θ_0. It is obvious that:

$$\sin(\theta_h + \beta) > 0 \tag{8.174}$$

or

$$0 < \theta_h + \beta < \pi \tag{8.175}$$

or

$$-\beta < \theta_h < \pi - \beta \tag{8.176}$$

Accounting for the above refinements, the ranges now become:

$$0 < r_0 < \infty \tag{8.177}$$

$$0 < \theta_0 < \tfrac{1}{2}\pi + \phi - \beta \tag{8.178}$$

and

$$\tfrac{1}{2}\pi + \phi - \alpha < \theta_h < \pi - \beta \tag{8.179}$$

These restrictions should further reduce the efforts needed in the optimization.

8.4 Special spiral-slope configurations

The discussions presented in Section 8.3 pertain essentially to failure mechanisms with the ending at the toe of the slope. However, for special cases, it is possible that the spiral may terminate at some distance vertically above the toe, or even stretched horizontally away from the toe.

8.4.1 Sagging spiral

Before discussing the special cases mentioned above, it is worth noting yet another possibility, the case of a sagging spiral (Fig. 8.13). A spiral will be termed '*sagging*' if its point vertically farthest away from the origin (M in Fig. 8.13) is not its endpoint E. This point of the largest vertical distance is a stationary point in the spiral:

$$y = r\sin\theta = r_0 \exp[(\theta - \theta_0)\tan\phi]\sin\theta \tag{8.180}$$

This point which corresponds to the maximum of y, is determined by solving the equation:

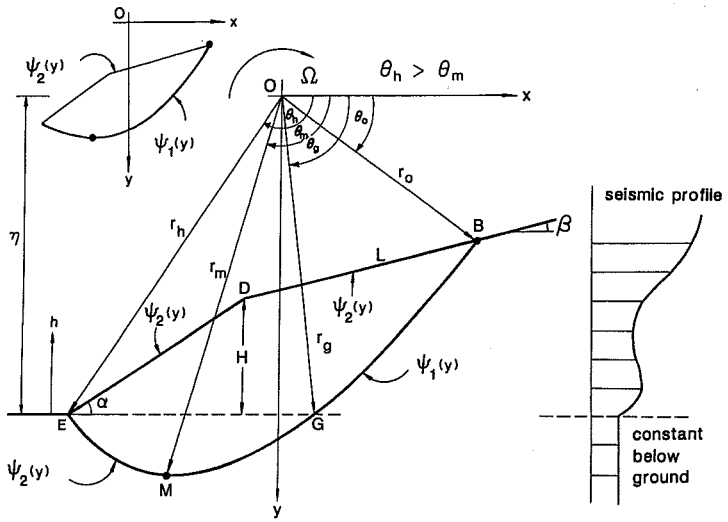

Fig. 8.13. Sagging spiral.

$$\frac{dy}{d\theta} = r_0 \exp[(\theta - \theta_0) \tan\phi] (\tan\phi \sin\theta + \cos\theta) = 0 \tag{8.181}$$

The solution is:

$$\theta_m = \tfrac{1}{2}\pi + \phi \tag{8.182}$$

From this, a criterion can be set to determine whether a given spiral is sagging or not. Clearly, we have:

ordinary spiral: $\theta_h \leq \theta_m$

sagging spiral: $\theta_h > \theta_m$

In view of the possibility of having a sagging spiral failure surface, it is important that the analytical procedure developed for ordinary spiral failure surfaces be re-examined to determine its applicability to the case of sagging spirals. That the procedure is equally applicable to both cases is easily demonstrated. We note that the evaluation of the external work rate contributed by the soil block B-M-E-D-B (Fig. 8.13), defined by the spiral and part of the perimeter of the slope, is equivalent to the

evaluation of the area inside two curves $\psi_1(y)$ and $\psi_2(y)$ (Section 8.2). In the case of the ordinary spiral, the external work rate is calculated formally:

$$\dot{W}_1 = \int d\dot{W}_{1x} + \int d\dot{W}_{1y} \qquad \text{for } y_B < y < y_E \text{, with boundary } \psi_1(y) \tag{8.183}$$

$$\left.\begin{aligned} \dot{W}_2 &= \int d\dot{W}_{2x} + \int d\dot{W}_{2y} \qquad \text{for } y_B < y < y_D \\ \dot{W}_3 &= \int d\dot{W}_{3x} + \int d\dot{W}_{3y} \qquad \text{for } y_D < y < y_E \end{aligned}\right\} \text{with boundary } \psi_2(y) \tag{8.184}$$

For the case of a sagging spiral (Fig. 8.13), it is convenient to truncate the portion of $\psi_1(y)$ at point M, and add the remaining portion of the curve to $\psi_2(y)$, such that:

$$(\dot{W}_1)_1 = \int d\dot{W}_1 \qquad \text{for } y_B \leq y \leq y_m \text{, with boundary } \psi_1(y)$$

$$(\dot{W}_1)_2 = \int d\dot{W}_1 \qquad \text{for } y_E \leq y \leq y_m \text{, with boundary } \psi_2(y)$$

with

$$\dot{W}_1 = (\dot{W}_1)_1 + (\dot{W}_1)_2 \tag{8.185}$$

$$\left.\begin{aligned} \dot{W}_2 &= \int d\dot{W}_2 \qquad \text{for } y_B < y < y_D \text{, with boundary } \psi_2(y) \\ W_3 &= \int dW_3 \qquad \text{for } y_D < y < y_E \text{, with boundary } \psi_2(y) \end{aligned}\right. \tag{8.186}$$

Therefore:

$$\begin{aligned} \dot{W}_E &= \int_{\theta_0}^{\theta_m} d\dot{W}_1 - \int_{\theta_h}^{\theta_m} d\dot{W}_1 - \int_{y_B}^{y_D} d\dot{W}_2 - \int_{y_D}^{y_E} d\dot{W}_3 \\ &= \int_{\theta_0}^{\theta_m} d\dot{W}_1 + \int_{\theta_m}^{\theta_h} d\dot{W}_1 - \int_{y_B}^{y_D} d\dot{W}_2 - \int_{y_D}^{y_E} d\dot{W}_3 \\ &= \int_{\theta_0}^{\theta_h} d\dot{W}_1 - \int_{y_B}^{y_D} d\dot{W}_2 - \int_{y_D}^{y_E} d\dot{W}_3 \end{aligned} \tag{8.187}$$

Formally, this is the same as Eq. (8.129). Thus, the same formula may be treated for both the case of the sagging spiral and the ordinary spiral. In the latter case, the formula is applicable only when the entire length of the spiral is above the ground level.

The exception taken in the last statement is justified by the constant seismic force beneath the ground level; in contrary to the variation of the seismic coefficient above the ground, with the elevation. This essentially divides the seismic coefficients into two regions (Fig. 8.13):

$$k_x(h) = \begin{cases} a_0 & \text{for } h \le 0 \\ a_0 + \sum_{j=1}^{m} a_j h^j & \text{for } h > 0 \end{cases} \tag{8.188}$$

$$k_y(h) = \begin{cases} b_0 & \text{for } h \le 0 \\ b_0 + \sum_{j=1}^{n} b_j h^j & \text{for } h > 0 \end{cases} \tag{8.189}$$

or

$$k_x(y) = \begin{cases} a_0 & \text{for } y \ge \eta \\ \sum_{j=0}^{m} \nu_j y^j & \text{for } y < \eta \end{cases} \tag{8.190}$$

$$k_y(y) = \begin{cases} b_0 & \text{for } y \ge \eta \\ \sum_{j=0}^{n} \mu_j y^j & \text{for } y < \eta \end{cases} \tag{8.191}$$

A close examination of the geometry of the earthslope and the possible combinations of relative position between the slope and the spiral failure surface reveals that there are basically four major categories of spiral failure mechanism. These are illustrated in Fig. 8.14 and are categorized as follows:

(i) Normal:
- (a) The spiral terminates at the toe and there is no sagging ($\theta_h \le \theta_m$, $\eta = r_h \sin\theta_h$).
- (b) The spiral ends some elevations above the ground and there is no sagging ($\theta_h \le \theta_m$, $\eta > r_h \sin\theta_h$).
- (c) The spiral is sagging, but its end is raised and it has no point below the ground ($\theta_h > \theta_m$, $\eta > r_m \sin\theta_m$).

(ii) Partially sunken: The spiral is sagging; despite the elevation of its end above the ground, part of its length is below the ground ($\theta_h > \theta_m$, $r_h \sin\theta_h < \eta < r_m \sin\theta_m$).

(iii) Sunken: The spiral is sagging, ends at the toe, and the portion between the end and a certain point is completely below the ground ($\theta_h > \theta_m$, $r_h \sin\theta_h = \eta < r_m \sin\theta_m$, $d = 0$).

(iv) Stretched: The spiral is sagging, ends some horizontal distance d away from the toe, and the portion between the end and a certain point is completely grounded ($\theta_h > \theta_m$, $d > 0$, $r_h \sin\theta_h = \eta < r_m \sin\theta_m$).

8.4.2 Raised spiral

A spiral which has its end at an elevation above the toe of the slope is hereby referred to as a *raised spiral*. Typical slopes are shown in Fig. 8.14, (i.b), (i.c) and (ii). For such a spiral, the two simultaneous equations, Eqs. (8.117) and (8.118), governing the dimensions of the rotating block are unchanged. In fact, only minor modifications of the formulations need be made.

The modified expression for η is:

$$\eta = r_0 \exp[(\theta_h - \theta_0)\tan\phi] \sin\theta_h + H_T \tag{8.192}$$

where H_T is the height of the raised spiral terminal. Corresponding changes in the expressions (8.137) to (8.141) for H are:

$$H = \frac{c}{\gamma} F(r_0, \theta_0, \theta_h, H_T) \tag{8.193}$$

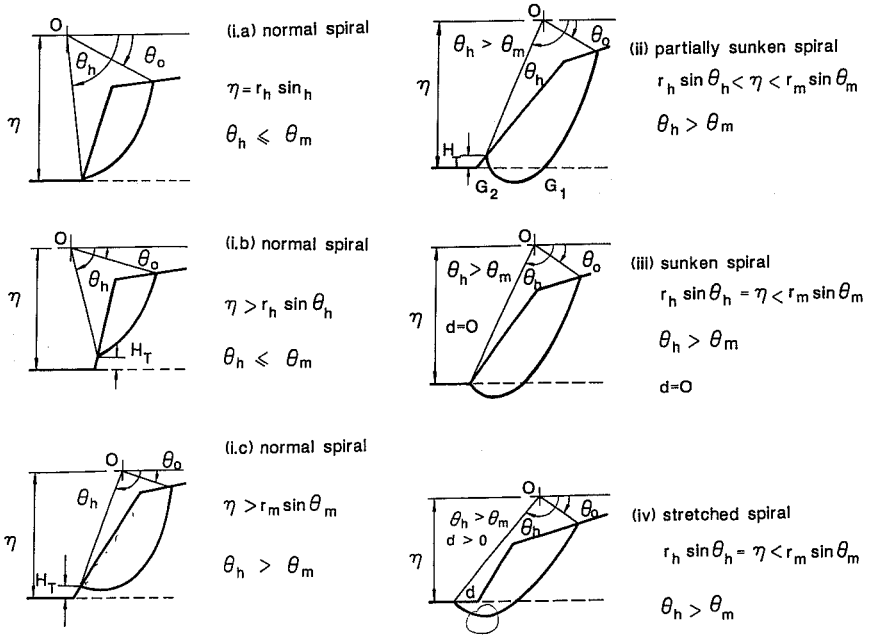

Fig. 8.14. Four major categories of spirals.

with

$$F(r_0,\theta_0,\theta_h,H_T) = H_T\frac{\gamma}{c} + \frac{\sin\alpha\{\exp[(\theta_h-\theta_0)\tan\phi]\,\sin(\theta_h+\beta) - \sin(\theta_0+\beta)\}[e^{2(\theta_h-\theta_0)\tan\phi}-1]}{2\tan\phi\,\sin(\alpha-\beta)\,[f_{1x}-f_{2x}-f_{3x}+\frac{1}{2}(f_{1y}-f_{2y}-f_{3y})]} \tag{8.194}$$

such that:

$$H^* \le \frac{c}{\gamma}N^* \tag{8.195}$$

where

$$N^* = \min[F(r_0,\theta_0,\theta_h,H_T)] = F(r_0^*,\theta_0^*,\theta_h^*,H_T^*) \tag{8.196}$$

In addition, r_0^*, θ_0^*, θ_h^*, H_T^* must satisfy the conditions:

$$\frac{\partial F}{\partial r_0}=0,\quad \frac{\partial F}{\partial\theta_0}=0,\quad \frac{\partial F}{\partial\theta_h}=0,\quad \frac{\partial F}{\partial H_T}=0 \tag{8.197}$$

These modifications are sufficiently general and would include the toe spiral as a special case ($H_T = 0$). When the raised spiral qualifies for the first category as a normal spiral, no modification is needed.

For the spiral of the third category (Fig. 8.14.iii), the sunken spiral, the raised height is zero, but the spiral cuts through the ground level once. Referring to the angle corresponding to the ground level point G (Fig. 8.13) of the spiral as θ_g, the external work rate (gross) can be modified as:

$$\int_{\theta_0}^{\theta_h} d\dot{W}_1 = \int_{\theta_0}^{\theta_g} d\dot{W}_{1A} + \int_{\theta_g}^{\theta_h} d\dot{W}_{1B} \tag{8.198}$$

where

$$\int_{\theta_0}^{\theta_g} d\dot{W}_{1A} = \gamma\Omega r_0^3\left[f_{1x}(r_0,\theta_0,\theta_h)\Big|_{\theta_0}^{\theta_g} + \tfrac{1}{2}f_{1y}(r_0,\theta_0,\theta_h)\Big|_{\theta_0}^{\theta_g}\right] \tag{8.199}$$

$$\int_{\theta_g}^{\theta_h} d\dot{W}_{1B} = \int_{\theta_g}^{\theta_h}\gamma\Omega a_0 r^3\,[\sin^2\theta\cos\theta\tan\phi + \sin\theta\cos^2\theta]d\theta +$$

$$\tfrac{1}{2}\int_{\theta_g}^{\theta_h}\gamma\Omega b_0 r^3\,[\sin\theta\cos^2\theta\tan\phi + \cos^3\theta]d\theta$$

$$= \gamma\Omega r_0^3\left[f_{1x}^B(r_0,\theta_0,\theta_h)\Big|_{\theta_g}^{\theta_h} + \tfrac{1}{2}f_{1y}^B(r_0,\theta_0,\theta_h)\Big|_{\theta_g}^{\theta_h}\right] \tag{8.200}$$

with

$$f_{1x}^B(r_0,\theta_0,\theta_h)\Big|_{\theta_g}^{\theta_h} = r_0^{-3}a_0\varrho^3\left\{I[3\tan\phi,\,1]\Big|_{\theta_g}^{\theta_h} - I[3\tan\phi,\,3]\Big|_{\theta_g}^{\theta_h} + \tan\phi\,J[3\tan\phi,\,2]\Big|_{\theta_g}^{\theta_h}\right\} \tag{8.201}$$

$$f_{1y}^B(r_0,\theta_0,\theta_h)\Big|_{\theta_g}^{\theta_h} = r_0^{-3}b_0\varrho^3\left\{J[3\tan\phi,\,0]\Big|_{\theta_g}^{\theta_h} - J[3\tan\phi,\,2]\Big|_{\theta_g}^{\theta_h} + \tan\phi\,I[3\tan\phi,\,1]\Big|_{\theta_g}^{\theta_h} - \tan\phi\,I[3\tan\phi,\,3]\Big|_{\theta_g}^{\theta_h}\right\} \tag{8.202}$$

Thus, the earlier equations for $\dot{W}_1$, Eqs. (8.108) and (8.109) can still be used, as long as the Eqs. (8.110) and (8.111) are modified as:

$$f_{1x}(r_0,\theta_0,\theta_h)\Big|_{\theta_0}^{\theta_h} = f_{1x}(r_0,\theta_0,\theta_h)\Big|_{\theta_0}^{\theta_g} + f_{1x}^B(r_0,\theta_0,\theta_h)\Big|_{\theta_g}^{\theta_h} \tag{8.203}$$

$$f_{1y}(r_0,\theta_0,\theta_h)\Big|_{\theta_0}^{\theta_h} = f_{1y}(r_0,\theta_0,\theta_h)\Big|_{\theta_0}^{\theta_g} + f_{1y}^B(r_0,\theta_0,\theta_h)\Big|_{\theta_g}^{\theta_h} \tag{8.204}$$

The ground point angle θ_g can be found from the following equation derived from the geometry:

$$G_1 = r_0\,e^{(\theta_h-\theta_0)\tan\phi}\sin\theta_h - r_0\,e^{(\theta_g-\theta_0)\tan\phi}\sin\theta_g = 0 \tag{8.205}$$

The elevation is to be carried out with the Newton's iterative root finding method:

$$\theta_g^{(n+1)} = \theta_g^{(n)} - G_1/G_1' \tag{8.206}$$

$$G_1' = \frac{dG_1}{d\theta_g} = r_0\,e^{(\theta_g-\theta_0)\tan\phi}(\tan\phi\,\sin\theta_g + \cos\theta_g) \tag{8.207}$$

The superscripts stand for the iteration number. For the initiation of the iteration process, or at the zero-th iteration, $\theta_g^{(0)}$ can be estimated by assuming that:

$$\theta_h - \theta_m \simeq \theta_m - \theta_g \tag{8.208}$$

So

$$\theta_g^{(0)} = 2\theta_m - \theta_h = \pi + 2\phi - \theta_h \tag{8.209}$$

Since the possibility of divergency exists in Newton's method, the following bounds will assure that such possibility will be eliminated:

$$\theta_0 < \theta_g < \theta_m \tag{8.210}$$

For the spiral of the second category, the partially sunken spiral (Fig. 8.14,ii), the raised height is non-zero and the spiral cuts through the ground level twice. Referring to the angles corresponding to the ground level points G_1 and G_2 as θ_{g1} and θ_{g2}, respectively, we have the following expressions for the functions f_{1x} and f_{1y} associated with the gross external work rate:

$$f_{1x}(r_0,\theta_0,\theta_h)\Big|_{\theta_0}^{\theta_h} = f_{1x}(r_0,\theta_0,\theta_h)\Big|_{\theta_0}^{\theta_{g1}} + f_{1x}^{B}(r_0,\theta_0,\theta_h)\Big|_{\theta_{g1}}^{\theta_{g2}} + f_{1x}(r_0,\theta_0,\theta_h)\Big|_{\theta_{g2}}^{\theta_h} \tag{8.211}$$

$$f_{1y}(r_0,\theta_0,\theta_h)\Big|_{\theta_0}^{\theta_h} = f_{1y}(r_0,\theta_0,\theta_h)\Big|_{\theta_0}^{\theta_{g1}} + f_{1y}^{B}(r_0,\theta_0,\theta_h)\Big|_{\theta_{g1}}^{\theta_{g2}} + f_{1y}(r_0,\theta_0,\theta_h)\Big|_{\theta_{g2}}^{\theta_h} \tag{8.212}$$

The angles θ_{g1} and θ_{g2} can be found from the following equation of geometric consideration:

$$G_2 = r_0\, e^{(\theta_h - \theta_0)\tan\phi} \sin\theta_h + H_T - r_0\, e^{(\theta_g - \theta_0)\tan\phi} \sin\theta_g = 0 \tag{8.213}$$

As before, the evaluation formula is Newton's iterative formula:

$$\theta_{g1,2}^{(n+1)} = \theta_{g1,2}^{(n)} - G_2/G_2' \tag{8.214}$$

where

$$G_2' = G_1' \tag{8.215}$$

The initial estimation for θ_{g1} and θ_{g2} are made in a similar procedure as before:

$$\theta_{g1}^{(0)} = 2\theta_m - \theta_h \tag{8.216}$$

and

$$\theta_{g2}^{(0)} = 2\theta_m - \theta_{g1} \tag{8.217}$$

Their safety ranges for convergency are:

$$\theta_0 < \theta_{g1} < \theta_m \tag{8.218}$$

$$\theta_m < \theta_{g2} < \theta_h \tag{8.219}$$

8.4.3 Stretched spiral

When the end of a spiral is stretched a horizontal distance d away from the toe, the two simultaneous equations for geometry are changed to:

$$r_0 \cos\theta_0 - r_h \cos\theta_h - H/\tan\alpha - d - L\cos\beta = 0 \tag{8.220}$$

$$r_h \sin\theta_h - r_0 \sin\theta_0 - H - L\sin\beta = 0 \tag{8.221}$$

Solving these equations simultaneously, we obtain:

$$L = [r_0 \sin(\theta_0 + \alpha) - r_h \sin(\theta_h + \alpha) - d\sin\alpha]/\sin(\alpha - \beta) \tag{8.222}$$

and

$$H = [r_h \sin(\theta_h + \beta) - r_0 \sin(\theta_0 + \beta) + d\sin\beta\sin\alpha]\sin\alpha/\sin(\alpha - \beta)$$

with:

$$0 \le d < \infty;\quad \theta_m < \theta_h < \pi - \beta \tag{8.223}$$

Accordingly, for the formulation of x_E used in Eq. (8.116), modification is necessary:

$$x_E = r_h \cos\theta_h + d \tag{8.224}$$

where it is noted that $r_h \cos\theta_h$ is negative because θ_h is larger than $\pi/2$.

Also, since the spiral is sagging, the formulation for $\dot{W}_1$ must be modified as in Eqs. (8.198) to (8.204) for the sunken spiral. Eq. (8.137) now becomes:

$$H = \frac{c}{\gamma} F(r_0,\theta_0,\theta_h,d) \tag{8.225}$$

where

$$F(r_0,\theta_0,\theta_h,d) = \frac{d\sin\beta\sin\alpha}{\sin(\alpha-\beta)}\frac{\gamma}{c} +$$

$$\frac{\sin\alpha\,[e^{(\theta_h-\theta_0)\tan\phi}\sin(\theta_h+\beta)-\sin(\theta_0+\beta)]\,[e^{2(\theta_h-\theta_0)\tan\phi}-1]}{2\tan\phi\sin(\alpha-\beta)\,[f_{1x}-f_{2x}-f_{3x}+\frac{1}{2}(f_{1y}-f_{2y}-f_{3y})]} \tag{8.226}$$

The critical height H^* of the stretched slope is:

$$H^* \le \frac{c}{\gamma}N^* \tag{8.227}$$

where

$$N^* = \min[F(r_0,\theta_0,\theta_h,d)] = F(r_0^*,\theta_0^*,\theta_h^*,d^*) \tag{8.228}$$

such that r_0^*, θ_0^*, θ_h^*, d^* satisfy the conditions:

$$\frac{\partial F}{\partial r_0}=0,\quad \frac{\partial F}{\partial\theta_0}=0,\quad \frac{\partial F}{\partial\theta_h}=0,\quad \frac{\partial F}{\partial d}=0 \tag{8.229}$$

In addition, since a stretched spiral is necessarily a sagging spiral, the range for θ_h must be restricted as:

$$\theta_m < \theta_h < \pi-\beta \tag{8.230}$$

The other ranges and constraints for the simple toe spiral still apply.

8.4.4 The most critical slip surface for a given earthslope

The determination of the critical height for a slope of given geometry and soil properties is useful in that it provides valuable criteria for the safety design of earthslope structures. However, for an existing earthslope, it would be more vital to be able to predict the most critical failure surface under a given seismic load. Investigations of the cumulative soil mass displacement of a slope during an earthquake, similar to those suggested by Newmark (1965) and Seed (1967) may be carried out. This will be presented in Chapter 10.

To accommodate the analysis of the critical slip surface, in particular to determine the location of the probable failure of the existing slope, only a few modifications have to be made to the analysis presented in the preceding sections. Foremost, we have to set:

$$\eta = r_0\sin\theta_0 + L\sin\beta + H \tag{8.231}$$

where H is the height of the given slope and L is as defined in Eq. (8.119). In addition, H_T, the elevation of the end point of the spiral above the ground, is now no longer an independent variable, but is given as:

$$H_T = \eta - r_h\sin\theta_h \tag{8.232}$$

With these changes introduced, the rest of the formulations for the critical height of a toe-spiral can be used as discussed in the preceding section.

As for H^*, it is now defined as the vertical distance between the knee of the slope and the end of the most critical spiral. It can thus be used to specify the dimension of the most critical rotating block of soil mass.

In addition to the modifications to the formulations, an additional physical constraint must be recognized, namely:

$$H \ge H^* \tag{8.233}$$

Adding this extra constraint to the original constraints assures that the height of the potential failure surface is not higher than the physical height of the slope.

8.5 Calculated results and discussions

In order that the formulations developed in this study can be readily applicable to related investigations, computer coding has been implemented. A listing of the computer program and some selected sample outputs are given in the appendices of the paper by Chen et al. (1984). An in-house optimization subroutine BIASLIB, developed by the Purdue University School of Mechanical Engineering (Root and Ragsdell, 1977) was used in the program. The program itself has been subjected to testings and debuggings, and should contains a minimum of residual errors.

A total of nine cases were investigated and presented in the forthcoming. Their results are tabulated.

8.5.1 Static case

The first two of these cases deal with a static situation, with gravity as the sole influence force. The stability factors associated with dead-weight induced collapse were calculated. For the static case, the loading profiles for the vertical and horizontal components are:

$$k_y(h) = 1.0 \tag{8.234}$$

TABLE 8.1
Stability factor $N^* = H^* (\gamma/c)$ for dead-weight induced failure, through non-stretched spirals. Loading profiles: $k_x = 0$, $k_y = 1$

ϕ	β	α	N^*	$N^{*,a}$	$\frac{\gamma}{c} L^*$	$\frac{\gamma}{c} r_0^*$	θ_0^*	θ_h^*	θ_g^*
0	0	30	6.43	(6.51)	6.54	11.70	0.288	2.156	0.986
		60	5.25	(5.25)	4.37	7.73	0.327	1.581	1.561
		90	3.83	(3.83)	3.50	10.02	0.479	1.003	–
5	0	30	9.14	(9.13)	5.75	14.98	0.427	2.048	1.259
		60	6.16	(6.16)	4.17	8.41	0.386	1.563	–
		90	4.19	(4.19)	3.47	10.77	0.529	1.026	–
10	0	30	13.50	(13.50)	5.58	21.31	0.571	1.986	1.497
		60	7.26	(7.26)	4.04	9.25	0.447	1.561	–
		90	4.58	(4.58)	3.44	11.56	0.579	1.062	–
	10	30	12.99	(12.89)	11.89	27.67	0.671	1.942	1.544
		60	6.99	(6.99)	5.17	9.96	0.445	1.562	–
		90	4.47	(4.47)	3.92	10.45	0.521	1.105	–
15	0	30	21.67	(21.69)	5.77	34.93	0.732	1.939	1.725
		60	8.63	(8.63)	3.96	10.31	0.512	1.568	–
		90	5.02	(5.02)	3.42	12.35	0.630	1.081	–
	10	30	21.16	(21.14)	9.26	36.60	0.730	1.945	1.718
		60	8.38	(8.38)	4.87	10.86	0.506	1.580	–
		90	4.91	(4.91)	3.82	11.19	0.577	1.122	–
20	0	30	41.22	(41.22)	6.46	73.65	0.917	1.891	–
		60	10.39	(10.39)	3.91	11.68	0.581	1.580	–
		90	5.51	(5.50)	3.40	13.30	0.684	1.110	–
	10	30	40.69	(40.69)	8.93	73.61	0.904	1.896	–
		60	10.16	(10.16)	4.68	12.13	0.573	1.587	–
		90	5.40	(5.40)	3.75	12.01	0.634	1.144	–
	20	30	38.81	(38.64)	18.63	76.15	0.887	1.909	–
		60	9.79	(9.74)	7.31	16.01	0.669	1.570	–
		90	5.24	(5.24)	4.38	11.18	0.586	1.188	–
25	0	30	120.64	(119.9)	11.74	300.15	1.160	1.820	–
		60	12.74	(12.74)	3.89	13.55	0.655	1.595	–
		90	6.06	(6.06)	3.39	14.30	0.739	1.141	–
	10	30	119.33	(119.4)	12.02	286.17	1.139	1.824	–
		60	12.52	(12.52)	4.57	13.92	0.647	1.599	–
		90	5.95	(5.95)	3.68	12.91	0.692	1.169	–
	20	30	117.28	(117.4)	22.88	294.68	1.138	1.823	–
		60	12.14	(12.14)	5.91	14.74	0.646	1.605	–
		90	5.80	(5.80)	4.22	11.95	0.647	1.203	–
30	0	60	16.04	(16.04)	3.90	16.24	0.735	1.612	–
		90	6.69	(6.69)	3.37	15.42	0.794	1.173	–
	10	60	15.82	(15.82)	4.50	16.54	0.727	1.614	–
		90	6.59	(6.59)	3.63	13.99	0.754	1.195	–

TABLE 8.1 (*continued*)

ϕ	β	α	N^*	$N^{*,a}$	$\frac{\gamma}{c} L^*$	$\frac{\gamma}{c} r_0^*$	θ_0^*	θ_h^*	θ_g^*
	20	60	15.47	(15.47)	5.64	17.20	0.724	1.617	–
		90	6.44	(6.44)	4.09	12.86	0.711	1.222	–
	30	60	14.78	(14.78)	8.41	19.09	0.737	1.623	–
		90	6.22	(6.22)	4.95	12.20	0.672	1.258	–
35	0	60	20.94	(20.94)	3.94	20.43	0.822	1.630	–
		90	7.42	(7.42)	3.36	16.70	0.851	1.205	–
	10	60	20.73	(20.73)	4.49	20.69	0.815	1.631	–
		90	7.32	(7.32)	3.58	15.26	0.816	1.222	–
	20	60	20.40	(20.40)	5.51	21.22	0.811	1.633	–
		90	7.19	(7.19)	4.04	15.27	0.800	1.234	–
	30	60	19.78	(19.78)	7.67	22.57	0.814	1.635	–
		90	6.98	(6.99)	4.70	13.08	0.739	1.272	–
40	0	60	28.92	(28.91)	4.03	27.69	0.918	1.647	–
		90	8.29	(8.29)	3.33	17.84	0.906	1.239	–
	10	60	28.71	(28.71)	4.56	27.91	0.913	1.648	–
		90	8.19	(8.19)	3.54	16.58	0.878	1.252	–
	20	60	28.39	(28.39)	5.50	28.37	0.908	1.649	–
		90	8.06	(8.06)	3.90	15.41	0.847	1.268	–
	30	60	27.82	(27.82)	7.35	29.40	0.907	1.650	–
		90	7.87	(7.87)	4.55	15.42	0.830	1.279	–
	40	60	26.46	(26.45)	12.05	31.82	0.908	1.654	–
		90	7.56	(7.56)	5.73	13.69	0.779	1.320	–

ϕ, β and α in degrees; θ_0^*, θ_h^* and θ_g^* in radians.
[a] Data published by Chen et al. (1969) and Chen (1975).

$$k_x(h) = 0.0 \tag{8.235}$$

Data for this simple loading are in abundance. The purpose here is to provide an indication on how good results from the new model agree with the existing ones. Such a comparison is possible because the present model is quite general and that the dead-weight collapse is but one special case. As shown in Tables 8.1 and 8.2, the stability factors are in good agreement with the published values (Chen, 1975), both for the nonstretched and the stretched spirals.

Also listed in these two tables are the coordinates and dimensional parameters of the spirals. These parameters are useful because they provide valuable insight into the estimation of the coordinates of the most critical spiral for a slope of similar geometry and properties. The estimation corresponds to the choice of a feasible star-

TABLE 8.2
Stability factor $N^* = (\gamma/c)H^*$ for dead-weight induced failure, through stretched spirals. Loading profiles: $k_x = 0$, $k_y = 1$.

ϕ	β	α	N^*	$N^{*,a}$	$\frac{\gamma}{c}L^*$	$\frac{\gamma}{c}r_0^*$	θ_0^*	θ_h^*	θ_g^*	$\frac{\gamma}{c}d^*$
0	0	15	5.60	(5.53)	42.85	56.64	0.349	2.688	0.456	40.34
		30	5.56	(5.53)	32.81	39.77	0.332	2.657	0.484	30.36
		45	5.53	(5.53)	51.48	57.75	0.352	2.685	0.456	49.05
5	0	15	14.38	(14.38)	10.15	45.67	0.627	2.242	1.053	5.90
		30	9.13	(9.13)	6.09	15.21	0.402	2.119	1.184	1.30
		45	7.35	(7.35)	4.69	9.97	0.372	1.817	1.498	0.00
	5	15	13.71	(13.71)	18.49	50.97	0.646	2.239	1.056	7.42
		30	8.83	(8.83)	8.76	16.93	0.407	2.174	1.126	2.80
		45	7.18	(7.18)	5.62	10.52	0.379	1.825	1.490	0.00

ϕ, β and α in degrees; θ_0^*, θ_h^* and θ_g^* in radians.
[a] Data from Chen (1975).

TABLE 8.3
Stability factor $N^* = (\gamma/c)H^*$ for constant seismic horizontal component. Loading profiles: $k_x = 0.325$, $k_y = 1$

ϕ	β	α	N^*	$N^{*,a}$	$\frac{\gamma}{c}L^*$	$\frac{\gamma}{c}r_0^*$	θ_0^*	θ_h^*	θ_g^*
10	0	30	4.98	(4.98)	12.80	16.86	0.882	2.107	1.367
		60	4.32	(4.32)	5.26	9.40	0.781	1.669	–
		90	3.22	(3.22)	3.56	13.57	0.839	1.178	–
20	0	30	8.83	(8.83)	6.94	17.32	0.949	2.058	1.776
		60	5.63	(5.63)	4.53	10.26	0.885	1.665	–
		90	3.65	(3.65)	3.35	17.53	0.962	1.217	–
30	0	60	7.44	(7.44)	4.20	11.78	1.008	1.697	–
		90	4.13	(4.13)	3.14	18.65	1.058	1.284	–
40	0	60	10.25	(10.25)	4.01	14.19	1.142	1.743	–
		90	4.66	(4.65)	2.93	21.31	1.166	1.349	–

ϕ, β and α in degrees; θ_0^*, θ_h^* and θ_g^* in radians.
[a] Data from Chen et al. (1978).

ting point for the optimization process. This optimization process can be quite sensitive to the choice taken.

8.5.2 Cases of constant and linear pseudo-seismic profiles

Tables 8.3 and 8.4 present the results for the cases of constant and linear pseudo-seismic profiles. The constant seismic profile is taken so that:

$$k_y(h) = 1.0 \tag{8.236}$$

$$k_x(h) = 0.325 \tag{8.237}$$

Again, the stability factors obtained from the present analysis are in good agreement with the published values (Chen et al., 1978).

It should be noted that for the linear profile, the profile itself is not the same for each slope. Instead, shorter slopes have steeper profiles as tall slopes have more gentle ones. This is due to the fact that the first published data (Chen et al., 1978) for a linear profile were obtained by imposing on the slopes a maximum of four zones of equal thickness. These zones are of different seismic coefficient values

TABLE 8.4
Stability factor $N^* = (\gamma/c)H^*$ for linear seismic horizontal profile. Loading profiles: $k_x = 0.225 + b_1^a h$, $k_y = 1$

ϕ	β	α	b_1^a	N^*	$N^{*,b}$	$\frac{\gamma}{c}L^*$	$\frac{\gamma}{c}r_0^*$	θ_0^*	θ_h^*	θ_g^*	$\frac{\gamma}{c}d^*$
10	0	30	0.0388	5.24	(5.16)	10.96	18.26	0.941	2.005	1.478	0.0
		60	0.0468	4.25	(4.27)	5.50	10.91	0.856	1.635	–	
		90	0.0635	3.13	(3.15)	3.59	16.39	0.888	1.168	–	
20	0	30	0.0221	9.09	(9.06)	8.25	22.49	1.064	1.998	1.840	0.0
		60	0.0362	5.50	(5.53)	4.83	12.29	0.970	1.638	–	
		90	0.0562	3.54	(3.56)	3.35	18.95	0.990	1.222	–	
30	0	60	0.0275	7.22	(7.28)	4.55	14.67	1.101	1.673	–	
		90	0.0500	3.98	(4.00)	3.12	19.47	1.080	1.292	–	
40	0	60	0.0201	9.87	(9.97)	4.44	18.65	1.243	1.720	–	
		90	0.0447	4.47	(4.47)	2.88	18.42	1.166	1.369	–	

ϕ, β, α in degrees; θ_0^*, θ_h^* and θ_g^* in radians.
[a] Imposing four equi-thickness zones of different coefficients (0.25, 0.30, 0.35, 0.40) indiscriminate of slope heights in effect results in the variation of seismic profile with the size of the slope.
[b] Data from Chen et al. (1978).

($k_{x1} = 0.25$, $k_{x2} = 0.30$, $k_{x3} = 0.35$, $k_{x4} = 0.40$) to approximate the original profile of linear variation (Fig. 8.2b). Such a zone-restricting technique, which distributes the seismic load linearly through the slope height, tends to subject shorter slopes to heavier seismic loadings.

While it is necessary to ascertain the validity of the philosophy underlying this technique, we dispense with the philosophical arguments and still use the published data to check the results of the present study. For this comparative study, we first identify the equation of the seismic profile for the slope configuration for a published critical height. Thus, if the seismic coefficients for the slope are of the form:

$$k_y(h) = 1.0 \tag{8.238}$$

$$k_x(h) = b_0 + b_1 h \tag{8.239}$$

we may use equivalent data from the published data by arbitrarily fixing the following conditions:

$$\text{At } H^*/8\text{: } k_x(H^*/8) = b_0 + b_1(H^*/8) = 0.25 \tag{8.240}$$

$$\text{At } 7H^*/8\text{: } k_x(7H^*/8) = b_0 + b_1(7H^*/8) = 0.40 \tag{8.241}$$

Solving these equations simultaneously, the coefficients b_0 and b_1 are determined:

$$b_0 = 0.225, \quad b_1 = 0.20/H^* \tag{8.242}$$

This, of course, reflects the inverse relationship between the height of the slope and the seismic loading intensity. With the loading profile for each slope calculated as indicated above, the critical height can be analyzed using the new model formulated. Calculated results compare well with the previous published data as shown in Table 8.4.

8.5.3 Cases of nonlinear pseudo-seismic profiles

The data in Table 8.5 reflect the reductions in critical heights resulting from a more realistic seismic profile (Fig. 8.15). This profile was given by Seed and Martin (1966), and Seed (1967) for earthdams up to 300 feet tall. The equation of the profile can be approximated, between 0 and 50 feet of height, as:

$$k_y(h) = 1.0 \tag{8.243}$$

$$k_x(h) = 0.0057 + 0.0084\,h - 0.000076\,h^2 + 0.00000032\,h^3 \tag{8.244}$$

which is sufficiently accurate for the slope configurations studied. The data obtained are shown to be larger (from 1.5 to 2.5 times) than those for the constant profile of 0.325 in Table 8.3. On the other hand, they are less than those for the static case, as expected.

TABLE 8.5

Stability factor $N^* = (\gamma/c)H^*$ for the general average horizontal profile. Loading profiles: $k_x = 0.0057 + 0.0084\,\mathrm{h} - 0.000076\,\mathrm{h}^2 + 0.00000032\,\mathrm{h}^3$, $k_y = 1$

ϕ	β	α	N^*	$\frac{\gamma}{c}L^*$	$\frac{\gamma}{c}r_0^*$	θ_0^*	θ_h^*	θ_g^*	Comment
0	0	30	6.12	7.00	12.02	0.349	2.123	1.019	
			5.15	36.97	44.02	0.365	2.648	0.494	$(\gamma/c)\overset{*}{d} = 34.0$
		60	5.07	4.55	8.03	0.377	1.523	–	
			5.07	46.96	53.53	0.380	2.658	0.484	$(\gamma/c)\overset{*}{d} = 47.2$
		90	3.75	3.53	10.33	0.504	1.008	–	
			5.06	50.05	53.54	0.380	2.660	0.481	$(\gamma/c)\overset{*}{d} = 47.2$
10	0	30	11.63	6.29	20.65	0.647	1.963	1.522	
		60	6.87	4.24	9.61	0.509	1.555	–	
		90	4.45	3.48	12.29	0.616	1.055	–	
20	0	30	23.67	8.04	48.55	0.985	1.904	–	
		60	9.48	4.16	12.08	0.658	1.575	–	
		90	5.28	3.44	14.69	0.733	1.111	–	
	20	30	9.55	98.29	122.15	1.124	1.922	1.919	$(\gamma/c)H_T^* = 0.00022$
			10.59	100.0	144.37	1.174	1.921	1.919	$(\gamma/c)\overset{*}{d} = 8.46$
		60	8.72	7.60	14.70	0.681	1.608	–	
		90	5.00	4.54	11.74	0.631	1.202	–	
30	0	60	13.58	4.25	16.39	0.831	1.611	–	
		90	6.31	3.40	17.55	0.851	1.174	–	
	20	60	12.88	6.70	18.21	0.835	1.623	–	
		90	6.06	4.22	13.87	0.766	1.232	–	
40	0	60	20.58	4.57	25.15	1.035	1.656	–	
		90	7.63	3.37	22.26	0.981	1.239	–	
	20	60	19.84	6.82	27.05	1.037	1.661	–	
		90	7.39	4.02	17.24	0.913	1.278	–	
	40	60	7.64	76.23	80.73	1.197	1.819	–	$(\gamma/c)H_T^* = 0.00001$
		90	6.84	6.42	15.16	0.855	1.350	–	

ϕ, β and α in degrees; θ_0^*, θ_h^* and θ_g^* in radians.

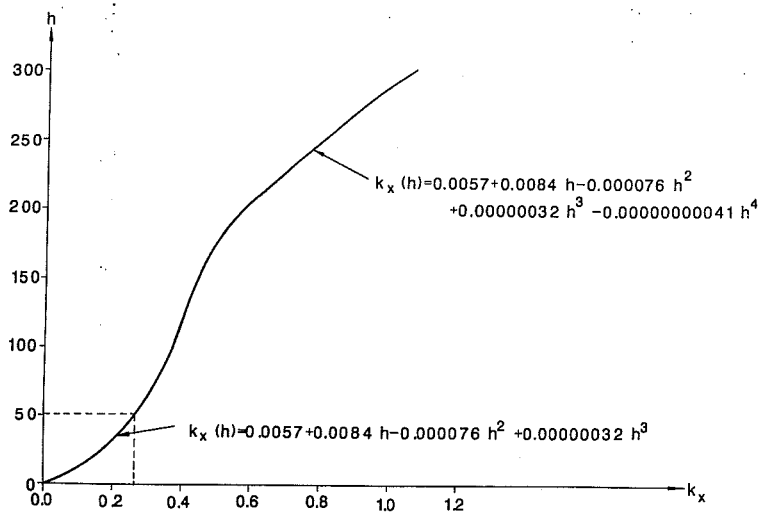

Fig. 8.15. The general average seismic profile (horizontal).

Tables 8.6 and 8.7 exhibit data corresponding, respectively, to the following loading profiles:

$$k_y(h) = 1.0 + 0.1k_x(h) \tag{8.245}$$

$$k_x(h) = 0.0057 + 0.0084\,h - 0.000076\,h^2 + 0.00000032\,h^3 \tag{8.246}$$

and

$$k_y(h) = 1.0 + 0.5k_x(h) \tag{8.247}$$

$$k_x(h) = 0.0057 + 0.0084\,h - 0.000076\,h^2 + 0.00000032\,h^3 \tag{8.248}$$

These calculations were made to understand the effect of a weak vertical seismic component on the critical height. The results indicate that while there are decreases in the values for an increase of the vertical component, these decreases are generally not too significant. This insignificant effect can be observed for a vertical component as strong as half the magnitude of the horizontal one. There are also relatively no significant change in the spiral coordinates. These small changes may be due to the fact that the two component profiles were assumed to be similar. Therefore, any statements extracted from these two tables may not be general enough to warrant

TABLE 8.6
Stability factor $N^* = (\gamma/c)H^*$ for the general profile oriented at a direction of arctan (0.1) with the horizon. Loading profiles: $k_x = 0.0057 + 0.0084\,h - 0.000076\,h^2 + 0.00000032\,h^3$, $k_y = 1. + 0.1\,k_x$

ϕ	β	α	N^*	$\frac{\gamma}{c}L^*$	$\frac{\gamma}{c}r_0^*$	θ_0^*	θ_h^*	θ_g^*	$\bar{d} = \frac{\gamma}{c}d^*$ or $\bar{h} = \frac{\gamma}{c}H_T^*$
0	0	30	6.10	6.97	11.98	0.349	2.123	1.019	
			5.15	35.20	42.34	0.362	2.646	0.495	$\bar{d}$ = 32.73
		90	3.74	3.53	10.33	0.505	1.008	–	
20	0	30	23.51	7.93	47.94	0.982	1.905	–	
		90	5.27	3.43	14.57	0.732	1.112	–	
	20	30	9.27	100.8	136.42	1.168	1.891	–	$\bar{h}$ = 0.773
		90	4.99	4.54	11.74	0.632	1.202	–	
40	0	60	20.45	4.51	24.84	1.032	1.656	–	
		90	7.60	3.36	22.34	0.982	1.238	–	
	40	60	7.61	76.08	79.81	1.195	1.821	–	$\bar{h}$ = 0.0021
		90	6.81	6.41	15.15	0.856	1.350	–	

ϕ, β and α in degrees; θ_0^*, θ_h^* and θ_g^* in radians.

TABLE 8.7
Stability factor $N^* = (\gamma/c)H^*$ for the general profile oriented at a direction of arctan (0.5) with the horizon. Loading profiles: $k_x = 0.0057 + 0.0084\,h - 0.000076\,h^2 + 0.00000032\,h^3$, $k_y = 1. + 0.5\,k_x$

ϕ	β	α	N^*	$\frac{\gamma}{c}L^*$	$\frac{\gamma}{c}r_0^*$	θ_0^*	θ_h^*	θ_g^*	$\bar{d} = \frac{\gamma}{c}d^*$ or $\bar{h} = \frac{\gamma}{c}H_T^*$
0	0	30	6.02	6.89	11.82	0.349	2.124	1.018	
			5.14	31.13	37.74	0.352	2.639	0.502	$\bar{d}$ = 28.47
		90	3.70	3.50	10.33	0.508	1.006	–	
20	0	30	22.91	7.49	45.53	0.970	1.911	–	
		90	5.20	3.38	14.40	0.731	1.111	–	
	20	30	9.02	98.15	122.05	1.129	1.920	–	$\bar{h}$ = 0.011
		90	4.92	4.48	11.61	0.633	1.202	–	
40	0	60	19.97	4.32	23.73	1.024	1.658	–	
		90	7.48	3.31	21.91	0.981	1.238	–	
	40	60	7.53	75.46	78.23	1.192	1.823	–	
		90	6.69	6.33	14.96	0.858	1.351	–	

ϕ, β and α in degrees; θ_0^*, θ_h^* and θ_g^* in radians.

TABLE 8.8
Location of the most critical slip surface for a slope of 30 feet in height. Loading profiles: $k_x = 0.0057 + 0.0084\,h - 0.000076\,h^2 + 0.00000032\,h^3$, $k_y = 1$. Height of the slope: $H = 30$ ft.

ϕ	β	α	$\frac{\gamma}{c}H^*$	$\frac{\gamma}{c}H_T^*$	$\frac{\gamma}{c}L^*$	$\frac{\gamma}{c}r_0^*$	θ_0^*	θ_h^*	θ_g^*
0	0	30	3.10	26.90	27.87	21.74	0.602	2.353	–
		90	3.20	26.80	3.73	11.30	0.643	1.081	–
20	0	30	17.17	12.83	7.05	32.34	0.943	1.960	–
		90	4.32	25.68	3.41	16.99	0.872	1.162	–
	20	30	4.89	25.11	49.09	43.78	0.966	2.046	–
		90	4.03	25.97	4.99	11.20	0.741	1.308	–
40	0	60	16.22	13.78	4.30	19.85	1.055	1.686	–
		90	5.86	24.14	3.19	24.79	1.097	1.288	–
	40	60	4.65	25.35	46.24	34.82	1.084	1.894	–
		90	5.05	24.95	8.10	13.97	0.959	1.487	–

ϕ, β and α in degrees; θ_0^*, θ_h^* and θ_g^* in radians.
* Values calculated for a (c/γ) ratio of 1.

TABLE 8.9
Location of the most critical slip surface for a slope of 50 feet in height. Loading profiles: $k_x = 0.0057 + 0.0084\,h - 0.000076\,h^2 + 0.00000032\,h^3$, $k_y = 1$. Height of the slope: $H = 50$ ft.

ϕ	β	α	$\frac{\gamma}{c}H^*$	$\frac{\gamma}{c}H_T^*$	$\frac{\gamma}{c}L^*$	$\frac{\gamma}{c}r_0^*$	θ_0^*	θ_h^*	θ_g^*
0	0	30	2.03	47.97	21.49	14.92	0.491	2.489	–
		90	2.96	47.04	3.82	11.13	0.693	1.131	–
20	0	30	11.18	38.82	6.78	21.06	0.936	2.023	–
		90	3.90	46.10	3.39	17.70	0.931	1.193	–
	20	30	3.44	46.56	34.03	26.29	0.878	2.111	–
		90	3.60	46.40	5.42	10.74	0.793	1.386	–
40	0	60	12.22	37.78	4.12	16.09	1.107	1.719	–
		90	5.09	44.91	3.06	26.95	1.159	1.317	–
	40	60	3.49	46.51	34.77	22.26	1.020	1.933	–
		90	2.95	47.05	29.46	26.06	1.118	1.812	–

ϕ, β and α in degrees; θ_0^*, θ_h^* and θ_g^* in radians.
* Values calculated for a (c/γ) ratio of 1.

the omission of the vertical component profile in future works, as they might be quite different in real life. More detailed investigations concerning the vertical loading should be made in the future when such profiles are available.

Tables 8.8 and 8.9 are the tabulations of the locations of the most critical slip surface in slopes of different configurations. The height of the slope was given as 30 feet in Table 8.8 and 50 feet in Table 8.9. Under loadings specified by Eqs. (8.243) and (8.244), the soil near the top of the slope experiences the worst conditions and is the most likely place for a spiral to develop. The two tables reflect this fact and also the reductions in spiral heights as a result of the more intense loading of a taller slope.

In all these tables, some more or less common features can be observed. They are:

1. Stretched spirals are present only in slopes with low angle of internal friction, ϕ, and small slope angle α;
2. Sagging spirals are also found only when ϕ and α are small, but their ranges are usually larger than those of the stretched ones;
3. Partially sunken spirals have not been studied completely so far.

A close examination reveals a relatively general pattern for the variations of the spiral coordinates for similar configurations and loading conditions. This may be helpful in choosing the feasible starting points for future analyses with the computer coding.

8.6 Concluding remarks

This chapter discusses and develops a more general and consistent mathematical model for the analysis of the instability of earthslopes under seismic loads. By recognizing the disadvantages of existing models and with a better understanding of the nature of an earthquake's influences, such a more involved model has been successfully formulated. The treatment of several possibilities has been categorized such that a better insight into the influence of the slope geometry on the spiral failure mechanism can be gained. By looking into the possible changes seismic loads may have on the shape of the most critical slip surface, far-reaching conclusions may be drawn. For instance, in the derivation of the slip surface equation, it could be observed that the inhomogeneity and anisotropy in the cohesion of the soil has no effect on the critical shape. In fact, the only controlling factor on the shape of the slip surface is the internal friction angle ϕ.

Most important of all is the flexibility inherent in the present formulation to account for the variations of the seismic forces along the height. In considering both vertical and horizontal components for the seismic loads, not only is the variation of magnitude of the seismic force with height, but also the variation of the direction of the seismic force accountable. Such loading profiles, if interpreted wisely and

with care, can also be used to allow the variation of the specific weight of the soil along the height.

To facilitate the adaption of the present model to future analyses related to seismic-infirmed earthslopes, computer coding of the tedious formulations has been implemented, and results of fairly simple cases have been studied. These data constitute two main functions: to provide indicators of agreement between results of the present model and previous established models, and to provide further information relating to the seismic loadings that were not available previously. Of importance are the tables of the spiral coordinates for the different cases studied. They not only show the general patterns of the variation of the coordinates, but also provide good indications for estimating the initial coordinates for the spiral optimization process. Thus, the iterative algorithm of the optimization subroutine (used in the computer program) can be initiated in the right direction, resulting in the expedited analysis, cutting down on run time and cost, as well as preventing convergence onto local minimum.

The ability to predict and estimate the relative location of the most critical failure surface in an earthslope of given property, geometry, and height is even more significant. It allows for the cumulative displacement analysis proposed by Newmark (1965) and Seed (1967) to be developed.

All in all, the computer model developed in this chapter is a step forward in recent efforts to understand better the seismic effects on the stability of earthslopes. It is, nevertheless, quite idealized with respect to the actual time variation feature of the seismic forces, and the changes in soil properties. The changes in properties are results of compaction, pore water pressure variation, liquefaction, seepage forces, nonlinear post-elastic responses, hysteretic strain behaviors, etc., caused by the loadings.

In the following chapter, the present formulation will be extended to account for the inhomogeneity and anisotropy of the soil cohesion. It is obvious from the present study that the varying cohesion has no effect on the spiral equation, and it does not enter in the equations of external work rate. Thus, all is needed is a modification of the internal energy dissipation rate equation to account for two cohesion profiles, one with respect to the elevation, the other with respect to the orientation. Such modification is similar to that obtained previously by Chen (1975) and will not induce much changes in the formulations or the computer coding.

In Chapter 10, an extensive computer program to incorporate the hazards of a slope at different time intervals during the occurrence of an earthquake will be attempted. Such coding will include the examination of the seismic profiles at different intervals, to see if displacements along a well defined slip surface are inflicted or not. The displacements at the end of each interval will be integrated to determine the total displacement after the quake. This is essentially the new approach to the assessment of seismic slope hazards proposed by Newmark (1965) and Seed (1967).

However, no specific method of identifying the slip surface was mentioned in these earlier articles. The present study has provided part of the answer. The method developed for identifying the most critical slip surface for a slope of given height (such as those in Tables 8.8 and 8.9) can be used to determine the progressive development and movement of the failure surface in the course of the quake.

References

Ambraseys, N.N. and Sarma, S.K., 1967. The response of earth dams to strong earthquakes. Geotechnique, 17: 181–213.

Chen, W.F., 1975. Limit Analysis and Soil Plasticity. Elsevier, Amsterdam, The Netherlands, 638 pp.

Chen, W.F., 1977. Mechanics of slope failure and landslides. Proc. Advisory Meeting on Earthquake Engineering and Landslides, U.S-Republic of China Cooperative Science Program, Taipei, Taiwan, August 29–Sept. 2, pp. 219–232.

Chen, W.F., 1980. Plasticity in soil mechanics and landslides. J. Eng. Mech. Div., ASCE, 106(EM3): 443–464.

Chen, W.F. and Koh, S.L., 1978. Earthquake-induced landslide problems. Proc. Central Am. Conf. on Earthquake Eng., San Salvador, El Salvador, January 9–14, Envo, PA, pp. 665–685.

Chen, W.F., Giger, M. and Fang, H.Y., 1969. On the limit analysis of stability of slopes, soil and foundations. Jpn. Soc. Soil Mech. Found. Eng., 9(4): 23–32.

Chen, W.F., Chang, C.J. and Yao, J.T.P., 1978. Limit analysis of earthquake-induced slope failure. Proc. 15th Annual Meeting, Soc. Eng. Sci., R.L. Sierakowski (Ed.), December 4–6, Gainesville, Florida, pp. 533–538.

Chen, W.F., Chan, S.W. and Koh, S.L., 1984. Upper bound limit analysis of the stability of a seismic-infirmed earthslope. In: A.S. Balasubramaniam, S. Chandra and D.T. Bergado (Editors), Proc. Symp. Geotechnical Aspects of Mass and Material Transportation, Bangkok, 1984. Balkema Publishers, Rotterdam, The Netherlands, 1987, pp. 373–428.

Koh, S.L. and Chen, W.F., 1978. The prevention and control of earthquakes. Proc. U.S.-S.E. Asia Symp. on Eng. for Nat'l. Hazards Protection, Manila, Philippines, Sept. 1977; Univ. Illinois Press.

Newmark, N.M., 1965. Effects of earthquakes of dams and embankments. Geotechnique, 15(2): 137–160.

Prater, E.G., 1979. Yield acceleration for seismic stability of slopes. J. Geotech. Eng. Div., ASCE, 105(GT5): 682–687.

Root, R.R. and Ragsdell, K.M., 1977. BIAS: A nonlinear programming code in Fortran IV. User's Manual, Design Group, School of Mech. Eng., Purdue Univ., West Lafayette, IN.

Seed, H.B., 1967. Slope stability during earthquakes. J. Soil Mech. Found. Div., ASCE, 93(SM4): 299–323.

Seed, H.B. and Martin, G.R., 1966. The seismic coefficient in earth dam design. J. Soil Mech. Found. Div., ASCE, 92(SM3): 25–58.

Chapter 9

SEISMIC STABILITY OF SLOPES IN NONHOMOGENEOUS, ANISOTROPIC SOILS AND GENERAL DISCUSSIONS

9.1 Introduction

As mentioned in the preceding chapter, the conventional method for evaluating the effect of an earthquake load on the stability of a slope uses the so-called *'pseudo-static method'*. In this method, the inertia force is treated as an equivalent concentrated horizontal force, i.e., the pseudo-static force, at some critical point (usually the center of gravity) of the critical sliding mass. The inadequacies of the method for slope stability analysis have been discussed in various papers by many authors (e.g., Chen, 1982). Despite these criticisms, the pseudo-static method continues to be used by consulting geotechnical engineers because it is required by the building codes, it is easier and less costly to apply, and satisfactory results have been obtained since 1933. This method will continue to be popular until an alternative method can be shown to be a more reasonable approach.

In the first part of this chapter, we shall extend the upper bound technique of limit analysis for the seismic stability of slopes to account for the *nonhomogeneity* and *anisotropy* of the soil cohesion. The Mohr-Coulomb yield condition is described by two parameters, cohesion c and friction angle ϕ. Here, as in Chapter 7, we shall assume that only the parameter c is nonhomogeneous and anisotropic. The friction angle ϕ is assumed to remain homogeneous and isotropic throughout the calculations, i.e., a constant value for a given type of slope. The term *'nonhomogeneity'* of cohesion implies a variation of c with respect to depth z and the term *'anisotropy'* of cohesion implies a variation of c with respect to direction at a particular point. It has been shown from the preceding chapter that the variation of cohesion has no effect on the spiral mechanism, and it will not enter in the equation for the external rate of work. Thus, all we need here is a modification of the equation for the rate of internal energy dissipation.

For simplicity, we assume in this chapter a uniform distribution of lateral acceleration with respect to depth, and we use the Mohr-Coulomb failure criterion with constant ϕ but variable c. In the following, a brief description of the two terms 'nonhomogeneity' and 'anisotropy' follows a rigorous analysis capable of dealing with a general slope. Extensive numerical studies of slopes made using this analysis are then presented. Details of this development are given in the paper by Chen and Sawada (1983).

In the later part of this chapter, the assessment of seismic stability of slopes will be discussed. This discussion includes the mechanics of earthquake-induced landslides, the applicability of some dynamic properties of soils to earthquake loadings, and the selection of appropriate analysis methods. The salient features of the most widely used methods proposed by Newmark (1965) and Seed (1966) for the analysis and design of the slides of dams and embankments induced by earthquake motions are briefly introduced. This introduction provides the necessary background information for the assessment of seismic displacement of slopes described in Chapter 10.

9.2 Log-spiral failure mechanism for a nonhomogeneous and anistropic slope

The term 'nonhomogeneous soil' implies only the cohesion strength, c, which is assumed to vary linearly with depth (Fig. 9.1c). Figure 9.2 summarizes diagrammatically some of the simple cutting in normally consolidated clays with several forms of cohesion strength distribution being considered previously by several investigators. (Taylor, 1948; Gibson and Mogenstern, 1962; Odenstad, 1963; Reddy and Srinivasan, 1967).

The term *'anisotropic soil'* implies here the variation of the cohesion strength, c,

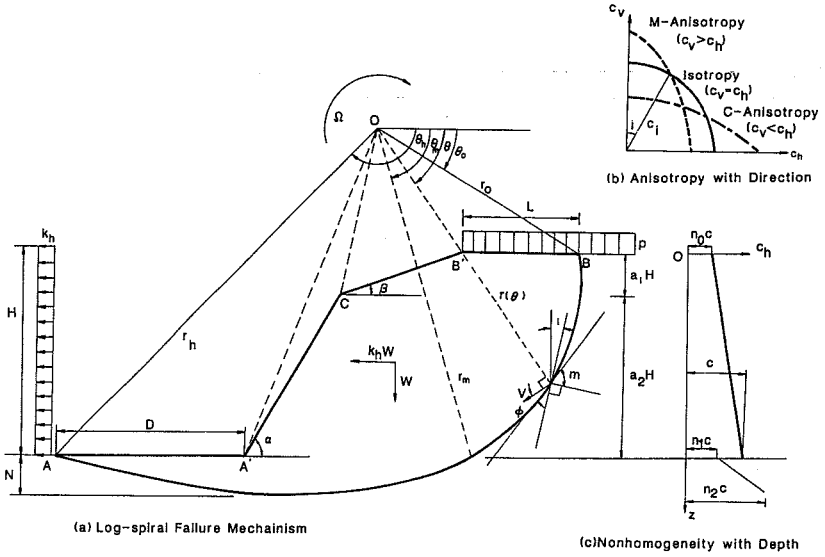

Fig. 9.1. Failure mechanism for a nonhomogeneous and anisotropic slope.

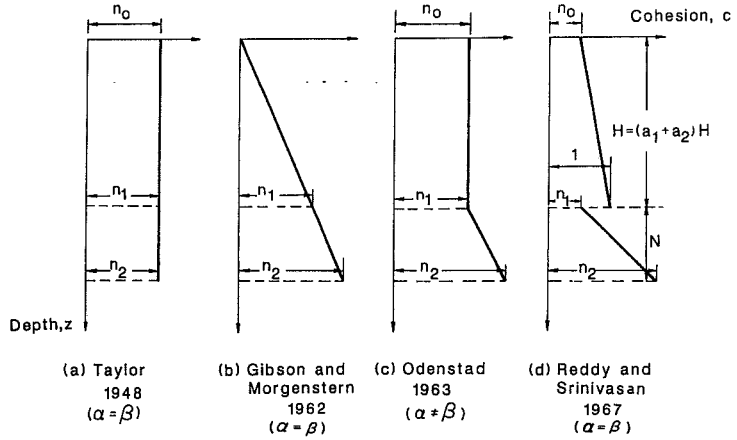

Fig. 9.2. Some types of linear variations of cohesion with depth.

with direction at a particular point. The anisotropy with respect to cohesion strength, c of the soil has been studied by several investigators. (Taylor, 1948; Odenstad, 1963; Lo, 1965; Reddy and Srinivasan, 1967). It is found that the variation of cohesion strength, c, with direction approximates to the curve shown in Fig. 9.1b. In this section, the variation of the apparent friction angle ϕ is not considered with respect to either the nonhomogeneity or the anisotropy. In the following we assume that the cohesion strength c_i, with its major principal stress inclined at an angle i with the vertical direction, is given by the same equation as Eq. 7.1:

$$c_i = c_h + (c_v - c_h)\cos^2 i \tag{9.1}$$

where c_h and c_v are the cohesion strength in the horizontal and vertical directions, respectively. These cohesion strengths may be termed as *'principal cohesion strengths'* (Lo, 1965). For example, the vertical cohesion strength, c_v can be obtained by taking vertical soil samples at any position and being investigated with the major principal stress applied in the same direction. The ratio of the principal cohesion strengths c_h/c_v, denoted by $\varkappa$, is assumed to be the same at all points in the medium. $c_i = c_h = c_v$ (or $\varkappa = 1.0$) is an isotropic material. In Fig. 9.1a, the angle m is the angle between the failure plane and the plane which is normal to the direction of the major principle cohesion strength kept at an angle i with the vertical direction. This angle, according to Lo's test (1965), is found to be independent of the angle of rotation of the major principal stress.

The geometrical relations L/r_0, H/r_0 and N/r_0 in Fig. 9.1a can be expressed in the forms:

$$\frac{L}{r_0} = \cos\theta_0 - \cos\theta_h \exp[(\theta_h - \theta_0)\tan\phi] - \frac{D}{r_0} - \frac{H}{r_0}(a_1 \cot\beta + a_2 \cot\alpha) \tag{9.2}$$

$$\frac{H}{r_0} = \sin\theta_h \exp[(\theta_h - \theta_0)\tan\phi] - \sin\theta_0 \tag{9.3}$$

$$\frac{N}{r_0} = \cos\phi \exp\left[\left(\frac{\pi}{2} + \phi - \theta_0\right)\tan\phi\right] - \sin\theta_0 - \frac{H}{r_0} \tag{9.4}$$

where a_1, a_2, D and N are defined in Fig. 9.1a. The rate of external work done by the region A-A′-C-B′-B-A can be obtained from the algebraic summation of $\dot{W}_1 - \dot{W}_2 - W_3 - \dot{W}_4 - \dot{W}_5$. Herein, $\dot{W}_1$, $\dot{W}_2$, $\dot{W}_3$, $\dot{W}_4$ and $\dot{W}_5$ represent the rates of external work done by the soil weight in the region O-A-B, O-B′-B, O-C-B′, O-A′-C an O-A-A′, respectively.

These expressions are:

$$\dot{W}_1 = \gamma r_0^3 \Omega \left[\frac{1}{3(1 + 9\tan^2\phi)}\{(3\tan\phi\cos\theta_h + \sin\theta_h)\exp[3(\theta_h - \theta_0)\tan\phi] - 3\tan\phi\cos\theta_0 - \sin\theta_0\}\right] = \gamma r_0^3 \Omega G_1 \tag{9.5}$$

$$\dot{W}_2 = \gamma r_0^3 \Omega \tfrac{1}{6}\sin\theta_0 \frac{L}{r_0}\left(2\cos\theta_0 - \frac{L}{r_0}\right) = \gamma r_0^3 \Omega G_2 \tag{9.6}$$

$$\dot{W}_3 = \gamma r_0^3 \Omega \left[\frac{a_1}{3}\frac{H}{r_0}\left\{\cos^2\theta_0 + \frac{L}{r_0}\left(\frac{L}{r_0} - 2\cos\theta_0\right) + \sin\theta_0 \cot\beta\left(\cos\theta_0 - \frac{L}{r_0}\right) - \frac{a_1}{2}\frac{H}{r_0}\cot\beta\left(\cos\theta_0 + \frac{L}{r_0} - \sin\theta_0\cot\beta\right)\right\}\right] = \gamma r_0^3 \Omega G_3 \tag{9.7}$$

$$\dot{W}_4 = \gamma r_0^3 \Omega \frac{a_2}{3}\frac{H}{r_0}\left[(\cos^2\theta_h + \cot\alpha \sin\theta_h \cos\theta_h)\exp[2(\theta_h - \theta_0)\tan\phi] + \left(\frac{D}{r_0}\cot\alpha\sin\theta_h + \frac{a_2}{2}\frac{H}{r_0}\sin\theta_h \cot^2\alpha + 2\frac{D}{r_0}\cos\theta_h + \frac{a_2}{2}\frac{H}{r_0}\cot\alpha\cos\theta_h\right)\exp[(\theta_h - \theta_0)\tan\phi] + \left(\frac{D}{r_0}\right)^2\right] = \gamma r_0^3 \Omega G_4 \tag{9.8}$$

$$\dot{W}_5 = \gamma r_0^3 \Omega \tfrac{1}{6}\frac{D}{r_0}\sin\theta_h\left[\left\{2\cos\theta_h \exp[2(\theta_h - \theta_0)\tan\phi] + \frac{D}{r_0}\right\}\exp[(\theta_h - \theta_0)\tan\phi]\right] = \gamma r_0^3 \Omega G_5 \tag{9.9}$$

Similarly, the rate of external work done by the inertia force on the soil weight can be found by a simple summation of $\dot{W}_6 - \dot{W}_7 - \dot{W}_8 - \dot{W}_9 - \dot{W}_{10}$. Herein, $\dot{W}_6$, $\dot{W}_7$, $\dot{W}_8$, $\dot{W}_9$ and $\dot{W}_{10}$ represent the rates of of external work done by the inertia force due to sliding soil weight in regions O-A-B, O-B′-B, O-C-B′, O-A′-C and O-A-A′, respectively.

These expressions are as follows:

$$\dot{W}_6 = k_h \gamma r_0^3 \Omega\left[\frac{1}{3(1 + 9\tan^2\phi)}\{(3\tan\phi\sin\theta_h - \cos\theta_h)\exp[3(\theta_h - \theta_0)\tan\phi] - 3\tan\phi\sin\theta_0 + \cos\theta_0\}\right] = k_h \gamma r_0^3 \Omega G_6 \tag{9.10}$$

$$\dot{W}_7 = \frac{k_h \gamma r_0^3 \Omega}{3}\left\{\frac{L}{r_0}\sin^2\theta_0\right\} = k_h \gamma r_0^3 \Omega G_7 \tag{9.11}$$

$$\dot{W}_8 = k_h \gamma r_0^3 \Omega\left[\frac{a_1}{3}\frac{H}{r_0}\left\{\sin\theta_0 + \frac{a_1}{2}\left(\frac{H}{r_0}\right)\right\}\left(\cos\theta_0 + \sin\theta_0\cos\beta - \frac{L}{r_0}\right)\right] = k_h \gamma r_0^3 \Omega G_8 \tag{9.12}$$

$$\dot{W}_9 = -\frac{k_h \gamma r_0^3 \Omega}{3}\left[\sin\theta_h \cos\theta_h\left(\sin\theta_0 + \frac{H}{r_0}\right)\exp[2(\theta_h - \theta_0)\tan\phi] + \exp[(\theta_h - \theta_0)\tan\phi]\left[\sin\theta_h \frac{D}{r_0}\left(\sin\theta_0 + \frac{H}{r_0}\right) - \cos\theta_h\left\{\sin\theta_0 + (a_2 + 1)\frac{H}{r_0} + \left(\frac{a_2 H}{r_0}\right)^2\right\}\right] - \frac{D}{r_0}\left\{\sin\theta_0 + (a_2 + 1)\frac{H}{r_0} + \left(\frac{a_2 H}{r_0}\right)^2\right\} - a_2\cot\alpha\frac{H}{r_0}\left\{\sin\theta_0 + (1 - a_2)\frac{H}{r_0}\right\}\left(\sin\theta_0 + \frac{H}{r_0}\right)\right] = k_h \gamma r_0^3 \Omega G_9 \tag{9.13}$$

$$\dot{W}_{10} = k_h \gamma r_0^3 \Omega\left\{\tfrac{1}{3}\frac{D}{r_0}\sin^2\theta_h \exp[2(\theta_h - \theta_0)\tan\phi]\right\} = k_h \gamma r_0^3 \Omega G_{10} \tag{9.14}$$

The rate of external work due to the surcharge boundary pressure p and its associated inertia force are found to be:

– due to the surcharge load pL

$$p\, r_0^2\Omega \left\{ \frac{L}{r_0} \cos\theta_0 - \frac{L}{2r_0} \right\} = p\, r_0^2\Omega\, f_p \tag{9.15}$$

– due to the inertia force of the surcharge load pL

$$k_h'\, p\, r_0^2\Omega \left\{ \frac{L}{r_0} \sin\theta_0 \right\} = p\, r_0^2\Omega\, f_q \tag{9.16}$$

where the factor $k_h' = \chi k_h$ is the seismic coefficient for the surcharge load pL. The inertia response of the surcharge load pL caused by the earthquake is represented by $k_h' pL$.

The total rates of internal energy dissipation along the discontinuous logspiral failure surface AB is found by multiplying the differential area $r\, d\theta/\cos\phi$ by c_i times the discontinuity in velocity, $V\cos\phi$, across the surface and integrating over the whole surface AB. Since the layered clays possess different values of c_i, the integration is therefore carried out into two parts:

$$\int_{\theta_0}^{\theta_h} c_i\, (V\cos\phi)\, \frac{r\, d\theta}{\cos\phi} = \int_{\theta_0}^{\theta_m} (c_i)_I\, r_0 V_0 \exp[2(\theta - \theta_0)\tan\phi] d\theta + \int_{\theta_m}^{\theta_h} (c_i)_{II}\, r_0\, V_0 \exp[2(\theta - \theta_0)\tan\phi] d\theta \tag{9.17}$$

The log-spiral angle, θ_m at the level of the toe, and the logspiral angle, θ_h at the exit of the spiral, are related from the geometric configuration shown in Fig. 9.1a as

$$\sin\theta_m \exp[\theta_m \tan\phi] = \sin\theta_h \exp[\theta_h \tan\phi] \tag{9.18}$$

Referring to Eq. (9.1) and the geometry of Fig. 9.1, $(c_i)_I$ and $(c_i)_{II}$ can be expressed as:

– in the region θ_0 and θ_m

$$(c_i)_I = \left\{ 1 + \frac{1 - \varkappa}{\varkappa} \cos^2 i \right\} c \left\{ n_0 + \frac{1 - n_0}{H/r_0} (\sin\theta \exp[(\theta - \theta_0)\tan\phi] - \sin\theta_0) \right\} \tag{9.19}$$

– in the region θ_m and θ_h

$$(c_i)_{II} = \left\{ 1 + \left(\frac{1 - \varkappa}{\varkappa} \right) \cos^2 i \right\} c \left\{ n_1 + \frac{n_2 - n_1}{N/r_0} (\sin\theta \exp[(\theta - \theta_0)\tan\phi] - \sin\theta_m \exp[(\theta_m - \theta_0)\tan\phi]) \right\} \tag{9.20}$$

where $\varkappa = c_h/c_v$, $i = \theta + \Phi$, $\Phi = -(\pi/2 + \phi - m)$ and n_0, n_1 and n_2 are defined in Fig. 9.1c. After integration and some simplifications, Eq. (9.17) reduces to:

$$\int_{\theta_0}^{\theta_h} c_i (V\cos\phi) \frac{r\, d\theta}{\cos\phi} = c\, r_0^2\Omega\, Q \tag{9.21}$$

in which c is the cohesion of soil at the level of the toe (see Fig. 9.1), and:

$$Q = Q_1 + Q_2 + Q_3 \tag{9.22}$$

The functions Q_1, and Q_2 and Q_3 are:

$$Q_1 = \frac{n_0}{\exp(2\theta_0 \tan\phi)} \left| B + \left(\frac{1 - \varkappa}{\varkappa} \right) E \right|_{\theta_0}^{\theta_m} + \frac{n_1}{\exp(2\theta_0 \tan\phi)} \left| B + \left(\frac{1 - \varkappa}{\varkappa} \right) E \right|_{\theta_m}^{\theta_h} \tag{9.23}$$

$$Q_2 = \frac{1 - n_0}{\left(\frac{H}{r_0} \right) \exp(3\theta_0 \tan\phi)} \left| A - B \sin\theta_0 \exp[\theta_0 \tan\phi] \right. + \left(\frac{1 - \varkappa}{\varkappa} \right) C - E \sin\theta_0 \exp[\theta_0 \tan\phi] \Big|_{\theta_0}^{\theta_m} \tag{9.24}$$

$$Q_3 = \frac{n_2 - n_1}{\left(\frac{N}{r_0} \right) \exp(3\theta_0 \tan\phi)} \left| A - B \sin\theta_m \exp[\theta_m \tan\phi] \right. + \left(\frac{1 - \varkappa}{\varkappa} \right) C - E \sin\theta_m \exp[\theta_m \tan\phi] \Big|_{\theta_m}^{\theta_h} \tag{9.25}$$

in which:

$$A = \frac{(3\tan\phi \sin\theta - \cos\theta)}{1 + 9\tan^2\phi} \exp[3\theta \tan\phi] \tag{9.26}$$

$$B = \frac{\exp[2\theta \tan\phi]}{2\tan\phi} \tag{9.27}$$

$$C = \frac{\exp[3\theta \tan\phi]}{2}\left[\frac{3\tan\phi \sin\theta - \cos\theta}{1 + 9\tan^2\phi}\right.$$

$$+ \cos 2\Phi \left\{\frac{\tan\phi \sin 3\theta - \cos 3\theta}{6(1 + \tan^2\phi)} + \frac{\cos\theta - 3\tan\theta \sin\theta}{2(1 + 9\tan^2\phi)}\right\}$$

$$\left. - \sin 2\Phi \left\{\frac{\sin\theta + 3\tan\phi \cos\theta}{2(1 + 9\tan^2\phi)} - \frac{\sin 3\theta + \tan\phi \cos 3\theta}{6(1 + \tan^2\phi)}\right\}\right] \quad (9.28)$$

$$E = \frac{\exp[2\theta \tan\phi]}{2}\left[\frac{1}{2\tan\phi}\right.$$

$$\left. + \frac{\cos 2\Phi (\tan\phi \cos 2\theta + \sin 2\theta) - \sin 2\Phi (\tan\phi \sin 2\theta - \cos 2\theta)}{2(1 + \tan^2\phi)}\right] \quad (9.29)$$

By equating the total rates of external work, Eqs. (9.5) to (9.16) to the total rate of internal energy dissipation, Eq. (9.21) and assuming $k_h' = \chi k_h$, we obtain:

$$k_h = F(\theta_0, \theta_h, D/r_0)$$

$$= \frac{c(Q_1 + Q_2 + Q_3) - \gamma r_0(G_1 - G_2 - G_3 - G_4 - G_5) - pf_p}{\gamma r_0(G_6 - G_7 - G_8 - G_9 - G_{10}) + \chi pf_q} \quad (9.30)$$

The function $F(\theta_0, \theta_h, D/r_0)$ has a minimum value and, thus, indicates a least upper bound, when θ_0,θ_h, and D/r_0 satisfy the following conditions:

$$\frac{\partial F}{\partial \theta_0} = 0, \quad \frac{\partial F}{\partial \theta_h} = 0, \quad \frac{\partial F}{\partial D/r_0} = 0 \quad (9.31)$$

Thus, the *yield acceleration factor,* k_c is denoted as:

$$k_c = \text{Min } F(\theta_0, \theta_h, D/r_0) \quad (9.32)$$

9.3 Numerical results and discussions

9.3.1 Calculated results

Extensive numerical results for the yield acceleration factor k_c were reported by Chen and Sawada (1983) using a computer program developed at Purdue University. Details of the program are given elsewhere by Chen and Sawada (1982). The optimization technique reported by Sigel (1975) was used to minimize the function of Eq. (9.32) without calculating the derivatives. The results are summarized in Tables 9.1 to 9.7 and Fig. 9.3. Some of the solutions are compared in Tables 9.1 and 9.2 with the existing limit equilibrium solutions.

Table 9.1 compares the critical heights, H_c, obtained by the limit equilibrium method with those obtained by the present limit analysis for anistropic slopes with constant shear strength (Lo, 1965). Here, as in Lo's work, the value of m is taken to be 55° and the values of friction angle ϕ and acceleration k_h are put nearly equal to zero so that the statical log-spiral failure surface reduces to the circular one. Generally speaking, both results are in a good agreement.

Table 9.2 compares the cases of anisotropic slopes with shear strength increasing linearly with depth (Fig. 9.2b). In this way, the critical heights, H_c, can be compared with those obtained previously by Lo (1965) using the limit equilibrium method. A good agreement is again observed.

TABLE 9.1
Comparison of critical height: H_c for anisotropic soil with constant shear strength

		Curved failure surface		
Slope angle (degree) $\alpha = \beta$	Anisotropy factor χ	Limit equilibrium ϕ circle*, (1)	Limit analysis Log-spiral, (2)	Ratio (1)/(2)
90	1.0	95.75	110.57	0.870
	0.9	–	–	–
	0.8	–	–	–
	0.7	–	–	–
	0.6	–	–	–
	0.5	–	–	–
70	1.0	119.75	136.62	0.877
	0.9	118.00	132.36	0.892
	0.8	116.25	128.14	0.907
	0.7	114.50	123.89	0.924
	0.6	112.25	119.12	0.942
	0.5	110.25	114.92	0.960
50	1.0	142.00	142.00	1.000
	0.9	138.50	137.50	1.007
	0.8	133.75	129.40	1.034
	0.7	129.75	125.50	1.054
	0.6	127.25	120.75	1.054
	0.5	121.25	116.50	1.041

* Lo (1965).

TABLE 9.2
Comparison of critical height: H_c for anisotropic soil with shear strength increasing linearly with depth

Slope angle (degree) $\alpha = \beta$	Anisotropy factor $\varkappa$	Curved failure surface: Limit equilibrium ϕ circle*, (1)	Curved failure surface: Limit analysis Log-spiral, (2)	Ratio (1)/(2)
90	1.0	50.00	60.97	0.820
	0.9	50.00	60.45	0.827
	0.8	50.00	60.30	0.829
	0.7	50.00	59.40	0.842
	0.6	50.00	58.85	0.850
	0.5	50.00	58.35	0.857
70	1.0	69.25	72.10	0.961
	0.9	68.25	72.06	0.947
	0.8	67.25	70.77	0.950
	0.7	66.25	70.40	0.941
	0.6	65.25	70.20	0.930
	0.5	62.50	68.68	0.910
50	1.0	94.50	103.70	0.911
	0.9	91.50	100.50	0.911
	0.8	89.00	98.00	0.908
	0.7	86.25	95.40	0.904
	0.6	82.75	92.40	0.896
	0.5	79.25	89.50	0.886
30	1.0	137.50	135.50	1.015
	0.9	–	–	–
	0.8	125.00	127.00	0.984
	0.7	–	–	–
	0.6	–	–	–
	0.5	104.50	114.00	0.917

* Lo (1965).

TABLE 9.3
Yield acceleration factor k_c with constant stability number N_s and surcharge p

Anisotropy factor $\varkappa$	$p = 0$ $k_h'/k_h = 0$	$p = 120$ psf $k_h'/k_h = 0$	$p = 120$ psf $k_h'/k_h = 0.5$
1.0	0.477	0.455	0.450
0.9	0.457	0.436	0.431
0.8	0.437	0.417	0.413
0.7	0.416	0.399	0.394
0.6	0.396	0.380	0.376
0.5	0.377	0.361	0.357

$p = 5.75$ kPa.

Figure 9.3 illustrates graphically the k_c-values of anisotropy case normalized by the corresponding k_c-value of isotropy case with C-anisotropy type (or $\varkappa > 1$) and M-anisotropy type (or $\varkappa < 1$) as shown in Fig. 9.1b (Lo, 1965).

Some typical results for the yield acceleration k_c corresponding to the general case of nonhomogeneous and anisotropic soil are tabulated in Tables 9.3 to 9.7. Table 9.3 gives the yield acceleration factor k_c with constant stability number N_s and surcharge p. The others consider (see Fig. 9.2) Taylor's model (1948), Gibson and Mogenstern's model (1962), Odenstad's model (1963), and Reddy and Srinivasan's model (1967), in which the angle m between the failure plane and the major principal plane as shown in Fig. 9.1a is taken to be $\pi/4 + \phi/2$.

9.3.2 General remarks

A practical approach to obtain effectively the stability solutions of nonhomogeneous and anisotropic slopes under an earthquake loading has been established (Fig. 9.3). Herein, the upper-bound techniques of limit analysis have been applied to obtain the yield acceleration factor for different cohesion strength distributions. The formulation of the problem is seen to be rather straightforward and simple. The numerical results are found to be in a good agreement with the existing limit equilibrium solutions. It can therefore be concluded that the upper-bound techniques of limit analysis provide a convenient and effective method for the analysis for seismic stability of nonhomogeneous and anisotropic slopes.

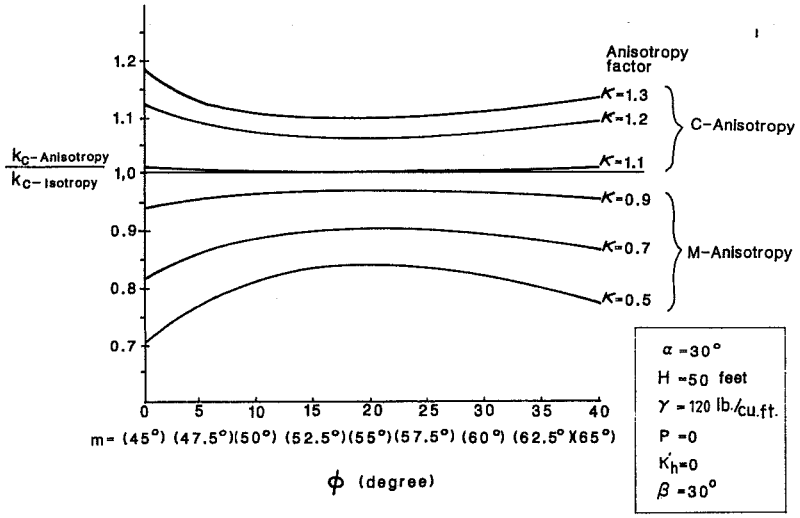

Fig. 9.3. Variation of $k_{c\text{-anisotropy}}/k_{c\text{-isotropy}}$ with ϕ.

TABLE 9.4
Anisotropic but homogeneous soil: Taylor model (1948) with constant c_v (ϕ = constant, $\alpha = \beta$), $n_0 = 1.0$, $n_1 = 1.0$, $n_2 = 1.0$

Friction angle ϕ (°)	Anisotropy factor x	Yield acceleration factor: k_c			
		$\alpha = 30°$	$\alpha = 50°$	$\alpha = 70°$	$\alpha = 90°$
C-anisotropy type	1.3	0.290	0.285	0.282	0.280
	1.2	0.275	0.270	0.268	0.266
	1.1	0.260	0.256	0.253	0.252
0.0	1.0	0.246	0.241	0.239	0.237
($m = 45°$)	0.9	0.231	0.227	0.225	0.223
	0.8	0.216	0.212	0.211	0.209
M-anisotropy	0.7	0.201	0.198	0.196	0.195
type	0.6	0.187	0.184	0.182	0.181
	0.5	0.172	0.169	0.168	0.167
C-anisotropy type	1.3	0.361	0.356	0.354	0.352
	1.2	0.346	0.342	0.339	0.337
	1.1	0.331	0.327	0.325	0.323
5.0	1.0	0.316	0.312	0.310	0.309
($m = 47.5°$)	0.9	0.301	0.297	0.296	0.294
	0.8	0.286	0.283	0.281	0.280
M-anisotropy	0.7	0.271	0.268	0.267	0.266
type	0.6	0.256	0.253	0.252	0.251
	0.5	0.240	0.239	0.238	0.237
C-anisotropy type	1.3	0.459	0.454	0.451	0.449
	1.2	0.433	0.438	0.435	0.434
	1.1	0.432	0.422	0.420	0.418
10.0	1.0	0.411	0.407	0.405	0.403
($m = 50°$)	0.9	0.394	0.391	0.389	0.388
	0.8	0.378	0.375	0.374	0.373
M-anisotropy	0.7	0.362	0.359	0.358	0.357
type	0.6	0.346	0.344	0.343	0.342
	0.5	0.329	0.328	0.327	0.326
C-anisotropy type	1.3	0.739	0.729	0.725	0.721
	1.2	0.717	0.707	0.704	0.701
	1.1	0.695	0.686	0.683	0.680
20.0	1.0	0.673	0.666	0.662	0.660
($m = 60°$)	0.9	0.651	0.645	0.641	0.639
	0.8	0.629	0.623	0.621	0.619
M-anisotropy	0.7	0.607	0.602	0.600	0.598
type	0.6	0.585	0.581	0.579	0.578
	0.5	0.562	0.560	0.558	0.557

Before we proceed to describe the methods for a valid assessment of the seismic stability of slopes in the following chapter, it is necessary to mention here that the success in developing a practical method for a valid assessment of the hazard of slope failure and landslides requires the considerations of the structure of the slope and its water saturation as well as the physical properties of the soils comprising the slope. Supplemental data on the local earthquake activity, climatic and hydrologic conditions of the region, and the history of local landslides should also be collected. Estimates of the slope stability must be based on the results of these investigations (Chen, 1977). The effects of these factors on the stability of slopes from the viewpoint of soil mechanics will be described in the forthcoming.

TABLE 9.5
Anisotropic and nonhomogeneous soil: Gibson and Morgenstern Model (1962) for c_v increasing linearly with depth $n_0 = 0$, $n_1 = 1.0$

Friction angle ϕ (°)	Anisotropy factor x	Yield acceleration factor: k_c			
		$\alpha = 30°$	$\alpha = 50°$	$\alpha = 70°$	$\alpha = 90°$
	1.0	0.231	0.227	0.226	0.224
	0.9	0.216	0.213	0.211	0.210
	0.8	0.201	0.199	0.197	0.196
0.0	0.7	0.186	0.184	0.183	0.182
($m = 45°$)	0.6	0.172	0.170	0.169	0.168
	0.5	0.157	0.155	0.155	0.154
	1.0	0.303	0.300	0.299	0.298
	0.9	0.288	0.286	0.284	0.283
	0.8	0.273	0.271	0.270	0.269
5.0	0.7	0.258	0.256	0.255	0.255
($m = 47.5°$)	0.6	0.243	0.242	0.241	0.241
	0.5	0.228	0.227	0.227	0.226
	1.0	0.399	0.396	0.394	0.393
	0.9	0.383	0.380	0.379	0.378
10.0	0.8	0.367	0.365	0.364	0.363
($m = 50°$)	0.7	0.350	0.349	0.348	0.348
	0.6	0.344	0.333	0.332	0.332
	0.5	0.318	0.318	0.317	0.317
	1.0	0.659	0.653	0.650	0.648
	0.9	–	0.632	0.629	0.628
20.0	0.8	–	0.611	0.609	0.608
($m = 60°$)	0.7	–	0.590	0.588	0.587
	0.6	–	0.569	0.568	0.567
	0.5	–	0.548	0.547	0.547

TABLE 9.6
Anisotropic and nonhomogeneous soil: Odenstad Model (1963) for c_v increasing linearly with depth (ϕ = constant, $\alpha \neq \beta$), $n_0 = 1.0$, $n_1 = 1.0$, $n_2 = 1.5$.

Friction angle ϕ (°)	Anisotropy factor $\varkappa$	Yield acceleration factor: k_c			
		$\alpha = 30°$	$\alpha = 50°$	$\alpha = 70°$	$\alpha = 90°$
	1.0	0.329	0.323	0.320	0.318
	0.9	0.311	0.305	0.302	0.300
0.0	0.8	0.293	0.287	0.284	0.282
(m = 45°)	0.7	0.274	0.269	0.266	0.264
	0.6	0.255	0.250	0.248	0.246
	0.5	0.237	0.232	0.230	0.228
	1.0	0.395	0.389	0.386	0.383
	0.9	0.376	0.370	0.367	0.365
5.0	0.8	0.356	0.351	0.349	0.347
(m = 47.5°)	0.7	0.337	0.332	0.330	0.328
	0.6	0.318	0.314	0.311	0.310
	0.5	0.299	0.295	0.293	0.292
	1.0	0.486	0.480	0.477	0.474
	0.9	0.465	0.460	0.457	0.455
10.0	0.8	0.445	0.439	0.437	0.435
(m = 50°)	0.7	0.424	0.419	0.416	0.415
	0.6	0.403	0.399	0.396	0.395
	0.5	0.382	0.379	0.377	0.376
	1.0	0.741	0.732	0.727	0.724
	0.9	0.713	0.705	0.701	0.698
20.0	0.8	0.686	0.678	0.675	0.672
(m = 60°)	0.7	0.658	0.652	0.648	0.646
	0.6	0.631	0.625	0.622	0.620
	0.5	0.603	0.598	0.595	0.593

9.4 Mechanics of earthquake-induced slope failure

Earthquake accelerations cause a temporary increase in shearing stress, τ, within a soil mass and at the same time significantly decrease the shearing strength, s, in some materials such as water saturated sand. If the existing slope is already in a near-critical stress condition, the earthquake will trigger the landslide. If, as a result of cyclic loading due to accelerations, the pore-water pressure in a mass of undrained cohesionless soil increases to the point where it is equal to the externally applied pressures, the soil loses completely its shearing strength and the soil is said to *liquefy*. If liquefaction occurs along a large portion of the potential sliding surface,

the landslide movements will be very extensive and the motion is termed a *flow slide*. The action of the pore-water pressure, u, in a landslide can be compared to that of a hydraulic jack. The greater the pore-water pressure, the greater is the part of the total weight of sliding mass which is carried by the water, and as soon as the pore-water pressure becomes equal to the normal pressure, the sliding mass 'floats' and a flow slide occurs.

In many cases a liquefied zone may not be extensive so that sliding occurs partly through liquefied soil and partly through non-liquefied soil along the slip surface. In such cases, the strength of the nonliquefied soil may be sufficient to prevent sliding as soon as the inertia forces due to earthquake ground motions stop. The

TABLE 9.7
Anisotropic and nonhomogeneous soil: Reddy and Srinivasan Model (1967) for c_v increasing linearly with depth (ϕ = constant, $\alpha = \beta$), $n_0 = 0.5$, $n_1 = 0.7$, $n_2 = 1.5$

Friction angle ϕ (°)	Anisotropy factor $\varkappa$	Yield acceleration factor: k_c			
		$\alpha = 30°$	$\alpha = 50°$	$\alpha = 70°$	$\alpha = 90°$
	1.0	0.304	0.298	0.295	0.293
	0.9	0.286	0.281	0.278	0.276
0.0	0.8	0.268	0.263	0.261	0.259
(m = 45°)	0.7	0.250	0.245	0.243	0.242
	0.6	0.232	0.228	0.226	0.225
	0.5	0.213	0.210	0.209	0.207
	1.0	0.372	0.368	0.364	0.362
	0.9	0.354	0.350	0.347	0.345
5.0	0.8	0.335	0.331	0.329	0.327
(m = 47.5°)	0.7	0.317	0.313	0.311	0.310
	0.6	0.298	0.295	0.293	0.292
	0.5	0.280	0.277	0.276	0.275
	1.0	0.467	0.461	0.459	0.456
	0.9	0.447	0.442	0.440	0.438
10.0	0.8	0.428	0.423	0.421	0.419
(m = 50°)	0.7	0.409	0.404	0.402	0.401
	0.6	0.390	0.385	0.383	0.382
	0.5	0.369	0.365	0.364	0.363
	1.0	0.739	0.730	0.725	0.722
	0.9	0.712	0.704	0.700	0.697
20.0	0.8	0.685	0.678	0.674	0.672
(m = 60°)	0.7	0.658	0.652	0.649	0.647
	0.6	0.631	0.626	0.624	0.622
	0.5	0.605	0.600	0.598	0.597

movements involved in such cases are relatively small compared to the size of the slide mass (Seed, 1968). This is usually referred to as *landslide due to liquefaction*.

Liquefaction can only persist as long as high pore-water pressures persist in a soil. For some materials such as a medium-dense cohesionless soil, liquefaction may be developed initially over a small deformation range but the material stiffens rapidly as a result of the property of *dilation* at large deformation. This behavior of dilation reduces the pore-water pressure and results in a self-stabilizing effect against large movements. Similarly, if drainage can occur rapidly in the soil, large displacements of landslides during earthquake due to soil liquefaction can not develop. Some case studies of landslides due to liquefaction and flow slides are reviewed by Seed (1968), among many others.

No slide can take place unless the factor of safety or the ratio '$\bar{s}/\bar{\tau}$' between the average shearing resistance, $\bar{s}$, of the ground and the average shearing stress, $\bar{\tau}$, on the potential surface of sliding has previously decreased from an initial value greater than one to unity at the instant of the slide. For most slides, the change of the ratio is rather gradual, which, in turn, results in a gradual progressive type of deformation process for material located above the potential surface of sliding and some downward movements of all points located on the surface of the potential sliding mass. The differential downward movements of the slope which proceeds the slide may be detectable by a careful measurement. Further, this relative displacement is likely to cause tension cracks along the upper boundary of the slide area. This phenomenon may be used as an indication of a possible disaster of slope failure or landslides. Sometimes, these effects are such that they are conspicuous enough to attract the attention of animals (Terzaghi, 1950).

The only slope failures and landslides which occur suddenly as a result of an almost instantaneous decrease of shearing strength, s, and instantaneous increase of shearing stress, τ, are those due to earthquakes by liquefaction. Earthquakes alone without extensive liquefaction can produce only a cumulative finite displacement as the magnitude of each cycle of the acceleration increases, decreases and reverses. Since the inertia forces are developed in such short periods of time, the factor of safety of a slope may drop below unity several times during an earthquake with a cumulative finite displacement resulting, but the earthquake produces no 'failure' in the conventional sense of a major collapse or change in configuration. However, for a certain soil, if an earthquake leads to a simultaneous soil liquefaction along the potential surface of sliding and this liquefied zone extends to a free surface, the extensive lateral movements and shape change of a slope, characteristic of flow slides, will be inevitable and the slope fails or collapses completely.

The conventional method for evaluating the effect of an earthquake shock on the stability of a slope is to determine its minimum dynamic factor of safety against sliding using the rigid-block-type of motion. In the analysis the inertia force is

treated as an equivalent concentrated horizontal force, F, which is expressed as the product of a *seismic coefficient*, k, and the weight, W, of the potential sliding mass. The magnitude of the dynamic shear stress, τ, is determined by simple statics such as the slice method (Morgenstern and Price, 1965). The values of the dynamic factor of safety against sliding is then determined by comparing the average shearing stress, $\bar{\tau}$, along the potential surface of sliding to that of the average shearing resistance, $\bar{s}$, of the material mobilized, with due regard to the considerable reduction in shearing strength of the material owing to the dynamic effects on the pore-water pressures.

The numerical value of the seismic coefficient, k, depends on the intensity of the earthquake. This empirical value is in the range of $0.05-0.15$ for most engineers designing earth dams in the United States, but somewhat higher values are used in Japan, ranging from 0.12 to 0.25, depending on the location of the dam, the type of foundation and the possible downstream effects of damage caused by an earthquake. Some analytical procedures in obtaining these values will be described later.

The magnitude of the dynamic shearing resistance depends on the current state of initial stresses along the potential surface of sliding before the earthquake, the magnitude of increase and decrease in shearing stresses and the number of their stress cycles during the earthquake and slope drainage conditions. At the present time, there is no analytical material model available for determining the dynamic shearing stress resistance under the above-mentioned conditions, although analytical modeling to this problem of dynamic properties of soil is in a very active stage of research and development (Chen and Baladi, 1985). In such a situation, the only engineering recourse is to attempt to determine the soil strength characteristics in the laboratory for soil samples taken from the field and prepare them as closely as possible to the field conditions and test them under the conditions applicable in a given design earthquake. This procedure will have to be used until a more satisfactory strength and deformation model becomes available. A brief review of some dynamic properties of soil as applicable to earthquake loading is summarized in the following.

9.4.1 Dynamic shearing resistance of soils

During an earthquake, the soil along a potential surface of sliding is subjected to a series of alternating shearing stresses which vary in magnitude in a rather random fashion, in addition to the initial shearing stresses due to the weight of the earth slope. The dynamic effects of earthquake motions on soil shearing resistance involve mainly the change of pore-water pressure, which, in turn, is a function of the volume change of the material. In general, it is the undrained shearing resistance that is of importance in an earthquake. For highly permeable materials, however, the drained shearing resistance may be appropriate.

At the present time little analytical work has been done concerning the mechanism of pore-water pressure build-up under given cyclic loading conditions except, that we know from laboratory tests that are markedly different from those developed under static loading conditions, depending on the type of soils considered (Chen, 1980). So long as the strains are relatively small, for many soils, the stress strain curve for a soil sample in a pulsating loading is the same as for a single application of stress as shown in Fig. 9.4. However, for some soils after a certain strain has been reached the stress may drop from the original virgin curve as the pore-water pressure builds up progressively during each cycle of loading, which in turn reduces the shearing resistance of the material. This is illustrated by the dotted line in Fig. 9.4. For the case of saturated sand, the development of pore-water pressures can be equal to the applied confined pressure after some number of cycles. As soon as this happens, the effective stresses become zero and the soil 'floats'. The soil loses all of its strength. This is known as *liquefaction*. Conditions for the possible development of liquefaction for a soil under cyclic loading depend on the magnitude and number of stress cycles, the initial density and stresses, and drainage situation. In general, laboratory tests show that (Seed, 1968):

1. the larger the magnitude of the applied cyclic stresses, the fewer the number of cycles required to induce liquefaction;
2. the magnitude of the cyclic stresses required to induce liquefaction increases rapidly with increase in initial density;
3. the higher the confining pressure the greater the cyclic shearing stress required to induce liquefaction; and
4. the larger the ratio of initial shearing stress to initial confining pressure acting on the same plane, the greater the cyclic shearing stress required to induce liquefaction in a given number of cycles.

Experimentally determined relations between these variables for the conditions of liquefaction of a *saturated sand* under a cyclic loading are reported by Seed (1968), among many others. However, only limited data is available for clay types of soils,

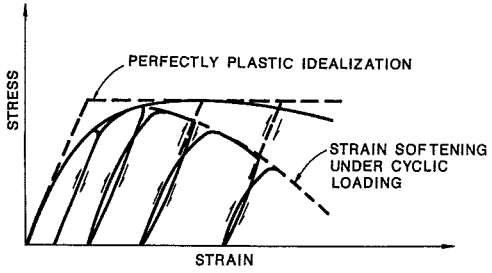

Fig. 9.4. Stress-strain relations for ideal and real soils under pulsating soils.

and it appears to indicate that liquefaction problems are not likely to develop in plastic soils such as soft clay, even for strain cycles with an amplitude as large as 2%.

9.4.2 Seismic coefficient

The seismic coefficient is a simple engineering means of designating the complex dynamic effects induced by earthquake motions by a single static equivalent force. The static equivalent force may be chosen to represent: (1) the maximum or average inertia force developed on the soil mass during the design earthquake; or (2) the maximum or average deformations of the embankment developed during the design earthquake. The value of the seismic coefficient depends of course on its precise meaning or definition.

If a dam is assumed to behave as a *rigid body*, the accelerations will of course be uniform throughout the dam and equal at all times to the ground accelerations. Probable intensities of maximum acceleration for major earthquakes in California are about $0.3-0.5\ g$. Thus, it may be argued that the design seismic coefficient, k, should reflect this maximum ground acceleration, $k = 0.3-0.5$. However, this simplified approach assumes that the horizontal acceleration kg acts permanently on the slope material and in one direction only. This conception of earthquake effects on slopes is obviously not correct because, the reduction in stability of a slope only exists during the short period of time for which the unfavorable direction of inertia force is induced. As soon as the ground acceleration is reversed, the direction of the inertia forces is also reversed with a corresponding increase in stability of the slope. During the period of the unfavorable direction of inertia force, the factor of safety may drop below unity and some permanent displacements can occur but this movement will be arrested as soon as the magnitude of the acceleration decreases or is reversed.

For most stable soils such as clays with a low degree of sensitivity, in a plastic state, or dense sand above the water table, the overall effect of a series of large but brief inertia forces causes only a cumulative displacement of the embankment but the slope will not fail even with a severe permanent displacement. The factor of safety of the section after the earthquake will be just about the same as it was before the earthquake. Hence the effects of earthquakes on embankment stability should be assessed also in terms of the displacements they produce. This was first proposed by Newmark (1965), and Seed (1966) subsequently presented improved methods of analysis based on this concept which requires the complete time history of the inertia forces acting on the embankment during the earthquake. This will be described later.

Since soils are not rigid, the magnitude of the acceleration in a dam will vary depending on the material properties and damping characteristics of the dam as well

as the nature of the ground motions. To assess the effect of dam flexibility on the design seismic coefficient, Mononobe et al. (1936) assumed the dam consisting of a series of infinitely thin horizontal slices which are connected to each other by linearly elastic shear springs and viscous damping devices and obtained *visco-elastic* response solutions. Subsequent developments by others extend this analysis to include the variation of horizontal response over both the length and height of the dam, the dam resting on an elastic layer of finite thickness instead of a rigid foundation, and a variation of increasing shear modulus as the cube root of the depth. Application of these solutions leads to a distribution of seismic coefficient varying from a maximum value at the crest of the embankment to zero at the base.

In the 1960's, Seed and Martin (1966) determined the average seismic coefficients based on the concept of *visco-elastic* response solutions which represent the entire time history of the inertia force to which the embankment has been subjected by any given ground motion. It was concluded in their evaluation that, in designating seismic coefficients for design purposes, it is important to differentiate between dams of different heights and different material characteristics, as well as different positions of the potential slide mass with the embankment section. For example, for a 100-ft-high embankment subjected to EL CENTRO earthquake (shear wave velocity = 1000 FPS, 20% critical damping, 15 significant cycles of force, with a predominant frequency of 3.3 cycles per second), the following equivalent maximum seismic coefficients operative over different portions of the embankment are shown in Table 9.8 (Seed and Martin, 1966). Suggested values for the seismic coefficients appropriate for other cases are also given in the same reference.

9.4.3 Rigid-plastic analysis

As mentioned previously, for some soils, their stress-strain behavior may be approximated by two straight lines as shown by the dashed lines in Fig. 9.4. A hypothetical material exhibiting this property of continuing plastic flow at constant stress is called *ideally plastic* or *perfectly plastic* material. The yield stress level used in an analysis may be chosen to represent the average stress in an appropriate range of strain applicable to an earthquake condition.

TABLE 9.8
Equivalent maximum seismic coefficients of embankment

Extent of potential slide mass	Equivalent maximum seismic coefficient
Upper quarter of embankment	0.4
Upper half of embankment	0.35
Upper three quarters of embankment	0.30
Full height of embankment	0.25

The simplest type of motion of slope failures or landslides associated with this perfectly plastic idealization is the rigid-block-type of sliding separated by narrow transition layer. The two most important cases of rigid body sliding for a dam subjected to an earthquake as observed in the field are shown in Fig. 9.5 (Newmark, 1965). The two slip surfaces as indicated in Fig. 9.5, marked curve 'a' and curve 'b', are the result of successive ground motions, with the net result of a major settlement at the crest. This has been observed in several old dams which may not have been designed to have adequate earthquake resistance (Newmark, 1965). For some cases, natural soil strata can lose part or almost all of their shearing resistance under shock conditions, as the result of liquefaction. Under such conditions, motion of the dam as a rigid block along the base can occur, as indicated in Fig. 9.5, line 'c'. A typical example of this type of failure for natural embankments which slide major distances on sensitive clay strata or on loose sand layers has been observed in the Anchorage earthquake (Newmark, 1965; Seed, 1968).

Once a failure mechanism has been assumed, values of the dynamic factor of safety against sliding can be determined by conventional analysis or by limit analysis with due consideration of inertia forces due to earthquake and dynamic shearing strengths of material whose values may be considerably reduced owing to the dynamic effects on the pore pressures.

As pointed out by Newmark (1965), the effects of earthquakes on embankment stability should also be assessed in terms of the deformations they produce rather than depending mainly on the concept of minimum factor of safety. In estimating the magnitude of displacements, Newmark (1965) proposed a simple method which assumes that the slipping of a mass of soil along a failure surface is analogous to the slipping of a rigid block on an inclined plane. Thus, it is necessary to determine the *yield acceleration* at which slippage will just begin to occur, and the actual acceleration generated by the earthquake for the sliding mass. When the induced acceleration exceeds the yield acceleration, movement will occur and the magnitude

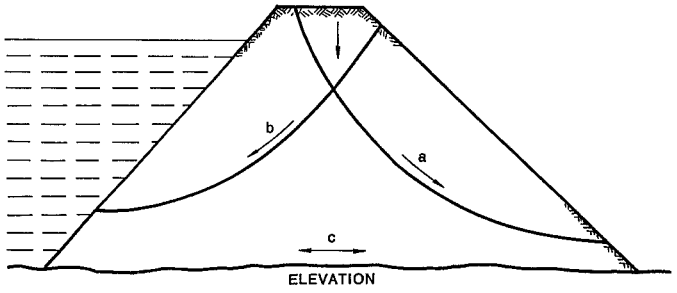

Fig. 9.5. Possible mechanisms of failures of an earth dam in an earthquake.

of displacements may be evaluated by double integration of that part of the acceleration history above the yield acceleration. The applicability of this procedure for cohesionless soil has been examined by Seed and his associates at Berkeley (see Seed, 1966). It was concluded that if the yield acceleration can be accurately evaluated and due allowance is made for a variation in yield acceleration with increasing slope displacement, Newmark method provides a reasonably good estimate of slope displacement induced by an earthquake.

This appears to be the case for the analyses of displacements resulting from surface sliding of the downstream slope and the analyses of displacements of the upstream slope when the reservoir is empty (see Fig. 9.5). Under such conditions, the main part of the sliding surface is developed essentially in dry or partly saturated cohesionless soils for which the pore pressures has negligible magnitude. However, for the analyses of displacements of the upstream slope with water in the reservoir, the determination of the yield acceleration in the saturated cohesionless soil requires an assessment of the progressive change in pore-water pressures during the period of the earthquake. At the present time, this is still not possible. The only engineering recourse is to estimate the pore-water pressures form the results of simulated-earthquake loading tests in the laboratory for the samples taken from the field. This latter procedure has been proposed by Seed (1966).

In short, the slope stability of embankments during earthquakes should be assessed in terms of embankment displacements as well as the factor of safety against sliding. The method of displacement analysis proposed by Newmark is simple to apply for dry or partly saturated cohesionless soils for which rigid body motion occurred on a well-defined slip surface. In the case of saturated cohesionless soils in which pore pressure changes may occur during the earthquake, special types of laboratory tests in which soil samples are subjected to simulated field conditions are needed. This requires the consideration of the time history of inertia forces developed in a dam during an earthquake as well as the initial stresses on soil elements along any potential failure surface before the earthquake. A step-by-step analytical procedure in estimating these stresses along with the laboratory test procedure is given by Seed (1966).

For cohesive soils for which large deformations approaching failure can occur under pulsating load conditions even when the maximum applied stress is somewhat less than the static strength of the soil, a *broad shear zone* within the embankment will contribute to the overall displacements of the embankment. At the present time, no means is available for integrating these deformations to determine the slope displacements and overall change in slope configuration. Nevertheless, Seed's procedure is still valid and can be applied to calculate the factor of safety against sliding for such slopes, once the shearing strength along the potential failure plane has been evaluated by laboratory tests appropriate to an earthquake condition.

References

Chen, W.F., 1977. Mechanics of slope failure and landslides, Proc. Advisory Meeting on Earthquake Engineering and Landslides, US-ROC Cooperative Science Program, Taipei, Taiwan, R.O.C., August 29 – Sept. 2, pp. 219 – 232.

Chen, W.F., 1980. Plasticity in soil mechanics and landslides. J. Eng. Mech. Div., ASCE, 106(EM3): 443 – 464.

Chen, W.F., 1982. Soil mechanics, plasticity and landslides. In: R.T. Shield and G. Dvorak (Editors), Special Anniversary Volume on Mechanics of Material Behavior to Honor D.C. Drucker. Elsevier, Amsterdam, pp. 31 – 58.

Chen, W.F. and Baladi, G.Y., 1985. Soil Plasticity: Theory and Implementation. Elsevier, Amsterdam, 230 pp.

Chen, W.F. and Sawada, T., 1982. Seismic stability of slope in nonhomogeneous, anistropic soils. Structural Engineering Report No. CE-STR-82-25, School of Civil Engineering, Purdue University, West Lafayette, IN, 108 pp.

Chen, W.E. and Sawada, T., 1983. Earthquake-induced slope failure in nonhomogeneous, anisotropic soils. Soils Foundations, Jpn. Soc. Soil Mech. Found. Eng., 23(2): 125 – 139.

Gibson, R.F. and Morgenstern, N.R., 1962. A note on the stability of cutting in normally consolidated clays. Geotechnique, 12(3): 212 – 216.

Lo, K.Y., 1965. Stability of slopes in anisotropic soils. J. Soil Mech. Found. Div., ASCE, 91(SM4): 85 – 106.

Mononobe, N., Takata, A. and Matumura, M., 1936. Seismic stability of the earth dam. Proc., 2nd Congress on Large Dams, Washington, D.C., Vol. IV.

Morgenstern, N.R. and Price, V.E., 1965. The analysis of the stability of general slip surfaces. Geotechnique, 15(1): 79 – 93.

Newmark, N.M., 1965. Effect of earthquakes on dams and embankments. Geotechnique, 15(2): 139 – 160.

Odenstad, S., 1963. Correspondence. Geotechnique, 13(2): 166 – 170.

Reddy, A.S. and Srinivasan, R.J., 1967. Bearing capacity of footing and layered clays. J. Soil Mech. Found. Div., ASCE, 93(SM2): 83 – 98.

Seed, H.B., 1966. A method for earthquake-resistant design of earth dams. J. Soil Mech. Found. Div., ASCE, 92(SM1): 13 – 41.

Seed, H.B., 1968. Landslides during earthquakes due to soil liquefaction. J. Soil Mech. Found. Div., ASCE, 94(SM5): 1055 – 1122.

Seed, H.B. and Martin, G.R., 1966. The seismic coefficient in earth dam design. J. Soil Mech. Found. Div., ASCE, 92(SM3): 25 – 58.

Sigel, R.A., 1975. STABL User Manual, Joint Highway Research Project, JHRP-75-9, School of Civil Engineering, Purdue University, West Lafayette, IN, 112 pp.

Taylor, D.W., 1948. Fundamental of Soil Mechanics. John Wiley and Sons, New York, NY, 700 pp.

Terzaghi, K., 1950. Mechanics of Landslides, Engineering Geology Volume, The Geological Society of America, November, pp. 83 – 123.

Chapter 10

ASSESSMENT OF SEISMIC DISPLACEMENT OF SLOPES*

10.1 Introduction

In current seismic stability analysis of slopes, there are two basic approaches, one is the conventional *pseudo-static analysis* and the other is the *stress-strain analysis*. With the advent of the finite-element technique and knowing the material properties, the cross-section of the slope, and the time history of acceleration of a design earthquake, it is possible to analyze the section for deformation and safety by computing the stresses and strains in the structure. However, a complete progressive failure analysis of stress and strain in a soil mechanics problem by using the stress-strain approach is too complicated for practical applications.

The most important feature of seismic stability analysis is the estimation of the seismic loads which will cause slippage of the soil mass and the overall movements of the sliding soil mass throughout an earthquake. However, the traditional pseudo-static approach is too crude to predict the behavior of a slope under earthquake loading condition. In this traditional analysis, the pseudo-static inertia force is applied as an equivalent permanent concentrated horizontal force, i.e., the pseudo-static force, acting at some critical point (usually the center of gravity) of the critical sliding mass (Chen, 1980). Earthslopes are then analyzed with the calculation of the factor of safety when this inertia force is considered. If the factor of safety is less than unity, the slope is considered to be unsafe. In reality, however, the reduction in the stability of the slope exists only during the short period of time for which the inertia force is acting. Thus, during the earthquake, the factor of safety may drop below unity a number of times which will induce some movements of the failure section of a slope, but this may not cause the collapse of a slope. Thus, the stability of slopes should depend on the cumulative displacements developed during an earthquake. Newmark (1965) first proposed the important concept that the seismic stability of slopes should be evaluated in terms of the displacements rather than the traditional concept of minimum factor of safety.

After carefully investigating the influence of the earthquake on the stability of the slope and upon the awareness of the drawbacks and deficiences of currently available methods, an effective, practical and relatively accurate analytical pro-

* This chapter is based on the Ph.D. thesis by C.J. Chang (1981) and the paper by Chang, Chen, and Yao (1984).

cedure which extends the present pseudo-static method, is proposed herein for the analysis of earthslope stability subjected to earthquake loading. The necessary steps are outlined in the forthcoming.

In estimating the magnitude of displacement, we assume that the slipping of a mass of soil along a failure surface is analogous to the slipping of a rigid block on an inclined plane. Thus, it is necessary to determine the yield acceleration at which slippage will just begin to occur, and to compare it with actual acceleration generated by the earthquake for the sliding mass. When the induced acceleration exceeds the yield acceleration, rigid-body-type of slope movement will occur and the magnitude of displacements can be evaluated by double integration of that part of the acceleration history above the yield acceleration. The applicability of this procedure for cohesionless soil has been examined by Seed and his associates at Berkeley (1966). It was concluded that if the yield acceleration can be accurately evaluated and due allowance is made for a variation in yield acceleration with increasing slope displacement, the proposed method provides a reasonably good estimate of slope displacement induced by an earthquake.

It should be noted that the Newmark's analytical procedure can not account for the dynamic effects of pore-water pressures built-up and the possible loss of shear strength of soil owing to liquefaction during an earthquake shaking, but it will probably provide a satisfactory result, whenever the major portion of the sliding surface, that develops the resistance to sliding in a slope, is made of either clays with a low degree of sensitivity, dense sand either above or below the water table, or loose sand above the water table.

In this chapter, the yield acceleration of slopes is first computed by using the upper-bound techniques of pseudo-static limit analysis method. Based on the calculated yield acceleration and its associated failure mechanism, Newmark's concept is then used to evaluate the displacements of earth slopes during an earthquake.

10.2 Failure mechanisms and yield acceleration

The possible failure modes of slope include the *infinite* slope failure and the *local* slope failure. The former is the sliding parallel to the earth surface or the bedrock in a very wide range. The latter, however, is due to the surcharge boundary loads and any other conditions that may change the possible occurrence of parallel sliding. The critical mode of failure depends on the properties of soil, slope angle, magnitude and direction of inertia force, and thickness of the soil overlying the bedrock. The slope is considered unstable when either an infinite slope failure or a local slope failure occurs.

This section is concerned with the calculation of the critical or yield horizontal inertia force corresponding to the *yield acceleration factor,* k_c, at which a condition of incipient slope movement is possible along the potential sliding surface. Here, as

in Chapter 9, the computation of the yield acceleration factor by using the upper-bound limit analysis is based on the following conditions: plane strain condition; pseudo-static earthquake loading; uniform horizontal distribution of lateral acceleration; Mohr-Coulomb criterion for failure with constant c and ϕ, homogeneous and isotropic slope.

10.2.1 Infinite slope failure

Figure 10.1 shows an infinite slope. We assume that the slope is very wide in the direction normal to the cross-section, and consider only the stresses that act in the plane of the cross-section. Further, the slopes are relatively long and presumably homogeneous and isotropic. Thus, if the horizontal inertia force is uniformly distributed along the slope, the stresses on any vertical planes at same depth below the surface should be equal. Thus, sliding is likely to begin at any depth, depending on the properties of the soil, magnitude of inertia force and slope angle, α.

Referring now to Fig. 10.1, the rate of external work done by soil weight and the inertia force, respectively, are:

$$\dot{W}_\gamma = \gamma\,(d/\cos\alpha)\,V\sin(\alpha - \phi) \tag{10.1}$$

and

$$\dot{W}_E = k_h\,\gamma\,(d/\cos\alpha)\,V\cos(\alpha - \phi) \tag{10.2}$$

where γ is the unit weight of soil, ϕ is the internal friction angle of soil, V is the discontinuous velocity vector of sliding block, k_h is the *horizontal seismic coefficient* of inertia force, and d is the perpendicular depth of soil stratum overlying bedrock (Fig. 10.1).

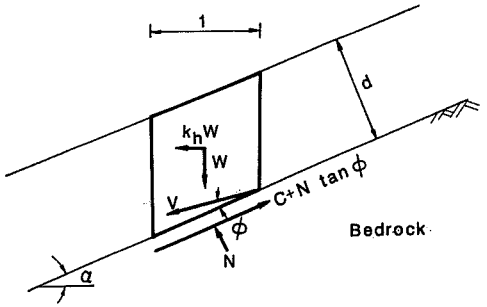

Fig. 10.1. Analysis of infinite slope.

The internal rate of dissipation of energy along the slip surface is:

$$D = c\,(1/\cos\alpha)\,V\cos\phi \tag{10.3}$$

Equating the sum of the external rates of work, Eqs. (10.1) and (10.2), to the rate of internal energy dissipation, Eq. (10.3), yields:

$$k_c = k_h = \frac{c/(d\gamma\cos\alpha) - \tan\alpha + \tan\phi}{(1 + \tan\phi\tan\alpha)} \tag{10.4}$$

10.2.2 Plane failure mechanism of local slope failure

The construction of structures on an infinite slope changes the geometric and stress conditions. Thus, the local slope failure may be more critical than that of the parallel sliding. For local slope failure, the plane slip surface and the logarithmic spiral slip surface of angle ϕ are the two popular surfaces of velocity discontinuity that are permitted in the limit analysis for a rigid-body motion relative to a fixed surface.

Figure 10.2 shows the first of the two possible failure mechanisms – plane failure mechanism.

In this figure, region ABC translates as a rigid body with the relative velocity V to the rigid body below the discontinuous surface AC. The failure mechanism is assumed to end at point A in Fig. 10.2 with height H. The assumed failure mechanism can be specified by two variables θ and L, where θ is the angle of slip surface with respect to the horizontal line and L is related to H by:

$$L = \frac{H\sin(\alpha - \theta)}{\sin\alpha\sin\theta} \tag{10.5}$$

The rate of internal energy dissipation along the surface AC is:

$$D = c\,(H/\sin\theta)\,V\cos\phi \tag{10.6}$$

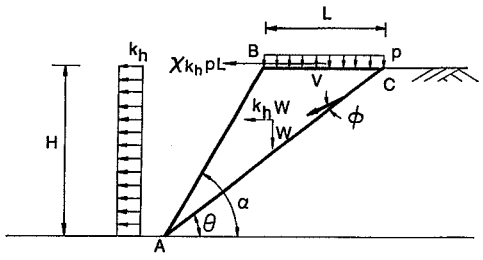

Fig. 10.2. Translational local slope failure mechanism.

The external rate of work done by soil weight, surcharge loads, and the inertia forces, respectively, are:

$$\dot{W}_\gamma = \tfrac{1}{2}\gamma H L V\sin(\theta - \phi) \tag{10.7}$$

$$\dot{W}_p = p L V\sin(\theta - \phi) \tag{10.8}$$

$$\dot{W}_{E,\gamma} = k_h \tfrac{1}{2}\gamma H L V\cos(\theta - \phi) \tag{10.9}$$

and

$$\dot{W}_{E,p} = k_h' p L V\cos(\theta - \phi) \tag{10.10}$$

where k_h' is the seismic coefficient corresponding to the surcharge load p whose magnitude can be related to k_h by:

$$k_h'/k_h = \chi \tag{10.11}$$

k_h'/k_h can be greater or less than unity.

By equating the external and internal rates of work, we obtain the expression for k_h as:

$$k_h = \frac{\dfrac{\cos\phi}{\cos(\theta - \phi)}\left[\dfrac{\sin\alpha}{\sin(\alpha - \theta)} - \dfrac{p}{c}\dfrac{\sin(\theta - \phi)}{\cos\phi} - \dfrac{N_s}{2}\dfrac{\sin(\theta - \phi)}{\cos\phi}\right]}{\dfrac{N_s}{2} + \dfrac{p\chi}{c}} \tag{10.12}$$

where N_s, the stability factor, is equal to $\gamma H/c$. The yield acceleration factor k_h has the minimum value k_c, when θ satisfies the condition:

$$\frac{dk_h}{d\theta} = 0 \tag{10.13}$$

Solving this equation and substituting the θ-value thus obtained into Eq. (10.12) yield a least upper-bound k_c for the yield acceleration factor for plane failure mechanism.

When no surcharge exists, Eq. (10.12) can be reduced to:

$$k_h = \frac{\cos\phi}{\cos(\theta - \phi)}\left[\frac{2}{N_s}\frac{\sin\alpha}{\sin(\alpha - \theta)} + \frac{\sin(\phi - \theta)}{\cos\phi}\right] \tag{10.14}$$

10.2.3 Log-spiral failure mechanism of local slope failure

The motion of plane failure mechanism is a translational type. In this section, we consider a rotational log-spiral failure mechanism as shown in Fig. 10.3. The region ABC rotates as a rigid body about the center of rotation O with the angular velocity Ω relative to the materials below the logarithmic failure surface AC. As shown in Fig. 10.3, the parameters H, θ_0 and θ_h are used to specify the failure mechanism.

The geometrical relations of H/r_0 and L/r_0 can be expressed as follows:

$$\frac{H}{r_0} = \sin\theta_h \exp[(\theta_h - \theta_0)\tan\phi] - \sin\theta_0 \tag{10.15}$$

$$\frac{L}{r_0} = \frac{\sin(\alpha + \theta_0) - \exp[(\theta_h - \theta_0)\tan\phi]\sin(\theta_h + \alpha)}{\sin\alpha} \tag{10.16}$$

For the failure mechanism passing through the toe, the internal dissipation of energy occurred along the discontinuity surface AC is:

$$D = \int_{\theta_0}^{\theta_h} (cV\cos\phi)\frac{r\,d\theta}{\cos\phi}$$

$$= \frac{cr_0^2\Omega}{2\tan\phi}\{\exp[2(\theta_h - \theta_0)\tan\phi] - 1\} = cr_0^2\Omega f_c \tag{10.17}$$

The rate of external work due to soil weight for region ABC can be found by a simple algebraic summation $\dot{W}_1 - \dot{W}_2 - \dot{W}_3$, in which $\dot{W}_1$, $\dot{W}_2$ and $\dot{W}_3$ are the

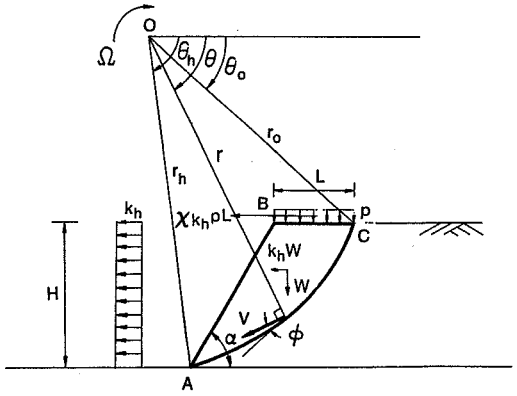

Fig. 10.3. Rotational local slope failure mechanism.

rates of work done by the soil weight in regions OAC, OBC and OAB, respectively:

$$\dot{W}_1 = \frac{\gamma r_0^3\Omega}{3(1 + 9\tan^2\phi)}\{(3\tan\phi\cos\theta_h + \sin\theta_h)\exp[3(\theta_h - \theta_0)\tan\phi]$$

$$- 3\tan\phi\cos\theta_0 - \sin\theta_0\} = \gamma r_0^3\Omega f_1 \tag{10.18}$$

$$\dot{W}_2 = \frac{\gamma r_0^3\Omega}{6}\frac{L}{r_0}\left(2\cos\theta_0 - \frac{L}{r_0}\right)\sin\theta_0 = \gamma r_0^3 f_2^{\Omega} \tag{10.19}$$

$$\dot{W}_3 = \frac{\gamma r_0^3\Omega}{6}\exp[(\theta_h - \theta_0)\tan\phi]\left[\sin(\theta_h - \theta_0) - \frac{L}{r_0}\sin\theta_h\right]\left\{\cos\theta_0 - \frac{L}{r_0}\right.$$

$$\left. + \cos\theta_h\exp[(\theta_h - \theta_0)\tan\phi]\right\} = \gamma r_0^3\Omega f_3 \tag{10.20}$$

Similarly, the rate of external work done by the inertia force due to soil weight can be found by the summation $\dot{W}_4 - \dot{W}_5 - \dot{W}_6$, in which $\dot{W}_4$, $\dot{W}_5$ and $\dot{W}_6$ are the rates of work done by the inertia force due to soil weight in regions OAC, OBC and OAB, respectively:

$$\dot{W}_4 = \frac{\gamma r_0^3\Omega k_h}{3(1 + 9\tan^2\phi)}\{(3\tan\phi\sin\theta_h - \cos\theta_h)\exp[3(\theta_h - \theta_0)\tan\phi]$$

$$- 3\tan\phi\sin\theta_0 + \cos\theta_0\} = k_h\gamma r_0^3\Omega f_4 \tag{10.21}$$

$$\dot{W}_5 = \frac{k_h\gamma r_0^3\Omega}{6}\frac{L}{r_0}2\sin^2\theta_0 = k_h\gamma r_0^3\Omega f_5 \tag{10.22}$$

$$\dot{W}_6 = \frac{k_h\gamma r_0^3\Omega}{6}\exp[(\theta_h - \theta_0)\tan\phi]\left[\sin(\theta_h - \theta_0) - \frac{L}{r_0}\sin\theta_h\right]\{\sin\theta_0$$

$$+ \sin\theta_h\exp[(\theta_h - \theta_0)\tan\phi]\} = k_h\gamma r_0^3\Omega f_6 \tag{10.23}$$

The external rates of work due to surcharge boundary loads and their inertia forces are:

$$pL\Omega\left(r_0\cos\theta_0 - \frac{L}{2}\right) = pr_0^2\Omega\frac{L}{r_0}\left(\cos\theta_0 - \frac{L}{2r_0}\right) = pr_0^2\Omega f_p \tag{10.24}$$

and

$$\chi\, k_h\, p\, L\, \Omega(r_0 \sin\theta_0) = \chi\, k_h\, p\, r_0^2\, \Omega\, \frac{L}{r_0} \sin\theta_0 = \chi\, k_h\, p r_0^2\, \Omega\, f_q \tag{10.25}$$

Equating the rate of internal energy dissipation to the external rate of work gives:

$$k_h = \frac{f_c - N_s \dfrac{f_1 - f_2 - f_3}{\sin\theta_h \exp[(\theta_h - \theta_0)\tan\phi] - \sin\theta_0} - \dfrac{p}{c} f_p}{N_s \dfrac{f_4 - f_5 - f_6}{\sin\theta_h \exp[(\theta_h - \theta_0)\tan\phi] - \sin\theta_0} + \dfrac{\chi p}{c} f_q} \tag{10.26}$$

where N_s, the stability factor, is equal to $\gamma H/c$ and the functions f's are defined as above, which are all functions of θ_0, θ_h.

k_h is the upper-bound solution of the yield acceleration factor of the logspiral failure mechanism. By taking the first derivatives of Eq. (10.26) with respect to θ_0 and θ_h, respectively, and equating them to zero, i.e.:

$$\frac{\partial k_h}{\partial \theta_0} = 0 \text{ and } \frac{\partial k_h}{\partial \theta_h} = 0 \tag{10.27}$$

and solving Eq. (10.27), we obtain the critical values of θ_0 and θ_h. Substituting θ_0 and θ_h values so obtained to Eq. (10.26), we have the least upper-bound for the yield acceleration factor, $k_c = \min(k_h)$, of the rotational log-spiral failure mechanism.

When no surcharge exists, Eq. (10.26) can be reduced to:

$$k_h = \frac{\dfrac{f_c}{N_s} - \dfrac{f_1 - f_2 - f_3}{\sin\theta_h \exp[(\theta_h - \theta_0)\tan\phi] - \sin\theta_0}}{\dfrac{f_4 - f_5 - f_6}{\sin\theta_h \exp[(\theta_h - \theta_0)\tan\phi] - \sin\theta_0}} \tag{10.28}$$

The yield acceleration factor of the log-spiral failure mechanism generally gives a lower value than that of the plane failure mechanism. Thus, the log-spiral failure mechanism generally controls the local slope failure.

The value of γ in N_s is the unit weight of sliding soil mass. If the soil is partially saturated or submerged, the yield acceleration factor, k_h, can be evaluated by introducing an average unit weight of the sliding mass or directly calculating the inertia effect including the consideration of saturation on the energy-balance equation.

Computer programs developed at Purdue University using the aforementioned analytical procedures are listed at the end of this chapter. Some selected sample outputs have been obtained by this program. The results are tabulated in Table 10.1 and illustrated graphically in Figs. 10.4 and 10.5.

From the results in Table 10.1b, we can see that the log-spiral failure surface is more critical than the plane failure surface. It appears that the surcharge loading has little effect on the yield acceleration factor. This is due to the fact that the surcharge is only a small fragment when compared to the sliding mass in this case with height $H = 100$ ft.

Table 10.2 presents a comparison of the limit equilibrium solutions with the upper-bound limit analysis solutions. The limit equilibrium solutions are run by a computer program STABL (Sigel, 1975) with which the simplified Janbu method of slices (Janbu, 1957) and circular failure surface are adopted to find the factor of safety of a slope.

In the use of STABL program, only the factor of safety of slopes can be assessed. Besides, log-spiral failure surface is not included and χ is always assumed equal to zero. Thus, in order to compare the limit analysis solutions with the solutions obtained by STABL, we assume χ equals to zero and use k_c, obtained by the limit analysis method, as input data to find the corresponding factor of safety. The factor

TABLE 10.1
Yield acceleration factor, k_c, of infinite slope failure and local slope failure with $c = 900$ psf, $\phi = 40°$, and $\gamma = 120$ pcf

(a) k_c of infinite slope failure with $d = 50$ feet

$\alpha°$	15	30	45	60	75
k_c	0.593	0.293	0.028	*	*

* The slope has already failed before imposing any seismic force.

(b) k_c of local slope failure with $H = 100$ ft, $\phi = 40°$, $c = 1800$ psf and $\gamma = 120$ pcf

	$p = 0$		$p = 120$ psf, $\chi = 0$		$p = 120$ psf, $\chi = 0.5$	
$\alpha°$	Plane	Logspiral	Plane	Logspiral	Plane	Logspiral
15	1.111	0.926	1.126	0.928	1.115	0.925
30	0.951	0.819	0.961	0.820	0.951	0.817
45	0.759	0.677	0.764	0.677	0.757	0.674
60	0.560	0.516	0.562	0.514	0.556	0.511
75	0.353	0.333	0.350	0.329	0.347	0.326
90	0.124	0.116	0.116	0.108	0.115	0.107

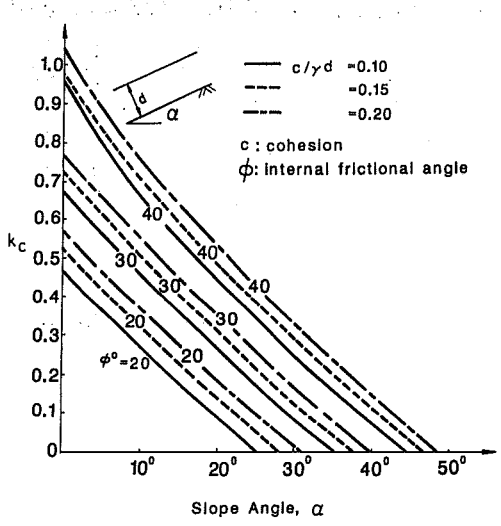

Fig. 10.4. Yield acceleration factor, k_c, of infinite slope failure as a function of slope angle α.

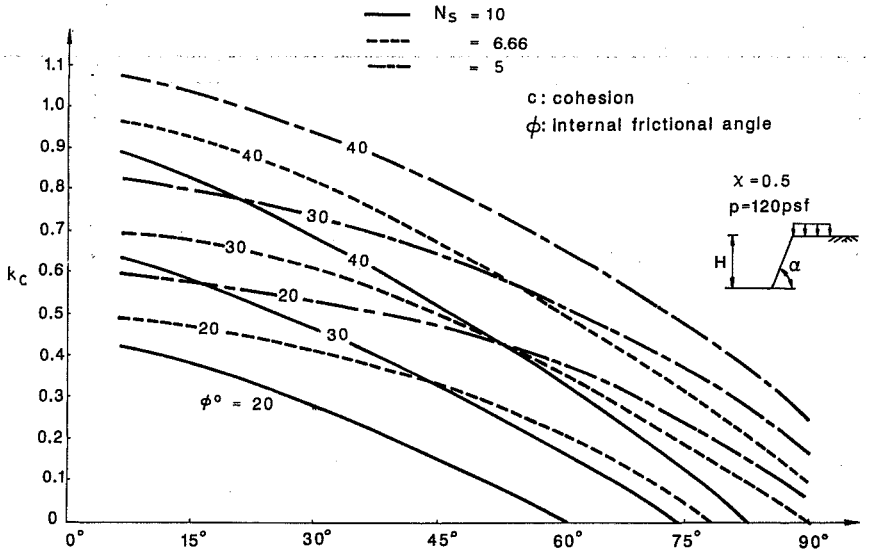

Fig. 10.5. Yield acceleration factor, k_c, of logspiral failure mechanism as a function of slope angle α.

TABLE 10.2

Factor of safety obtained by the limit equilibrium method with H = 100 ft, ϕ = 40°, c = 1800 psf, γ = 120 pcf, p = 120 psf and χ = 0

α°	15	30	45	60	75	90
Factor of safety	0.920	0.885	0.891	0.933	1.006	1.025

of safety thus obtained is listed in Table 10.2. The factor of safety so obtained should be very close to unity as checked by the limit analysis. However, due to the difference in failure surfaces assumed, i.e., circular surface in the limit equilibrium method and the logspiral surface in the limit analysis method, the results are somewhat different.

10.3 Assessment of seismic displacement of slopes

10.3.1 General description

In 1965, Newmark first proposed the basic elements of a procedure for evaluating the potential displacements of an embankment due to an earthquake shaking. Newmark envisaged that sliding would be imminent once the inertia forces on a potential failure block were large enough to overcome the yield resistance and that movement would stop when the initial forces were reversed (Newmark, 1965). In his analysis, a soil mass moving downward along a failure surface under inertia force due to earthquake shaking is considered to be analogous to a rigid block acted on by an external force sliding on an inclined plane as shown in Fig. 10.6. Thus, the movements of slope would begin to occur if the inertia force induced by earthquake on a potential slide mass exceeds the yield acceleration. The failure mechanism and corresponding yield acceleration must be determined first so that the analogous inclined plane and external force can be simulated. Subsequently, the overall displacements of a failure slope under earthquake loads can be assessed (Chen et

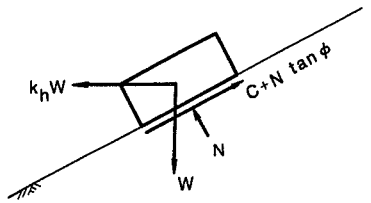

Fig. 10.6. Rigid block on an inclined plane.

al. 1978; Chen, 1980). This can be achieved in the following steps (Chang et al. 1984):

1. Calculate the yield acceleration at which slippage will just begin to occur.
2. Apply various values of the pseudo-static force to the slope. These values are obtained from a discretized accelerogram of an actual or simulated earthquake.
3. According to the yield acceleration and accelerogram of an earthquake, the time history of velocity of the sliding soil mass of a slope can be calculated. The magnitude of displacements can be evaluated by integrating all the positive velocity.
4. Determine the 'stability' of the slope on the basis of this estimated total displacement by rigid body sliding.

The computation of the yield acceleration by the upper bound techniques of limit analysis has been described in the preceding Sections. Based on this yield acceleration and its associated failure mechanism, the equation of motion for the estimation of displacements along the potential failure surface is developed in this Section.

Newmark's concept implies that movements would stop when the inertia forces were reversed. Actually, the velocity could remain positive even if the inertia forces were reversed or the inertia forces were not reversed but less than the yield resistance on the potential failure surface. Positive velocity thereby causes sliding on the surface. On the other hand, the velocity could be negative even though the inertia forces were greater than the yield resistance. It all depends on the magnitude and direction of both the velocity and the inertia force. Besides, as also indicated by Newmark, the uphill resistance may be taken as infinitely large without serious error in the calculations. In this situation, ground motions in the direction of the downward slope tend to move the mass downhill, but ground motions in the upward direction along the slope leave the mass without relative additional motion except where the ground motions are extremely large in magnitude. Thus, the negative velocity or velocity heading uphill is not allowed in this analysis.

Accordingly, by computing an acceleration at which the inertia forces become sufficiently high to cause yielding to begin and integrating the effective velocity on the sliding mass as a function of time, ultimately, displacements of the slope can be evaluated. Thus, the slope failure can be judged on the basis of the overall displacement caused throughout the earthquake.

10.3.2 Numerical procedure

The resistance to earthquake shock of a block of soil that slides along a surface is a function of the shearing resistance of the material under the conditions applicable in the earthquake (Newmark, 1965). However, in this section we shall assume that the resistance to sliding does not change during the earthquake. The calculation based on the assumption that the whole moving mass moves as a single

rigid body with resistance mobilized along the sliding surface may proceed by the following steps:

Step 1

Select a design earthquake with time history of acceleration. A constant time interval may be chosen to designate the time and subsequently estimate all the corresponding accelerations. The acceleration within a time interval is assumed to be linear but not necessarily constant.

Step 2

The inertia forces, caused by the accelerations, tend to reduce the stability of the slope. Once the induced acceleration, $k_h g$, is greater than the yield acceleration, $k_c g$, the movement of the failure section will occur. Based on the computed yield acceleration and the accelerations obtained from the accelerogram of the design earthquake, calculate the motion acceleration, $\ddot{x}$, of the sliding block.

The motion acceleration, $\ddot{x}$, acting on the sliding block for different failure mechanisms can be calculated, respectively, as follows:

(a) Infinite slope failure

Referring to Fig. 10.7, when $\ddot{x}_1 = 0$, $k_h = k_c$:

$$W_1 \cos\alpha - k_c W_1 \sin\alpha = N_1 \tag{10.29}$$

$$W_1 \sin\alpha + k_c W_1 \cos\alpha = C + (N_1 - U_1) \tan\phi \tag{10.30}$$

and when $k_h \neq k_c$;

$$W_1 \cos\alpha - k_h W_1 \sin\alpha = N_2 - F_1 \sin\phi \tag{10.31}$$

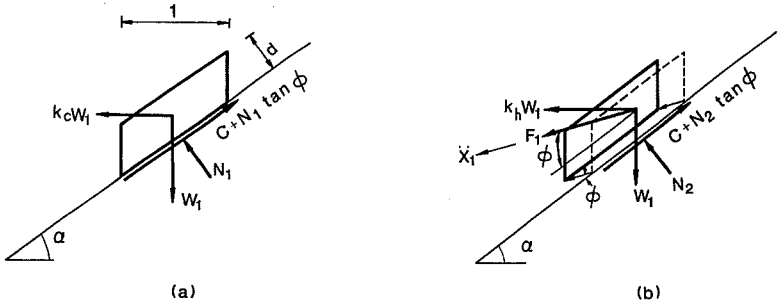

Fig. 10.7. (a). Equilibrium of forces on resting block (infinite slope). (b). Forces on sliding block (infinite slope).

$$W_1 \sin\alpha + k_h W_1 \cos\alpha - [C + (N_2 - U_2)\tan\phi] = F_1 \cos\phi \qquad (10.32)$$

where, W_1 is the weight of the sliding block of unit length, i.e., $\gamma\, d/\cos\alpha$, C is the total cohesion; N_1, N_2 are the normal forces, U_1, U_2 are the pore-water forces for the cases mentioned above respectively, and F_1 is the force acting in the direction of motion.

Assuming $U_1 = U_2$, from the cancellation of N_1 and N_2 from Eqs. (10.29) to (10.32), and using the relation $F_1 = (W_1/g)\,\ddot{x}_1$, we obtain:

$$\ddot{x}_1 = (k_h - k_c)\, g \cos(\phi - \alpha) \qquad (10.33)$$

(b) Local plane failure

Referring to Fig. 10.8, when $\ddot{x}_2 = 0$: $k_h = k_c$;

$$W_2 \cos\alpha - k_c W_2 \sin\alpha + pL\cos\alpha - \chi k_c pL \sin\alpha = N_3 \qquad (10.34)$$

$$W_2 \sin\alpha + k_c W_2 \cos\alpha + pL \sin\alpha + \chi k_c pL \cos\alpha = C + (N_3 - U_3)\tan\phi \qquad (10.35)$$

and when $k_h \neq k_c$:

$$W_2 \cos\alpha - k_h W_2 \sin\alpha + pL\cos\alpha - \chi k_h pL \sin\alpha = N_4 - F_2 \sin\phi \qquad (10.36)$$

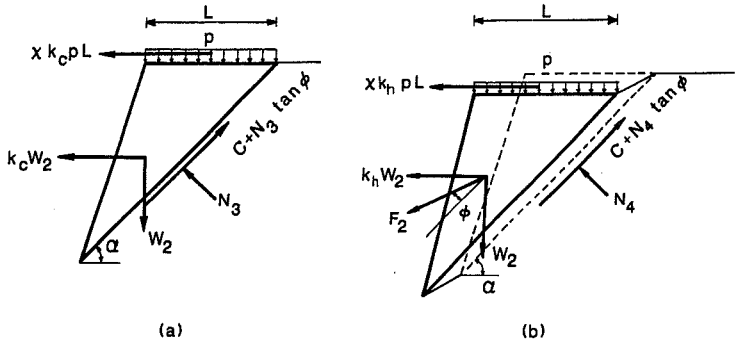

Fig. 10.8. (a). Equilibrium of forces on resting block (plane failure surface). (b). Forces on sliding block (plane failure surface).

$$W_2 \sin\alpha + k_h W_2 \cos\alpha + pL\sin\alpha + \chi\, k_h\, pL \cos\alpha - [C + (N_4 - U_4)\tan\phi] = F_2 \cos\phi \qquad (10.37)$$

where W_2 $(= \gamma H\, L/2)$ is the weight of the sliding wedge of plane failure mechanism N_3, N_4 are the normal forces; U_3, U_4 are the pore-water forces for the cases mentioned above respectively, and F_2 is the force acting in the direction of motion.

Assuming $U_3 = U_4$, from the cancellation of N_3 and N_4 from Eqs. (10.34) to (10.37), and using the relation $F_2 = (W_2/g)\,\ddot{x}_2$, we obtain:

$$\ddot{x}_2 = (k_h - k_c)\, g \cos(\phi - \alpha)\left(1 + \frac{\chi\, pL}{W_2}\right) \qquad (10.38)$$

(c) Local log-spiral failure

Referring to Fig. 10.9, when $\ddot{\theta} = 0$, $k_h = k_c$:

$$k_c \gamma r_0^3 (f_4 - f_5 - f_6) + \gamma r_0^3 (f_1 - f_2 - f_3) + \chi\, k_c\, p\, r_0^2 f_q + p\, r_0^2 f_p = c\, r_0^2 f_c - \int_{\theta_0}^{\theta_h} u_1 r^2 \tan\phi \, d\theta \qquad (10.39)$$

in which the f's are defined in the preceding sections.

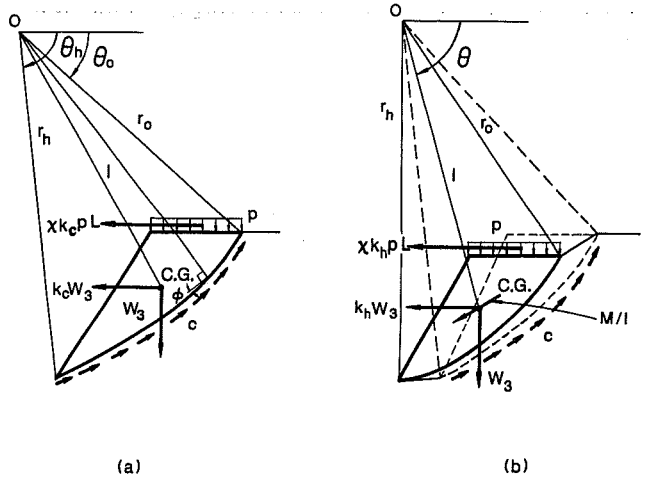

Fig. 10.9. (a). Equilibrium of forces on resting block (logspiral failure surface). (b). Forces on sliding block (logspiral failure surface).

When $k_h \neq k_c$:

$$k_h \gamma r_0^3 (f_4 - f_5 - f_6) + \gamma r_0^3 (f_1 - f_2 - f_3) + \chi k_h p r_0^2 f_q + p r_0^2 f_p = c r_0^2 f_c - \int_{\theta_0}^{\theta_h} u_2 r^2 \tan\phi \, d\theta + M \tag{10.40}$$

where u_1, u_2 are the pore-water pressure distributions along the failure surface for the cases mentioned above, respectively.

Assuming $u_1 = u_2$ and substituting Eqs. (10.39) and (10.40) into $M = (W_3/g) \ddot{\theta} l^2$, we obtain:

$$\ddot{\theta} = (k_h - k_c) g[\gamma r_0^3 (f_4 - f_5 - f_6) + \chi p r_0^2 f_q]/(W_3 l^2) \tag{10.41}$$

in which

W_3 = weight of the sliding block of log-spiral failure mechanism

$$= \frac{\gamma r_0^2}{2} \left\{ \frac{\exp[2(\theta_h - \theta_0)\tan\phi] - 1}{2\tan\phi} - \frac{L}{r_0} \sin\theta_0 - \left[\sin(\theta_h - \theta_0) - \frac{L}{r_0} \sin\theta_h \right] \exp[(\theta_h - \theta_0)\tan\phi] \right\} \tag{10.42}$$

M = moment taken about center O

l = arm length of $M = \sqrt{[\gamma r_0^3 (f_1 - f_2 - f_3)]^2 + [\gamma r_0^3 (f_4 - f_5 - f_6)]^2}/W_3$

Step 3

Using the results of step (2), starting from the beginning of the earthquake, find the first positive motion acceleration $\ddot{x}_i$ (or $\ddot{\theta}_i$), with which the downhill movement will start to occur at time t_i. If $\ddot{x}_i$ is the first positive motion acceleration, then $\ddot{x}_{i-1}$ at t_{i-1} must be negative except in a special case in which $\ddot{x}_{i-1} = 0$. Thus, it needs to calculate time t, at which $\dot{x} = 0$ and motion velocity $\dot{x}$ will start to increase from zero. By linear interpolation, we obtain:

$$t = \frac{-\ddot{x}_{i-1}(t_i - t_{i-1})}{(\ddot{x}_i - \ddot{x}_{i-1})} + t_{i-1} \tag{10.43}$$

at time t, when the induced acceleration exceeds the yield acceleration, the motion velocity of the slide block increases from zero and the motion displacement x occurs.

Step 4

The motion velocity, $\dot{x}_i$ at time t_i can be calculated as:

$$\dot{x}_i = \tfrac{1}{2} \ddot{x}_i (t_i - t) \tag{10.44}$$

Knowing $\dot{x}_i$, the motion velocity $\dot{x}_{i+1}$ at time t_{i+1} can similarly be calculated as

$$\dot{x}_{i+1} = \dot{x}_i + \tfrac{1}{2} (\ddot{x}_i + \ddot{x}_{i+1})(t_{i+1} - t_i) \tag{10.45}$$

In this calculation, $\ddot{x}_{i+1}$ is obtained from Eq. (10.33), (10.38) or (10.41). Using the same procedure, all the velocities corresponding to all the selected time instants can be calculated. Besides, as Newmark pointed out, the uphill resistance may be taken as infinitely large without causing serious errors in the calculations. In this situation, ground motions in the direction of the downward slope tend to move the mass downhill, but ground motions in the upward direction along the slope leave the mass without relative additional motion except where these are extremely large in magnitude. Thus, the sliding block can only move downhill with positive velocity, regardless of the direction of the acceleration.

If the acceleration changes from negative to positive and the velocity changes from positive to negative during a time interval, by referring to Fig. 10.10, in addi-

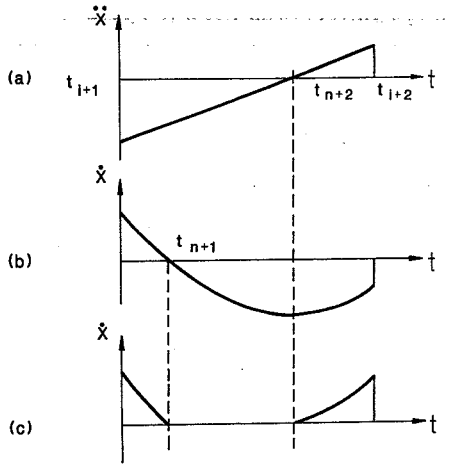

Fig. 10.10. Motion of failure block on slope with a positive velocity at t_{i+1} and negative velocity at t_{i+2}. (a). Negative acceleration at t_{i+1} and positive acceleration at t_{i+2}. (b). If negative velocity is permissible. (c). If negative velocity is not permissible.

tion to time t_{n+1}, time t_{n+2} also needs to be computed. The time t_{n+1}, at which $\dot{x}$ becomes zero can be computed by using the following relationship:

$$\dot{x}_{n+1} = \dot{x}_{i+1} + \frac{(\ddot{x}_{i+2} - \ddot{x}_{i+1})(t_{n+1} - t_{i+1})^2}{2(t_{i+2} - t_{i+1})} + \ddot{x}_{i+1}(t_{n+1} - t_{i+1}) = 0 \tag{10.46}$$

Solving for $t_{n+1} - t_{i+1}$, thus gives:

$$(t_{n+1} - t_{i+1}) = \frac{-\ddot{x}_{i+1} \pm \left[\ddot{x}_{i+1}^2 - \frac{2(\ddot{x}_{i+2} - \ddot{x}_{i+1})\dot{x}_{i+1}}{(t_{i+2} - t_{i+1})}\right]^{\frac{1}{2}}}{\frac{(\ddot{x}_{i+2} - \ddot{x}_{i+1})}{(t_{i+2} - t_{i+1})}} \tag{10.47}$$

Only one solution of the two obtained from Eq. (10.47) is reasonable, at which the velocity is zero and displacement ceases. Because, as mentioned earlier, the velocity cannot be negative, the velocity after time t_{n+1} is zero rather than negative. This zero velocity will remain until time t_{n+2}. During t_{n+1} and t_{i+2} whenever motion acceleration becomes positive the failure block will move again, and the time is t_{n+2}, at which the failure block move downward again, t_{n+2} can be expressed as follows:

$$t_{n+2} = \frac{-\ddot{x}_{i+1}(t_{i+2} - t_{i+1})}{(\ddot{x}_{i+2} - \ddot{x}_{i+1})} + t_{i+1} \tag{10.48}$$

Thus, during the time period from t_{i+1} to t_{i+2}, two nonconsecutive displacements can be calculated.

When the acceleration changes from negative to positive and the velocities at times t_{i+1} and t_{i+2} are positive, as shown in Fig. 10.11, it is necessary to check the velocity at time t_{n+2} so that the velocity actually occurs as sketched in Fig. 11.11b or c. The velocity from t_{i+1} to t_{i+2} must be all positive provided that $\dot{x}_{n+2}$ is positive, otherwise, a procedure similar to that described previously for finding t_{n+1} and t_{n+2} should be used.

When the acceleration changes from positive at time t_{i+1}, and the velocity at time t_{i+2} is positive, or the accelerations are all positive during the time interval from t_{i+1} to t_{i+2}, we can calculate the deformation by proceeding to step (5) directly. If the velocity at t_{i+2} is negative in the former case, as shown in Fig.

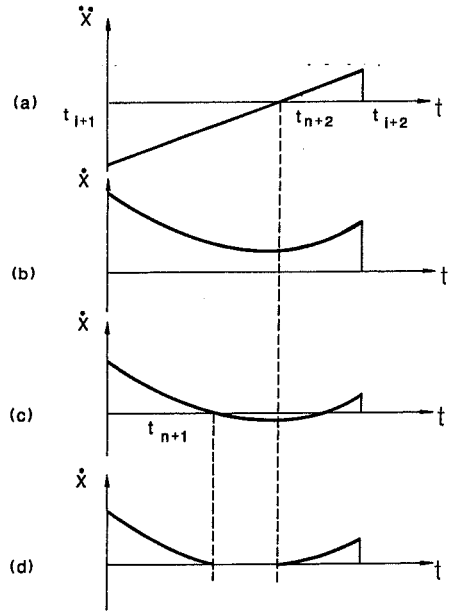

Fig. 10.11. Motion of failure block on a slope with positive velocity at both t_{i+1} and t_{i+2}. (a). Negative acceleration at t_{i+1} and positive acceleration at t_{i+2}. (b). Velocity is all positive. (c). Velocity is negative between t_{n+1} and t_{n+2}, if negative velocity is permissible. (d). Velocity is zero between t_{n+1} and t_{n+2}, if negative velocity is not permissible.

10.12, the time t_{n+1}, at which the velocity becomes zero should be calculated as follows:

$$t_{n+1} = t_{i+1} - \frac{\ddot{x}_{i+1} + \left[\ddot{x}_{i+1}^2 - 2\frac{\ddot{x}_{i+2} - \ddot{x}_{i+1}}{t_{i+2} - t_{i+1}}\dot{x}_{i+1}\right]^{\frac{1}{2}}}{\frac{\ddot{x}_{i+2} - \ddot{x}_{i+1}}{t_{i+2} - t_{i+1}}} \tag{10.49}$$

Finally, when the accelerations at both t_{i+1} and t_{i+2} are negative, the time t_{n+1}, at which the velocity becomes zero can also be calculated in a similar manner as that of Eq. (10.49).

Step 5

Based on the accelerations and velocities between two times, e.g., t_i and t_{i+1}, the displacement of the failure section between t_i and t_{i+1}, thereby can be calculated as:

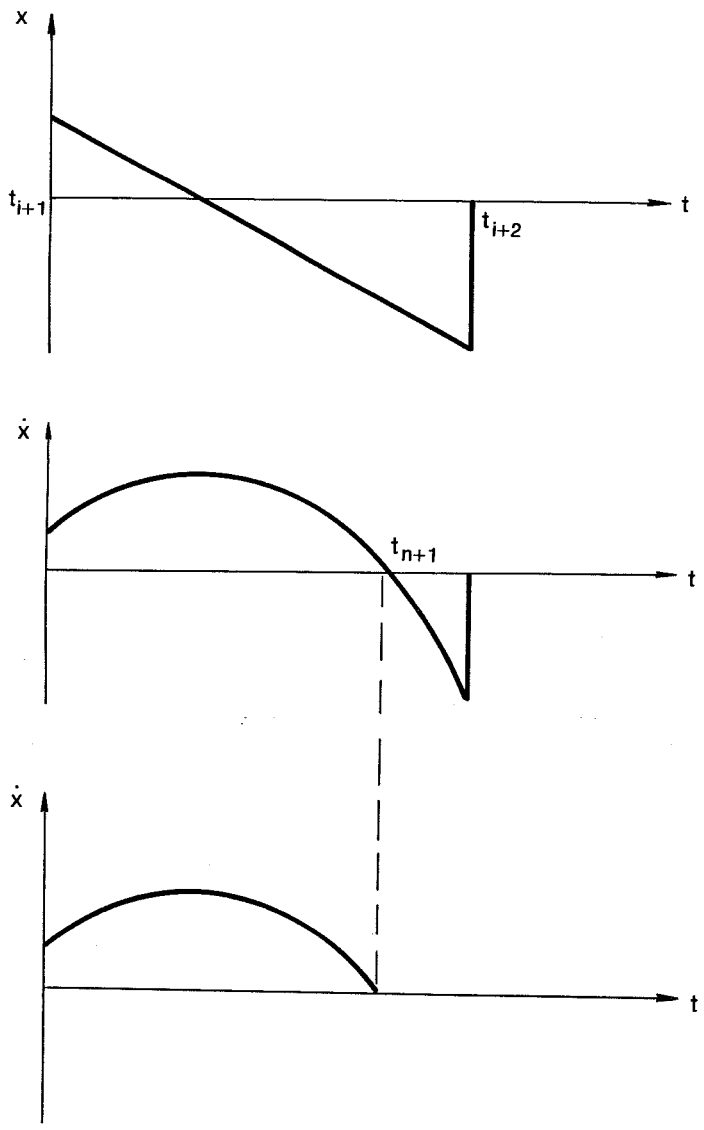

Fig. 10.12. Motion of failure block on a slope. (a). Positive acceleration at t_{i+1}, negative acceleration at t_{i+2}. (b). If negative velocity is permissible. (c). If negative velocity is not permissible.

$$x_{i+1} = x_i + \dot{x}_i (t_{i+1} - t_i) + \tfrac{1}{6}(2\ddot{x}_i + \ddot{x}_{i+1})(t_{i+1} - t_i)^2 \qquad (10.50)$$

Similar procedures will be performed to find the overall displacement until the end of the earthquake.

10.3.3 Numerical results

A computer program using the aforementioned analytical procedure has been developed at Purdue University and is listed at the end of this chapter. The problem as shown in Fig. 10.13 is considered. The design earthquake record selected is the Pasadena earthquake (1952) scaled to 0.15 g, as shown in Fig. 10.15. After solving the problem, the yield acceleration factor for the log-spiral failure mechanism is found to be 0.01764. For simplicity, we shall assume this yield acceleration factor to be constant during the earthquake.

Two diagrams of displacements at the top of failure surface versus time are shown in Fig. 10.14. From the result, we can see that the displacement increases sharply during the range close to the positive peak acceleration, and that the displacement at the top in both directions are rather close. This is due to the fact that the value of θ_0 is 43.65°, that is close to 45°. Actually, the displacement in any point along the failure surface can be obtained by introducing the corresponding angle θ.

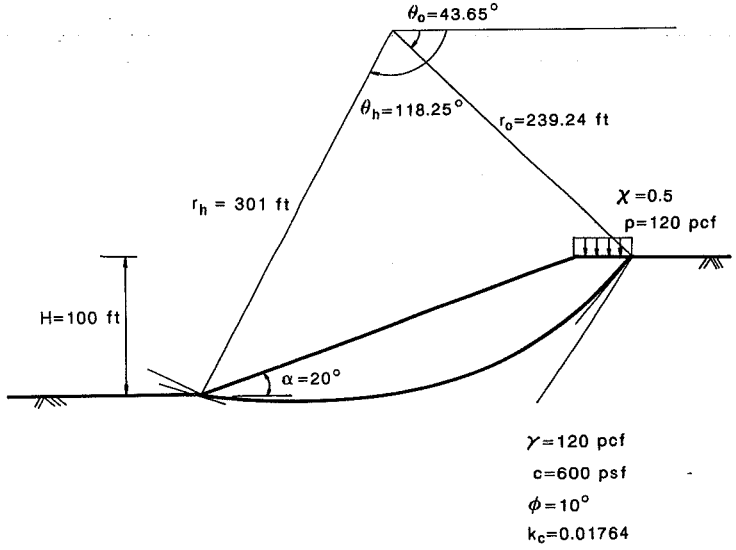

Fig. 10.13. Example problem.

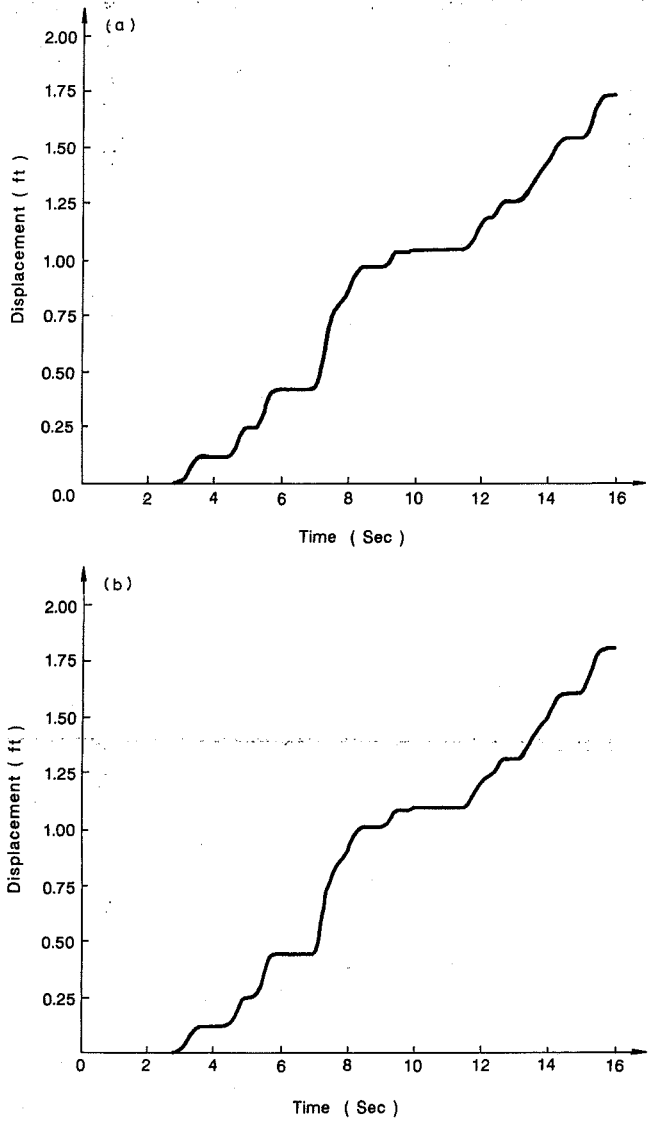

Fig. 10.14(a). Horizontal displacement at the top of the failure surface. (b). Vertical displacement at the top of the failure surface.

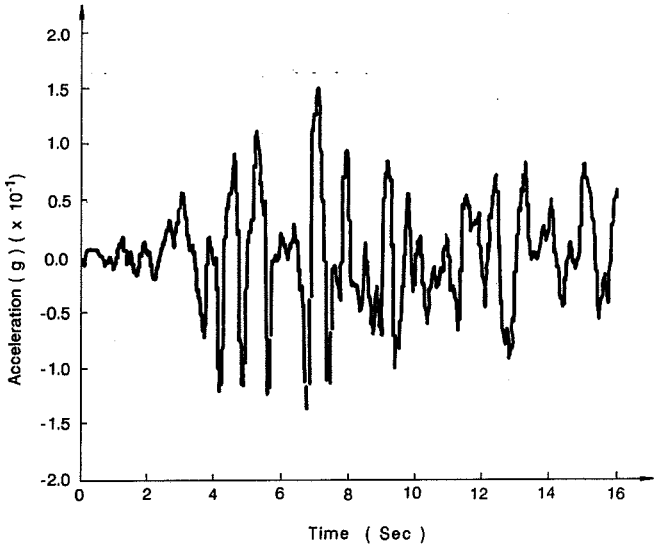

Fig. 10.15. Time history of acceleration of Pasadena earthquake.

10.4 Summary

This Chapter attempts to develop a practical method to effectively analyze the stability of earth slopes under earthquake loading. The proposed approach is an extension and modification of the pseudo-static method of slope stability analysis. It is a pseudo-static approach and not a dynamic analysis. Thus, it should be viewed only as a useful and practical computational tool. The corresponding computer program listing for the modified pseudo- static approach are given in Appendices. The following two parts of work are presented in this chapter:

1. The determination of failure mechanisms and corresponding yield accelerations.
2. The assessment of seismic displacement with Newmark's analytical procedure.

In the first part of the work, the limit analysis method is used to determine the critical failure surface and its yield acceleration of earth slopes subjected to earthquake loads. In this analysis the acceleration is assumed to be uniform throughout the depth of the slope. However, because the slope is not rigid, acceleration is not really uniform throughout the slope. The distribution of seismic coefficient is therefore a function of the height of a slope. This is the subject of study of Chapter 8. Using the concept of superposition, the variation of the horizontal pseudo-static force throughout the depth of the slope can be incorporated. The critical state of a slope against collapse with nonuniform seismic coefficients thus can be determined.

The concept of superposition can be used not only to handle the variation of acceleration throughout slopes but also to solve the multi-layer property of a slope. However, to apply the concept of superposition to multi-layer slopes the compatibilities of failure surfaces among all the layers have to be satisfied. According to the associated flow rule of limit analysis, the shape of the failure surface is directly related to the frictional angle ϕ and for a multi-layer slope, the angle ϕ is different for each layer. Thus, to find the critical state of nonhomogeneous slope, some studies have been made by Chen and Sawada (1983).

The failure surface is assumed here to pass through the toe. In some cases, the failure surface may pass below the toe. For simplicity, we consider that the inclination on the upper part of slope is horizontal. If the slope has an inclined upper part and the failure surface may pass below the toe, the procedure described in this chapter for analyzing the seismic response of slope during earthquake can still be applied. Details of this general formulation are not given here. The related equations for a general slope without the seismic effect can be found in the book by Chen (1975).

For seismic slope stability analysis, in addition to calculating the yield acceleration and failure mechanism of a slope after a given earthquake, the effect of earthquake on the displacements of a slope must also be assessed. Based on the calculated yield acceleration and its corresponding failure mechanism, Newmark's analytical procedure is used to assess the soil displacements of the earth slope which is subjected to a design earthquake. It is the magnitude of the displacement which forms the basis for assessing the stability and adequacy of the section and not the seismic factor of safety. This is the second part of the work as described in the later part of this Chapter.

The method is particularly useful in cases where the yield resistance of the soil can be reliably determined and therefore for the analysis of cases where pore-water pressures do not change significantly as the earthquake motions continue or shear displacements occur. This leads to the conclusion that the pseudo-static analysis procedure provides an acceptable method of analysis for some types of soil, which do not build up large pore pressures or cause significant strength loss due to earthquake shaking and associated displacements.

In fact, the Newmark analytical procedure for assessing the seismic displacement of a slope is based on the effective stress method. If the pore-water pressure does not change significantly or the induced pore-water pressure can be appropriately evaluated during an earthquake, this procedure can be effectively applied for analyzing the seismic displacement of a slope with saturated soils. Sarma (1975) attempted to use pore-pressure parameters to evaluate the seismic displacement of earth dams based on an effective stress analysis.

In the evaluation of the seismic displacement of a slope during earthquake, the theory of perfect plasticity together with its associated flow rule of Mohr-Coulomb

material are assumed. This may overestimate the volume change for some soils such as sands. A similar procedure can be applied for different types of soil models. Furthermore, even if there exist some limitations in the present procedure, we can extend and modify the present procedure to make it more suitable to the analysis of the related geotechnical engineering problems.

References

Chang, C.J., 1981. Seismic Safety Analysis of Slopes. Ph.D. Thesis, School of Civil Engineering, Purdue University, West Lafayette, IN, 125 pp.

Chang, C.J., Chen, W.F. and Yao, J.T.P., 1984. Seismic displacements in slopes by limit analysis. J. Geotech. Eng., ASCE, 110(7): 860–874.

Chang, C.J., Chen, W.F. and Yao, J.T.P., 1985. Evaluation of seismic factor of safety of a submarine slope by limit analysis, Proc. 1983 Symposium on Marine Geotechnology and Near Shore/Offshore Structures, Shanghai, China, Tongi University Press, pp. 262–295.

Chen, W.F., 1975. Limit Analysis and Soil Plasticity. Elsevier Amsterdam, 630 pp.

Chen, W.F., 1980. Plasticity in soil mechanics and landslides. J. Eng. Mech. Div., ASCE, 106(EM3): 443–464.

Chen, W.F. and Sawada, T., 1983. Earthquake-induced slope failure in nonhomogeneous anisotropic soils. Soils Found., Jpn. Soc. Civ. Eng., 23(2): 125–139.

Chen, W.F., Chang, C.J. and Yao, J.T.P., 1978. Limit analysis of earthquake-induced slope failure. In: R.L. Seirakowski (Editor), Proc. 15th Annual Meeting of the Society of Engineering Science. University of Florida, Gainesville, FL, pp. 533–538.

Janbu, N., 1957. Earth pressure and bearing capacity by generalized procedure of slices. Proc. 4th Int. Conference on Soil Mechanics, 2, pp. 207–212.

Newmark, N.W., 1965. Effects of earthquake on dams and embankments. The Fifth Rankine Lecture of the British Geotechnical Society. Geotechnique, 15(2): 137–160.

Sarma, S.K., 1975. Seismic stability of earth dams and embankments. Geotechnique 25(4): 743–761.

Seed, H.B., 1966. A method for earthquake resistance design of earth dams. J. Soil Mech. Found. Div., ASCE, 92(SM1): 13–41.

Sigel, R.A., 1975. STABL User Manual, Joint Highway Research Project, JHRP-75-9. School of Civil Engineering, Purdue University, West Lafayette, IN, 112 pp.

APPENDICES: Program Listings

Appendix 1: Plane Failure Surface

```
c-------------------------------------------------------------
c This program can be used to obtain the yield acceleration
c factor for plane failure surface
 -----------------------------------------------
c      h  : height of slope (ft)
c      c  : cohesion of soil (psf)
c      f  : friction angle of soil (degree)
c      a  : slope angle (degree)
```

```
c      p  : uniform surcharge (psf)
c      x  : seismic coefficient of surcharge
c      xns: stability factor (= #rh/c)
c      r  : average unit weight of soil
c      x1,x2,dx
c         : minimum,maximum values and interval of angle
c           respectively in the process of searching for
c           the yield acceleration factor
c      xmin
c         : critical value of yield acceleration factor
c      xa : failure surface angle corresponding to xmin
c-------------------------------------------------------------
       read*,h,c,f,a
       read*,p,x,r
       xns=r*h/c
c----- 1st-round trial
       x1=0.05*a
       x2=0.95*a
       f=f/57.2958
       a=a/57.2958
       dx=1.
       call xx(x1,x2,dx,a,f,c,p,x,xns,xa,xmin)
c----- 2nd-round trial
       x1=xa-1.
       x2=xa+1.
       dx=0.05
       call xx(x1,x2,dx,a,f,c,p,x,xns,xa,xmin)
c----- 3rd-round trial
       x1=xa-0.05
       x2=xa+0.05
       dx=0.001
       call xx(x1,x2,dx,a,f,c,p,x,xns,xa,xmin)
       print*,xa,xmin
       stop
       end
c-----subroutine to search for the critical value
       subroutine xx(x1,x2,dx,a,f,c,p,x,xns,xa,xmin)
       xmin=3.
       xa=90.
       m=(x2-x1)/dx
       do 10 i=1,m+1
       bb=x1+(i-1)*dx
       b=bb/57.2958
       b1=cos(f)/cos(b-f)
       b2=sin(a)/sin(a-b)
       b3=p*sin(f-b)/(c*cos(f))
       b4=0.5*xns*sin(f-b)/cos(f)
       t1=b1*(b2+b3+b4)
       b5=0.5*xns+x*p/c
       xkc=t1/b5
       if(xkc-xmin.lt.0.and.xkc.gt.0.) then
       xmin=xkc
```



```
       xa=bb
       else
       go to 10
       endif
    10 continue
       return
       end
```

Appendix 2: Logspiral Failure Surface

```
c-------------------------------------------------------------
c This program can be used to obtain the yield acceleration
c factor for logspiral failure surface
 ------------------------------------------------
c      h  : height of slope (ft)
c      c  : cohesion of soil (psf)
c      f  : friction angle of soil (degree)
c      a  : slope angle (degree)
c      s1 : the 1st-round trial value of theta 0, (60 - 120)
c      p  : uniform surcharge (psf)
c      x  : seismic coefficient of surcharge
c      xns: stability factor (= #rh/c)
c      r  : average unit weight of soil
c      x1,x2
c         : minimum, maximum values of theta 0 respectively
c           in the process of searching for the yield
c           acceleration factor
c      y1,y2
c         : minimum, maximum values of theta h respectively
c           in the process of searching for the yield
c           acceleration factor
c      da : interval of theta 0 and theta h in the process
c           of searching for the yield accleration factor
c      r0 : the distance between the rotation center and the
c           top of failure surface
c      lr : ratio of surcharge length to r0
c      smin
c         : critical value of yield acceleration factor
c      xx : the value of theta 0 corresponding to smin
c      yy : the value of theta h corresponding to smin
c-------------------------------------------------------------
       real lr
       read*,h,c,f,a,s1
       read*,p,x,r,ss
       xns=r*h/c
c----- 1st-round trial
       x1=-0.2*a
       x2=s1
       y1=90-0.6*a
       y2=175
       da=1.0
```

```
      a=a/57.2958
      f=f/57.2928
      call vx(x1,x2,y1,y2,da,a,f,p,c,x,xns,xx,yy,smin,ss)
c---- 2nd-round trial
      x1=xx-1
      x2=xx+1
      y1=yy-1
      y2=yy+1
      da=0.05
      call vx(x1,x2,y1,y2,da,a,f,p,c,x,xns,xx,yy,smin,ss)
      xx1=xx/57.2958
      yy1=yy/57.2958
      tt=(yy1-xx1)*tan(f)
      r0=h/(sin(yy1)*exp(tt)-sin(xx1))
      lr=(sin(a+xx1)-exp(tt)*sin(a+yy1))/sin(a)
      print*,xx,yy,smin,r0,lr
      stop
      end
c---- subroutine to search for the critical value
      subroutine vx(x1,x2,y1,y2,da,a,f,p,c,x,xns,xx,yy
     1,smin,ss)
      real lr
      xx=90
      yy=180
      smin=3.
      m=(x2-x1)/da
      n=(y2-y1)/da
      do 10 i=1,m
      aa1=x1+(i-1)*da
      a1=aa1/57.2958
      do 10 j=1,n
      aa2=y1+(j-1)*da
      a2=aa2/57.2958
      t1=(a2-a1)*tan(f)
      t2=3.*(1.+9*tan(f)*tan(f))
      ck=sin(a2)*exp(t1)-sin(a1)
      if(ck.lt.0.0) go to 10
      lr=(sin(a+a1)-exp(t1)*sin(a+a2))/sin(a)
      if(lr.lt.0.0) go to 10
      fc=(exp(2.*t1)-1)/(2.*tan(f))
      f1=((3.*tan(f)*cos(a2)+sin(a2))*exp(3.*t1)-(3.*tan(
     1f)*cos(a1)+sin(
     1a1)))/t2
      f2=lr*(2.*cos(a1)-lr)*sin(a1)/6.
      f3=exp(t1)*(sin(a2-a1)-lr*sin(a2))*(cos(a1)-lr+cos(
     1a2)*exp(t1))/6.
      f4=((3.*tan(f)*sin(a2)-cos(a2))*exp(3.*t1)-(3.*tan(
     1f)*sin(a1)-cos(a1)))/t2
      f5=lr*sin(a1)*sin(a1)/3.
      f6=exp(t1)*(sin(a2-a1)-lr*sin(a2))*(sin(a1)+sin(a2)
     1*exp(t1))/6.
      fp=lr*(cos(a1)-0.5*lr)
```



```
      fq=lr*sin(a1)
      b1=fc-xns*(f1-f2-f3)/(sin(a2)*exp(t1)-sin(a1))-p*
     1fp/c
      b2=ss*xns*(f4-f5-f6)/(sin(a2)*exp(t1)-sin(a1))+x*
     1p*fq/c
      xkc=b1/b2
      if(xkc-smin.lt.0.and.xkc.gt.0.) then
      smin=xkc
      xx=aa1
      yy=aa2
      else
      go to 10
      endif
   10 continue
      return
      end
```

Appendix 3: Limit Analysis During Earthquake

```
c-------------------------------------------------------------
This program can be used to analyze the response of
slopes by limit analysis method during earthquake (EQ)
 -------------------------------------------------------
c     ug(i): acceleration for EQ record or motion of
c            slope mass
c     d(i) : accumulated rotation of slope mass during EQ
c     v(i) : angular velocity of slope mass during EQ
c     dx(i): displacement in horizontal direction for some
c            specified point along failure surface
c     dy(i): displacement in vertical direction for some
c            specified point along failure surface
c     m1   : length of acceleration,no. of EQ record input
c     mm   : no. of lines of EQ record input (mm=m1/8)
c     dt   : time interval
c     scale: scaling factor of EQ
c     h    : height of slope (ft)
c     c    : cohesion of soil (psf)
c     f    : friction of soil (degree)
c     a    : slope angle (degree)
c     a1   : theta 0 (degree)
c     a2   : theta h (degree)
c     xkc  : yield accel. factor
c     p    : surcharge loading (psf)
c     x    : seismic factor of surcharge
c     xns  : stability factor (= rh/c)
c     r    : average unit weight of soil (pcf)
c     r0   : the distance between the rotation center and
c            the top of failure surface
c     cc   : coefficient in Eq. 10.41 after the induced
c            accleration factor substracted by yield
c            acceleration factor
```

```
c      rx    : the distance between the rotation center and
c              the specified point along failure surface
c      theta: the value of angle from the horizontal
c             direction corresponding to rx
c-------------------------------------------------------------
       dimension ug(900),d(900),v(900)
       dimension dx(900),dy(900)
       read*,m1,mm
       read*,dt,scale
c----- input earthquake record
       do 10 i=1,mm
       read(5,20) (ug(j),j=i*8-7,i*8)
   20  format(8f9.6)
   10  continue
c-------------------------------------------------------------
c----- scaling earthquake record
       ugmax=0.
       do 30 i=1,m1
       if(abs(ug(i))-ugmax.gt.0.) ugmax=abs(ug(i))
   30  continue
       ratio=scale/ugmax
       do 40 i=1,m1
   40  ug(i)=ratio*ug(i)
c----- input the required data for slope geometry, etc.
       read*,h,c,f,a,a1,a2,r0
       read*,p,x,r,xkc
       read*,theta
       xns=r*h/c
c----- open files for saving the displacement
       open(8,file='t1',status='new')
       open(9,file='t2',status='new')
       b=b/57.2958
       f=f/57.2928
       a1=a1/57.2958
       a2=a2/57.2958
       theta=theta/57.2958
       rx=r0*exp(tan(theta-a1))
c----- find the value of cc (defined above)
       call vx(a1,a2,a,f,h,p,c,x,r,xns,cc)
c----- set initial values of followings as zero
       do 50 i=1,m1
       d(i)=0.
       v(i)=0.
       dx(i)=0.
       dy(i)=0.
   50  continue
c----- substract accel. of earthquake by yield accel.
       do 60 i=1,m1
       ug(i)=(ug(i)-xkc)*cc
   60  continue
c----- search for time at which the positive movement starts
       do 70 i=1,m1
```



```
       if(ug(i).gt.0.) then
       k=i
       go to 80
       else
       go to 70
       endif
   70  continuebr
c----- compute the accumulated angular rotation
   80  tx=-dt*ug(k-1)/(ug(k)-ug(k-1))
       v(k)=0.5*ug(k)*(dt-tx)
       d(k)=ug(k)*(dt-tx)*(dt-tx)/6.0
       mx=m1-1
       do 90 j=k,mx
       v(j+1)=v(j)+0.5*(ug(j)+ug(j+1))*dt
       if(ug(j).gt.0.0.and.ug(j+1).gt.0.) go to 100
       if(ug(j).gt.0.0.and.ug(j+1).le.0.) go to 200
       if(ug(j).le.0.0.and.ug(j+1).gt.0.) go to 300
       if(ug(j).le.0.0.and.ug(j+1).le.0.) go to 350
  100  d(j+1)=d(j)+v(j)*dt+(2*ug(j)+ug(j+1))*dt*dt/6.0
       go to 90
  200  if(v(j+1).ge.0) go to 100
       b1=(ug(j+1)-ug(j))/dt
       tn=-(ug(j)+sqrt(ug(j)*ug(j)-2.*b1*v(j)))/b1
       d(j+1)=d(j)+v(j)*tn+(2.*ug(j)+tn*b1)*tn*tn/6.
       v(j+1)=0.
       go to 90
  300  if(v(j+1).le.0) go to 301
       b1=(ug(j+1)-ug(j))/dt
       tn3=-ug(j)/b1
       vm=v(j)+0.5*ug(j)*tn3
       if(vm.le.0) go to 301
       go to 100
  350  if(v(j+1).ge.0.) go to 100
       b1=(ug(j+1)-ug(j))/dt
       if(b1.lt.0.0001) then
       tn=-v(j)/ug(j)
       go to 351
       else
       go to 352
       endif
  352  b2=sqrt(ug(j)*ug(j)-2.*b1*v(j))
       tn=(-ug(j)-b2)/b1
  351  v(j+1)=0.
       d(j+1)=d(j)+v(j)*tn+(2.*ug(j)+tn*b1)*tn*tn/6.0
       go to 90
  301  b1=(ug(j+1)-ug(j))/dt
       b2=sqrt(ug(j)*ug(j)-2.*b1*v(j))
       tn1=(-ug(j)+b2)/b1
       tn2=(-ug(j)-b2)/b1
       if(tn1-tn2.gt.0) tn=tn2
       tn=tn1
       d(j+1)=d(j)+v(j)*tn+(2.*ug(j)+tn*b1)*tn*tn/6.0
```

```
      tn3=-ug(j)/bl
      v(j+1)=0.5*ug(j+1)*(dt-tn3)
      d(j+1)=d(j+1)+ug(j+1)*(dt-tn3)*(dt-tn3)/6.0
   90 continue
c---- compute the accumulated displacement
      do 400 j=1,ml
      dx(j)=rx*d(j)*sin(theta)
      dy(j)=rx*d(j)*cos(theta)
  400 continue
      do 500 j=1,ml
      tt=dt*(j-1)
      write(8,501) tt,dx(j)
      write(9,501) tt,dy(j)
  500 continue
  501 format(10x,2f10.7)
      stop
      end
c---- subroutine to search for the value of cc
      subroutine vx(a1,a2,b,f,h,p,c,x,r,xns,cc)
      real lr,l
      t1=(a2-a1)*tan(f)
      t2=3.*(1.+9*tan(f)*tan(f))
      lr=(sin(b+a1)-exp(t1)*sin(b+a2))/sin(b)
      fc=(exp(2.*t1)-1)/(2.*tan(f))
      f1=((3.*tan(f)*cos(a2)+sin(a2))*exp(3.*t1)-(3.*tan(
     1f)*cos(a1)+sin(
     1a1)))/t2
      f2=lr*(2.*cos(a1)-lr)*sin(a1)/6.
      f3=exp(t1)*(sin(a2-a1)-lr*sin(a2))*(cos(a1)-lr+cos(
     1a2)*exp(t1))/6.
      f4=((3.*tan(f)*sin(a2)-cos(a2))*exp(3.*t1)-(3.*tan(
     1f)*sin(a1)-cos(
     1a1)))/t2
      f5=lr*sin(a1)*sin(a1)/3.
      f6=exp(t1)*(sin(a2-a1)-lr*sin(a2))*(sin(a1)+sin(a2)
     1*exp(t1))/6.
      fp=lr*(cos(a1)-0.5*lr)
      fq=lr*sin(a1)
      r0=h/(sin(a2)*exp(t1)-sin(a1))
      x1=r*r0*r0*r0*(f4-f5-f6)+x*p*r0*r0*fq
      w=0.5*r*r0*r0*(0.5*(exp(2.*t1)-1)/tan(f)-lr*sin(a1)
     1-(sin(a2-a1)-lr
     1*sin(a2))*exp(t1))
      x2=r*r0*r0*r0*(f1-f2-f3)
      x3=r*r0*r0*r0*(f4-f5-f6)
      l=sqrt(x2*x2+x3*x3)/w
      cc=32.2*x1/(w*l*l)
      return
      end
```


Chapter 11

STABILITY ANALYSIS OF SLOPES WITH GENERALIZED FAILURE CRITERION

11.1 Introduction

In many practical problems, such as the frozen gravel embankments, concepts adopted recently in offshore arctic engineering, sufficient experimental data have shown that the frozen gravel follows a highly nonlinear failure criterion, but it is difficult to obtain experimental data on its deformations. As a result, finite-element methods cannot be applied directly to solve such problems because of a lack of specific information about the behavior of this material under *in situ* conditions. Fortunately, our main interest here is the overall stability of slopes, not the detailed history of stresses and deformations. Limit analysis methods, together with a nonlinear failure criterion, provide a powerful tool to engineers to obtain approximate solutions under this situation.

All methods of stability analysis in soil mechanics are highly dependent on the particular failure mechanism chosen for the problem. The selection of a proper failure mechanism is therefore of great importance for properly assessing the collapse load. It has been shown by the variational calculus that the logarithmic spiral rotational failure mechanism utilized in the upper-bound limit analysis solution is the appropriate failure surface for a rigid-body type of rotational sliding mechanism (Chen and Snitbhan, 1975). However, this conclusion is true only for the material that follows the *linear* Mohr-Coulomb failure criterion. We cannot immediately apply the linear limit analysis method to *nonlinear* failure problems. It is necessary therefore to investigate the soil stability problems and to develop practical solution methods based upon a generalized failure criterion. This is described in the present Chapter.

When the failure criterion in σ-τ space is a straight line, the logarithmic spiral rotational failure mechanism utilized in both the limit analysis and limit equilibrium solutions can be obtained directly without the information about the normal stress distribution along the failure surface. When the failure criterion is nonlinear, however, the calculation of the internal dissipation of energy along the slip surface is influenced by the normal stress distribution. In this case, the variational calculus can be used to obtain solutions of stability problems in soil mechanics. In 1970, Chen suggested to use the variational calculus to obtain the normal stress distribution along the slip surface for stability problems in soil mechanics. Afterwards,

Chen and Snitbhan (1975) applied the variational method to obtain the shape of the slip surface and its corresponding normal stress distribution of a vertical slope. Baker and Garber (1977) suggested a similar variational approach to solve bearing-capacity problems. Baker (1981) extended the same approach to include both the tensile strength and tension cracks in slope stability problems.

Baker and Frydman (1983) appear to be the first to discuss the effect of nonlinearity of a generalized failure criterion on the upper-bound solution procedure. They applied the variational calculus to formulate the bearing capacity of a strip footing on the upper surface of a slope under the nonlinear failure case. Two solution procedures are suggested. One is based on minimization with four unknown parameters. Another is based on solving a system of four simultaneous equations. Both solution procedures proposed by Baker and Frydman, however, are not realistic except in very special cases. Zhang and Chen (1987) adopted the same variational calculus, developed an inverse solution procedure, and obtained numerical results for the critical height of an embankment. Liu et al. (1989) recently developed a new effective solution procedure called *the combined method*, suitable for the slope stability problems with a generalized nonlinear failure criterion. By this method, they obtained extensive numerical results for the critical height of slopes and the bearing capacity of a strip footing on the upper surface of a slope, and extended the method to obtain solutions of the stability of layered frozen gravel embankments.

In this Chapter, the variational calculus approach in the limit analysis of strip footings is first introduced. A solution procedure suitable for the analysis of slope stability problems is then explained, and finally, a realistic engineering problem involving a layered analysis with nonlinear failure criterion, is described.

11.2 Variational approach in limit analysis and the combined method

The solution procedure required in an upper-bound limit analysis consists of the following steps. First, a class of kinematically admissible collapse mechanisms is postulated in terms of some geometrical variables. Second, for a set of values of the geometrical variables, an estimate of the collapse load is obtained by equating the rate of external work to the rate of internal dissipation. The estimate of the collapse load is expressed in terms of the geometrical variables defining the collapse mechanism. Third, the lowest value of these estimates represents the least upper-bound value for this class of collapse mechanisms. Probably, other classes of collapse mechanisms may be considered, and the least upper-bound obtained from all classes of assumed mechanisms is taken as the *best* estimate of the true collapse load.

The application of the variational calculus approach to the upper-bound limit analysis provides a systematic procedure to find the lowest value of the collapse load

required in the third step. To this end, we shall develop a more rigorous approach and obtain both the failure surface and the critical stress distribution that will provide a more complete result of the stability problems in soil mechanics.

To focus our attention on the implication of the nonlinearity of the failure criterion on the stability analysis, we shall take here the simplest type of kinematically admissible discontinuous velocity field, that is, a single rigid-body rotation along a surface of velocity discontinuity. The soil is assumed to be isotropic and homogeneous and no pore-water pressure exists. The variational calculus approach developed in the forthcoming considers the general case of bearing capacity of a strip footing on the upper surface of a slope (Fig. 11.1). The failure criterion of the soil can generally be expressed as:

$$\tau = f(\sigma) \tag{11.1}$$

where σ and τ are the normal and shear stresses on the failure surface respectively (Fig. 11.2). If the plastic normal strain rate $\dot{\epsilon}^p$ and the plastic shear strain rate $\dot{\gamma}^p$ are superimposed on the σ-τ space, the plastic strain rate vector ($\dot{\epsilon}^p$, $\dot{\gamma}^p$) should be normal to the yield curve at the yield stress state. In Fig. 11.2, the plastic strain rate vector is seen making an angle ϕ_t, the tangential friction angle, with the plastic shear strain rate vector $\dot{\gamma}^p$, where:

$$\tan \phi_t = \frac{d\tau}{d\sigma} = \frac{df(\sigma)}{d\sigma} \tag{11.2}$$

The upper-bound method requires that the rate of external work be equated to the rate of internal dissipation for all plastically deformed zones. This requirement may be expressed as:

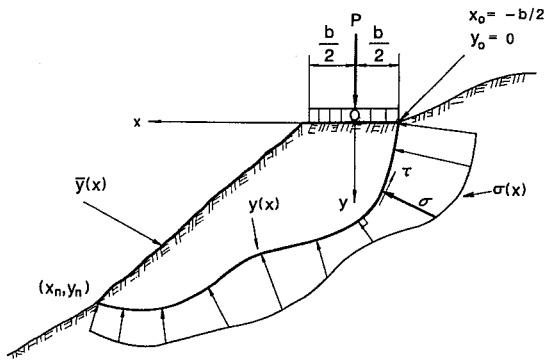

Fig. 11.1. A strip footing on a slope surface.

$$W(P, \eta_i) = \int_V D(\eta_i)\, dV \tag{11.3}$$

where W is the rate of external work, P is the applied load, η_i are a set of geometrical parameters defining the failure mechanism, and D is the rate of dissipation of energy per unit volume.

For the present purpose, it is more convenient to write Eq. (11.3) in the form:

$$Q(P, \eta_i) = \int_V D(\eta_i)\, dV - W(P, \eta_i) = 0 \tag{11.4}$$

where Q may be defined as the total work of the system at collapse.

Considering the equilibrium of the rigid body shown in Fig. 11.1, the total virtual work of the sliding mass may be written as:

$$Q = \dot{u} H + \dot{v} V + \dot{\Omega} M = 0 \tag{11.5}$$

where M is the resultant moment about some reference point. H, V are the resultant horizontal and vertical forces acting on the rigid body. $\dot{\Omega}$ is the rate of virtual rotation of the rigid body. $\dot{u}$ and $\dot{v}$ are the rates of horizontal and vertical virtual displacements of the reference point. In the present case, the reference point is taken at point 0 in Fig. 11.1, through which the external load P is applied.

Referring to Figs. 11.1 and 11.3, the resultant horizontal, vertical forces and moment with respect to 0 can be written as:

$$H = \int_s (\sigma \cos\theta - \tau \sin\theta)\, ds \tag{11.6}$$

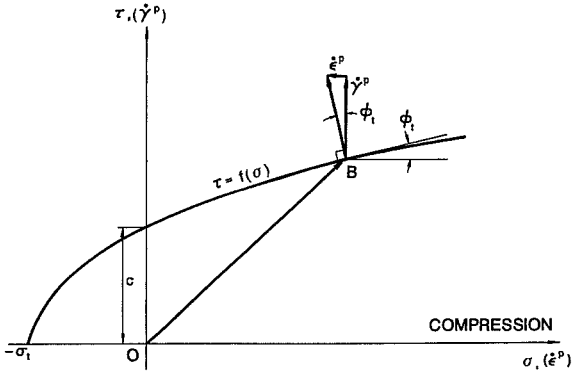

Fig. 11.2. A nonlinear yield criterion and its associated flow rule.

$$V = -\int_s (\sigma \sin\theta + \tau \cos\theta)\, ds + \int_{x_0}^{x_n} (y - \bar{y})\, \gamma\, dx + P \tag{11.7}$$

$$M = \int_s [(\sigma \cos\theta - \tau \sin\theta)\, y + (\sigma \sin\theta + \tau \cos\theta)\, x]\, ds - \int_{x_0}^{x_n} \gamma\, (y - \bar{y})\, x\, dx \tag{11.8}$$

where $y = y(x)$ is the equation describing the discontinuous surface, i.e., the slip surface along which the nonlinear yield condition (11.1) is satisfied. $\sigma = \sigma(x)$ and $\tau = \tau(x)$ are the normal and shear stress distributions along the slip surface $y(x)$, respectively (Fig. 11.1). x_0 and x_n are the end points of $y(x)$. s is the arc length along $y(x)$, and the angle θ satisfies:

$$\cot\theta = \frac{dy}{dx} \tag{11.9}$$

The equation $\bar{y} = \bar{y}(x)$ describes the soil surface, and γ is the unit weight of the soil.

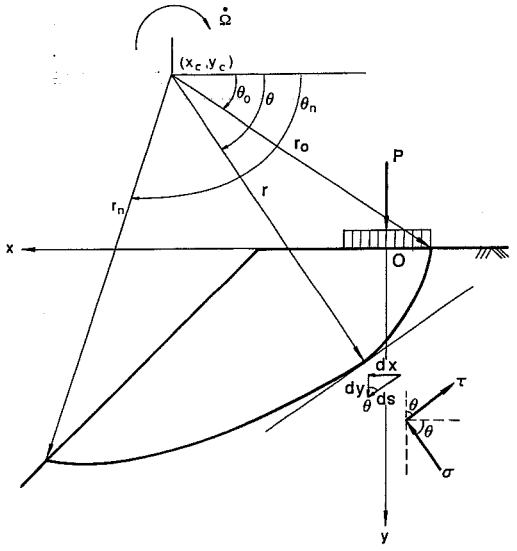

Fig. 11.3. The kinematic constraints of the slope.

Re-arranging the integrations in Eqs. (11.6) to (11.8), we have:

$$H = \int_{x_0}^{x_n} \left(\sigma \frac{dy}{dx} - \tau\right) dx \tag{11.10}$$

$$V = \int_{x_0}^{x_n} \left[-\left(\sigma + \tau \frac{dy}{dx}\right) + (y - \bar{y})\,\gamma\right] dx + P \tag{11.11}$$

$$M = \int_{x_0}^{x_n} \left[\left(\sigma + \tau \frac{dy}{dx}\right) x - (y - \bar{y})\,\gamma\, x + \left(\sigma \frac{dy}{dx} - \tau\right) y\right] dx \tag{11.12}$$

Taking $\dot{v}$ as unity and defining:

$$V_1 = V - P \tag{11.13}$$

Equation (11.5) may be solved for P and yields:

$$P + (V_1 + H\,\dot{u} + M\,\dot{\Omega}) = 0 \tag{11.14}$$

Substituting Eqs. (11.10) to (11.12) into Eq. (11.14), and assuming $\dot{\Omega} \neq 0$, we obtain:

$$P = \int_{x_0}^{x_n} \left\{\left[\sigma + \tau \frac{dy}{dx} - (y - \bar{y})\,\gamma\right] - \dot{u}\left(\sigma \frac{dy}{dx} - \tau\right) + \dot{\Omega}\left[-\left(\sigma + \tau \frac{dy}{dx}\right) x + (y - \bar{y})\,\gamma\, x - \left(\sigma \frac{dy}{dx} - \tau\right) y\right]\right\} dx$$

or

$$P = \int_{x_0}^{x_n} \dot{\Omega}\,(\tau\, g_1 + \sigma\, g_2 - \gamma\, g_3)\, dx \tag{11.15}$$

where:

$$g_1 = \left(\frac{\dot{u}}{\dot{\Omega}} + y\right) + \frac{dy}{dx}\left(\frac{1}{\dot{\Omega}} - x\right) \tag{11.16}$$

$$g_2 = \left(\frac{1}{\dot{\Omega}} - x\right) - \frac{dy}{dx}\left(\frac{\dot{u}}{\dot{\Omega}} + y\right) \tag{11.17}$$

$$g_3 = \left(\frac{1}{\dot{\Omega}} - x\right)(y - \bar{y}) \tag{11.18}$$

Now the problem becomes a typical problem in variational calculus. The integral g in:

$$P = G[y(x), \sigma(x), dy/dx, \dot{u}, \dot{\Omega}] = \int_{x_0}^{x_n} g\, dx \tag{11.19}$$

is stationary when its first variation vanishes. In Eq. (11.19), G is the functional relation between the load P and the unknown functions $y(x)$, $\sigma(x)$, dy/dx, $\dot{u}$, and $\dot{\Omega}$.

From Eq. (11.14), we can conclude that G represents the work done by the body forces (soil weight) and the dissipated work along the slip surface. G is not related to the external load P. The least upper bound value P can therefore be obtained by minimizing this functional relation with respect to the parameters η_i defining the failure mechanism. This minimization process must also be subjected to the constraint conditions: the failure mechanism is kinematically admissible. This procedure can be summarized in the following equations:

$$P_{\min} = \underset{\eta_i}{\text{Min}}\,[G] \tag{11.20}$$

$$K(\eta_i) = 0 \tag{11.21}$$

where $P_{\min}$ is the minimum value of P, and $K(\eta_i)$ represents the kinematic constraints.

If the $\dot{u}$ and $\dot{\Omega}$ have been chosen, then we can use the Euler equation to obtain the necessary conditions for the stationary requirement. One of these conditions is:

$$\frac{\delta G}{\delta \sigma} = \frac{\partial g}{\partial \sigma} = 0 \tag{11.22}$$

where δ is the variational operator. Eq. (11.22) can be rewritten as:

$$\left[\left(\frac{\dot{u}}{\dot{\Omega}} + y\right) + \frac{dy}{dx}\left(\frac{1}{\dot{\Omega}} - x\right)\right]\frac{df(\sigma)}{d\sigma} + \left[\left(\frac{1}{\dot{\Omega}} - x\right) - \frac{dy}{dx}\left(\frac{\dot{u}}{\dot{\Omega}} + y\right)\right] = 0 \tag{11.23}$$

where $f(\sigma)$ is given by Eq. (11.1).

Using the polar coordinate transformation (Fig. 11.3):

$$x = x_c - r\cos\theta \tag{11.24}$$

$$y = y_c + r\sin\theta \tag{11.25}$$

The polar coordinate system r and θ centers at point (x_c, y_c). By the definitions of $\dot{\Omega}$, $\dot{u}$, and $\dot{v}$, we have:

$$x_c\,\dot{\Omega} = \dot{v} = 1 \tag{11.26}$$

$$(-y_c)\,\dot{\Omega} = \dot{u} \tag{11.27}$$

i.e.

$$x_c = \frac{1}{\dot{\Omega}} \tag{11.28}$$

$$y_c = -\frac{\dot{u}}{\dot{\Omega}} \tag{11.29}$$

Using Eqs. (11.24), (11.25), (11.28), and (11.29), Eq. (11.23) can be simplified to the form:

$$\frac{dr}{d\theta} = r\frac{df(\sigma)}{d\sigma} \tag{11.30}$$

Similarly, the other necessary condition can be found by the condition:

$$\frac{\delta G}{\delta y} = \frac{\partial g}{\partial y} - \frac{d}{dx}\left[\frac{\partial g}{\partial\left(\frac{dy}{dx}\right)}\right] = 0 \tag{11.31}$$

i.e.:

$$2\tau - \gamma\left(\frac{1}{\dot{\Omega}} - x\right) + \left(\frac{\dot{u}}{\dot{\Omega}} + y\right)\frac{d\sigma}{dx} - \left(\frac{1}{\dot{\Omega}} - x\right)\frac{d\tau}{dx} = 0 \tag{11.32}$$

and this equation can be simplified by the transformation to the polar coordinate shown in Fig. 11.3:

$$\frac{d\sigma}{d\theta} + 2\tau - \gamma\, r\cos\theta = 0 \tag{11.33}$$

Equations (11.30) and (11.33) are the two necessary conditions for a minimum solution of the problem. However, by the upper bound theorem of limit analysis, the existence of such a minimum solution is guaranteed. Thus, there is no need to study the nature of the stationary point using the second variation.

Equations (11.30) and (11.33) constitute a pair of simultaneous differential equations for the determination of the functional forms of $r(\theta)$ and $\sigma(\theta)$. Obviously, four boundary conditions are needed.

According to the Peano's theorem, the solution of Eqs. (11.30) and (11.33) can always be written in the forms:

$$r = r(\theta \mid A, B, \dot{u}, \dot{\Omega}) \tag{11.34}$$

$$\sigma = \sigma(\theta \mid A, B, \dot{u}, \dot{\Omega}) \tag{11.35}$$

in which, A, B are the two integration constants and $\dot{u}$, $\dot{\Omega}$ define the origin of the polar coordinate system. Note that Eqs. (11.34) and (11.35) do not imply the existence of explicit forms of solutions for $r(\theta)$ and $\sigma(\theta)$ along the failure plane. It only emphasizes the dependence of the solutions on the four unknown parameters A, B, $\dot{u}$, $\dot{\Omega}$. By substituting Eqs. (11.34) and (11.35) into Eqs. (11.20) and (11.21), we can write the general solution in the form:

$$P_{\min} = \min_{A,\,B,\,\dot{u},\,\dot{\Omega}} [G(A, B, \dot{u}, \dot{\Omega})] \tag{11.36}$$

$$K(A, B, \dot{u}, \dot{\Omega}) = 0 \tag{11.37}$$

Thus, the solution procedure for the stability problem is based on the minimization of the functional G with respect to the parameters, A, B, $\dot{u}$, and $\dot{\Omega}$ satisfying the kinematic constraints (11.37).

The parameters, A, B in fact depend on the boundary conditions. For example, as shown in Fig. 11.1, the slip surface starts at the footing edge, i.e., $x_0 = -b/2$ and $y_0 = 0$. For an assumed set of values of σ_0, $\dot{u}$, and $\dot{\Omega}$, the pair of simultaneous differential equations, Eqs. (11.30) and (11.33), can be converted to an initial value problem, and we can obtain the distributions of the functions $r(\theta)$ and $\sigma(\theta)$ by a formal numerical method without difficulty.

According to Eq. (11.19), this minimization can also be achieved by considering the conditions $\partial G/\partial\dot{u} = 0$ and $\partial G/\partial\dot{\Omega} = 0$. From Eqs. (11.14) and (11.19), we have:

$$\left(\frac{\partial G}{\partial \dot{u}}\right) = H = 0 \tag{11.38}$$

$$\left(\frac{\partial G}{\partial \dot{\Omega}}\right) = M = 0 \tag{11.39}$$

Therefore, the minimization of G (or P) with respect to $\dot{u}$ and $\dot{\Omega}$ is equivalent to the satisfaction of the equilibrium conditions $H = 0$, $M = 0$. Furthermore, from Eq. (11.5), we also have $V = 0$, it follows that the minimization of G (or P) is equivalent to enforce the equilibrium requirement. In other words, we can use the equilibrium conditions $H = 0$ and $V = 0$ to check the minimum value G (or P) so obtained in a numerical procedure.

Introducing the equilibrium function:

$$F = \sqrt{H^2 + V^2} \tag{11.40}$$

The general procedure of the variational calculus approach can now be summarized as follows (Wang and Liu, 1988):

$$P_{\min} = \min_{\theta_0, \sigma_0, \dot{u}, \dot{\Omega}} [G] \tag{11.41}$$

$$F = 0 \tag{11.42}$$

$$\tau = f(\sigma) \tag{11.43}$$

$$K(\theta_0, \sigma_0, \dot{u}, \dot{\Omega}) = 0 \tag{11.44}$$

It is worth to note the following points:

(1) The proposed combined method is neither a conventional upper-bound method nor a conventional lower-bound method. It combines the upper-bound and lower-bound methods together. The assumed admissible velocity field not only satisfies the kinematic constraints and the yield criterion, but also satisfies the equilibrium equations. The combined method appears to lead to the best solution within the framework of rigid-body sliding and perfect plasticity for the material.

(2) The kinematic collapse mechanism so obtained satisfies the associated flow rule. For example, the necessary condition (11.30) is in fact the normality requirement for a rigid-body rotation. As shown in Fig. 11.4, Δ_n and Δ_t are normal and tangential components of the plastic velocity vector Δ to the slip surface respectively. From Fig. 11.4 and Eqs. (11.2) and (11.30), we find:

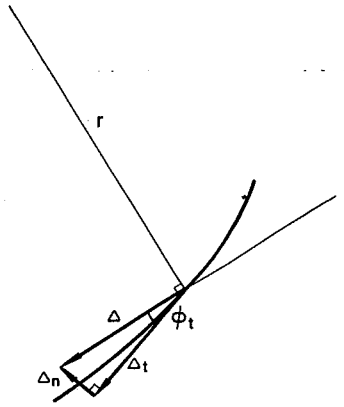

Fig. 11.4. Geometric significance of the plastic velocity vector Δ.

$$\frac{\Delta_n}{\Delta_t} = \tan\phi_t = \frac{1}{r}\left(\frac{dr}{d\theta}\right) \tag{11.45}$$

which implies that the plastic velocity vector, Δ, at the slip surface acts at an angle ϕ_t to the surface.

11.3 Stability analysis of slopes

In the preceding section, we have introduced the variational calculus approach in the limit analysis and the combined method by an illustrative example, i.e., the bearing capacity of a strip footing on the upper surface of a slope (Fig. 11.1). In the following, we shall discuss the general solution procedure. Since it is possible that when $P = 0$, the soil mass can still slide under its own weight, the critical height of a slope must also be considered in the analysis. To find the critical height of a slope, we can use the same solution procedure as we did for the bearing capacity of a strip footing on the upper surface of a slope, but let $P = 0$ and let the starting point of the slip surface flexible.

11.3.1 The solution procedure for the bearing capacity of a strip footing on the upper surface of a slope

As shown in Fig. 11.5, the solution procedure can be summarized as follows:

Step 1: Input soil property data and known slope geometric parameters of the strip footing on a slope.

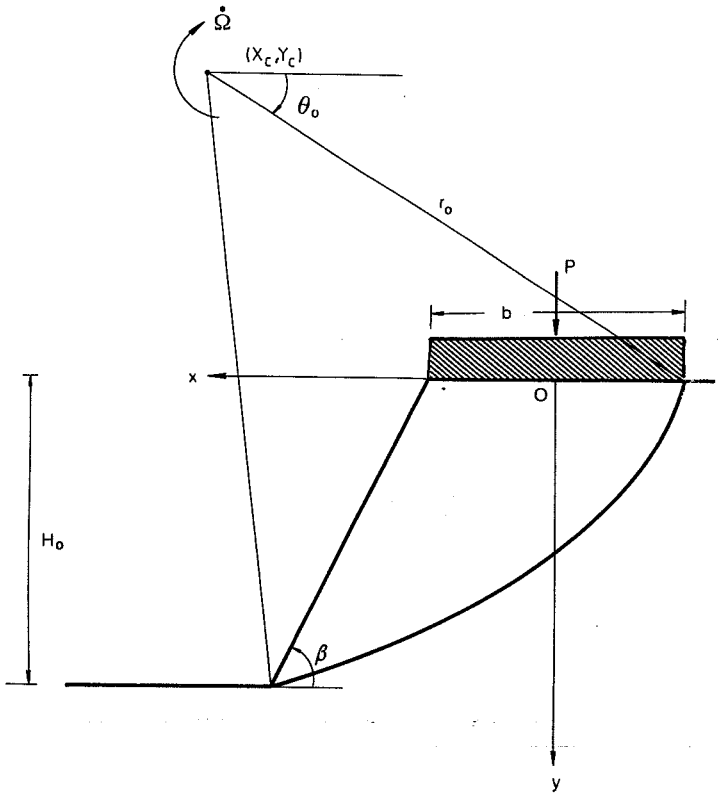

Fig. 11.5. Bearing capacity problems with slope angle β.

Step 2: Assume the initial normal stress σ_0.
Step 3: Assume the coordinates of the rotation center (x_c, y_c), and calculate the initial radius r_0 and the initial angle θ_0.
Step 4: Select the step size $\Delta\theta$. Using a numerical method to calculate the values of $r(\theta)$ and $\sigma(\theta)$ from Eqs. (11.30) and (11.33), until the slip surface reaches the slope surface.
Step 5: Calculate the resultant horizontal and vertical forces H and V by the numerical integration.
Step 6: Use an optimization method to repeat Step 3 to Step 5, until $F = \sqrt{H^2 + V^2}$ is very close to zero.
Step 7: Calculate the external load P from Eq. (11.15) and the corresponding coordinates of the exit point of the slip surface (x_n, y_n).

Step 8: Change the initial normal stress σ_0, repeat Step 3 to Step 7 until P_{min} is found.
Step 9: Output the results.

11.3.2 The solution procedure for the critical height of slopes

As shown in Fig. 11.6, there is no external load, and the length L is unknown. Thus, we have:
Step 1: Input soil property data and the known slope geometric parameters.
Step 2: Assume the length L.
Step 3: Assume the initial normal stress σ_0.
Step 4: Assume the coordinates of the rotation center (x_c, y_c), and calculate the initial radius r_0 and the initial angle θ_0.
Step 5: Select the step size $\Delta\theta$. Using a numerical method to calculate the values of $r(\theta)$ and $\sigma(\theta)$ from Eqs. (11.30) and (11.33) until the slip surface reaches the slope surface.
Step 6: Calculate the resultant horizontal and vertical forces H and V and the load P by the numerical integration.
Step 7: Use an optimization method to repeat Step 4 to Step 6, until the load P reaches a minimum value.
Step 8: Calculate the equilibrium function F when P is a minimum value.
Step 9: Change σ_0, and repeat Step 3 to Step 8, until F is very close to zero.
Step 10: Determine the coordinates of the exit point of the slip surface (x_n, y_n). Let the height of slope $H_0 = y_n$.
Step 11: Change L, and repeat Step 2 to Step 10, until the minimum H (H_{min}) is found.
Step 12: Output $H_{cr} = H_{min}$.

11.3.3 Numerical results

Define the *stability factor* N_s as:

$$N_s = H_{cr}\frac{\gamma}{c} \tag{11.46}$$

where c is the nominal cohesion of the nonlinear failure curve shown in Fig. 11.2. The height H_{cr} is the critical value of the slope as shown in Fig. 11.6. The following three-parameter failure criterion is used. A similar criterion has been used previously by Zhang and Chen (1987):

$$\tau = f(\sigma) = c\left(1 + \frac{\sigma}{\sigma_t}\right)^m \tag{11.47}$$

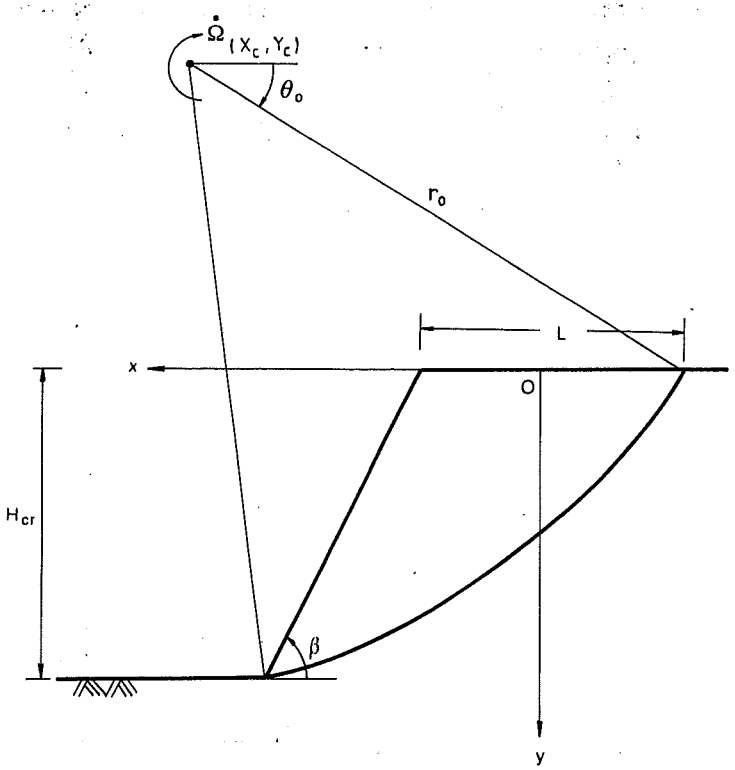

Fig. 11.6. Critical height problem.

TABLE 11.1
Comparison of the N_s-values for the combined method with the linear limit analysis

	β	90°	80°	70°	60°	50°
1	Linear limit analysis (Chen, 1975)	5.50	6.75	8.13	10.39	13.45
2	Nonlinear method					
	(a) c = 0.01 MPa, γ = 0.0016 kg/cm^3	5.50	6.71	8.23	10.35	13.63
	Relative error (%)	0.00	0.59	1.23	0.38	1.34
	(b) c = 0.015 MPa, γ = 0.0024 kg/cm^3	5.46	6.68	8.22	10.28	13.30
	Relative error (%)	0.72	1.00	1.11	1.06	1.12

Note: The Mohr-Coulomb criterion with ϕ = 20° is used in both cases.

where c is the nominal cohesion of soil. $\sigma_t = c/\tan\phi$. ϕ is the nominal angle of internal friction of soil. m is the nonlinear coefficient. It can be seen that when m = 1, Eq. (11.47) reduces to the well-known linear Mohr-Coulomb failure criterion.

Comparison of the present numerical results for the linear case with the existing limit analysis solutions (Chen, 1975) is given in Fig. 11.7 and Table 11.1. It is seen that the agreement is good and in most cases, the combined method gives lower solutions. From Table 11.1, if we change the values of c and γ, and keep γ/c constant,

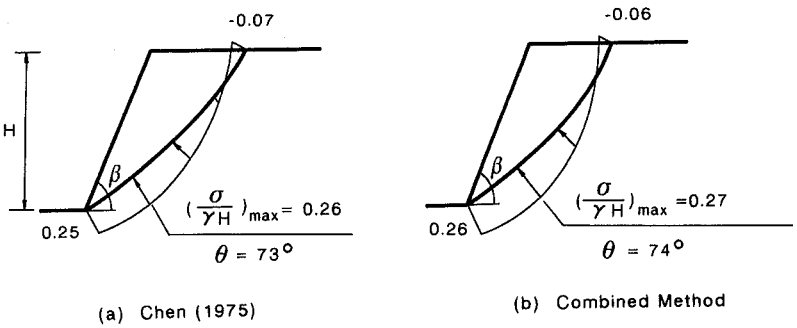

Fig. 11.7. Comparison of the distributions of the normal stresses (β = 70°, ϕ = 20°).

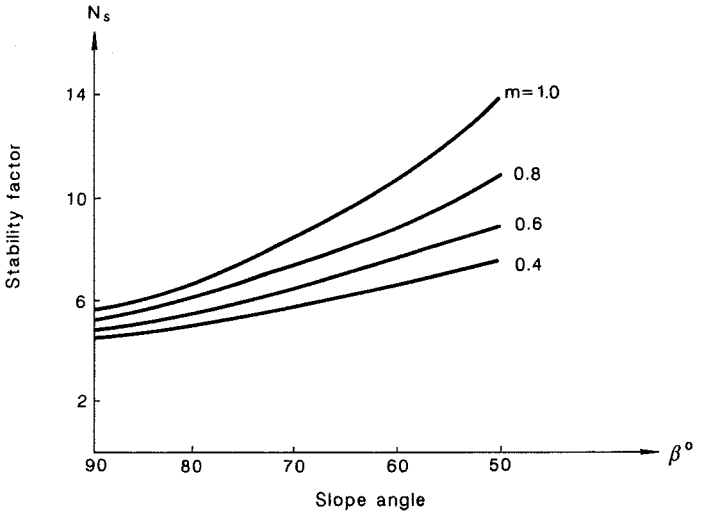

Fig. 11.8. The relationship between N_s and β (ϕ = 20°, c = 0.01 MPa, γ = 0.0016 kg/cm^3).

the combined method leads to different answers, while the analysis for a linear failure criterion leads to the same answer.

Effect of the nonlinear coefficient m on the stability factor N_s

Values of the stability factor N_s corresponding to constant values of the nominal cohesion c and the nominal angle of internal friction ϕ with the nonlinear coefficient m varying from 0.4 to 1.0 are given in Fig. 11.8 (ϕ = 20°, c = 0.01 MPa, and

TABLE 11.2
Influence of the nonlinear coefficient m on the bearing capacity P (unit: kN/m)

	β:	90°	80°	70°	60°	50°
	H_0 (cm):	300	350	400	450	500
	b (cm):	200	200	250	250	300
m	1.0	7.89	13.19	28.94	47.81	102.00
	0.8	3.47	7.67	14.72	24.51	50.53
	0.6	*	*	0.61	4.19	14.59
	0.4	*	*	*	*	*

* Note P is negative.

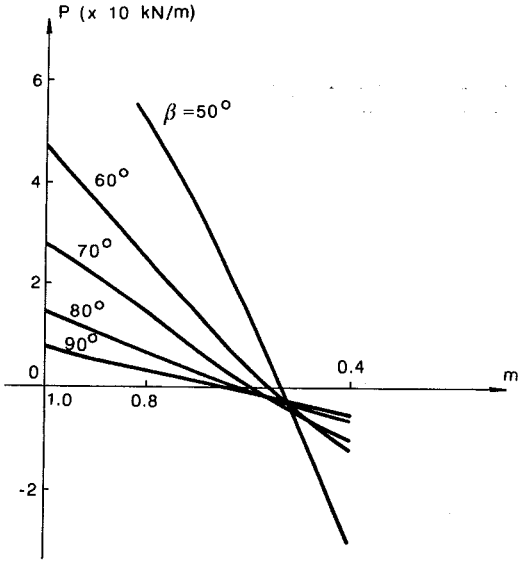

Fig. 11.9. The relationship between P and m.

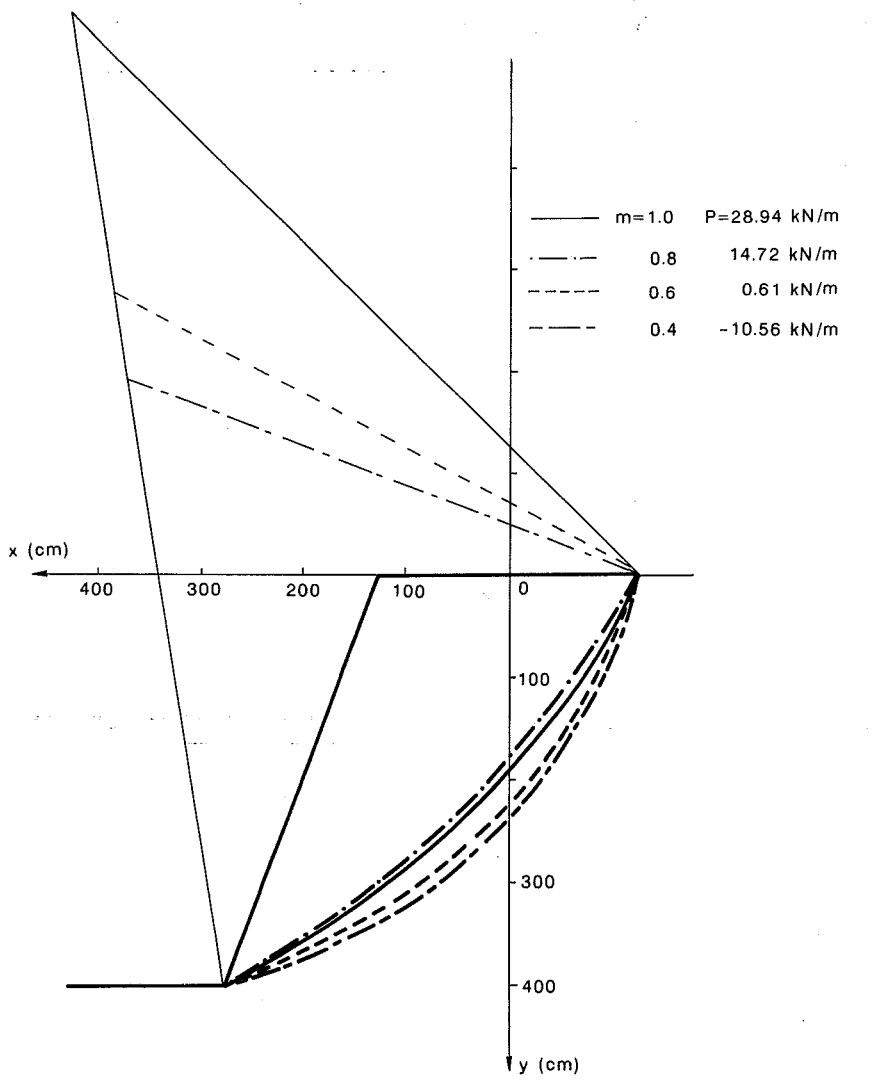

Fig. 11.10. The failure mechanisms for bearing capacity problems (β = 70°, H_0 = 400 cm, b = 250 cm).

$\gamma = 0.0016\ \text{kg/cm}^3$). It is observed that the stability factor N_s decreases significantly with a decrease in the nonlinear coefficient m, especially in the range of less slope angle β.

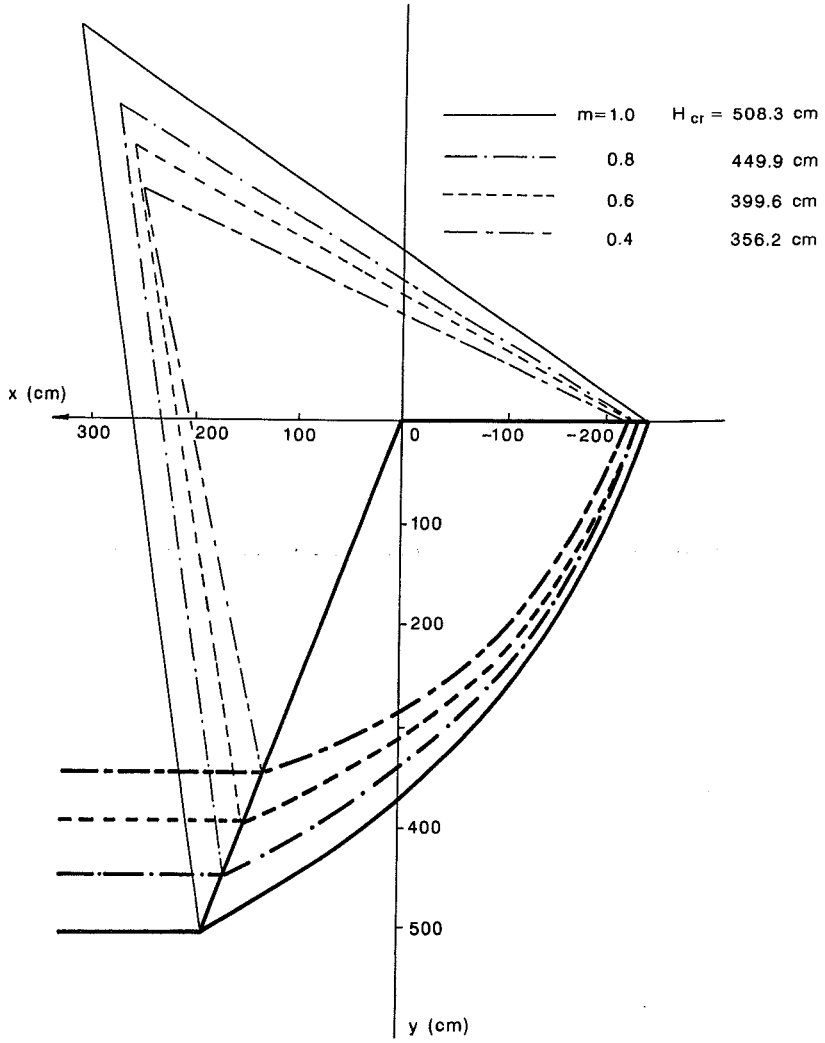

Fig. 11.11. The failure mechanisms for critical height of slopes ($\beta = 70°$).

Effect of the nonlinear coefficient m on the bearing capacity

As shown in Fig. 11.5, Table 11.2 gives the relationship between the bearing capacity P and the nonlinear coefficient m. According to Fig. 11.9 and Table 11.2, it can be seen that when β = constant, the bearing capacity of slope decreases with a decrease in the nonlinear coefficient m.

Effect of the nonlinear coefficient m on the failure mechanisms

Figure 11.10 shows that when $\beta = 70°$, $H_0 = 400$ cm, $b = 250$ cm, even when the bearing capacity has been reached, the effect of m on the failure mechanisms is still not obvious. From Fig. 11.11, it is found that when $\beta = 70°$, the critical height of slope decreases with a decrease in the nonlinear coefficient m.

Effect of the nonlinear coefficient m on the distribution of normal stresses

Figures 11.12 and 11.13 give the distributions of normal stresses for both the critical height and the bearing capacity, respectively. In general, when m decreases, the normal compressive stress increases somewhat. For the bearing capacity problems, the initial normal compressive stress σ_0 decreases with a decrease in the coefficient m.

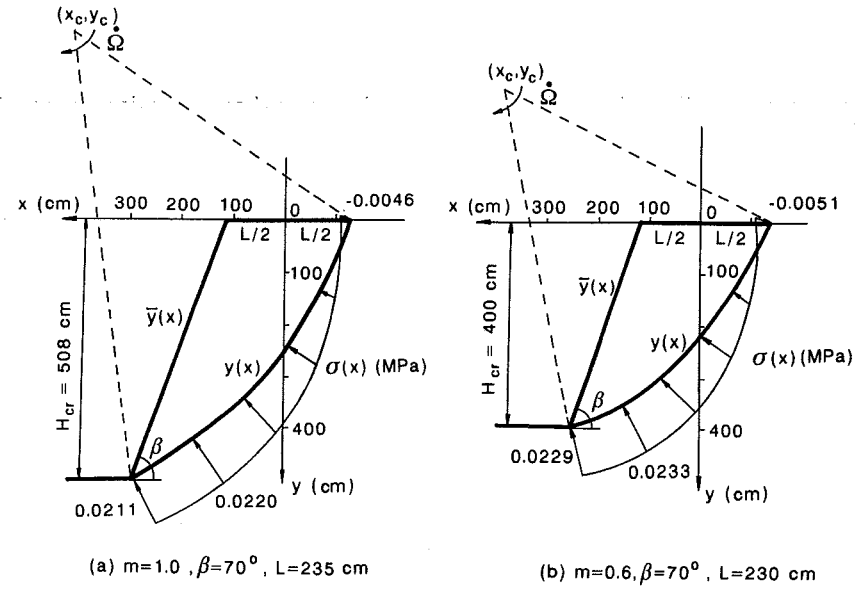

Fig. 11.12. Normal stress distributions of the critical height of slopes.

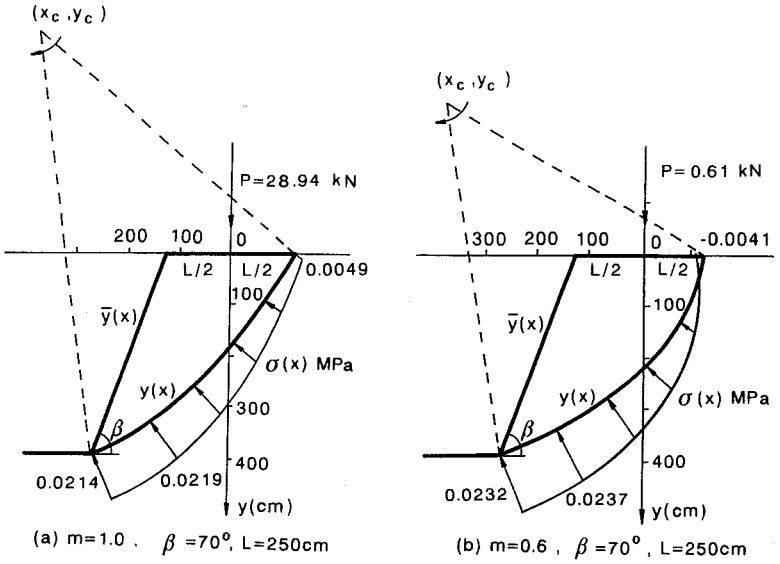

Fig. 11.13. Normal stress distributions of the bearing capacity of footing on slopes.

11.4 Layered analysis of embankments

In reality, every mass of soil exhibits some anisotropy and some nonhomogeneity. The slope under consideration is usually made of several different soils. In practice, we may treat this as a composite slope made of different layers, and in each layer, the soil can be treated as an isotropic and homogeneous medium. In this section, we shall extend the combined method to the stability problem of layered slopes (Liu et al., 1989).

As an illustrative example, we consider the particular cross section of embankments consisting of several layers (Fig. 11.14). The load includes the ice bump pressure p and the surcharge pressure q. In many cases, the ice sheet or flow will seriously damage the embankment surface and even cause the sliding failure of the shoulder. In the following discussion, we shall assume the ice pressure p causes the sliding failure of the slope.

Referring to the rigid body sliding failure in Fig. 11.14 and neglecting the interface slips between different layers, we shall derive in the forthcoming the governing equation similar to that of Eq. (11.5). Referring to Figs. 11.15 and 11.19, we have the following geometrical relationships:

$$ds\cos\theta = dx \tag{11.48}$$

$$ds\sin\theta = dy \tag{11.49}$$

The horizontal force along ds is:

$$-\sigma\,ds\sin\theta - \tau\,ds\cos\theta = -\sigma\frac{dx}{\cos\theta}\sin\theta - \tau\frac{dx}{\cos\theta}\cos\theta$$

$$= -\sigma\tan\theta\,dx - \tau\,dx = -\left(\sigma\frac{dy}{dx} + \tau\right)dx \tag{11.50}$$

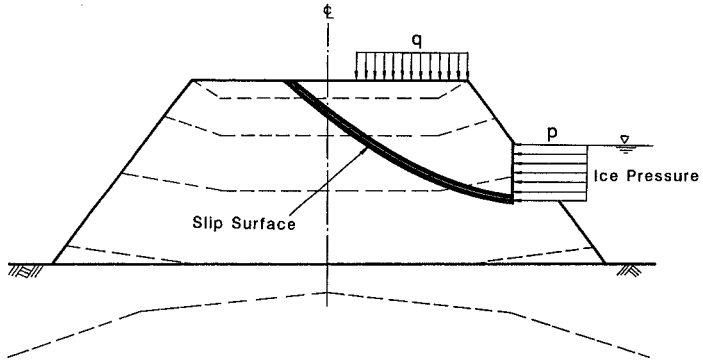

Fig. 11.14. Typical layered embankment.

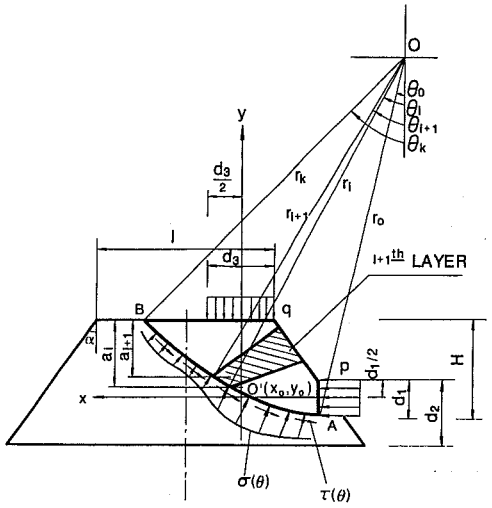

Fig. 11.15. Calculation scheme of the embankment.

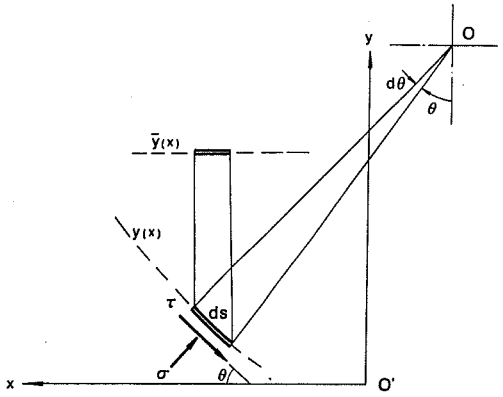

Fig. 11.16. Geometric relationship on the slip surface.

Similarly, in the vertical direction, we obtain:

$$\left[-\tau\frac{\mathrm{d}y}{\mathrm{d}x}+\sigma-(\bar{y}-y)\,\gamma\right]\mathrm{d}x \tag{11.51}$$

Integrating from x_B to x_A, we obtain:

$$H=-\int_{x_B}^{x_A}\left(\tau+\frac{\mathrm{d}y}{\mathrm{d}x}\sigma\right)\mathrm{d}x+p\,d_1 \tag{11.52}$$

$$V=\int_{x_B}^{x_A}\left[\left(-\tau\frac{\mathrm{d}y}{\mathrm{d}x}+\sigma\right)-(\bar{y}-y)\,\gamma\right]\mathrm{d}x-q\,d_3 \tag{11.53}$$

The moment equilibrium of the mass with respect to the point O′ (Fig. 11.15) is:

$$M=\int_{x_B}^{x_A}\left[-\left(\tau\frac{\mathrm{d}y}{\mathrm{d}x}-\sigma\right)x-(\bar{y}-y)\,\gamma\,x+\left(\tau+\sigma\frac{\mathrm{d}y}{\mathrm{d}x}\right)y\right]\mathrm{d}x \tag{11.54}$$

Let $\dot{\Omega}\neq 0$ and $\dot{u}=1$. Substituting Eqs. (11.52) to (11.54) into Eq. (11.5), we find:

$$p=\int_{x_B}^{x_A}\frac{\dot{\Omega}}{d_1}\left\{\left[\left(\frac{1}{\dot{\Omega}}-y\right)+\frac{\mathrm{d}y}{\mathrm{d}x}\left(\frac{\dot{v}}{\dot{\Omega}}+x\right)\right]\tau+\left[\frac{\mathrm{d}y}{\mathrm{d}x}\left(\frac{1}{\dot{\Omega}}-y\right)-\frac{\dot{v}}{\dot{\Omega}}+x\right)\right]\sigma$$

$$+\gamma\,(\bar{y}-y)\left(\frac{\dot{v}}{\dot{\Omega}}+x\right)\Bigg\}\mathrm{d}x+\frac{\dot{v}}{d_1}\,q\,d_3 \tag{11.55}$$

Now the problem reduces to:

$$p=G\left[y(x),\,\sigma(x),\,\frac{\mathrm{d}y}{\mathrm{d}x},\,\dot{v},\,\dot{\Omega}\right]=\int_{x_0}^{x_n}g^*\,\mathrm{d}x \tag{11.56}$$

Similarly, introducing:

$$F=(H^2+V^2)^{\frac{1}{2}}=0 \tag{11.57}$$

the solution procedure becomes:

$$P_{\min}=\operatorname*{Min}_{\eta_i}[G] \tag{11.58}$$

$$F=0 \tag{11.59}$$

$$\tau=f(\sigma) \tag{11.60}$$

$$K(\eta_i)=0 \tag{11.61}$$

Using the following coordinate transformation (Fig. 11.15):

$$x=-\frac{\dot{v}}{\dot{\Omega}}+r\sin\theta \tag{11.62}$$

$$y=\frac{1}{\dot{\Omega}}-r\cos\theta \tag{11.63}$$

the necessary conditions for the determination of the minimum ice pressure p are:

$$\frac{\mathrm{d}r}{\mathrm{d}\theta}=r\frac{\mathrm{d}f(\sigma)}{\mathrm{d}\sigma} \tag{11.64}$$

and

$$\frac{d\sigma}{d\theta} + 2\tau + \gamma r \sin\theta = 0 \tag{11.65}$$

In the present case, we shall assume the slip surface begins at Point A (Fig. 11.15). If r_0 and θ_0 are assumed, the location of the Point 0 is known as:

$$(x_0, y_0) = \left(-\frac{\dot{v}}{\dot{\Omega}}, \frac{1}{\dot{\Omega}}\right) \tag{11.66}$$

Assume the normal stress σ_0 at Point A. Thus, the necessary conditions (11.64) and (11.65) can be treated as a pair of simultaneous differential equations with initial values. Many numerical methods can be used to find the slip surface and the corresponding normal stress distribution by a step-by-step process. Then, the value p can be obtained from Eq. (11.55). To find the minimum ice pressure p, we reassume the initial values of r_0, θ_0, and σ_0 and repeat the above procedure. The minimum p can usually be found by using an available optimization program.

In the layered stability analysis, several different layers must be considered in Eq. (11.55). The following expressions may be used for the evaluation of Eq. (11.55) in such a case.

We divide Eq. (11.55) into three parts as:

$$p_I = \int_{x_B}^{x_A} \frac{\dot{\Omega}}{d_1}\left\{\left[\left(\frac{1}{\dot{\Omega}} - y\right) + \frac{dy}{dx}\left(\frac{\dot{v}}{\dot{\Omega}} + x\right)\right]\tau + \left[\frac{dy}{dx}\left(\frac{1}{\dot{\Omega}} - y\right) - \left(\frac{\dot{v}}{\dot{\Omega}} + x\right)\right]\sigma\right\} dx \tag{11.67}$$

$$p_b = \int_{x_B}^{x_A} \frac{\dot{\Omega}}{d_1}\gamma(\bar{y} - y)\left(\frac{\dot{v}}{\dot{\Omega}} + x\right)dx \tag{11.68}$$

and

$$p_q = \dot{v}\frac{d_3}{d_1}q \tag{11.69}$$

where p_I is the part of p carried by the internal stresses along the slip surface. p_b is the part of ice pressure carried by the body force (the soil weight), and p_q is the part by the surcharge load.

For layered soil, by superposition, Eq. (11.68) can be written as:

$$p_b = \frac{1}{d_1}\sum_i (p_b)_i = \frac{1}{d_1}\sum_i \dot{\Omega}\gamma_i S_i \tag{11.70}$$

where γ_i and S_i are the unit weight and the area moment of layer i, respectively.

The calculation for S_i in Eq. (11.70) is outlined in the following. Referring to Fig. 11.17, we first calculate $(S)_{125}$, and $(S)_{123765}$, and then use the following relationship:

$$(S)_{23765} = (S)_{123765} - (S)_{125} \tag{11.71}$$

to find $(S)_{23765}$. In this way, S_i values for different layers can be obtained.

In what follows, we shall only consider a common case, in which the interfaces between different layers are approximately straight lines, and $q = 0$. For convenience, the definition of the interface MN with the end points M and N is necessary. As shown in Fig. 11.18, starting from $A(x_0, y_0)$, following the surface of the em-

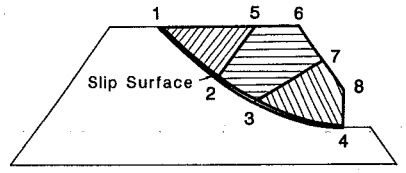

Fig. 11.17. Basic idea of layered analysis.

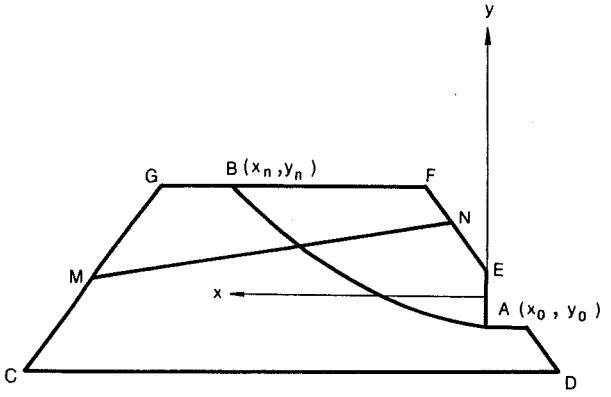

Fig. 11.18. Definition of M and N.

bankment counterclockwise, the first intersection point with an intersurface is called N, the other one is called M.

To calculate S_i, computer program will be used, considering the triangular type (Fig. 11.19a) and sector type (Fig. 11.19b). For the triangular type, we can develop a subroutine to calculate the centroid location and the area by the coordinates of three vertexes. For the sector type, the numerical integration can be used, such as:

$$S_{012} = \frac{1}{3}\int_{\theta_1}^{\theta_2} r^3(\theta)\sin\theta\,\mathrm{d}\theta \tag{11.72}$$

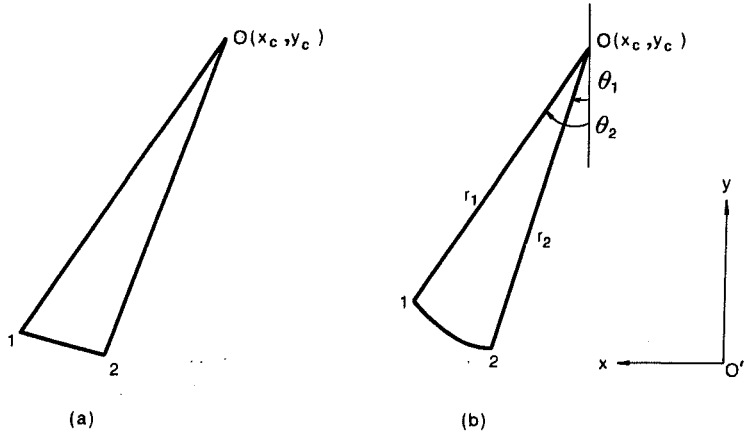

Fig. 11.19. The triangular type and sector type.

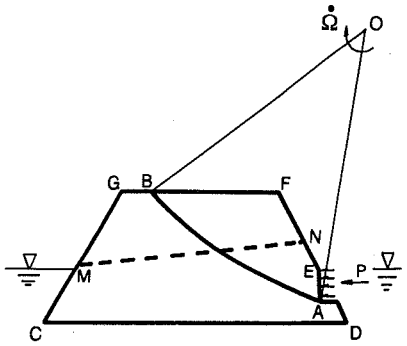

Fig. 11.20. Type I.

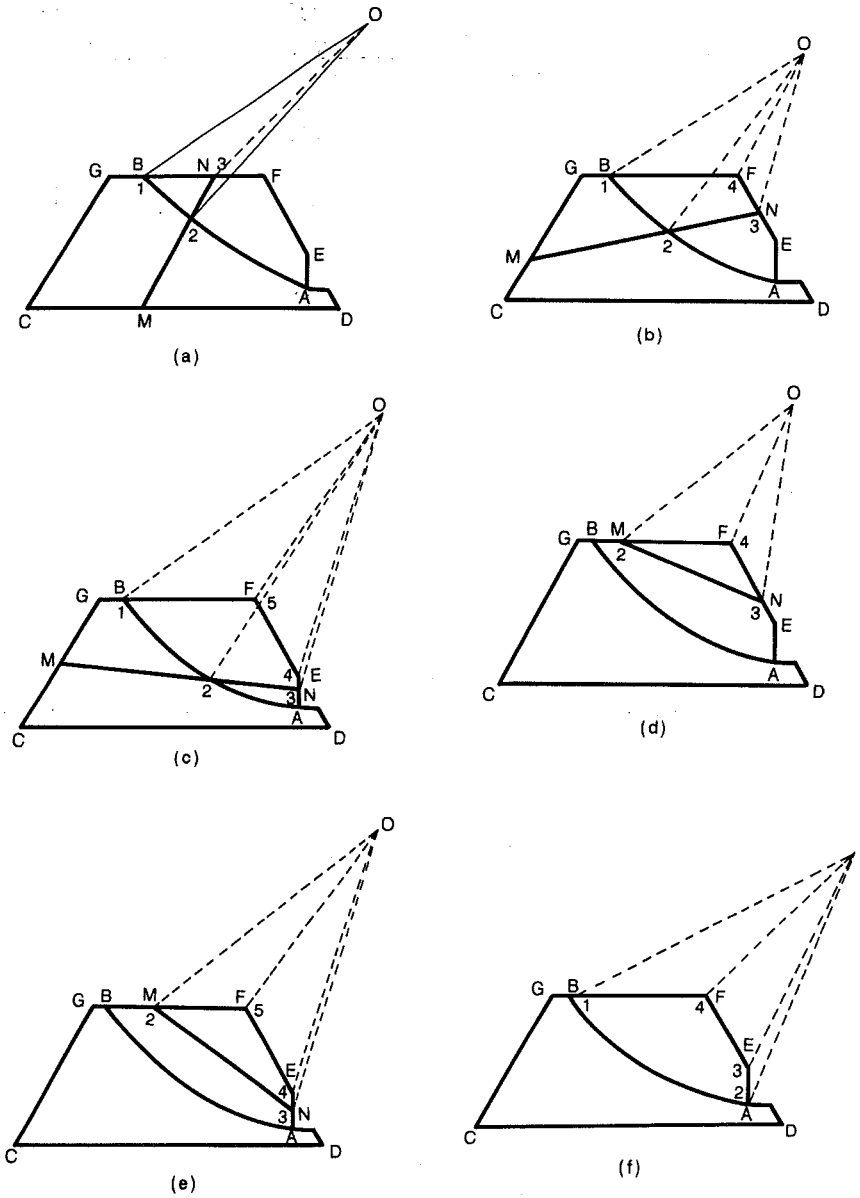

Fig. 11.21. Six cases in Type I.

According to the different distribution of layers, three different locations of the failure surface end B(x_n, y_n) will be considered. For each location of B(x_n, y_n) there exist several cases depending on the location of MN.

(1) Type I

As shown in Fig. 11.20, the point B is located between F and G, i.e., on the upper surface of the embankment. Based on the locations of M and N, there exist six cases.

(a) M is located between BGCD, and N between FB (Fig. 11.21a):

$$S_{123} = S_{012} - S_{013} - S_{032} \tag{11.73}$$

(b) M is located between BGCD, and N between EF (Fig. 11.21b):

$$S_{1234} = S_{012} + S_{023} - S_{014} - S_{043} \tag{11.74}$$

(c) M is located between BGCD, and N between AE (Fig. 11.21c):

$$S_{12345} = S_{012} + S_{023} - S_{015} - S_{054} - S_{043} \tag{11.75}$$

(d) M is located between FB, and N between EF (Fig. 11.21d):

$$S_{234} = S_{023} - S_{024} - S_{043} \tag{11.76}$$

(e) M is located between FB, and N between AE (Fig. 11.21e):

$$S_{2345} = S_{023} - S_{025} - S_{054} - S_{043} \tag{11.77}$$

(f) There is no intersection between MN and the failure surface (Fig. 11.21f).

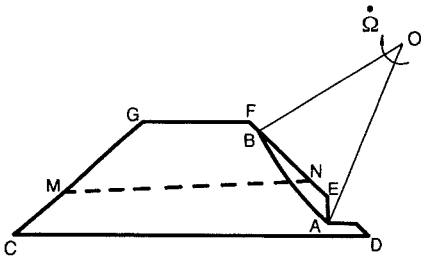

Fig. 11.22. Type II.

(2) Type II

As shown in Fig. 11.22, point B is located between E and F, i.e., on the right surface of the embankment. There are three cases exist.

(a) N is located between EF (Fig. 11.23a):

$$S_{123} = S_{012} + S_{023} - S_{013} \tag{11.78}$$

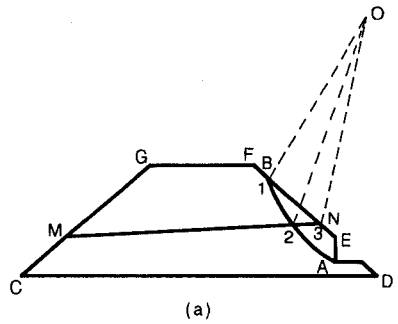

(a)

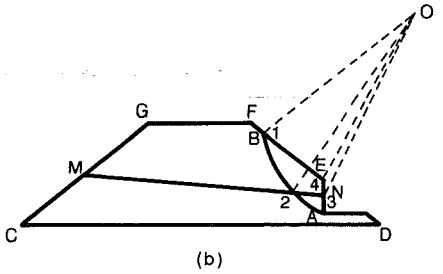

(b)

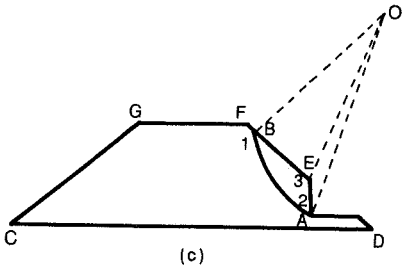

(c)

Fig. 11.23. Three cases in Type II.

(b) N is located between AE (Fig. 11.23b):

$$S_{1234} = S_{012} + S_{023} - S_{014} - S_{043} \tag{11.79}$$

(c) There is no intersection between MN and the failure surface (Fig. 11.23c).

(3) Type III

Point B is located between G and C, i.e., on the left surface of the embankment. There exist ten cases. But in practice not all cases will occur, especially when FG (Fig. 11.18) or α (Fig. 11.15) is not small. Details of this development will not be given here. The procedure for this program can be stated in the following steps:

Step 1. Input soil property data and known embankment geometric parameters.

Step 2. Assume the initial normal stress σ_0.

Step 3. Assume the initial parameters of the rotation center x_c and y_c, and calculate the initial radius r_0 and the initial angle θ_0.

Step 4. Choose step length $\Delta\theta$, and calculate the values of $r(\theta)$ and $\sigma(\theta)$ of Eqs. (11.64) and (11.65) until the slip surface reaches the embankment surface by Runge Kutta method. Note that when the failure surface reaches a different layer the corresponding layer property data should be used and the relative position numbers should also be recorded.

Step 5. Considering different layers, calculate S_i, the resultant horizontal force, H, the vertical force V, and the external load p by a numerical integration. Check the equilibrium function F.

Step 6. Repeat Step 3 and Step 5 until the equilibrium function F is close to zero by an optimization method.

Step 7. Record the $p = p(\theta_0)$ when F is close to zero.

Step 8. Change σ_0, and repeat Step 3 to Step 6 again until $p_{\min}$ is satisfactory.

Step 9. Output the calculation results.

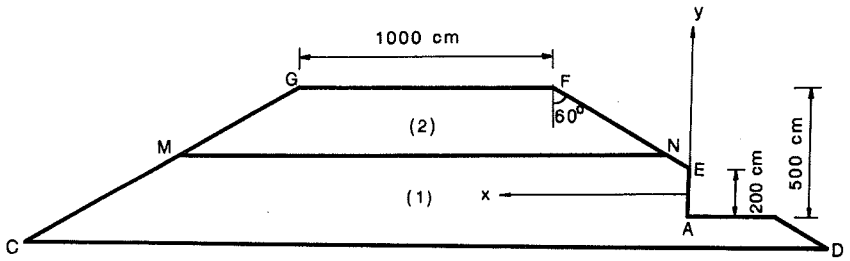

Fig. 11.24. A two-layered embankment example.

As an example, we consider a two-layered embankment (Fig. 11.24) in three cases:

Case <1>: $c_1 = 0.01$ MPa , $\phi_1 = 20°$
$\gamma_1 = 0.0016$ kg/cm^3, $m_1 = 1.0$

$c_2 = 0.01$ MPa , $\phi_2 = 20°$
$\gamma_2 = 0.0016$ kg/cm^3, $m_2 = 1.0$

Case <2>: $c_1 = 0.02$ MPa , $\phi_1 = 10°$,
$\gamma_1 = 0.0016$ kg/cm^3, $m_1 = 1.0$

$c_2 = 0.01$ MPa , $\phi_2 = 20°$
$\gamma_2 = 0.0018$ kg/cm^3, $m_2 = 1.0$

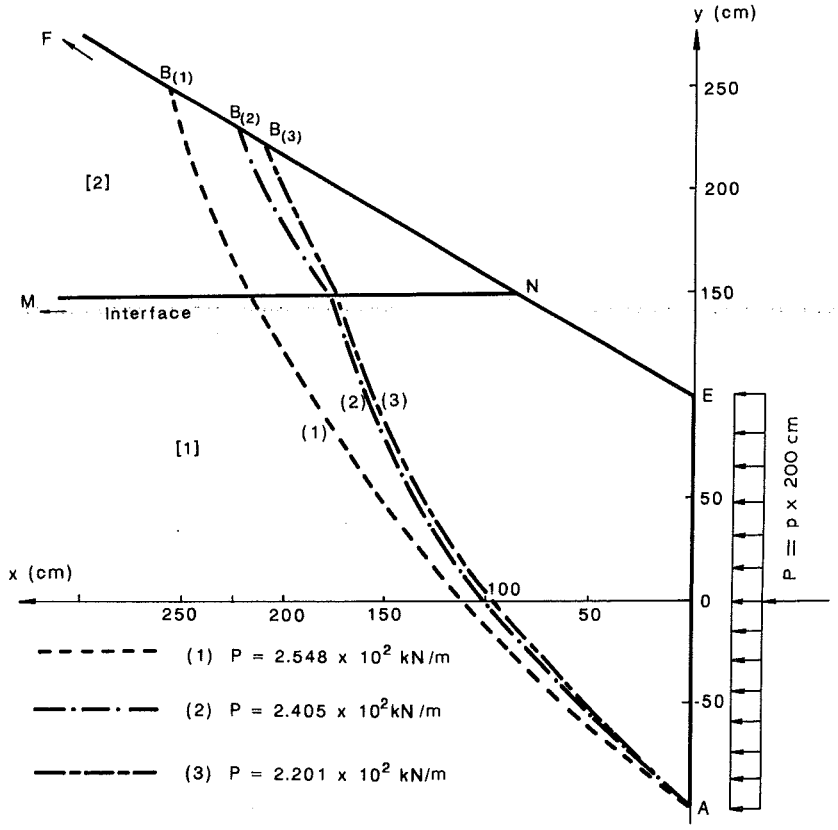

Fig. 11.25. Failure mechanisms of the layered embankment example.

Case <3>: $c_1 = 0.02$ MPa , $\phi_1 = 10°$,
$\gamma_1 = 0.0016$ kg/cm^3, $m_1 = 0.8$

$c_2 = 0.01$ MPa , $\phi_2 = 20°$,
$\gamma_2 = 0.0018$ kg/cm^3, $m_2 = 0.8$

The results of this calculation are shown in Table 11.3 and Fig. 11.25. It can be seen that Case <1> is in fact a single-layered embankment, its failure surface is continuously smooth. In Case <2> or Case <3>, the reduction of ϕ causes a decrease of the bearing capacity, even though c and γ increase. From Fig. 11.25, it is seen that the failure surface can not remain smooth. Comparing Case <3> with Case <2>, the bearing capacity is found to decrease by an amount of about 8.5%.

11.5 Summary

(1) The linear limit analysis procedure is generally limited to the linear Mohr-Coulomb criterion. The extended nonlinear procedure which is called the combined method herein is valid for both linear and nonlinear failure criteria. This procedure yields not only the mechanism of rotational discontinuity, but also its associated stress distribution along the slip surface.

(2) One of the necessary conditions used in the extended procedure is the normality condition.

(3) The combination of the variational calculus and the optimization method provides an effective solution procedure, that is convenient for solving various stability problems in soil mechanics including the layered analysis of embankment.

(4) For the special case of a linear failure criterion the present results reduce to those obtained previously by the linear limit analysis, but in addition, the associated normal stress distribution along the slip surface is also obtained.

TABLE 11.3
Layered embankment example

Case	P (kN/m)	σ_0 (MPa)	σ_n (MPa)	(x_c,y_c) (cm)	(x_n,y_n) (cm)
<1>	254.8	0.1050	0.0069	(−572,258)	(261,251)
<2>	240.5	0.1066	0.0083	(−397,262)	(224,229)
<3>	220.1	0.0998	0.0083	(−395,282)	(212,223)

References

Baker, R. and Garber, M., 1977. Variational approach to slope stability. Proc., 9th ICSMFE, Vol. 2, Tokyo, pp. 8–12.

Baker, R., 1981. Tensile strength, tension cracks, and stability of slopes. Soil Found. 21(2): 1–17.

Baker, R. and Frydman, S., 1983. Upper bound limit analysis of soil with non-linear failure criterion. Soil Found., Jpn., 23(4): 34–42.

Chen, W.F., 1970. Discussion on Circular and Logarithmic Spiral Slip Surfaces, by Eric Spencer. J. Soil Mech. Found. Div., ASCE, 96(SM1): 324–326.

Chen, W.F. and Snitbhan, N., 1975. On slip surface and slope stability analysis. Soil Found., Jpn., 15(3): 41–49.

Garber, M. and Baker, R., 1977. Bearing capacity by variational method. J. Geotech. Eng. Div., ASCE, 103(GT-11): 1209–1225.

Chen, W.F., 1975. Limit Analysis and Soil Plasticity. Elsevier, Amsterdam, The Netherlands, 638 pp.

Liu, X.L., Wang, Q.Y. and Chen, W.F., 1989. Layered Analysis with Generalized Failure Criterion. Computers Structures, 33(4): 1117–1123.

Wang, Q.Y. and Liu, X.L., 1988. Limit analysis based on variational method. Proc. Int. Conf. of Engineering Problems of Regional Soils, Beijing, China, pp. 469–472.

Zhang, X.J. and Chen, W.F., 1987. Stability analysis of slopes with general non-linear failure criterion. Int. J. Numer. Anal. Methods Geomech., 11: 33–50.

SUBJECT INDEX

AUTHOR INDEX